LBL-26455
UC-400

MATERIALS AND CHEMICAL SCIENCES DIVISION

Annual Report 1988

July 1989

Lawrence Berkeley Laboratory
University of California
Berkeley, California 94720

Prepared for the
U.S. Department of Energy under Contract DE-AC03-76SF00098

DISCLAIMER

LBL-26455

MATERIALS AND CHEMICAL SCIENCES DIVISION

Annual Report 1988
July 1989

Norman E. Phillips, Division Director
Mark Alper, Associate Division Director
Rolf H. Muller, Associate Division Director
Conway V. Peterson, Associate Division Director

Lawrence Berkeley Laboratory
University of California
Berkeley, California 94720

Materials Sciences

Chemical Sciences

Fossil Energy

Energy Storage Systems

Health and Environmental Sciences

Exploratory Research and Development Funds

Work for Others

Appendices

Contents

APPENDICES

REMARKS BY THE DIVISION DIRECTOR

The merger of MMRD and CAM has been fully implemented during the past year. CAM is now a Center within MCSD, retaining its mission to do industry-relevant research. Administratively, the merger makes it easier to transfer scientific personnel in and out of CAM as the directions of the CAM programs evolve. Several MMRD programs that were closely related to CAM programs have been transferred to CAM in order to foster greater collaboration between Investigators. The programs transferred are Structure-Property Relationships in Semiconductor Materials, Jack Washburn, Investigator; and Solid-State and Surface Reactions, Gabor A. Somorjai, Investigator (both supported by DOE's Division of Materials Sciences); Catalytic Hydrogenation of CO, Alexis T. Bell, Investigator (supported by DOE's Division of Chemical Sciences); and Fundamental Studies of Catalytic Gasification, Heinz Heinemann, Investigator (supported by DOE's Office of Fossil Energy). Two other MMRD programs transferred to CAM at the same time—Fundamental Studies of Chemical Properties and Processing of Advanced Ceramics, Lutgard De Jonghe, Investigator; and Environmentally Affected Crack Growth in Engineering Materials, Robert O. Ritchie, Investigator—will be combined with another MMRD program, Ceramic Interfaces, Andreas Glaeser, Investigator, to become the CAM Ceramic Processing Program, under the overall direction of Lutgard De Jonghe. Glaeser's program will be transferred to CAM in October 1989; at that time the Ceramic Processing Program will officially become the sixth CAM program. The combination of these programs will give CAM an independent ceramics program again.

The Advanced Materials Laboratory (AML), the second new LBL building to be occupied by MCSD staff, was completed by May 31, 1989, the scheduled completion date. By that date, the equipment purchased with building funds had been installed and accepted, and the process of moving in was well under way. Major occupants of the AML will be the CAM Electronic Materials and High-T_c Superconductivity Programs. Other MCSD programs housed in the AML include Studies at the Metal/Solution Interface with X Rays (Philip Ross, Investigator); Growth Mechanisms at Heterointerfaces (Marjorie Olmstead, Investigator); and Photoelectron Spectroscopy (David Shirley, Investigator). The Center for X-Ray Optics, a program in the Accelerator and Fusion Research Division (AFRD), occupies the fourth floor of the AML.

A large fraction of the equipment funds for the AML was used to purchase apparatus for fabrication and characterization of thin films, including MOCVD (metal-organic chemical vapor deposition) and CBE (chemical-beam epitaxy) apparatus. This equipment brings an entirely new capability to LBL, one that will contribute in important ways to a number of research projects.

Even with construction complete, however, the AML continues to require considerable attention from both the Division and Laboratory administrations. During the years since the building was designed, the awareness of hazards associated with certain chemicals has become more widespread, with consequent changes in the building code. As a result, our new laboratory does not meet code! Thus, some modifications will have to be made, and planning for these is under way. Specific plans are for changes in ventilation controls, the installation of alarm and sensor systems, and the training of building occupants in dealing with the hazards associated with the research in the building. Although these changes represent a considerable complication and expense, they will contribute significantly to improving safety in the AML.

Several new projects were initiated in 1988, and there were significant changes in the status of several others. Structure Determination at the Metal/Solution Interface, with Philip Ross as Investigator, a project started with LBL Director's Exploratory Research and Development Funds (ERF), received regular DOE/BES funding. Other projects that were continued with a second year of ERF funding included Matter at Megabars of Pressure, with Peter Yu, Marvin Cohen, and Raymond Jeanloz as Investigators; Electron Electric Dipole Moment, with Harvey Gould as Investigator; and Novel Materials from Nanocrystalline Aggregates, with Ulrich Dahmen and Kenneth Westmacott as Investigators. A number of high-T_c research projects were also supported by ERF funds. These include Thin Film Superconductors, with Ian Brown as Investigator;

Thin Film High-T_c Superconductors, with John Clarke as Investigator; Fabrication of Ceramic Superconductors, with Lutgard De Jonghe as Investigator, and High-Temperature Superconductors, with Don Morris as Investigator. All of these high-T_c ERF projects are sponsored by MCSD, although Ian Brown is a member of ARFD, and Don Morris is in the Physics Division. (Some contributions by MCSD investigators to the research on high-T_c superconductivity are included in this Annual Report; an overview of the program appears in the CAM Annual Report.)

J.W. Evans, who is Chairman of UCB's Materials Sciences and Mineral Engineering Department, as well as an MCSD Investigator, and I appointed a new committee, the Committee to Strengthen Materials Sciences at Berkeley. The committee will identify promising areas for growth or new directions in LBL/UCB materials sciences research. Members of the committee are Gareth Thomas (Chairman), Robert O. Ritchie, Eugene E. Haller, Neil Bartlett, Leo M. Falicov, and John R. Whinnery. All but Whinnery are MCSD investigators.

As of May 1, 1989, there were a total of 581 MCSD staff: 83 Investigators, 29 other scientists, 55 postdoctoral associates, 282 graduate students, 28 undergraduate students, 43 administrative/clerical staff, 33 technical staff, and 28 guests. During the calendar year 451 refereed journal articles were published by MCSD investigators. Students working with MCSD investigators received 11 M.S. and 46 Ph.D. degrees.

The year saw small reductions in the budget (over and above losses associated with inflation) in most budget categories. The exception was high-T_c research, which did experience real growth, both in BES and OESD funds.

The honors received by MCSD Investigators in calendar year 1988 included:

- Neil Bartlett was awarded the Prix Moissan and the American Chemical Society Award for Distinguished Service in the Advancement of Inorganic Chemistry.
- Alex Bell was elected a Fellow of the American Association for the Advancement of Science.
- Leo Brewer received the Henry B. Linford Award for Distinguished Teaching from the Electrochemical Society.
- Marvin Cohen was appointed a Miller Research Professor of the University of California at Berkeley.
- Robert Connick received the Berkeley Medal.
- Didier de Fontaine received a Japan Society for Promotion of Science Fellowship.
- Leo Falicov was elected a foreign member of the Royal Danish Academy of Physics Faculty.
- Harvey Gould was elected a Fellow of the American Physical Society.
- Ron Gronsky was elected a scientific member of the Böhmische Physical Society.
- Yuan Lee was elected a Fellow of the American Association for the Advancement of Science. He received the Leland J. Haworth Distinguished Scientist award from Brookhaven National Laboratory. He was named Alumnus of the Year by the California Alumni Association, and a Corresponding Member of the Göttingen Academy of Sciences, Federal Republic of Germany.
- C. Bradley Moore received the first Inter-American Photochemical Society Award in Photochemistry.
- Donald Olander was the Lady Davis Visiting Professor at Technion, Israel.
- Alexander Pines won the 1988 E.O. Lawrence Award of the U.S. Department of Energy. He was elected to the National Academy of Sciences, was the Burke Lecturer for the Royal Society of Chemistry, won a Guggenheim Fellowship, and was appointed a Miller Research Professor of the University of California at Berkeley.
- Kenneth Pitzer received the Rossini Lectureship, the annual award of the Commission on Thermodynamics of the International Union of Pure and Applied Chemistry.
- John Prausnitz was elected a Fellow of the American Academy of Arts and Sciences.
- Richard Saykally received the E.K. Pyler Prize for Molecular Spectroscopy from the American Physical Society, the Bomen-Michelson Award from the Coblenz Society, and the Merci-Frost Lectureship from the University of British Columbia.
- Peter Schultz received an Alfred P. Sloan fellowship and the NSF Waterman Award.
- Glenn Seaborg was one of three recipients of the Energy for Mankind Award for 1988, sponsored by the Global Energy Society for the Eradication of Poverty and Hunger. He also received the Vannevar Bush Award from the National Science Foundation.
- David Shirley received an Alexander von Humboldt Senior U.S. Scientist award.

- Gabor Somorjai received the Peter Debye Award in Physical Chemistry.
- Andrew Streitwieser received the Arthur C. Cope Award from the American Chemical Society.
- Doros Theodorou received an NSF Presidential Young Investigator award.

Norman E. Phillips
Division Director
Materials and Chemical Sciences Division

Materials Sciences

METALLURGY AND CERAMICS

STRUCTURE OF MATERIALS

Structure and Properties of Transformation Interfaces*

Ronald Gronsky, Investigator

INTRODUCTION

The modern science of materials devotes increasing attention to the role of solid-state interfaces; they completely dominate the behavior of thin-film electronic devices, and they strongly influence the behavior of composite materials as well as bulk ceramic and metallic alloys. This program seeks a fundamental understanding of the role of interfaces in materials by applications of high-resolution electron microscopy to determine local interfacial structure and composition, by theoretical modeling to relate these parameters to actual atomic structure and composition, and by correlations with interfacial-specific properties, including conductivity, diffusivity, ductility, mobility, and reactivity.

Significant attention has been given this past year to various interfaces in the new high-T_c superconductor materials. Planar defects, twins, and grain boundaries are examples of internal interfaces that act as rather serious obstacles to the commercial implementation of these materials, no matter how high their critical temperatures. The continued emphasis in this program is to understand interfacial atomic structure and transformation behavior.

*This work is supported by the Director, Office of Energy Research, Office of Basic Energy Sciences, Materials Sciences Division, of the U.S. Department of Energy under Contract No. DE-AC03-76SF00098.

1. Grain Boundaries in YBCO Oxide Superconductors (Publications 2, 3, 5, 19, 21, and 22)

H.W. Zandbergen,† C.J.D. Hetherington, G. Thomas, and R. Gronsky

It is now well established that grain boundaries are the most problematic microstructural constituents in the new oxide superconductors, particularly with respect to their ability to carry high critical currents. The problem stems from the severely anisotropic nature of the orthorhombic crystal structure in YBCO ($YBa_2Cu_3O_{7-\delta}$), necessitating connectivity of the CuO planes for conduction of the supercurrent. This study has given attention to the atomic structure of grain boundaries, mapping out atomic positions in the boundary vicinity by direct imaging in the Atomic Resolution Microscope (ARM) and other microscopes, and verification of atomic models through computer simulation and processing.

During this past year, it has been found that (1) very few boundaries in properly fabricated materials have amorphous, insulating grain-boundary phases of the type that occur in fluxed, sintered ceramics; (2) many grain boundaries have a contiguous atomic structure that is an abruptly terminated variation of normal stacking (see Figure 1-1), leading to possible insulating layers of a crystalline variety; (3) double CuO layer defects nucleate at grain boundaries in the same manner as free surfaces, leading to bifurcation of conduction planes at grain junctions; (4) the high frequency of occurrence of (001) grain-boundary planes is associated with precursor 90° rotation twins in the tetragonal phase of YBCO; and (5) specimen-preparation procedures for electron microscopy of grain boundaries in these materials must include precautions that guard against the formation of intercalation defects, particularly the double CuO plane variety.

†Present address: Gorlaeus Laboratories, State University of Leiden, 2300 RA, Leiden, The Netherlands.

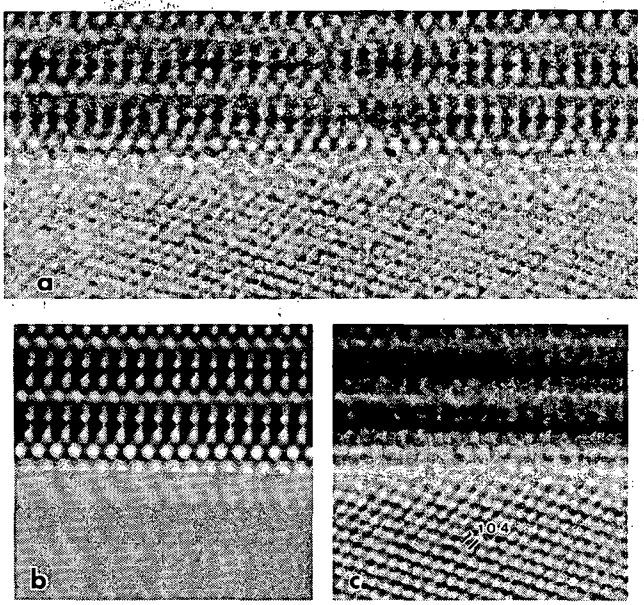

Figure 1-1. (a) Atomic-resolution micrograph of a grain boundary in YBCO, boundary plane parallel to (001) of the upper grain. (b) Processed version of the upper grain. (c) Processed version of the lower grain. Comparisons with calculated images reveal that the upper grain terminates on a BaO_x layer, leaving a partial unit cell at the grain boundary, which may act as an insulating layer. (XBB 8711-4633)

2. On the Structure of $(CuO)_2$ Double Layers in Superconducting $YBa_2Cu_3O_{7-\delta}$ (Publications 6 and 12)

H.W. Zandbergen,† K. Wang, R. Gronsky, and G. Thomas

Detailed high-resolution electron-microscopy studies were applied to identify the atomic structure of the planar defects formed in YBCO ($YBa_2Cu_3O_{7-\delta}$) as a result of exposure to oxygen. The analysis involved computer simulation of images and comparisons with experimental images, evaluated at the atomic level through side-by-side matching of intensity-line scans across image pairs. This process is illustrated in Figure 2-1. The best fit between experimental and calculated images was obtained for the model in which Cu-O-Cu-O... chains occur in the direction of the displacement required to accommodate the extra CuO layer. This means that a shift along the **b** axis of the orthorhombic cell will leave the oxygen atoms at their original positions, whereas a shift along the **a** axis will lead to a rearrangement of the oxygen atoms in both CuO planes, such that the Cu atoms will occupy the originally vacant sites. Only in this way can the planar fourfold coordination of Cu be maintained.

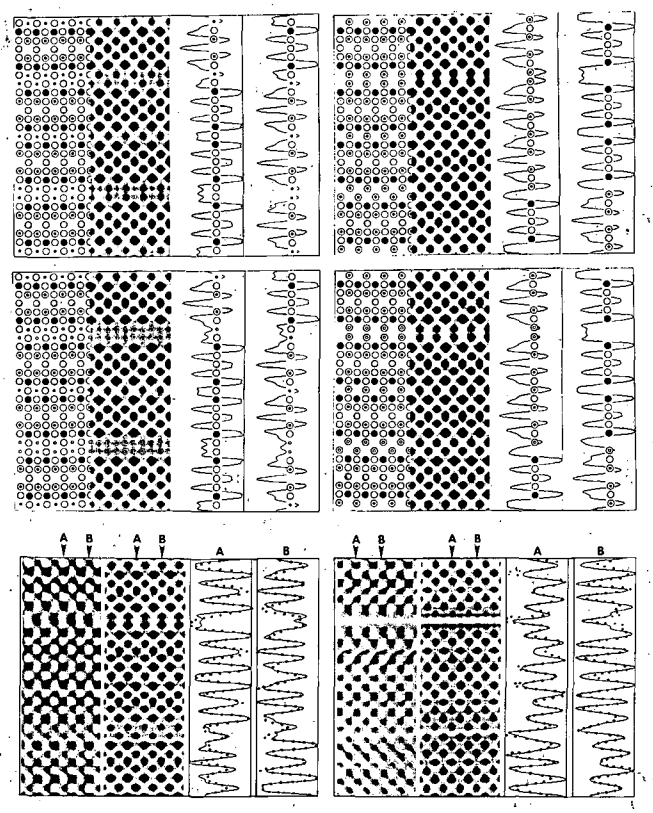

Figure 2-1. Comparisons of the atomic structure of the double CuO layer defect when viewed along [100] (left column) and [010] (right column) directions. The top two structures are those resulting from an a/2 shift of the crystal across the defect plane, and the middle two structures from a b/2 shift. In the bottom two blocks, experimental and calculated images are compared. The line-scan intensity profiles are representative of a 0.075-nm-wide line through positions A and B indicated in the bottom two blocks. Full lines give calculated data, dotted lines the observed intensity variations in the experimental images. The experimental parameters are: specimen thickness, 2 nm; objective aperture, 6 nm^{-1}; accelerating voltage, 100 kV; spherical-aberration coefficient, 2.8 mm; beam-divergence angle, 0.6 mrad. (XBL 8712-5391)

A secondary result of this study was that the presence of oxygen in the conduction planes could be detected directly in the images. Differences were observed at the location of oxygen-bearing columns of atoms along the beam direction when the specimen was imaged in a [100] direction as compared to a [010] direction. The was only possible because the performance of the microscope was sufficient to discriminate all cation positions, i.e., Ba, Y, and Cu.

†Present address: Gorlaeus Laboratories, State University of Leiden, 2300 RA, Leiden, The Netherlands.

3. Work In Progress

Continuing work is listed by thesis topic, followed by the graduate students responsible for the

research: metallic contacts to $YBa_2Cu_3O_{7-\delta}$," M. Tidjani; grain-boundary structure in $YBa_2Cu_3O_{7-\delta}$," L. Yamamoto; the semiconductor interface to $YBa_2Cu_3O_7$ thin films, K. Atwal; structural transitions and effect of transition-metal doping in $Bi_2SrCa_2Cu_2O_{8+\delta}$ superconductors, C. Burmester, M. Fendorf, and K. Fortunati (work supported by DARPA through TCSUH); corrosion susceptibility and grain boundaries in stainless steel, C. Willis; and multilayers for x-ray optical applications, T. Nguyen. Postdoctoral scientist Judith Ulan is investigating the microstructure of new zeolites in collaboration with S-Cal® and Georgia Tech.

1988 PUBLICATIONS AND REPORTS

Refereed Journals

1. R. Gronsky, "Spectroscopic Information from High Resolution Images," Ultramicroscopy **24**, 155 (1988); LBL-23387.
2. H.W. Zandbergen, R. Gronsky, and G. Thomas, "High Resolution Electron Microscopy Study of Grain Boundaries in Sintered $YBa_2Cu_3O_{7-\delta}$," Physica C **153–155**, 1002 (1988); LBL-24588.
3. H.W. Zandbergen, R. Gronsky, and G. Thomas, "Surface Decomposition of Superconducting $YBa_2Cu_3O_{7-\delta}$," Phys. Status Solidi A **105**, 207 (1988); LBL-23854.
4. A. Meike, H.-R. Wenk, M.A. O'Keefe, and R. Gronsky, "Atomic Resolution Microscopy of Carbonates. Interpretation of Contrast," Phys. Chem. Miner. **15**, 427 (1988).
5. H.W. Zandbergen, R. Gronsky, and G. Thomas, "Atomic Structure of (001) Grain Boundaries and (001) Surfaces in $YBa_2Cu_3O_{7-\delta}$," J. Electr. Spectr. Tech. **13**, 307 (1988); LBL-25800.
6. H.W. Zandbergen, R. Gronsky, and G. Thomas, "On the Structure of $(CuO)_2$ Double Layers in Superconducting $YBa_2Cu_3O_{7-\delta}$," Nature **331**, 596 (1988); LBL-24671.
7. J. Ding, B. Lee, R. Gronsky, J. Washburn, D. Chin, and T. Van Duzer, "High-Temperature Stability of Nb/GaAs and NbN/GaAs Interfaces," Appl. Phys. Lett. **52**, 135 (1988); LBL-23970.
8. B. Lee, R. Gronsky, and E.D. Bourret, "Dislocation Loops and Precipitates Associated with Excess Arsenic in GaAs," J. Appl. Phys. **64**, 114 (1988); LBL-24363.
9. R.W. Siegel, S. Ramasamy, H. Hahn, L. Zongquan, L. Ting, and R. Gronsky, "Synthesis, Characterization and Properties of Nanophase TiO_2," J. Mater. Res. **3**, 1376 (1988).

Other Publications

10. R. Csencsits, "Microstructural Evolution of an Iron Silicate Catalyst with Thermal and Hydrothermal Treatments," in *Proc. 46th Annual Meeting Electron Microscopy Society of America*, G.W. Bailey, Ed., San Francisco Press, Inc., 1988, p. 710; LBL-25171.
11. R. Csencsits, C.E. Lyman, and R. Gronsky, "X-Ray Emission Spectroscopy Study of Iron Silicate Catalyst FeZSM-5," in *Proc. 46th Annual Meeting Electron Microscopy Society of America*, G.W. Bailey, Ed., San Francisco Press, Inc., 1988, p. 712; LBL-25172.
12. H.W. Zandbergen, R. Gronsky, K. Wang, and G. Thomas, "Simulation and Processing of High Resolution Images of Defects and Interfaces in Superconducting $YBa_2Cu_3O_{7-\delta}$," Mat. Res. Soc. Symp. Proc. **99**, 553 (1988); LBL-24140.
13. R. Csencsits and R. Gronsky, "Preparation of Zeolites for TEM Using Microtomy," Mat. Res. Soc. Symp. Proc. **115**, 103 (1988); LBL-24116.
14. R. Csencsits, R. Gronsky, V. Nair, and R. Szostak, "Electron Microscopy Study of Morphology and Composition of a Ferrisilicate Catalyst," Mat. Res. Soc. Symp. Proc. **111**, 155 (1988); LBL-24117.
15. R. Gronsky, "An Overview of North American User Facilities for Electron Microscopy in the Physical Sciences," in *Proc. 46th Annual Meeting Electron Microscopy Society of America*, G.W. Bailey, Ed., San Francisco Press, Inc. 1988, p. 802; LBL-25861.
16. R. Gronsky, M. Fendorf, K. Fortunati, P. Hor, R.-L. Meng, and C.W. Chu, "Modulated Structure of Superconducting $Bi_2SrCa_2Cu_2O_{8+\delta}$," in *Proc. 46th Annual Meeting Electron Microscopy Society of America*, G.W. Bailey, Ed., San Francisco Press, Inc., 1988, p. 874; LBL-25844.
17. M.K. Kundmann and R. Gronsky, "Plasmon Lineshape Analysis in EELS of Semiconductors," in *Proc. 46th Annual Meeting Electron Microscopy Society of America*, G.W. Bailey, Ed., San Francisco Press, Inc., 1988, p. 500; LBL-25204.

LBL Reports

18. R. Csencsits and R. Gronsky, "Vitrification of Zeolite Y in the TEM," Zeolites (in press); LBL-22549.
19. H.W. Zandbergen, C.J.D. Hetherington, and R. Gronsky, "Sample Preparation of $YBa_2Cu_3O_7$ for High Resolution Electron Microscopy," J. Superconductivity (in press); LBL-24614.
20. R. Csencsits and R. Gronsky, "Microstructural Study of an Iron Silicate Catalyst Using Electron Microscopy," in *Proc. ACS Symposium on Preparation and Characterization of Catalysts* (in press); LBL-25173.
21. H.W. Zandbergen, R. Gronsky, and G. Thomas, "The Atomic Structure at Grain Boundaries, the Cause of Low Critical Currents in Sintered

$YBa_2Cu_3O_{7-\delta}$," in *Proc. EUREM Congress*, York, U.K., Sept. 1988 (in press); LBL-25800.

22. H.W. Zandbergen, R. Gronsky, and G. van Tendeloo, "Atomic Structure of Grain Boundaries in $YBa_2Cu_3O_{7-\delta}$ and $LaBaCaCu_3O_{7-\delta}$," submitted to J. Superconductivity; LBL-26397.
23. B.-T. Lee, R. Gronsky, and E. Bourret, "Transmission Electron Microscopy Study of Arsenic Precipitates in GaAs: Morphology and Orientation Relationship with the Matrix," submitted to J. Cryst. Growth; LBL-26568.
24. B.-T. Lee (Ph.D. Thesis), "Characterization of As-Grown and Annealed GaAs: Structural Defects and Electrical Properties," LBL-25604.
25. R. Csencsits (Ph.D. Thesis), "A Study of the Structure and Composition of an Iron Silicate Catalyst," LBL-26258.

Invited Talks

26. R. Gronsky, "TEM at Atomic Resolution," Indo-U.S. Workshop on Advanced Techniques for Microstructural Characterization, Bombay, India, Jan. 11–15, 1988.
27. R. Gronsky, "Structural Properties and Twins," Panel Discussion (televised by National Technological University), DOE/BES/DMS Information Meeting on High Temperature Superconductors, Sandia National Laboratories, Albuquerque, NM, Jan. 25–26, 1988.
28. R. Gronsky, "Low Temperature Ceramics, High Temperature Superconductors," American Ceramics Society, Northern California Section Meeting, Hayward, CA, Mar. 1, 1988.
29. R. Gronsky, "History of Superconductivity," Industrial Liaison Program Conference, University of California at Berkeley, Mar. 9, 1988.
30. R. Gronsky, "High Resolution Electron Microscopy Study of Grain Boundaries in Superconducting $Ba_2Cu_3O_{7-\delta}$," Materials Research Society Spring Meeting, Reno, NV, Apr. 4–7, 1988
31. R. Gronsky, "High Resolution Electron Microscopy of the New Oxide Superconductors," Frontiers of Electron Microscopy in Materials Science, Oak Brook, IL, May 16–19, 1988.
32. R. Gronsky, "Transmission Electron Microscopy Methods," Scanning Electron Microscopy School, University of California at Davis University Extension, Aug. 21–26, 1988.
33. R. Gronsky, "Transmission Electron Microscopy of Interfaces at Atomic Resolution," Technological Transfer Symposium on Interfaces in Materials: Synthesis and Properties, Pacific Northwest Laboratory, Richland, WA, Sept. 19–20, 1988.
34. R. Gronsky, "Transformation Interfaces," Department of Materials Science and Mineral Engineering, University of California at Berkeley, Oct. 6, 1988.
35. R. Gronsky, "Atomic Level Characterization of High Temperature Superconductors: A Tutorial," American Ceramics Society, Pacific Coast Regional Meeting, San Francisco, CA, Oct. 23–26, 1988.
36. R. Gronsky, "Transmission Electron Microscopy," Workshop on First Order Displacive Phase Transformations, Oakland, CA, Oct. 24–28, 1988.

Microstructure, Properties, and Alloy Design: Inorganic Materials*

Gareth Thomas, Investigator

INTRODUCTION

This is a multicomponent, interdisciplinary program in advanced inorganic materials involving fundamental quantitative studies of the structure-property relationships in technologically significant materials involved in energy and conservation. All tasks involve characterization of both structure and composition at the highest levels of spatial (transmission electron microscopy) and chemical (spectroscopy) resolutions in order to understand the complexities of structure-chemistry-processing-property relationships, without which alloy design is impossible. Specific tasks include: (a) effect of microalloying on structure properties and processing of duplex martensitic-austenitic composite steels designed for optimum toughness (terminating in 1989); (b) magnetic materials: ceramics, and permanent and hard rare-earth magnets; and (c) high-critical-temperature superconducting ceramics.

The overall objectives are to understand structure-property relations so as to design new materials, or to better utilize existing materials and processing routes for industrial practice and to realize materials and energy conservation.

STEELS

The demise of the steel industry in the United States is a reflection of both management and research limitations. The need for improving quality and properties of steels without large capital investment is thus critical. In addition, cost savings by improved processing, minimizing alloying, and reducing or eliminating heat treatments should be a prime factor in the research philosophy. The purpose of this alloy-design program has been to optimize the above factors with emphasis on dual-phase low-carbon steels and the medium-carbon microcomposite steels already designed under this project. In particular, transferring laboratory techniques to existing hot-mill practice (hot plate, bars, and wire rod are specific examples) has been successfully achieved. All projects have now been completed, and this alloy design project is terminated. It must be noted that research interest by students in ferrous metallurgy has rapidly declined, especially by U.S. students in recent times. We have a manpower shortage in the metallurgical industries that is continuing to become a severe national problem now that many foreigners return to their home countries (especially Korea and Taiwan).

MAGNETIC MATERIALS

1. Magnetization Reversal in Nucleation-Controlled Magnets. 1. Theory (Publication 20)

R. Ramesh and K. Srikrishna

A statistical model, based on earlier models of Brown[1] and McIntyre,[2] has been developed to examine the magnetization reversal of domain-wall nucleation-controlled permanent magnets such as sintered Fe-Nd-B and $SmCo_5$. Using a Poisson distribution of the defects on the surface of the grains, a "weakest link statistics" type model has been developed. The model has been used to calculate hysteresis loops for sintered Fe-Nd-B type polycrystalline magnets. It is shown that the intrinsic coercivity measured for a bulk magnet should vary inversely as the logarithm of the surface area of the grain. The effect of demagnetizing field has been incorporated by a mean-field-type approximation, to calculate the overall nucleation field from the intrinsic coercivity. The theoretically calculated hysteresis loops are in excellent agreement with the overall form of those experimentally determined for similar nucleation-controlled magnets. The model also predicts that for an inhomogeneous grain-size distribution, such as a bimodal distribution, kinks will be observed in the second quadrant of the hysteresis loops.

1. W.D. Brown, J. Appl. Phys. **33**, 3022 (1962).
2. D.A. McIntyre, J. Phys. D **3**, 1430 (1970).

*This work was supported by the Director, Office of Energy Research, Office of Basic Energy Sciences, Materials Sciences Division, of the U.S. Department of Energy under Contract No. DE-AC03-76SF00098.

2. Magnetization Reversal in Nucleation-Controlled Magnets. II. Effect of Grain Size and Size Distribution on Intrinsic Coercivity of Fe-Nd-B Magnets (Publication 21)

R. Ramesh, G. Thomas, and B.M. Ma

Results of experiments to study the effect of grain size and grain-size distribution on the intrinsic coercivity and the hysteresis loop of sintered Fe-Nd-B magnets have been obtained. It is shown that the intrinsic coercivity decreases as the average grain size of the magnet is increased. It is also shown that the intrinsic coercivity decreases linearly with the logarithm of the square of the grain size. This is consistent with the predictions made based on the statistical model developed in abstract 1. An increase in the sintering temperature leads to an increase in the average grain size, which consequently leads to a narrower hysteresis loop and lower intrinsic coercivity compared to magnets sintered at a lower temperature. It is also shown that a heterogeneous grain-size distribution, such as a bimodal distribution, causes kinks to appear in the second quadrant of the hysteresis loop. By examining magnets with different fractions of large grains, the prediction that the magnitude of the kinks increases with the volume fraction of the large grains was verified experimentally.

3. Characterization of Microstructures in Recording Head Materials (Publication 51)

T. Huynh and G. Thomas

Polycrystalline $Ba_2(Cu_{0.8}Zn_{1.2})Fe_{12}O_{22}$ for high-frequency VTR heads exhibits large anisotropy and high permeability on its c-planes at high frequencies. The ferrite grains have been magnetically oriented during processing. Characterization of grain-boundary structures with transmission electron microscopy (TEM) and analytical electron microsocpy (AEM) has shown that some triple grain junctions have a high concentration of Cu. Ba-deficient second-phase particles have been observed and characterized by convergent-beam electron diffraction (CBED). Twins and dislocations have also been observed. The effects of the microstructural defects on the magnetic properties of the materials could not be studied using Lorentz electron microscopy, as domains could not be imaged, suggesting that this material behaves as a single-domain "particle."

4. Microstructural and Magnetic Characterization in Soft Magnetic Fe-Si-Al Sendust Alloys (Publication 47)

J.D. Kim and G. Thomas

Microstructure and its effect on magnetic domain structure and domain-wall motion have been studied by TEM to understand the role of microstructure in determining the magnetic properties of a soft magnetic Sendust alloy.

The B2 $\rightarrow$ DO_3 phase transition in an $Fe_3Si_{0.6}Al_{0.4}$ Sendust alloy commenced on cooling below 1,030°C and followed a nucleation-and-growth process, developing a two-phase structure. However, since the phase transition could not be suppressed by quenching, the microstructure at room temperature consisted of single-phase DO_3. However, as-quenched microstructures from the two-phase region showed interfacial superlattice dislocations bound with antiphase domain boundaries (APBs). These superlattice dislocations have a Burgers vector of the $1/2<100>$ type, consistent with their being misfit interfacial dislocations.

From *in situ* studies by Lorentz imaging of domain-wall motion, it was shown that the interactions of domain walls with individual dislocations and APBs are not sufficiently strong to be observed, as domain walls passed straight across them. However, grain boundaries act as strong pinning sites for domain walls and closure domains formed at holes, leading to a retardation of the domain-wall motion.

A suggestion for improving Sendust for recording heads is therefore to have clean, nonporous alloys, preferably single crystals, but if not, crystals with very large grain size.

5. Microstructures and Dielectric Properties at the Morphotropic Phase Boundary (MPB) of the $PbTiO_3-PbZrO_3$ System (Publication 10)

T. Yamamoto, K. Okazaki, M.L. Dass, and G. Thomas

Microstructures and dielectric properties near the MPB of the $PbTiO_3-PbZrO_3$ system have been investigated. The coexistence of both tetragonal (T) and rhombohedral (R) phases has been confirmed in the MPB of the $Pb(Zr_{0.53}Ti_{0.47})O_3$ specimen by convergent-beam diffraction (CBD) techniques. In the case of PZT, the point groups of the ferroelectric T and R crystal symmetries are 4mm and 3m,

respectively. In CBD, the intensity variations in the diffracted beams provide a wealth of information. The [100] CBD patterns obtained from the T [$Pb(Zr_{0.45}Ti_{0.55})O_3$] and R [$Pb(Zr_{0.35}Ti_{0.65})O_3$] phases are shown in Figures 5-1 and 5-2, respectively. In the case of CBD patterns from the T phase, the intersection of Kikuchi lines within the [010] Kikuchi band (shown by the arrow in Figure 5-1) is symmetric only with respect to the mirror along [001]. On the other hand, the intersections of Kikuchi lines in the CBD pattern of the R phase (Figure 5-2) are symmetrical only in the indicated [110] planes. Figures 5-3 and 5-4 show the bright-field images obtained from both the T and R phases. These phases do not coexist in any one grain but only in each independent grain in the MPB specimen. The domain structures are almost similar in either case, and these phases can thus only be identified by CBD analysis, not by images.

SUPERCONDUCTING CERAMICS

In 1988 much effort using the Atomic Resolution Microscope (ARM) and Analytical Electron Microscope (AEM) was devoted to studies of the alkaline-earth Bi-Cr-Ca-Cu-O and Bi(Pb)-Sr-Ca-Cr-O superconductors. The results were reported separately (see the National Center for Electron Microscopy section in this Annual Report), and the published papers are listed in the accompanying publications list.

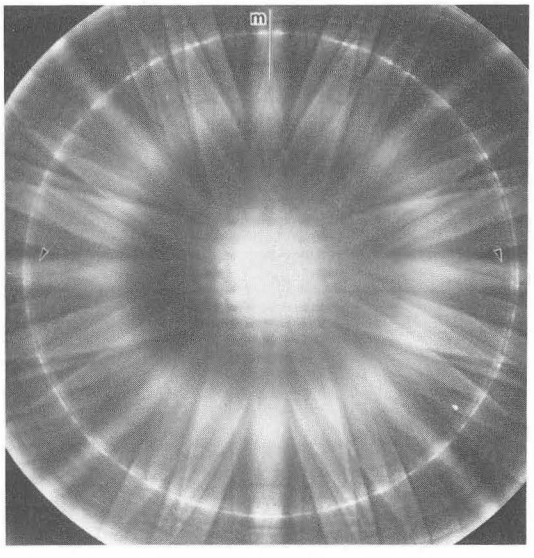

Figure 5-1. [100] ZAP obtained from the T phase obtained at liquid-nitrogen temperature with a mirror symmetry. Symmetry-breaking Kikuchi-line intersections are indicated by arrows. (XBB 874-2644)

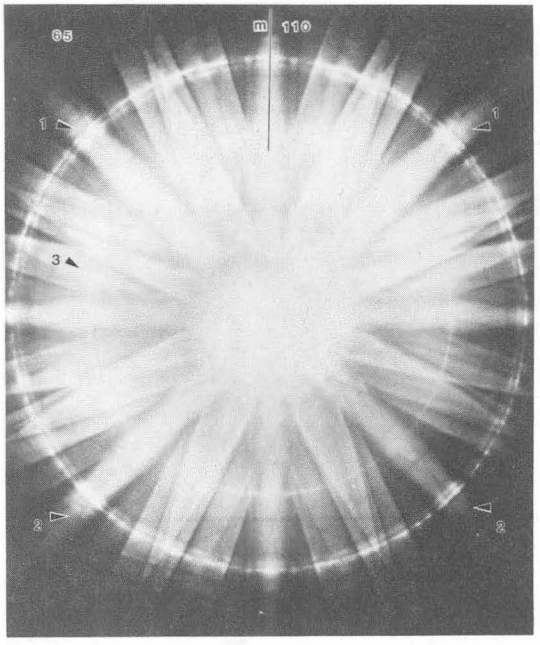

Figure 5-2. <001> ZAP obtained from the R phase obtained at liquid-nitrogen temperature with a mirror symmetry. The symmetry-breaking Kikuchi-line intersections are indicated by arrows 1 and 2. An inner ring indicated by arrow 3 is caused by the phase transformation of the R phase. (XBB 850-8341)

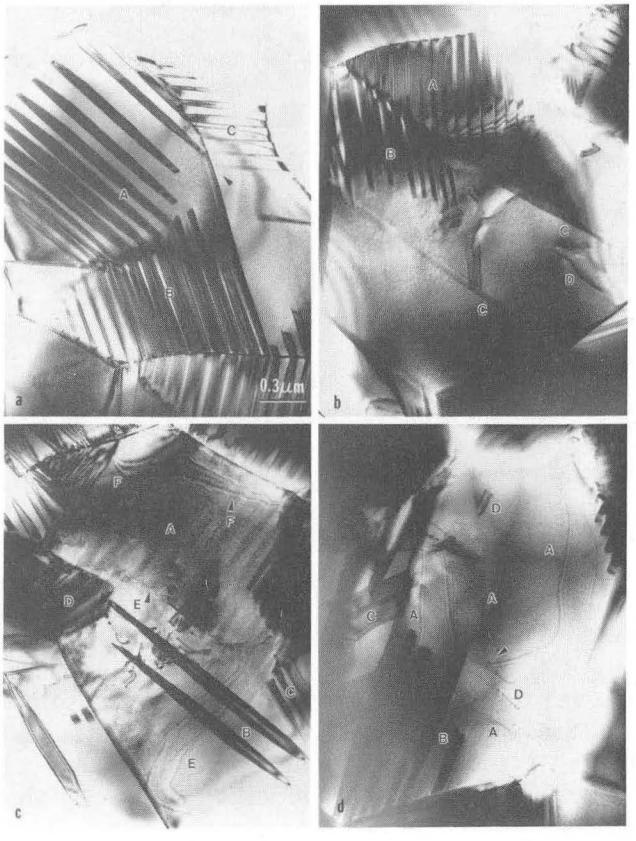

Figure 5-3. A set of micrographs of typical domain configurations observed in the T phase [$Pb(Zr_{0.45}Ti_{0.55})O_3$]. (XBB 870-8538A)

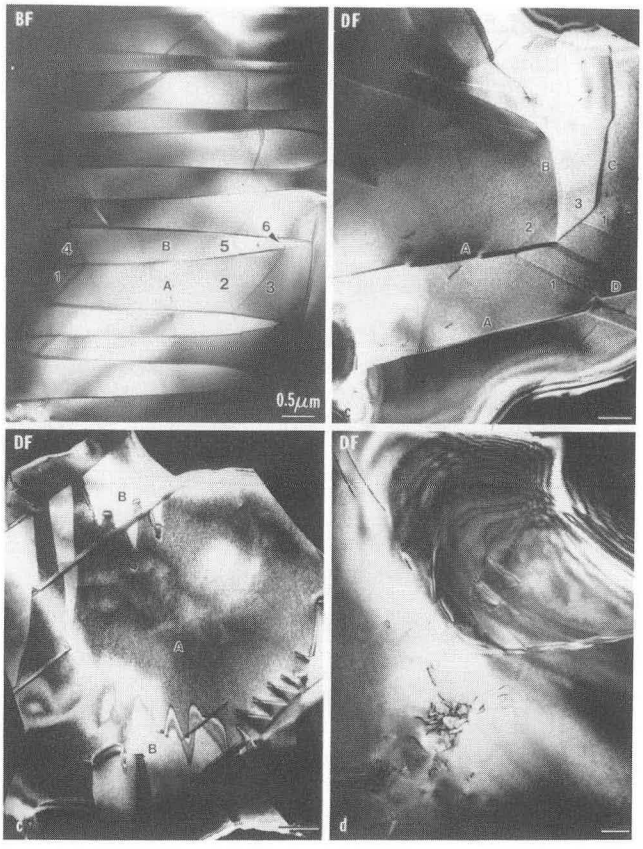

Figure 5-4. A set of micrographs of typical domain configurations observed in the R phase [$Pb(Zr_{0.65}Ti_{0.35})O_3$]. (XBB 870-8539A)

6. Work in Progress

Current Research on Hard Rare-Earth Magnets

Sintering of $Fe_{14}Nd_2B$ with $Dy_{80}Al_{20}$. The microstructure, composition, and magnetic properties of $Fe_{14}Nd_2B$ sintered magnets with Dy-Al additions have been characterized using AEM, scanning electron microscopy (SEM), and with a vibrating sample magnetometer (VSM). Magnets provided by B.M. Mao of Crucible Research Corp. were prepared by mixing powders of $Fe_{14}Nd_2B$ with 8 wt% additions of $Dy_{80}Al_{20}$ alloys of eutectic composition. Since Dy-Al melts at 800°C and sintering is carried out 1000°C, Dy and Al transport is enhanced through liquid-phase transport. Additional isothermal heat treatments were performed at 600°C for 8 hours, 15 hours, and 40 hours, followed by air cooling in an effort to further modify the alloy distribution.

SEM results reveal that the material has a multiphase microstructure with the matrix having a composition consistent with $Fe_{14}Nd_2B$. Microdiffraction carried out in the AEM confirmed that the matrix phase was indeed tetragonal $Fe_{14}Nd_2B$. The grain-boundary phase was found to be Nd rich and predominantly fcc, with a_o = 5.2 Å, consistent with a variant of Nd_2O_3, as has been previously reported. The monoclinic variant of Nd_2O_3 has been detected infrequently. A Dy-rich amorphous phase was also observed at multiphase junctions. Compositional profiles conducted across matrix/grain-boundary phase interfaces reveal that Dy does segregate into the matrix. Dy and Al segregation to matrix grain boundaries is observed as well. A Dy-rich phase of unknown structure has been observed infrequently at fcc/matrix interfaces. The structure of this phase is still being determined. In the sample treated for 15 hours, a tetragonal Al-rich phase was observed infrequently.

Cobalt-Modified $Fe_{14}Nd_2B$ Magnets

It is well known that the substitution of cobalt for iron raises the Curie temperature T_c of the hard magnetic $Nd_2Fe_{14}B$ phase and enhances the thermostability in the temperature range that is important for technical applications. Thus the objective of the experiments was to determine the number, composition, and structure of the grain-boundary phases in melt-spun $Nd_{17}Fe_{77}B_6$ and $Nd_{15}(Fe_{1-x}Co_x)_{77}B_8$ permanent magnets using analytical and high-resolution TEM.

In samples without Co, the overall microstructure is similar to that observed by other workers, although very few grain boundaries are laced with an amorphous phase. The grain-boundary phase is crystalline and has an fcc structure with a nominal composition of $Nd_{75}Fe_{25}$, in general agreement with earlier work. For the Co-substituted sample, two other fcc phases have been observed. One of them has a lattice parameter of 7.3Å and a composition of $Nd(FeCo)_2$ (see Figure 6-1), while the other has a lattice parameter of 5.4 Å and a composition of $Nd_{20}(Fe_{1-x}Co_x)_{80}$. This 5.4-Å fcc phase is a new phase in this alloy system, heretofore unobserved, although the composition is close to that of Nd_6Fe_{23} (fcc, a = 12.1 Å). The Co content of the 7.3-Å fcc phase is significantly higher than that of the alloy, suggesting that Co stabilizes the 7.3-Å fcc phase by preferentially partitioning into it. The volume fraction of these two fcc phases increases with increasing Co content of the alloy, and for x = 0.5, some of the matrix grains are surrounded by the grain-boundary phases (see Figure 6-2). In all cases, the $Nd_{1.1}Fe_4B_4$ phase was never observed. The

Figure 6-1. High-resolution image of the 7.3-Å $Nd(FeCo)_2$ grain-boundary phase (marked by arrows). (XBB 888-7740)

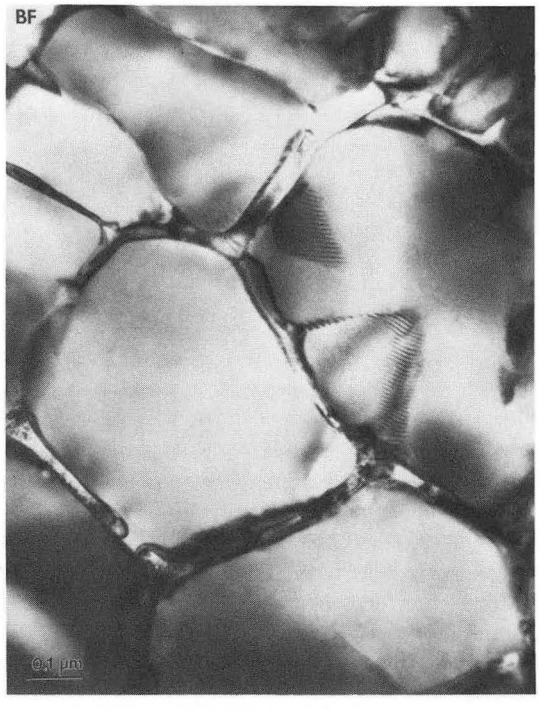

Figure 6-2. High-resolution image illustrating the almost complete surrounding of the matrix by the grain-boundary phase in $Nd_{15}(Fe_{0.5}Co_{0.5})_{77}B_8$. (XBB 880-9685)

increase in the iHc of the magnet up to x = 0.3 Co can be explained by the increase in the fraction of the grain boundary phases leading to better pinning of the domain walls. In this composition range from x = 0 to x = 0.3 Co, the effective anisotropy field of the matrix phase does not change appreciably. For higher values of x, the iHc drops, since the anisotropy field of the matrix phase drops significantly for Co contents greater than 0.4 (see Figure 6-3).

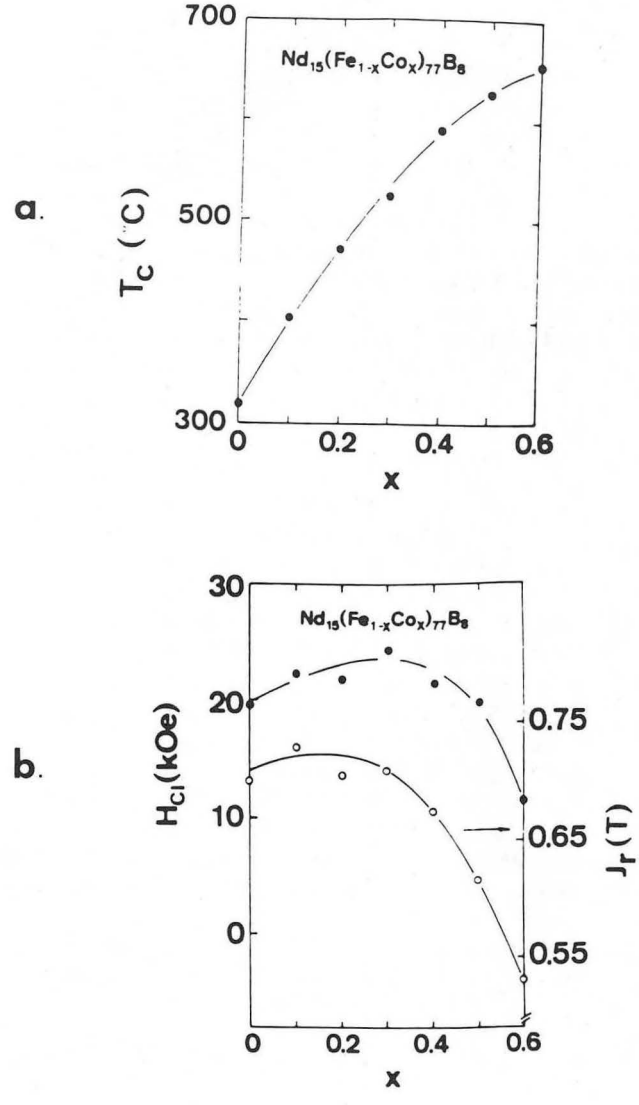

Figure 6-3. (a) Curie temperature as a function of Co content x in optimally quenched $Nd_{15}(Fe_{1-x}Co_x)_{77}B_8$. (b) Coercivity iHc and remanence $J_r(T)$ of optimally quenched ribbons vs Co content x. (XBL 889-3196)

1988 PUBLICATIONS AND REPORTS

Refereed Journals

1. H.W. Zandbergen, R. Gronsky, and G. Thomas, "Surface Decomposition of Superconducting $YBa_2Cu_3O_{7-\delta}$," Phys. Stat. Sol. (a) **105**, 207 (1988); LBL-23854.
2. H.M. Ho, G. Thomas, C.N. Schooley, and J.S. Gau, "Cross-Sectioning Magnetic Thin Films for TEM," Mat. Res. Soc. Symp. Proc. **115**, 149 (1988); LBL-23565.
3. T.R. Dinger, R.S. Rai, and G. Thomas, "Crystallization Behavior of a Glass in the Y_2O_3-SiO_2-AlN System," J. Am. Ceram. Soc. **71**, 236 (1988); LBL-23251.†
4. R. Ramesh, G. Thomas, S.M. Green, M.L. Rudee, and H.L. Lu, "Structure and Composition of the 115°K Superconducting Phase in the Bi-Ca-Sr-Cu-O System," Appl. Phys. Lett. **53**, 520 (1988); LBL-25076.
5. R. Ramesh, C.J.D. Hetherington, S.M. Green, C. Jiang, M.L. Rudee, and H.L. Luo, "Further Evidence for the Presence of c = 38.2 Å phase in a Bi-Ca-Sr-Cu-O Superconductor," Appl. Phys. Lett. **53**, 615 (1988); LBL-25103.
6. H.W. Zandbergen and G. Thomas, "Defect Characterization in Sintered $YBa_2Cu_3O_{7-\delta}$ by HREM," Inst. Phys. Conf. Ser. No. 93, **2**, Chap. 13, p. 259 (1988); LBL-25786.
7. D. Schryvers, K. Srikrishna, and G. Thomas, "Electron Microscopy Study of a Mullite Compound; a Combination of HREM, CBED, and EDX," Inst. Phys. Conf. Ser. No. 93, **2**, Chap. 14, p. 553 (1988).†
8. H.W. Zandbergen, R. Gronsky, and G. Thomas, "The Atomic Structure at Grain Boundaries, the Cause of Low Critical Currents in Sintered $YBa_2Cu_3O_{7-\delta}$," Inst. Phys. Conf. Ser. No. 93, **2**, Chap. 6, p. 257 (1988); LBL-25578.
9. H.W. Zandbergen, R. Gronsky, and G. Thomas, "High Resolution Electron Microscopy Study of Grain Boundaries in Sintered $YBa_2Cu_3O_{7-\delta}$," Physica **C153–155**, 1002 (1988).
10. T. Yamamoto, K. Ozazaki, M.L. Dass, and G. Thomas, "Microstructures and Dielectric Properties at the Morphotropic Phase Boundary (MPB) of $PBTiO_3-PbZrO_3$ System," Ferroelectrics **81**, 331 (1988); LBL-24209.
11. R. Ramesh and G. Thomas, "Effect of Quench Rate on the Intrinsic Coercivity of Iron–Rare Earth–Boron Permanent Magnets," Acta Metall. **36**, 3137 (1988); LBL-24218.
12. R. Ramesh, G. Thomas, S.M. Green, Y. Mei, C. Jiang, and H.M. Luo, "Microstructure of Pb-modified Bi-Ca-Sr-Cu-O Superconductor," Appl. Phys. Lett. **53**, 1759 (1988); LBL-25557.
13. R. Ramesh and G. Thomas, "Polytypoid Structure of Pb-modified Bi-Ca-Sr-Cu-O Superconductor," Phys. Rev. B **38**, 7070 (1988); LBL-25276.
14. H.W. Zandbergen, R. Gronsky, K. Wang, and G. Thomas, "On the Structure of $(CuO)_2$ Double Layers in Superconducting $YBa_2Cu_3O_{7-\delta}$," Nature **331**, 596 (1988); LBL-24671.
15. H.W. Zandbergen and G. Thomas, "HREM Investigations of Defects in Sintered Polycrystalline $YBa_2Cu_3O_{7-\delta}$," Phys. Stat. Sol. (a) **107**, 825 (1988).
16. D. Schryvers, K. Srikrishna, G. Thomas, and M.A. O'Keefe, "An Electron Microscopy Study of the Atomic Structure of a Mullite in a Reaction Sintered Composite," J. Mat. Res. **3**, 1355 (Nov./Dec. 1988).†
17. G. Thomas, R. Ramesh, and C.J.D. Hetherington, "Electron Microscopy of Bi-Ca-Sr-Cu-O High T_c Superconductors," JEOL News **26E**, 2 (1988).
18. C.J.D. Hetherington, R. Ramesh, M.A. O'Keefe, R. Kilaas, G. Thomas, S.M. Green, and H.L. Luo, "High Resolution Electron Microscopy of the c = 30.5 Å and c = 38.2 Å Polytypoids in the Bi-Ca-Sr-Cu-O Superconductor," Appl. Phys. Lett. **53**, 1016 (1988); LBL-25320.
19. H.W. Zandbergen and G. Thomas, "Grain Boundaries in Sintered $YBa_2Cu_3O_{7-\delta}$," Acta Crystallogr. A **44**, 772 (1988); LBL-24603.
20. R. Ramesh and K. Srikrishna, "Magnetization Reversal in Nucleation Controlled Magnets. Part I: Theory," J. Appl. Phys. **64**, 6406 (1988); LBL 25094.
21. R. Ramesh, G. Thomas, and B.M. Ma, "Magnetization Reversal in Nucleation Controlled Magnets. Part II: Effect of Grain Size and Size Distribution on Intrinsic Coercivity of Fe-Nd-B Magnets," J. Appl. Phys. **64**, 6416 (1988); LBL-25094.
22. H.W. Zandbergen, R. Gronsky, and G. Thomas, "The Atomic Structure at (001) Grain Boundaries and (001) Surfaces in $YBa_2Cu_3O_{7-\delta}$," J. Electron Spectrosc. Tech. **13**, 307 (1988); LBL-25800.
23. J.S. Gau, H.M. Ho, and G. Thomas, "Magnetic Properties of CO–20%Ni Thin Films Evaporated near the Grazing Angle," IEEE Trans. Magn. **24**, 2994 (1988).†
24. R. Ramesh, G. Thomas, G. Van Tendeloo, S.M. Green, and H.L. Luo, "New Modulated Structure in Pb-Doped Bi-Ca-Si-Cu-O Superconductor," Appl. Phys. Lett. **53**, 2220 (1988); LBL-25422.
25. H.W. Zandbergen, R. Gronsky, and G. Thomas, "High Resolution Electron Microscopy Study of Grain Boundaries in Superconducting $YBa_2Cu_3O_{7-\delta}$," in *Proc. MRS Meeting*, Spring 1988, Apr. 4–8, 1988, Reno, NV; Physica **C153**, 1000 (1988).
26. R. Ramesh, G. Thomas, S.M. Green, C. Jiang, Y. Mei, and H.L. Luo, "Bi-Ca-Sr-Cu-O Superconductors: The Connectivity Issue," in *Proc. Applied Superconductivity Conf.*, San Francisco, CA, Aug. 22–25, 1988; IEEE Trans. Magn. **25**, 2360 (1989); LBL-25842.
27. R. Ramesh, J.K. Chen, G. Thomas, and L.K. Rabenberg, "Microstructure and Properties of Rare Earth Magnets," in *Proc. ASM Fall Meeting, Symposium on Hard and Soft Magnets,* 1988, p. 1; LBL-24129.

Other Publications

28. K. Srikrishna, G. Thomas, and J.S. Moya, "Analytical Electron Microscopy of the Glassy Phase in Mullite/Zirconia Composities," in *Ceramic Microstructures '86*, J.A. Pask and A.G. Evans, eds., Plenum, New York, 1988, p. 111.
29. G. Thomas, J.K. Kim, D. Manojlovic, and R. Milovic, "Development of High Strength and Toughness Microcomposite HSLA Fe/Cr/Mn/C Steel with and without Nb," in *Processing, Microstructure and Properties of HSLA Steels*, A.J. DeArdo, Ed., 1988, p. 339; LBL-23968.
30. H.W. Zandbergen, R. Gronsky, K. Wang, and G. Thomas, "Simulation and Processing of High Resolution Images of Defects and Interfaces in Superconducting $YBa_2Cu_3O_7$," in *Conf. Proc. MRS 1987 Fall Meeting*, Boston, MA, Dec. 1, 1987; Mat. Res. Soc. Symp. Proc. **99**, 553 (1988); LBL-24140.
31. H.W. Zandbergen, R. Gronsky, and G. Thomas, "High Resolution Electron Microscopy Study of Grain Boundaries in $YBa_2Cu_3O_{7-\delta}$," in *Proc. Int. Conf. on HT Superconductors and Materials Mechanisims of Superconductivity*, Interlaken, Switzerland, Feb. 29–Mar. 4, 1988; LBL-24588abs.
32. R. Ramesh, H.M. Ho, G. Thomas, and A.E. Berkowitz, "Microstructure of Nano-Crystalline γ-Fe_2O_3 Particulate Recording Medium," in *Proc. AIME Meeting*, Lake Tahoe, CA, Mar. 9–11, 1988.†
33. G. Thomas, "Grain Boundaries and Interfaces: Some Applications of Electron Microscopy and Microanalysis," in *Ceramic Microstructures '86*, J.A. Pask and A.G. Evans, eds., 1988, p. 55.
34. J.W. McCauley, K.M. Krishnan, R.S. Rai, G. Thomas, A. Zangvill, R.W. Doser, and N.D. Corbin, "Anion Controlled Microstructures in the Al_2O_3-AlN System," in *Ceramic Microstructures '86*, J.A. Pask and A.G. Evans, eds., 1988, p. 577.
35. G. Thomas, "Electron Microscopy in Materials Science," in *Proc. IVth Asia-Pacific Conf. and Workshop on Electron Microscopy*, Bangkok, Thailand, July 26–Aug. 4 1988, V. Mangclavira, J.W. Banchoendhevakul, and P. Ingkanium, eds., p. 27; LBL-25001.
36. K. Srikrishna, G. Thomas, and J.S. Moya, "Sintering Additives for Mullite/Zirconia Composites," Advances in Ceramics **24**, 277 (1988).†
37. G. Thomas, R. Ramesh, and C.J.D. Hetherington, "Electron Microscopy of Bi-Ca-Sr-Cu-O High T_c Superconductors," JEOL News, **26E**, 2 (1988).
38. K. Srikrishna (Ph. D. Thesis), "Toughening Mechanisms in Mullite Zirconia Composites."

LBL Reports

39. R. Ramesh, G. Thomas, and B.M. Ma, "Dy-Al Sintering Additive: Effect on Microstructure and Magnetic Properties of Fe-Nd-B Magnets," in *Conf. Proc. MRS Int. Meeting*, Toyko, Japan, June 1988 (in press); LBL-24401.
40. J.D. Kim, T. Huynh, and G. Thomas, "Characterization of Microstructures in Recording Materials: $Fe_3Si_{0.6}Al_{0.4}$ Alloy and $Ba_2(Cu_{0.8}Zn_{1.2})\ Fe_{12}O_{22}$," in *Conf. Proc. MRS. Int. Meeting*, Tokyo, Japan, June 1988 (in press); LBL-24402.
41. T. Huynh and G. Thomas, "Characterization of Barium Ferrite Recording Materials," in *Conf. Proc. MRS. Int. Meeting*, Tokyo, Japan, June 1988 (in press); LBL-25359.
42. G. Thomas, "Transmission Electron Microscopy: Imaging of Materials," in *Proc. ASM Congress*, Chicago, IL, Sept. 26–30, 1988 (in press); LBL-26144.
43. C.J.D. Hetherington, R. Ramesh, M.A. O'Keefe, R. Kilaas, and G. Thomas, "High Resolution Electron Microscopy and Image Simulation Studies of Superconducting Polytypoid in Bi-Ca-Sr-Cu-O Ceramics," in *Proc. MRS Fall Meeting*, Boston, MA, Nov. 1988 (in press); LBL-25579.
44. C.J.D. Hetherington, E.C. Nelson, K. Westmacott, R. Gronsky, and G. Thomas, "The Berkeley Atomic Resolution Microscope," in *Proc. MRS Fall Meeting*, Boston, MA, Nov. 1988 (in press); LBL-25797abs.
45. R. Ramesh, G. Thomas, S.M. Green, Y. Mei, C. Jiang, and H.L. Luo, "Liquid Phase Sintering and Zero Resistance above 100°K in Bi-Ca-Sr-Cu-O Superconductors," in *Proc. MRS Fall Meeting*, Boston, MA, Nov. 1988 (in press); LBL-25403.
46. J.D. Kim and G. Thomas, "Characterization of Microstructures in Recording Materials: $Fe_3Sr_{0.6}Al_{0.4}$ Alloy," in *Proc. MRS Fall Meeting*, Boston, MA, Nov. 1988 (in press); LBL-25362.
47. J.D. Kim (Ph.D. Thesis), "Microstructural and Magnetic Characterization in Soft Magnetic Fe-Si-Al (Sendust) Alloy," LBL-26334.
48. J. Kim (Ph.D. Thesis), "Nb Modification of Microcomposite Fe/C/Cr/Mn Steel," LBL-26145.
49. L.M. Dass (Ph.D Thesis), "Characterization of Microstructure and Domain Configuration of Lead Zirconate Titanate (PZT) Ceramics," LBL-26375.
50. H.M. Ho (Ph.D. Thesis), "Characterization of Co-Ni Oblique Incidence Thin Films for Recording Media Application," LBL-27121.
51. T. Huynh (M.S. Thesis), "Microstructure and Magnetic Properties of $Ba_2Cu_{0.8}Zn_{1.2}Fe_{12}O_{22}$," LBL-25968.
52. G. Thomas and R. Ramesh, "Atomic Imaging and Microanalysis of Ceramics," in *Conf. Proc. American Ceramic Society Meeting*, San Francisco, CA, Oct. 24, 1988 (in press); LBL-26319.
53. C. Koestler, R. Ramesh, C.J. Echer, and G. Thomas, "Microstructure of Melt Spin Nd-Fe-Co-B Magnets," Acta Metall. (in press); LBL-26156.
54. H.M. Ho, J.S. Gau, and G. Thomas, "Domain Structure and Microstructure of Co-Ni-Oblique Incident Thin Films," J. Appl. Phys. (in press); LBL-25914.
55. R. Ramesh, G. Thomas, and B.M. Ma, "Improvements in Intrinsic Coercivity of Sintered Fe-Nd-B Magnets by the Introduction of Non-Magnetic Dispersoids," Acta Metall. (in press); LBL-25648.

56. R. Ramesh, G. Thomas, R.L. Meng, P.H. Hor, and C.W. Chu, "Electron Microscopy of a Gd-Ba-Cu-O Superconductor," J. Mat. Res. (in press); LBL-25405.
57. L.H. Chan, G. Thomas, and J.S. Gau, "Magnetic Properties and Microstructure of Co-Cr Bulk Alloys," J. Magn. Magn. Mater. (in press); LBL-25266.

Invited Talks

58. G. Thomas, "Interfacial Defects in Structual and Superconducting Ceramics," Madrid, Spain, Jan. 8, 1988.
59. G. Thomas, "Electron Microscopy Studies of Superconducting Oxides," Industrial Liaision Meeting, University of California at Berkeley, Mar. 9, 1988.
60. G. Thomas (speaker), S. Miyasato, and V. Radmilovic, "Electron Microscopy of Al-Li-Cu and Al-Li-Mg Alloys," 1988 Al-Li Symposium, Westec '88, ASM International Meeting, Los Angeles, CA, Mar. 21–24, 1988.
61. G. Thomas, "Design of Strong, Tough Steel Plates," Swedish Steel Co., Oxelosund, Sweden, May 10, 1988
62. G. Thomas, "Alloy Design of Steel Plates and Rods," Avaco Steel Co., Stockholm, Sweden, May 10, 1988.
63. R. Ramesh, B.M. Ma, and G. Thomas (speaker), "Dy-Al Sintering Additive: Effect on Microstructure and Magnetic Properties of Fe-Nd-B Magnets," MRS International Meeting, Toyko, Japan, June 1988.
64. T. Hyunh and G. Thomas (speaker), "Characterization of Barium Ferrite Recording Materials," MRS International Meeting, Toyko, Japan, June 1988.
65. J.D. Kim and G. Thomas, "Characterization of Microstructures in Recording Materials: $Fe_3Si_{0.6}Al_{0.4}$ Alloys," MRS International Meeting, Toyko, Japan, June 1988.
66. G. Thomas, as President of IFSEM, presided over the 9th APEM Regional Conference and Workshop on Electron Microscopy: "Electron Microscopy in Materials Science," Plenary Lecture, Fourth Asia-Pacific Conference and Workshop on Electron Microscopy, Bangkok, Thailand, July 26–Aug. 4, 1988.
67. G. Thomas, "Transmission Electron Microscopy: Imaging of Materials," ASM International World Congress '88, Chicago, IL, Sept. 26–30, 1988.
68. G. Thomas, "Microcomposite Duplex HSLA Steel for High Strength and Toughness," World Materials Congress, Chicago, IL, Sept. 29, 1988.
69. G. Thomas, "Microstructural and Microanalytical Analyses of Ceramic Materials," World Materials Congress, Chicago, IL, Sept. 29, 1988.
70. G. Thomas (speaker) and R. Ramesh, "Atomic Imaging and Microanalysis of Ceramics," American Ceramic Society, Pacific Coast Meeting, San Francisco, CA, Oct. 24–27, 1988.
71. G. Thomas, "Microstructural Aspects in Magnetic Materials," invited chairman, DOE Workshop on Magnetic Materials, Santa Rosa, CA, Nov. 14–19, 1988.
72. G. Thomas, "Atomic Resolution of Structural and Superconducting Ceramics," plenary lecture, Spain-Portugal Joint Meeting on Electron Microscopy, Lisbon, Portugal, Dec. 13–15, 1988.
73. G. Thomas, "High Resolution Electron Microscopy of Structural and Superconducting Ceramics," Kyocera Ceramics Central Research Lab., Kagoshima, Japan, Dec. 20, 1988.

---

†Supported by the National Science Foundation.

Solid-State Phase-Transformation Mechanisms*

Kenneth H. Westmacott, Investigator

INTRODUCTION

This research is directed towards obtaining an atomic-level understanding of the structural factors that govern phase changes and phase stability. Transmission electron microscopy techniques, particularly high-voltage and high-resolution microscopy, are employed to characterize phase changes and to infer the atomic rearrangements occurring during a transformation. By studying alloy systems characterized by strains of different signs and magnitudes, the fundamental mechanisms for a broad range of phase transformations are being identified. It has been possible to predict precipitate morphologies (growth directions, habit planes, orientation relationships, substructure, twinning, etc.) from first principles and to relate them to nucleation and growth processes. Extension of the principles from simple model alloy systems to more complex materials is now in progress.

1. The Formation of Hexagonal Silicon at Twin Intersections (Publication 8)

U. Dahmen, C. Hetherington, P. Pirouz,† and K.H. Westmacott

From studies of the microstructure of the heavily deformed zones of hot-indented silicon, it has been postulated that the formation of an observed hexagonal form of silicon has its origin in multiple twinning. A model has been developed, one feature of which is the prediction that under strict plane-strain conditions the region of twin intersection will be forced into hexagonal close-packed stacking to accommodate the strain of crossing twins. Direct confirmation of this prediction has been obtained by high-resolution microscopy performed on NCEM's Atomic Resolution Microscope, as illustrated in Figure 1-1. The hexagonal ABAB atom stacking is clearly visible in the region marked H, which lies at the intersection of twin 1 and twin 2. A schematic diagram showing the lattice changes induced by a sequence of twinning operations given in Figure 1-2 may be compared directly with the observed structure.

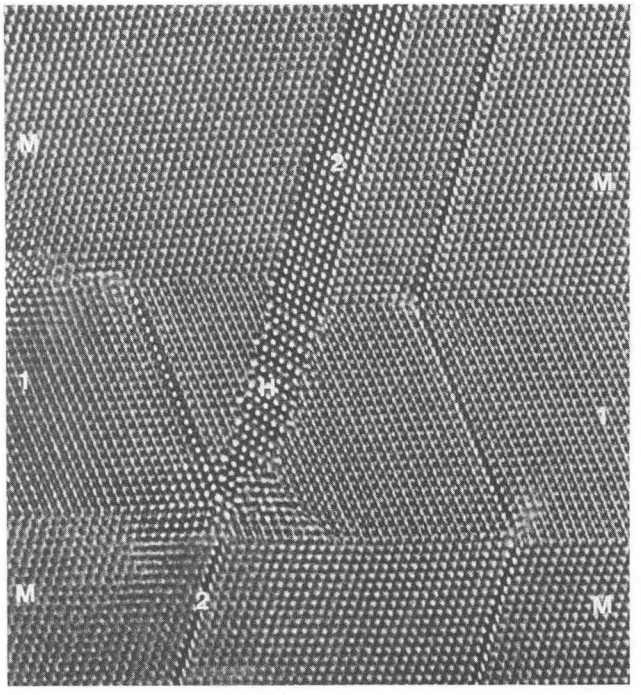

Figure 1-1. High-resolution micrograph taken at 800 kV of two intersecting twins in single-crystal silicon indented at 400°C. Matrix labeled M, twins labeled 1 and 2, hexagonal phase labeled H. A slight crystal misorientation is responsible for the variation in the images of the matrix and the two twins. (XBB 880-9626)

*This work was supported by the Director, Office of Energy Research, Office of Basic Energy Sciences, Materials Sciences Division, of the U.S. Department of Energy under Contract No. DE-AC03-76SF00098.

†Permanent address: Case Western Reserve University, Cleveland, OH 44106.

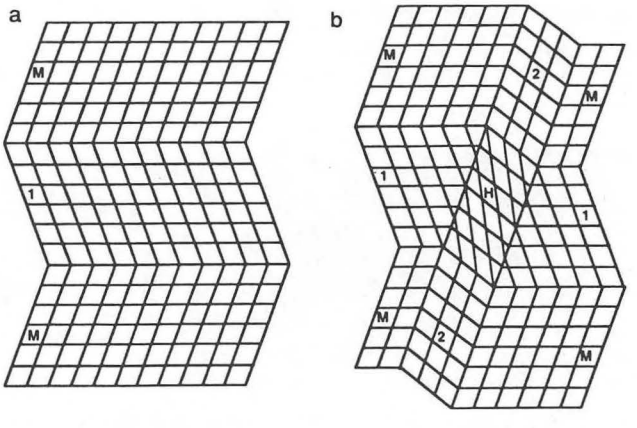

Figure 1-2. Schematic diagram showing single twin in (a) being intersected by a second twin in (b). Strain accommodation causes the region of the intersection to transform to hexagonal stacking. Matrix labeled M, twins labeled 1 and 2, hexagonal phase labeled H. (XBL 893-1200)

The Coprecipitation of Cr_3P and Cr in Cu (Publications 5 and 10)

M.J. Witcomb,† U. Dahmen, and K.H. Westmacott

During TEM studies on Cu-Cr alloys previously considered to be simple binaries, it was found that a minor secondary precipitate phase was also present. Through electron diffraction, EDS, microprobe analyses, and high-resolution imaging, the additional phase was identified as bct Cr_3P and related to the presence of trace amounts of P in the alloys. It was concluded, however, that the phosphide particles precipitate on the primary Cr laths only after they are well-developed. Thus, earlier quantitative analyses of Cr precipitate morphologies in Cu remain valid. Dark-field micrographs illustrating the interesting morphological relationship between the Cr precipitate and the Cr_3P particle are given in Figure 2-1. In (a) and (b) the Cr and Cr_3P are respectively imaged independently, while (c) shows the composite shape when both are imaged simultaneously.

†Permanent address: Electron Microscope Unit, University of the Witwatersrand, WITTS 2050, South Africa.

3. Work in Progress

A series of papers on the nature and origin of the diamond hexagonal phase in silicon is being prepared for publication (in collaboration with P. Pirouz of Case Western Reserve University).

A comprehensive high-resolution study of germanium precipitation from aluminum has been completed and is being written up for publication. It is shown that multiple twinning of the precipitates is the thread linking the many different precipitate morphologies that are observed. A high-resolution analysis of the fcc/bcc interfaces between matrix and precipitation in a Cu-Cr alloy is being undertaken to complete a detailed study of precipitate crystallography in this classical fcc/bcc alloy system (in collaboration with M.J. Witcomb, University of the Witwatersrand, Johannesburg, South Africa).

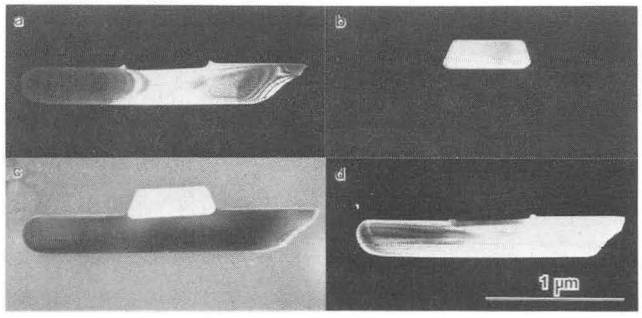

Figure 2-1. Dark-field analysis of an extracted Cr lath precipitate with attached Cr_3P particle. The interface between the two phases is seen edge-on in (a). (XBB 888-7338)

1988 PUBLICATIONS AND REPORTS

Refereed Journals

1. U. Dahmen, K.H. Westmacott, and M.J. Witcomb, "Morphology of Cr Precipitates in an Overaged Cu–0.3% Cr Alloy," Scripta Metall. **22**, 1897 (1988); LBL-25749.
2. U. Dahmen, M.J. Witcomb, and K.H. Westmacott, "Accurate Habit Plane Determination of Lath-Shaped Cr Precipitates in Cu," EMSSA Proc. **18**, 185 (1988); LBL-25883abs.
3. U. Dahmen and K.H. Westmacott, "The Use of Symmetry in the TEM Analysis of Phase Transformation," EMSSA Proc. **18**, 5 (1988); LBL-25880abs.
4. P. Pirouz, R. Chaim, and U. Dahmen, "Hexagonal Silicon, a Stress-Induced Martensitic Transformation," MRS Symp. Proc. **104**, 133 (1987).

Other Publications

5. M.J. Witcomb, U. Dahmen, and K.H. Westmacott, and "The Co-Precipitation of Cr_3P and Cr in Cu," in *Proc. 46th Annual Meeting EMSA*, G.W. Bailey, Ed., San Francisco Press, 1988, p. 764; LBL-24953.
6. K.H. Westmacott, U. Dahmen, A. Thorel, and J.-Y. Laval, "Precipitation in a (Mg) Partially Stabilized Zirconia During Aging at 1000°C," in *Ceramic Microstructures '86*, J. Pask and A. Evans, eds., Plenum Publishing Corp., 1988, p. 831; LBL-22140.
7. U. Dahmen, J. Douin, C.J.D. Hetherington, and K.H. Westmacott, "High Resolution Electron Microscopy of Interfaces in Topotaxial and Epitaxial Reactions," MRS Symposium on High Resolution Microscopy of Materials, Boston, MA, Dec. 1988; LBL-26545.

LBL Reports

8. U. Dahmen, K.H. Westmacott, C. Hetherington, and P. Pirouz, "The Formation of Hexagonal Silicon at Twin Intersection," Scripta Metall. (in press); LBL-26233.
9. U. Dahmen, K.H. Westmacott, P. Pirouz, and R. Chaim, "On the Origin of {511} Plates of Hexagonal Silicon," submitted to Acta Metall.; LBL-24930.
10. M.J. Witcomb, U. Dahmen, and K.H. Westmacott, "The Coprecipitation of Cr_3P and Cr in Cu," Ultramicroscopy (in press); LBL-24953abs.
11. U. Dahmen, "Transmission Electron Microscope Characterization of Precipitates," Ultramicroscopy (in press); LBL-24660abs.

National Center for Electron Microscopy*

Gareth Thomas, Ronald Gronsky, and Kenneth H. Westmacott, Investigators

INTRODUCTION

The National Center for Electron Microscopy (NCEM) provides advanced facilities for electron-optical characterization of materials. Its resident staff operate, maintain, design, and develop equipment and software, making it available to all Center users, and in addition conduct their own forefront research on problems in the materials sciences.

Central to NCEM are two unique high-voltage electron microscopes, a 1.5-MeV machine (the High-Voltage Electron Microscope, or HVEM), which is the most powerful in the U.S., and a 1-MeV machine (the Atomic Resolution Microscope, or ARM), which offers the best resolution in the world (better than 1.6 Å). These instruments are backed by "feeder" microscopes (for specimen screening, preliminary experiments, and complementary microchemical analysis), by specimen-preparation facilities, and by image-processing and analysis facilities, all within the same building and exclusively dedicated to electron microscopy.

The 200-keV analytical microscope (AEM) is fully utilized in support of Center research. Current projects on the instrument include standard analyses as well as the development and refinement of new techniques (e.g., electron-energy-loss spectroscopy and convergent-beam electron diffraction) and software for quantification. The NCEM computer system is designed to assist interpretation of electron microscope images in three ways: (1) real-time enhancement of live video-rate TV images from the electron microscopes under control of the microscope operator; (2) interactive *a posteriori* processing of stored experimental images at a work station hosted by the computer; and (3) matching experimental images to ones simulated from a proposed model structure at a work station controlled by the host computer, in order to confirm (or reject) the suitability of the model.

Both operations (2) and (3) are running and available for use by users at a two-station Gould IP8500 image processor controlled by the microVAX. For implementation of operation (3), a second microVAX is available to control sets of DataCube modules that will digitize a video image in real time, store it in memory, and average it over a (selected) time interval to improve the signal-to-noise ratio, and display the enhanced image on the microscope operator's monitor. A small-array processor (MCS ZIP3232) provides background correction and the capability to present the operator with the diffractogram of the image.

Guidance for NCEM is provided by a steering committee, chaired by J.J. Hren (North Carolina State University). Its present members are C.W. Allen (Argonne National Laboratory), J. Barry (Arizona State University), U. Dahmen (LBL), T. Hayes (LBL), D.G. Howitt (University of California, Davis), F. Ponce (Xerox Palo Alto Research Center), L.E. Thomas (Battelle Pacific Northwest Laboratory), M.M.J. Treacy (Exxon R&D), and the investigators on this project. Meetings are held yearly.

Research projects at the Center cover a wide spectrum, including phase-transformation studies in metals, ceramics, and minerals; high-T_c superconductors; semiconductor devices; catalyst and amorphous-metal investigations; and biological medical-science applications.

Ongoing research projects at NCEM are listed in Table 1-1.

Some examples of recent research at the Center are listed below.

1. The Berkeley Atomic Resolution Microscope—an Update (Publication 84)

C.J.D. Hetherington, E.C. Nelson, K.H. Westmacott, R. Gronsky, and G. Thomas

Recent modifications to the JEOL ARM-1000 microscope have markedly enhanced its performance. The point resolution limit at 1000 kV is confirmed by optical diffractograms down to 1.7 Å, and there are firm indications of contrast transfer down to 1.4 Å. The unique tilting capability of the ARM, ±40° biaxial tilt over the 800-kV to 1000-kV range, is preserved at this resolution. This paper presents the measured imaging parameters and results on resolution tests.

*This work was supported by the Director, Office of Energy Research, Office of Basic Energy Sciences, Materials Sciences Division, of the U.S. Department of Energy under Contract No. DE-AC03-76SF00098.

Table 1-1
NCEM Research Proposals (active during 1988)

Principal Investigator	Affiliation	Title
HVEM		
J. Bastacky	LBL/UC Berkeley	The phagocytic process involved in uptake of coal-combustion particulates (fly ash) by pulmonary macrophage cells
L. Blackburn	NASA Langley	Effect of indium additions on precipitation in Al-Cu-Li-Zr alloys
T. Cass	Hewlett-Packard	Defect structures in semiconductor devices
J.A. Cornie	MIT	Tayloring and modeling interfaces in metal-matrix composites
U. Dahmen	LBL/UC Berkeley	Characterization of nanocrystals by TEM
J. Dash	Portland State University	Phase transformation induced by high pressures and temperatures in a ballistic compressor
D. de Fontaine	LBL/UC Berkeley	*In situ* observation of the Devil's staircase in long-period superstructures of binary alloys
L. De Jonghe	LBL/UC Berkeley	Structure of Si_3N_4 and SiC whiskers coated with metal oxides or polymers
J.W. Evans	LBL/UC Berkeley	Thermal oxidation of InP; dynamic transmission electron microscopy
R. Fisher	LBL/Wolverhampton, UK	Critical-voltage studies of alloys
D. Frear	Sandia National Laboratory	Microstructural study of Al thin films
		Microstructure of solder interconnections in electronic packaging polymers
R. Gronsky	LBL/UC Berkeley	*In situ* oxidation study of the Y/Ba/Cu/O superconductors
J. Hardin	Duke University	An HVEM analysis of filopodial structure and function during sea urchin gastrulation
H. Heinemann	LBL	Gasification of graphite catalyzed by KOH:MgO
J. Howe	Carnegie-Mellon University	*In situ* studies of precipitate growth by a terrace-ledge-kink mechanism
D. Howitt	UC Davis	Structural study of thin-film ceramics
V. Jayaram	UC Santa Barbara	Microstructural study of rapidly solidified powders
M. Libera	IBM Almaden	Microstructural properties of multilayer thin films for phase-change optical recording
Z. Liliental-Weber	LBL	Study of the kinetics of Au crystallite formation on the periphery of Au Schottky contacts
M. Madden	Intel	Analysis of single-bit failures in VSLICs
W. Mayer	Domain Technologies	(Proprietary)
A. Meike	LBL/UC Berkeley	Characterization of stress-induced defects in minerals in relation to enhanced aqueous dissolution

Table 1-1 (continued)

Principal Investigator	Affiliation	Title
J.W. Morris, Jr.	LBL/UC Berkeley	Fatigue-crack propagation mechanisms of structural alloys at cryogenic temperatures
		Dislocation substructures and work-hardening in bcc polycrystalline metals
V. Polito	UC Davis	High-voltage EM study of the ultrastructure of freeze-substituted pollen tubes in Pyrus communis L
D. Olander	LBL/UC Berkeley	Electron-irradiation-induced amorphization of precipitates in Zircaloy
L.E. Rehn	Argonne National Laboratory	Comparison of electron- and ion-irradiation-induced grain growth in gold films
R.O. Ritchie	LBL/UC Berkeley	Dynamic studies of deformation and failure in SiC-aluminum metal-matrix composites
M. Ruhle	UC Santa Barbara	Bridging mechanisms of toughening in whisker-reinforced ceramics
T.H. Sanders	Georgia Tech.	Deformation behavior in Al-Li-Zr alloys
A.W. Searcy	LBL/UC Berkeley	TEM studies of decomposition reactions
G. Shiflet	U. Virginia	HVEM of pearlite in a Fe-C-Mn alloy
W. Stacy	Philips	Transistor pipes
L. Tanner	LLNL	Study of metastable phase formation in Cu-Zr and Al-Ni
M.A. Taylor	UC Davis	Hydration of Portland cement in environmental cell
Gareth Thomas	LBL/UC Berkeley	*In situ* studies of plastic deformation in Al-Li base alloys
		A systematic study of Cu-Ni thin films for magnetic recording media
George Thomas	Sandia National Laboratory	*In situ* oxidation studies on stainless steel
		Gases in metals
R. Wenk	LBL/UC Berkeley	Phase transformation in silica minerals
		Dislocation properties of silicate garnets
K.H. Westmacott	LBL/UC Berkeley	Dynamic hot-stage studies of precipitate development in interstitial and substitutional alloys
M.C. Williams	LBL/UC Berkeley	*In situ* study of strain deformation of block copolymer microstructures
C. Wong	GM	Effects of oxidation-reduction treatments on the morphology of supported rhodium catalysts
ARM		
L. Blackburn	NASA Langley	Effect of indium additions on precipitation in Al-Cu-Li-Z
D. Blake	NASA Ames	HREM observation of interstellar diamonds in meteorites

Table 1-1 (continued)

Principal Investigator	Affiliation	Title
H. Chan	Ceracon Ltd.	High-pressure consolidation of $YBa_2Cu_3O_{7-x}$ superconductor powder
J. Cornie	MIT	Tayloring and modeling interfaces in metal matrix composites
U. Dahmen	LBL	Characterization of nanocrystals by HREM
J. Goral	SERI	High-resolution structural study of $YBa_2Cu_3O_{7-x}$
		Ordering in GaInP
R. Gronsky	LBL/UC Berkeley	Atomic mechanisms of precipitate plate growth
		Quasicrystals
		Defects in oxide superconductors
J. Howe	Carnegie-Mellon University	Atomic-resolution studies of shearable coherent precipitates in Al-Li alloy
		Atomic-resolution microscopy of interfaces in intermetallic-matrix composites
		Atomic-resolution studies of {225} martensite-austenite interfaces
A. Jankowski	LLNL	Interfacial structure of short-period multilayers
W. Kriven	U. Illinois	TEM characterization of modulated structures in $CaO-Dy_2O_3$ solid solutions
J.Y. Laval	CNRS, Paris	Atomic structure of internal interfaces in covalent materials
C. Lyman	Lehigh University	ARM of copper crystallites via methanol synthesis Cu/ZnO catalyst
		HREM study of zirconia-based eutectics
I. Mackinnon	U. New Mexico	High-resolution imaging of boron carbides
K. Merkle	Argonne National Laboratory	Study of tilt grain boundaries in NiO
M. Mills	Sandia, Livermore	Core structure of screw superdislocations in Ni_3Al
J.W. Morris	LBL/UC Berkeley	Analysis of fine microstructure in Al-Sc-(RE)
G.B. Olson	MIT	Fine structure of martensitic interfaces
F. Ponce	Xerox	Structure of early stages of growth in GaAs/Si epitaxy
G. Shiflet	U. Virginia	HREM growth ledges on T1 (Al_2CuLi) plates
		HR studies of interfacial pearlitic structures in a Fe-C-Mn alloy
R. Sinclair	Stanford	Structure of twin interfaces in TiNi
M. Suenaga	Brookhaven National Laboratory	Twin boundaries in $YBa_2Cu_3O_7$
L. Tanner	LLNL	HRTEM studies of pretransformation microstructures in metallic alloys
		Study of metastable formation in Cu-Zr and Al-Ni

Table 1-1 (continued)

Principal Investigator	Affiliation	Title
Gareth Thomas	LBL/UC Berkeley	HREM on glasses
		Structure of PFZ in Al-Li alloys
		Atomic imaging of structure and defects in high-T_c superconductors
George Thomas	Sandia, Livermore	Structure of high-T_c superconductors
		Structure of grain boundaries in metals
H.L. Wenk	LBL/UC Berkeley	Superstructure identification in carbonate minerals
U. Dahmen, K.H. Westmacott, and J. Douin	LBL	Studies of precipitate morphologies and interfaces
AEM		
K. Krishnan	LBL/UC Berkeley	Determination of the composition of the icosahedral phase in Al-Mn alloys at high spatial resolution
		Processing and microstructural characterization of the crystalline phases in the Al_2O_3-AlNd system
		Applications and development of channeling enhanced microanalysis
		Compound semiconductor contact metallizations
K. Krishnan and C. Echer	LBL/UC Berkeley	Experimental determination of UTW K-factors for low-atomic-number elements
Z. Liliental-Weber, J. Washburn, and R. Gronsky	LBL/UC Berkeley	Ohmic and Schottky Au contacts on GaAs
R. Ramesh, J. Chen, and G. Thomas	LBL/UC Berkeley	Role of grain-boundary phases in Fe-Nd(B) permanent magnets
M. Sattler, A.T. Bell, and P.N. Ross	LBL/UC Berkeley	EDX characterization and electron microdiffraction of submicron catalyst particles of TiO_2 on SiO_2, Pt and Pt_3Co on C, and Rh on La_2O_3 and SiO_2
J. Kouvetakis, K. Krishnnan, and N. Bartlett	LBL/UC Berkeley	EELS analysis of B-C-N chemically vapor deposited crystallites
		Characterization of new graphite-like materials ($C_xB_yN_z$) by electron energy loss spectroscopy
E. Kamenetzky, L. Tanner, and W. Johnson	LBL/UC Berkeley, LLNL/ Caltech	Solid-state amorphization reactions; glass formation by particle melting in a Cu-Ti alloy
		Solid-state amorphization reactions; nucleation of glass at grain boundaries, Ni on Zr
		Solid-state amorphization reactions; kinetics of glass formation in Ni-Zr multilayers
Gareth Thomas and V. Radmilovic	LBL/UC Berkeley	Structure of PFZ in Al-Li alloys
D. Blake	NASA Ames	Characterization of carbonaceous phases contained in meteorites and interplanetary dust particles

Table 1-1 (continued)

Principal Investigator	Affiliation	Title
J. Goral, K. Jones, and M. Al-Jassim	SERI	Characterization of interfacial island inclusions formed during CVD deposition of InAs (InP) on GaAs substrate and subsequently capped with GaAs
V. Radmilovic and T. Devine	LBL/UC Berkeley	Characterization of type 308 and 304 stainless steel weldment that showed intergranular stress-corrosion cracking in the heat-altered-zone region
		Characterization of inclusions contained in Al-Li alloys
J. Bastacky	LBL/UC Berkeley	Microchemical analysis of alveolar walls in the human lung
E. Kamenetzky	LLNL	Characterization of glass nucleation in the grain boundaries of Ni-Zr layers during solid-state amorphization reactions
R. Spontak	LBL/UC Berkeley	Characterization of microstructure resulting from microphase-separated block copolymers composed of polysiloxane and polymide
W. Hirt and K. Krishnan	LBL/UC Berkeley	Channeling-enhanced microanalysis of a metastable intermediate phase between pure calcite and pure dolomite
K. Srikrishna	LBL/UC Berkeley	Characterization of oxygen content in aluminum oxynitride ceramics
M. Sattler	LLNL	Characterization of small precipitates in Ce- and Nd-doped $Gd_3Sc_2Ga_3O_{12}$ single crystals contaminated with Ir and Cr
W. Hirt	LBL/UC Berkeley	EDX and EELS characterization of pyroxene
D. Frear	Sandia, Albuquerque	Microstructural characterization of Cu distribution in deposited and annealed Al–2%Cu magnetron-sputtered thin films
D. Jian-Zhong and R. Fisher	LBL	Microstructural characterization of evaporated chromium films
A. Meike	LBL/UC Santa Cruz	Microchemical analysis of trace pigment observed on an Egyptian carved limestone head (ca. 2400 B.C.) to determine whether they were painted with Egyptian orpiment containing arsenic
N. Thadani	NM Inst. Mining Technology	Microstructural characterization of shock-synthesized B_4C and TiB_2 ceramics, and aluminides of Ni and Nb
J. Douin, U. Dahmen, and K.H. Westmacott	LBL	Microstructural characterization of precipitates in aluminum—1% germanium alloy
C. Ortiz and K. Krishnan	IBM San Jose/LBL	Microstructural characterization of Fe-oxide magnetic recording media
M. Witcomb and U. Dahmen	U. Witwatersrand, South Africa/ LBL	Microstructural characterization of Cr precipitates in copper-chromium alloys
T. Epicier	INSA, France/LBL	Characterization of dislocations in W_2C and Al_2TiO_5 after high-voltage electron irradiation

Table 1-1 (continued)

Principal Investigator	Affiliation	Title
D. Callahan and Gareth Thomas	LBL/UC Berkeley	Characterization of oxygen and nitrogen content in aluminum nitride ceramic
N. Merk and L. Tanner	LLNL/LBL	Phase characterization of arc-melted and extruded Cu-Zr alloy
G. Holland and K. Krishnan	LBL/UC Berkeley	Chemical and structural phase characterization of microcrystalline FeW_2S_7 alloy
A. Fox	Wolverhampton, UK/LBL	Dislocation characterization of solid-state bonding of copper to glass
C. Koestler and Gareth Thomas	UC Berkeley	Microstructural characterization of Fe-Co-Nd-B melt-spun magnets containing various Co contents
R. Csencsits and R. Gronsky	LBL/UC Berkeley	Chemical and structural characterization of submicron iron-rich second-phase particles in iron silicate molecular sieve
L. Blackburn	NASA Langley	Microstructural investigation into the effects of cadmium, indium, and tin additions to Al-Cu-Li alloys
COMPUTER PROJECTS		
R.S. Rai and M.A. O'Keefe	LBL/UC Berkeley	Processing of images of phases of yttrium disilicate
		Simulation of phases in $Y_2Si_2O_7$
Z. Liliental-Weber and M.A. O'Keefe	LBL/UC Berkeley	Processing of images of GaAs antiphase boundaries
M. Sattler and M.A. O'Keefe	LBL/UC Berkeley	Processing of images of catalysts (anatase/rutile on amorphous Si)
I. Chan and M.A. O'Keefe	Chevron/LBL	Processing to detect Pt clusters in Y-zeolite
R. Kilaas, K. Krishnan, and R. Rai	LBL/UC Berkeley	Image simulation and processing of 32H AlN/Al_2O_3 images
J.Y. Laval and R. Kilaas	LBL/CNRS, Paris	Silicon nitride and interface simulation
H. Zandbergen and R. Kilaas	LBL/UC Berkeley	Simulation of defects in high-T_c superconductors
M.L. Sattler and M.A. O'Keefe	LBL/LLNL	Simulation of anatase/rutile particles on amorphous SiO_2
N. Schryvers and R. Kilaas	LBL/LLNL	Simulation of "tweed" image of NiAl
U. Dahmen and M.A. O'Keefe	LBL/UC Berkeley	Simulation of metastable phases in zirconia
C.J. Jou and R. Kilaas	LBL/UC Berkeley	Oxygen vacancies in $YBa_2Cu_3O_{7-d}$
N. Merk	LBL/LLNL	Diffraction pattern calculation in CuZr–NiAl
M. Stampfer	LBL	Quantification in energy-loss spectroscopy
C. Hetherington	LBL	ARM characterization (CTFs, on-line ODM)
		Al grain-boundary processing (SEMPER)
C. Hetherington, M.A. O'Keefe, R. Kilaas, and A. Fox	LBL/Wolverhampton, UK	Wedge crystal study of experimental image vs calculated image

Table 1-1 (continued)

Principal Investigator	Affiliation	Title
C. Hetherington and U. Dahmen	LBL	Hexagonal silicon and hexagonal/cubic interface
J. Douin and U. Dahmen	LBL	Interface simulation in Al/Si–AlGe
T. Epicier, R. Kilaas, and K. Krishnan	INSA, Lyon, France/LBL	Studies of mullite; studies of C_6O cluster
M.A. O'Keefe and R. Kilaas	LBL	Simulation of Al grain boundaries
R. Ramesh, C. Hetherington, and M.A. O'Keefe	LBL/UC Berkeley	Simulations of modified BCSCO high-T_c superconductors
M.A. O'Keefe and M. Sattler	LBL/LLNL	Simulation of multilayer structures
J. Wong and M.A. O'Keefe	LBL/LLNL	Simulation of substituted high-T_c superconductors
M.A. O'Keefe and D. Blake	LBL/NASA Ames	Interstellar diamond processing
Z. Liliental-Weber and M.A. O'Keefe	LBL	Inversion boundaries in GaAs grown on Si
A. Motta and J. Turner	LBL/UC Berkeley	Computer-intensity analysis of diffraction patterns from Zircaloy
U. Dahmen and J. Turner	LBL	Diffraction pattern profiles of MgOH
		Image processing of ICB aluminum grain boundaries to determine periodicity
		Image processing of models for the determination of crystal misorientations represented in the optical diffractograms
R. Ramesh and J. Turner	LBL/UC Berkeley	HREM image processing of the $Bi_2Sn_2Ca_2Cu_3O_4$ superconductor
T. Epicier and J. Turner	LBL/INSA, Lyon, France	Fourier filtering of HREM images of mullite

A striking demonstration of the utility of the high-angle tilting stage is provided by the micrographs in Figure 1-1. These show atomic-resolution images of the same island of GaAs (deposited on a Si substrate) viewed along two <110> directions separated by a 90° tilt.

2. High-Resolution Electron Microscopy (HREM) of Interfaces in Topotaxial and Epitaxial Reactions (Publication 39)

U. Dahmen, J. Douin, C.J.D. Hetherington, and K.H. Westmacott

In the study of interfaces, HREM is most useful when the interface is viewed edge-on while both crystals are accurately aligned along low-index zone axes. The formation of such interfaces by epitaxy or topotaxy is the natural means of obtaining structures that can be usefully analyzed by HREM. Furthermore, there is intense interest in understanding the atomic structure of such interfaces in a variety of technologically important materials. This contribution addresses such structures produced by thermal decomposition, precipitation reactions, and ionized cluster-beam deposition, and reports on the structural investigation of symmetrical and asymmetrical grain boundaries, precipitate/matrix interfaces, internal defect structure of precipitates, and nanocrystalline composites. A micrograph illustrating the clarity of interface images now attainable with the Atomic Resolution Microscope is given in Figure 2-1. The periodic structure along a Σ99 symmetrical grain boundary in an Al bicrystal is resolved at a level where detailed comparison with theory is now possible.

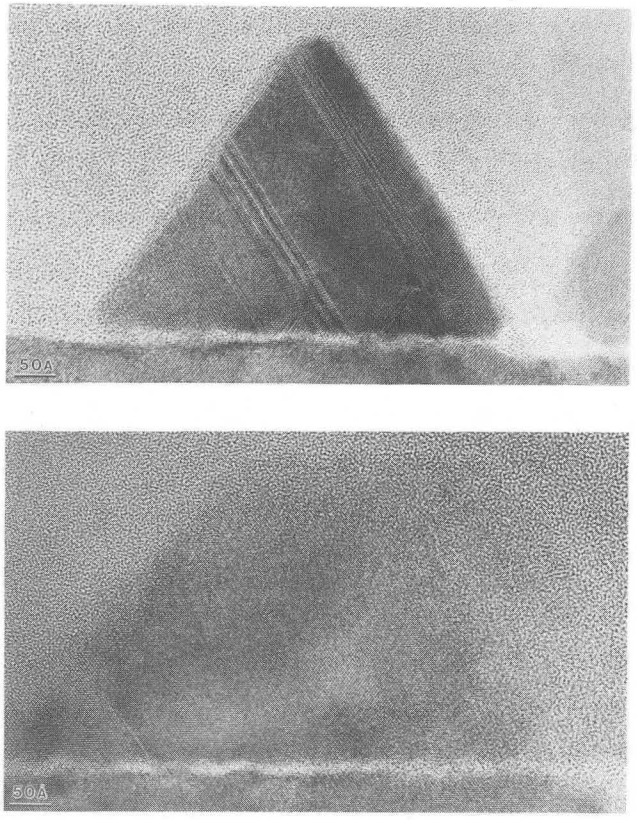

Figure 1-1. Top: GaAs island on (001) Si viewed down [110]. The sample was prepared as a [100] cross section and tilted +45°. Bottom: The same GaAs island on (001) Si; here it is tilted −45° to be viewed down [110]. Note the information that can be obtained from the two images on island morphology and defect distribution. Sample from Dr. F.A. Ponce. (XBB 891-593)

3. High-Resolution Electron Microscopy and Image-Simulation Studies of Superconducting Polytypoids in Bi-Ca-Sr-Cu-O Ceramics (Publication 83)

C.J.D. Hetherington, R. Ramesh, M.A. O'Keefe, R. Kilaas and G. Thomas

High-resolution electron microscopy of two superconducting polytypoids has been carried out, and image simulation and matching have been used to investigate their structures. We have confirmed the stacking sequence of the cations in the c = 30.5-Å polytypoid as Bi-Bi-Sr-Cu-Ca-Cu-Sr-Bi-Bi ..., while the 37-Å polytypoid contains one additional set of

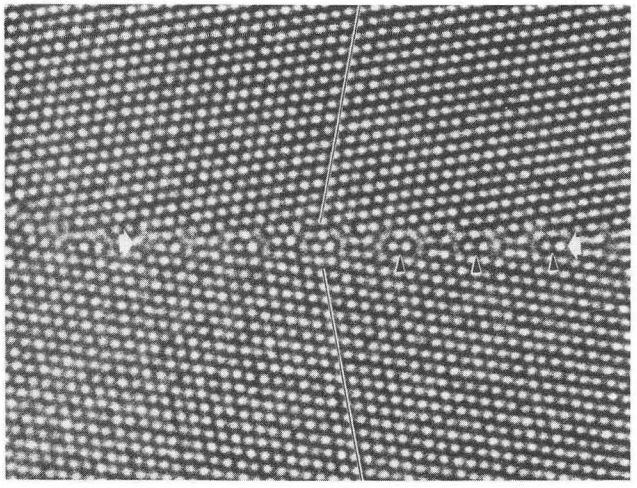

Figure 2-1. High-resolution image of a typical facet on an Al<110> grain boundary in symmetrical orientation. The periodic atomic arrangements along the boundary are indicated by black arrows. (XBB 889-8856)

Cu + Ca layers in each half of the unit cell. Figure 3-1 shows an example of a micrograph taken on the ARM that identified a region as a uniform 37-Å polytypoid. We have also examined the possibility that the HREM images can give further information about the structures using image processing and simulation. The results suggest that (i) in some regions Bi replaces Ca, (ii) the oxygen atoms in the Bi bilayers are located at the face centers of the Bi sublattice, and (iii) the central Cu-O layer in the 37-Å polytypoid may be oxygen deficient.

4. Atomic Structure of Grain Boundaries and Surfaces in $YBa_2Cu_3O_{7-\delta}$ and $LaBaCaCu_3O_{7-\delta}$ (Publication 101)

H.W. Zandbergen,[†] R. Gronsky, and G. van Tendeloo[‡]

High-resolution electron-microscopy studies of grain boundaries and fractured surfaces in both the tetragonal and orthorhombic phases of dense (> 90%) $YBa_2Cu_3O_{7-\delta}$ and tetragonal $LaBaCaCu_3O_{7-\delta}$ have been conducted. Grain boundaries in polycrystalline $YBa_2Cu_3O_{7-\delta}$ are found to be frequently parallel to a (001) plane of one of the adjacent grains, with a structure similar to that of the (001) surface of fractured $YBa_2Cu_3O_{7-\delta}$. Matching of experimental and calculated images shows the outermost surface layer in this compound is a deformed BaO layer. Both grain boundaries and fractured surfaces in $LaBaCaCu_3O_{7-\delta}$ show no such tendency for preferential orientation of the interface plane. Results indicate that the low critical currents observed in sintered materials are caused by textured grain growth in combination with the atomic structure of the grain boundary plane, and the intercalation of off-stoichiometric species near the grain boundary.

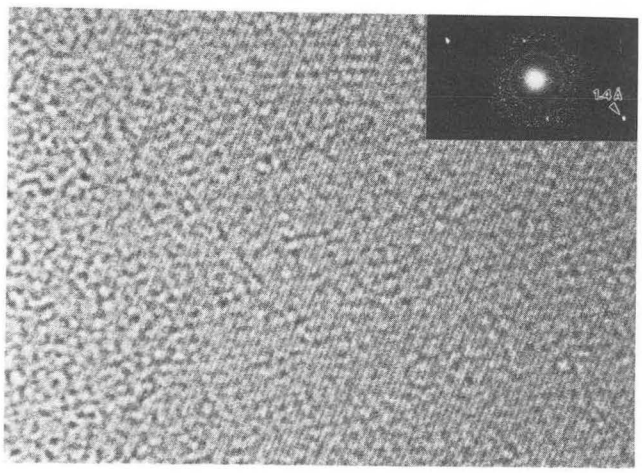

Figure 3-1. [110] zone-axis Atomic Resolution Microscope image (800 kV) of the r = 3 polytypoid showing the stacking sequence of Bi-Bi-Sr-Cu-Ca-Cu-Sr-Bi-Bi. (XBB 891-591)

[†]Permanent address: Gorlaeus Laboratories, State University of Leiden, 2300 RA Leiden, The Netherlands.

[‡]Permanent address: Antwerp University, RUCA, B-2020, Antwerp, Belgium.

5. Transmission Electron Microscopy (TEM) Characterization of Precipitates (Publication 90)

U. Dahmen

This paper reviews the methods and principles underlying the structural and morphological characterization of precipitates by TEM. Precipitate contrast mechanisms are reduced to the better-known contrast behavior of crystal defects, such as dislocation loops, dipoles, and stacking faults. Because of their importance, basic techniques of controlled specimen tilting and the analysis of double diffraction are treated in some detail. The remainder of this paper concentrates on more advanced concepts in precipitate characterization, not available in textbooks. Emphasis is placed on the use of crystal symmetry in practical problems of precipitate analysis, on the relationship between transformation strains of the real and the reciprocal lattice, and on the connection between transformation strain and morphology. These concepts are illustrated with selected examples.

6. Transmission Electron Microscope Study of Arsenic Precipitates in GaAs: Morphology and Orientation Relationship with the Matrix (Publication 102)

B.-T. Lee[†] R. Gronsky, and E.D. Bourret

Precipitates in several GaAs crystals with different properties were studied with transmission electron microscopy to reveal their identity, their orientation relationship with the matrix, and their morphology. Most of them were identified as elemental rhombohedral As with a tetrahedral shape bounded by GaAs {111} planes. Some of the As precipitates showed a simple orientation relationship with the matrix: (0001)As ∥ (111)GaAs and [1120]As ∥ [110]GaAs. It was found that this orientation rela-

tionship yields a high degree of structural coherence between the two phases and is responsible for the observed tetrahedral precipitate shape. Other As particles associated with dislocations showed a less coherent orientation relationship, with a few-degree variation from the above relationship, likely due to strain around the dislocation core.

[†]Present address: Department of Metallurgy, Chonnam National University, Kwang Ju 505, Seoul, Republic of Korea.

7. Electron-Energy-Loss Spectroscopy (EELS): Fundamentals and Applications in the Characterization of Minerals (Publication 53)

K.M. Krishnan

The combined use of an energy-loss spectrometer and an analytical electron microscope with fine probe-forming capabilities provides a wealth of information about the sample at high spatial resolution. Fundamental principles governing the physics of the interaction between the fast electron and a thin foil sample, to account for the fine structure in the inelastically scattered fast-electron distribution (EELS), are reviewed. General application of EELS is in the area of microanalysis of low-atomic-number elements ($Z > 11$), where it significantly complements the more widely used energy-dispersive x-ray (EDX) spectroscopy. However, a careful analysis of the low-loss plasmon oscillations and the fine structure in the core-loss edges can provide additional information related to the bonding and electronic structure of the sample. An illustration of this is presented from our study of Cδ diamond residue from the Allende carbonaceous chondrite. The combination of EELS with channeling effects can provide specific site-occupation/valence information in crystalline materials. Details of this novel crystallographic method are outlined and illustrated with an example of the study of chromite spinels.

8. Microstructure of Melt-Spun Nd-Fe-Co-B Magnets (Publication 103)

C. Koestler, R. Ramesh, C.J. Echer, and G. Thomas

We report results on microstructural characterization of melt-spun $Nd_{17}Fe_{77}B_6$ and $Nd_{15}(Fe_{1-x}Co_x)_{77}B_8$ ribbons using-high resolution electron microscopy, x-ray microanalysis, and microdiffraction. In general, the microstructure consists of the hard magnetic $Nd_2Fe_{14}B$ phase and one or more grain-boundary phases. In all these materials, no $Nd_{1.1}Fe_4B_4$ phase was observed. The grain-boundary phase in the Co-free samples appears mainly at multigrain junctions and is a Nd-rich, crystalline (fcc) phase, whereas the Co-containing specimens comprise two different fcc grain-boundary phases. The structural and microchemical data indicate that these are likely to be ferromagnetic and that they contain significantly less Nd than the grain-boundary phase of the Co-free samples. The average matrix grain diameter is about 80 nm, but there are always some areas in every specimen where the grain diameter is very small (about 20 nm) or very large (more than 300 nm), causing differences in the size of the grain-boundary phases both at the triple grain junctions and between the grains.

9. Structure and Bonding of Diamond and Diamond-Like Materials: Microanalytical Characterization at High Spatial Resolution (Publication 86)

K.M. Krishnan, D.F. Blake,[†] F. Freund,[†] and R.J. Lipari[‡]

Recent developments in the synthesis of single-phase diamond films and the observation of nanometer-scale diamond-like particles in meteoritic residues have generated much interest in the characterization of these materials. Of particular interest is the evaluation of parameters such as degree of crystallinity, defects, homogeneity, grain size, impurity content, bonding, electronic structure, etc. With the incorporation of fine probe-forming systems in an Analytical Electron Microscope (AEM) and the development of related diffraction, spectroscopic, and imaging methods, it is possible to obtain precisely such structural and chemical information at high spatial resolution. Here we summarize the results of our studies of explosively compacted diamond particles, microwave plasma-enhanced chemical-vapor-deposition diamond films, and diamond-like residues of extraterrestrial carbon (Cd residue) by microdiffraction, EDX spectroscopy, and EELS, all using nanometer-scale electron probes, and by electron spectroscopy for chemical analysis, a complementary bulk spectroscopic method. However, the characterization of the Cd residue is particularly emphasized.

[†]Permanent address: NASA/Ames Research Laboratory, Moffett Field, CA 94305.

[‡]Permanent address: Surface Science Laboratory, Mountain View, CA 94043.

10. Characterization of Electron-Beam-Induced Damage Structures in Natural Fluorite, CaF_2, by Analytical Electron Microscopy (Publication 81)

D.F. Blake,[†] L.F. Allard,[‡] C.J. Echer, and F. Freund[†]

Naturally occurring fluorite, CaF_2, develops a particular highly ordered damage structure when exposed to the primary beam in the transmission electron microscope (TEM). This structure has been variously described as "ordered defect aggregates," a "superlattice array of voids," and "Ca colloids produced by beam-induced loss of fluorine from the fluorite structure." During a reconnaissance study of optical anisotropy in natural fluorite, we observed this structure under a variety of instrumental conditions. The electron-beam-induced damage structure in fluorite is described, and, based on these new data, suggestions are made of its mechanism.

[†]Permanent address: Planetary Biology Branch, NASA/Ames Research Center, Moffett Field, CA 94035.

[‡]Permanent address: High Temperature Materials Laboratory, Martin Marietta Energy Systems, Oak Ridge National Laboratory, Oak Ridge, TN 38731.

11. The Design of a Computer Image System for Simulation and Processing of TEM Images: Hardware and Software (Publication 104)

R. Kilaas and M.A. O'Keefe

With images being the central theme in both simulation and processing, the traditional computer setup of a text terminal connected to a heavily used mainframe computer is turning out not to be an optimum choice for these types of applications. Breakthroughs in computer technology are producing far less expensive setups that can rival the turnaround time of their bigger siblings and provide a level of interaction not previously possible. The process of designing an integrated environment is, however, complicated by incompatible hardware and software. In an effort to guide anyone desiring to acquire their own workstation for simulation and processing of TEM images, two systems are discussed. One system has been designed with performance in mind; the other system designed for low cost. Both hardware and software components are discussed, with emphasis on optimum matching of each to the other.

12. Multislice Calculations: "Slicing" and Those Upper Laue Layer Interactions (Publication 52)

R. Kilaas

The relationship between the inclusion of upper Laue layer interactions in multislice calculations and the method of subdividing the unit cell has been studied in detail. Four different approaches are compared, and it is shown that two of the methods are capable of producing scattering out of the zeroth-order Laue zone. In order to demonstrate the differences between the methods, calculations were carried out on two distinct systems, BiTe and $MgAl_2O_4$.

13. Critical-Voltage Estimates of Lithium Depletion in Precipitate-Free Zones (PFZs) in Al-Li Base Alloys (Publication 98)

V. Radmilovic,[†] A.G. Fox, R.M. Fisher, and G. Thomas

Since the effects of PFZs were first examined in high-strength Al-Mg-Zn alloys, much attention has been paid to PFZs and their deleterious effects, especially with respect to the mechanical behavior, fracture, and stress-corrosion cracking, in a wide range of conventional high-strength Al-base alloys, as well as in the newer high-strength Al-Li alloys for aerospace applications. The difficulties of spectroscopic analysis for Li (mainly because of its low atomic number) are well known. An alternative technique for compositional analysis, although indirect, that can be utilized by high-voltage electron microscopy is that of the so-called "critical voltage" effect, by which it should be possible to measure the percent of Li to within 3%. The 1.5-MeV HVEM with liquid-nitrogen stage available at NCEM is necessary for such analyses. Several alloys based on Al-2% Li with and without 2.5% Cu were studied in the overaged condition. The chemical analyses of alloys A and B shown in Table 13-1 indicate that the lithium contents of the center of the grains in both alloys are very nearly the same in both the as-quenched and overaged conditions. This allows a comparison between the critical-voltage measurements made on the two alloys so that possible Li depletion at PFZs can be confirmed. In spite of the unavoidably large errors, the V_c^{222} measurements on alloy B suggest

that there is lithium depletion at PFZs (see Table 13-1).

†Present address: University of Belgrade, Department of Metallurgy, Karnegijeva 4, Belgrade, Yugoslavia.

14. Inversion Boundaries in GaAs Grown on Si (Publication 97)

Z. Liliental-Weber, M.A. O'Keefe, and J. Washburn

Inversion boundaries in GaAs grown on Si were investigated by high-resolution transmission electron microscopy. These boundaries were found to microscopically follow {110} planes, even when they appeared macroscopically along other planes, such as {111}. High-resolution micrographs from edge-on {110} inversion boundaries were taken in [110] and [100] projections. In certain areas, shifts of the images of {111} and {200} planes across the boundaries were observed. Image simulations confirmed that the visibility of these shifts can only be observed for specific imaging conditions and within a limited range of sample thickness.

15. Dislocation Microstructures on Flat and Stepped Si Surfaces: Guidance for Growing High-Quality GaAs on (100) Si Substrates (Publication 18)

Y.H. Lo,† M.C. Wu,† H. Lee,† S. Wang,† and Z. Liliental-Weber

Type-I dislocations at the GaAs/Si interface are beneficial, because they effectively relax the mismatched stress but do not propagate into the GaAs film. Accordingly, the best way to grow a low-defect-density GaAs film on a Si substrate is to form as many as possible type-I dislocations or, equivalently, to suppress other kinds of defects. This high-resolution transmission electron microscopy study shows that most of the type-I dislocations are formed at the double step on a Si surface. It is further determined that the silicon surface steps are mainly caused by the substrate's tilting instead of heating before growth. Based on our study, the (100) Si substrate with double steps along both [110] and [110] axes provides the best condition for growing low-defect-density GaAs on Si substrates.

†Permanent address: Department of Electrical Engineering and Computer Sciences, and Electronic Research Laboratory, University of California, Berkeley, CA 94720.

Table 13-1
Calculated and Experimental Critical Voltages (V_c) for Al-Li Alloys

Sample	Temp. (K)	V_c^{222} (kV)	V_c^{400} (kV)	%Li (at)	%Li (wt)
Alloy A as quenched (calculated)	293	478	994.5	8.9	2.45
Alloy B as quenched (calculated)	293	477	990.	8.7	2.37
Alloy B (overaged; in PFZ)	293	465 ± 15	—	5.3	1.40
Alloy B (overaged; in grain center)	293	475 ± 30	—	8.3	2.30
Alloy A (overaged; in grain center)	293	480 ± 10	1000 ± 25	9.8	2.70
Alloy A (overaged; in grain center)	253	500 ± 7.5	—	9.8	2.70
Al (as quenched)	293	465 ± 10	975 ± 15	5.3	1.40
Al (as quenched)	92	535 ± 10	1110 ± 15	5.3	1.40
A2 (as quenched)	293	475 ± 10	990 ± 15	8.1	2.20
A2 (as quenched)	92	550 ± 10	1140 ± 15	8.1	2.20

16. A TEM Study of Microstructures Associated with Solution Cleavage in Limestone (Publication 20)

A. Meike[†] and H.-R. Wenk[†]

Microstructures associated with clay-filled seams in the Scaglie Rossa limestone from the Umbria-Marche Apennines, Italy, were characterized with high-voltage transmission electron microscopy (TEM) in order to study one of the mechanisms that presently falls under the heading of "pressure solution." Only seams that formed after lithification, often called "solution" or "spaced" cleavage, were examined. Although some observations supported suggestions that much of the clay in the solution cleavage seam could be authigenic, this report focuses primarily on the limestone microstructures. No evidence of plastic deformation could be observed around the seams with an optical microscope. However, the TEM-resolved dislocations concentrated within limited areas of single grains. Comparisons with experimentally deformed calcite microstructures and with computer simulations of TEM dislocation contrast allowed further interpretation of the character and density of dislocations. Dislocation concentrations were frequently associated with voids and pits. The pits and voids were usually elongate in a calcite dislocation slip plane and were interpreted as dissolution features. These and other observations suggested that selective dissolution of localized dislocation tangles was responsible for solution cleavage formation. Similar microstructures associated with stress-corrosion cracking have been interpreted elsewhere as evidence of plastic-strain-enhanced heterogeneous dissolution. Further interpretations indicated that a solution cleavage surface grows laterally like a fracture tip.

[†]Permanent address: Department of Geology and Geophysics, University of California, Berkeley, CA 94720.

17. Rapid Solidification of Alumina-Zirconia Eutectic and Hypoeutectic Alloys (Publication 74)

T. Whitney,[†] V. Jayaram,[†] C.G. Levi,[†] and R. Mehrabian[†]

A technique has been developed to produce rapidly solidified fine powders of binary ceramic alloys by electrohydrodynamic (EHD) atomization. Eutectic (42.5 wt%) and hypoeutectic (17 wt%) alumina-zirconia mixtures were prepared by colloidal chemistry methods, extruded, and sintered to form thin rods that were subsequently atomized. Powders from tens of nanometers to the hundred-micrometer range were produced in this manner. Scanning and high-voltage transmission electron microscopy of these materials revealed a variety of microstructures, including completely amorphous particles, single-phase microcrystalline solid solutions, and two-phase mixtures of Al_2O_3 and ZrO_2. Although zirconia appeared predominantly in the monoclinic form, alumina exhibited a multiplicity of metastable crystal structures, including cubic spinel (γ), orthorhombic ordered spinel (δ), and monoclinic (θ). Microstructure evolution is discussed in terms of composition and particle size, hence achievable supercooling, with particular emphasis on phase selection and solute redistribution.

[†]Permanent address: Materials Department, Mechanical and Environmental Engineering, University of California, Santa Barbara, CA 94106.

18. An Electron Microscopy Study of the Atomic Structure of a Mullite in a Reaction-Sintered Composite (Publication 23)

D. Schryvers, K. Srikrishna, M.A. O'Keefe, and G. Thomas

The mullite matrix of a reaction-sintered mullite/zirconia composite has been characterized by various electron microscopy techniques. The mullite was determined to be stoichiometrically $Al_{4.76}Si_{1.23}O_{9.61}$ (1.7:1 mullite), with a disordered vacancy structure and *Pbam* symmetry. The atomic structure of the mullite has been described in terms of an average unit cell.

19. Interphase Composition Profile in Sb/SBS Block Copolymers, Measured with Electron Microscopy, and Microstructural Implications (Publication 24)

R.J. Spontak,[†] M.C. Williams,[†] and D.A. Agard[d]

The behavior of microphase-separated block copolymers has major contributions from the mixed interphase existing between the two homogeneous phases. However, relatively little has been known

about the interphase itself, and in particular, its composition profile has never been measured directly. Here we have used quantitative transmission electron microscopy to acquire the shape of the volume-fraction composition profile across this interphase. Measurements were made on four styrene (S)/butadiene (B) block copolymers having structure SBS (three) and SB (one), with molecular weights 1.0–2.3 $\times$ 10^5 g/mol and overall volume compositions of 0.24–0.38 styrene. Results, averaged over the four samples, depict an asymmetric interphase profile rich in styrene (54 vol%), in agreement with new differential scanning calorimetry data and with dynamic mechanical testing studies of others. This profile is then used in an equilibrium thermodynamic theory (which extends earlier work by adding an enthalpic "Debye" term that accounts for molecular interactions beyond nearest neighbors) to predict various microstructural and thermal properties of the bulk polymer. Excellent agreement with reported data is obtained for the predicted interphase thickness and interphase volume fraction and for predictions of the repeat distance for lamellar SB copolymers.

†Permanent address: Department of Chemical Engineering, University of California, Berkeley, CA 94720.

‡Permanent address: Department of Biochemistry and Biophysics, University of California, San Francisco, CA 94143.

20. The Preparation of Mechanically Alloyed Powders for TEM Examination (Publication 82)

E.A. Kamenetzky,† M. Wall,† R. Castro,†· and L.E. Tanner†

TEM specimens of mechanically alloyed elemental Ni and Nb powders are prepared by a new procedure. The alloyed powders are mixed with smaller Al powders and fill an aluminum ring (3-mm outer diameter). This composite is cold pressed together, with the Al powders taking most of the deformation. The compacted specimen can be mechanically thinned. Electropolishing and ion milling can then proceed by standard methods with special precautions to minimize differential polishing or milling rates.

The microstructural aspects of the formation of an amorphous phase by high-energy ball milling of these powders have been studied. After 6 hr each particle transforms to a heterogeneous layered composite of particles of one element in the matrix of the other. Particle size ranges from 15 to 90 nm. Mechanical alloying for 36 hr results in the formation of an apparently uniform phase interspersed with a few small (4–30 nm) elemental crystalline particles. The uniformity of composition and the presence of C, O, and Fe were studied by EDX and EELS.

†Permanent address: Chemistry and Materials Science Department, Lawrence Livermore National Laboratory, Livermore, CA 94550.

21. Structure of δ_2-$Y_2Si_2O_7$ Confirmed by Processing and Simulation of Atomic Resolution Images (Publication 89)

R.S. Rai,† M.A. O'Keefe, and G. Thomas

Although high-resolution images of δ_2-$Y_2Si_2O_7$ are extremely "noisy" due to the presence of a non-crystalline glassy phase, it is possible to extract the periodic component of the image sufficiently well to enable a structural model based on diffraction information to be confirmed by matching of experimental and simulated images. This procedure can be carried out even for the case of a crystal tilted off exact orientation, provided that a sufficiently thin crystal edge can be found. In this case, high-resolution TEM imaging has confirmed the model postulated for the structure of the phase δ_2-$Y_2Si_2O_7$. High resolution electron micrographs of δ_2-$Y_2Si_2O_7$, obtained with NCEM's ARM, were processed by masking the diffractogram of the digitized image in Fourier space and applying an inverse transform in order to reveal details obscured by amorphous contrast originating in the glassy matrix. When these processed experimental images were compared with images simulated from postulated models (SHRLI images); close agreement was obtained. Figure 21-1 demonstrates how the match between the simulated image and the processed image (insert) confirms the postulated model, and shows that the large black spots are at the positions of the yttrium atoms in the structure.

†Present address: Metallurgical Engineering and Materials Science, Carnegie Mellon University, Pittsburgh, PA 15213.

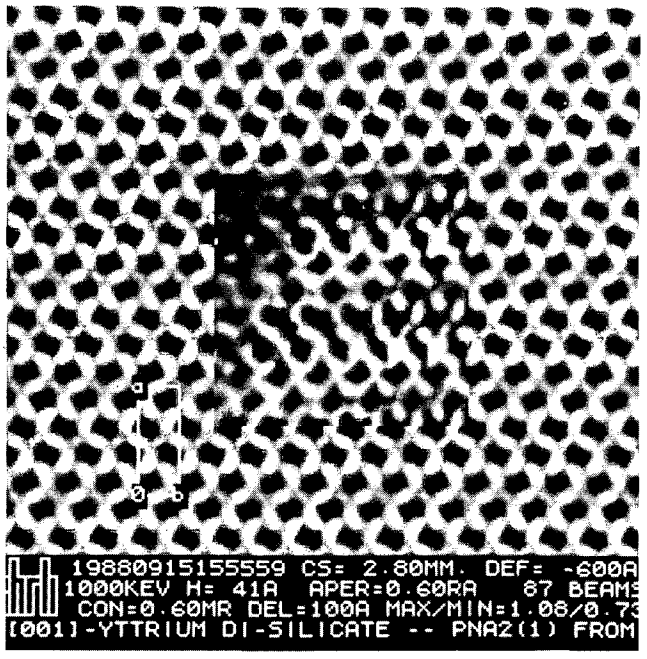

Figure 21-1. Thin-crystal processed image inset into an image simulated for ARM conditions at a defocus of 600 Å and a specimen thickness of 41 Å. The unit cell is marked. The inserted processed image matches the simulation best at its right edge. (XBB 892-928)

1988 PUBLICATIONS AND REPORTS

Refereed Journals

1. D. Blake, F. Freund, K. Krishnan, C. Echer, C. Hetherington, R. Shipp, T. Bunch, A. Tielens, R.J. Lipari, and S. Chang, "The Nature and Origin of Interstellar Diamond," Nature **332**, 611 (1988).
2. R. Csencsits and R. Gronsky, "Vitrification of Zeolite Y in the TEM," Zeolites **8**, 122 (1988); LBL-22549.
3. U. Dahmen, M.J. Witcomb, and K.H. Westmacott, "Morphology of Cr Precipitates in an Overaged Cu–0.3% Cr Alloy," Scripta. Metall. **22**, 1867 (1988); LBL-25749.
4. C. d'Anterroches, H.N. Yakupoglu, T.L. Lin, R. Fathauer, and P. Grunthaner. "Transmission Electron Microscopy Study of the Formation of Epitaxial $CoSi_2$/Si (111) by a Room Temperature Codeposition Technique," Appl. Phys. Lett. **52**, 434 (1988).
5. J. Ding, Z. Liliental-Weber, E.R. Weber, J. Washburn, R.M. Fourkas, and N.W. Cheung, "The Structure and Electrical Properties of TiN/GaAs Schottky Contacts," Appl. Phys. Lett. **52**, 2160 (1988); LBL-23970.
6. J. Ding, B. Lee, R. Gronsky, J. Washburn, D. Chin, and T. van Duzer, "High-Temperature Stability of Nb/GaAs and NbN/GaAs Interfaces," Appl. Phys. Lett. **52**, 135 (1988); LBL-23970.
7. A.G. Fox and R.M. Fisher, "The Origin of the High Elastic Modulus in Al-Li Alloys," J. Mat. Sci. Lett. **7**, 301 (1988).
8. A.G. Fox and R.M. Fisher, "Low-Angle Atomic Scattering Factors and the Charge Density of Beryllium," Philos. Mag. **B57**, 197 (1988).
9. A.G. Fox and R.M. Fisher, "A Summary of the Low Angle X-Ray Atomic Scattering Factors Which Have Been Measured by the Critical Voltage Effect in High Energy Electron Diffraction (HEED)," Aust. J. Phys. **41**, 461 (1988).
10. R. Gronsky, "Spectroscopic Information from High Resolution Images," Ultramicroscopy **24**, 155 (1988); LBL-23387.
11. V. Jayaram, "Some Observations of Microstructural Changes in Alumina Induced by Ti Inhomogeneities," J. Mater. Res. **3**, 764 (1988).
12. V. Jayaram, "The Precipitation of Alpha-TiO_2 from Supersaturated Solutions of Ti in Alumina. Crystal Structure and Morphology," Philos. Mag. **A57**, 525 (1988).
13. M.G. Kim, U. Dahmen, and A.W. Searcy, "Shape and Size of Crystalline MgO Particles Formed by the Decomposition of $Mg(OH)_2$," J. Am. Ceram. Soc. **71**, C373 (1988); LBL-22159.
14. K.M. Krishnan, "Atomic Site and Species Determinations Using Channelling and Related Effects in AEM," in *Limits of Submicron Spectroscopy,* J. Hren and M.J. Kersker, eds.; Ultramicroscopy **24**, 125 (1988); LBL-22305.
15. C.G. Levi, V. Jayaram, J.J. Valencia, and R. Mehrabian, "Phase Selection in Electrohydrodynamic Atomization of Alumina," J. Mater. Res. **3**, 969 (1988); LBL-25069.
16. Z. Liliental-Weber, E.R. Weber, J. Washburn, and L. Parechanian-Allen, "On the Use of Convergent Beam Electron Diffraction for Identification of Antiphase Boundaries in GaAs Grown on Si," Ultramicroscopy **26**, 59 (1988); LBL-25069.
17. T.L. Lin, J. Fathauer, P.J. Grunthaner, and C. d'Anterroches, "A Room Temperature Codeposition Technique for Pinhole Reduction in Epitaxial $CoSi_2$ on Si (111)," Appl. Phys. **52**, 804 (1988).
18. Y.H. Lo, M.C. Wu, H. Lee, S. Wang, and Z. Liliental-Weber, "The Dislocation Microstructure on Flat and Stepped Si Surfaces: Guidance for Growing High Quality GaAs on (100) Si Substrates," Appl. Phys. Lett. **52**, 1386 (1988); LBL-24476.
19. A. Meike, H.-R. Wenk, M.A. O'Keefe, and R. Gronsky, "Atomic Resolution Microscopy of Carbonates, Interpretation of Contrast," Phys. Chem. Minerals **15**, 427 (1988).
20. A. Meike and H.-R. Wenk, "A TEM Study of Microstructures Associated with Solution Cleavage in Limestone," Tectonophysics **154**, 137 (1988).
21. A. Meike, "Heterogeneous Deformation Resulting from Stress Gradients in Calcite Single Crystals," Phys. Chem. Minerals **16**, 148 (1988).
22. R. Ramesh, G. Thomas, S.M. Green, Y. Mei, C. Jiang, and H.L. Luo, "Microstructure of Pb-

Modified Bi-Ca-Sr-Cu-O Superconductor," Appl. Phys. Lett. **53**, 1759 (1988); LBL-25557.
23. D. Schryvers, K. Srikrishna, M.A. O'Keefe, and G. Thomas, "An Electron Microscopy Study of the Atomic Structure of a Mullite in a Reaction-Sintered Composite," J. Mater. Res. **3**, 1355 (1988).
24. R.J. Spontak, M.C. Williams, and D.A. Agard, "Interphase Composition Profile in SB/SBS Block Copolymers, Measured with Electron Microscopy, and Microstructural Applications," Macromolecules **21**, 1377 (1988).
25. R.J. Spontak, M.C. Williams, and D.A. Agard, "Three-Dimensional Study of Cylindrical Morphology in a Styrene-Butadiene-Styrene Block Copolymer," Polymer **29**, 387 (1988).
26. S. Takeda, J. Kulik, and D. de Fontaine, "One-Dimensional Long Period Superstructures in Cu_3Pd Observed by High Resolution Electron Microscopy," J. Phys. F: Met. Phys. **18**, 1387 (1988); LBL-24132.
27. H.-R. Wenk, H.-R., S.J. Shaffer, and G. Van Tendeloo, "Planar Defects in Low Temperature Quartz," Physica Stat. Solidi, Amelinckx Vol. (a) **107**, 799 (1988).
28. T. Yoshiie, Y. Satoh, H. Taoka, S. Koijima, and M. Kiritani, "Detection and Analysis of Microscopically Invisible Cascade Defects in 14 MeV Neutron Irradiated Aluminum and Iron," J. Nucl. Mater. **155–157**, 1098 (1988).
29. H.W. Zandbergen, R. Gronsky, and G. Thomas, "Surface Decomposition of Superconducting $YBa_2Cu_3O_7$," Phys. Stat. Sol. (a) **105**, 207 (1988); LBL-23854.
30. H.W. Zandbergen, R. Gronsky, K. Wang, and G. Thomas, "On the Structure of $(CuO)_2$ Double Layers in Superconducting $YBa_2Cu_3O_7$," Nature **331**, 596 (1988); LBL-24671.
31. H.W. Zandbergen, R. Gronsky, and G. Thomas, "High Resolution Electron Microscopy Study of Grain Boundaries in Sintered $YBa_2Cu_3O_{7-\delta}$," Physica **C153–155**, 1002 (1988).

Other Publications

32. D.M. Ague, H.-R. Wenk, and E. Wenk, "Deformation Microstructures and Lattice Orientations of Plagioclase in Gabbros from Central Australia," submitted to Geophys. Monogr. H. Heard volume.
33. M.M. Al Jassim, J.P. Goral, P. Sheldon, and K.M. Jones, "Heteronucleation and Growth of InAs and GaInAs on GaAs," in *Proc. 1988 MRS Fall Meeting* (in press).
34. H.W. Chan, D.G. Howitt, and A. Harker, "Microstructures of Simulated ICPP Nuclear Waste," J. Am. Ceram. Soc. (in press).
35. R. Csencsits, "Microstructural Evolution of an Iron Silicate Catalyst with Thermal and Hydrothermal Treatments," in *Proc. 46th Annual Meeting EMSA*, Milwaukee, WI, Aug. 7–12, 1988, G.W. Bailey, Ed., San Francisco Press, Inc., 1988, p. 710.
36. U. Dahmen and K.H. Westmacott, "TEM Characterization of Nanocrystals Produced by Decomposition Reactions," in *Proc. Northern California Section of the Metallurgical Society 1988 Pacific Regional Meeting*, Micrometallurgy '88, Lake Tahoe, CA, March 1988; LBL-24077abs.
37. U. Dahmen, "High Resolution Imaging of Near-Σ = 17 Tilt Boundaries in Aluminum," EMSSA Proc. **18**, 147 (1988); LBL-25879abs.
38. U. Dahmen and K.H. Westmacott, "The Use of Symmetry in the TEM Analysis of Phase Transformations," EMSSA Proc. **18**, 5 (1988); LBL-25880abs.
39. U. Dahmen, J. Douin, C.J. Hetherington, and K.H. Westmacott, "HREM of Interfaces in Topotaxial and Epitaxial Reactions," in *MRS Symp. Proc. on High Resolution Microscopy of Materials*, Boston, MA, 1988; LBL-26545.
40. M.L.A. Dass and G. Thomas, "Characterization of Microstructure and Domains in Lead Zirconate Titanate Ceramics," in *Proc. Gordon Research Conf. on Solid State Studies in Ceramics*, Plymouth, NH, July 27–31, 1987; LBL-23237.
41. M.L.A. Dass and G. Thomas, "Convergent-Beam Electron Diffraction Studies of Domains in Rhombohedral Phase of Lead Zirconate Titanate Ceramics," in *Proc. Microbeam Analysis Society Conf.*, Kona, Hawaii, July 13–17, 1987; LBL-23055.
42. M.L.A. Dass and G. Thomas, "Study of Microstructure and Domains in Rhombohedral Phase of PZT Ceramic," in *Proc. 40th Pacific Coast Regional Meeting*, American Ceramic Society, San Diego, CA, Nov. 1–4, 1987; LBL-23552abs.
43. D. de Fontaine, A. Finel, S. Takeda, and J. Kulik, "Application of the ANNNI Model to Long-Period Superstructures in Some Noble Metal Alloys," in *Proc. Met. Soc. A.I.M.E.*, February 1985, Noble Metal Alloys, Massalski, Bennett, Pearson, and Chang, eds., 1988, p. 49.
44. L.B. Goodwin and H.-R. Wenk, "Intracrystalline Folding and Cataclasis in Biotite," submitted to Tectonophysics.
45. J.P. Goral, M.M. Al-Jassim, J.M. Olson, and A. Kibbler, "TEM and TED Studies of Ordering in GaInP," in *Epitaxy of Semiconductor Layered Structures*, Mat. Res. Soc. Symp. Proc. **102**, 583 (1988).
46. P. Grodzinski, J.H. Mazur, A. Nouhi, R. Stirn, and R. Sudharsanan, "Growth of CdTe Thin Films on Polar and Nonpolar Semiconductor Substrates by Metalorganic Chemical Vapor Deposition," MRS Symp. Proc. **144** (in press).
47. R. Gronsky, "TEM at Atomic Resolution," in *Proc. Workshop on "Advanced Techniques for Microstructural Characterization,"* Bombay, India, Jan. 11–15, 1988; LBL-23363abs.
48. R. Gronsky, "Transformation Interfaces at Atomic Resolution," in *Proc. Phase Transformations Conf.*, 1987, The Institute of Metals, Cambridge, England (in press); LBL-23354abs.
49. M. Hirata, S. Takeda, and K. Fujii, "Characterization of Defects in GaP, GaAs and $GaAs_{1-x}P_x$ Elec-

troluminescent Diodes by Transmission Electron Microscopy," Mat. Res. Soc. Symp. Proc. **104**, 495 (1988).

50. A.F. Jankowski, L.R. Schrawyer, M.A. Wall, and D.M. Makowiecki, "Interfacial Bonding in W/C and W/B4C Multilayers," in *Proc. Topical Conf. "Probing Nanometer Scale Properties of Surfaces and Interfaces,"* J. Vac. Sci. Technol. A (in press).
51. R. Kilaas, "Interactive Software for Simulation of High Resolution TEM Images," in *Microbeam Analysis 1987*, MAS Conference, Kona, HI, July 13–17, 1987, R.H. Geiss, Ed., San Francisco Press, 1988, p. 293; LBL-23259.
52. R. Kilaas, "Multislice Calculations: 'Slicing' and Those Upper Laue Interactions," in *Proc. 46th Annual Meeting EMSA*, Milwaukee, WI, Aug. 7–12, 1988, G.W. Bailey, Ed., San Francisco Press, Inc., 1988; LBL-24976.
53. K.M. Krishnan, "Electron Energy-Loss Spectroscopy: Fundamentals and Applications in Mineral Characterization," in *Proc. Annual Meeting American Cheical Society* (in press).
54. K.M. Krishnan and M.T. Stampfer, "Background Modelling Alternatives in Electron Energy-Loss Spectroscopy and Their Implications on Microanalysis," in *Proc. 46th Annual Meeting EMSA*, Milwaukee, WI, Aug. 7–12, 1988, G.W. Bailey, Ed., San Francisco Press, Inc., 1988; LBL-25203.
55 K.M. Krishnan, C.J. Echer, L.E. Tanner, and R. Schaffer, "Compositional Variation of Icosahedral Al-Mn," J. Mat. Res. (in press).
56. M.K. Kundmann and R. Gronsky, "Plasmon Lineshape in EELS of Semiconductors," in *Proc. 46th Annual Meeting EMSA*, Milwaukee, WI, Aug. 7–12, 1988, G.W. Bailey, Ed., San Francisco Press, Inc., 1988; LBL-25204.
57. Q. Li, J. Megusar, L.J. Masur, and J.A. Cornie, "A High Resolution Transmission Electron Microscopy Study of the SiC Coated Graphite Fiber/Aluminum Composite," submitted to Mat. Sci. Eng. A.
58. Z. Liliental-Weber, N. Newman, J. Washburn, E.R. Weber, and W.E. Spicer, "The Influence of Contamination on the Structure and Barrier Height in Cr/GaAs Schottky Contacts," submitted to Appl. Phys. Lett.
59. Z. Liliental-Weber, M.A. O'Keefe, and J. Washburn, "Lattice Imaging of Antiphase Boundaries in GaAs Grown on Si," in *Proc. 46th Annual Meeting EMSA*, Milwaukee, WI, Aug. 7–12, 1988, G.W. Bailey, Ed., San Francisco Press, Inc., 1988, p. 598.
60. T.L. Lin, R. Fathauer, P.J. Grunthaner, and D. d'Anterroches, "Reduction of Pinhole Density in Epitaxial $CoSi_2$ Films," in *Proc. 2nd Internat. Symp. "Silicon Molecular Beam Epitaxy,"* Vol. 88-8, The Electrochemical Society, Inc., 1988, p. 259.
61. J. Megusar, Q. Li, J.A. Cornie, and K.H. Westmacott, "*In situ* HVEM Study of Fracture in the SiC Coated Graphite Fiber/Aluminum Composite," 12th Annual Conference on Composites and Advanced Ceramics, Cocoa Beach, FL, Jan. 17–20, 1988; in *Ceramic Engineering and Science Proc.*, July–Aug. 1988, pp. 1031; LBL-24898.
62. M.A. O'Keefe, D. Blake, F. Freund, C. Hetherington, and J. Turner, "Enhancement of Structure Images of Interstellar Diamond Microcrystals by Image Processing," in *Proc. 46th Annual Meeting EMSA*, Milwaukee, WI, Aug. 7–12, 1988, G.W. Bailey, Ed., San Francisco Press, Inc., 1988, p. 836.
63. M.A. O'Keefe and M.L. Sattler, "Identification of Periodic Structure Characterized from Amorphous Support by Simulation and Processing Techniques," in *Proc. 46th Annual Meeting EMSA*, Milwaukee, WI, Aug. 7–12, 1988, G.W. Bailey, Ed., San Francisco Press, Inc., 1988; LBL-25004.
64. D. Schryvers, K. Srikrishna, and G. Thomas, "Electron Microscopy Study of a Mullite Compound: a Combination of HREM, CBED and EDX," Inst. Phys. Conf. Ser. No. 93; Vol. 2, Chap. 14, EUREM 88, York, England, 1988.
65. P. Sheldon, M.M. Al-Jassim, K.M. Jones, J.P. Goral, and G.B. Yacobi, "Structural and Electrical Characterization of InAs Grown on GaAs Substrates Grown by MBE," J. Vac. Sci. Technol. A. (in press).
66. R.J. Spontak and M.C. Williams, "Microstructural and Bulk Characterization of Two Poly(Siloxane-Imide) Multiblock Copolymers," J. Appl. Polym. Sci. (in press).
67. R.J. Spontak and M.C. Williams, "Using Dynamic TEM to Study Thermal and Strain-Induced Effects on Block Copolymer Microstructures," in *Proc. Analytical Electron Microscopy–1987*, D. Joy, Ed., San Francisco Press, Inc., San Francisco, 1988, p. 159.
68. G. Thomas, "Electron Microscopy in Materials Science," in *Proc. IVth Asia-Pacific Conference and Workshop on Electron Microscopy*, Bangkok, Thailand, 1988, p. 27.
69. G. Thomas, R. Ramesh, and C.J.D. Hetherington, "Electron Microscopy of Bi-Ca-Sr-Cu-O High T_c Superconductors," JEOL News **26E**, 2 (1988).
70. A. Thorel, *Structure atomique des Interfaces dans les ceramiques a base de silicium,* Bulletin de Liaison, Centre des Materiaux Pierre Marie Fourt, École des Mines de Paris, October 1988, p. 4.
71. K.H. Westmacott, "Up Close: the National Center for Electron Microscopy at the Lawrence Berkeley Laboratory," MRS Bulletin, 1988; LBL-24809.
72. K.H. Westmacott, U. Dahmen, A. Thorel, and J.Y. Laval, "Precipitation in a (Mg) Partially Stabilized Zirconia during Aging at 1000°C," in *Ceramic Microstructures '86*, J. Pask and A. Evans, Eds., Plenum, 1988, p. 831; LBL-22140.
73. K.H. Westmacott, and U. Dahmen, "The National Center for Electron Microscopy at Berkeley: an Update," in *Proc. 46th Annual Meeting EMSA*, Milwaukee, WI, Aug. 7–12, 1988, G.W. Bailey, Ed., 1988, p. 812; LBL-24952abs.
74. T. Whitney, V. Jayaram, C.G. Levi, and R. Mehrabian, "Rapid Solidification of Alumina-Zirconia Eutectic and Hypoeutectic Alloys," in *Solidification*

Processing of Eutectic Alloys, D.M. Stefanescu, G.J. Abbaschian, and R.J. Bayuzick, eds., The Metallurgical Society, 1988, p. 199.

75. M.J. Witcomb, U. Dahmen, and K.H. Westmacott, "The Coprecipitation of Cr_3P and Cr in Cu," in *Proc. 46th Annual Meeting EMSA*, Milwaukee, WI, Aug. 7–12, 1988, G.W. Bailey, Ed., San Francisco Press, Inc., 1988, p. 764; LBL-24953abs.
76. M.J. Witcomb, U. Dahmen, and K.H. Westmacott, "The Coprecipitation of Cr_3P and Cr in Cu," Ultramicroscopy (in press).
77. M.J. Witcomb, U. Dahmen, and K.H. Westmacott, "Accurate Habit Plane Determination of Lath-Shaped Cr-Precipitates in Cu," EMSSA Proc. **18**, 185 (1988); LBL-25883abs.
78. C. Wong and R.W. McCabe, "The Effects of High-Temperature Oxidation and Reduction on the Structure and Activity of Rhodium/Alumina Catalysts," submitted to J. Catal.
79. H. Zandbergen and G. Thomas, "Defect Characterization in Sintered $YBa_2Cu_3O_{7-\delta}$ by HREM," Inst. Phys. Conf. Ser. No. 93: Vol. 2, Chap. 6, EUREM 88, York, England, 1988; LBL-25577.
80. U. Dahmen, C.J. Hetherington, P. Pirouz, and K.H. Westmacott, "The Formation of Hexagonal Silicon at Twin Intersections," submitted to Scripta Metall.
81. D.F. Blake, L.F. Allard, C.J. Echer, and F. Freund, "Characterization of Electron-Beam Induced Damage Structures in Natural Fluorite, CaF_2, by Analytical Electron Microscopy," in *Proc. Microbeam Analysis Society*, Milwaukee, WI, Aug. 1988, p. 129.
82. E.A. Kamenetzky, M. Wall, R. Castro, and L.E. Tanner, "The Preparation of Mechanically Alloyed Powders for TEM Examination," Mat. Res. Soc. Symp. Proc. **115**, 167 (1988).

LBL Reports

83. C. Hetherington, R. Ramesh, M.A. O'Keefe, R. Kilaas, and G. Thomas, "High Resolution Electron Microscopy and Image Simulation Studies of Superconducting Polytypoids in Bi-Ca-Sr-Cu-O Ceramics," MRS Fall Meeting, Boston, MA, Nov. 1988; LBL-25798.
84. C.J.D. Hetherington, C. Nelson, K.H. Westmacott, R. Gronsky, and G. Thomas, "The Berkeley Atomic Resolution Microscope—an Update," MRS Fall Meeting, Boston, MA, Nov. 1988; LBL-25797.
85. K.M. Krishnan, "Channelling Enhanced Microanalysis: a High Resolution Analytical Technique for Atomic Site and Species Determination," Indo-U.S. Workshop: "Advanced Techniques for Microstructural Characterization," Bombay, India, Jan. 11–15, 1988; to be published in Mat. Sci. Forum, Trans. Tech. Publications; LBL-24317.
86. K.M. Krishnan, D.F. Blake, F. Freund, and R.J. Lipari, "Structure and Bonding of Diamond and Diamond-Like Materials: Characterization at High Spatial Resolution," MRS. Symp. "Diamond and Diamond-Like Material Synthesis," Reno, NV, Apr. 5–8, 1988; LBL-25268.
87. K.M. Krishnan, J. Kouvetakis, T. Sasaki, and N. Bartlett, "Characterization of Newly Synthesized Novel Graphite Films," MRS Symp. "Better Ceramics Through Chemistry," Reno, NV, Apr. 5–8, 1988; LBL-25269.
88. Z. Liliental-Weber, E.R. Weber, J. Washburn, T.Y. Liu, and H. Kroemer, "Suppression of Defect Propagation in Heteroepitaxial Structures by Strained Layer Superlattices," in *Proc. NATO Advanced Study Institute from the Workshop "Heterostructures on Si: One Step Further with Silicon,"* Cargese, France, May 15–20, 1988; LBL-25780.
89. R.S. Rai, M.A. O'Keefe, and G. Thomas, "δ_2-$Y_2Si_2O_7$ Structure Confirmed by Processing and Simulation of Atomic Resolution Images," MRS Conference, Boston, MA, Nov. 29, 1988; LBL-26336.
90. U. Dahmen, "Transmission Electron Microscope Characterization of Precipitates," Ultramicroscopy (in press); LBL-24460abs.
91. T.R. Dinger, R.S. Rai, and G. Thomas, "Crystallization Behavior of a Glass in the Y_2O_3-SiO_2-AlN System," submitted to J. Am. Ceram. Soc.; LBL-23213.
92. A.G. Fox, M.A. O'Keefe, and M.A. Tabbernor, "Relativistic Hartree-Fock X-Ray and Electron Atomic Scattering Factors at High-Angles," submitted to Acta Crystallogr.; LBL-26387.
93. R. Gronsky, "Atomic Resolution Imaging of Interfaces," XIIth Western Regional Meeting for Electron Microscopy and Microbeam Analysis, Concord, CA, June 24–27, 1987; J. Electron Microsc. Tech. (in press); LBL-23289abs.
94. C.J. Jou, R. Kilaas, and J. Washburn, "Oxygen Vacancies and Twin Boundaries in $YBa_2Cu_3O_{7-\delta}$ Superconductors," submitted to Phys. Rev. Lett.; LBL-25149.
95. C.J. Jou, J. Washburn, Z. Liliental-Weber, and R. Gronsky, "The Morphology and the Electrical Properties of the Ag/GaAs Contacts," submitted to J. Electrochem. Soc.; LBL-23033.
96. C.J. Jou, R. Kilaas, and J. Washburn, "Formation of Coherent Twins in High-T_c $YBa_2Cu_3O_{7-\delta}$ Superconductors," submitted to J. Mat. Res.; LBL-26065.
97. Z. Liliental-Weber, M.A. O'Keefe, and J. Washburn, "Inversion Boundaries in GaAs Grown on Si," submitted to Ultramicroscopy; LBL-25779.
98. V. Radmilovic, A.G. Fox, R.M. Fisher, and G. Thomas, "Lithium Depletion in Precipitate Free Zones (PFZ's) in Al-Li Base Alloys," submitted to Scripta Metall.; LBL-25603.
99. G. Thomas and R. Ramesh, "Atomic Imaging and Microanalysis of Ceramics," submitted to Proc. Amer. Ceram. Soc. Conf., San Francisco, Oct. 1988; LBL-26319.
100. H.W. Zandbergen and G. Thomas, "Grain Boundaries in Sintered $YBa_2Cu_3O_{7-\delta}$," submitted to Acta Crystallogr. B; LBL-24603.
101. H.W. Zandbergen, R. Gronsky, and G. van Tendeloo, "Atomic Structure of Grain Boundaries and Surfaces in $YBa_2Cu_3O_{7-\delta}$ and

$LaBaCaCu_3O_{7-\delta}$," submitted to J. Superconductivity; LBL-26397.

102. B.-T. Lee, R. Gronsky, and E.D. Bourret, "Transmission Electron Microscope Study of Arsenic Precipitates in GaAs: Morphology and Orientation Relationship with the Matrix," submitted to J. Crystal Growth; LBL-26568.
103. C. Koestler, R. Ramesh, C. Echer, and G. Thomas, "Microstructure of Melt Spin Nd-Fe-Co-B Magnets," submitted to Acta Metall.; LBL-26156.
104. R. Kilaas and M.A. O'Keefe, "The Design of a Computer System for Simulation and Processing of TEM Images: Hardware and Software," submitted to TMS Annual Meeting, Las Vegas, NV, Feb. 1989; LBL-26772.

Invited Talks

105. R. Csencsits and R. Gronsky, "Microstructural Study of an Iron Silicate Catalyst using Electron Microscopy," American Chem. Soc. Meeting, Los Angeles, CA, Sept. 26–28, 1988; LBL-25173.
106. U. Dahmen, "TEM Characterization of Precipitates," 46th Annual EMSA Meeting, Milwaukee, WI, Aug. 1988.
107. U. Dahmen, "Electron Microscopy Characterization of Interfaces," Symposium on Interface Science and Engineering, World Materials Congress, Chicago, IL, Sept. 1988.
108. U. Dahmen, "Interfacial Structure and Semicoherent Precipitation of Interstitial Phases," International Conference on Bainite, World Materials Congress, Chicago, IL, Sept. 1988.
109. U. Dahmen, "High Resolution Electron Microscopy of Topotaxial and Epitaxial Interfaces," Symposium on High Resolution Microscopy of Materials, Fall Meeting, MRS, Boston, MA, Dec. 1988.
110. U. Dahmen, "Orientation Relationships in Precipitation Systems," CSIR, Pretoria, South Africa, Dec. 1988.
111. U. Dahmen, "The Use of Symmetry in the TEM Analysis of Phase Transformations," EMSSA keynote lecture, Durban, South Africa, Dec. 1988.
112. U. Dahmen, "Structural Precipitate Analysis by TEM," EMSSA tutorial, Durban, South Africa, Dec. 1988.
113. U. Dahmen, "Atomic Structure of Near $\Sigma 17$ Grain Boundaries in Al," EMSSA, Durban, South Africa, Dec. 1988.
114. U. Dahmen, "The Use of Symmetry in the TEM Analysis of Phase Transformations," University of the Witwatersrand, Johannesburg, South Africa, Dec. 1988.
115. U. Dahmen, "Recent Applications of Electron Microscopy at the NCEM," University of Port Elizabeth, South Africa, Dec. 1988.
116. U. Dahmen, "Orientation Relationships in Precipitation Systems," University of Cape Town, South Africa, Dec. 1988.
117. U. Dahmen and K.H. Westmacott, "The Berkeley Atomic Resolution Microscope," MRS Meeting, Boston, MA, Nov. 27–Dec. 2, 1988.
118. K.M. Krishnan, "Channelling Enhanced Microanalysis: an Emerging Technique for Atomic Site and Species Determinations in Analytical Electron Microsocpy," Indo-U.S. workshop on advanced techniques for microstructural characterization, Bombay, India, Jan. 11–15, 1988.
119. K.M. Krishnan, "Background in Electron Energy-Loss Spectroscopy: Signal Processing Alternatives and Their Implications on Microanalysis," EMSA/MAS Annual Meeting, Milwaukee, WI, Aug. 1988.
120. K.M. Krishnan, "Electron Energy-Loss Spectroscopy: Fundamentals and Applications in Mineral Characterization," American Chemical Society Annual Meeting, Los Angeles, CA, Sept. 1988.
121. K.M. Krishnan, "Bonding in Novel Graphite and the Nature of Interstellar Diamonds: Recent Experimental Investigations," Physics Department Colloquium, Banaras Hindu University, Varanasi, India, Jan. 1988; Indian Institute of Science, Bangalore, India, Jan. 1988; LBL-24329abs.
122. K.M. Krishnan, "Microanalytical Electron Microscopy: Techniques and Applications in Materials Science," Metallurgy Department Colloquium, Banaras Hindu University, Varanasi, India, Jan. 1988.
123. K.M. Krishnan, "Advances in the Characterization of Ceramics by Imaging, Diffraction and Spectroscopy," Indian Institute of Science, Bangalore, India, Feb. 1988; LBL-24331abs.
124. K.M. Krishnan, "Advanced Analytical Electron Microscopy in Materials Science," Defense Metallurgical Research Laboratory, Hyderabad, India, Feb. 1988.
125. K.M. Krishnan, "Microanalytical Electron Microscopy and Related Spectroscopies: Fundamentals and Applications in Materials Science," MICROMAT 88, Annual Meeting, Brazilian Electron Microscopy Society, Sao Paulo, Brazil, Oct. 1988.
126. K.M. Krishnan, "Structure Property Relations and the Characterization of Materials by Imaging, Diffraction and Spectroscopy," Pontifica Universidade Catolica, Rio de Janeiro, Brazil, Oct. 1988.
127. C.J.D. Hetherington, "The Atomic Resolution Microscope," Northern California Crystal Growers' Technical Dinner Meeting, Santa Clara, CA, Nov. 1988.
128. C.J.D. Hetherington, "High Resolution Studies on the Berkeley Atomic Resolution Electron Microscope," Liverpool University, United Kingdom, May 1988.
129. M.A. O'Keefe, "Using Simulation and Processing to Interpret HREM Images," Lawrence Livermore National Laboratory, Livermore, CA, Mar. 1988.
130. M.A. O'Keefe, "TEM Image Analysis by Processing and Simulation," Department of Materials Science and Mineral Engineering, University of California at Berkeley, Apr. 1988.

131. M.A. O'Keefe, "High Resolution TEM Image Analysis," NCSEM/WCMAS Joint Meeting, Syntex Research Co., Palo Alto, CA, May 1988.
132. M.A. O'Keefe, "Image Analysis at the NCEM," Arizona State University, Tempe, Oct. 1988.
133. M.A. O'Keefe, "TEM Image Analysis by Processing and Simulation," Department of Materials Science and Mineral Engineering, University of California at Berkeley, Nov. 1988.
134. G. Thomas, "Electron Microscopy of Al-Li-Cu and Al-Li-Mg Alloys," Westec '88, Los Angeles, CA, Mar. 1988.
135. G. Thomas, "Dy-Al Sintering Additive: Effect on Microstructure and Magnetic Properties of Fe-Nd-B Magnets," MRS International Meeting, Tokyo, Japan, June 1988.
136. G. Thomas, "Structural Ceramics," and "New Alkaline Earth Superconductors," Postech, Seoul, Republic of Korea, June 1988.
137. G. Thomas, "Electron Microscopy in Materials Science," Fourth Asia-Pacific Conference and Workshop on Electron Microscopy, Bangkok, Thailand, July–Aug. 1988.
138. G. Thomas, "Atomic Imaging and Spectroscopy of Ceramic," 41st Pacific Coast Meeting, American Ceramic Society, San Francisco, CA, Oct. 1988.
139. G. Thomas, "Microstructural Aspects in Magnetic Materials," DOE Workshop on Magnetic Materials, Santa Rosa, CA, Nov. 1988.
140. G. Thomas, "Atomic Resolution of Structural and Superconducting Ceramics," Spain-Portugal Joint Electron Microscopy Meeting, Lisbon, Portugal, Dec. 1988.
141. G. Thomas, "High Resolution Electron Microscopy of Structural and Superconducting Ceramics," Kyocera Ceramics Central Research Laboratories, Kagoshima, Japan, Dec. 1988.
142. K.H. Westmacott, "Structure of Grain Boundaries in ICB Aluminum," Intermediate Voltage Electron Microscopy Meeting, Saclay, France, Mar. 1988.
143. K.H. Westmacott, "The National Center for Electron Microscopy at Berkeley: an Update," 46th Annual EMSA Meeting, Milwaukee, WI, Aug. 1988.
144. K.H. Westmacott, "Facilities and Research at the NCEM," EMSA Fall Meeting, Chicago, IL Sept. 25–28, 1988; LBL-25839abs.
145. K.H. Westmacott, "Grain Boundaries in ICB Aluminum," U.S./Japan Cooperation Meeting, Berkeley, CA, Oct. 1988.
146. K.H. Westmacott, "The Berkeley Atomic Resolution Microscope," MRS Meeting, Boston, MA, Nov. 1988.

In Situ Investigation of Gas-Solid Reactions by Electron Microscopy*

James W. Evans, Investigator

INTRODUCTION

This work is concerned with microstructural aspects of the reactions between gases and solids that are important in materials science. Of particular interest are the nucleation, growth, epitaxy, and chemical nature of solid products formed from the parent phase. Experimental tools used in this investigation include the environmental cells in the high-voltage transmission electron microscopes at LBL, which permit observation and electron-diffraction studies of reaction products as they are formed. Conventional transmission electron microscopy of cross-sectioned reacted samples is used to obtain additional information on the morphology and chemistry of phases occurring at the reaction front. Auxiliary techniques, such as secondary-ion mass spectroscopy (SIMS), also play a role in this investigation.

In 1988 the focus of this investigation has been on the oxidation of III-V compound semiconductor materials, particularly gallium arsenide and indium phosphide. Oxidation is a well-established technique in the processing of silicon, the most widely used semiconductor material; dielectric layers can readily be formed on silicon in this way. This straightforward method of producing dielectric layers has so far eluded the processors of III-V compound semiconductors. Additional work has been performed on the annealing of $YBa_2Cu_3O_{7-\delta}$.

1. Oxidation of Indium Phosphide (Publications 1 and 4)

O.R. Monteiro and J.W. Evans

Despite industrial interest in producing a dielectric layer on indium phosphide, its thermal oxidation is not fully understood. This article describes some results obtained from observing the oxidation reaction inside a transmission electron microscope. At temperatures between 450 and 600°C, In_2O_3 and $InPO_4$ are produced. Polycrystalline In_2O_3 appears to be produced during simultaneous incongruent vaporization, which takes place above 362°C. At the early stages of the reaction, $InPO_4$ grows epitaxially on the InP, but later it transforms into polycrystalline $InPO_4$.

2. Oxidation of Gallium Arsenide (Publications 2 and 4)

O.R. Monteiro and J.W. Evans

This study has been concerned with the effect of dopants on the oxidation of gallium arsenide. Here we present some results of transmission electron microscopy (TEM) and SIMS of thermally oxidized gallium arsenide with different types of dopants. At temperatures below 400°C an amorphous oxide is formed. Oxidation at temperatures between 500°C and 600°C initially produces an epitaxial film of γ-Ga_2O_3. As the reaction proceeds, this film becomes polycrystalline and then transforms to β-Ga_2O_3. This film contains small crystallites of As_2O_5 in the case of Si-doped and Te-doped materials, and some As_2O_3 and As_2O_5 in the case of Cr-doped GaAs. SIMS results showed that in both cases, arsenic accumulates at the interface, and the reduced solubility of As in GaAs results in precipitation of hexagonal As. The chromium-doped and other gallium arsenides also exhibit different oxidation kinetics.

3. TEM Studies on the Annealing of $YBa_2Cu_3O_{7-\delta}$ (Publication 3)

O R. Monteiro and S.M. Johnson[†]

Annealing in oxygen-rich atmosphere at intermediate temperatures (400–600°C) has been proven necessary to provide the appropriate microstructure of the superconducting $YBa_2Cu_3O_{7-\delta}$. The symmetry of the orthorhombic phase requires that if more than one type of twin plane is present within a grain, a distorted region should exist inside the multiple-twinned grain. This distorted region hinders the tetragonal-to-orthorhombic transformation and may account for some retained tetragonal phase inside an otherwise orthorhombic grain. Figure 3-1 shows the advancement of two twin regions (tips indicated by arrows) from the grain boundary into an adjacent grain of $YBa_2Cu_3O_{7-\delta}$. A

*This work was supported by the Director, Office of Energy Research, Office of Basic Energy Sciences, Materials Sciences Division, of the U.S. Department of Energy under Contract No. DE-AC03-76SF00098.

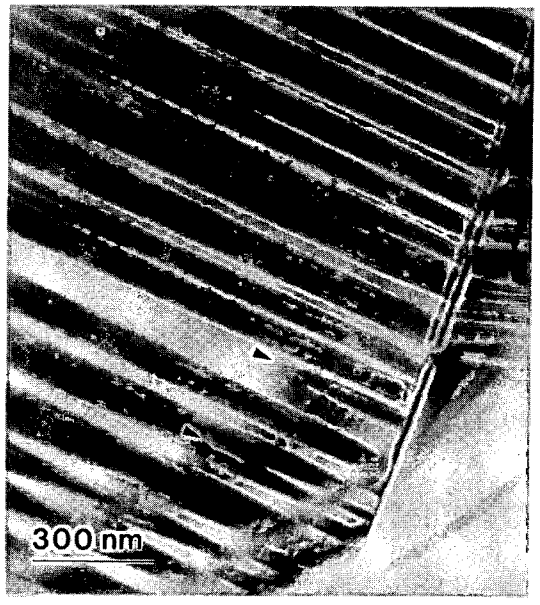

Figure 3-1. Advancement of two twin regions (tips indicated by arrows) from the grain boundary into an adjacent grain of the superconductor $YBa_2Cu_3O_{7-\delta}$ following two hours of annealing at 500°C in flowing oxygen at atmospheric pressure. (XBB 880-11525)

physical model describing the formation of such regions, and their eventual transformation into low-angle grain boundaries after long annealing, is presented. Extended annealing at intermediate temperatures apparently leads to the formation of planar faults in off-stoichiometric samples. Transmission electron-microscope image contrast and energy-dispersive x-ray analyses of highly defective regions suggested these defects to be extra $CuO_x(x = 1,2)$ layers that result from the slight copper enrichment in the $YBa_2Cu_3O_{7-\delta}$ used here. These extra layers tend to form near grain boundaries or free surfaces, where oxygen is readily available.

---

†Permanent address: SRI International, Menlo Park, CA 94025.

4. Work In Progress

Investigations are in progress on the oxidation of porous silicon and on the reaction of silicon with tungsten hexafluoride.

1988 PUBLICATIONS AND REPORTS

Refereed Journals

1. O.R. Monteiro and J.W. Evans, "Thermal Oxidation of Indium Phosphide," J. Electrochem. Soc. **135**, 2366 (1988); LBL-23467.

LBL Reports

2. O.R. Monteiro and J.W. Evans, "Thermal Oxidation of Gallium Arsenide," LBL-24989.
3. O.R. Monteiro and S M. Johnson, "TEM Studies of the Annealing of $YBa_2Cu_3O_{7-\delta}$," LBL-26442.
4. O.R. Monteiro (Ph.D. Thesis), "Thermal Oxidation of III-V Compound Semiconductors," LBL-26337.

Local Atomic Configurations in Solid Solutions*

Didier de Fontaine, Investigator

INTRODUCTION

This investigation is concerned with ordering phenomena in alloys, and the recent emphasis has been on long-period ordered superstructures (modulated structures) in binary fcc alloys. Two systems have been studied in detail: Cu-Pd and Ag-Mg. Structural observations have been carried out using the Atomic Resolution Microscope at LBL's National Center for Electron Microscopy (NCEM), and the nature of the periodic antiphase boundaries present in these alloys has been characterized. In addition, a systematic investigation of long- and short-range order in Cu-Pd has been undertaken using *in situ* variation of temperature and radiation dose in the High Voltage Electron Microscope at NCEM. Other work on the Cu-Pd system, using standard electron microscopy techniques, is directed toward clarification of the equilibrium phase diagram. Concerning the theoretical aspect of this project, a statistical mechanics model for modulated structures in alloys has been proposed and solved within the mean-field approximation. Results show agreement with some real systems. Also, the mechanism governing the distinction between sharp and diffuse antiphase boundaries has been elucidated. New work will focus on the nature of ordered structures in the technologically important Al-Ti system and related ternaries.

1. Mean-Field Theory of Long-Period Superstructures on the fcc Lattice (Publication 3)

J. Kulik† and D. de Fontaine

An Ising model with long-range competing interactions on the fcc lattice is examined in mean-field theory. The competition of the interaction parameters is characterized by a parameter k, and a phase diagram in the (T,k) plane is presented. Long-period superstructures are obtained as ordered states. Results are compared with the ordered structures observed in Ag_3Mg. Figure 1-1 shows calculated stability regions of indicated polytypes as a function of wavenumber q and temperature T (in K).

*This work was supported by the Director, Office of Energy Research, Office of Basic Energy Sciences, Materials Sciences Division, of the U.S. Department of Energy under Contract No. DE-AC03-76SF00098.

†Present address: Department of Physics, University of Houston, Houston, TX 77004.

2. Concentration Waves in Cu-Pd: Fermi Surface vs Entropy Effects (Publication 6)

J. Kulik† and D. de Fontaine

Restoration of short-range order (SRO) in Cu-Pd alloys has been observed after samples were initially disordered using the electron beam in a high-voltage (1.5-MeV) electron microscope. Complete disorder under the beam action is observed at 100 K. SRO reappears at temperatures of 150 K and higher due to beam-induced kinetics. Diffuse peaks of SRO scattered intensity appear at positions [q 10] and equivalent in the first Brillouin zone of the disordered fcc lattice. The value of q is known to be dependent on Fermi surface effects, but we also

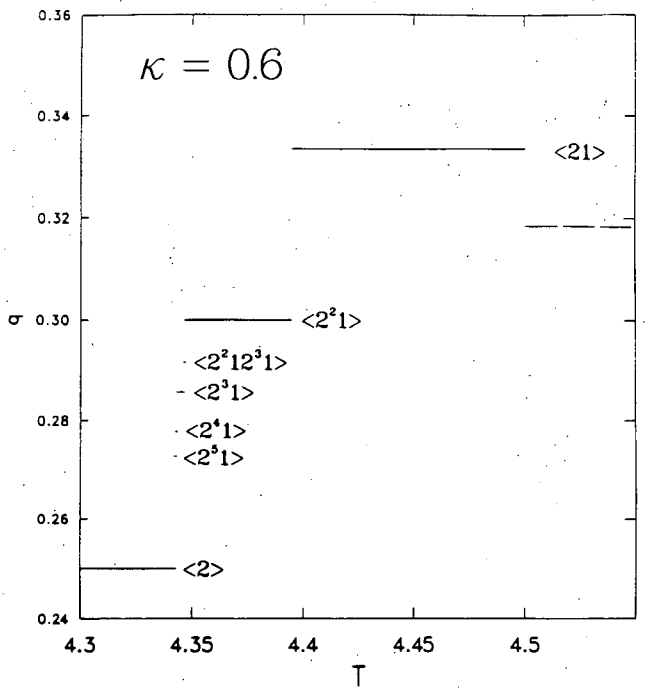

Figure 1-1. Calculated stability regions of indicated polytypes as a function of wavenumber q and temperature T (in K). (XBL 894-1494)

observe a weak temperature dependence in the value of q over the temperature range 150 to 400 K. We discuss a possible origin of this phenomenon in terms of entropy effects.

[†]Present address: Department of Physics, University of Houston, Houston, TX 77004.

3. A Gorsky-Bragg-Williams Approach to the Study of Long-Period Superlattice Phases in Binary Alloys (Publication 4)

G. Ceder, M. De Graef,[†] L. Delaey,[†] J. Kulik,[‡] and D. de Fontaine

The influence of the shape of the reciprocal-space potential on the relative stability of long-period superlattice (LPS) phases in binary alloys is discussed in a Gorsky-Bragg-Williams approximation. First, for a certain class of LPS phases, the set of pair-interaction parameters is reduced to a similar set of parameters that characterize only the essential aspects of the reciprocal-space potential. Minimization of the free energy for different LPS phases is then used to extract some general tendencies, such as the change of wave vector towards the potential minimum (with increasing temperature) and the increasing stability of complex phases with deepening of the potential minimum.

[†]Permanent address: Department of Metallurgy and Materials Science, Catholic University of Leuven, Belgium.

[‡]Present address: Department of Physics, University of Houston, Houston, TX 77004.

4. Work in Progress

Portions of the Cu-Pd equilibrium phase diagram are poorly known, particularly in the vicinity of one- and two-dimensional long-period superstructure phase regions. Conventional and high-resolution TEM are currently being used to determine phase boundaries accurately.

1988 PUBLICATIONS AND REPORTS

Refereed Journals

1. D. de Fontaine, "Simple Models for the Omega Phase Transformation," Metall. Trans. A **19A**, 169 (1988); LBL-21555.
2. S. Takeda, J. Kulik, and D. de Fontaine, "One-Dimensional Long Period Superstructures in Cu_3Pd Observed by High Resolution Electron Microscopy," J. Phys. F: Met. Phys. **18**, 1387 (1988); LBL-24132.
3. J. Kulik and D. de Fontaine, "Mean Field Theory of Long Period Superstructures on the F.C.C. Lattice," J. Phys. C: Solid State Phys. **21**, L291 (1988); LBL-24264.

LBL Reports

4. G. Ceder, M. De Graef, L. Delaey, J. Kulik, and D. de Fontaine, "A Grosky-Bragg-Williams Approach to the Study of Long-Period Superlattice Phases in Binary Alloys," accepted by Phys. Rev. B; LBL-26724.

Invited Talks

5. J. Kulik, S. Takeda, and D. de Fontaine, "Periodic Antiphase Structures in Ordered Alloys," AIME Annual Meeting, Phoenix, AZ, Jan. 25, 1988.
6. J. Kulik and D. de Fontaine, "Concentration Waves in Cu-Pd: Fermi Surface Entropy Effects," APS Annual Meeting, New Orleans, LA, Mar. 23, 1988.

Alloy Theory*

D. de Fontaine and L.M. Falicov, Investigators

INTRODUCTION

Temperature-composition phase diagrams are of great practical interest as they constitute useful "maps" of thermodynamic systems such as binary, ternary..., etc., alloys. These diagrams are generally determined experimentally, but the exciting possibility now exists of deriving certain classes of phase diagrams virtually from first principles. This possibility rests on the very significant advances that have been made recently in the two relevant areas of alloy theory — electronic-band-structure calculations and statistical thermodynamics. The purpose of this project is to combine the latest electronic structure and statistical thermodynamic calculations in integrated packages in order to produce phase diagrams from a minimum amount of empirical information and to compare various approximate computational methods with one another. A temperature-composition diagram for the Ti-Rh system has been derived that agrees remarkably well with the temperature-composition diagram determined empirically. The same theoretical techniques are also being applied successfully to vacancy ordering in the high-T_c superconductors. It has also been proved that for some systems, and probably for many, inclusion of many-body effects beyond the mean-field or density-functional approximations should be taken carefully into account.

1. A Direct Method of Obtaining Effective-Pair Interactions in Binary Alloys (Publication 3)

A. Berera, H. Dreysse,[†] L.T. Wille,[‡] and D. de Fontaine

It is shown that effective-pair interactions (EPI) in disordered binary alloys can be calculated accurately and reliably by direct averaging over a small number of randomly selected configurations within the framework of the recursion method. This approach is illustrated on a canonical tight-binding Hamiltonian and relies on the "orbital peeling" technique to calculate energy differences directly, without large subtractive cancellations. The results are checked for convergence, as a function of both the number of configurations and the number of levels of the continued fraction, and they are also compared with more elaborate calculations. The main advantages of such a real-space method are the computational simplicity and the possibility to treat deviations from lattice periodicity.

*This work was supported by the Director, Office of Energy Research, Office of Basic Energy Sciences, Materials Sciences Division, of the U.S. Department of Energy under Contract No. DE-AC03-76SF00098.

[†]Permanent address: Department of Physics, University of Nancy, France.

[‡]Permanent address: Department of Physics, Florida Atlantic University, Boca Raton, FL 33431.

2. Thermodynamics of Oxygen Ordering in $YBa_2Cu_3O_z$ (Publication 4)

L.T. Wille,[†] A. Berera, and D. de Fontaine

The ordering in the Cu-O basal plane of $YBa_2Cu_3O_z$ is investigated as a function of oxygen content and temperature. Several phase diagrams are calculated by means of the cluster variation method applied to asymmetric two-dimensional Ising models. The interaction parameters selected guarantee the stability of the orthorhombic structures near $z = 7$, and, for certain choices, also include a double-cell phase around $z = 6.5$. O-Cu-O correlations are investigated as a function of temperature and concentration. Calculated orthorhombic-to-tetragonal transition temperatures and concentrations for various oxygen partial pressures are in excellent agreement with recent experimental data (see Figure 2-1).

[†]Permanent address: Department of Physics, Florida Atlantic University, Baco Raton, FL 33431.

3. *Ab Initio* Calculations of Ordered Intermetallic Phase Equilibria (Publication 19)

M. Sluiter,[†] D. de Fontaine, X.Q. Guo,[‡] R. Podloucky,[‡] and A.J. Freeman[‡]

General procedures for computing alloy phase equilibria from *ab initio* electronic structure calculations are reviewed and applied to the Al-Li phase diagram. Free energies were calculated by the cluster variation method in the tetrahedron approximation for the fcc and bcc lattices and ordered superstructures. Input was provided by first-principles

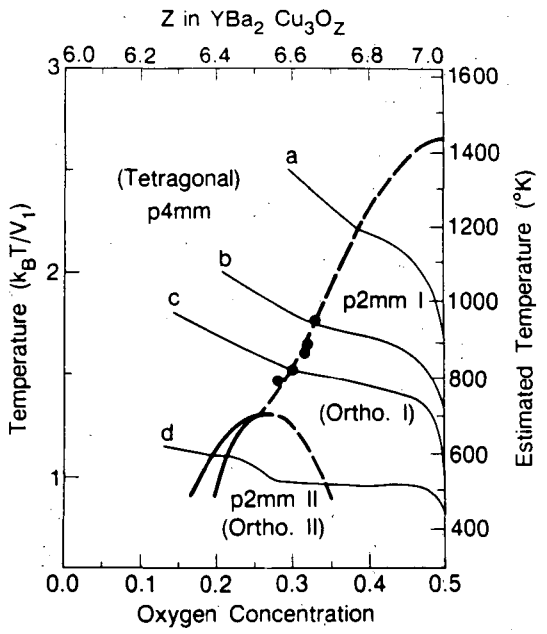

Figure 2-1. $YBa_2Cu_3O_z$ psuedo-binary phase diagram calculated by the cluster-variation method. Ortho. I is the 90 K and Ortho. II the 60 K superconducting phase. Dashed lines are second-order transitions, continuous lines are first-order phase boundaries. Fine lines represent oxygen partial-pressure isotherms at (a) 400 atm, (b) 1 atm, (c) 0.2 atm, and (d) 0.001 atm. Filled circles are order-disorder transition points determined experimentally. (XBL 894-1495)

FLAPW calculations. The computed phase diagram for both stable and metastable structures agrees remarkably well with the experimental one.

---

†Present address: Lawrence Livermore National Laboratory, Livermore, CA 94550.

‡Permanent address: Department of Physics, Northwestern University, Evanston, IL.

4. Phase Stability of Ternary Alloys in the Four-Sublattice Bragg-Williams Approximation (Publication 5)

D.C. Chrzan and L.M. Falicov

A full Bragg-Williams calculation of a four-sublattice face-centered-cubic ternary alloy was carried out. It corresponds to elements that, similarly to Cu, Ag, and Au, form disparate binaries: one pair that strongly segregates, one pair that forms strongly ordered compounds, and a third pair that forms only weakly ordered binaries. The obtained diagrams are internally consistent, have a sensible temperature evolution towards disorder, and present a variety of behaviors that include ordered and disordered homogeneous single phases, and regions of heterogeneous two- and three-phase mixtures. Although not realistic, the calculation gives a good starting point for more sophisticated models that may include short-range correlations and a better thermodynamic treatment.

5. Many-Body Small-Cluster Theory of bcc Fe, Co, and the Fe-Co Alloy (Publication 6)

E.C. Sowa and L.M. Falicov

An exact solution for a two-site crystal model, the smallest body-centered-cubic crystal, was developed for cobalt, iron, and the virtual-crystal iron-cobalt alloy. The model consists of five d-like orbitals per site spin, with interatomic hopping terms and an onsite Coulomb interaction of the fullest generality allowed by atomic symmetry. The ground-state spin polarization per atom is found to begin at 2 for cobalt, rise to 2.5 for the iron-cobalt alloy, and drop back down to 2 for iron. This behavior, which mimics the peak in the Slater-Pauling magnetization curve for this system, is dominated by one-electron properties rather than by the Coulomb interaction. The many-body energy-level spectra and intracluster charge and spin fluctuations are also computed.

6. Work in Progress

The general method of calculating effective-pair interactions in binary alloys has been extended to surface regions. It is thereby proposed to predict which component segregates to the free surface. Monte Carlo methods are being used to study oxygen/vacancy ordering in the "chain" plane of $YBa_2Cu_3O_x$. Low-temperature metastable ordered states are found for anisotropic second-neighbor pair interactions ($V_2 \neq V_3$). For the symmetric case ($V_2 = V_3$), proposed by other investigators, no such ordered states are found.

An exactly solvable model mimicking the properties of (001) antiphase boundaries in the face-centered-cubic substitutional alloys (Ising or, equivalently, antiferromagnets) with only nearest-neighbor interactions is being developed. It has been already proved exactly that in the thermodynamic limit, antiphase boundaries are unstable at all temperatures. It may be conjectured that antiphase boundaries are unstable for all thermodynamics systems with dimension greater than one. Antiphase boundaries are found at equilibrium in three-

dimensional systems with sizes on the order of those used in Monte Carlo simulations of the Ising model. The implications of this unusual size effect are being studied.

1988 PUBLICATIONS AND REPORTS

Refereed Journals

1. L.T. Wille and D. de Fontaine, "Ground State Analysis of Ordered Superstructures in the Basal Plane of $YBa_2Cu_3O_z$," Phys. Rev. B **37**, 2227 (1988); LBL-23900.
2. A. Berera, L.T. Wille, and D. de Fontaine, "Oxygen-Vacancy Ordering in the $YBa_2Cu_3O_z$ Basal Plane Studied by the Cluster Variation Method," J. Stat. Phys.: Short Commun. **50**, 1245 (1988); LBL-24261.
3. A. Berera, H. Dreysse, L.T. Wille, and D. de Fontaine, "A Direct Method of Obtaining Effective Pair Interactions in Binary Alloys," J. Physics F: Met. Phys. **18**, L49 (1988); LBL-24935.
4. L.T. Wille, A. Berera, and D. de Fontaine, "Thermodynamics of Oxygen Ordering in $YBa_2Cu_3O_z$," Phys. Rev. Lett. **60**, 1065 (1988); LBL-24581.
5. D.C. Chrzan and L.M. Falicov, "Phase Stability of Ternary Alloys in the Four-Sublattice Bragg-Williams Approximation," Phys. Rev. B **37**, 3894 (1988); LBL-24227.
6. E. Sowa and L.M. Falicov, "Many-Body Small-Cluster Theory of bcc Fe, Co, and the Fe-Co Alloy," Phys. Rev. B **37**, 8707 (1988); LBL-24124.
7. D.C. Chrzan and L.M. Falicov, "Incommensurable Magnetic Surface Structures for MnO-type Antiferromagnetic Insulators," Phys. Rev. Lett. **61**, 1509 (1988); LBL-25336.

Other Publications

8. L.T. Wille, A. Berera, D. de Fontaine, and S.C. Moss, "Vacancy Ordering in the Basal Plane of $YBa_2Cu_3O_z$," Mat. Res. Soc. Symp. Proc. **99**, 535 (1988); LBL-24263.
9. D. de Fontaine, "The Cluster Variation Method and the Calculation of Alloy Phase Diagrams," in *Proc. NATO Advanced Study Institute on Alloy Phase Stability*, Maleme, Crete, June 13–27, 1988; LBL-24934.
10. A. Berera, L.T. Wille, and D. de Fontaine, "Thermodynamics of Oxygen-Vacancy Ordering in $YBa_2Cu_3O_z$," in *Proc. Int. Conf. on High-Temperature Superconductors and Materials and Mechanisms of Superconductivity*, Interlaken, Switzerland, Feb. 29–Mar. 4, 1988; Physica C **153–155**, 598 (1988); LBL-24936.
11. L.M. Falicov, "Superconductivity: Phenomenology," in *Proc. First Topsøe School on Superconductivity*, Risø National Laboratory, Roskilde, Denmark, 1988, Risø Publication M-2756, p. 7.

LBL Reports

12. H. Dreysse, A. Berera, L.T. Wille, and D. de Fontaine, "Determination of Effective Cluster Interactions in Random Alloys by Configurational Averaging," accepted by Phys. Rev.; LBL-25659.
13. A. Berera and D. de Fontaine, "Oxygen-Vacancy Phase Equilibria in $YBa_2Cu_3O_z$ Calculated by the Cluster Variation Method," accepted by Phys. Rev. B1: Condensed Matter; LBL-25449.
14. D.C. Chrzan and L.M. Falicov, "Theoretical Phase Stability of Incommensurable Spin Structures on the (001) Surfaces of MnO-type Antiferromagnetic Insulators," LBL-25875.
15. D.C. Chrzan and L.M. Falicov, "Theoretical Phase Stability of Incommensurable Spin Structures on the (001) Surfaces of MnO-type Antiferromagnetic Insulators," LBL-26313.

Invited Talks

16. D. de Fontaine, "Psuedo Binary Phase Diagram of the High-Temperature Superconductor $YBa_2Cu_3O_z$," special lecture at the Fifth Meeting of the Japanese Committee for Alloy Phase Diagrams.
17. L.T. Wille, S.C. Moss, and D. de Fontaine, "Ordered Superstructures in the Basal Plane of $YBa_2Cu_3O_z$," TMS Fall Meeting Topical Symposium, Materials Science of High Temperature Superconductors I, Cincinnati, OH, Oct. 1987.
18. A. Berera, H. Dreysse, L.T. Wille, and D. de Fontaine, "Effective Pair Interactions for Alloy Phase Stability Calculations," APS Meeting, New Orleans, LA, Mar. 25, 1988.
19. M. Sluiter, D. de Fontaine, X.Q. Guo, R. Podloucky, and A.J. Freeman, "*Ab Initio* Calculations of Ordered Intermetallic Phase Equilibria," MRS, Boston, MA, Nov. 1988.
20. D. de Fontaine, "First Principles Calculations of Thermodynamic Equilibria in Alloys," 24th Semi-Annual Bay Area Symposium on High-Temperature Science and Technology, Stanford University, Stanford, CA, Nov. 19, 1988.
21. D. de Fontaine, "Vacancy Ordering in Superconductors," Materials Science Symposium, John Cahn 60th Birthday Celebration, National Bureau of Standards, Jan. 15, 1988; Naval Research Laboratory, Washington, DC, Jan. 15, 1988; IBM Almaden Research Center, San Jose, CA, Apr. 28, 1988.
22. D. de Fontaine, "Order-Disorder Transformations in $YBa_2Cu_3O_z$," Fukuoka University, Fukuoka, Japan, June 6, 1988; Osaka University, Osaka, Japan, June 10, 1988; Kyoto University, Kyoto, Japan, June 13, 1988; Nagoya University, Nagoya, Japan, June 14, 1988; Nagoya Institute of Technology, Nagoya, Japan, June 15, 1988; Japanese Committee for Alloy Phase Diagrams, June 17, 1988; Tohoku University, Tohoku, Japan, June 20, 1988; Hokkaido University, Hokkaido, Japan, June 22, 1988; Institute for Solid State Physics, Tokyo University, Tokyo, Japan, June 24, 1988.

23. L.M. Falicov, "The Challenge of the New Materials," San Martin Theater, Buenos Aires, Argentina, June 2, 1988.
24. L.M. Falicov, "Superconductivity: Phenomenology," 1st Topsøe Summer School on Superconductivity, Risø, Roskilde, Denmark, June 20, 1988.
25. L.M. Falicov, "Models for High Temperature Superconductivity," 1st Topsøe Summer School on Superconductivity, Risø, Roskilde, Denmark, June 22, 1988.
26. L.M. Falicov, "Highly Correlated Metals: A Small-Cluster Approach," Annual Meeting, Materials and Chemical Sciences Division, LBL, Feb. 10, 1988.
27. L.M. Falicov, "Highly Correlated Metals: A Small-Cluster Approach to Heavy Fermions," Department of Applied Physics, Stanford University, Stanford, CA, Mar. 10, 1988.
28. L.M. Falicov, "Highly Correlated Metals: Heavy Fermions," Physics Colloquium, University of California, Santa Cruz, Mar. 31, 1988; Oak Ridge National Laboratory, Oak Ridge, TN, Nov. 3, 1988; VII Congress of the Costa Rican Physics Association, San Jose, Costa Rica, Nov. 25, 1988.
29. L.M. Falicov, "1988: Open Problems in Condensed Matter Physics," Physics Colloquium, the Balseiro Institute, Bariloche, Argentina, June 1, 1988; Physics Department, University of Santiago, Chile, Sept. 12, 1988; VII Congress of the Costa Rican Physics Association, San Jose, Costa Rica, Nov. 24, 1988.
30. L.M. Falicov, "Photoemission in Solids," VII Congress of the Costa Rican Physics Association, San Jose, Costa Rica, Nov. 24, 1988.

PHYSICAL PROPERTIES

High-Temperature Reactions*

Alan W. Searcy, Investigator

INTRODUCTION

The central purposes of this program are to develop and to experimentally test thermodynamic and kinetic models of important processes in materials science. A theoretical breakthrough has been the reconciliation of the kinetics to the thermodynamics of equilibria among edge, surface, and bulk molecules in crystalline particles. The new understanding of the thermodynamics in particles makes it possible to evaluate the previously neglected roles of ledge nucleation and growth in sintering of crystalline particles and in exaggerated grain growth. New expressions for sintering and grain growth are consistent with important experimental observations that are inconsistent with predictions of classical surface thermodynamic theory. A theory for sintering in temperature gradients has been obtained as a consequence of extending the new thermodynamic approach to nonisothermal systems. Tests of various theoretical predictions are in progress.

1. The Influence of Temperature Gradients on Transition Temperatures: Predictions from Alternate Models (Publication 5)

A.W. Searcy

Theoretical studies under this project in recent fiscal years demonstrated that equilibrium of crystalline particles with the vapor requires that $\mu_a - \mu_v = \mu_g$, where μ_a, μ_v, and μ_g are the chemical potentials of atoms in the crystal, of vacancies, and of gaseous atoms. This relation indicates that local thermodynamic activities of crystals are sensitive to changes in the local vacancy concentrations. When the relation is introduced into equations for solids placed in a temperature gradient under circumstances that lead to zero net flux exchanges, the prediction emerges that transition temperatures for solids can be changed by measurable amounts. Such a possibility had not previously been suggested.

*This work was supported by the Director, Office of Energy Research, Office of Basic Energy Sciences, Materials Sciences Division, of the U.S. Department of Energy under Contract No. DE-AC03-76SF00098.

2. The Influence of Temperature Gradients on the Melting Point of Tin (Publication 6)

D. Beruto,† R. Botter,‡ and A.W. Searcy

Isothermal and nonisothermal steady-state experiments were performed with tin in a graphite crucible equipped with seven thermocouples of carefully determined heights relative to interface positions in imposed temperature gradients. The experiments confirm the predictions of the previous paper that a measurable change in melting temperature could result from a gradient through the solid; the melting temperature decreased 1.7 ± 0.8 K when the temperature drop through the solid tin was 40 K.

†Permanent address: LBL and University of Genoa, Italy.
‡Permanent address: University of Genoa, Italy.

3. Comparison of Sizes Calculated for MgO Crystals from X-Ray Diffraction (XRD) Line Broadening to Transmission Electron Microscopy (TEM) Observations (Publication 7)

M.G. Kim, M.J. Cima, and A.W. Searcy

It is shown by examples that for some decomposition reactions XRD line-broadening measurements overestimated the product particle sizes. Particle sizes of MgO from decomposition of $MgCO_3$ and of $Mg(OH)_2$ in vacuum were calculated from XRD line-broadening experiments for comparison to direct observations of particle dimensions by TEM. When $MgCO_3$ is decomposed, the MgO forms with a range of orientations, and the MgO particle sizes calculated

from line broadening, 4.5 ± 0.8 nm, agreed reasonably well with TEM observations, 3.2 ± 0.8 nm. When $Mg(OH)_2$ is decomposed, the MgO particles are all aligned, and the smallest reported XRD cross sections are more than twice the cross sections directly observed, 0.8 to 2.4 nm. Furthermore, although the cross sections observed by TEM for MgO formed from flakes of $Mg(OH)_2$ decomposed in vacuum are independent of the size of the parent $Mg(OH)_2$ flake, the apparent size of the aligned MgO particles calculated from XRD data increase with thickness of the parent flakes.

4. The Formation of Barium Titanate Ceramics by Solid-State Reaction (Publication 8)

J. Bierach

Investigations of the industrially important $BaCO_3-TiO_2$ reaction have commonly reported that, while $BaTiO_3$ forms readily, nucleation barriers inhibit formation of $Ba_4Ti_{13}O_{30}$ and $BaTi_4O_9$, which are stable phases with compositions between $BaTiO_3$ and TiO_2. A computer-assisted evaluation of the variations in XRD peak positions and intensities with time of heating of $BaTiO_3$ with TiO_2 shows that these two intermediate phases also form readily. They are present in low quantities and have probably been overlooked because of overlap of major XRD peaks with those of reactants and of $BaTiO_3$.

1988 PUBLICATIONS AND REPORTS

Refereed Journals

1. M.G. Kim, U. Dahmen, and A.W. Searcy, "Shape and Size of Crystalline MgO Particles Formed by the Decomposition of $Mg(OH)_2$," J. Am. Ceram. Soc. **71**, C-373–C-375 (1988); LBL-22159.
2. D. Beruto, M.G. Kim, and A.W. Searcy, "Microstructure and Reactivity of Porous and Ultrafine CaO Particles with CO_2," High Temp.–High Press **20**, 25 (1988); LBL-22158.
3. D. Beruto, R. Botter, and A.W. Searcy, "The Influence of Thermal Cycling on Densification: Further Tests of a Theory," Ceramic Trans. **1B**, G.L. Messing, E.R. Fuller, and H. Hausner, eds., American Ceram. Soc., Westerville, OH, 1988, p. 911; LBL-24196.

Other Publications

4. A.W. Searcy and D. Beruto, "Theory and Experiments for Isothermal and Non-Isothermal Sintering," Science of Ceramics **14**, D. Taylor, Ed., Inst. of Ceramics, Stoke-on-Trent, Staffs., U.K., 1988, p. 1; LBL-23220.

LBL Reports

5. A.W. Searcy, "The Influence of Temperature Gradients on Transition Temperatures: Predictions from Alternate Models," LBL-24943.
6. D. Beruto, R. Botter, and A.W. Searcy, "The Influence of Temperature Gradients on the Melting Point of Tin," LBL-26000.
7. M.G. Kim, M.J. Cima, and A.W. Searcy, "Comparison of Sizes Calculated for MgO Crystals from XRD Line Broadening to TEM Observations," LBL-26391.
8. J. Bierach (M.S. Thesis), "The Formation of Barium Titanate Ceramics by Solid State Reaction," LBL-26519.

Invited Talks

9. A.W. Searcy, D.J. Meschi, and D. Beruto, "The Kinetics of Neck Growth and Pore Closure in Faceted Solids," Symposium on Sintering of Advanced Ceramics, National Meeting, American Ceramic Society, Cincinnati, OH, May 3, 1988.
10. A.W. Searcy, "Surprising Effects of Temperature Gradients and Temperature Changes in Solids: Observations and Explanations," Departmental Seminar, Materials Science and Mineral Engineering, University of California at Berkeley, Oct. 13, 1988.
11. A.W. Searcy, "A Theory for Sub-Eutectic Melting at Solid-Solid Interfaces," Joint Basic Science Division and Pacific Coast Regional Meeting, American Ceramic Society, San Francisco, CA, Oct. 25, 1988.

Ceramic Interfaces*

Andreas M. Glaeser, Investigator

INTRODUCTION

Numerous properties of ceramics depend strongly on microstructure, necessitating control of microstructural characteristics developed during processing. This research program focuses on improving our understanding of processes that dictate the microstructural changes occurring during processing and utilization. A broad range of model experiments utilizing photolithographically introduced, microdesigned, intragranular, or intergranular pore/flaw structures have been developed and applied to studies of the kinetics of interfacial processes. Phenomena amenable to study include: pore–grain boundary separation, pore coarsening or elimination, faceting (surface-energy anisotropy), and high-temperature crack healing. In addition, microstructure development in model compacts formed from an "ideal," nominally monodispersed, chemically synthesized titania powder is being examined by applying transmission electron microscopy to ultramicrotomed sections of heat-treated compacts. The effects of crystallization, polymorphic phase transformations, and particle substructure on microstructural evolution are being studied.

1. Applications of Microdesigned Interfacial Pore Structures to Kinetic Studies in Ceramics (Publications 3, 7–9)

J. Rödel and A.M. Glaeser

A broad range of new model experiments for systematic study of processes that dictate microstructural evolution during sintering and high-temperature use of ceramics has been developed and applied to fundamental kinetic studies of alumina. Photolithographically introduced controlled-geometry surface structures are transformed into interfacial pore structures via hot pressing. Bicrystals of controlled misorientation, single-crystal/polycrystal ensembles, and polycrystal/polycrystal ensembles with microdesigned interfacial pore structures can be produced.

Low-misorientation bicrystals with controlled-diameter, controlled-aspect-ratio pore channels have been used to study the effects of geometrical parameters and surface crystallography on the morphological evolution of pore channels in alumina at 1800°C. Channels at various stages of evolution are shown in Figure 1-1. The critical (minimum) aspect ratio for breakup into multiple pores, the kinetics of breakup, and the apparent surface diffusivity were all sensitive to the interfacial crystallography. Channels lying parallel to the basal and prismatic planes behaved differently, as did channels lying along differing directions within a given boundary plane.

A technique for investigating the elimination and coarsening of model pore arrays was developed. Photolithography affords precise control over the size, shape, spatial distribution, and spatial density of interfacial pores. As a result, the effects of variations in each of these parameters on the densification or coarsening behavior can be evaluated. Furthermore, via control of the grain-boundary misorientation, the possibility exists of separating the contributions of grain boundary and lattice transport to these processes. Effects of interfacial reactions and dopants on process rates are also amenable to study.

Preliminary studies of high-temperature crack healing have been conducted. The morphological evolution of rectangular crack-like flaws, $\approx 200\ \mu m \cdot 100\ \mu m \cdot 0.18\ \mu m$, in low-twist-angle basal- and prismatic-plane twist boundaries during annealing at 1800°C has been studied. Two distinct *crystallographically dictated* modes of morphological evolu-

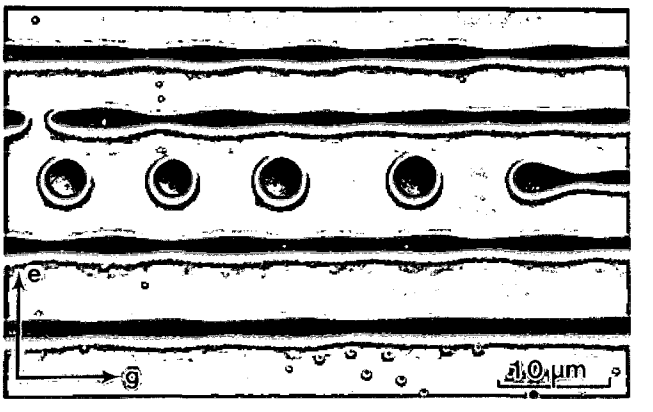

Figure 1-1. Illustration of pore-channel evolution during high-temperature annealing. SEM micrograph of bicrystal fracture surface with 5-channel array. Channels 1 through 5 (top to bottom) have diameters of 1.1, 1.1, 0.9, 1.3, and 1.7 μm, respectively. The sample was annealed for 25 hr at 1800°C. Scaling-law effects are evident. (XBB 884-3395)

*This work was supported by the Director, Office of Energy Research, Office of Basic Energy Sciences, Materials Sciences Division, of the U.S. Department of Energy under Contract No. DE-AC03-76SF00098.

from line broadening, 4.5 ± 0.8 nm, agreed reasonably well with TEM observations, 3.2 ± 0.8 nm. When $Mg(OH)_2$ is decomposed, the MgO particles are all aligned, and the smallest reported XRD cross sections are more than twice the cross sections directly observed, 0.8 to 2.4 nm. Furthermore, although the cross sections observed by TEM for MgO formed from flakes of $Mg(OH)_2$ decomposed in vacuum are independent of the size of the parent $Mg(OH)_2$ flake, the apparent size of the aligned MgO particles calculated from XRD data increase with thickness of the parent flakes.

4. The Formation of Barium Titanate Ceramics by Solid-State Reaction (Publication 8)

J. Bierach

Investigations of the industrially important $BaCO_3-TiO_2$ reaction have commonly reported that, while $BaTiO_3$ forms readily, nucleation barriers inhibit formation of $Ba_4Ti_{13}O_{30}$ and $BaTi_4O_9$, which are stable phases with compositions between $BaTiO_3$ and TiO_2. A computer-assisted evaluation of the variations in XRD peak positions and intensities with time of heating of $BaTiO_3$ with TiO_2 shows that these two intermediate phases also form readily. They are present in low quantities and have probably been overlooked because of overlap of major XRD peaks with those of reactants and of $BaTiO_3$.

1988 PUBLICATIONS AND REPORTS

Refereed Journals

1. M.G. Kim, U. Dahmen, and A.W. Searcy, "Shape and Size of Crystalline MgO Particles Formed by the Decomposition of $Mg(OH)_2$," J. Am. Ceram. Soc. **71**, C-373–C-375 (1988); LBL-22159.
2. D. Beruto, M.G. Kim, and A.W. Searcy, "Microstructure and Reactivity of Porous and Ultrafine CaO Particles with CO_2," High Temp.–High Press **20**, 25 (1988); LBL-22158.
3. D. Beruto, R. Botter, and A.W. Searcy, "The Influence of Thermal Cycling on Densification: Further Tests of a Theory," Ceramic Trans. **1B**, G.L. Messing, E.R. Fuller, and H. Hausner, eds., American Ceram. Soc., Westerville, OH, 1988, p. 911; LBL-24196.

Other Publications

4. A.W. Searcy and D. Beruto, "Theory and Experiments for Isothermal and Non-Isothermal Sintering," Science of Ceramics **14**, D. Taylor, Ed., Inst. of Ceramics, Stoke-on-Trent, Staffs., U.K., 1988, p. 1; LBL-23220.

LBL Reports

5. A.W. Searcy, "The Influence of Temperature Gradients on Transition Temperatures: Predictions from Alternate Models," LBL-24943.
6. D. Beruto, R. Botter, and A.W. Searcy, "The Influence of Temperature Gradients on the Melting Point of Tin," LBL-26000.
7. M.G. Kim, M.J. Cima, and A.W. Searcy, "Comparison of Sizes Calculated for MgO Crystals from XRD Line Broadening to TEM Observations," LBL-26391.
8. J. Bierach (M.S. Thesis), "The Formation of Barium Titanate Ceramics by Solid State Reaction," LBL-26519.

Invited Talks

9. A.W. Searcy, D.J. Meschi, and D. Beruto, "The Kinetics of Neck Growth and Pore Closure in Faceted Solids," Symposium on Sintering of Advanced Ceramics, National Meeting, American Ceramic Society, Cincinnati, OH, May 3, 1988.
10. A.W. Searcy, "Surprising Effects of Temperature Gradients and Temperature Changes in Solids: Observations and Explanations," Departmental Seminar, Materials Science and Mineral Engineering, University of California at Berkeley, Oct. 13, 1988.
11. A.W. Searcy, "A Theory for Sub-Eutectic Melting at Solid-Solid Interfaces," Joint Basic Science Division and Pacific Coast Regional Meeting, American Ceramic Society, San Francisco, CA, Oct. 25, 1988.

Ceramic Interfaces*

Andreas M. Glaeser, Investigator

INTRODUCTION

Numerous properties of ceramics depend strongly on microstructure, necessitating control of microstructural characteristics developed during processing. This research program focuses on improving our understanding of processes that dictate the microstructural changes occurring during processing and utilization. A broad range of model experiments utilizing photolithographically introduced, microdesigned, intragranular, or intergranular pore/flaw structures have been developed and applied to studies of the kinetics of interfacial processes. Phenomena amenable to study include: pore–grain boundary separation, pore coarsening or elimination, faceting (surface-energy anisotropy), and high-temperature crack healing. In addition, microstructure development in model compacts formed from an "ideal," nominally monodispersed, chemically synthesized titania powder is being examined by applying transmission electron microscopy to ultramicrotomed sections of heat-treated compacts. The effects of crystallization, polymorphic phase transformations, and particle substructure on microstructural evolution are being studied.

1. Applications of Microdesigned Interfacial Pore Structures to Kinetic Studies in Ceramics (Publications 3, 7–9)

J. Rödel and A.M. Glaeser

A broad range of new model experiments for systematic study of processes that dictate microstructural evolution during sintering and high-temperature use of ceramics has been developed and applied to fundamental kinetic studies of alumina. Photolithographically introduced controlled-geometry surface structures are transformed into interfacial pore structures via hot pressing. Bicrystals of controlled misorientation, single-crystal/polycrystal ensembles, and polycrystal/polycrystal ensembles with microdesigned interfacial pore structures can be produced.

Low-misorientation bicrystals with controlled-diameter, controlled-aspect-ratio pore channels have been used to study the effects of geometrical parameters and surface crystallography on the morphological evolution of pore channels in alumina at 1800°C. Channels at various stages of evolution are shown in Figure 1-1. The critical (minimum) aspect ratio for breakup into multiple pores, the kinetics of breakup, and the apparent surface diffusivity were all sensitive to the interfacial crystallography. Channels lying parallel to the basal and prismatic planes behaved differently, as did channels lying along differing directions within a given boundary plane.

A technique for investigating the elimination and coarsening of model pore arrays was developed. Photolithography affords precise control over the size, shape, spatial distribution, and spatial density of interfacial pores. As a result, the effects of variations in each of these parameters on the densification or coarsening behavior can be evaluated. Furthermore, via control of the grain-boundary misorientation, the possibility exists of separating the contributions of grain boundary and lattice transport to these processes. Effects of interfacial reactions and dopants on process rates are also amenable to study.

Preliminary studies of high-temperature crack healing have been conducted. The morphological evolution of rectangular crack-like flaws, $\approx$200 μm·100 μm·0.18 μm, in low-twist-angle basal- and prismatic-plane twist boundaries during annealing at 1800°C has been studied. Two distinct *crystallographically dictated* modes of morphological evolu-

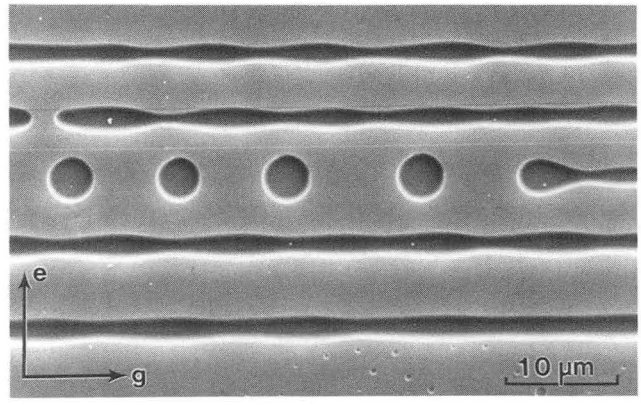

Figure 1-1. Illustration of pore-channel evolution during high-temperature annealing. SEM micrograph of bicrystal fracture surface with 5-channel array. Channels 1 through 5 (top to bottom) have diameters of 1.1, 1.1, 0.9, 1.3, and 1.7 μm, respectively. The sample was annealed for 25 hr at 1800°C. Scaling-law effects are evident. (XBB 884-3395)

*This work was supported by the Director, Office of Energy Research, Office of Basic Energy Sciences, Materials Sciences Division, of the U.S. Department of Energy under Contract No. DE-AC03-76SF00098.

tion were identified; previous studies of crack healing had attributed the difference in healing mode to residual stress effects.

A model experiment has been developed that allows the study of pore drag and pore-boundary separation under conditions of constant density. Photolithography, ion-beam etching, and hot pressing were used to generate microdesigned interfacial pore arrays, consisting of pores of controlled size and spacing, in alumina. An example of a sapphire-polycrystal interface migrating under the influence of pore drag is illustrated in Figure 1-2. Results from an investigation of pore drag suggest that the surface diffusivity in MgO-doped alumina exceeds that in undoped alumina by a factor of 2 to 9 at 1600°C. The condition for pore-boundary separation depended strongly on pore spacing; the influence zone of pores was several microns wide. Concurrent studies of the grain-boundary mobility showed that the migration rate of basal-plane sapphire into undoped alumina is lower than that into MgO-doped alumina. To our knowledge, we are the first to provide an experimentally determined "map" of pore-boundary separation conditions for a ceramic material.

2. Work in Progress

Previous work characterizing microstructural evolution in chemically synthesized titania powders established the importance of phase transformations that occur within nanometer diameter particles, at low temperatures, and at low relative densities. Current efforts are focused on developing and improving ultramicrotomy procedures for preparation of foils for high-resolution transmission electron microscopy (TEM) studies, and subsequent characterization of microstructural evolution within annealed, low-density powder compacts.

The techniques for embedding ceramic-powder compacts in resins for ultramicrotomy were not well established. Several methods were employed, some with a failure rate of over 50%. Infiltration and curing procedures were developed that produced material suitable for ultramicrotomy. In addition, procedures for producing a suitably sized tip on the embedded compact were devised.

Compacts constituted of nominally monodispersed, ≈0.37-μm-diameter titania powders have been annealed for times ranging from 6 min to 122 hr at temperatures from 400°C to 825°C, microtomed, and then studied by TEM. A low-magnification TEM micrograph of a microtomed sample is shown in Figure 2-1.

Results confirm that the as-prepared ≈0.37-μm-diameter powders consist of fine 7-nm-diameter amorphous primary particles. During annealing at 400°C, crystallization occurs. TEM reveals the presence of anatase crystallites (in agreement with previous measurements); however, TEM diffraction patterns indicate that *brookite* also forms. Crystallite coarsening and rutile formation initiate at a temperature between 400°C and 500°C. Anneals at temperatures between 500°C and 600°C are accompanied by gradual disappearance of the brookite and anatase phases. Experiments suggest that the phase content,

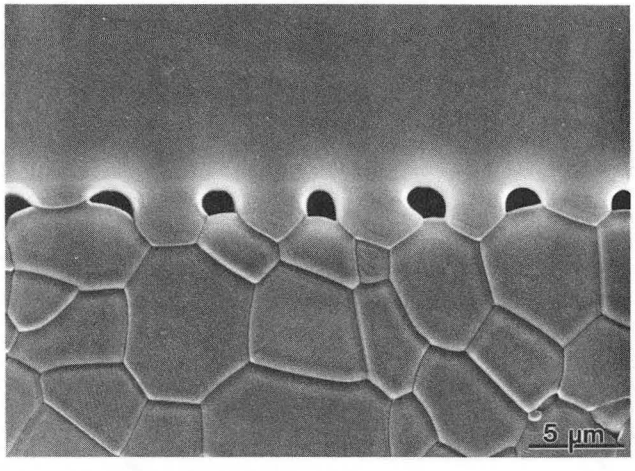

Figure 1-2. Cross section taken perpendicular to a single-crystal-sapphire/polycrystalline-alumina interface, illustrating the effect of pore drag. Note the distortion of the pore shape. Pore size and spacing are controlled using photolithographic methods and ion-beam etching. (XBB 8810-9938)

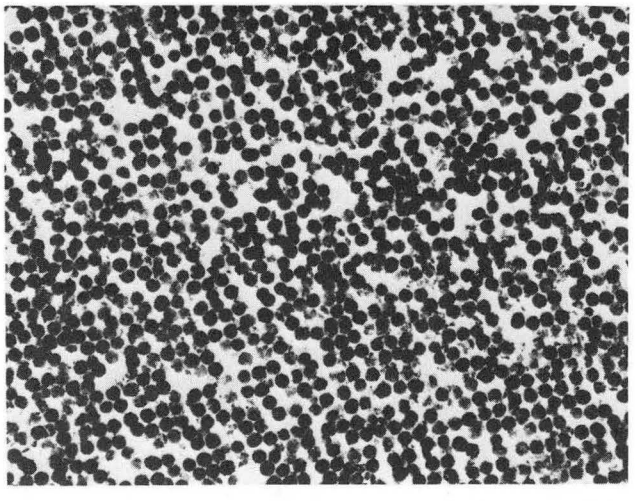

Figure 2-1. Low-magnification TEM micrograph of a microtomed section of a compact formed from nominally monodispersed, chemically synthesized titania particles. In this particular case, the microtome slice was parallel to a nearly close-packed plane within the compact. (XBB 880-11106)

grain size, and degree of grain growth or phase-transformation-front propagation across interparticle necks during higher-temperature ($\geq$650°C) annealing are highly sensitive to thermal pretreatment in the 400°C to 500°C temperature range.

Previous work on pore-boundary interactions in alumina studied the growth of basal plane sapphire into MgO-doped and undoped polycrystalline aluminas. Work utilizing prismatic-plane sapphire is in progress, in an effort to understand the effects of MgO on migration rates and pore-boundary separation conditions for grain boundaries of differing structure.

1988 PUBLICATIONS AND REPORTS

Refereed Journals

1. L.H. Edelson and A.M. Glaeser, "Effects of Thermal Pretreatment on Coarsening of Nominally Monodispersed Titania," J. Am. Ceram. Soc. **71**, C198 (1988); LBL-23358.
2. L.H. Edelson and A.M. Glaeser, "The Role of Particle Substructure in the Sintering of Monosized Titania" J. Am. Ceram. Soc. **71**, 225, (1988); LBL-23367.
3. J. Rödel and A.M. Glaeser, "A Technique for Investigating The Elimination and Coarsening of Model Pore Arrays," Mater. Lett. **6**, 351 (1988); LBL-24970.
4. W.C. Carter, "The Forces and Behavior of Fluids Constrained by Solids," Acta Metall. **36**, 2283 (1988); LBL-24694.
5. T.S. Oh, J. Rödel, R.M. Cannon, and R.O. Ritchie, "Ceramic/Metal Interfacial Crack Growth: Toughening by Controlled Microcracks and Interfacial Geometries," Acta Metall. **36**, 2083 (1988); LBL-24285.

Other Publications

6. R.M. Cannon, T.S. Oh, J. Rödel, A.M. Glaeser, and R.O. Ritchie, "Effects of Near Interfacial Microstructure on Toughness and Subcritical Crack Growth in Ceramic/Metal Systems," in *Interfaces in Polymer, Ceramic, and Metal Matrix Composites*, H. Ishida, Ed., Elsevier Science, New York, 1988, p. 567; LBL-24799.

LBL Reports

7. J. Rödel and A.M. Glaeser, "Application of Controlled Interfacial Pore Structures to Kinetic Studies in Alumina," to appear in *Interfacial Structures, Properties and Design*, Mat. Res. Soc. Proc. **122**, Pittsburgh, PA, 1988; LBL-25010.
8. J. Rödel and A.M. Glaeser, "Morphological Evolution of Pore Channels in Alumina," to appear in *Proc. Int. Symp. Sintering of Advanced Ceramics*; LBL-25147.
9. J. Rödel and A.M. Glaeser, "Pore Drag in Alumina," to appear in *Proc. Int. Symp. Sintering of Advanced Ceramics*; LBL-25147.
10. R.M. Cannon, T.S. Oh, J. Rödel, A.M. Glaeser, and R.O. Ritchie, "Toughening of Ceramic-Metal Interfaces Using Patterned Arrays of Near-Interfacial Pores," J. Am. Ceram. Soc. (in press); LBL-24407.

Invited Talks

11. J. Rödel, "Generation of Controlled Interfacial Pore Structures and their Application to Kinetic Studies in Alumina," MRS Spring Meeting, Reno, NV, April 5–9, 1988.
12. J. Rödel, "Pore Drag in Alumina," Annual Meeting, American Ceramic Society, Cincinnati, OH, May 1–5, 1988.
13. A.M. Glaeser, "The Morphological Evolution of Pore Channels in Alumina," Annual Meeting, American Ceramic Society, Cincinnati, OH, May 1–5, 1988.

SOLID-STATE PHYSICS

EXPERIMENTAL RESEARCH

Far-Infrared Spectroscopy*

Paul L. Richards, Investigator

INTRODUCTION

Improvements in infrared technology are making possible increases in the sensitivity of many types of infrared and millimeter wave measurements. In this project, improved types of infrared sources, spectrometers, and detectors are being developed. Also, improved infrared techniques are being used to do experiments in areas of fundamental and applied infrared physics where their impact is expected to be large. Infrared experiments in progress include: measurements of the far-infrared absorptivity of the new high-T_c superconductors, measurements of the infrared emission spectra of molecules chemically adsorbed on metal surfaces, measurements of the infrared spectra of one-dimensional conductors, and measurements of the heat capacity of monolayers of adsorbates on metal films. Developments in infrared technology include: development of thin-film high-T_c superconducting bolometers for detecting x-ray, infrared, and microwave radiation; development of superconducting thin-film quasiparticle detectors and mixers for near-millimeter wavelengths that approach quantum-limited sensitivity; and development of a new source for broadly tuned far-infrared spectroscopy based on harmonic generation from microwave oscillators.

1. The High-T_c Superconducting Bolometer (Publication 17)†

P.L. Richards, S. Verghese, T.H. Geballe,‡ and S.R. Spielman‡

A description is given of the optimization of a bolometric infrared detector that uses the resistive transition of a high-T_c film as the thermometer. The performance of a liquid nitrogen (LN)-cooled far-infrared bolometer operated with a cooled low-pass filter is computed for the ideal case of a noise-free readout, as is shown in Figure 1-1. The theory is then extended to include various contributions to the readout noise. Measurements are presented of the low-frequency noise near T_c in current-biased films of $ErBa_2Cu_3O_7$, which show that useful performance can be achieved. Comparisons are made with other infrared detection technologies that show that practical high-T_c bolometers will be especially useful for wavelengths longer than the ~20-μm cutoff of LN-cooled photovoltaic detectors. Potential applications include far-infrared laboratory spectroscopy and passively cooled space observations of bright sources such as the earth.

*This work was supported by the Director, Office of Energy Research, Office of Basic Energy Sciences, Materials Sciences Division, of the U.S. Department of Energy under Contract No. DE-AC03-76SF00098.

†This work was supported by the Director's Exploratory Research and Development Funds of the Lawrence Berkeley Laboratory under Contract No. DE-AC03-76SF00098.

‡Stanford University collaborators.

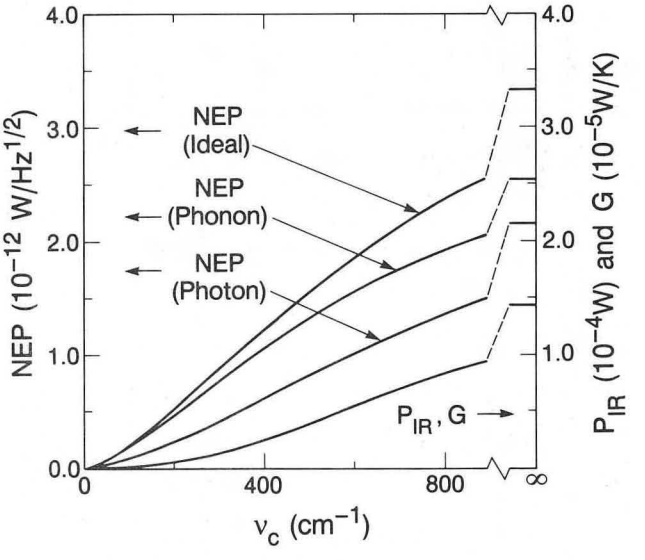

Figure 1-1. Infrared power loading P_{IR} and thermal conductance G for an ideal thermal infrared detector plotted as a function of the cutoff frequency ν_c of the cold low-pass filter. The detector is assumed to view 300-K background radiation with a throughput $A\Omega = 10^{-2}$ srcm^2 and perfect optical efficiency and to operate 10 K above the heat-sink temperature. The NEP of the ideal detector is shown, along with the separate contributions from phonon noise and photon noise. (XBL 889-7593)

2. Feasibility of the High-T_c Superconducting Bolometer (Publication 18)[†]

P.L. Richards, J. Clarke, R. Leoni, P. Lerch, S. Verghese, M.R. Beasley,[‡] T.H. Geballe,[‡] R.H. Hammond,[‡] P. Rosenthal,[‡] and S.R. Spielman[‡]

A design analysis is given for a bolometric infrared detector that uses the resistive transition of a high-temperature superconductor as the temperature-sensing element, and LN as a coolant. The measured low-frequency noise for highly oriented c-axis films shown in Figure 2-1 causes little or no degradation of the performance. With the incoming radiation chopped at 10 Hz, a noise equivalent power (NEP) in the range $(1-20) \times 10^{-12}$ $WHz^{-1/2}$ should be achievable. These values compare favorably with the NEP of other detectors operating at or above LN temperatures for wavelengths greater than 20 μm.

[†]This work was supported by the Director's Exploratory Research and Development Funds of the Lawrence Berkeley Laboratory under Contract No. DE-AC03-76SF00098.

[‡]Stanford University collaborators.

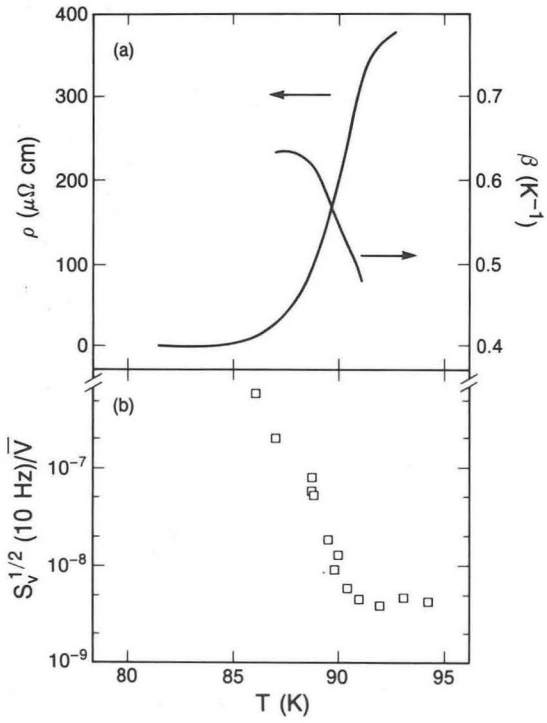

Figure 2-1. (a) Resistivity and temperature coefficient β of a YBCO film as a function of temperature, both measured with I = 1 mA. (b) Normalized noise $S_V^{1/2}(10Hz)/\overline{V}$ as a function of temperature measured with I = 10 mA. (XBL 889-7584)

3. Bias-Induced Nonlinearities in Neutron-Transmutation-Doped Germanium at ^{4}He Temperatures (Publication 19)

T.W. Kenny, P.L. Richards, I.S. Park, J.W. Beeman, and E.E. Haller[†]

Measurements have been made of the electrical properties of neutron-transmutation-doped (NTD) Ge commonly used for thermometers at and below ^{4}He temperatures. Once the effects of changes in lattice temperature due to electrical heating are removed, the results can be separated into two categories: those related to electrical nonlinearities, and those related to internal time constants.

The electrical nonlinearities were investigated by measuring the resistance of well heat-sunk thermometers as a function of applied bias voltage. These measurements showed that the form of the dependence of the resistance on the applied voltage is consistent with the predictions for variable-range hopping in the presence of a Coulomb gap. In order to fit all of the data precisely, it was necessary to assign a temperature dependence to the hopping length that is not in good agreement with theoretical predictions. Our results are consistent with previous investigations on similar materials.

The internal time constants were investigated by measuring the resistance oscillation that occurs when the thermometers are attached to a substrate undergoing a temperature oscillation. The amplitude of the resistance oscillation was measured as a function of the frequency of the temperature oscillation for several thermometers attached to the same substrate. The results of measurements at 2.3 K for samples labeled NTD-1 through NTD-4 are shown in Figure 3-1.

The mechanism for the internal time constant is not understood. A relationship between the internal time constant and the bias-induced nonlinearities appears likely because of their appearance together in several distinct systems dominated by hopping conductivity.

Both of these experimental results have implications for the use of these thermometers as the sensing element in various detectors.

[†]Samples for this study were provided by the group led by Prof. E.E. Haller. Haller's work is supported by the Director, Office of Energy Research, Office of Health and Environmental Research, U.S. Department of Energy under Contract No. DE-AC03-76SF00098.

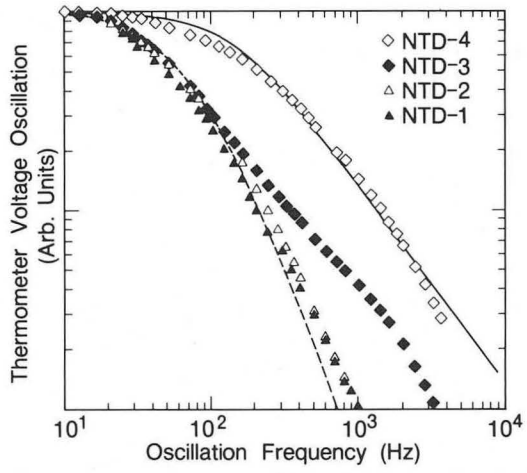

Figure 3-1. Measured amplitude of the voltage oscillation of the thermometer plotted as a function of the frequency of the applied thermal oscillation for four thermometers mounted on the same substrate. The solid line is the expected rolloff for the 1.3-msec time constant of the apparatus, while the dashed line is the product of the rolloff from this 1.3-msec time constant and the rolloff from a 4-msec time constant. This additional time constant $\tau_2 \approx$ 4 msec is evidence for an internal relaxation effect in NTD-1 and NTD-2. Electrical RC times become important in all curves after the first decade of rolloff. (XBL 884-7368)

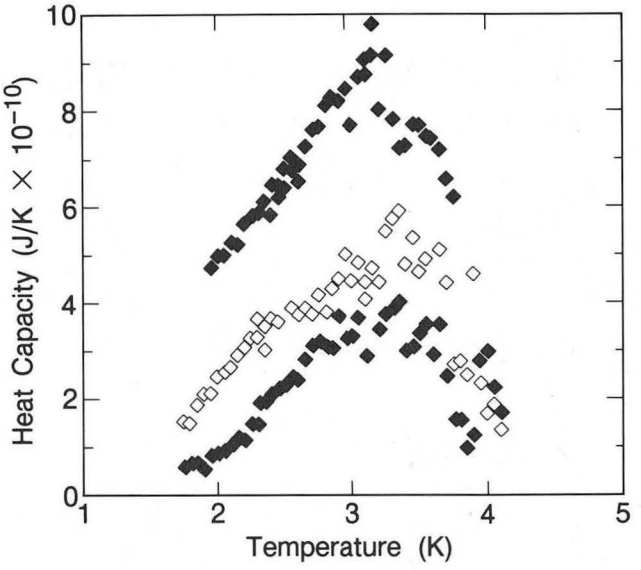

Figure 4-1. Heat capacity of three coverages of ^{4}He adsorbed on sapphire. The heat capacity of the bare calorimeter has already been subtracted. The heat capacity has a temperature-dependent component that is the same for all coverages investigated, and a temperature-independent component that increases with coverage. The temperature dependence above 3.3 K is dominated by desorption of the adsorbed ^{4}He. (XBL 8810-7666)

4. Heat-Capacity Measurements of Submonolayer ^{4}He Films Adsorbed on Sapphire (Publication 16)

W. Kenny and P.L. Richards

We have built a novel microcalorimeter for studies of the heat capacity of submonolayers and multilayers physisorbed on a variety of substrates. We have completed a series of measurements of the heat capacity of ^{4}He submonolayers adsorbed on the optically polished, chemically cleaned sapphire. This study is of practical importance to the operation of composite infrared bolometers that are similar in construction to the calorimeter.

The measured temperature dependence of the heat capacity for three different coverages of ^{4}He is shown in Figure 4-1. The heat capacity has a temperature-dependent component that is the same for all coverages investigated, and a temperature-independent component that increases with coverage. One interpretation is that the temperature-dependent component is due to the solidification of ^{4}He near impurities on the surface, and that the temperature-independent component is due to a dilute gas phase that occupies the rest of the surface. The sharp decreases in heat capacity above 3.3 K are due to desorption of ^{4}He from the calorimeter.

Measurements of the heat capacity of ^{4}He submonolayers adsorbed on Ag films are currently under way. This investigation has already shown that ^{4}He submonolayers on Ag exist in a two-dimensional gas phase between 2.3 and 3.5 K. The current series of measurements, which have been extended down to 1.8 K through improvements in the apparatus, will explore the expected deviations from the two-dimensional gas-phase behavior that arise due to either second-virial-coefficient corrections to the ideal-gas law or the formation of two-dimensional solid phases.

5. Millimeter Wave Quasioptical SIS Mixers (Publication 15)

Q. Hu, C.A. Mears, P.L. Richards, and F.L. Lloyd

We have tested the performance of planar superconductor-insulator-superconductor (SIS) mixers with log-periodic antennas at near-millimeter and submillimeter wave frequencies from 90 to 360 GHz. The large $\omega R_N C$ product ($\sim$10 at 90 GHz) of our Nb/NbO_x/Pb-In-Au junctions requires an integrated inductive tuning element such as the ones shown in Figure 5-1 to resonate the junction capacitance at the operating frequencies. We have used

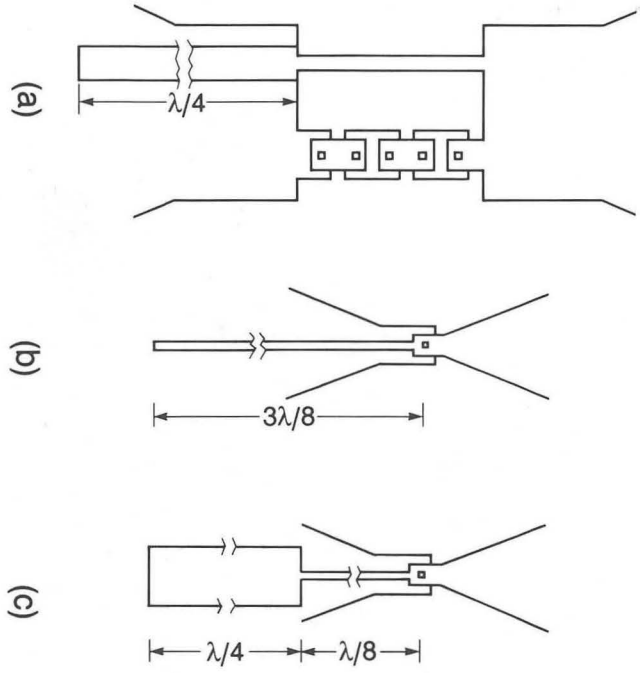

Figure 5-1. Diagrams of SIS junctions with tuning elements: (a) Five-junction array with inductive tuning wire. (b) Single junction with open-ended microstrip stub. (c) Single junction with rf shorted-end microstrip stub. (XBL 888-7506)

two types of integrated tuning element, both of which were designed with the aid of measurements using a Fourier transform spectrometer. Preliminary results indicate that the tuning elements can give very good mixer performance up to at least 200 GHz, as is shown in Figure 5-2. An inductive wire in parallel with a five-junction array gives a minimum mixer noise temperature of 115 K (DSB) at 90 GHz with a full-width half-maximum (FWHM) bandwidth of 8 GHz. An open-ended microstrip stub in parallel with a single junction gives minimum mixer noise temperatures of 150 and 200 K (DSB) near 90 and 180 GHz with FWHM bandwidths of 4 and 3 GHz, respectively. The relatively high mixer noise temperatures compared to those of waveguide SIS mixers in a similar frequency range are attributed mainly to the losses in our optical system, which is being improved.

6. Numerical Simulation of Experimental Data from Planar SIS Mixers with Integrated Tuning Elements (Publication 14)

C.A. Mears, Q. Hu, and P.L. Richards

We have used the full Tucker quantum theory of mixing, including the quantum susceptance, to fit data from planar lithographed mm-wave mixers with bow-tie antennas and integrated RF coupling elements. The quality of the fit obtained is shown in Figure 6-1. Essentially perfect fits to pumped IV curves have been obtained. The deduced imbedding admittances agree well with those independently calculated from the geometry of the antenna and matching structures. We find that the quantum susceptance is essential to the fit and thus to predictions of the mixer performance. For junctions with

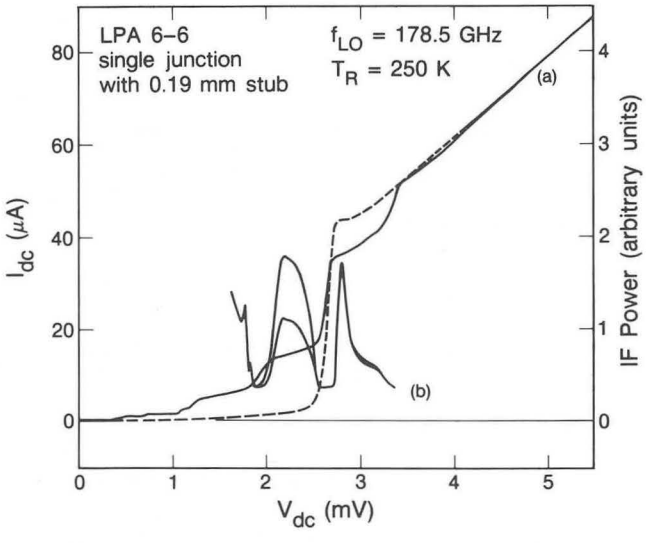

Figure 5-2. (a) IV curves of a pumped (solid line) and unpumped (dashed line) junction. (b) IF power as a function of dc bias voltage. The top curve is for the hot (300 K) load, and the bottom curve is for the cold (77 K) load. (XBL 888-7502)

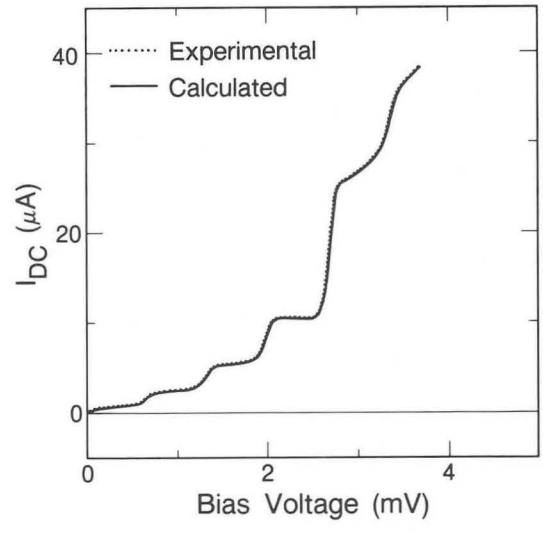

Figure 6-1. Experimental and calculated pumped IV curve. The experimental data points are offset upward by 0.02 μA. The LO frequency is 161 GHz. (XBL 887-7497)

moderately sharp gap structures, the quantum susceptance is especially important in the production of steps with low and/or negative dynamic conductance.

7. Superconducting Components for Infrared and Millimeter Wave Receivers (Publication 20)

P.L. Richards and Q. Hu

A review is given of the superconducting components that have been developed for infrared and millimeter wave receivers. A brief description is given of the scientific principles on which each device is based, followed by a discussion of the performance that has been achieved in terms of the appropriate figures of merit. Finally, comments are made about the possibility that useful device performance can be achieved by using the new high-T_c oxide superconductors. This review emphasizes photon-assisted quasiparticle tunneling and the SIS quasiparticle mixer, which is the only superconducting component to find substantial applications at infrared or millimeter wavelengths. Descriptions are given of the SIS quasiparticle direct detector, the Josephson-effect oscillator, the Josephson-effect parametric amplifier, and the various superconducting bolometers, for which practical applications appear possible. The less promising Josephson-effect detector and mixer and also the various ideas for superconducting photon detectors are described because of the current interest in possible high-T_c versions of these devices.

8. Work in Progress

Direct bolometric absorptivity measurements of high-T_c superconductors will be perfected so as to provide high accuracy over a wide far-infrared spectral range from $\sim$3 to 1200 cm^{-1}. The refurbishment of the spectrometer begun in 1988 will be completed. Attention will be given to errors arising from multiple thermal time constants, absolute normalization, standing waves, etc. Accuracy will be checked by measuring both normal and low-T_c superconducting metals whose absorptivity is known. Systematic measurements on films from a variety of sources will be in progress.

The search for information about energy-relaxation mechanisms in molecule-metal vibrational modes will be continued using our novel infrared-emission apparatus. The linewidth of the carbon-metal mode of CO on Ni(100) will be measured as a function of temperature. The one data point available is consistent with theories of multiphonon relaxation. A study of the temperature dependence could confirm the only known example of this mechanism, which is predicted to be of general importance.

The search for the far-infrared optical phason mode in the charge-density-wave compounds TaS_3 and $K_{0.3}MoO_3$ will be continued.

1988 PUBLICATIONS AND REPORTS

Refereed Journals

1. M.S. Sherwin, P.L. Richards, and A. Zettl, "Temperature Dependent Far Infrared Reflectance of La-(Sr,Ca)-Cu-O: BCS Electrodynamics but Uncertain Energy Gap," Phys. Rev. B **37**, 1587 (1988); LBL-24160.

Other Publications

2. P.L. Richards, "Spectrum of the Microwave Background," Comets to Cosmology Proceedings, London 1987, in *Lecture Notes in Physics*, Vol. 297, A. Lawrence, Ed., Springer-Verlag, Berlin, Heidelberg, 1988, p. 289.†
3. D.W. Face, W.R. McGrath, P.L. Richards, and D.E. Prober, "Accurate Experimental and Theoretical Comparison Between Superconducting Mixers Showing Strong and Weak Quantum Effects," ISEC'87 Extended Abstracts, 1987, p. 286.‡
4. W.R. McGrath, P.L. Richards, D.W. Face, D.E. Prober, and F.L. Lloyd, "Accurate Experimental and Theoretical Comparisons Between SIS Mixers Showing Weak and Strong Quantum Effects," J. Appl. Phys. **63**, 2479 (1988).‡
5. T. Matsumoto, S. Hayakawa, H. Matsuo, H. Murakami, S. Sato, A.E. Lange, and P.L. Richards, "The Submillimeter Spectrum of the Cosmic Background Radiation," Astrophys. J. **329**, 567 (1988).§
6. S. Hayakawa, T. Matsumoto, H. Matsuo, H. Murakami, S. Sato, A.E. Lange, and P.L. Richards, "Cosmological Implication of a New Measurement of the Submillimeter Background," Publ. Astron. Soc. Japan **39**, 941 (1987).§
7. L. Xizhi, P.L. Richards, and F.L. Lloyd, "SIS Quasiparticle Mixers with Bow-Tie Antennas," Int. J. IR MM Waves **9**, 101 (1988).‡
8. Q. Hu, C.A. Mears, P.L. Richards, and F.L. Lloyd, "Measurement of Integrated Tuning Elements for SIS Mixers with Fourier Transform Spectrometer," Bull. Am. Phys. Soc. **33**, 223 (1988).‡
9. Q. Hu. C.A. Mears, P.L. Richards, and F.L. Lloyd, "Measurement of Integrated Tuning Elements for SIS Mixers with a Fourier Transform Spectrometer," Int. J. IR MM Waves **9**, 303 (1988).‡

10. T.W. Kenny and P.L. Richards, "Heat Capacity Measurements of Gas Phase ^{4}He Adsorbed on Evaporated Silver Films," Bull. Am. Phys. Soc. **33**, 264 (1988); LBL-24503abs.
11. T.W. Kenny, P.L. Richards, I.S. Park, J.W. Beeman, and E.E. Haller, "Bias Dependent Nonlinearities in Neutron-Transmutation-Doped Germanium at ^{4}He Temperatures," Bull. Am. Phys. Soc. **33**, 232 (1988); LBL-24504abs.[‖]
12. M.S. Sherwin, P.L. Richards, and A. Zettl, "Far Infrared Reflectance of La-(Sr,Ca)-Cu-O: BCS Electrodynamics but Uncertain Energy Gap," Bull. Am. Phys. Soc. **33**, 451 (1988); LBL-24502abs.[**]

LBL Reports

13. M.S. Sherwin (Ph.D. Thesis), "Far Infrared Linear Response of Charge Density Wave Conductors and High T_c Superconductors," LBL-25404.[**]
14. C.A. Mears, Q. Hu, and P.L. Richards, "Numerical Simulation of Experimental Data from Planar SIS Mixers with Integrated Tuning Elements," IEEE Trans. Magn. **MAG-25** (in press); LBL-25813.[††]
15. Q. Hu, C.A. Mears, P.L. Richards, and F.L. Lloyd, "MM Wave Quasioptical SIS Mixers," IEEE Trans. Magn. **MAG-25** (in press); LBL-25814.[††]
16. T.W. Kenny and P.L. Richards, "Heat Capacity Measurements of Submonolayer ^{4}He Films Adsorbed on Sapphire," submitted to Surf. Sci.; LBL-26517.
17. P.L. Richards, S. Verghese, T.H. Geballe, and S.R. Spielman, "The High T_c Superconducting Bolometer," IEEE Trans. Magn. **MAG-25** (in press); LBL-25812.[‡‡]
18. P.L. Richards, J. Clarke, R. Leoni, P. Lerch, S. Verghese, M.R. Beasley, T.H. Geballe, R.H. Hammond, P. Rosenthal, and S.R. Spielman, "Feasibility of the High T_c Superconducting Bolometer," Appl. Phys. Lett. (in press); LBL-26113.[‡‡]
19. T.W. Kenny, P.L. Richards, I.S. Park, E.E. Haller, and J.W. Beeman, "Bias Induced Nonlinearities in Neutron Transmutation Doped Germanium at ^{4}He Temperatures," Phys. Rev. B. (in press); LBL-25633.[‖]
20. P.L. Richards and Q. Hu, "Superconducting Components for Infrared and Millimeter Wave Receivers," in *Proc. IEEE* (in press); LBL-26169.[††]
21. Q. Hu and P.L. Richards, "Quasiparticle Mixers and Detectors," chapter in *Modern Superconducting Devices*, Academic Press (in press); LBL-26535.[††]

Invited Talks

22. P.L. Richards, "Excess Infrared Flux in the Microwave Background," National Radio Science Meeting, Boulder, CO, Jan. 7, 1988.
23. P.L. Richards, "Rocket Measurements of the Cosmic Submillimeter Background," Physics Colloquium, U.S. Naval Postgraduate School, Monterey, CA, Jan. 22, 1988.
24. P.L. Richards, "Far Infrared and Submillimeter Devices," Radio Research Laboratory, Tokyo, Japan, Feb. 3, 1988; Advanced Telecommunications Research Institute International, Osaka, Japan, Feb. 10, 1988.
25. P.L. Richards, "The Cosmic Microwave Background," Institute for Space and Astronautical Sciences, Tokyo, Japan, Feb. 5, 1988; Physics Colloquium, Kyoto University, Kyoto, Japan, Feb. 10, 1988.
26. P.L. Richards, "Superconducting Detectors for Infrared and Millimeter Waves," Conference on Lasers and Electro-Optics (CLEO'88), Anaheim, CA, Apr. 25, 1988; One Day Workshop on Superconductivity and Microwaves, New York, NY, May 22, 1988.
27. P.L. Richards, "Infrared Detectors for the Advanced Light Source," Workshop on Scientific Applications of the Infrared Free Electron Laser, LBL, Oct. 31–Nov. 1, 1988.
28. P.L. Richards, "Superconducting Detectors for Infrared and Millimeter Waves," Conference on the Science and Technology of Thin-Film Superconductors, Colorado Springs, CO, Nov. 18, 1988.
29. P.L. Richards, "New Messages from the Early Universe," 26th Annual Briefing on New Horizons in Science, Council for the Advancement of Science Writing, Inc., Boulder, CO, Dec. 1, 1988.

[†]Supported in part by the U.S. National Aeronautics and Space Administration.

[‡]Supported in part by the U.S. Air Force Office of Scientific Research.

[§]Supported by the National Science Foundation and the California Space Institute.

[‖]Collaboration with Prof. E.E. Haller, whose research is supported by the Engineering Division of the Lawrence Berkeley Laboratory.

[**]Collaboration with Prof. Zettl, whose research is supported by the National Science Foundation.

[††]Supported in part by the U.S. Department of Defense.

[‡‡]Supported by DOE Exploratory Research and Development Funds.

Experimental Solid-State Physics and Quantum Electronics*

Y.R. Shen, Investigator

INTRODUCTION

This program involves theoretical and experimental research on laser interaction with matter. New nonlinear optical techniques are developed for studies of materials, both in the condensed-matter phase and in the gas phase. Current projects include (1) exploration of optical second-harmonic generation as a surface probe for noncentrosymmetric media; (2) development of sum-frequency generation for surface vibrational spectroscopy of adsorbed molecules at liquid/solid, air/metal, and air/semiconductor interfaces; (3) study of vibrational modes, including the local modes of benzene using the infrared-ultraviolet (IR-UV) double-resonance spectroscopic technique on supersonically cooled molecular beams; (4) far-UV high-resolution photoionization spectroscopic study of water molecules in a supersonically cooled beam; and (5) theoretical study of the localization of multivibrational excitations in a one-dimensional boson system with on-site random anharmonicity.

1. Optical Second-Harmonic Generation as a Surface Probe for Noncentrosymmetric Media (Publication 5)

T. Stehlin, M. Feller, P. Guyot-Sionnest, and Y.R. Shen

In recent years, optical second-harmonic generation (SHG) has proved to be an effective and sensitive tool for studies of a large variety of surface and interface properties. It has yielded, for example, information about structural and electronic properties of metal and semiconductor surfaces. However, experiments so far have been restricted to substrates with inversion symmetry, since then SHG is forbidden in the bulk but allowed at the surface, giving this technique its unique surface specificity. We show in the present work that, with proper polarization combinations, this restriction to media with inversion symmetry can be relaxed. SHG can then be used as an effective surface probe with submonolayer sensitivity for all interfaces accessible by light. For demonstration, we have studied with SHG the adsorption of Sn on GaAs, since semiconductor-metal interfaces are of great interest in fundamental as well as applied semiconductor research. Figure 1-1 is an illustration of the results.

*This work was supported by the Director, Office of Energy Research, Office of Basic Energy Sciences, Materials Sciences Division, of the U.S. Department of Energy under Contract No. DE-AC03-76SF00098.

2. Variational Spectroscopy of a Silane Monolayer at Air/Solid and Liquid/Solid Interfaces Using Sum-Frequency Generation (Publication 10)

P. Guyot-Sionnest, R. Superfine, J.H. Hunt, and Y.R. Shen

The understanding of liquid/solid interfaces is of central importance in surface science and technology. For decades, they have been studied by methods such as contact-angle measurements, capacitance measurements, and liquid chromatography, yielding mostly information on the macroscopic level. Techniques so successful at probing vacuum/solid interfaces are generally inapplicable here. The recently developed optical SHG technique does allow one to

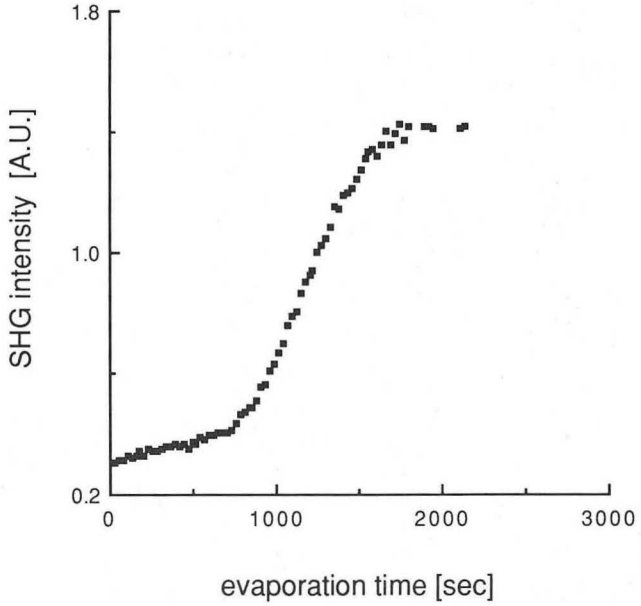

Figure 1-1. SH signal as a function of evaporation time of Sn on GaAs (100). The $p_{in} - p_{out}$ geometry with the (100) axis in the plane of incidence was used. (XBL 8711-4863)

probe various types of interfaces, including liquid/solid and liquid/liquid, but it is incapable of a selective study of adsorbed molecules via their vibrational spectroscopy. As a remedy, our group recently extended SHG to infrared-visible sum-frequency generation (SFG) for surface vibrational spectroscopic studies. We report here the first application of SFG to a liquid/solid interface. Although infrared techniques have been applied to probe the liquid/solid interface, SFG, being intrinsically surface sensitive, will allow the study of a much wider range of geometries and substrates.

The system we chose to study is OTS adsorbed at the interfaces between fused silica and different solvents. We present the first application of infrared-visible SFG to studies of liquid/solid interfaces. The spectra in the CH stretch region of OTS were measured and compared (see Figure 2-1). In every case, it was found that the OTS molecules were oriented with the alkane chains normal to the surface. Little difference was seen between polar and nonpolar liquids, although in the methanol case, the methanol molecules also appeared to adsorb at the interface. Our result is at variance with the picture assumed in liquid chromatography, but the difference could be understood from the different surface densities. We were able to monitor *in situ* the adsorption of OTS on fused silica in real time. This work demonstrates clearly the enormous potential of surface SFG for studies of liquid/solid interfaces. It is therefore expected that the technique will find applications in many areas of surface science.

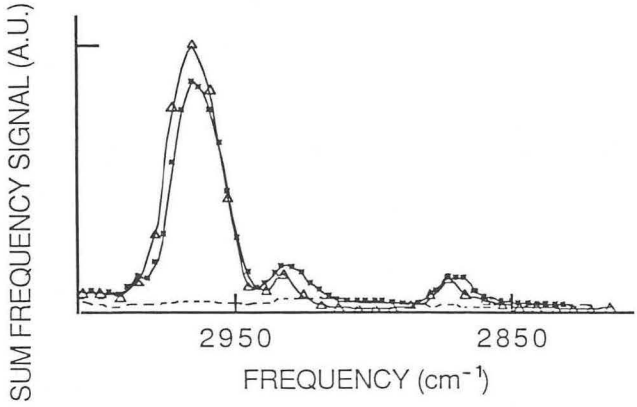

Figure 2-1. SFG spectra at different interfaces in the (p_{vis}, p_{IR}) polarization combination. Dashes: silica-hexadecane interface. Solid squares: silica-OTS-CCl_4 interfaces. Triangles: silica-OTS-hexadecane interface. The dashed and solid lines are guides for the eye. (XBL 894-1496)

3. Surface Vibrational Spectroscopy of Molecular Adsorbates on Metals and Semiconductors by Infrared-Visible SFG (Publication 9)

R. Superfine, P. Guyot-Sionnest, J.H. Hunt, C.T. Kao, and Y.R. Shen

Surface vibrational spectroscopy is of central importance for surface studies. Most of the existing spectroscopic techniques, unfortunately, have serious limitations. Our recently developed infrared-visible SFG technique has a number of clear advantages over existing techniques. Like optical SHG, SFG is highly surface-specific and is applicable to all interfaces accessible by light. With the help of ultrashort pump pulses, it has the potential of monitoring *in situ* surface dynamics, surface reactions, and intermediate transient species with picosecond time resolution. In several recent publications, we have successfully demonstrated the possibility of using SFG to obtain vibrational spectra of monolayers of molecules adsorbed at air/liquid, air/glass, and liquid/glass interfaces. However, to many researchers, studies of molecules adsorbed on metals and semiconductors are far more interesting because of their relevance to surface catalysis and surface preparation of electronic devices.

We have tried the SF surface spectroscopic technique on metals and semiconductors. We use the molecular adsorbate octadecyltrichlorosilane (OTS) as an example. The spectra of CH stretches of OTS on Si and Al and ethylidyne on Rh(111) are presented as examples (see Figure 3-1). The signal-to-noise ratio in the present experiment was not optimized. By choosing a proper beam geometry, we can anticipate an improvement of one order of magnitude in our SF signal. This should make the technique extremely attractive for future dynamic studies of selective molecules adsorbed on metals and semiconductors.

4. Vibrational and Electronic Spectroscopy of Pyridine and Benzene Adsorbed on the Rh(111) Crystal Surface (Publication 1)

C.M. Mate, G.A. Somorjai, H.W.K. Tom, X.D. Zhu, and Y.R. Shen

The interaction of aromatic molecules with metal surfaces has recently been the subject of several investigations. Much of this interest is

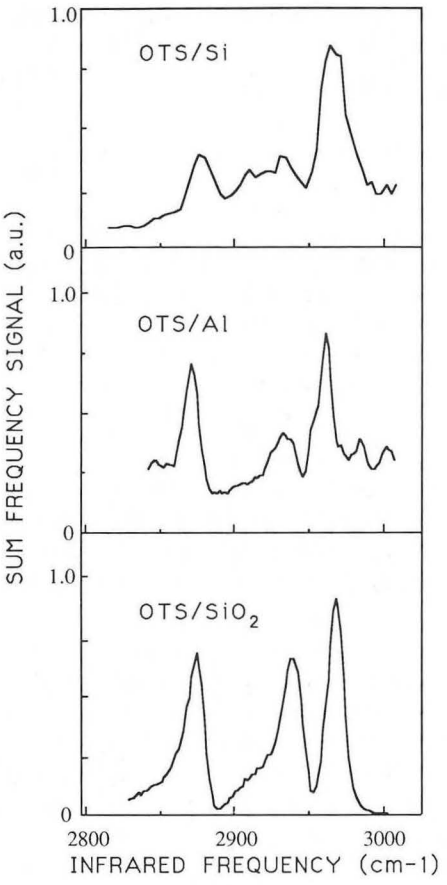

Figure 3-1. Sum-frequency spectra of OTS on freshly evaporated aluminum and OTS on glass, as described in the text. (XBL 894-1497)

derived from the importance of aromatic molecules, such as fuels, chemicals, and lubricants, that are produced and utilized by technologies where surface phenomena play a dominant role. For example, aromatic compounds are desirable products of heterogeneous catalytic reactions in the refining of crude oil into high-octane fuels. In lubrication, aromatic compounds are frequently used as functional groups in extreme-pressure additives, even though their role is not understood. Therefore, a molecular-scale understanding of how aromatic molecules interact with metal surfaces should be of considerable importance.

We report the vibrational and electronic spectra for pyridine and benzene adsorbed on the Rh(111) crystal surface obtained by high-resolution electron-energy-loss spectroscopy (HREELS). Low-energy electron diffraction (LEED), thermal-desorption spectroscopy (TDS), and optical SHG have also been used to provide complementary information. Pyridine adsorption on Rh(111) was studied over the 77–450 K temperature range. At 77 K, multilayers of pyridine are observed with a vibrational spectrum similar to that of liquid pyridine. Between 185 and 230 K, HREELS and TDS indicate that both physisorbed and chemisorbed pyridine species are present on the surface. The physisorbed species desorbs at 295 K, while the chemisorbed species is stable until it decomposes on the surface at 400 K. We propose that the chemisorbed species is an α-pyridyl complex, as TDS indicates partial dehydrogenation of this pyridine surface species. Electronic energy-loss spectra for both benzene and pyridine adsorbed at 310 K show only a weak transition centered at $\sim$ 4 eV. The absence of prominent $\pi \rightarrow \pi^*$ transitions, which are readily observed for multilayers of benzene adsorbed on Rh(111), implies that the π orbitals are strongly involved in the chemisorption bond of these molecules with the Rh(111) surface.

5. Local Modes of Benzene and Benzene Dimer, Studied by Infrared-Ultraviolet Double Resonance in a Supersonic Beam (Publication 3)

R.H. Page, Y.R. Shen, and Y.T. Lee

We have reported on what we believe to be the first high-resolution, state-selective study of local modes in a relatively large molecule—benzene. The technique we used was a combination of rotational cooling in a supersonic beam expansion and multilevel, state-selective saturation spectroscopy. There is no doubt that the room-temperature local-mode overtone spectra of large molecules previously published have had inhomogeneous congestion. Broad "rotational envelopes" and "hot bands" appear to be the culprits. Linear absorption measurements on room-temperature samples simply cannot uncover the wealth of detail present in the spectra.

Many suspected but heretofore undetected perturbations between the local and other vibrational modes obviously occur. Judging from the appearances of the overtone spectra of the monomer and dimer, we conclude that the local-mode description of the benzene C-H stretches applies to $\nu \geq 3$. Perturbation-matrix elements change from $\sim$ 25 cm^{-1} at $\nu = 1$ to $\sim$ 0.004 cm^{-1} at $\nu = 3$. Our linewidth measurements show that the lifetimes of the C-H stretching vibration exceed a few psec, even at a total energy of $\sim$ 8800 cm^{-1}. This is an accordance with lifetime data on other vibrational modes of benzene excited to similar energies. In the

absence of direct lifetime measurements of the local-mode states, these lifetime estimates based on the measured linewidths are likely to be only a lower bound.

Our measurements of the C-H stretching spectra of the benzene dimer could help to resolve questions concerning its intermolecular potential, structure, and vibrational predissociation lifetime. New lines around the C-H stretching fundamental band have been observed. Certainly, the dimer's vibrational predissociation lifetime is in excess of a few psec at 3000 cm^{-1} vibrational energy.

6. Infrared-Ultraviolet Double-Resonance Studies of Benzene Molecules in a Supersonic Beam (Publication 2)

R.H. Page, Y.R. Shen, and Y.T. Lee

We have used the powerful, elegant double-resonance technique to study a prototype intermediate-size molecule (benzene) cooled in a supersonic expansion. The thorough work that has already been done on the $\tilde{X}$ vibrations and the $\tilde{A} \leftarrow \tilde{X}$ transition of benzene allowed us to make decisive assignments of several IR-pumping-induced UV transitions. With these assignments, we were able to confirm, in a qualitative way, Pliva's analysis of the C-H stretching Fermi tetrad in the $\tilde{X}$ state. Also, we provided a determination of the gas-phase value of ν'_{19}, the IR-active C-H bend, and the first observation in the $\tilde{A}$ state of ν_3, the "C-H libration," and of ν_{20}, the IR-active C-H stretch. The values of these frequencies are found to be $\nu'_{19} \cong 1045$ cm^{-1}, $\nu'_3 \approx 1327$ cm^{-1}, and $\nu'_{20} \approx 3084$ cm^{-1}.

A thorough understanding of the first excited state of a simple phenyl system could prove useful in several situations. Vibrations and their anharmonicity are thought to be important in mediating radiationless transitions. Radiationless decay is not thoroughly characterized in either the $\tilde{X}$ or $\tilde{A}$ states of benzene. Also, the electronic properties of phenyls help to determine the qualities of many molecules of photophysical and photochemical interest. For example, phenyl rings form the basis of many (e.g., laser) dyes. Enhancements in lasing efficiency and photochemical stability could perhaps be engineered with better knowledge of excited-state geometries and forces.

7. High-Resolution Photoionization Spectrum of Water Molecules in a Supersonic Beam (Publication 4)

R.H. Page, R.J. Larkin, Y.R. Shen, and Y.T. Lee

We have obtained high-resolution ($\sim$ 1.5 cm^{-1}) photoionization spectra of supersonically cooled (T_{rot} $\sim$ 50 K) H_2O and D_2O in the 1000–900 Å range. The light source, which used the technique of frequency tripling in a pulsed free jet of gas, is described briefly. Spectra are rotationally resolved. Vibrationally excited autoionizing Rydberg series converging to the ground electronic $[\tilde{X}; (1b_1)^{-1}]$ state of the molecular ion are detected. This may well be the first example of a highly resolved Rydberg spectrum of a stable polyatomic atomic molecule. From the convergence limit, the ionization potential H_2O is determined to be 101,777 $\pm$ 7 cm^{-1}. Intensities of the Rydberg-state autoionization signals are smaller than predicted with known Franck-Condon factors, indicating that predissociation is a competitive decay channel. Rydberg-state lifetimes are $\sim$ 1 psec, deduced from homogeneous linewidths. Autoionizing features from Rydberg states associated with the ion's quasilinear $\tilde{A}$ $(3a_1)^{-1}$ state are observed with linewidths above 10 cm^{-1}, indicating that their lifetimes are less than $\sim$ 0.5 psec. Rotational assignments of some of the bands in this linear $\leftarrow$ bent transitions show that the Rydberg and ionic-state geometries are nearly identical. A consistent assignment of the controversial bending (ν_2) quantum number and Rydberg series quantum defect $\delta = -0.037$ have been provided.

8. Localization of Multivibrational Excitations (Publication 7)

M.S. Wartak, L.H. Yang, C.Y. Fong, and Y.R. Shen

The problem of localization in fermion systems has received a great deal of attention in the last two decades. However, the parallel behavior in the boson systems has rarely been discussed. In reality, multiple excitations can readily occur in a boson system; the appearance of localization of multiple excitations in a boson system is also not uncommon. The existence of local vibrational modes in a polya-

tomic molecule, for example, has recently stimulated a tremendous amount of interest. The possibility of observing localized multiple vibrational excitations in molecular liquids and solids is very intriguing. In weakly bonded molecular polymers or clusters, how well the multiple vibrational excitations are localized can be a subject of fundamental importance. In all these cases, it will be very interesting if it is possible to identify the physical mechanism that causes the localization.

We have studied the localization of multivibrational states in the one-dimensional boson system with onsite random anharmonicity. By introducing site basis states (local representation), we were able, in the limit of $\Delta/\bar{\Gamma} \ll 1$, where Δ is the coupling interaction between the nearest neighbors and $\bar{\Gamma}$ is the average on site anharmonic energy, to reduce to problem to Anderson-like model for a one-dimensional electron system with diagonal disorder. Assuming a Cauchy distribution for onsite anharmonicity, we have calculated the degree of localization. It is shown that the degree of localization increases with the increase of randomness.

9. Work in Progress

Optical SHG is being used to study laser thermal desorption of molecules from metal surfaces. Combining the technique with conventional thermal desorption should allow an unambiguous determination of the preexponential factor and the desorption energy. Two interfering laser beams can create a monolayer grating of adsorbed molecules on a surface by laser desorption. This can be monitored by the multiorder diffraction of SHG from the surface. The technique is being used to probe the grating profile. As the molecules diffuse on the surface and the grating smears out, the diffraction signal decays away. The results lead to a determination of the surface-diffusion constant of the molecules. Anisotropy in surface diffusion can also be probed.

1988 PUBLICATIONS AND REPORTS

Refereed Journals

1. C.M. Mate, G.A. Somorjai, H.W.K. Tom, X.D. Zhu, and Y.R. Shen, "Vibrational and Electronic Spectroscopy of Pyridine and Benzene Adsorbed on the Rh(111) Crystal Surface," J. Chem. Phys. **88**, 441 (1988); LBL-23628.
2. R.H. Page, Y.R. Shen, and Y.T. Lee, "Infrared-Ultraviolet Double Resonance Studies of Benzene Molecules in a Supersonic Beam," J. Chem. Phys. **88**, 5362 (1988); LBL-23769.
3. R.H. Page, Y.R. Shen, and Y.T. Lee, "Local Modes of Benzene and Benzene Dimer, Studied by Infrared-Ultraviolet Double Resonance in a Supersonic Beam," J. Chem. Phys. **88**, 4621 (1988); LBL-24007.
4. R.H. Page, R.J. Larkin, Y.R. Shen, and Y.T. Lee, "High Resolution Photoionization Spectrum of Water Molecules in a Supersonic Beam," J. Chem. Phys. **88**, 2249 (1988); LBL-24158.
5. T. Stehlin, M. Feller, P. Guyot-Sionnest, and Y.R. Shen, "Optical Second Harmonic Generation as a Surface Probe for Non-centrosymmetric Media," Opt. Lett. **13**, 389 (1988); LBL-24366.
6. P. Guyot-Sionnest and Y.R. Shen, "Bulk Contribution in Surface Second Harmonic Generation," Phys. Rev. B **38**, 7985 (1988); LBL-24703.
7. M.S. Wartak, L.H. Yang, C.Y. Fong, and Y.R. Shen, "Localization of Multivibrational Excitations," Phys. Rev. B **37**, 10350 (1988); LBL-24824.
8. R. Blumel, J.M. Chen, E. Peik, W. Quint, S. Schleich, Y.R. Shen, and H. Walther, "Phase Transitions of Stored Laser-Cooled Ions," Nature **334**, 309 (1988).
9. R. Superfine, P. Guyot-Sionnest, J.H. Hunt, C.T. Kao, and Y.R. Shen, "Surface Vibrational Spectroscopy of Molecular Adsorbates on Metals and Semiconductors by Infrared-Visible Sum-Frequency Generation," Surf. Sci. (Letters) **200**, L445 (1988); LBL-24434.
10. P. Guyot-Sionnest, R. Superfine, J.H. Hunt, and Y.R. Shen, "Vibrational Spectroscopy of a Silane Monolayer at Air/Solid and Liquid/Solid Interfaces using Sum-Frequency Generation," Chem. Phys. Lett. **144**, 1 (1988); LBL-24434.
11. X.D. Zhu, T. Rasing, and Y.R. Shen, "Surface Diffusion of CO on Ni(111) Studied by Diffraction of Optical Second-Harmonic Generation off a Monolayer," Phys. Rev. Lett. **61**, 2883 (1988); LBL-25970.

Other Publications

12. X.D. Zhu, T. Rasing, and Y.R. Shen, "Laser-Induced Desorption of CO on Ni(111): Determination of Desorption Preexponential Factor and Head of Adsorption," Bull. Am. Phys. Soc. **33**, 819 (1988); LBL-24437abs.
13. R. Blumel, J.M. Chen, E. Peik, W. Quint, W. Schleich, Y.R.Shen, and H. Walther, "Phase Transitions of Stored Laser-Cooled Ions," in *Proc. Conference on Atomic Physics*, Paris, France, 1988, p. 199.
14. T. Stehlin, M. Feller, P. Guyot-Sionnest, and Y.R. Shen, "Can Optical Second Harmonic Generation be Used as a Surface Probe for Noncentrosymmetric Media," Bull. Am. Phys. Soc. **33**, 1647 (1988); LBL-25549abs.
15. Y.R. Shen, "Nonlinear Optics and Surface Science," Bull. Am. Phys. Soc. **33**, 1647 (1988); LBL-25550abs.

LBL Reports

16. Y.R. Shen, "Nonlinear Optical Techniques for Surface Studies," in *Proc. NATO Advanced Study Institute on Interfacial Spectro-electrochemistry,* Canary Islands, Spain, July 13–15, 1988 (in press); LBL-25002.
17. Y.R. Shen and G. Yang, "Theory of Self-Phase Modulation and Spectral Broadening," LBL-25040.
18. X.D. Zhu, T. Rasing, and Y.R. Shen, "Laser-Induced Thermal Desorption of CO on Ni(111): Determination of Pre-exponential Factor and Head of Desorption," Chem. Phys. Lett. (in press:); LBL-25189.
19. R-P. Pan, H.D. Wei, and Y.R. Shen, "Optical Second Harmonic Generation from Magnetized Surfaces," Phys. Rev. B (in press); LBL-26093.
20. Y.R. Shen, "Surface Second Harmonic and Sum-Frequency Generation: A Novel Optical Probe for Surface Studies," Nature (in press); LBL-26099.
21. X.D. Zhu and Y.R. Shen, "Generation and Detection of a Monolayer Grating: CO on Ni(111)," Opt. Lett. (in press); LBL-26276.

Invited Talks

22. X.D. Zhu, T. Rasing, and Y.R. Shen, "Laser-Induced Thermal Desorption of CO on Ni(111): Determination of Desorption Preesponential Factor and Heat of Adsorption," March Meeting, American Physical Society, New Orleans, LA, Mar. 21–25, 1988.
23. Y.R. Shen, "Nonlinear Optics and Surface Science," Texas Christian University, Fort Worth, TX, Apr. 18, 1988.
24. Y.R. Shen, "Nonlinear Optical Studies of Interfaces," 173rd Meeting, The Electrochemical Society, Atlanta, GA, May 15–16, 1988.
25. Y.R. Shen, "Nonlinear Optics and Liquid Crystals," Bell Communications Research, Red Bank, NJ, May 20, 2988.
26. Y.R. Shen, "Nonlinear Optical Studies of Monolayers and Films," Exxon Research and Engineering Co., Annandale, NJ, May 23, 1988.
27. Y.R. Shen, "Nonlinear Optics for Surface Studies," AT&T Bell Laboratories, Murray Hill, NJ, May 24, 1988.
28. Y.R. Shen, "Nonlinear Optical Techniques for Surface Studies," NATO Advanced Study Institute on Interfacial Spectroelectrochemistry, Canary Islands, Spain, July 3–15, 1988.
29. P. Guyot-Sionnest, R. Superfine, J.H. Hunt, and Y.R. Shen, "Sum-Frequency Generation for Surface Vibrational Spectroscopy," Topical Meeting on Laser Materials and Spectroscopy, Shanghai, People's Republic of China, July 25–27, 1988.
30. Y.R. Shen, "Surface Nonlinear Optical Processes," Adriatico Research Conference, The Applications of Lasers in Surface Science, Trieste, Italy, Aug 23–26, 1988.
31. Y.R. Shen, "Nonlinear Optics and Surface Science," IVth International Laser Science Conference, Atlanta, GA, Oct. 2–6, 1988.
32. Y.R. Shen, "Nonlinear Optics at Interfaces," Symposium on Nonlinear Optics and Ultrafast Phenomena—Photonics, Chicago, IL, Oct. 9–14, 1988.
33. Y.R. Shen, "Surface Spectroscopy by IR-VIS Sum Frequency Generation," LBL/BNL Workshop on Scientific Opportunities of the IRFEL, Berkeley, CA, Oct. 31, 1988.
34. X.D. Zhu and Y.R. Shen, "Dynamic Gratings on Surface Monolayers," Xth International Conference on Lasers and Applications, Lake Tahoe, CA, Dec. 5–9, 1988.

Nonlinear Excitations in Solid-State Systems*

Carson D. Jeffries, Investigator

INTRODUCTION

The central objectives of this program are to experimentally study nonlinear phenomena in solid-state systems and to develop models that can explain and predict the observed behavior. This report describes experiments and analysis of spin waves in ferrites and of plasma waves in Ge rods. Present emphasis is on the novel nonlinear electrodynamics exhibited by high-temperature superconductors of the copper oxide type. The origin of the nonlinearities lies in the microstructures of these ceramic materials: superconducting grains in contact through weak links. Observed generic behavior includes very high-order odd harmonic generation in zero dc field; even harmonics in nonzero field; and, at high harmonics and high pump power, very sharp power dips periodic in the dc field, due to flux quantization. Models are developed that semiquantitatively explain the observed behavior and help characterize the material. This work has a bearing on the problem of high critical currents in high magnetic fields, as well as on the origin of the superconductivity.

1. Spin-Wave Dynamics in a Ferrimagnetic Sphere (Publications 1–4)

P.H. Bryant, C.D. Jeffries, and K. Nakamura

An experimental study has been made of the interaction between spin-wave modes excited in a sphere of yttrium iron garnet by pumping the Suhl subsidiary absorption at 9.2 GHz with the dc field parallel to [111]. The dynamical behavior of the magnetization is observed under high resolution by varying two control parameters, dc field ($580\ \text{Oe} < H < 2100\ \text{Oe}$) and microwave pump power ($1\ \text{mW} < P < 200\ \text{mW}$). Within this parameter space, quite varied behavior is found: (i) onset of the Suhl instability occurs by excitation of a single spin-wave mode with very narrow linewidth (<0.5 G); (ii) when two or more modes are excited, interactions lead to auto-oscillations with a systematic dependence of frequency (10^4–10^6 Hz) on pump power, these oscillations displaying period doubling to chaos; (iii) quasiperiodicity, locking, and chaos occur when three or more modes are excited; (iv) abrupt transition to wide-band power spectra (i.e., turbulence) occurs with hysteresis; and (v) irregular relaxation oscillations and aperiodic spiking behavior occur. A theoretical model has been developed from first principles, using the plane-wave approximation and including anisotropy effects, obtaining the lowest-order nonlinear interaction terms between the excited modes. Bifurcation behavior has been examined, and dynamical behavior has been numerically computed and compared to the experimental data, explaining a number of features. A theory has been developed regarding the nature of the experimentally observed relaxation oscillations and spiking behavior based on the interaction of "weak" and "strong" modes, and this theory has been demonstrated in the numerical simulations.

*This work was supported by the Director, Office of Energy Research, Office of Basic Energy Sciences, Materials Sciences Division, of the U.S. Department of Energy under Contract No. DE-AC03-76SF00098.

2. Multifractal Structure of Attractors at the Quasiperiodic Transition to Chaos for Electron-Hole Plasma Instability in Ge (Publication 7)

Y. Kim

The scaling structure of attractors at the transition from quasiperiodicity to chaos has been studied for an electron-hole plasma instability in Ge crystal. The scaling function f(a) spectrum calculated from the time series of the plasma current oscillation at the onset of chaos is in good agreement with that of a circle-map model. The experimental power spectrum also confirms that the transition to chaos is well described by the circle map. The extrinsic noise effect on the f(a) spectrum is discussed by using the circle map.

3. Symmetry Breaking and Nonlinear Electrodynamics in the Ceramic Superconductor $YBa_2Cu_3O_7$ (Publication 5)

C. Jeffries, Q.H. Lam, Y. Kim, L.C. Bourne, and A. Zettl

For bulk samples of the ceramic superconductor $YBa_2Cu_3O_7$ in a radiofrequency magnetic field and

in a dc magnetic field H_o, we observe novel nonlinear behavior, including very high-order odd-harmonic generation if $H_o = 0$ (see Figure 3-1). If $H_o \neq 0$, there is additional even-harmonic generation. The even-harmonic power displays a very sharp dip at $H_o \sim 0$, of width $\sim 100\ \mu G$. This and related behavior can be semiquantitatively understood by modeling the system as a suitably averaged collection of flux-quantized supercurrent loops containing Josephson junctions.

4. Harmonic Generation and Flux Quantization in Granular Superconductors (Publication 6)

Q.H. Lam and C.D. Jeffries

Simple dynamical models of granular superconductors are used to compute the generation of harmonic power in ac and dc magnetic fields. In zero order, the model is a single superconducting loop, with or without a weak link. The sample-average power is predicted by averaging over suitable distribution functions for loop areas and orientations in a dc magnetic field. In a first-order model, inductance and resistance are also included. In all models the power at high harmonics shows strikingly sharp dips periodic in the dc field, revealing flux quantization in the prototype loops.

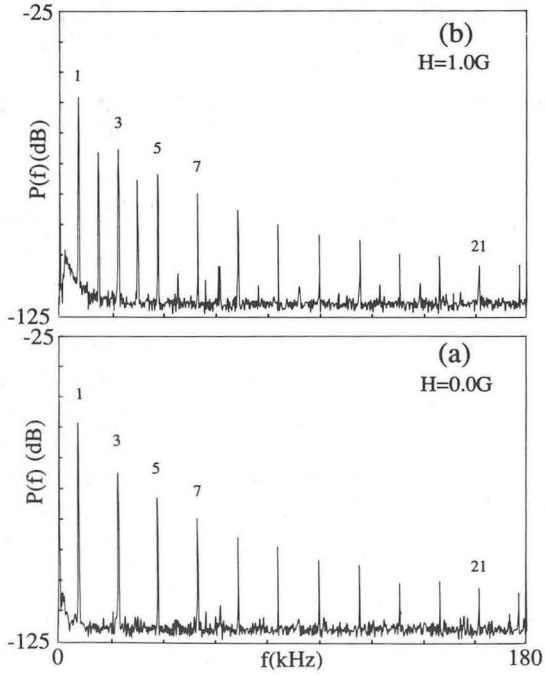

Figure 3-1. Power spectra for powdered $YBa_2Cu_3O_7$ at T = 77 K, driven by an ac field at $f_o = 7.7$ kHz, of amplitude $H_1 \approx 14$ G. (a) dc field $H_o = 0.0$ G. Odd harmonics, n = 3,5,..., are generated. (b) In a parallel dc field $H_o = 1.0$ G, even harmonics, n = 2,4,..., also appear, owing to symmetry breaking by the dc field. The unit of the vertical scale is $P(db) = 20 \log_{10} V_s + 13$, where V_s is the rms signal voltage. (XBL 891-360)

5. Nonlinear Electrodynamics in the Granular Superconductor $YBa_2Cu_3O_7$: Experiments and Interpretation (Publication 8)

C.D. Jeffries, Q.H. Lam, Y. Kim, C.M. Kim, A. Zettl, and M.P. Klein

For bulk samples of superconducting $YBa_2Cu_3O_7$ powder and pellets subject to a dc magnetic field H_o and a parallel ac magnetic field H_1 at frequency $f \sim 10^3$ to 10^5 Hz, we report data on the generated harmonic power P(nf) up to harmonic $n \approx 40$, finding: (1) if $H_o = 0$, only odd harmonics are generated; (2) if $H_o = 0$, even harmonics are additionally generated; (3) for H_1 sufficiently large ($\gtrsim 10$ Oe) and n large, then P(nf) vs H_o displays sharp and deep periodic dips, revealing a remarkably consistent and reproducible macroscopic flux quantization for the bulk sample. These data, as well as the relative intensities of the harmonic power, are found to be in semiquantitative agreement with detailed numerical predictions of a dynamical model of the material as a suitably averaged ensemble of prototype flux quantized loops with weak links (see Figures 5-1 and 5-2). At lower values of H_1, additional structure is observed, related to fluxon pinning and depinning.

6. Work in Progress

Much remains to be done to understand the complex and interesting problem of the electrodynamics of granular superconductors. The phenomena reported here are believed to be generic to $YBa_2Cu_3O_7$. Similar studies are under way on other compounds (e.g., $Bi_4Sr_3Cu_7O_x$), as well as on a variety of forms, including films, single crystals, and powders and sintered pellets with different grain sizes and methods of preparation. The harmonic-generation studies are sensitive probes of the electrodynamic properties and the microstructure, and may be useful in characterizing materials. The theoretical models are being broadened to take account of the sample geometry, critical state, and fluxon pinning and motion.

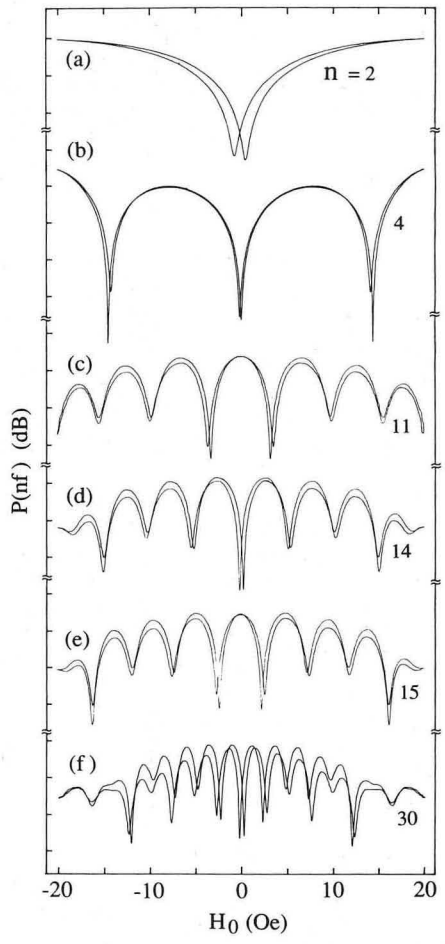

Figure 5-1. Relative harmonic power (10 dB/div) of P(nf) vs H_o, scanned at a uniform rate, for a sample of powdered $YBa_2Cu_3O_7$ at T = 77 K, f = 28 kHz, H_1 = 23 Oe. (a) to (f) show data for selected representative harmonics n. Shown are two scans, the arrows denoting the direction of time increase. The sharp dips are a consequence of flux quantization of an ensemble of supercurrent loops in the granular sample, and are to be compared to Figure 5-2. (XBL 8812-4191)

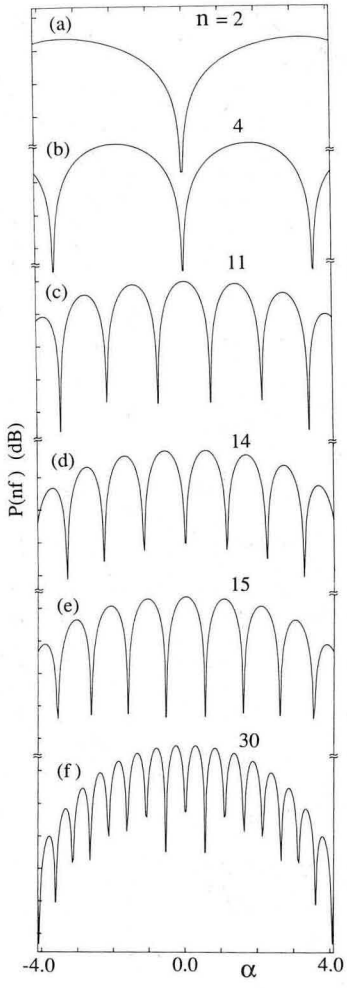

Figure 5-2. Relative harmonic power (10 dB/div) of P(nf) vs α, computed from the model, where $\alpha \equiv 2\pi SH_o/\phi_o$, where S is an effective loop area and ϕ_o is the flux quantum. (XBL 8812-4300)

1988 PUBLICATIONS AND REPORTS

Refereed Journals

1. P. Bryant, C. Jeffries,† and K. Nakamura, "Spin-Wave Turbulence," Nucl. Phys. B (Proc. Suppl.) **2**, 25 (1987); LBL-23041.
2. P. Bryant, C. Jeffries,† and K. Nakamura, "Spin-Wave Nonlinear Dynamics in an Yttrium Iron Garnet Sphere," Phys. Rev. Lett. **60**, 1185 (1988); LBL-24471.
3. C. Jeffries,† P. Bryant, and K. Nakamura, "Nonlinear Dynamics of Spin Waves," J. Appl. Phys. **64**, 5382 (1988); LBL-25409.
4. P. Bryant, C. Jeffries,† and K. Nakamura, "Spin-Wave Dynamics in a Ferrimagnetic Sphere," Phys. Rev. A **38**, 4223 (1988); LBL-24470.
5. C. Jeffries,† Q.H. Lam, Y. Kim, L.C. Bourne, and A. Zettl, "Symmetry Breaking and Nonlinear Electrodynamics in the Ceramic Superconductor $YBa_2Cu_3O_7$," Phys. Rev. B **37**, 9840 (1988); LBL-24874.

LBL Reports

6. Q.H. Lam and C.D. Jeffries,† "Harmonic Generation and Flux Quantization in Granular Superconductors," accepted by Phys. Rev. B; LBL-26227.
7. Y. Kim, "Multifractal Structure of Attractors at the Quasiperiodic Transition to Chaos for Electron-Hole Plasma Instability in Ge," accepted by Phys. Rev. A; LBL-26200.
8. C.D. Jeffries,† Q.H. Lam, Y. Kim, C.M. Kim, A. Zettl, and M.P. Klein, "Nonlinear Electrodynamics in the Granular Superconductor $YBa_2Cu_3O_7$: Experiments and Interpretation," accepted by Phys. Rev. B; LBL-26624.

Invited Talks

9. C.D. Jeffries,[†] "Nonlinear Dynamics in a YIG Sphere," Fourth Joint MMM-Intermag Conference, Vancouver, B.C., July 12–15, 1988.

[†]Supported in part by U.S. Office of Naval Research under Contract No. N00014-86-K-0154.

Time-Resolved Spectroscopies in Solids*

Peter Y. Yu, Investigator

INTRODUCTION

The purpose of this project is to use picosecond and subpicosecond laser pulses generated by modelocked dye lasers to study ultrafast interactions between elementary excitations in solids. An understanding of these interactions, such as between electrons and phonons and among electrons, is important in the design of new generations of fast electronic devices. Nonequilibrium phonons and electron-hole plasmas are excited in semiconductors such as GaAs by picosecond and subpicosecond laser pulses. Their subsequent expansion and cooling are monitored as a function of time by techniques such as photoluminescence and Raman scattering. The influence of defects, impurities, carrier confinement, and external perturbations such as strain are also investigated.

The effects of pressure on the electrical and optical properties of solids are also studied using diamond anvil high-pressure cells. The effect of pressure on defect levels in semiconductors and at semiconductor interfaces has been studied by capacitance techniques such as deep-level transient spectroscopy (DLTS) and photocapacitance techniques.

1. Optical Characterization of Epitaxial GaAs Films Grown on Si (Publications 1, 2, and 6)

Y. Huang and P.Y. Yu

Epitaxial GaAs films grown on Si are one of the most extensively studied heteroepitaxial systems. From the technological point of view, the system promises to combine the desirable optoelectronic properties of GaAs for optical communication with the well-established Si technology. From the materials science point of view, it poses interesting challenges because of the differences in the lattice constants and ionicities between GaAs and Si. Although the quality of GaAs film grown on Si is still far inferior to GaAs films grown on GaAs substrates, methods of growing high-quality epitaxial GaAs films on Si are continuously being proposed. Optical techniques such as photoluminescence and light scattering have been shown to be fast, nondestructive, and sensitive in characterizing these thin-film samples. In collaboration with Prof. S. Wang's group, defects in epitaxial GaAs films grown on Si by molecular-beam epitaxy (MBE) have been studied optically. One proposed method of reducing stress and defects in this heteroepitaxial system is to use selective-area MBE growth in which crystalline GaAs is surrounded by polycrystalline GaAs. Using photoluminescence at 77 K, the thermal stress and crystal quality of narrow strips of GaAs (width varying between 4 and 100 μm) fabricated by both selective-area MBE and chemical etching have been studied. The presence of polycrystalline GaAs surrounding crystalline GaAs had no measurable effect on the thermal stress in the crystalline region. However, in chemically etched GaAs strips grown on Si, the thermal stress decreased monotonically with strip width and became constant for strip width below 7 μm. In strips with width <7 μm, the photoluminescence spectra became polarized. A theoretical analysis of the degree of polarization indicated that the stress distribution in these narrower strips was uniaxial instead of biaxial, as found in the broader strips.

2. Effect of Pressure on the DX Centers in GaAs and Related GaAlAs Semiconductor Alloys (Publications 4, 8, 13, and 14)

M. Li,† W. Shan, and P.Y. Yu

Recently there has been much interest in the properties of a deep center known as the DX center found in GaAs and GaAlAs alloys. The pressure dependence of the activation energies for both capture and emission in these centers has been measured. The results are consistent with the large-lattice relaxation model for the structure of these centers. The behavior of these centers with a direct band gap was compared with the behavior of centers with an indirect band gap. When the band gap is direct, carriers are captured into the DX centers through the L valleys, while carriers are captured through the X valleys when the band gap is indirect.

*This work was supported by the Director, Office of Energy Research, Office of Basic Energy Sciences, Materials Sciences Division, of the U.S. Department of Energy under Contract No. DE-AC03-76SF00098.

†Present address: Graduate School, University of Science and Technology of China, Beijing, People's Republic of China.

3. Reduction of Persistent Photoconductivity due to DX Centers in GaAs by Boron (Publications 12 and 15)

M. Li,† W. Shan, and P.Y. Yu

Persistent photoconductivity in n-type GaAlAs and in GaAs under pressure has been attributed to deep centers known as DX centers. In studying these centers in GaAs contaminated by boron during liquid-encapsulated Czochralski growth, it was discovered that boron could reduce persistent photoconductivity in the DX center by decreasing its capture barrier height. This effect of boron was confirmed by implanting B into GaAs that did not contain B. An explanation of this effect of B is still lacking. Boron is an isovalent impurity in GaAs and is known to be electrically inactive in GaAs or GaAlAs alloys. A plausible explanation is that isovalent impurities such as B may reduce the lattice relaxation surrounding the donor atoms and hence minimize the effect of persistent photoconductivity. This finding may have significant impact on GaAs technology in making high-electron-mobility transistor (HEMT) devices practical.

†Present address: Graduate School, University of Science and Technology of China, Beijing, People's Republic of China.

4. Pressure Dependence of Schottky Barrier at the Pt/GaAs Interface (Publications 5 and 17)

W. Shan, M. Li,† and P.Y. Yu

It has been proposed that the pinning of the Fermi level in the middle of the band gap of GaAs and other III-V semiconductors results from intrinsic defects, such as EL2, or extrinsic defects created by the metal overlayers. This hypothesis has been tested by measuring the pressure dependence of the Schottky barrier height formed by Pt on GaAs and comparing the pressure coefficient with those of the known defects in GaAs. It was found that the Schottky barrier followed the valence band as a function of pressure. This result rules out defects such as EL2 as being responsible for the Schottky barrier. On the other hand, this result was consistent with other intrinsic defects, such as E3 and E4, as responsible for pinning the Fermi level.

†Present address: Graduate School, University of Science and Technology of China, Beijing, People's Republic of China.

5. Pressure Dependence of Defect Centers at the [111] Si/SiO_2 Interface (Publication 11)

W. Shan and P.Y. Yu

Defects at the Si/SiO_2 interface are very important for Si electronic devices and have been studied extensively. An amphoteric paramagnetic center, known as the P_b center, has been identified by electron-spin resonance and electrical measurements. Two models have been proposed to explain the origin of the P_b center. On model involves a threefold coordinated Si with a dangling bond, while the other model suggested a overcoordinated Si with a "floating bond." Edwards predicted that the one-to-two-hole transition of the P_b center would shift toward the valence band for a dangling bond and toward the conduction band for the floating bond. In collaboration with Dr. Noble Johnson of Xerox Palo Alto Research Center, the pressure dependence of the one-to-two-hole transition of the P_b center has been determined using the diamond anvil cell and constant-capacitance DLTS. The transition was found to shift toward the valence band at a rate of about -1.2 meV/kbar, in good quantitative agreement with the predictions of the dangling-bond model.

1988 PUBLICATIONS AND REPORTS

Refereed Journals

1. H.P. Lee, S. Wang, Y.H. Huang, and P.Y. Yu, "Photoluminescence Studies of Selective-Area Molecular Beam Epitaxy of GaAs Film on Si Substrate," Appl. Phys. Lett. **52**, 215 (1988).
2. Y. Huang, P.Y. Yu, H. Lee, and S. Wang, "Characterization of GaAs Film Grown on Si Substrate by Photoluminescence at 77 K," Appl. Phys. Lett. **52**, 579 (1988); LBL-24554.
3. Y. Huang and P.Y. Yu, "A Variable Band Pass Filter with High Rejection Ratio for Raman Scattering," Rev. Sci. Instrum. **59**, 190 (1988); LBL-23957.
4. P.Y. Yu and M. Li, "Comment on 'New Evidence of Small Lattice Relaxation for the DX Center in $Al_xGa_{1-x}As$'," Appl. Phys. Lett. **52**, 1645 (1988).
5. W. Shan, M.F. Li, P.Y. Yu, W.L. Hansen, and W. Walukiewicz, "Pressure Dependence of Schottky Barrier Height at Pt/GaAs Interface," Appl. Phys. Lett. **53**, 974 (1988); LBL-25653.
6. H.P. Lee, X. Liu, H. Lin, J.S. Smith, S. Wang, Y.-H. Huang, P. Yu, and Y.-Z. Huang, "Tensile Stress Variations of Chemically Etched GaAs Films Grown on Si Substrate," Appl. Phys. Lett. **53**, 2394 (1988).

7. P.Y. Yu, "Thermalization of Excitons," Prog. Solid State Chem. **18**, 201 (1988); LBL-24762.
8. M.F. Li, W. Shan, P.Y. Yu, W.L. Hansen, E.R. Weber, and E. Bauser, "Pressure Dependence of the DX Center in GaAlAs:Te in the Vicinity of the b-X Cross-over," Appl. Phys. Lett. **53**, (1988); LBL-25568.
9. D. Erskine, P.Y. Yu, and S.C. Freilich, "High Pressure Visible Spectroscopy of Polyimide Film," J. Polymer Sci. C **26**, 465 (1988); LBL-24553.

Other Publications

10. P.Y. Yu and C. Kittel, "Polyexcitons in Ultrapure Silicon," Nature **332**, 783 (1988).
11. N.M. Johnson, W. Shan, and P.Y. Yu, "Pressure Dependence of the P_b Center at the $<111>$ Si-SiO_2 Interface," Phys. Rev. B **39**, 3431 (1989); LBL-26396.
12. M.F. Li, P.Y. Yu, W. Shan, W. Hansen, and E.R. Weber, "Effect of Boron on the Pressure Induced Deep Donors in GaAs:Si," LBL-25329.
13. M.F. Li, W. Shan, P.Y. Yu, W.L. Hansen, E.R. Weber, and E. Bauser, "Lattice Relaxation of the DX Centers in $Ga_{1-x}Al_xAs$ and of the Pressure-induced Deep Donors in GaAs," in *Defects in Electronic Materials*, MRS Symp. Proc. Vol. 104, M. Stavola, S.J. Pearton and G. Davies, eds., MRS, Pittsburgh, PA, 1988, p. 573; LBL-24523.

Invited Talks

14. M.F. Li, P.Y. Yu, W. Shan, W.L. Hansen, and E.R. Weber, "A Comparison of the Pressure-induced Deep Donors in GaAs:Si and the DX Centers in GaAlAs:Si Alloys," presented at the 19th International Conference on the Physics of Semiconductors, Warsaw, Poland, Aug. 1988; LBL-25689.
15. M.F. Li, P.Y. Yu, W. Shan, W.L. Hansen, and E.R. Weber, "Reduction of Capture Barrier Height of Pressure-induced Deep Donors (DX Center) in GaAs:Si," presented at the 15th International Conference on Defects in Semiconductors, Budapest, Hungary, Aug. 1988; LBL-25692.
16. M.F. Li, W. Shan, P.Y. Yu, W.L. Hansen, E.R. Weber, and E. Bauser, "Pressure Dependence of the DX Center in $Al_{0.35}Ga_{0.65}As$:Te," presented at the 15th International Conference on Defects in Semiconductors, Budapest, Hungary, Aug. 1988; LBL-25690.
17. W. Shan, M.F. Li, P.Y. Yu, W.L. Hansen, and W. Walukiewicz, "Pressure Dependence of Schottky Barrier Height at Pt/GaAs Interface," presented at the 15th International Conference on Defects in Semiconductors, Budapest, Hungary, Aug. 1988; LBL-25691.
18. P.Y. Yu, "Superconductivity and Other Studies of Electrical Properties," Gordon Research Conference on Research at High Pressures, Meriden, NH, June 28, 1988.†
19. P.Y. Yu, "Ultrafast Processes in Semiconductors and Devices," Physics Lecture Series, Department of Physics, San Jose State University, San Jose, CA, Oct. 6, 1988.

†Also supported by the Director's Exploratory Research and Development Fund of Lawrence Berkeley Laboratory under Contract No. DE-AC03-76SF00098.

Superconductivity, Superconducting Devices, and 1/f Noise*

John Clarke, Investigator

INTRODUCTION

DC Superconducting QUantum Interference Devices (SQUIDs) based on a niobium technology are applied to a wide variety of applications, including geophysics, nuclear magnetic resonance, and the study of noise in high-temperature superconductors. Measurements on high-temperature superconductors such as YBaCuO, BiCaSrCuO, or TlCaBaCuO yield information concerning the dependence of the low-frequency magnetic-flux noise on temperature and the microstructure of the materials, and guide the design of devices operating at liquid-nitrogen temperatures. Measurements of voltage noise at the resistive transition of superconductors yield information on the nature of the transition and are used to design superconducting bolometers. Sensitive SQUID amplifiers involving a tuned input circuit and a novel Q-spoiler are used to detect nuclear magnetic resonance (NMR) and nuclear quadrupole resonance (NQR) in the frequency range 20–50 MHz. This system is being applied to magnetic resonance of surface layers. SQUIDs with superconducting input circuits are able to detect zero-field NMR or NQR at frequencies as low as 20 kHz in organic and amorphous materials. These data provide information on the magnetic fields and electric-field gradients at the active nuclei. Submicron tunnel junctions are being investigated at ultralow temperatures to test new theories of macroscopic quantum phenomena such as Bloch oscillations.

1. Flux Noise in Thin Films (Publications 5 and 19)

M.J. Ferrari, M. Johnson, J. Clarke, P.A. Rosenthal,† R.H. Hammond,† and M.R. Beasley†

One of the earliest applications of the high-T_c thin films is to SQUIDs. A SQUID consists of a superconducting loop interrupted by one or two Josephson junctions. The voltage produced by the SQUID is periodic in the applied magnetic flux. The device is an exceedingly sensitive detector of flux and has wide-ranging applications, from biomagnetism to geophysics. High-T_c SQUIDs made at IBM and elsewhere exhibit high levels of low-frequency noise, and the present project was designed to investigate the origin of this noise. In the experiment, a thin film of $YBa_2Cu_3O_7$ (YBCO), made at Stanford, was patterned into a 1-mm-square washer with a 200-μm-square hole in the middle. The film was mounted very close to a conventional Nb-based SQUID, the whole assembly being surrounded by a vacuum can. The SQUID was maintained at 4.2 K, while the temperature of the film could be raised to the transition temperature of the YBCO. Any flux noise generated in the film was measured by the SQUID. It was found that high levels of 1/f flux noise (where f is frequency) were generated by the YBCO films in the frequency range studied, $1–10^3$ Hz. The magnitude of the noise increased with temperature, as shown in Figure 1-1. Furthermore, at a given temperature the magnitude of the noise decreased as the quality of the film was improved. In Figure 1-1, the data with squares were obtained from a polycrystalline film with $T_c = 47$ K, those with triangles from a mixed a- and c-axis film with $T_c = 85$ K and a critical current (J_c) of 2×10^4 A cm^{-2} at 4.2 K, and those with circles from a predominantly c-axis film with $T_c = 85$ K and $J_c = 5 \times 10^6$ A cm^{-2}. The noise arises from the thermally activated hopping of flux vortices, possibly trapped at grain boundaries. From these

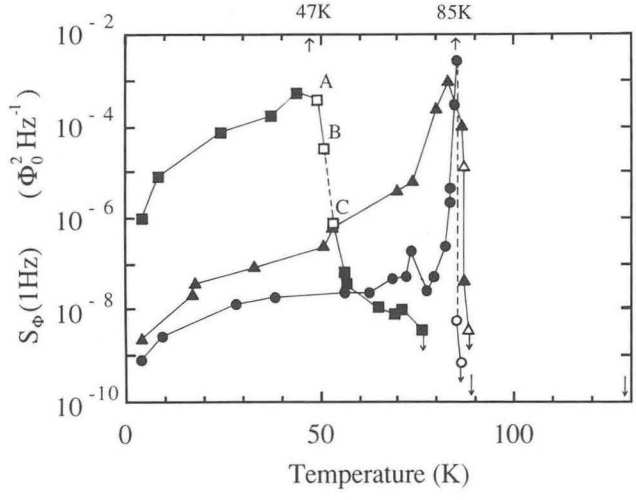

Figure 1-1. Spectral density of flux noise at 1 Hz vs temperature for three samples of YBCO. (XBL 889-3440)

*This work was supported by the Director, Office of Energy Research, Office of Basic Energy Sciences, Materials Sciences Division, of the U.S. Department of Energy under Contract No. DE-AC03-76SF00098.

results, one concludes that to obtain low noise, one must fabricate SQUIDs and circuits connected to them of very high quality films.

---

†Permanent address: Department of Applied Physics, Stanford University, Stanford, CA 94305.

2. Noise at the Resistive Transition: Bolometers (Publications 17 and 18)

P. Lerch, R. Leoni, J. Clarke, S. Verghase, P.L. Richards, M.R. Beasley,† T.H. Geballe,† R.H. Hammond,† P.A. Rosenthal,† and S.R. Spielman†

In the mid-1970s, Clarke, Richards, Hoffer, and Yeh developed a very sensitive far-infrared bolometer involving a thin film of aluminium at the midpoint of the superconducting transition. The bolometer consists of a substrate, coated with an absorbing film on one side, suspended in a vacuum can by leads providing weak thermal contact to the heat bath. When radiation falls on the bolometer, the resulting increase in temperature is detected by the increase in the resistance of the aluminium film, which serves as a very sensitive thermometer. The advent of high-T_c superconductivity opens up the possibility of operating a transition-edge bolometer at temperatures above the boiling point of liquid N_2 (77 K), and this project was aimed at investigating the noise limitations in this application.

Thin films of YBCO, made at Stanford, were patterned into narrow strips, with four terminals to enable one to measure the resistance and voltage noise at constant current. Each sample was mounted on a brass block suspended in a vacuum can immersed in liquid N_2. The temperature of the block could be raised above that of the bath with a resistive heater, and the resistance of the film was measured as a function of temperature. The spectral density of the voltage noise $S_v(f)$ was measured as a function of bias current I and of temperature through the resistive transition. $S_v(f)$ varied approximately as I^2/f through the transition. Figure 2-1 shows $S_v^{1/2}(10\ \text{Hz})/\bar{V}$, where $\bar{V} = I\bar{R}$ and $\bar{R}$ is the average value of the resistance, vs temperature T for two films.

Sample A was a polycrystalline film with a semiconducting behavior at temperatures above a broad transition, while film B was epitaxially grown and showed a metallic behavior above a relatively narrow transition. We see from Figure 2-1 that the normalized voltage noise is substantially lower in B than

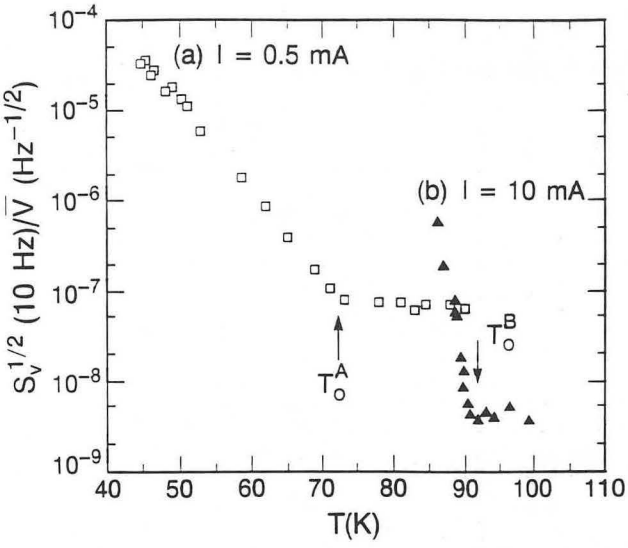

Figure 2-1. Normalized voltage noise $S_v^{1/2}$ (10 Hz) /$\bar{V}$ vs temperature for two samples of YBCO. (XBL 888-7517)

in A. From these data and measurements of dR/dT, we find that the temperature resolution set by 1/f noise can be as high as 10^{-8} K $Hz^{-1/2}$ at 10 Hz.

The measured 1/f noise is sufficiently low that a superconducting bolometer based on a YBCO thermometer looks extremely promising. An optimization procedure indicates that it should be possible to fabricate bolometers operating at 90 K with noise equivalent powers (NEP) in the range $(1–20) \times 10^{-12}$ $WHz^{-1/2}$. These values compare very favorably with the NEP of other detectors operating at or above liquid N_2 temperatures for wavelengths greater than 20 μm.

---

†Permanent address: Department of Applied Physics, Stanford University, Stanford, CA 94305.

3. Low-Field Nuclear Magnetic Resonance with SQUID Amplifiers (Publication 21)

N.Q. Fan, J. Clarke, E.L. Hahn, A. Bielecki, and A. Pines

An NMR spectrometer based on a dc SQUID has been developed for frequencies below 250 kHz. The primary goal of this spectrometer is to perform NMR in zero magnetic field. As a preliminary demonstration, however, we have used the spectrometer to observe NMR in ^{195}Pt at 4.2 K with applied magnetic fields of a few tens of gauss.

The configuration of the spectrometer is shown in Figure 3-1. The flux-locked loop can track signals

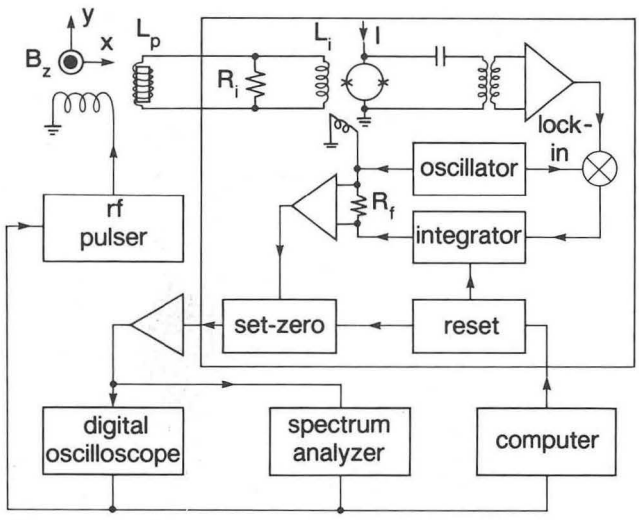

Figure 3-1. Experimental configuration of low-field NMR spectrometer. (XBL 888-7514)

at frequencies up to 250 kHz. After the radio-frequency pulse in the transmitter coil is turned off, the integrator in the feedback loop is reset, and the voltage across the feedback resistor R_f is held at zero until the feedback circuit has stabilized. When the feedback circuit is enabled, the precessing nuclear spins in the sample induce an oscillating magnetic flux in the pickup coil that is coupled into the SQUID via a superconducting transformer. The signal from the flux-locked loop is filtered, amplified, and transmitted to the digital oscilloscope for time-domain analysis and the spectrum analyzer for frequency-domain analysis. The entire system is computer controlled.

The spin of the ^{195}Pt nucleus is 1/2, and its gyromagnetic ratio is 0.95 kHz gauss^{-1}. It has a T_2 of 1.1 msec and a T_1 of 10 msec. We carried out the NMR experiments in magnetic fields ranging from 30 gauss to 200 gauss, applying a radiofrequency pulse every 0.5 sec to initiate the free-induction decay (FID). Typically, the pulse was about 2 gauss peak-to-peak and 0.4 msec long. Experimental results in a 60-gauss field are shown in Figure 3-2: (a) is the real-time trace of the average of 256 FID signals, while (b) is the square of the Fourier transform of the average of 40 FID signals. The measured resonant frequency is 54.75 kHz. The high sensitivity achieved in this experiment implies that it should be possible to make a direct detection of the zero-field NMR signal from amorphous and polycrystalline materials.

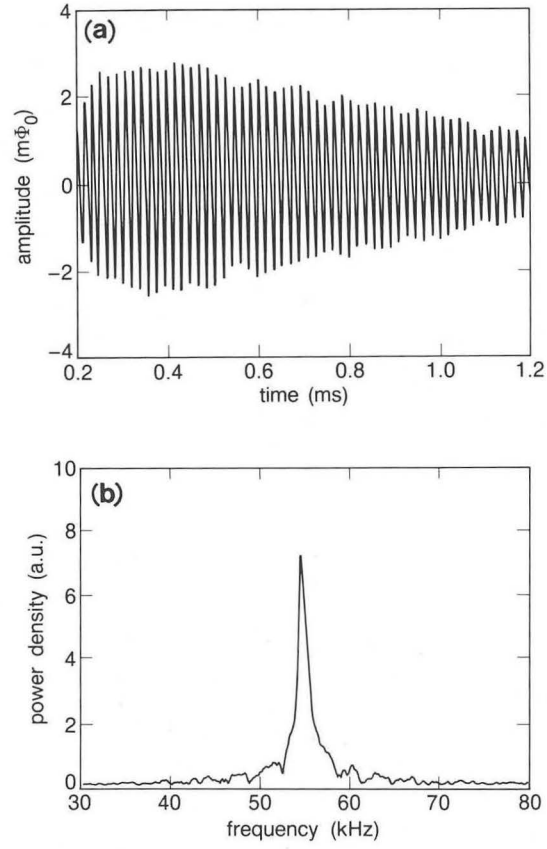

Figure 3-2. Observation of low-field NMR in ^{195}Pt powder at 60 gauss: (a) free-induction decay (expressed in units of flux in the SQUID), and (b) the square of the Fourier transform of the free-induction decay. (XBL 888-7513)

4. Hot-Electron Effect in the dc SQUID (Publications 12, 16, and 20)

F.C. Wellstood, C. Urbina, and J. Clarke

The noise energy of the dc SQUID at frequencies above the 1/f noise region scales as the temperature T, reflecting the fact that the noise originates as Nyquist noise in the resistors shunting the two Josephson junctions. We have studied the noise of SQUIDs cooled in a dilution refrigerator to temperatures as low as 20 mK. We found that the white-noise energy $S_\phi(f)/2L$ of typical devices flattened out at a value corresponding to a bath temperature of 150 mK, even though the SQUID was cooled to 20 mK; here, $S_\phi(f)$ is the spectral density of the flux noise, and L is the inductance of the SQUID loop.

A detailed investigation of this saturation showed that it arose from heating of the electrons in the shunt resistors by the current biasing the SQUID. The bottleneck in the cooling process turns out to be

the rate at which the electrons can transfer energy to the phonons, which are at or very near to the bath temperature. It can be shown under certain simplifying assumptions that the electron temperature T_e is given by $P = \Sigma\Omega(T_e^5 - T_p^5)$, where P is the power dissipated in the shunts, which have volume Ω, T_p is the phonon temperature, and Σ is a proportionality constant, found experimentally to be $(2.4 \pm 0.6) \times 10^9\ WK^{-5}\ m^{-3}$.

We have been able to reduce the heating significantly by attaching a large cooling fin to each shunt. The fins are made of the same metal as the shunts, Au (25% Cu), and are about $0.4 \times 0.4\ mm^2$ in area. Hot electrons from the shunts diffuse into the fins, where they exchange energy with large numbers of cooler electrons and phonons, thereby cooling very rapidly. Figure 4-1 shows the noise energy in units of $\hbar$ vs the bath temperature for two conventional SQUIDs and two SQUIDs with cooling fins. We see that the noise energies for the former flattened out at about 15 $\hbar$, while those of the latter decreased to about 4 or 5 $\hbar$ at 20 mK. We note that similar effects are expected in any dc SQUID operated at temperatures below 100 to 200 mK, and that it will be necessary to use cooling fins to take advantage of operation at lower bath temperatures.

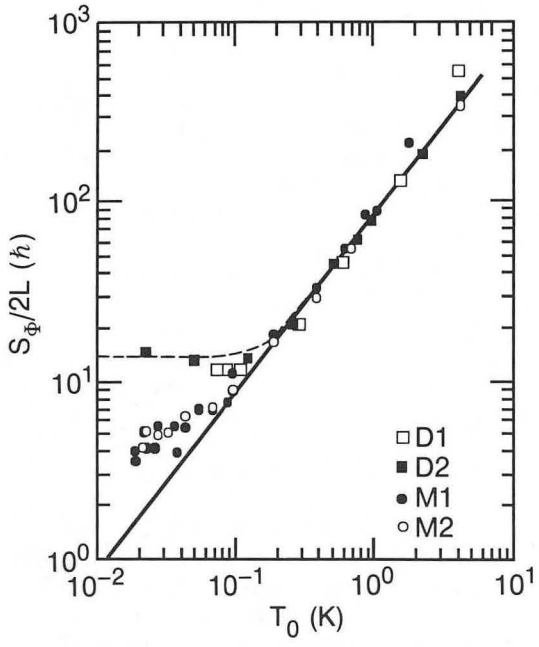

Figure 4-1. Flux-noise energy vs bath temperature for two conventional SQUIDs, D1 and D2, and two SQUIDs with cooling fins, M1 and M2. The solid line is the prediction of the theory, assuming heating is negligible. (XBL 891-5012)

1988 PUBLICATIONS AND REPORTS

Refereed Journals

1. J. Clarke, A.N. Cleland, M.H. Devoret, D. Esteve, and J.M. Martinis, "Quantum Mechanics of a Macroscopic Degree of Freedom: The Phase Difference across a Josephson Tunnel Junction," Science **239**, 992 (1988); LBL-24144.
2. A.N. Cleland and J.M. Martinis, "Measurement of the Effect of Moderate Dissipation on Macroscopic Quantum Tunneling," Phys. Rev. B Rapid Commun. **37**, 5950 (1988); LBL-23877.
3. J. Clarke, "Small-scale Analog Applications of High-Transition-Temperature Superconductors," Nature **333**, 29 (1988); LBL-25001.
4. B. Savo, F.C. Wellstood, and J. Clarke, "Response to Comment on 'Low-Frequency Excess Noise in Nb-Al_2O_3-Nb Josephson Tunnel Junctions'," Appl. Phys. Lett. **52**, 2001 (1988); LBL-25190.
5. M.J. Ferrari, M. Johnson, F.C. Wellstood, J. Clarke, P.A. Rosenthal, R.H. Hammond, and M.R. Beasley, "Magnetic Flux Noise in Thin-Film Rings of $YBa_2Cu_3O_{7-d}$," Appl. Phys. Lett. **53**, 695 (1988); LBL-25352.
6. J. Clarke and R.H. Koch, "The Impact of High-Temperature Superconductivity on SQUID Magnetometers," Science **242**, 217 (1988).
7. M.H. Devoret, J.M. Martinis, D. Esteve, and J. Clarke, "Macroscopic Quantum Mechanics Experiments," Helvetica Physica Acta **61**, 622 (1988); LBL-24693.
8. T. Sleator, E.L. Hahn, M.B. Heaney, C. Hilbert, and J. Clarke, "Nuclear Quadrupole Induction of Atomic Polarization," Phys. Rev. B **38**, 8609 (1988); LBL-25191.
9. E.A. Nichols, H.F. Morrison, and J. Clarke, "Signals and Noise in Measurements of Low Frequency Geomagnetic Fields," J. Geophys. Res. **93**, 743 (1988); LBL-24325.
10. J. Pelz, J. Clarke, and W.E. King, "Flicker (l/f) Noise in Copper Films due to Radiation-Induced Effects," Phys. Rev. B **38**, 371 (1988); LBL-25192.
11. D.J. Scalapino, D.R. Clarke, J. Clarke, R.E. Schwall, A.F. Clark, and D.K. Finnemore, "New Research Opportunities in Superconductivity," Cryogenics **28**, 711 (1988).

Other Publications

12. F.C. Wellstood, C. Urbina, and J. Clarke, "Hot Electron Effect in a dc SQUID at 20 mK," Bull. Am. Phys. Soc. **33**, 263 (1988); LBL-24439abs.
13. J. Clarke, "The Impact of High-T_c Superconductivity on Superconducting Quantum Interference Devices," Bull. Am. Phys. Soc. **33**, 461 (1988); LBL-24441abs.
14. J. Clarke, C. Hilbert, E.L. Hahn, and T. Sleator, U.S. Patent No. 4,733,182, Mar. 22, 1988: Josephson Junction Q-Spoiler.

LBL Reports

15. J. Pelz (Ph.D. Thesis), "Flicker (l/f) Noise in Copper Films Due to Radiation-Induced Defects," LBL-24568.
16. F.C. Wellstood (Ph.D. Thesis), "Excess Noise in the dc SQUID; 4.2 K to 20 mK," LBL-26443.
17. P.L. Richards, J. Clarke, R. Leoni, P. Lerch, S. Verghase, M.R. Beasley, T.H. Geballe, R.H. Hammond, P.A. Rosenthal, and S.R. Spielman, "Feasibility of the High T_c Superconducting Bolometer," accepted by Appl. Phys. Lett.; LBL-26113.
18. P.A. Rosenthal, R.H. Hammond, M.R. Beasley, R. Leoni, P. Lerch, and J. Clarke, "Low Frequency Resistance Fluctuations in Films of High Temperature Superconductors," accepted by IEEE Trans. Magn.; LBL-26235.
19. M.F. Ferrari, M. Johnson, F.C. Wellstood, J. Clarke, P.A. Rosenthal, R.H. Hammond, and M.R. Beasley, "Flux Noise and Creep in YBCO Thin Films," accepted by IEEE Trans. Magn.; LBL-26237.
20. F.C. Wellstood, C. Urbina, and J. Clarke, "Hot Electron Effect in the dc SQUID," LBL-26236.
21. N.Q. Fan, M.B. Heaney, J. Clarke, D. Newitt, L.L. Wald, E.L. Hahn, A. Bielecki, and A. Pines, "Nuclear Magnetic Resonance with dc SQUID Preamplifiers," LBL-26234.
22. J. Clarke, "SQUID Concepts and Systems," LBL-26444.
23. J. Clarke, "Principles and Applications of SQUIDs," LBL-26445.
24. J. Clarke, "SQUIDs: Principles, Noise and Applications," LBL-26446.

Invited Talks

25. J. Clarke, "Effects of Dissipation on Macroscopic Quantum Tunneling and Quantized Energy Levels," Gordon Conference on Superconducting Films, Oxnard, CA, Jan. 13, 1988.
26. J. Clarke, "Macroscopic Quantum Tunneling and Quantized Energy Levels in Josephson Tunnel Junctions," Department of Physics, Caltech, Pasadena, CA, Jan. 28, 1988.
27. J. Clarke, "Impact of High-T_c Superconductivity on SQUIDs," International Superconductor Applications Convention, Los Angeles, CA, Feb. 17, 1988.
28. J. Clarke, "The Impact of High-T_c Superconductivity on Superconducting Quantum Interference Devices," March Meeting, American Physical Society, New Orleans, LA, Mar. 21–25, 1988.
29. J. Clarke, "High-T_c Superconductivity, SQUIDs and Brains," Annual Scientific and Dinner Meeting, Gastroenterology Division, University of California at San Francisco, Mar. 30, 1988.
30. J. Clarke, "Superconducting Quantum Interference Device," 26th Annual Northern California–Western Nevada Junior Science and Humanities Symposium, Lawrence Hall of Science, Berkeley, CA, Apr. 7, 1988.
31. J. Clarke, "Superconducting Electronics," Workshop on Research Opportunities in Superconductivity, Copper Mountain, CO, Apr. 10–12, 1988.
32. J. Clarke, "Small Scale Applications of Superconductivity," President Reagan's Advisory Group on Superconductivity, New York, Apr. 19, 1988.
33. J. Clarke, "Impact of High-Temperature Superconductivity on SQUIDs," Department of Physics, University of Illinois, Urbana, Apr. 28, 1988.
34. J. Clarke, "Macroscopic Quantum Tunneling and Quantized Energy Levels in Josephson Tunnel Junctions," Department of Physics, University of Illinois, Urbana, Apr. 28, 1988.
35. J. Clarke, "Analog Superconducting Electronics," California State University, Sacramento, May 3, 1988.
36. F.C. Wellstood, "SQUIDs at MilliKelvin Temperatures," Low Temperature Physics Seminar, Stanford University, Stanford, CA, May 5, 1988.
37. J. Clarke, "SQUIDs: Yesterday, Today and Tomorrow," Physics of Materials and Devices, Harvard University, Cambridge, MA, May 14, 1988.
38. J. Clarke, "Research and Development of Superconductivity in the U.S.A.," 25th Anniversary Meeting, Metal Mining Agency of Japan, Tokyo, May 27, 1988; LBL-25360.
39. J. Clarke, "Progress on High Transition Temperature SQUIDs," International Superconductivity Technology Center, Tokyo, Japan, May 30, 1988.
40. J. Clarke, "The Impact of High Temperature Superconductivity on SQUIDs," 5th International Workshop on Future Electron Devices: Topical Meeting on High-Temperature Superconductivity Electron Devices, Miyagi-Zao, Japan, June 4, 1988; LBL-25257abs.
41. J. Clarke, "SQUID-Magnetometers," 1st Topsøe Summer School on Superconductivity, Risø, Roskilde, Denmark, June 20, 1988.
42. J. Clarke, "Present and Future SQUIDs," European Physical Society Workshop "SQUID: State of the Art, Perspectives and Applications," Rome, Italy, June 27, 1988.
43. J. Clarke, "SQUID Concepts and Systems I," NATO Advanced Study Institute: Superconducting Electronics, Il Ciocco, Italy, June 28, 1988.
44. J. Clarke, "SQUID Concepts and Systems II," NATO Advanced Study Institute: Superconducting Electronics, Il Ciocco, Italy, June 29, 1988.
45. J. Clarke, "SQUID Geophysics," NATO Advanced Study Institute: Superconducting Electronics, Il Ciocco, Italy, June 30, 1988.
46. J. Clarke "SQUID Amplifiers and Their Applications," NATO Advanced Study Institute: Superconducting Electronics, Il Ciocco, Italy, July 1, 1988.
47. J. Clarke, "Quantum Mechanics of a Macroscopic Degree of Freedom," Ohio State University, Columbus, OH, Oct. 18, 1988.
48. J. Clarke, "Analog Applications of High-T_c Superconductors," Second Canadian Symposium on High

Temperature Superconductivity, Vancouver, BC, Oct. 29, 1988.

49. J. Clarke, "SQUIDs (Superconducting QUantum Interference Devices)," conference on the Science and Technology of Thin-Film Superconductors, Colorado Springs, CO, Nov. 14, 1988.
50. J. Clarke, "SQUIDs, Brains and Gravity Waves," Society of Physics Students, University of California at Berkeley, Nov. 18, 1988.

Studies of the Metal/Solution Interface with X Rays*

Philip N. Ross, Investigator

INTRODUCTION

During the last two decades there have been great advances in the development of methods for the analysis of the structure of surfaces in ultrahigh vacuum (UHV), which has led to a detailed understanding of the chemistry of free surfaces. Further advances of comparable magnitude will be necessary to develop an equivalent level of understanding of structure at interfaces, particularly the technologically important cases of interfaces between condensed phases. In this work, we address the problem of structure determination at the metal/solution interface. Study of the metal/solution interface is relevant to technologies like metal corrosion, electrochemical energy conversion (fuel cells), and storage devices (batteries), and the rapidly growing new technology of electrolytic epilayers for photovoltaics, magnetic recording, and electro-optic devices.

The problem of structure determination at the interface between condensed phases is a difficult one. Most of the techniques developed for the study of solid surfaces in UHV cannot be applied to the interface between condensed phases, since they rely on the diffraction, scattering, or emission of electrons. The electrons scattered or emitted from the interface are too severely attenuated by the condensed phases for external detection and analysis. New techniques must be developed that utilize more penetrating, higher-momentum photons like x rays, gamma rays, or neutrons. We are pursuing the use of x rays, and especially x-ray diffraction, for structure determination at the metal/solution interface.

In recent years there have been several approaches to the development of surface-sensitive x-ray diffraction, including x-ray standing waves, direct-transmission diffraction from thin substrates, and grazing-incidence Bragg diffraction at the critical angle for total reflection (GID). The grazing-incidence geometry appears to be the most generally applicable technique for our purposes. GID is a very new surface tool that has been used only a few times, for some solid/solid interfaces (multilayers) and submonolayer metal/metal surfaces in UHV. Prior to this study, the application of GID to a solid/liquid interface was a totally new experiment.

*This work was supported by the Director, Office of Energy Research, Office of Basic Energy Sciences, Materials Sciences Division, of the U.S. Department of Energy under Contract No. DE-AC03-76SF00098.

1. An *In Situ* Grazing-Incidence X-Ray Diffraction Study of the Initial Stages of Electrochemical Growth of Lead on Silver (111) (Publication 3)

J. Kortright† and P. Ross

The first layer of lead atoms on Ag(111) electrodeposited from acetate or perchlorate solution forms a hexagonal close-packed 2D lattice (see Figure 1-1) that is incommensurate with the silver lattice due to the large atomic mismatch (~18%). The monolayer is stable over an ~180 mV region of electrochemical potential. Within this potential region, the 2D lattice constant is a function of potential, with Pb-Pb distance decreasing with increasing cathodic potential to a maximum compression of 2.8% (versus bulk Pb) at the onset of multilayer growth. The twist angle between the Pb and Ag(111) lattice vectors was 4.4° and was independent of potential. The Novaco-McTague theory of rotational epitaxy predicts a 6.5° angle for an atomic-size mismatch of 18%, and a change of 0.5° in twist angle even for a change in 2D lattice constant of only 1.5%. These deviations from theory are not understood but may come from buckling of the Pb layer along with compression. Because of the compressive strain, lead was not deposited epitaxially on this first layer but instead grew in multilevel islands oriented in the direction normal to the substrate but randomly

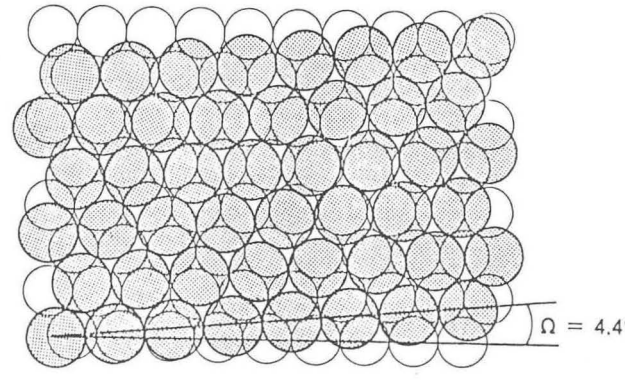

Figure 1-1. Schematic representation of one domain of the first layer of lead electrodeposited on Ag(111); open circles represent the silver atoms of the (111) surface, and shaded circles represent the lead atoms. The Pb monolayer is incommensurate, and one Pb atom is arbitrarily shown in a commensurate threefold hollow site. The rotational epitaxy angle Ω is 4.4°. (XBL 894-1259)

misoriented in the plane of the substrate. The initial underpotentially deposited monolayer (i.e., the strained epilayer) reconstructs after the deposition of approximately five "equivalent monolayers" of bulk lead. This apparently relieves the stress resulting from the lattice mismatch between the compressed monolayer and the bulk deposit. The deposition of a relatively thick layer, such as 100 monolayer equivalents, results in a (111) fiber texture structure.

---

†Permanent address: Center for X-Ray Optics, Accelerator and Fusion Research Division, LBL.

2. Potential-Dependent Reconstruction of Au(111) and (100) Surfaces in Solution (Publication 4)

M. Van Hove and P. Ross

GID experiments provided the first *in situ* evidence for the reconstruction of Au(111) in aqueous solution. The in-plane (2θ) scan (see Figure 2-1) clearly showed the appearance of superlattice reflections of periodicity $\sim a_0/20$, about the same as the superlattice periodicity of the ($\sqrt{3} \times 22$) reconstruction observed in UHV. This reconstruction is observed at potentials cathodic to the potential of zero charge (PZC) and is postulated to arise from the localization of electron density in the surface layer when solvated cations contact the surface at negative bias (potentials cathodic to the PZC).

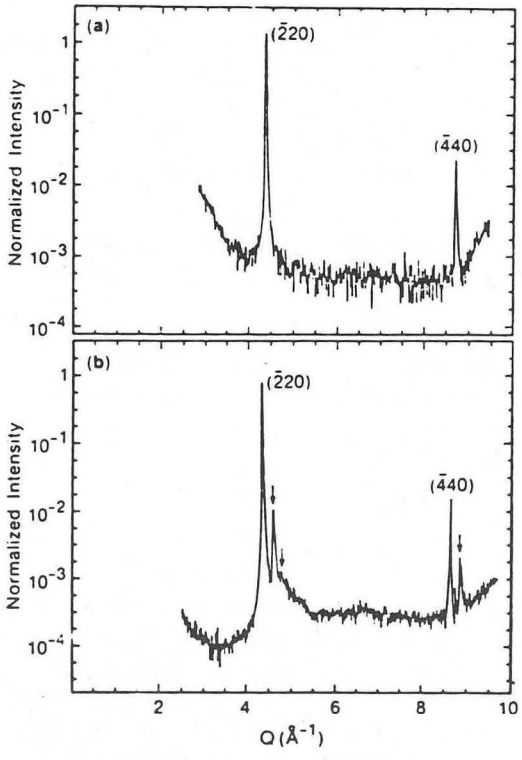

Figure 2-1. In-plane (2θ) scan of x rays scattered from a Au(111) crystal emersed in 0.3M HF + 0.1mM CsF solution at a potential 0.5 V anodic to the PZC (a); a potential 0.5 V cathodic to the PZC (b). (XBL 894-1260)

3. Work in Progress

The reconstruction of the Au(111) and (100) surfaces at potentials cathodic to the PZC into structures that appear to be related to the UHV reconstructions are being studied in detail using both x-ray reflectivity measurements and GID. The type of cation in the electrolyte, as well as the chemistry of the ion-metal interaction, is expected to play an important role in the reconstruction. Also of interest here are other metals whose clean low-index surfaces are not reconstructed in UHV but become reconstructed when alkali metals are placed on the surface, such as the (1 × 2) reconstructions of Ag(110), Pd(110), and Cu(110) caused by K adsorption. Such reconstructions may also occur on these surfaces at potentials cathodic to their PZCs in potassium-containing electrolyte, depending on the effect of solvation on the alkali-metal/noble-metal interaction; i.e., reconstruction may occur only in electrolytes with weakly solvated cations like Cs.

1988 PUBLICATIONS AND REPORTS

Refereed Journals

1. A. D'Agostino and P.N. Ross, "LEED-Electrochemical Analysis of Au Single Crystals: Stability of the UHV Prepared Surfaces of Au(111) and (100) in Aqueous Electrolyte," Surf. Sci. **185**, 88 (1987); LBL-21972.
2. O. Melroy, M. Toney, G. Borges, M. Samant, J. Kortright, P. Ross, and L. Blum, "Two-Dimensional Compressibility of Electrolytically Deposited Pb on Ag(111)," Phys. Rev. B **38**, 10962 (1988); LBL-24454.
3. O. Melroy, M. Toney, G. Borges, M. Samant, J. Kortright, P. Ross, and L. Blum, "An *In-Situ* GIXS Study of the Initial Stages of Electrochemical Growth of Pb on Ag(111)," J. Electroanal. Chem. **258**, 403 (1989); LBL-25510.

LBL Reports

4. P.N. Ross, "Potential Induced Structural Transformations of the Au(100) and (111) Surfaces," submitted to Surf. Sci.; LBL-24442.

THEORETICAL RESEARCH

Theoretical Studies of the Electronic Properties of Solid Surfaces*

L.M. Falicov, Investigator

INTRODUCTION

The purpose of this program is to study properties of solid surfaces. In particular, the interest is in determining (a) structural properties of surfaces, namely the organization and arrangement of atomic constituents at equilibrium; (b) constitutional properties of the surface, in particular the segregation properties of alloys at the surface as a function of crystal structure, surface orientation, nominal chemical composition, and temperature; (c) electronic structure of surfaces, in particular electron states and electron densities in the neighborhood of the surface; (d) vibronic properties of surfaces; (e) magnetic properties of surfaces, both in magnetic solids (ferromagnetic and antiferromagnetic) and in nonmagnetic solids that may develop a magnetic surface layer; and (f) chemical properties of solids—in particular their catalytic properties—as they are related to all the basic physical properties listed above.

A variety of theoretical techniques and models have been developed to focus on the various properties (band-structure models, many-body electron physics, numerical relaxation techniques), but the emphasis is on physical aspects and their implication to experiments rather than on techniques *per se*.

Since 1978 a collaboration has been established with Dr. Eugene Haller and his group to study a set of unusual impurities in very pure semiconductors. These impurities had never been seen before and include hydrogen complexes, lithium-based complexes, carbon-nitrogen complexes, and ordinary substitutional impurities in an unusual charge state.

*This work was supported by the Director, Office of Energy Research, Office of Basic Energy Sciences, Materials Sciences Division, of the U.S. Department of Energy under Contract No. DE-AC03-76SF00098.

1. Exact Solution of a Periodic-Cluster Hubbard Model with an Electron-Lattice Interaction (Publication 3)

C.R. Proetto† and L.M. Falicov

An exact solution of a modified Hubbard model for a tetrahedral cluster with periodic boundary conditions is presented. It includes a static electron-lattice interaction in which the intersite bond-hopping parameter is a function of the bond electron occupation. It is found that the intrasite Coulomb repulsion and the effective attractive electron-lattice interaction have, generally speaking, opposite (although not identical) effects. They cancel each other exactly along a line of singularities in parameter space. The state vectors are easily obtained analytically. A study is made of magnetic and superconducting static correlation functions as functions of the parameters. Various forms of anisotropic superconducting fluctuations are favored in the various regimes. There is an indication of possible states with coexisting nonuniform, nonisotropic superconductivity and antiferromagnetism caused by a "compromise" between the competing forces.

†Permanent address: Centro Atómico Bariloche, Comisión Nacional de Energía Atómica, 8400 Bariloche, Argentina.

2. Incommensurable Magnetic Surface Structures for MnO-Type Antiferromagnetic Insulators (Publication 4)

D.C. Chrzan and L.M. Falicov

A calculation of the magnetic (001) surface structure of an antiferromagnetic insulator with the MnO spin arrangement is reported. The calculation is based on classical spins with Heisenberg interactions that are (a) between second neighbors throughout the bulk and surface, (b) between nearest-neighbor spins at the surface layer, and (c) between nearest-neighbor spins in the first and second layers. It is found that, for a range of exchange parameters, incommensurable ground-state structures are obtained.

3. Heavy-Fermion System: Superconducting and Magnetic Fluctuations within a Periodic-Cluster Hubbard Model (Publication 5)

A. Reich and L.M. Falicov

An exact solution of an eight-site crystal model with periodic boundary conditions, a small face-centered-cubic crystal, is presented for the case of a heavy-fermion system. The model consists of (a) a single, fully symmetric orbital per site, with nearest-neighbor and second-nearest-neighbor hopping; (b) an infinite Coulomb repulsion between electrons on the same site; (c) antiferromagnetic superexchange interactions; and (d) band fillings near half filling (six, seven, and eight electrons per cluster). The superconducting and the antiferromagnetic correlations are studied and compared with the predictions of the noninteracting limit. The suitability of Bardeen-Cooper-Schrieffer and Gutzwiller approximate ground-state wave functions are quantitatively estimated.

4. Work in Progress

An exact solution of a four-site crystal model with periodic boundary conditions, a {001} thin film with face-centered-cubic crystal structure, is being developed for the nickel density of electron states, as would be measured in surface-sensitive valence-band photoemission. The object is to study modifications of the many-body electronic structure in the presence of surfaces. A realistic local-density-approximation one-electron structure and intrasite electron-electron interactions most generally allowed by atomic symmetry are used. The crystal-field effect in the nickel film will be examined. The photoemission spectrum will be calculated and compared with the bulk result. Physical conclusions for true nickel surface many-body states are expected to be obtained.

1988 PUBLICATIONS AND REPORTS

Refereed Journals

1. A. Reich and L.M. Falicov, "Heavy-Fermion System: an Exact Many-Body Solution to a Periodic-Cluster Hubbard Model," Phys. Rev. B **37**, 5560 (1988); LBL-24099.
2. L. Milans del Bosch and L.M. Falicov, "Extended One-Dimensional Hubbard Model: a Small-Cluster Approach," Phys. Rev. B **37**, 6073 (1988); LBL-23704.
3. C.R. Proetto and L.M. Falicov, "Exact Solution of a Periodic-Cluster Hubbard Model with an Electron-Lattice Interaction," Phys. Rev. B **38**, 1754 (1988); LBL-24642.
4. D.C. Chrzan and L.M. Falicov, "Incommensurable Magnetic Surface Structures for MnO-type Antiferromagnetic Insulators," Phys. Rev. Lett. **61**, 1509 (1988); LBL-25336.
5. A. Reich and L.M. Falicov, "Heavy-Fermion System: Superconducting and Magnetic Fluctuations Within a Periodic-Cluster Hubbard Model," Phys. Rev. B **38**, 11199 (1988); LBL-24794.
6. C. Chen, A. Reich, and L.M. Falicov, "Surface Properties of a Heavy-Fermion System: an Exact Many-Body Solution to a Periodic-Cluster Hubbard Model," Phys. Rev. B **38**, 12823 (1988); LBL-25600.

Other Publications

7. L.M. Falicov, "A Periodic Small-Cluster Approach to Many-Body Problems," in *Recent Progress in Many-Body Theories*, Vol. 1, Plenum, New York, 1988, p. 275; LBL-23894.
8. L.M. Falicov, "An Overview of Recent Developments in High-Temperature Superconductivity," in *Proc. Annual European ICASE-Seminar of 1987*, ICASE and FK, Copenhagen, 1988, p. 19; LBL-24323.
9. L.E. Oliveira and L.M. Falicov, "Energy Spectra of Shallow Donors and Acceptors in GaAs–$Ga_{1-x}Al_xAs$ Superlattices," in *Current Topics in Semiconductor Physics*, World Scientific, Singapore, 1988, p. 31; LBL-23492.

LBL Reports

10. M.L. Cohen and L.M. Falicov, "Comment on the Magnon Pairing Mechanism of Superconductivity in Cuprate Ceramics," submitted to Science; LBL-26089.
11. D.C. Chrzan and L.M. Falicov, "Theoretical Phase Stability of Incommensurable Spin Structures on the {001} Surfaces of MnO-Type Antiferromagnetic Semiconductors," accepted by Phys. Rev. B; LBL-25875.
12. H. Svensmark and L.M. Falicov, "Ginzburg-Landau Theory of Deformable Superconductors," submitted to Phys. Rev. B; LBL-26090.
13. J.K. Freericks and L.M. Falicov, "Dephasing Effects in a Two-Dimensional Magnetic-Breakdown-Linked Network: Magnesium," submitted to Phys. Rev. B; LBL-26182.
14. C. Chen, A. Reich, and L.M. Falicov, "Surface Properties of a Heavy Fermion System: an Exact Many-Body Solution to a Periodic-Cluster Hubbard Model," LBL-26312.
15. D.C. Chrzan and L.M. Falicov, "Theoretical Phase Stability of Incommensurable Spin Structures on the {001} Surfaces of MnO-Type Antiferromagnetic Semiconductors," LBL-26313.

16. H. Svensmark and L.M. Falicov, "Ginzburg-Landau Theory of Deformable Superconductors," LBL-26314.
17. J. Heyman, L. Falicov, and E.E. Haller, "Fano Resonances in Beryllium Doped Silicon," LBL-26357.

Invited Talks

18. L.M. Falicov, "The Challenge of the New Materials," San Martin Theater, Buenos Aires, Argentina, June 2, 1988.
19. L.M. Falicov, "Superconductivity: Phenomenology," First Topsøe Summer School on Superconductivity, Risø, Roskilde, Denmark, June 20, 1988.
20. L.M. Falicov, "Models for High Temperature Superconductivity," First Topsøe Summer School on Superconductivity, Risø, Roskilde, Denmark, June 22, 1988.
21. L.M. Falicov, "Highly Correlated Metals: a Small-Cluster Approach," Annual Review, Materials and Chemical Sciences Division, LBL, Feb. 10, 1988.
22. L.M. Falicov, "Highly Correlated Metals: a Small-Cluster Approach to Heavy Fermions," Department of Applied Physics, Stanford University, Stanford, CA, Mar. 10, 1988.
23. L.M. Falicov, "Highly Correlated Metals: Heavy Fermions," Physics Colloquium, University of California, Santa Cruz, Mar. 31, 1988; Oak Ridge National Laboratory, Oak Ridge, TN, Nov. 3, 1988; VII Congress, Costa Rican Physics Association, San Jose, Costa Rica, Nov. 25, 1988.
24. L.M. Falicov, "1988: Open Problems in Condensed Matter Physics," Physics Colloquium, the Balseiro Institute, Bariloche, Argentina, June 1, 1988; Physics Department, University of Santiago, Chile, Sept. 12, 1988; VII Congress, Costa Rican Physics Association, San Jose, Costa Rica, Nov. 24, 1988.
25. L.M. Falicov, "Photoemission in Solids," VII Congress, Costa Rican Physics Association, San Jose, Costa Rica, Nov. 24, 1988.

Theoretical Solid-State Physics*

Marvin L. Cohen, Investigator

INTRODUCTION

Some of the focus of the theoretical work was to foster and maintain collaborations with the experimental programs at LBL in high temperature superconductivity. In other areas the theoretical activity ranged from the development of new theoretical tools and approaches to materials development. In the latter category was the exploration of the use of high pressures for creating new systems and the theoretical analyses of data related to existing novel systems.

HIGH-TEMPERATURE SUPERCONDUCTIVITY

A close collaboration was established with the experimental research group directed by Alex Zettl. Some of the properties of high-temperature superconducting oxides that were examined are (1) the use of neutron diffraction to explore magnetic interactions, (2) transport properties such as resistivity and thermopower, and (3) the oxygen-substituted isotope effect.

Another area of investigation centered on the theoretical interpretation of photoemission data of high-temperature superconductors. The goal was to extract correlation parameters from satellite structures. The satellite observed at a binding energy of 12–13 eV below the Fermi level in the high-T_c oxide superconductors $La_{2-x}Sr_xCuO_4$ and $YBa_2Cu_3O_{7-\delta}$ is viewed as originating from a state with two holes bound at the same Cu site. As in the case of Ni metal, the satellite is caused by an intra-d-shell shakeup process into a Cu $3d^8$ final state, and its intensity is enhanced at resonance because of a super-Koster-Kronig transition. Based on the t-matrix approach for the hole self-energy, we have studied the effect of electronic correlations on the one-electron band structure. We examined the position of the satellite and found a large Coulomb interaction energy of ~5 eV at the Cu site when the experimental satellite position is duplicated by the theory. Since this energy is comparable with the 3d bandwidth, the two-hole bound state is a high-energy excitation. This indicates that in the ground state a creation of two holes at the Cu site is unlikely, and thus holes are formed at the O sites when Sr is substituted for La in La_2CuO_4 and when the oxidation is increased in $YBa_2Cu_3O_{7-\delta}$.

1. Calculation of Electronic and Structural Properties of BC_3 (Publication 3)

D. Tomanek, R.M. Wentzcovitch, S.G. Louie, and M.L. Cohen

The equilibrium geometry and electronic structure of the compound BC_3 is determined using the *ab initio* pseudopotential local-orbital approach and the local-density functional formalism. The boron-carbon compound BC_3 is a layered material with graphitic structure, where every fourth carbon atom is substituted by boron. The nearest-neighbor distances are predicted to be 1.42 Å for the C-C bond and 1.55 Å for the B-C bond. A monolayer of BC_3 is found to be a semiconductor, and the observed metallic behavior of the bulk sample arises from interactions between neighboring layers in BC_3 with AA and AB stacking. Based on total-energy calculations, we find BC_3 to be less stable than graphite for the structures investigated.

2. Atomic Arrangement and Electronic Structure of BC_2N (Publication 27)

A.Y. Liu, R.M. Wentzcovitch, and M.L. Cohen

Recently a hybrid of composition BC_2N has been synthesized using chemical vapor deposition (CVD) with BCl_3 and CH_3CN as the starting materials. X-ray diffraction indicates that this new material consists of irregularly stacked hexagonal sheets with an intralayer lattice constant (a = 2.44 Å) and an interlayer distance (c = 3.40 Å) very close to the values in graphite. Although the x-ray data do not yield the atomic arrangement within the planes, the fine structure in the electron-energy-loss core edges show that all three atomic species in BC_2N participate in sp^2-type bonding. Hence the atoms are expected to be

*This work was supported jointly by the Director, Office of Energy Research, Office of Basic Energy Sciences, Materials Sciences Division, of the U.S. Department of Energy under Contract No. DE-AC03-76SF00098, and by the National Science Foundation under Grant No. DMR88-18404.

arranged in planes of graphite-like hexagonal rings, with weak interplanar interactions. At this time, it is unclear whether BC_2N is semimetallic or semiconducting. While conductivity measurements of BC_2N indicate that it is a narrow-gap semiconductor, x-ray photoemission experiments suggest that it is metallic. Three possible geometries are investigated for the BC_2N monolayer. The calculations are done using the first-principles pseudopotential local-orbital method. The local-density approximation with the Wigner form of the exchange and correlation functional is used. The electronic wave function is expanded in a linear combination of Bloch sums of orbitals localized on the atomic sites.

3. *Ab Initio* Study of Graphite → Diamond-Like Transitions in BN (Publication 13)

R.M. Wentzcovitch, S. Fahy, M.L. Cohen, and S.G. Louie

The variation of the structural energy along two transition paths from the layered to the highly condensed phases of BN was investigated using the first-principles total-energy pseudopotential method. Along the structural paths considered, the symmetries of the initial layered phases have been maintained, leading from the rhombohedral and hexagonal graphitic phases, which differ in their stacking sequences, into the zincblende and wurtzite phases, respectively. Constraining the interlayer distances, the total energies were minimized by allowing the hexagonal rings to stretch and buckle into the chair conformation. The paths obtained in this way have activation-energy barriers approximately 40% smaller than those in graphite → diamond transitions of C, and approximately equal to 0.38 eV/pair for both processes considered when the zero-point-motion energy contribution is neglected. The charge densities indicate that strong bonding between the hexagonal layers occurs only in the final state of the transitions, after the barriers have been crossed, and the structures collapse into the tetrahedrally coordinated phases. From the point of view of electronic structure, at all stages along the transitions, BN displays gaps (calculated within the local-density approximation) larger than 3.5 eV, a minimum that is reached when the activation-energy barrier is near a maximum.

4. Structural and Electronic Properties of WC (Publication 19)

A.Y. Liu, R.M. Wentzcovitch, and M.L. Cohen

The results of a pseudopotential local-orbital calculation on hexagonal WC yields calculated lattice constants and cohesive energy in good agreement with experiment, and the calculated bulk modulus lies within the wide range of measured values. The band structure and Fermi surface obtained are also generally consistent with experimental data, and the Fermi level is found to lie in a deep minimum of the density of states. The calculated valence-electron charge density indicates that the bonding in WC consists of a metallic component similar to that found in solid W, and strong W-C bonds.

STRUCTURAL TRANSITIONS, HIGH-PRESSURE SUPERCONDUCTORS, AND BONDING PROPERTIES

5. Theoretical Model for the hcp-bcc Transition in Mg (Publication 5)

R.M. Wentzcovitch and M.L. Cohen

Using a first-principles total-energy pseudopotential method, we investigate the transition mechanism for a pressure-induced martensitic hcp → bcc transformation that occurs in Mg at pressures around 50 GPa. Two internal structural degrees of freedom are selected, and one lattice is transformed into the other by relaxing these two parameters continuously. One of the parameters characterizes the relative displacement of the hexagonal layers and corresponds to a transverse phonon at the Brillouin-zone edge A in the hexagonal structure. The other characterizes the distortion of the internal hexagonal angles and corresponds to uniform strain along one of the $[0010]_{hcp}$ directions. The interaction between these two distortion modes causes important anharmonic effects in the zone-edge phonon and provides a low-energy path for the structural transition. The small activation barrier at the transition indicates that quantum fluctuations between the two structures could be taking place.

6. Superconductivity in Primitive Hexagonal Germanium (Publication 4)

J.L. Martins and M.L. Cohen

We present a first-principles calculation of the electron-phonon coupling constant λ (mass-enhancement parameter) for the primitive hexagonal, high-pressure phase of Ge (75 GPa $<$ p $<$ 105 GPa). Using the calculated value of λ, we estimate the superconducting transition temperature T_c to be in the range of 2 to 7 K. We discuss the contributions to λ from the different phonon modes and its dependence on the phonon frequency, electron-phonon matrix elements, and Fermi-surface nesting. The results are compared with previous calculations for primitive hexagonal Si.

7. Theory of Electronic, Vibrational, and Superconducting Properties of fcc Silicon (Publication 7)

A.Y. Liu, K.J. Chang, and M.L. Cohen

We present a theoretical calculation of the properties of the fcc, high-pressure structural phase of Si. The electronic and phonon properties have been studied, and we predict that the system will be a free-electron-like metal with a very stiff lattice. In addition, we estimate the superconducting transition temperature to be approximately 2 K based on calculations of the electron-phonon coupling constant λ. Comparisons are made with the results of previous calculations for Al.

8. Determination of Diatomic Crystal Bond Lengths using Atomic s-Orbital Radii (Publication 20)

S.B. Zhang, M.L. Cohen, and J.C. Phillips

We develop a theory to determine the bond lengths of over 270 AB crystals having ZnS, NaCl, and CsCl structures, including intermetallic compounds. The first-principles pseudopotential s-orbital radius r_s is used, which contains no element-specific adjustable parameters. The good agreement found here between the calculated and measured bond lengths, along with the earlier successful applications of orbital radii for separating structures, illustrates the importance and usefulness of the orbital-radii scheme.

9. Quasiparticle Calculation of Valence-Band Offset of AlAs-GaAs(001) (Publication 9)

S.B. Zhang, D.Tomanek, S.G. Louie, M.L. Cohen, and M. S. Hybertsen

A first-principles quasiparticle theory for band offsets of heterojunctions is developed and used to compute the valence band offset ΔE_v for the prototypical AlAs-GaAs(001) interface. The result, ΔE_v = 0.53 $\pm$ 0.05 eV, is in good agreement with recent experimental values and in particular with the most recent photoluminescence data, ΔE_v = 0.56 $\pm$ 0.03 eV, for a sample grown by molecular-beam epitaxy. We show that there is a substantial many-body correction of 0.12 eV to the value of the valence-band offset calculated using local-density functional theory.

10. Jellium-Model Calculation for Dimer Decays of Potassium Clusters (Publication 10)

S. Saito and M.L. Cohen

We have calculated the total energies of n-atom potassium clusters K_n ($1 \leq n \leq 23$) using a jellium-sphere background model for the positive-ion cores and the local-spin-density-functional approximation for the valence electrons. We find that the K clusters with exoergic fission channels have low abundances in the experimental mass spectra, indicating the presence of thermal fissions of K_n. Most of the exoergic fissions are found to produce dimers, K_2, as one of the daughter clusters. We have studied the "dimer decay" of K_{10} in an attempt to explain why K_{10} is one of the least abundant clusters in the K_n mass spectra. Two overlapping jellium spheres with constant density are used for the positive background. The energy-barrier height for complete decay from the energy-minimum point is found to be 0.18 eV, which is a reasonable magnitude for thermal decay compared to the experimental temperature. The monomer decay of K_9 and the dimer decay of K_8 are found to have higher barriers.

NEW THEORETICAL TOOLS

11. Total Dielectric Function: Algebraic Sign, Electron-Lattice Response, and Superconductivity (Publication 11)

P.B. Allen, M.L. Cohen, and D.R. Penn

The interaction between two test charges in a solid can be described in terms of a total dielectric function that includes electronic and lattice polarization. Crystal stability requires the eigenvalues of ϵ^{-1} to be $\leqslant 1$. Some implications for superconductivity are discussed. A total dielectric function for the electron-lattice system is derived in the mean-field approximation, and its inverse is explicitly constructed. The low-lying poles of ϵ^{-1} give the correct phonon frequencies as determined by the usual dynamical matrix.

12. X_1 and X_3 States of Electrons and Phonons in Zincblende-Type Semiconductors (Publication 17)

R.M. Wentzcovitch, M. Cardona, M.L. Cohen, and N.E. Christensen

Despite the extensive experimental and theoretical characterization of the band structures of III-V zincblende semiconductors, the literature is still ambiguous in classifying the symmetries of the lowest conduction states at the X point in the Brillouin zone of these compounds. We present the symmetries of these states obtained by the first-principles pseudopotential and the linear muffin-tin orbital methods and label them consistently for this class of compounds. We also point out that analyses of the indirect optical absorption edge structure in compounds with the lowest conduction states at X (e.g., AlAs, AlSb, and GaP) reveal the symmetries of these states in agreement with theoretical predictions. This technique could also be used to determine these symmetries in other indirect-gap compounds or those that acquire an indirect gap $\Gamma \rightarrow X$ under reasonably modest pressures (e.g., GaAs).

13. Diagonalization of Large Matrices in Pseudopotential Band-Structure Calculations: Dual-Space Formalism (Publication 6)

J.L. Martins and M.L. Cohen

Combining iterative methods of calculating the eigenvectors of a Hermitian matrix with a matrix-multiplication technique using the fast-Fourier-transform algorithm, we present an efficient method of performing total-energy and band-structure calculations in crystals with the plane-wave local-pseudopotential formalism. The method can be viewed as a dual-space formalism where part of the calculation is performed in momentum space and another part in coordinate space. Significant savings in both computer time and memory are obtained. Results of calculations for molecular hydrogen with matrix sizes as large as 7200 are presented as an example.

1988 PUBLICATIONS AND REPORTS

Refereed Journals

1. U. Walter, S. Fahy, A. Zettl, S.G. Louie, M.L. Cohen, P. Tejedor, and A.M. Stacy, "Probing Electronic Density of States and Magnetic Interactions at the Rare-earth Site of $ErBa_2Cu_3O_7$," Phys. Rev. B **36**, 8899 (1987).
2. M.L. Cohen, "Theoretical Calculations of Phase Transitions in the Megabar Regime," Scripta Metall. **22**, 127 (1988).
3. D. Tomanek, R.M. Wentzcovitch, S.G. Louie, and M.L. Cohen, "Calculation of Electronic and Structural Properties of BC_3," Phys. Rev. B **37**, 3134 (1988); LBL-24507.
4. J.L. Martins and M.L. Cohen, "Superconductivity in Primitive Hexagonal Germanium," Phys. Rev. B **37**, 3304 (1988).
5. R.M. Wentzcovitch and M.L. Cohen, "Theoretical Model for the hcp-bcc Transition in Mg," Phys. Rev. B **37**, 5571 (1988).
6. J.L. Martins and M.L. Cohen, "Diagonalization of Large Matrices in Pseudopotential Band-Structure Calculations: Dual Space Formalism," Phys. Rev. B **37**, 6134 (1988).
7. A.Y. Liu, K.J. Chang, and M.L. Cohen, "Theory of Electronic, Vibrational, and Superconducting Properties of fcc Silicon," Phys. Rev. B **37**, 6344 (1988).

8. M.F. Crommie, A. Zettl, T.W. Barbee III, and M.L. Cohen, "Anisotropic Thermoelectric Power and Conductivity in Single Crystal $YBa_2Cu_3O_7$," Phys. Rev. B **37**, 9734 (1988).
9. S.B. Zhang, D. Tomanek, S.G. Louie, M.L. Cohen, and M.S. Hybertsen, "Quasiparticle Calculation of Valence Band Offset of AlAs-GaAs(001)," Solid State Commun. **66**, 585 (1988); LBL-24598.
10. S. Saito and M.L. Cohen, "Jellium-model Calculation for Dimer Decays of Potassiuim Clusters," Phys. Rev. B **38**, 1123 (1988).
11. P.B. Allen, M.L. Cohen, and D.R. Penn, "Total Dielectric Function: Algebraic Sign, Electron-Lattice Response, and Superconductivity," Phys. Rev. B **38**, 2513 (1988).
12. R.M. Wentzcovitch, M.L. Cohen, and S.G. Louie, "Comparative Study of the Density of States of Graphite and BC_3," Phys. Lett. A **131**, 457 (1988).
13. R.M. Wentzcovitch, S. Fahy, M.L. Cohen, and S.G. Louie, "*Ab Initio* Study of Graphite → Diamond-like Transitions in BN," Phys. Rev. B **38**, 6191 (1988).
14. R.M. Wentzcovitch, M.L. Cohen, S.G. Louie, and D. Tomanek, "σ-states Contribution to the Conductivity of BC_3" Solid State Commun. **67**, 515 (1988); LBL-24886.
15. L.C. Bourne, S. Hoen, M.F. Crommie, W.N. Creager, A. Zettl, M.L. Cohen, L. Bernardes, J. Kinney, and D.E. Morris, "Magnetic and Resistive Determination of the Oxygen Isotope Effect in $La_{1.85}Sr_{0.15}CuO_4$," Solid State Commun. **67**, 707 (1988).
16. A.Y. Liu and M.L. Cohen, "Theoretical Study of the Stability of Cubic WC," Solid State Commun. **67**, 907 (1988).
17. R.M. Wentzcovitch, M. Cardona, M.L. Cohen, and N.E. Christensen, "X_1 and X_3 States of Electrons and Phonons in Zincblende Type Semiconductors," Solid State Commun. **67**, 927 (1988).
18. K.J. Chang, M.L. Cohen, and D.R. Penn, "Electronic Correlations and Satellites in Superconducting Oxides," Phys. Rev. B **38**, 8691 (1988).
19. A.Y. Liu, R.M. Wentzcovitch, and M.L. Cohen, "Structural and Electronic Properties of WC," Phys. Rev. B **38**, 9483 (1988).
20. S.B. Zhang, M.L. Cohen, and J.C. Phillips, "Determination of Diatomic Crystal Bond Lengths Using Atomic s-orbital Radii," Phys. Rev. B **38**, 12085 (1988); LBL-26807.
21. T.W. Barbee III, M.L. Cohen, L.C. Bourne, and A. Zettl, "The Isotope Effect and Superconducting Oxides," J. Phys. C **21**, 5997 (1988); LBL-26755.
22. M.L. Cohen, "Theory of Bulk Moduli of Hard Solids," Mat. Sci. Eng. **A105/106**, 11 (1988); LBL-26751.

Other Publications

23. M.L. Cohen, "Future Trends in Calculating the Properties of Materials," in *Future Trends in Materials Sciences*, J. Keller, Ed., World Scientific, Singapore, 1988, p. 89.
24. M.L. Cohen, "The New High Temperature Superconductors," IEEE Trans. Nucl. Sci. **NS-35**, 22 (1988).
25. M.L. Cohen and J.R. Chelikowsky, *Electronic Structure and Optical Properties of Semiconductors*, Springer-Verlag, Berlin, 1988.
26. M.L. Cohen, "Superconduttivita ad 'alta temperatura'," Scienza and Tecnica **88/89**, 240 (1988).
27. A.Y. Liu, R.M. Wentzcovitch, and M.L. Cohen, "Atomic Arrangement and Electronic Structure of BC_2N," in *Graphite Intercalation Compounds: Science and Applications*, M. Endo, M. S. Dresselhaus, and G. Dresselhaus, eds., MRS, Pittsburg, 1988, p. 137.
28. D. Tomanek, S.B. Zhang, S.G. Louie, M.L. Cohen, and M.S. Hybertsen, "Calculation of Many-Body Effects in the Electronic Structure of GaAs–AlAs Superlattices," Bull. Am. Phys. Soc. **33**, 360 (1988).
29. R.M. Wentzcovitch, M.L. Cohen, D. Tomanek, and S.G. Louie, "Origin of the Improved Conductivity of BC_3," Bull. Am. Phys. Soc. **33**, 427 (1988).
30. S.B. Zhang, D. Tomanek, S.G. Louie, M.L. Cohen, and M.S. Hybertsen, "Many-body Effects on the Valence Band Offset of AlAs-GaAs(001)," Bull. Am. Phys. Soc. **33**, 475 (1988).
31. M.L. Cohen and S.B. Zhang, "Determining AB Crystal Structures Using Atomic s-radii," Bull. Am. Phys. Soc. **33**, 521 (1988).
32. R. Dandrea, M.L. Martins, and M.L. Cohen, "Electron-phonon Mass Enhancements in the Alkali Metals," Bull. Am. Phys. Soc. **33**, 772 (1988).
33. S. Saito and M.L. Cohen, "Jellium-model Calculation for Dimer-decay of Potassium Clusters," Bull. Am. Phys. Soc. **33**, 817 (1988).
34. M.L. Cohen, "High Temperature Superconductivity: Current Theoretical Situation," Institut de la Vie International Conf., *Proc. De la Physique Theorique a la Biologie,* Versailles, France, 1988.

LBL Reports

35. M.L. Cohen and L.M. Falicov, "Comment on the Magnon Pairing Mechanism of Superconductivity in Cuprate Ceramics," submitted to Science; LBL-26089
36. M.L. Cohen, "More on Crystals from First Principles," submitted to Nature; LBL-26365.
37. S.B. Zhang, D. Erskine, M.L. Cohen, and P.Y. Yu, "Metallic Properties of Orthorhombic High Pressure

of GaAs: Theory and Experiment," submitted to Solid State Commun.; LBL-26543.

38. T.W. Barbee III, A. Garcia, M.L. Cohen, and J.L. Martins, "Theory of High-Pressure Phases of Hydrogen," submitted to Phys. Rev. Lett.; LBL-26874.

Invited Talks

39 M.L. Cohen, "Predicting New Materials and Properties of Solids," Racah Institute of Physics, Hebrew University, Jerusalem, Israel, Jan. 3, 1988.

40. M.L. Cohen, "High Temperature Superconductivity: Theoretical Perspectives," IBM Almaden Research Center, San Jose, CA, Jan. 28, 1988.

41. M.L. Cohen, "Superconductivity," George Washington High School, San Francisco, CA, Feb. 23, 1988.

42. M.L. Cohen, "Predicting the Existence and Properties of New Materials," visit of CRAY CEO and Staff, University of California at Berkeley, Mar. 15, 1988.

43. M.L. Cohen, "The New High Temperature Superconductors," Department of Physics and Physical Science, California State University, Sacramento, Apr. 12, 1988.

44. M.L. Cohen, "High Temperature Superconductivity," Department of Physics, University of California at Santa Cruz, Apr. 14, 1988.

45. M.L. Cohen, "Microscopic Mechanisms of Superconductivity," Theoretical Physics Seminar, Department of Physics, University of California at Berkeley, May 9, 1988.

46. M.L. Cohen, "High Temperature Superconductivity: Current Theoretical Situation," Institut de la Vie International Conference on "De la Physique Théorique à la Biologie," Versailles, France, July 4, 1988.

47. M.L. Cohen, "Microscopic Mechanism of Superconductivity I," Université de Paris-Sud, LURE, Orsay, France, July 11, 1988.

48. M.L. Cohen, "Microscopic Mechanisms of Superconductivity II," Université de Paris-Sud, LURE, Orsay, France, July 11, 1988.

49. M.L. Cohen, "High Temperature Superconductivity," Berkeley Breakfast Club, Spenger's Restaurant, Berkeley, CA, Aug. 19, 1988.

50. M.L. Cohen, "High Temperature Superconductivity," Miller Institute for Basic Research in Science Lunch Seminars, Faculty Club, University of California at Berkeley, Sept. 27, 1988.

Surfaces, Chemisorption, and Theory of Solids*

Steven G. Louie, Investigator

INTRODUCTION

The goal of this work is to further basic understanding of the electronic and structural properties of solids and materials systems such as surfaces and interfaces. First-principles quantum mechanical calculations are carried out to obtain a microscopic understanding of realistic systems. The research effort encompasses the study of bulk materials, surfaces, chemisorption systems, and interfaces, and the formulation and development of new theoretical techniques for calculating ground-state and excited-state properties. Current projects include work on surface atomic and electronic structures, structural and vibrational properties of solids, electronic excitation spectra of solids, solid-solid structural phase transformations, and metal clusters.

1. Variational Quantum Monte Carlo Approach to Solids (Publications 8, 19, and 23)†

S. Fahy, X. Wang, and S.G. Louie

We have developed a new method of calculating the total energy and other ground-state properties of solids. The method employs nonlocal pseudopotentials in conjunction with the variational quantum Monte Carlo approach. Valence electron correlations are treated using the exact Coulomb interaction with a correlated many-electron wavefunction of the Jastrow-Slater form. The use of pseudopotentials for the electron-ion interaction removes from the problem the large fluctuations of electron energies in the core region that occur in quantum Monte Carlo all-electron schemes. The method is used to calculate the cohesive energy and structural properties of diamond and graphite and the ionization energy and electron affinity of various atoms. The results are in excellent agreement with experiment.

†Supported in part (graduate student salary) by NSF Grant No. DMR8319024.

*This work was supported by the Director, Office of Energy Research, Office of Basic Energy Sciences, Materials Sciences Division, of the U.S. Department of Energy under Contract No. DE-AC03-76SF00098.

2. Electron Excitations and Surface-State Energies at Semiconductor Surfaces (Publications 5, 17, 18, and 22)†

M.S. Hybertsen and S.G. Louie

A first-principles theory of the quasiparticle surface-state energies on semiconductor surfaces is developed. The surface properties are calculated using a repeated-slab geometry. Many-body effects due to the electron-electron interaction are represented by the electron self-energy operator, including the full-surface Green's function and local fields and dynamical screening effects in the Coulomb interaction. Calculated surface-state energies for the prototypical Si(111):As and Ge(111):As surfaces are presented. The calculated energies and dispersions for the occupied surface states (resonances) are in excellent agreement with recent angle-resolved photoemission data. Predictions are made for the position of empty surface states on both surfaces that may be experimentally accessible. The resulting surface-state gap at Γ for Si(111):As agrees with recent scanning-tunneling-spectroscopy and inverse-photoemission measurements. Comparison of the present results to eigenvalues from the local-density-functional calculation reveals substantial corrections for the gaps between empty and occupied surface states. This correction is found to depend on the character of the surface states involved.

†Supported in part (graduate student salary) by NSF Grant No. DMR8319024.

3. Quasiparticle Excitation Spectra of s-p Electron Metals (Publications 9 and 24)†

J.E. Northrup, M. Surh, M.S. Hybertsen, and S.G. Louie

The quasiparticle excitation spectrum is calculated for the s-p electron metals Li, Na, K, and Al by evaluation of the electron self-energy operator with use of a first-order expansion in the dressed Green's Function G and the screened Coulomb interaction W. The calculated quasiparticle energies for Na, K, and Al are in excellent agreement with angle-resolved photoemission experiments. For Na and K in particular, the occupied bandwidth is significantly narrower than the free-electron value, as found in experiment. Inclusion of exchange and correlation effects in the dielectric screening matrix is shown to

decrease the bandwidth relative to the random-phase approximation (RPA) result by a significant amount. Local-field effects, reflected in the off-diagonal elements of the dielectric matrix, are found to have little effect on the band structure of these simple metals.

†Supported in part (graduate student salary) by NSF Grant No. DMR8319024.

4. *Ab Initio* Calculation of Pressure Coefficients of Band Gaps of Silicon: Comparison of the LDA and Quasiparticle Results (Publication 21)†

X. Zhu, S. Fahy, and S.G. Louie

The pressure coefficients of band gaps of silicon are calculated using a first-principles quasiparticle approach. For comparison, the same quantities are also computed within the local-density approximation (LDA). In both cases, the calculations were performed for volumes corresponding to pressures between 0 and 150 kbar using *ab initio* norm-conserving pseudopotentials. The electron self-energy in the quasiparticle calculation is obtained using a first-order expansion in the dressed Green's function G and the screened Coulomb interaction W with local fields. The quasiparticle results show a linear dependence of changes in the band gaps on lattice constant, while the dependence on pressure deviates from linearity at high pressure. The LDA band-gap pressure coefficients, obtained using three commonly used exchange-correlation potential forms, are shown to be very close to the quasiparticle values for the whole range of crystal volumes considered. At some of the volumes considered, the LDA band gaps are negative. Both sets of pressure-coefficient results are in very good agreement with available experimental values for Si.

5. *Ab Initio* Study of Graphite → Diamond-Like Transitions in BN (Publication 7)†

R.M. Wentzcovitch, S. Fahy, M.L. Cohen, and S.G. Louie

The variation of the structural energy along two transition paths from the layered to the highly condensed phases of BN is investigated using the first-principles total-energy pseudopotential method. Along the structural paths considered, the symmetries of the initial layered phases have been maintained, leading from the rhombohedral and hexagonal graphitic phases, which differ in their stacking sequence, into zincblende and wurtzite phases, respectively. Constraining the interlayer distances, the total energies were minimized by allowing the hexagonal rings to stretch and buckle into the chair conformation. The paths obtained in this way have activation-energy barriers approximately 40% smaller than those in graphite → diamond transitions of C, and approximately equal to 0.38 eV/pair for both processes considered when the zero-point-motion energy contribution is neglected. The charge densities indicate that strong bonding between the hexagonal layers occurs only in the final state of the transitions, after the barriers have been crossed, and when the structures have collapsed into the tetrahedrally coordinated phases. From the point of view of electronic structure, at all stages along the transitions, BN displays gaps (calculated within the local-density approximation) larger than 3.5 eV, a minimum reached when the activation-energy barrier is near a maximum.

†Supported in part (graduate student salary) by NSF Grant No. DMR8319024.

6. Comparative Study of the Density of States of Graphite and BC_3 (Publication 6)

R.M. Wentzcovitch, M.L. Cohen, and S.G. Louie

Calculated results show important differences between the density of states (DOS) of the new layered materials BC_3, and that of graphite. The differences derive from the proposed structure of BC_3 and should provide evidence for the atomic arrangement in this material. Their signature seems to be present in electron-energy-loss (EELS) spectra and could be searched for in other types of experiments that probe the energy distribution of electrons, such as near-edge x-ray absorption fine-structure spectroscopy (NEXAFS).

7. Spin-Orbit Interaction Effects in Zincblende Semiconductors: *Ab Initio* Pseudopotential Calculations (Publication 20)†

M.F. Li, M.P. Surh, and S.G. Louie

Ab initio band-structure calculations have been performed for the spin-orbit interaction effects at the

top of the valence bands for GaAs and InSb. Relativistic, norm-conserving pseudopotentials are used with no correction made for the gaps from the LDA. The spin-orbit splitting at Γ and linear terms in the $\vec{k}$ dependence of the splitting are found to be in excellent agreement with existing experiments and previous theoretical results. The effective mass and the cubic splitting terms are also investigated.

---

†Supported in part (graduate student salary) by NSF Grant No. DMR8319024.

1988 PUBLICATIONS AND REPORTS

Refereed Journals

1. R.S. Becker, B.S. Swartzentruber, J.S. Vickers, M.S. Hybertsen, and S.G. Louie, "Geometric and Local Electronic Structure of Si(111)-As," Phys. Rev. Lett. **60**, 116 (1988); LBL-24343.†
2. S.B. Zhang, D. Tomanek, S.G. Louie, M.L. Cohen, and M.S. Hybertsen, "Quasiparticle Calculation of Valence Band Offset of AlAs-GaAs(001)," Solid State Commun. **66**, 585 (1988); LBL-24598.†
3. M.S. Hybertsen and S.G. Louie, "Model Dielectric Matrices for Quasiparticle Self-Energy Calculations," Phys. Rev. B **37**, 2733 (1988).‡
4. C. Kittel, S. Fahy, and S.G. Louie, "Magnetic Screening by a Thin Superconducting Surface Layer," Phys. Rev. B **37**, 642 (1988).‡
5. M.S. Hybertsen and S.G. Louie, "Theory of Quasiparticle Surface States in Semiconductor Surfaces," Phys. Rev. B **38**, 4033 (1988).†
6. R.M. Wentzcovitch, M.L. Cohen, and S.G. Louie, "Comparative Study of the Density of States of Graphite and BC_3," Phys. Lett. A **131**, 457 (1988).†
7. R.M. Wentzcovitch, S. Fahy, M.L. Cohen, and S.G. Louie, "*Ab initio* Study of Graphite→Diamond-like Transitions in BN," Phys. Rev. B **38**, 6191 (1988); LBL-24951.†
8. S. Fahy, X.W. Wang, and S.G. Louie, "Variational Quantum Monte Carlo Non-Local Pseudopotential Approach to Solids: Cohesive and Structural Properties of Diamond," Phys. Rev. Lett. **61**, 1631 (1988); LBL-25417.†
9. M. Surh, J.E. Northrup, and S.G. Louie, "Occupied Quasiparticle Bandwidth of K," Phys. Rev. B **38**, 5976 (1988); LBL-24887.†
10. S. Fahy, C. Kittel, and S.G. Louie, "Electromagnetic Screening by Metals," Am. J. Phys. **56**, 989 (1988).‡

Other Publications

11. S.G. Louie, "Calculating and Predicting the Properties of Materials," in *High Speed Computing: Scientific Applications and Algorithm Design*, R.B. Wilhelmson, Ed., Univ. of Illinois Press, Urbana, 1988, p. 112; LBL-21470.†
12. R.P. Andres, R.S. Averback, W.L. Brown, L.E. Brus, W.A. Goddard III, A. Kaldor, S.G. Louie, M. Moscovits, P.S. Peercy, S.J. Riley, R.W. Siegel, F. Spaepen, and Y. Wang, Department of Energy Panel Report on Clusters and Cluster-Assembled Materials.
13. S. Fahy and S.G. Louie, "Variational Quantum Monte Carlo Calculation of the Correlation Energies in Diamond and Graphite," Bull. Am. Phys. Soc. **33**, 278 (1988).†
14. D. Tomanek, S.B. Zhang, S.G. Louie, M.L. Cohen, and M.S. Hybertsen, "Calculation of Many-Body Effects in the Electronic Structure of GaAs-AlAs Superlattices," Bull. Am. Phys. Soc. **33**, 360 (1988).†
15. S.B. Zhang, D. Tomanek, S.G. Louie, M.L. Cohen, and M.S. Hybertsen, "Many-Body Effects on the Valence Band Offset of AlAs-GaAs(001)," Bull. Am. Phys. Soc. **33**, 475 (1988).†
16. S. Vickers, T. Klitsner, M.S. Hybertsen, S.G. Louie, R.S. Becker, and B.S. Swartzentruber, "Geometric and Electronic Structure of Si(111)-As," Bull. Am. Phys. Soc. **33**, 785 (1988).†

LBL Reports

17. S.G. Louie, "First-Principles Calculation of Quasiparticle Energies at Surfaces and Interfaces: Semiconductor Surface-State Spectra and Band Offsets," in *Proc. Solvay Conference on Surface Science,* Austin, TX, Dec. 1987 (in press); LBL-24467.†
18. M.S. Hybertsen and S.G. Louie, "First-Principles Theory of Semiconductor Surface State Energies," in *Proc. 19th Int. Conf. Physics of Semiconductors* (in press); LBL-25628.†
19. S. Fahy, X.W. Wang, and S.G. Louie, "Quantum Monte Carlo Calculation of the Properties of Atomic Carbon and Diamond," in *Proc. 19th Int. Conf. Physics of Semiconductors* (in press); LBL-25544.†
20. M.F. Li, M.P. Surh, and S.G. Louie, "Spin-Orbit Interaction Effects in Zincblende Semiconductors: *Ab initio* Pseudopotential Calculations," in *Proc. 19th Int. Conf. Physics of Semiconductors* (in press); LBL-25543.†
21. X. Zhu, S. Fahy, and S.G. Louie, "*Ab Initio* Calculation of Pressure Coefficients of Band Gaps of Silicon: Comparison of the LDA and Quasiparticle Results," Phys. Rev. B (in press); LBL-26082.†
22. S.G. Louie, "Theory of Ground- and Excited-State Properties of Solids, Surfaces, and Interfaces: Beyond Density Functional Formalism," in *Proc. '88 World Materials Congress, Symposium on Atomistic Modeling of Materials: Beyond Pair Potentials* (in press); LBL-26185.†
23. S.G. Louie, "Variational Quantum Monte Carlo Calculation of Materials Properties," in *Proc. 1988 Materials Research Society Meeting, Symposium T* (in press); LBL-26360.‡
24. J.E. Northrup, M.S. Hybertsen, and S.G. Louie, "Quasiparticle Excitation Spectrum for Nearly Free Electron Metals," submitted to Phys. Rev. B; LBL-26485.‡

Invited Talks

25. S.G. Louie, "Theoretical Methods in Cluster Studies," Department of Energy Meeting on Clusters and Nanophase Materials, Monterey, CA, Jan. 21, 1988.
26. S.G. Louie, "A Combined Variational Quantum Monte Carlo – *Ab initio* Pseudopotential Approach for Solid State Systems," International Workshop on Computational Condensed Matter Physics, Glion, Switzerland, Feb. 24, 1988.
27. S.G. Louie, "First-Principles Calculation of the Electronic Properties of Materials," Presentation to CEO of CRAY Corp., Berkeley, CA, Mar. 15, 1988.
28. S.G. Louie, "Quantum Monte Carlo Calculation of Materials Properties," Xerox PARC Physical Sciences Seminar, Palo Alto, CA, Aug. 26, 1988.
29. S.G. Louie, "Ground- and Excited-State Properties of Solids, Surfaces and Interfaces: Beyond Density Functional Formalism," World Materials Congress, Chicago, IL, Sept. 26, 1988.
30. S.G. Louie, "Recent Developments in Predicting the Electronic and Structural Properties of Materials," Condensed Matter Physics Seminar, Department of Applied Physics, Stanford University, Stanford, CA, Oct. 27, 1988.
31. S.G. Louie, "Theoretical Studies of the Atomic and Electronic Structure of Surfaces," Center for Advanced Materials Industrial Workshop, LBL, Nov. 3, 1988.
32. S.G. Louie, "Recent Progress in Predicting the Properties of Materials," Condensed Matter Physics Seminar, University of California at Berkeley, Nov. 9, 1988.
33. S.G. Louie, "Recent Progress in Predicting the Electronic and Structural Properties of Materials," Condensed Matter Physics Seminar, University of California, Irvine, Nov. 21, 1988.
34. S.G. Louie, "Quantum Monte Carlo Calculation of Materials Properties," Materials Research Society Meeting, Boston, MA, Nov. 28, 1988.

---

†Supported in part by NSF Grant No. DMR8319024.
‡Supported by NSF Grant No. DMR8319024.

MATERIALS CHEMISTRY

SYNTHESIS AND CHEMICAL STRUCTURE

Low-Temperature Properties of Materials*

Norman E. Phillips, Investigator

INTRODUCTION

The objective of this program is to obtain information that contributes to an understanding of the behavior of materials by the measurement of their low-temperature properties, particularly specific heats. There are numerous special cases in which specific-heat data provide either a test of theoretical models or values of important parameters that could not otherwise be obtained. Since much of the work is in the region below 1 K, where the temperature scale is not well established, and because accurate temperature determinations are important for specific-heat measurements, research is also conducted on methods of temperature measurement. An accurate temperature scale that extends to 5 mK has been developed for this region. The interest in high-T_c superconductors has led to an extension of the measurement capabilities to above 100 K. Recent specific-heat measurements include measurements on ^{3}He in the Fermi-liquid region that have established the correct values of important parameters; measurements on a number of heavy-fermion compounds, including three of the four known heavy-fermion superconductors and Th-doped UBe_{13}; and measurements on high-T_c superconductors that have demonstrated the reality of bulk superconductivity and given estimates of the electronic density of states.

Future objectives include additional studies on high-T_c superconductors, and specific-heat measurements at pressures to 20 kbar and in magnetic fields to 9 T on other heavy-fermion compounds.

*This work was supported by the Director, Office of Energy Research, Office of Basic Energy Sciences, Materials Sciences Division, of the U.S. Department of Energy under Contract No. DE-AC03-76SF00098.

1. Specific Heat of UPt_3: Evidence for Unconventional Superconductivity (Publication 10)

R.A. Fisher, S. Kim, B.F. Woodfield, N.E. Phillips, L. Taillefer,† K. Hasselbach,† J. Flouquet,† A.L. Giorgi,‡ and J. L. Smith‡

Two new samples of UPt_3 that show sharper superconducting transitions than any observed in the past have shown a distinct splitting of the specific-heat anomaly at the zero-field transition into two components separated by 60 mK (see Figure 1-1). From several lines of evidence, it has been concluded that the splitting is an intrinsic property of the superconductivity of UPt_3 and shows that the pairing cannot be purely s-wave. This result consti-

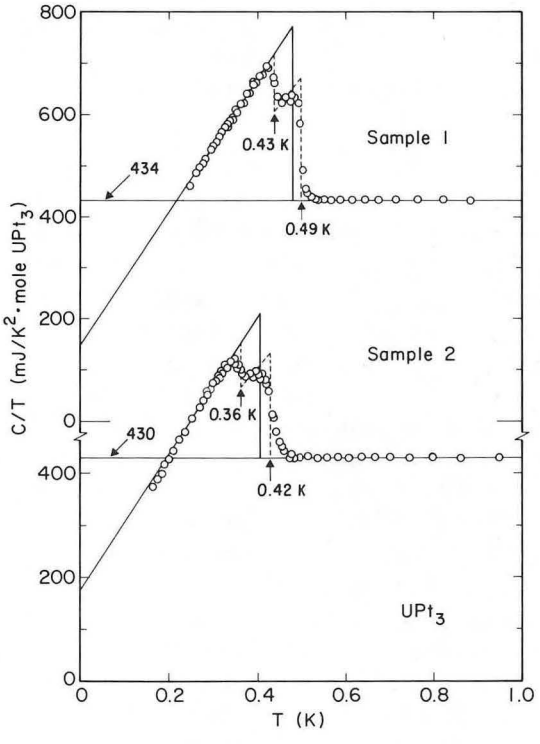

Figure 1-1. Specific heat of UPt_3 in the vicinity of the superconducting transition for samples 1 and 2. The dashed lines represent two ideally sharp transitions at T_a and T_b; the solid lines represent an ideally sharp single transition, with the same total entropy, at T_c. (XBL 8812-4279)

tutes a relatively direct indication that the superconductivity of UPt_3 differs from that of conventional BCS superconductors.

The parameters characterizing the superconducting-state specific heat have been correlated with those for a variety of other UPt_3 samples on the basis of a model in which a linear term in the specific heat and a finite density of states at the Fermi energy are produced by a pair-breaking mechanism, and the superconductivity is associated only with the remainder of the normal-state density of states. The correlation is internally consistent and gives values of the parameters for the fully superconducting material.

In the vicinity of 5 K, where μSR and neutron-scattering measurements show a very weak magnetic ordering, there is no effect, to within an accuracy of $\sim$ 0.1%, in the specific heat. This is a further indication that the magnetic ordering is extremely weak.

[†]CRTBT/CNRS, Grenoble, France.

[‡]Los Alamos National Laboratory, Los Alamos, NM 87545.

2. Pressure Dependence of the Specific Heat of Heavy-Fermion Compounds (Publication 8)

N.E. Phillips, R.A. Fisher, S.E. Lacy, C. Marcenat, J.A. Olsen, J. Flouquet,[†] A. Amato,[‡] D. Jaccard,[‡] Z. Fisk,[§] A.L. Georgi,[§] J.L. Smith,[§] and G.R. Stewart[‖]

The specific heats of $U_{0.97}Th_{0.03}Be_{13}$ and URu_2Si_2 have been measured under pressures to 9 kbar at temperatures between 0.4 and 25 K. Each of these materials shows both superconducting and antiferromagnetic ordering temperatures, and related parameters can contribute to an understanding of the relation between superconductivity and magnetism. In the case of $U_{0.97}Th_{0.03}Be_{13}$ at zero pressure, the superconducting transition occurs near 0.6 K, and there is a second specific-heat anomaly near 0.4 K. Under pressure, both ordering temperatures are lowered, and the entropy associated with the second is rapidly reduced with increasing pressure. The qualitative difference between the two pressure dependencies suggests that the two specific-heat anomalies are different in origin, consistent with μSR data that show weak magnetic ordering associated with the second. In the case of URu_2Si_2, there is a transition to an antiferromagnetic state, which involves moments of the order of a Bohr magnetron, at 17 K, and a superconducting transition, in the antiferromagnetic state, near 1.4 K. Both transitions are pressure dependent, but analysis of the results is not complete.

[†]CRTBT/CNRS, Grenoble, France.

[‡]Université de Genève, Switzerland.

[§]Los Alamos National Laboratory, Los Alamos, NM 87545.

[‖]University of Florida, Gainesville, FL 32611.

3. Specific Heat of $YBa_2Cu_3O_7$ (Publication 2)

R.A. Fisher, J.E. Gordon, S. Kim, N.E. Phillips, and A.M. Stacy

The specific heats of a number of new samples of YBCO made at LBL and also in other laboratories have been measured. Evidence for an intrinsic "linear" term, $\gamma(0)T$, in the zero field has continued to accumulate, but $\gamma(0)$ may be closer to 4.5 or 5 than the 6 or 7 mJ/mole·K_2 obtained in earlier measurements. There is no doubt that magnetic impurity phases contribute to the observed $\gamma(0)$, but it continues to appear that there is an intrinsic component that persists in the pure YBCO limit (but see abstract 4). This point is of considerable interest in connection with theory—the existence of a nonzero $\gamma(0)$ is an important prediction of one of the major theories.

4. Specific-Heat Measurements on Superconducting Bi-Ca-Sr-Cu and Tl-Ca-Ba-Ca Oxides: Absence of a Linear Term in the Specific Heat of Bi-Ca-Sr-Cu Oxides (Publication 3)

R.A. Fisher, S. Kim, S.E. Lacy, N.E. Phillips, D.E. Morris,[†] A.G. Markelz,[†] J.Y.T. Wei,[†] and D.S. Ginley[‡]

Measurements on a number of samples of Bi-Cu oxides have shown that $\gamma(0)$ is an order of magnitude smaller than in YBCO, and zero within the experimental uncertainty. The reason for this difference is not clear at this time, but even if $\gamma(0) \neq 0$ is an intrinsic property of all high-T_c oxide superconductors, it seems quite possible that it might assume different values in different materials. The Tl-Ca-Ba-Cu oxide investigated showed a linear term comparable to those found in YBCO (see Figure 4-1).

[†]Physics Division, LBL.

[‡]Sandia National Laboratories, Albuquerque, NM 87185.

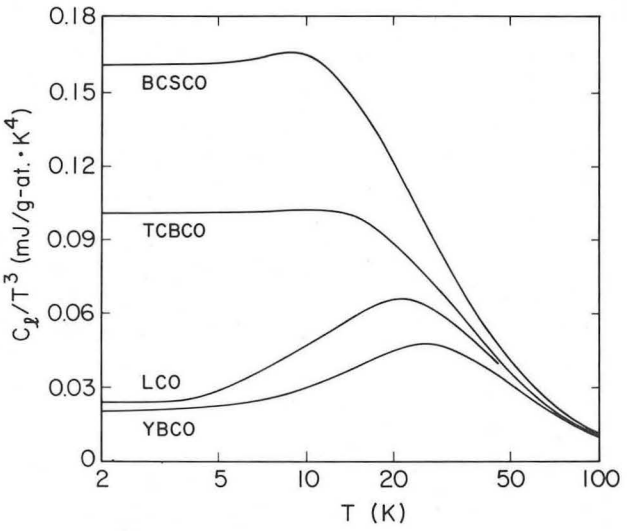

Figure 4-1. Lattice and electronic contributions to the specific heats of four Bi-Cu oxide samples and the one Tl-Cu oxide sample. (XBL 885-1818)

5. Specific-Heat Data of High-T_c Superconductors: Lattice and Electronic Contributions (Publication 9)

J.E. Gordon,† M.L. Tan,† R.A. Fisher, and N.E. Phillips

An analysis of high-temperature data for YBCO, in which the lattice specific heat is represented by an expansion in inverse powers of T, has been used to estimate γ (the normal-state value). The interesting result is that the value agrees approximately with those estimated from the "jump" in C at T_c (using BCS relations) and that obtained from γ(H) in the mixed state.

†Permanent address: Department of Physics, Amherst College, Amherst, MA 01002.

1988 PUBLICATIONS AND REPORTS

Refereed Journals

1. A.S. Edelstein, R.L. Holtz, D.J. Gillespie, M. Rubinstein, J. Tyson, N.E. Phillips, and R.A. Fisher, "Gd Interactions in (Ce,Gd)Al_3," Phys. Rev. B **37**, 7877 (1988); LBL-21789.
2. R.A. Fisher, J.E. Gordon, S. Kim., N.E. Phillips, and A.M. Stacy, "Specific Heat of $YBa_2Cu_3O_7$," Physica **C153–155**, 1092 (1988); LBL-24869.
3. R.A. Fisher, S. Kim. S.E. Lacy, N.E. Phillips, D.E. Morris, A.G. Markelz, J.Y.T. Wei, and D.S. Ginley, "Specific Heat Measurements on Superconducting Bi-Ca-Sr-Cu and Tl-Ca-Ba-Ca Oxides: Absence of a Linear Term in the Specific Heat of Bi-Ca-Sr-Cu Oxides," Phys. Rev. B **38**, 11942 (1988); LBL-25479.
4. C. Marcenat, R.A. Fisher, N.E. Phillips, and J. Flouquet, "Comparison of the Specific Heat of Heavy Fermion Cerium Compounds," J. Magn. Magn. Mater. **76–77**, 115 (1988); LBL-25763.
5. R.A. Fisher, N.E. Phillips, C. Marcenat, J. Flouquet, P. Haen, P. Lejay, and J.-M. Mignot, "Specific Heat of (Ce,La)Ru_2Si_2 in High Magnetic Fields," J. de Physique (Suppl. 12) **49**, 759 (1988); LBL-25764.

Other Publications

6. R.A. Fisher, J.E. Gordon, and N.E. Phillips, "Specific Heat of the High-T_c Oxide Superconductors: A Review," J. Superconductivity **1**, 233 (1988); LBL-25538.
7. R.A. Fisher, S.E. Lacy, C. Marcenat, J.A. Olsen, N.E. Phillips, Z. Fisk, A.L. Giorgi, J.L. Smith, and G.R. Stewart, "Low Temperature Specific Heat of UBe_{13}," in *Theoretical and Experimental Aspects of Valence Fluctuations and Heavy Fermions*, L.C. Gupta and S.K. Malik, eds., Plenum, NY, 1987, p. 345; LBL-22814.
8. N.E. Phillips, R.A. Fisher, S.E. Lacy, C. Marcenat, J.A. Olsen, J. Flouquet, A. Amato, D. Jaccard, Z. Fisk, A.L. Giorgi, J.L. Smith, and G.R. Stewart, "Pressure Dependence of the Specific Heat of Heavy-Fermion Compounds," in *Theoretical and Experimental Aspects of Valence Fluctuations and Heavy Fermions,* L.C. Gupta and S.K. Malik, eds., Plenum, NY, 1987, p. 141; LBL-22813.

LBL Reports

9. J.E. Gordon, M.L. Tan, R.A. Fisher, and N.E. Phillips, "Specific Heat Data of High-T_c Superconductors: Lattice and Electronic Contributions," submitted to Solid State Commun.; LBL-25845.
10. R.A. Fisher, S. Kim, B.F. Woodfield, N.E. Phillips; L. Taillefer, K. Hasselbach, J. Flouquet, A.L. Giorgi, and J.L. Smith, "Specific Heat of UPt_3: Evidence for Unconventional Superconductivity," submitted to Phys. Rev. Lett.; LBL-26456.

Invited Talks

11. N.E. Phillips, "Specific Heat of High-Temperature Superconductors," Conference on Theoretical Foundations of High-Temperature Superconductivity, Aspen, CO, Jan. 1988.
12. N.E. Phillips, "The Linear Term in the Specific Heat of High-Temperature Superconductors," CRTBT/CNRS, Grenoble, France, Feb. 1988.
13. N.E. Phillips, "Specific Heat of $YBa_2Cu_3O_7$," International Conference on High-Temperature Superconductors and Materials and Mechanisms of Superconductivity, Interlaken, Switzerland, Mar. 1988.

Electrochemical Processes*

Charles W. Tobias, Investigator

INTRODUCTION

This program is designed to advance the scientific foundations of electrochemical engineering and to broaden the range of useful applications of electrochemical transformations. Electrolysis processes have inherent advantages over thermochemical methods with respect to material yield and energy efficiency. However, in spite of their long history of economically significant applications, cell processes have not achieved their potential with respect to performance and range of applications in chemical synthesis, nor in energy conversion or storage. A major reason for this condition is the complex nature of transport phenomena in ionic media, as they are coupled to charge-transfer processes at the electrode surface.

- Multicomponent transport of charged species in solution is described by a mathematical model, and the composition at the surface experimentally determined, to clarify the mechanism of anomalous electrodeposition of magnetic alloys.
- In projects jointly directed with Dr. R.H. Muller, novel methods are explored for the reduction of mass-transfer resistance in high-rate applications, including in electroforming of metals, and in electroorganic synthesis. The effects of suspended inert solid particles in flowing electrolytes, on transport rates, and on electrocrystallization are determined and correlated.
- Stability analysis is used to gain insight into the development of roughness in the electrodeposition of metals. Current distribution on a profile is found by a perturbation technique accounting for ohmic, kinetic, capillary, and concentration overpotentials.

Applied research on the "Surface Morphology of Metals in Electrodeposition" and on "Engineering Analysis of Electrolytic Gas Evolution" is supported by the Assistant Secretary of Conservation and Renewable Energy, Office of Energy Storage and Distribution of the U.S. Department of Energy under Contract No. DE-AC03-76SF00098. Results are presented in this Report in the "Electrochemical Storage" Section.

*This work was supported by the Director, Office of Energy Research, Office of Basic Energy Sciences, Materials Sciences Division, of the U.S. Department of Energy under Contract No. DE-AC03-76SF00098.

1. Roughness Development in Metal Electrodeposition: Stability Theory (Publication 7)

D.P. Barkey, R.H. Muller, and C.W. Tobias

Electrodeposition of metals to thicknesses suitable for electroforming inevitably results in roughening of the deposit surface. Practical electrodeposits are polycrystalline and surface texture is amplified during deposition, resulting in macroscopic surface roughness. Roughness is a waste of material and in extreme cases leads to porous or noncoherent deposits. It arises because the process of electrodeposition is unstable to the development of protrusions that grow more rapidly than the surrounding surface.

A stability analysis of metal electrodeposition on a smooth surface has been formulated and applied to copper deposition on a rotating cylinder. Current distribution on a sinusoidal profile was found by a first-order perturbation technique accounting for ohmic, kinetic, capillary, and concentration overpotentials, and the derived current distribution was used to evaluate the rate of growth or decay of the perturbation. Growth rate was expressed as a function of three dimensionless parameters. The stability analysis correctly predicts trends in roughness spatial period as it depends on current density and fraction of limiting current. Relative to earlier efforts by Aogaki and by Landolt, the analysis improves agreement with experimental observations over a wide range of deposition conditions on the basis of quite fundamental considerations and without any adjustable parameters. However, while trends are correctly predicted, magnitudes of protrusion spacing are roughly twice those calculated by the present treatment.

Two factors may account for much of the discrepancy: nucleation and nonlinear terms in the boundary conditions. The observed surface textures were not faceted, and, therefore, crystalline anisotropy is probably not an important influence. Density of nucleation, however, places a lower limit on protrusion spacing and so could produce an unexpectedly large roughness spatial period. While the stability analysis may correctly estimate growth rates of protrusions, it cannot predict the character of underlying perturbations required for protrusion initiation. Higher-order terms and nucleation density could in principle be incorporated in a more com-

plete macroscopic stability analysis. The inclusion of fluctuations giving rise to surface perturbations requires a more mechanistic and microscopic approach.

2. Work in Progress

Anomalous Electrodeposition of Alloys.

It is known that certain metals interact when codeposited in such a way that their discharge kinetics are altered; the less noble metals deposit in preference to the more noble ones. Iron group metals, and zinc or palladium, are examples of such systems; when codeposited, the ratio of the less noble to the more noble metal is significantly higher in the deposit than in the solution phase. Despite the widespread occurrence and technical importance of these materials (e.g., thin magnetic films, corrosion protective layers, electronic devices), the mechanism of this behavior is not well understood. We have developed a mathematical model to describe the liquid-phase mass transport from basic principles. The rotating-disk electrode with its well-characterized hydrodynamics is used both in experiments and mathematical modeling. Homogeneous reactions, such as metal hydroxide ion formation, water dissociation, and buffering effects (e.g., boric acid), are included. The concentration profiles of all the species are calculated, and the interfacial values are used to evaluate more precisely the kinetic parameters of various electrode reactions. We have taken into account the discharge of both hydrogen ions and water during hydrogen evolution, and the discharge of both metal and metal-hydroxide ions during the metal deposition. Our first-order kinetic models (i.e., simple Butler-Volmer type without introducing any adsorption models) indicate that the difference in the discharge rate of metal-hydroxide ions and their dissociation constant are the key factors in the anomalous deposition behavior.

1988 PUBLICATIONS AND REPORTS

Other Publications

1. P.K. Andersen, R.H. Muller, and C.W. Tobias, "Enhancement of Mass Transfer to a Rotating Disk by Suspended Solids," Extended Abstracts of the Electrochemical Society, No. 278, May 1988, Atlanta, GA; LBL-24522.
2. D. Barkey, R.H. Muller, and C.W. Tobias, "Studies on High-Speed Electroforming," Extended Abstracts of the Electrochemical Society, No. 386, May 1988, Atlanta, GA; LBL-26024.
3. D. Barkey, R.H. Muller, and C.W. Tobias, "Stability Analysis of Metal Electrodeposition," Extended Abstracts of the Electrochemical Society, No. 325, Oct. 1988, Chicago, IL; LBL-26022.

LBL Reports

4. P.K. Andersen, R.H. Muller, and C.W. Tobias, "Enhancement of Mass Transfer to a Rotating Disk by Suspended Solids," accepted by J. Electrochem. Soc.; LBL-24522.
5. D. Barkey, R.H. Muller, and C.W. Tobias, "Studies in High Speed Electroforming," accepted by the Proceedings volume on *Electrochemistry in Mineral and Metal Processing*, The Electrochemical Society, 1988; LBL-23880.
6. D. Barkey, R.H. Muller, and C.W. Tobias, "Roughness Development in Metal Electrodeposition: I. Experimental Results," submitted to J. Electrochem. Soc.; LBL-26021.
7. D. Barkey, R.H. Muller, and C.W. Tobias, "Roughness Development in Metal Electrodeposition: II. Stability Theory," submitted to J. Electrochem. Soc.; LBL-26022.

Invited Talks

8. C.W. Tobias, "Novel Trends in Chemical Engineering Education in the USA," lecture and roundtable discussion, Technical University of Budapest, Hungary, May 25, 1988; Institute of Chemical Engineering, Veszprem, Hungary, May 20, 1988.
9. C.W. Tobias, "Technical Electrochemistry; The Engineering Side of Electrochemical Science," lecture to the Hungarian National Academy of Sciences, Budapest, Hungary, May 26, 1988.

HIGH-TEMPERATURE AND SURFACE CHEMISTRY

High-Temperature Thermodynamics*

Leo Brewer, Investigator

INTRODUCTION

The understanding of high-temperature chemistry is not only important for processes carried out at high temperature such as those of fusion and fission reactors and fossil-fuel power generators, but it is also important for the preparation and fabrication of ceramics, metals, semiconductors, superconductors, and many other materials. The understanding of high-temperature behavior is complicated by the occurrence of unusual species and phases that are often unstable at conventional temperatures. It is difficult to carry out measurements to obtain the data needed for the design of high-temperature systems. The experiments in progress are aimed at the testing or development of such predictive models.

Previous research of this program has led to the development of a variety of successful models of predictive capability for the behavior of gases, refractory containment materials, and of many metallic systems. At the present time the main thrust of the research is aimed at providing quantitative predictive models for the strongly interacting transition-metal alloys exhibiting generalized Lewis acid-base behavior. A variety of experimental methods are being used to characterize the thermodynamics of these systems.

1. Acid-Base Reactions of the Transition-Metal Alloys (Publications 1, 2, 3, and 10)

J. Bularzik,† M. Cima,‡ B. Ebbinghaus, J. Kouvetakis, and K. Krushwitz

The generalized Lewis acid-base theory describes the platinum-group metals Rh, Ir, Pd, or Pt as bases because of their nonbonding d-electron pairs that can be shared in the vacant d-orbitals of transition metals from the third to fifth groups and the lanthanides and actinides that are described as acids. A variety of techniques have been used to characterize these interactions and to develop a bonding model of general predictive capability. One procedure has been to use an electrochemical cell with solid electrolytes such as thoria doped with yttria to determine the partial molal Gibbs energies as a function of concentration. This method is limited to rather low temperatures, in the 800 to 1200°C range. For higher-temperature studies, gaseous-equilibria measurements have been made. Also, equilibration of nitrides and carbides with metallic phases have yielded useful data. The many oxides of Ti, V, and Nb have been used by equilibrating a pair of adjoining oxides such as $Nb_{12}O_{24}$ and NbO_2, which fix the Nb and O thermodynamic activities, with a platinum-group metal and analyzing the Nb content in the equilibrated metal phase.

The cell and oxide equilibration measurements that were previously carried out for combinations of 4d metals have now been extended to combinations of 3d acids with 4d and 5d bases. The literature on the thermodynamic properties of the oxides of Ti, V, and Nb has been reviewed and tabulations prepared to provide the data needed for evaluation of the oxide equilibration results. The crystal-field effect upon bonding of different d orbitals has been found to differ markedly for 3d, 4d, and 5d bases. For 3d metals such as Co and Ni, the nonbonding electron pairs of the pure metals are in orbitals that are so localized that the base strength of these metals is small. For the 5d metals such as Ir and Pt, all of the 5d orbitals are so extended that all of the nonbonding electron pairs of the pure metals can interact very strongly with acids such as Ti, Zr, V, or Nb. The 4d metals such as Rh and Pd show a very marked crystal-field effect, with a large change in localization of the d-orbitals as more of the orbitals are used in acid-base reactions. With small additions of acid that interacts with the most extended orbitals, the base strength is very high. With larger acid additions, more contracted orbitals of the base are used and the base strength rapidly decreases. Sufficient data have been obtained for combinations

*This work was supported by the Director, Office of Energy Research, Office of Basic Energy Sciences, Materials Sciences Division, of the U.S. Department of Energy under Contract No. DE-AC03-76SF00098.

of Ti, V, Nb, and Zr with Rh, Pd, Ir, and Pt to characterize the main features of the variation of base strength of 3d to 4d to 5d electron pairs.

---

†Present address: Department of Geological Science, Princeton University, Princeton, NJ 08544.

‡Present address: Department of Materials Sciences and Engineering, Massachusetts Institute of Technology, Cambridge, MA 02139.

2. Temperature-Stability Range of the Binary MoC Phase (Publication 10)

J. Kouvetakis†

Older compilations have described the Mo-C system in terms of the two phases Mo_2C and MoC, stable up to their melting points, although there had been reports of other phases. The definitive research of Rudy and associates in 1965–69[1] established two forms of Mo_2C, hexagonal $MoC_{0.6}$, stable above 1928 K, and cubic $MoC_{0.7}$, stable above 2233 K. The status of MoC (hexagonal WC type) was changed from that of a stable phase to that of a ternary phase requiring additional components for thermodynamic stability. In 1976, Shuster, Rudy, and Nowotny[2] extrapolated their data for phases containing C and Mo with Co, Fe, and W to suggest that MoC might be stable at temperatures below 1500 K, but this conclusion has not generally been accepted.

It is difficult to equilibrate the Mo-C system at temperatures below 1500 K. To clarify the question of the stability of MoC, heatings were carried out in a gradient furnace where samples could be annealed for many weeks in a range of temperatures. Also, small amounts of halogens were added to accelerate transport to crystal nuclei. Quenched samples of high-temperature carbides as well as Mo_2C or Mo with graphite were used as starting materials. The results demonstrate that MoC is thermodynamically stable at low temperatures and decomposes to Mo_2C and graphite above 1300 K. From consideration of equilibrium and calorimetric data, the thermodynamic properties of MoC can be established as $S^\circ_{298}/R = 4.41 \pm 0.3$ and $\Delta H^\circ_{298}/R = -3430 \pm 800$ K.

---

†Present address: IBM Corporation, T.J. Watson Research Center, Yorktown Heights, NY 10598.

1. E. Rudy, *Compendium of Phase Diagram Data*, Air Force Materials Laboratory, Wright-Patterson AFB, AFML-TR-65-2, Pt. V (June 1969).

2. J. Schuster, E. Rudy, and H. Nowotny, *Monatsh. Chem.* **107**, 1167 (1976).

3. Work in Progress

Additional data on the strength of generalized Lewis acid-base interactions is being obtained using high-temperature EMF cell measurements and ternary phase equilibria. These data are being combined with data from the literature to develop a model for characterizing these acid-base interactions for acids of the third to fifth groups, including the lanthanides and actinides and bases of the Ni-Pd, Co-Ir, and Fe-Os groups. Models are also being developed using data from the literature for interactions of the platinum metals, acting as acids, with nontransition metals such as Zn, Ga, and Si acting as bases.

1988 PUBLICATIONS AND REPORTS

Refereed Journals

1. M. Cima and L. Brewer, "Generalized Lewis Acid-Base Titration of Palladium and Niobium," Metall. Trans. B **19B**, 893 (1988); LBL-23613.
2. L. Brewer, "A Bonding Model for Strong Generalized Lewis Acid-Base Interactions in Intermetallics," Pure Appl. Chem. **60**, 281 (1988); LBL-23614.
3. L. Brewer and B. Ebbinghaus, "The Thermodynamics of Solid Oxides of Vanadium," Thermochim. Acta **129**, 49 (1988); LBL-24468.
4. L. Brewer, "Methods of Obtaining Thermodynamic Data," High Temp. Sci. **24**, 173 (1987); LBL-24469.
5. L. Brewer, "The Critical Evaluation of Typically Unreliable High-Temperature Data," Bull. Alloy Phase Diagrams **9**, 99 (1988); LBL-24701.

Other Publications

6. L. Brewer, "Bibliography on the High Temperature Chemistry and Physics of Materials, Vol. 32, Part 2: Gases: A: Spectroscopy of Interest to High-Temperature Chemistry. B: Reactions Between Gases and Condensed Phases," M. G. Hocking and V. Vasantasree, eds., IUPAC Commission on High Temperatures and Refractory Materials, London, 1988; LBL-26422.
7. L. Brewer, "Chemical Bonding Theory Applied to Metals," in *Alloying*, J. L. Walter, M. R. Jackson, and C. T. Sims, eds., ASM Int'l., 1988, p. 1; LBL-23612.

LBL Reports

8. L. Brewer, "Standard-State Gibbs Energies of the BCC, HCP, and CCP Structures of Metals," CALPHAD (in press); LBL-25878.
9. L. Brewer, "History of the Application of the Generalized Lewis Acid-Base Theory to Metals," J. Nucl. Mater. (in press); LBL-26942.

10. J. Kouvetakis (Ph.D. Thesis), with L. Brewer, "I. Stability Range of MoC(hP2). II. Thermodynamic Properties of Generalized Lewis Acid-Base Intermetallics," LBL-25340.

Invited Talks

11. L. Brewer and B. Ebbinghaus, "Thermodynamics of Vanadium Oxides and Intermetallics," Rocky Mountain Regional American Chemical Society Meeting, Las Vegas, NV, March 30, 1988.
12. L. Brewer, "Generalized Lewis Acid-Base Interactions at High Temperatures," Midwest Thermodynamic Symposium, Lake Geneva, WI, May 14–16, 1988.
13. L. Brewer, Linford Award Presentation, The Electrochemical Society Meeting, Atlanta, GA, May 16–19, 1988.
14. L. Brewer, "Standard-State Gibbs Energies of the BCC, HCP, and CCP Structures of Metals," CALPHAD XVII Conference, Berkeley, CA, July 10–15, 1988.
15. L. Brewer, J. Kouvetakis, B. Ebbinghaus, S. Leonard, and K. Krushwitz, "Intermetallic Thermodynamics from Oxide Equilibration," High Temperature Gordon Research Conference, Plymouth, NH, July 24–29, 1988.
16. L. Brewer, "The Extraordinary Reactivity of Platinum Group Metals," IBM T.J. Watson Research Center, Yorktown Heights, NY, Sept. 22–24, 1988.
17. L. Brewer, "History of the Application of the Generalized Lewis Acid-Base Theory to Metals," World Material Congress, Chicago, IL, Sept. 24–26, 1988.
18. L. Brewer, "The Nature of Bonding in Transition Metal Aluminides," High Temperature Materials Workshop, Wright-Patterson AFB, Dayton, OH, Dec. 14, 1988.

Materials Chemistry Problems in Nuclear Technology*

Donald R. Olander, Investigator

INTRODUCTION

This experimental research program has two principal objectives. The first is concerned with the chemical and physical behavior of materials of nuclear reactor systems, both fission and fusion. The experiments are designed to explore the fundamental processes that underlie the performance of these materials in their service environments, which are characterized by combinations of high temperature, intense radiation fields, and reactive gases or liquids. Solid-state diffusion in ceramic oxides, corrosion of metals for nuclear applications, and high-temperature vaporization of nuclear ceramics are investigated in this program.

The second direction of the project is the study of gas-solid chemical reactions such as corrosion or etching by the method of molecular beams coupled with mass spectrometry. The objective of these studies is to understand the kinetics and mechanisms of such reactions in clean, well-characterized systems. Systems studied include halogen reaction with metals and semiconductors, and atomic hydrogen etching of refractory materials.

1. Modulated Molecular-Beam Studies of the Surface Chemistry of Silicon Reaction with Reactive Gases (Publication 1)

D.R. Olander, M. Balooch, J. Abrefah, and W.J. Siekhaus[†]

The method of studying the kinetics of gas-solid surface reactions using modulated-molecular beams and mass-spectrometric detection is described. The modulated molecular-beam technique permits mechanistic study of gas-solid reactions that exhibit characteristic reaction times between 10 ms to 10 μs.

In situ direct-flight mass-spectrometric detection allows for determination of individual reaction product species.

Use of the method is greatly enhanced if related techniques, such as isotopic exchange, temperature-ramp thermal desorption, and surface spectroscopies, are brought to bear on the same reaction.

Low-pressure thermal cracking of silane on Si(111) proceeds along two parallel channels, neither of which involves atomic hydrogen as a surface intermediate.

Etching of Si(111) by atomic hydrogen gas exhibits a ~5% reaction probability at room temperature and may be rate-controlled by the reaction of a loosely bound hydrogen adlayer with surface SiH_x complexes, competing processes of recombination to produce H_2, and bulk solution-diffusion of surface-adsorbed H atoms becoming more important as the temperature is increased.

[†]Permanent address: Materials and Chemistry Department, Lawrence Livermore National Laboratory, Livermore, CA 94550.

2. Reaction and Thermal Accommodation of Gases with Liquid Uranium and Two Uranium Alloys (Publication 2)

D.R. Olander, M. Balooch, and W.J. Siekhaus[†]

The reactions and the thermal accommodation of CO, CO_2, N_2, CH_4, and C_2H_2 with liquid uranium and of CO, O_2, and H_2O with (U,Fe) and (U,Cr) alloys were studied by modulated molecular-beam mass-spectrometric methods using the appearance of a reaction product or the disappearance of the reactant to determine the reaction probability. temperatures up to 1500 K were investigated. The reaction probabilities of CO, N_2, and CH_4 were below the detection limit ($<10^{-3}$). The C_2H_2 and CO_2 reaction probabilities were found to be 0.7 and 0.03, respectively. Liquid uranium alloys exhibited the same reactivities with CO_2 and O_2 as pure uranium. The reaction probabilities of H_2O with the liquid alloys, however, were about a factor of two lower than that of uranium. The thermal-accommodation coefficient ranged from 0.1 for CO and CO_2, to 0.3 for C_2H_2 and CH_4, and to 0.6 for O_2 and H_2O.

[†]Permanent address: Materials and Chemistry Department, Lawrence Livermore National Laboratory, Livermore, CA 94550.

*This work was supported by the Director, Office of Energy Research, Office of Basic Energy Sciences, Materials Sciences Division, of the U.S. Department of Energy under Contract No. DE-AC03-76SF00098.

3. Release of Fission Products (Xe, I, Te, Cs, Mo, and Tc) from Polycrystalline UO_2 (Publication 3)

S.G. Prussin, D.R. Olander, W.K. Lau, and L. Hansson

The release of xenon, iodine, tellurium, cesium, molybdenum, and technetium from lightly irradiated, polycrystalline UO_2 has been studied in post-irradiation anneal experiments. The effective diffusion coefficients for cesium were found to be comparable to those for xenon and roughly an order of magnitude smaller than those for iodine and tellurium over the temperature range studied. Activation energies for diffusion of the more volatile elements as derived from analysis within the Booth model were 156 ± 45 (Xe), 122 ± 33 (I), 115 ± 11 (Te), and 99 ± 11 (Cs) kcal/mol. The activation energies for Mo and Tc found by a similar treatment were 353 ± 24 and 205 ± 42 kcal/mol, respectively, and are indicative of a fairly complex mechanism for release of these elements. The soluble ionic species Np^{4+}, Zr^{4+}, La^{3+}, and Nd^{3+} were completely retained in the UO_2.

4. Dissolution of Uranium Dioxide by Molten Zircaloy (Publications 4 and 5)

K.T. Kim and D.R. Olander

The morphology, reaction products, kinetics, and mechanisms of the reaction of UO_2 with Zircaloy were investigated in laboratory tests at temperatures between 1900 and 2200°C and times from 10 to 200 sec. To avoid unstable density gradients and the resulting bulk motion of the melt, a disk of UO_2 was used as the bottom of a crucible with walls of thoria to contain the liquid metal. Polished sections of the post-test specimens were examined by optical microscopy, scanning electron microscopy, Auger electron spectroscopy, and electron microprobe analysis.

The complicated structures observed in the quenched specimens, which contained up to seven distinct regions, could, with the aid of phase diagrams, be traced to a two-phase interaction region at high temperature. This region arose from inhomogeneous production of metallic uranium in the near-surface part of the oxide, which permitted rapid zirconium penetration of the oxide to depths of hundreds of microns.

Both the kinetic analysis of oxygen and the uranium migration into the melt were based on a diffusion model and utilized measured solubilities of these elements in the melt and data on UO_2 specimen thickness decrease and concentration distributions in the specimen.

Dissolution of the inner walls of UO_2 crucibles by molten Zircaloy was also studied. The reaction at the vertical wall was dominated by natural convection in the adjacent liquid. The composition and microstructure were uniform throughout the frozen melt. Most uranium dissolution occurred during an initial period of rapid transfer when the two-phase oxide-melt interfacial zone was absent. Mass-transfer theory successfully explained dissolution kinetics during this period.

The solubility of uranium in the melt depends strongly on the oxygen content of the latter, which must be determined by accounting for all sources. Application of the results to estimate fuel dissolution during severe fuel damage of nuclear reactor fuel elements showed that the liquefaction process reaches completion in about 100 sec at 2100°C.

5. Surface-Temperature Transients from Pulsed Laser Heating of UO_2 (Publication 6)

S.K. Yagnik and D.R. Olander

Surface heating of UO_2 by a pulsed laser was investigated theoretically and experimentally. Targets of solid uranium dioxide in vacuum were rapidly heated to peak temperatures of 3700 K, as measured by a fast-response automatic optical pyrometer. The measured target surface temperatures were compared with a one-dimensional heat-transport model that accounts for conduction and melting in the solid and ablation and radiation from the surface. Congruent vaporization of UO_2 was assumed. The measured temporal and spatial characteristics of the laser beam, as well as temperature-dependent physical and thermodynamic properties of UO_2, are used as input to the calculations. Agreement of the theory with the measurements was further validated by post-irradiation microscopic examination of the target surface. Additional tests were performed to qualitatively assess the attenuation of laser light and thermal radiation from the surface by the vapor blow-off from the target. This effect was found to be insignificant.

6. The Kinetics of Tungsten Etching by Atomic and Molecular Chlorine (Publication 7)

M. Balooch, D.S. Fischl, D.R. Olander, and W.J. Siekhaus[†]

The reactions of atomic and molecular chlorine with tungsten were studied by modulated-beam mass-spectrometric methods over the temperature range 300–1350 K. The atomic beam was generated by an RF plasma discharge. With both atomic and molecular beams, the main reaction product up to about 1000 K was WCl_4. The reaction probability with atomic chlorine was a factor of approximately ten higher than that obtained with molecular chlorine. The reaction was nonlinear with respect to Cl_2 intensity at low beam fluxes but approached linearity at high beam intensities. Above 1000 K the main reaction product was atomic chlorine. Its reaction probability increased rapidly with temperature; at 1300 K nearly complete dissociation of Cl_2 was observed. A kinetic model based on the Eley-Rideal mechanism was proposed and compared with the data.

[†]Permanent address: Materials and Chemistry Department, Lawrence Livermore National Laboratory, Livermore, CA 94550.

7. Laser-Pulse Vaporization of Uranium Dioxide and Other Refractory Materials (Publication 8)

D.R. Olander, S.K. Yagnik, and C.H. Tsai

The nature of the vapor produced by pulse surface heating of UO_2 and several other materials was investigated using normal-mode laser pulses with peak-power densities between 10^4 and 10^6 W/cm^2. Maximum surface temperatures measured by optical pyrometry ranged from 1900 to 4200 K. At temperatures below ~2400 K for UO_2, the vapor pulse followed the Hertz-Langmuir vacuum-vaporization theory. More energetic transients produced gas-dynamic blowoffs accompanied by significant supersaturation in the expanding plume. Neutron-activation analysis of the collected vapor indicated that the total quantity of liquid UO_2 evaporated in the pulse followed the Hertz-Langmuir formula. However, mass-spectrometric analysis of the emitted vapor showed large deviations in the quantity and waveform shape of the monomer species. These and other features of the blowoff were satisfactorily explained in terms of nucleation and growth of polymeric species. Although UO_2 clusters were undetectable by the mass spectrometer, polymers of MgO and ZrO_2 were observed.

8. Work in Progress

The reaction of chlorine with refractory metals is being investigated by the molecular-beam method.

The amorphization of intermetallic precipitates in Zircaloy is being studied by irradiation by high-energy electrons.

The high-temperature corrosion of Zircaloy by steam in the presence of hydrogen is being studied by a gravimetric technique. The solubility of hydrogen in Zircaloy is also being investigated.

Oxygen self-diffusion in the tetragonal high-temperature form of zirconia is being measured gravimetrically using the oxygen-isotope exchange method.

The interaction of iodine vapor with oxidized steel is being studied in a flow system with mass-spectrometric sampling.

The effect of grain size of UO_2 on the release of fission products is being investigated.

A simple mathematical technique for incorporating the heat effect of a phase change on moving-boundary heat-conduction problems is under investigation.

The combined effects of moving grain boundaries and solute diffusion into the lattice on solute transport by grain-boundary diffusion are being analyzed theoretically.

1988 PUBLICATIONS AND REPORTS

Refereed Journals

1. D.R. Olander, M. Balooch, and J. Abrefah, "Modulated Molecular-beam Studies of the Surface Chemistry of Silicon Reaction with Reactive Gases," J. Vac. Sci. Technol. **B5**, 1404 (1987); LBL-23205.
2. D.R. Olander, M. Balooch, and W.J. Siekhaus, "Reaction and Thermal Accommodation of Gases with Liquid Uranium and Two Uranium Alloys," High Temp. Sci. **24**, 21 (1987); LBL-23748.
3. S.G. Prussin, D.R. Olander, W.K. Lau, and L. Hansson, "Release of Fission Products (Xe, I, Te, Cs, Mo and Tc) from Polycrystalline UO_2," J. Nucl. Mater. **154**, 25 (1988); LBL-23786.
4. K.T. Kim and D.R. Olander, "Dissolution of Uranium Dioxide by Molten Zircaloy — I. Diffusion Controlled Reaction," J. Nucl. Mater. **154**, 85 (1988); LBL-23778.

5. K.T. Kim and D.R. Olander, "Dissolution of Uranium Dioxide by Molten Zircaloy — II. Convection-Controlled Reaction," J. Nucl. Mater. **154**, 102 (1988); LBL-23802.
6. S.K. Yagnik and D.R. Olander, "Surface Temperature Transients from Pulsed Laser Heating of UO_2," J. Nucl. Mater. **154**, 253 (1988); LBL-24022.
7. M. Balooch, D.S. Fischl, and D.R. Olander, "Kinetics of Tungsten Etching by Atomic and Molecular Chlorine," J. Electrochem. Soc. **125**, 2090 (1988); LBL-24255.
8. D.R. Olander, S.K. Yagnik, and C.H. Tsai, "Laser-pulse Vaporization of Uranium Dioxide and Other Refractory Materials," J. Appl. Phys. **64**, 2680 (1988); LBL-24405.

LBL Reports

9. D.K. Wilson (M.S. Thesis), "Oxidation and Reduction of Uranium Dioxide in Steam and Hydrogen," LBL-26406.
10. A.F. Motta and D.R. Olander, "Electron-Irradiation Induced Amorphization of Precipitates in Zircaloy," LBL-25370.
11. J. Abrefah and D.R. Olander, "Reaction of Atomic Hydrogen with Crystalline Silicon," LBL-26315.
12. J. Abrefah, D.F. Dooley, and D.R. Olander, "Reduction of UO_{2+x} by Atomic Hydrogen," LBL-26408.
13. D.R. Olander and Y.S. Kim, "A Simplified Approach to Transient Heat Conduction with Change of Phase," LBL-26409.
14. T. Wonnell (M.S. Thesis), "X Ray and TEM Characterization of the Uranium-Zirconium Alloy Fuel for the Integral Fast Reactor," LBL-26410.
15. F. Tehranian and D.R. Olander, "Laser-Pulse Vaporization of Uranium Carbide," LBL-24795.
16. Y. Eyal and D.R. Olander, "Leaching of Uranium and Thorium from Monazite—I. Initial Leaching," LBL-26411.
17. D.R. Olander and Y. Eyal, "Leaching of Uranium and Thorium from Monazite—II. Elemental Leaching," LBL-26412.
18. D.R. Olander and Y. Eyal, "Leaching of Uranium and Thorium from Monazite—III. Isotopic Fractionation," LBL-26413.
19. D.F. Sherman and D.R. Olander, "Hydrogen Dissolution and Release from Nonmetals—I. Uranium Dioxide," LBL-26414.

Invited Talks

20. D.R. Olander, "Effect of UO_2 Morphology Changes on the Transient Release of Volatile Fission Products from Severely Damaged LWR Fuels," Technion, Department of Nuclear Engineering, Haifa, Israel, Mar. 3, 1988.
21. D.R. Olander, "The Integral Fast Reactor Concept," Technion, Department of Nuclear Engineering, Haifa, Israel, Mar. 13, 1988.
22. D.R. Olander, "Post-Irradiation Annealing Studies of Fission Product Release from UO_2," Technion, Department of Nuclear Engineering, Haifa, Israel, Apr. 12, 1988.
23. D.R. Olander, "Investigation of Silicon Etching by the Modulated Molecular Beam Method," Technion, Department of Chemical Engineering, Haifa, Israel, Apr. 13, 1988.
24. D.R. Olander, "Nuclear Reactor Severe-Accident Chemistry and Academic Research," panel, Second Nuclear Reactor Severe-Accident Chemistry Symposium, Toronto, Ontario, June 7, 1988.
25. D.R. Olander, "Dissolution of Uranium Dioxide by Molten Zircaloy," Second Nuclear Reactor Severe-Accident Chemistry Symposium, Toronto, Ontario, June 7, 1988.
26. D.R. Olander, "Leaching of Uranium and Thorium from Monazite," Department of Nuclear Engineering, University of California at Berkeley, Sept. 19, 1988.
27. D.R. Olander, "Oxygen Self-Diffusion in Tetragonal Zirconia," 25th Semiannual Bay Area Conference on High Temperature Science and Technology, LBL, Nov. 9, 1988.

Electrochemical Phase Boundaries*

Rolf H. Muller, Investigator

INTRODUCTION

Nucleation and growth processes in the electrocrystallization of metals from aqueous media are investigated to advance the understanding of the propagation of deposit properties from the first atomic layers to macroscopic thicknesses. The effect of adsorbed molecules is studied in the early stages of deposition to gain insight into the action of leveling and brightening agents and their effect on the properties of thin-film metal deposits. Such agents are used on an empirical basis in technical electrodeposition, but for applications in new systems, a greater understanding of their function is necessary for their selection and the prediction of their effects.

New experimental techniques are developed and used for determining microtopographies and chemical constituents at deposit surfaces, particularly while they are immersed in the electrolyte: the development of microtopographies is followed *in situ* by scanning tunneling microscopy (STM) and *ex situ* by stylus profilametry with digital data analysis, and optical and electron microscopy. Adsorbed materials on electrode surfaces are determined *in situ* by Raman spectroscopy and spectroscopic ellipsometry, which are sensitive to monolayer coverages of some materials. Additives incorporated in metal deposits are determined *ex situ* by Auger electron spectroscopy (AES), x-ray photoelectron spectroscopy (XPS), and secondary-ion mass spectroscopy (SIMS). The results of measurements are compared to predictions of theoretical models.

Studies of electrochemical surface layers on battery electrode materials are reported under "Electrochemical Energy Storage." Research on electrochemical mass transfer, conducted in collaboration with C.W. Tobias, is reported in his section of this annual report, entitled "Electrochemical Processes."

*This work was supported by the Director, Office of Energy Research, Office of Basic Energy Sciences, Materials Sciences Division, of the U.S. Department of Energy under Contract No. DE-AC03-76SF00098.

1. STM Observations of the Electrodeposition of Copper (Publication 5)

M.J. Armstrong and R.H. Muller

Scanning tunneling microscopy (STM) has been used to investigate the electrocrystallization of metals with atomic resolution of surface topography. Parasitic currents to the Pt tunneling probe have been reduced to 10% of the tunneling current by the application of insulating coatings of polyvinylidine fluoride to the probe and by floating operation of electronic components. In order to avoid Faradaic currents between probe and surface, the probe potential was restricted to the range between Cu deposition and Pt oxidation. Software has been developed to digitally collect data in an array of 320 by 200 points and to display results in different forms: derivative-coded intensity has been found particularly effective to represent topographies.

Cu deposition on Pt(111) from 5mM $Cu(ClO_4)_2$, 0.5M $NaClO_4$ was followed by STM in a constant-tunneling-current (2 nA) mode with a sample-to-probe bias of -100 mV. Deposition rates under potential control were found to be highly nonuniform on a submicroscopic scale. The rate of deposit growth (at 50 mV), derived from the rate of vertical probe displacement between 1 and 1.5 min of deposition, was $\sim$1000Å/min in areas where nucleation had occurred. This rate was 40 times higher than that expected from the average current density of 0.1 mA/cm^2 on the entire electrode. Single and multiatomic steps between smooth regions in the deposit were found to be stable under cathodic potential control, but they disappeared at open circuit (see Figures 1-1 and 1-2). These observations illustrate changes that may occur during transfer of electrochemical specimens from the liquid phase.

2. STM of Cu Electrodeposited in the Presence of Benzotriazole (Publication 6)

M.J. Armstrong and R.H. Muller

Effects of the leveling agent benzotriazole (BTA) on the microtopography of copper deposited under controlled potentials on a Pt(111) surface have been investigated by continuous scanning with the probe of a STM during deposition from 10mM $Cu(ClO_4)_2$, 0.5M $NaClO_4$, pH 2, with and without 10μM BTA. The electrochemical cell contained an electrolyte volume of 0.05 ml, with reference and counter electrodes in separate cells connected by capillary tubing.

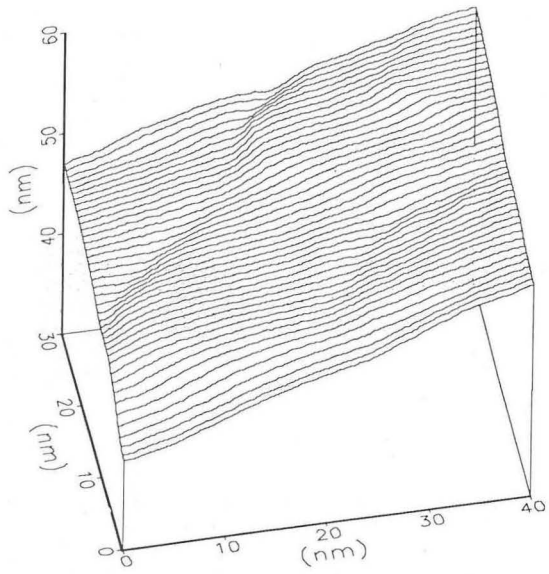

Figure 1-1. STM line plot of electrochemically deposited Cu on Pt(111) from 10mM $Cu(ClO_4)_2$, 0.5M $NaClO_4$, pH 2 after 5 min at −50 mV vs Cu. Single and multiatomic steps between atomically smooth regions. (XBL 889-3344)

Deposits from BTA-free electrolyte showed long-range order exceeding the width of the probe scan of 0.6 μm (see Figure 2-1), with the deposition occurring at the edges of crystal facets. In the presence of BTA, no faceting or long-range order was observed. Atomically smooth planes on the bare Pt surface, separated by 20-Å ledges, became wavy, with an amptitude of 5 Å and a period of about 200 Å, following a potential pulse of 0.5 sec to −500 mV vs

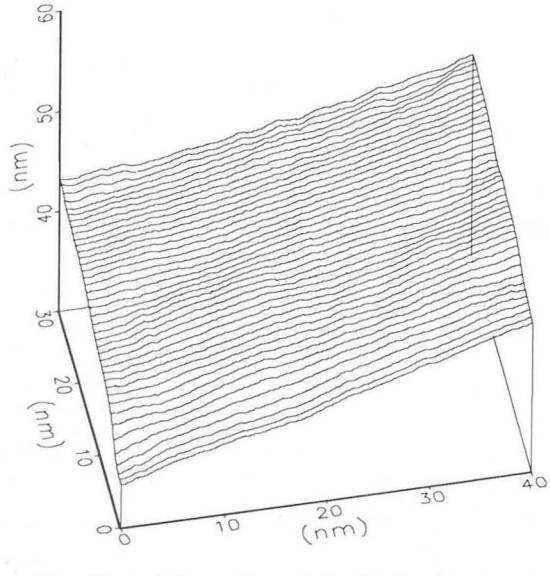

Figure 1-2. Deposit from Figure 1-1 after 1 min at open circuit. Note disappearance of most steps on the surface. (XBL 889-3343)

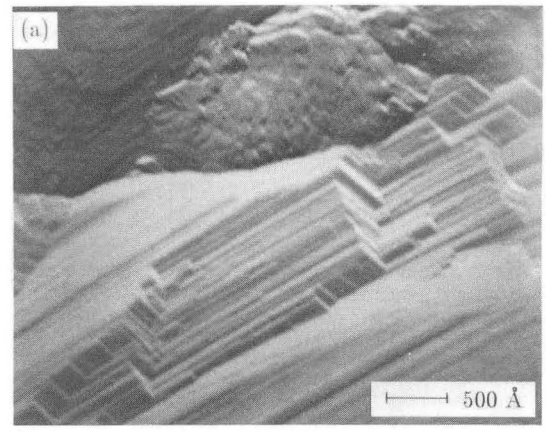

Figure 2-1. STM derivative-coded gray-scale image of electrochemically deposited Cu on Pt(111) from 10mM $Cu(ClO_4)_2$, 0.5M $NaClO_4$, pH 2 in the absence of BTA after 30 sec at −500 mV. Faceted crystals with long-range order. (XBB 8810-11213)

Cu (see Figure 2-2). This observation is proposed to represent the formation of the first monolayer of deposit in the form of islands. During subsequent deposition at −20 mV, elongated nuclei of 20 Å height and 500 Å width were observed after 90 sec of deposition.

3. Island Films Resulting From Ion Bombardment (Publication 7)

M.J. Armstrong and R.H. Muller

The ion bombardment of compact Pb films less than 100 nm thick has been found to result in a nonuniform removal of material and the formation of island films. This observation differs from the uniform removal on which the determination of

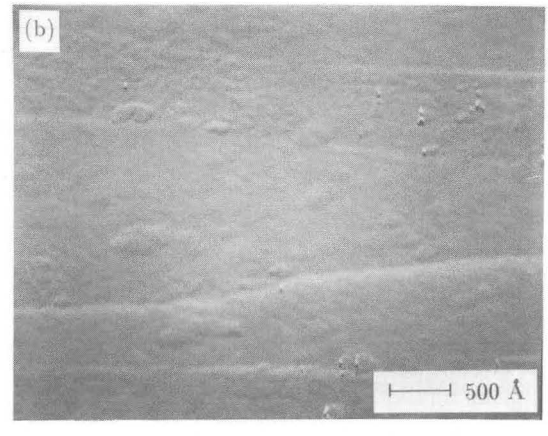

Figure 2-2. Cu deposited in the presence of 10μM BTA after 0.5 sec at −500 mV; other conditions as in Figure 2-1. Island growth of first monolayer. (XBB 8810-11211)

composition profiles by AES is based. The process is independent of the film preparation or the presence of an oxide overlayer. AES measurements interpreted in terms of surface coverage (rather than composition) agree well with ellipsometer measurements interpreted by the use of the coherent-superposition model for patchwise film coverage, developed earlier, thus supporting the validity of this optical model.

4. Studies on High-Speed Electroforming (Publication 1)

D.P. Barkey, R.H. Muller, and C.W. Tobias

Studies of high-speed copper electrodeposition have been undertaken to assess the potential for electroforming at rates comparable to those of shaping by mechanical means. The Fourier analysis of surface profiles of deposits showed a decrease in roughness amplitude and protrusion spacing with increasing current density at constant fraction of limiting current. These results agree with predictions based on the effect of mass-transport boundary layers that follow the contours of the larger surface features and are consistent with the observed higher nucleation density caused by higher kinetic overpotential.

5. Enhancement of Mass Transfer by Suspended Solids (Publication 2)

P.K. Andersen, R.H. Muller, and C.W. Tobias

Concentrated suspensions of inert solids have been found to increase mass transfer to a rotating disk by as much as fourfold. Enhancement increases with shear rate and is greatest for particles of size comparable to the thickness of the mass-transfer boundary layer. For small particles, a mechanism that involves microconvective vortices, which increase the dispersion of solutes and the dissipation of energy, is proposed. For particles much larger than the thickness of the mass-transfer boundary layer, transport enhancement is proposed to result from the formation of a particle-depleted slip layer at the electrode surface. The increased shear rate in this layer compared to that in a homogeneous suspension results in a thinning of the mass-transfer boundary layer.

1988 PUBLICATIONS AND REPORTS

Other Publications

1. D.P. Barkey, R.H. Muller, and C.W. Tobias, "Studies on High-Speed Electroforming," Electrochem. Soc. Meeting, Atlanta, GA, May 15–20, 1988, Ext. Abstr. 386.
2. P.K. Andersen, R.H. Muller, and C.W. Tobias, "Enhancement of Mass Transfer to a Rotating Disk by Suspended Solids," Electrochem. Soc. Meeting, Atlanta, GA, May 15–20, 1988, Ext. Abstr. 278; LBL-24522.
3. D.P. Barkey, R.H. Muller, and C.W. Tobias, "Stability Analysis of Metal Electrodeposition," Electrochem. Soc., Chicago, IL, October 9–14, 1988, Ext. Abstr. 325; LBL-26022.
4. D.P. Barkey, "Liquid Membrane Coated Ion-Exchange Column Solids," U.S. Patent 4,747,949.

LBL Reports

5. M.J. Armstrong and R.H. Muller, "STM Observations of Electrodeposited Copper under Potential Control and at Open Circuit," accepted by J. Electrochem. Soc.; LBL-26049.
6. M.J. Armstrong and R.H. Muller, "Scanning Tunneling Microscopy of Copper Electrodeposited in the Presence of Benzotriazole," LBL-26508.
7. M.J. Armstrong and R.H. Muller, "Island Films Resulting from Ion Bombardment: Spectroscopic Ellipsometry and Auger Electron Spectroscopy," accepted by J. Appl. Phys.; LBL-25447rev.
8. M.J. Armstrong and R.H. Muller, "Spectroscopic Ellipsometry of Ion-Bombarded Lead Films," LBL-25447.
9. D.P. Barkey, R.H. Muller, and C.W. Tobias, "Roughness Development in Metal Electrodeposition: I. Experimental Results," submitted to J. Electrochem. Soc.; LBL-26021.
10. D.P. Barkey, R.H. Muller, and C.W. Tobias, "Roughness Development in Metal Electrodeposition: II. Stability Theory," submitted to J. Electrochem. Soc.; LBL-26022.
11. D.P. Barkey, R.H. Muller, and C.W. Tobias, "Studies in High Speed Electroforming," accepted for publication in Proceedings volume *Electrochemistry in Mineral and Metal Processing*, The Electrochemical Society, 1988; LBL-23880.

Invited Talks

12. R.H. Muller, "Ellipsometry of Electrochemical Surface Layers," Electrochemical Society Meeting, Atlanta, GA, May 15–20, 1988, Ext. Abstr. 324.

13. R.H. Muller, "Optical Methods for the Study of Electrochemical Surface Layers and Electrochemical Processes," lecture course, Department of Applied Chemistry, Chongqing University, People's Republic of China (first foreign guest lecturer), Sept. 16–Oct. 15, 1988.

14. R.H. Muller, "Studies of Electrochemical Surface Layers," four lectures, Analysis and Testing Center for Physics and Chemistry, Chengdu University of Science and Technology, Chengdu, People's Republic of China, Oct. 10–11, 1988.

Nuclear Magnetic Resonance*

Alexander Pines, Investigator

INTRODUCTION

The goals of the nuclear magnetic resonance (NMR) program are the development of novel theory and experiments in magnetic resonance and the demonstration of their application to materials research. Recent techniques developed in our laboratory include multiple-quantum spectroscopy, zero-field NMR, iterative maps, double rotation (DOR), and SQUID magnetic resonance. Materials applications include clusters, semiconductors, oxides, liquid crystals, zeolites, and intercalated graphite.

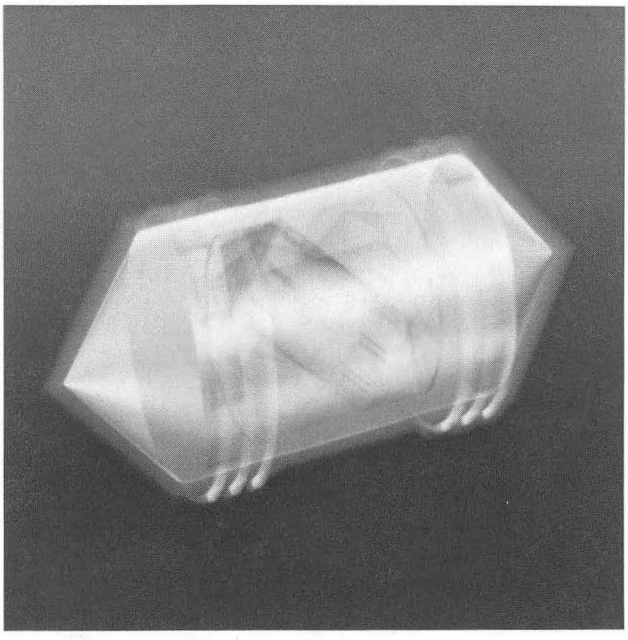

Double rotor (CBB 880-10988)

1. Oxygen-17 NMR in Solids

B. Chmelka, K.T. Mueller, A. Samoson, B. Sun, Y. Wu, and J.W. Zwanziger

It is widely lamented that despite its success with spin-1/2 nuclei such as carbon-13, silicon-29, and phosphorus-31, the popular NMR technique of magic-angle spinning (MAS) is restricted in its application to important quadrupolar nuclei such as oxygen-17, sodium-23, and aluminum-27, due to second-order broadening. Two new techniques, double rotation (DOR) and dynamic-angle spinning (DAS), involving the rotation of a sample around two axes, overcome these problems. Preliminary applications of the techniques include high-resolution NMR of sodium-23, and the observation of distinct oxygen-17 sites in solid oxides. Current work is under way on minerals, zeolites, and high-temperature superconductors.

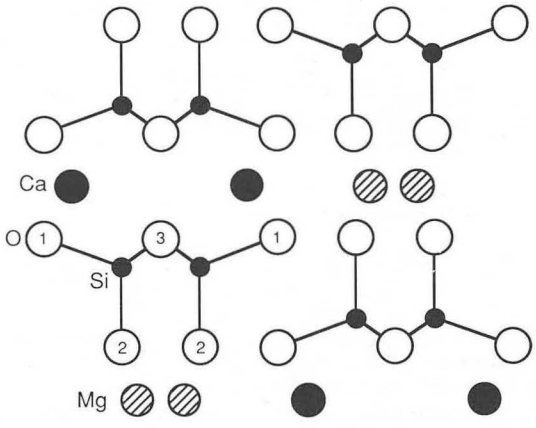

Figure 1-1. Structure of diopside, $CaMgSi_2O_6$, viewed as a projection along the tetrahedral chains. Oxygen is represented by open circles with the three distinct sites labeled. (XBL 891-197A)

*This work was supported by the Director, Office of Energy Research, Office of Basic Energy Sciences, Materials Sciences Division, of the U.S. Department of Energy under Contract No. DE-AC03-76SF00098.

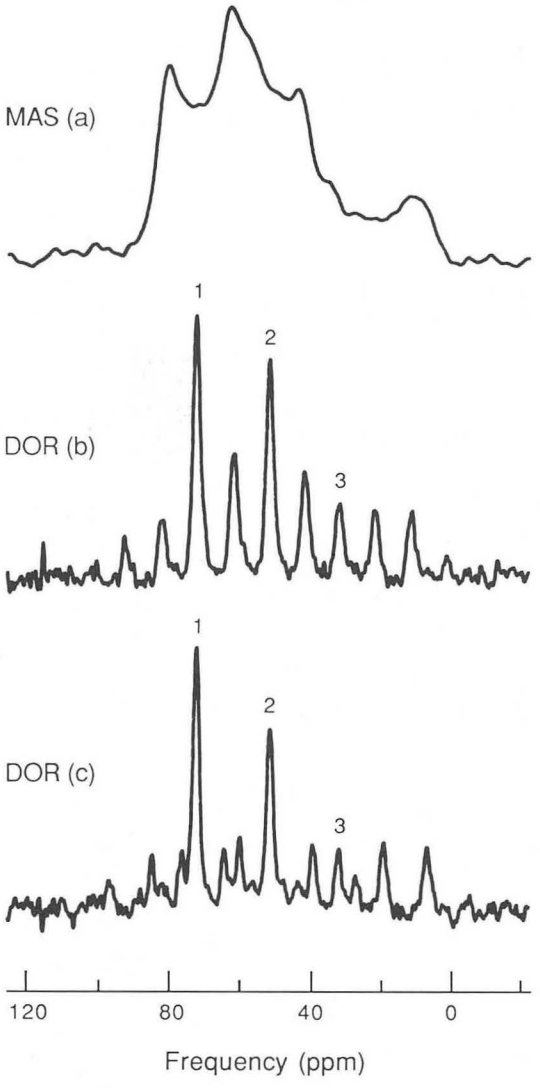

Figure 1-2. NMR spectra of oxygen-17 in a sample of diopside, under conditions of magic-angle spinning (MAS) (a), and in response to double rotation (DOR) with the outer rotor spinning at 540 Hz (b) and 680 Hz (c). The isotropic centerband peaks correspond to the three numbered oxygen sites in the top figure. (XBL 891-308A)

2. Berry's Phase for Spins

M. Koenig, K.T. Mueller, D. Suter, and J.W. Zwanziger

When a quantum system undergoes a cyclic evolution, it accumulates a geometric (Berry's) phase related to the topology of density matrix space and the geometry of the trajectory. These effects have been demonstrated by NMR interferometry and echo experiments; they are related to the (Pancharatnam) phases accumulated in a cycle of quantum measurements. Current work involves experiments that demonstrate for the first time the non-Abelian generalization of Berry's phase by transporting a degeneracy in a nonconical circuit. It is exciting that this is related to the notion of "incomplete" quantum measurement.

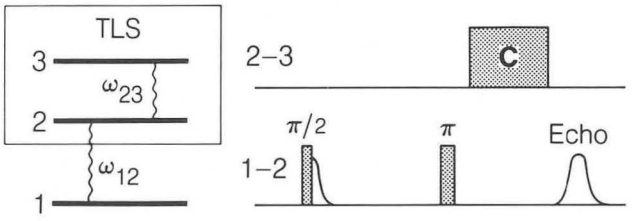

Figure 2-1. Schematic representation of the NMR interferometry experiment to demonstrate the Aharonov-Anandan generalization of Berry's phase. The 2–3 two-level system (TLS) undergoes a circuit C in projective Hilbert (density matrix) space, and the phase is determined by means of its effect on the echo produced by the coherent superposition of levels 1 and 2. (XBL 8711-9093A)

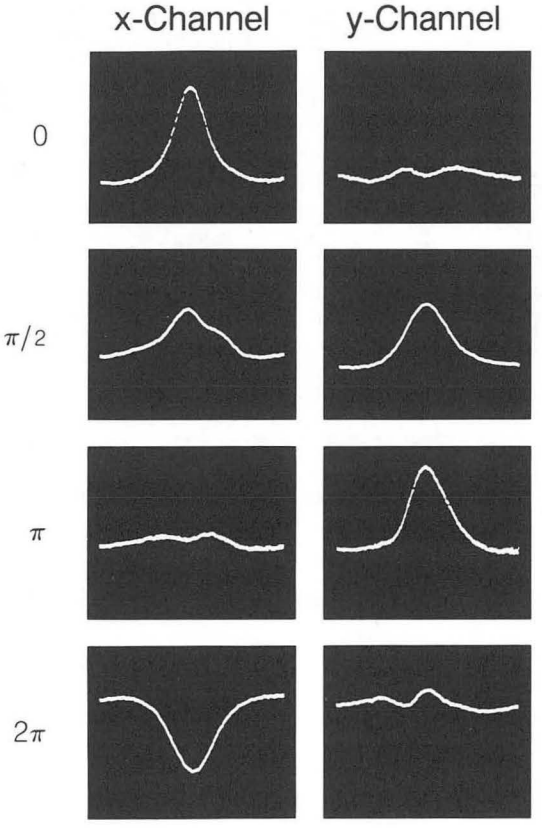

Figure 2-2. Oscilloscope traces of the 1–2 echoes detected in the two orthogonal (x,y) channels of a phase-sensitive detector at frequency ω_{12}. In this case, the 2–3 TLS undergoes circuits with solid angles $\Omega(C)$ equal to 0, $\pi/2$, π, and 2π. The Berry phase is $\Omega(C)/2$ and is invariant to area-preserving distortions of the circuit shape. (XBL 8711-4824A)

3. Clusters in Solids

D. Caplan, B. Chmelka, M. Koenig, J. Pearson, D. Raftery, and C. Schmidt

Two techniques are being further developed and used to "count" clusters and to characterize the distribution of atoms and molecules in solids. The first technique is multiple-quantum NMR, which involves the selective detection of spectroscopic events in which groups of n spins flip and groups of n radiofrequency quanta are absorbed or emitted.

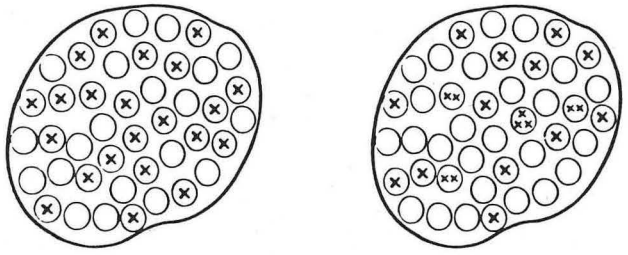

Figure 3-1. Two possible distributions for molecular guests adsorbed in NaY-zeolite supercages. The diagram to the left corresponds to a homogeneous guest dispersion, while that on the right represents a statistical distribution. (XBL 895-1690)

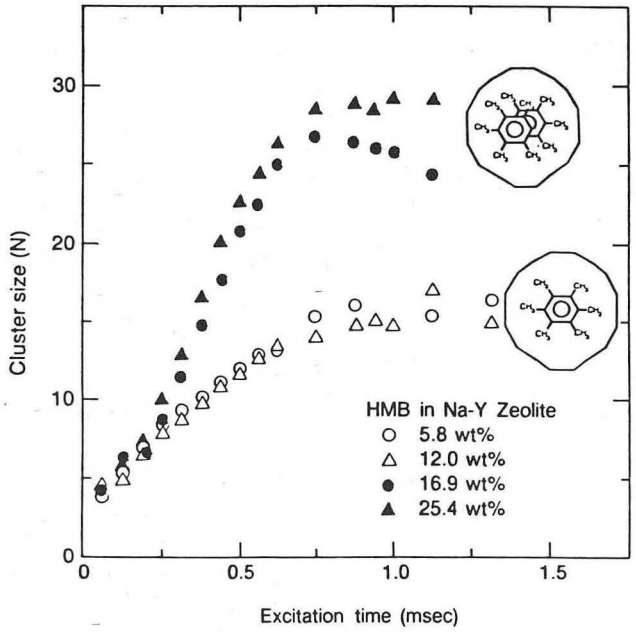

Figure 3-2. Proton multiple-quantum NMR results for hexamethylbenzene (HMB) adsorbed in NaY-zeolite. The data reveal the homogeneous nature of the HMB guest distribution as molecules preferentially enter empty supercages before increasing the occupancy of cavities already containing an adsorbed guest. (XBL 895-1689)

The second technique is xenon NMR, in which the spherical xenon atom is used as a sensitive probe of its surroundings. Problems being studied by these techniques include the distribution of molecules and metal particles in zeolite cavities, the dynamics of dilute spin systems, and molecules intercalated in graphite.

4. Multiple-Pulse NMR and Iterative Maps

H. Cho, K.T. Mueller, M. Rosen, S.P. Rucker, A.J. Shaka, and D.N. Shykind

Multiple-pulse schemes used in the extended excitation of spin systems are traditionally derived by average Hamiltonian theory and periodic application of a basic cycle. An alternative approach, stable over a wide range of instrument parameters, involves the application of iterative maps on SO(3). Fixed points of $U_{n+1} = F(U_n)$ are sought, where U are propagators that are then implemented by means of sophisticated pulse programmers and digital phase shifters. Recent applications include Carr-Purcell trains, spin-decoupling, bistable maps, and coherence transfer in two-dimensional spectroscopy.

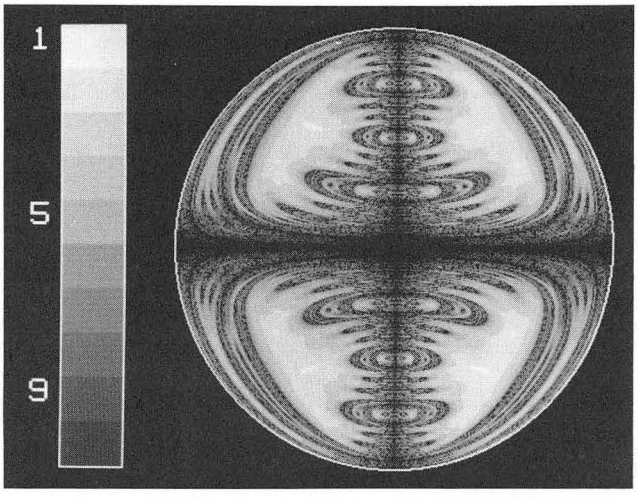

Figure 4-1. Two-dimensional basin image through a slice of SO(3) containing the z axis of the map specified by the scheme [0, 330, 60, 330, 0], preceded by the premapping step [0, 180, 90, 270, 90, 180, 0]. The basin shown is of the equator and can be identified by the light colored regions within the circle. The gray scale to the left assigns the correspondence between the shade at a point and the number of iterations necessary to map the point to the equator. Pulse sequences based on these maps can be used for frequency-selective excitation. (XBB 888-7859)

5. Zero-Field NMR

T. Jarvie, S. Matsui, B. Sun, and K. Takegoshi

In zero-field NMR, the magnetic field experienced by the sample is cycled between a high value (used for polarization and detection) and zero field, in which spin evolution occurs. This can produce sharp NMR spectra even for polycrystalline or disordered materials and has previously been used to study local symmetry in liquid crystals and correlated motions in hydrogen bonds of solid carboxylic acid dimers. Recent developments involve the application of pulses in zero field, the suppression of zero-frequency peaks, and two-dimensional correlations between high and zero field.

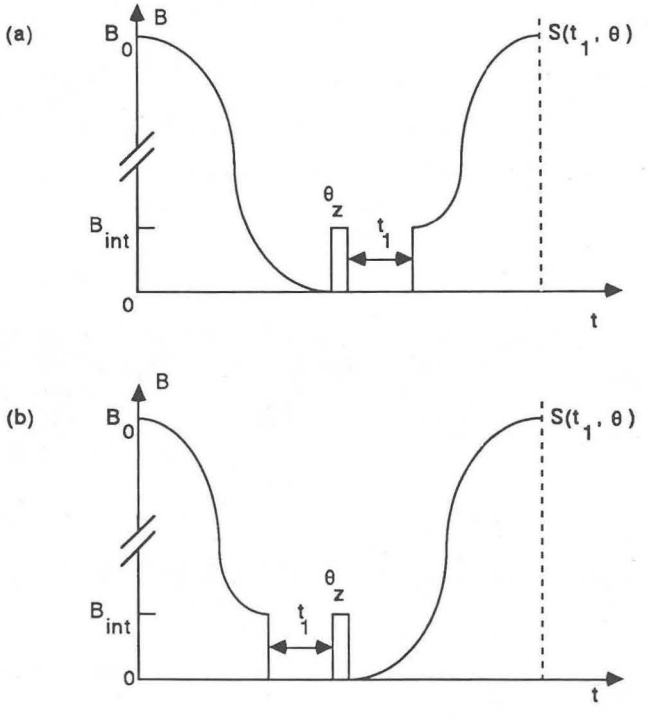

Figure 5-1. Field cycle for the zero-frequency suppression experiment. The sample is adiabatically removed from high field (4.2 T) to zero field. A dc magnetic-field pulse of angle θ_z initiates evolution, which proceeds for a time t_1. Termination of the evolution is caused by the sudden reapplication of an intermediate field (0.01 T) along the z axis. The sample is adiabatically remagnetized to high field, where the signal as a function of t_1 is measured. The maximum signal is achieved when θ_z is 50°. (XBL 8812-4274)

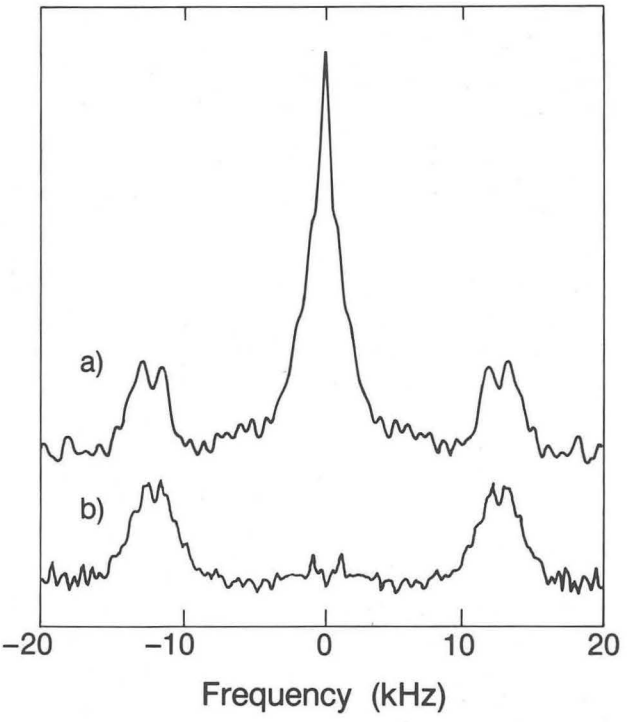

Figure 5-2. Zero-field NMR spectra of polycrystalline p-toluic acid without (a) and with (b) zero-frequency suppression. The splitting of lines at ~12 kHz arises from the correlated motions of hydrogens in the hydrogen bonds. (XBL 8812-9817)

6. SQUID Magnetic Resonance

J. Chang, C. Connor, and N.Q. Fan

In a collaborative project with J. Clarke and E.L. Hahn of MCSD and the University of California at Berkeley Physics Department, two new spectrometers have been designed for the direct detection of low-frequency magnetic resonance using dc Superconducting QUantum Interference Device (SQUID) detectors. Such devices enhance the detection sensitivity by many orders of magnitude. One spectrometer works in continuous-wave mode by detecting dc flux induced by a swept radiofrequency source, whereas the second detects the time-domain signal following a radiofrequency pulse. Using these spectrometers, low-frequency (typically less than 1 MHz) NMR and nuclear quadrupole resonance have been observed for deuterium in solid toluene-d3, boron-11 in glasses, aluminum-27 in crystalline sapphire, magnesium-25 in metallic magnesium, and quantum tunneling of methyl groups at low temperature.

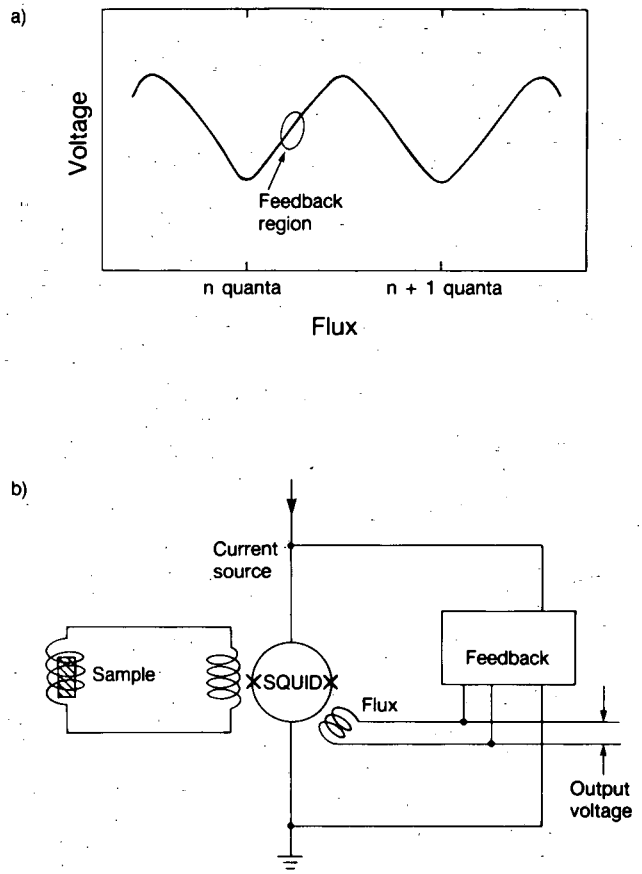

Figure 6-1. Voltage across the SQUID as a function of the number of flux quanta enclosed by the SQUID loop and feedback circuit used to measure the flux generated by magnetization of the sample. (XBL 8812-9768)

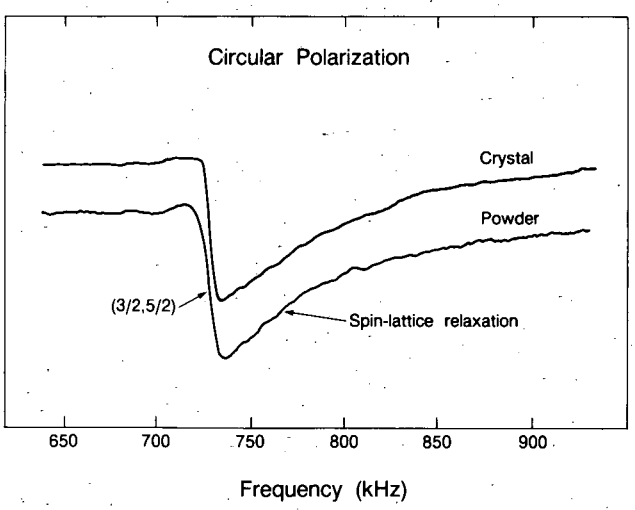

Figure 6-2. Response of aluminum-27 in single-crystal and powder samples of Al_2O_3 at zero field using circularly polarized radiation. Shown is the SQUID-detected magnetization induced by selectively exciting the $(-3/2, -5/2)$ transition, and exponential relaxation of the magnetization to the thermal equilibrium value. (XBL 8810-9770)

1988 PUBLICATIONS AND REPORTS

Refereed Journals

1. A.J. Shaka, D.N. Shykind, G.C. Chingas, and A. Pines, "Multiple-Pulse Sequences for Precise Transmitter Phase Alignment," J. Magn. Reson. **80**, 96 (1988); LBL-24027.
2. D. Suter, A. Pines, J.H. Lee, and G. Drobny, "Broadband Heteronuclear Spin Decoupling in Solids," Chem. Phys. Lett. **144**, 324 (1988); LBL-24170.
3. S.-B. Liu, J.F. Stebbins, E. Schneider, and A. Pines, "Diffusive Motion in Alkali Silicate Melts: An NMR Study at High Temperature," Geochim. Cosmochim. Acta **52**, 527 (1988); LBL-23806.
4. A.J. Shaka, C.J. Lee, and A. Pines, "Iterative Schemes for Bilinear Operators: Applications to Spin Decoupling," J. Magn. Reson. **77**, 274 (1988); LBL-23797.
5. D.N. Shykind, J. Baum, S.-B. Liu, A. Pines, and A.N. Garroway, "Phase-Incremented MQ-NMR Experiments," J. Magn. Reson. **76**, 149 (1988); LBL-23696.
6. R.J. Wittebort, M.G. Usha, D.J. Ruben, D.E. Wemmer, and A. Pines, "Observation of Molecular Reorientation in Ice by Proton and Deuterium Magnetic Resonance," J. Am. Chem. Soc. **110**, 56 (1988); LBL-24890.
7. D. Suter, K. Mueller, and A. Pines, "Study of the Aharonov-Anandan Quantum Phase by NMR Interferometry," Phys. Rev. Lett. **60**, 1218 (1988); LBL-24428.
8. B.F. Chmelka, L.C. de Menorval, S.-B. Liu, E.E. Petersen, C.J. Radke, R. Ryoo, and A. Pines, "Probing Metal Cluster Formation in NaY Zeolite by Xe-129 NMR," J. Am. Chem. Soc. **110**, 4465 (1988); LBL-24419.
9. A.J. Shaka, S.P. Rucker, and A. Pines, "Iterative Carr-Purcell Trains," J. Magn. Reson. **77**, 606 (1988); LBL-24424.
10. A. Samoson, E. Lippmaa, and A. Pines, "High Resolution Solid State NMR: Averaging of Second-Order Effects by Means of a Double Rotor," Mol. Phys. **65**, 1013 (1988); LBL-25684.
11. D. Suter and J. Pearson, "Experimental Classification of Multi-Spin Coherence under the Full Rotation Group," Chem. Phys. Lett. **144**, 328 (1988); LBL-24034.
12. J.B. Murdoch, J.F. Stebbins, I.S.E. Carmichael, and A. Pines, "A Silicon-29 Nuclear Magnetic Resonance Study of Silicon-Aluminum Ordering in Leucite and Analcite," Phys. Chem. Minerals **15**, 370 (1988); LBL-22552.

Other Publications

13. G.C. Chingas, C.J. Lee, E. Lippmaa, K.T. Mueller, A. Pines, A. Samoson, B.Q. Sun, D. Duter, and T. Terao, "New Angles in Sample Spinning," in *Proc.*

XXIVth Congress Ampere on Magnetic Resonance and Related Phenomena, J. Stankowski, N. Pislewski, and S. Idziak, eds., Poznan, Sept. 1988, p. D82; LBL-25391.

14. A. Pines, "Lectures on Pulsed NMR," in *Proc. 100th School of Physics "Enrico Fermi," B. Maraviglia, Ed., North Holland, Amsterdam, 1988, p. 43; LBL-22316.*
15. Double-Rotation NMR, U.S. Patent Application No. 227,729.

LBL Reports

16. S.P. Rucker and A.J. Shaka, "Broadband Homonuclear Cross Polarization in 2D NMR Using DIPSI-2," submitted to Mol. Phys.; LBL-26611.
17. J. Anandan, R.Y. Chaio, G. Chingas, K.M. Ganga, R.A. Harris, H. Jiao, A.S. Landsberg, A. Pines, and D. Suter, "Nonadiabatic Geometrical Phase in NMR and Optics," LBL-23410.
18. K. Takegoshi, T.P. Jarvie, D. Suter, D.B. Zax, and A. Pines, "Suppression of The Zero-Frequency Peak in Time-Domain Zero-Field NMR," submitted to Chem. Phys. Lett.; LBL-24429.
19. K. Takegoshi, T.P.Jarvie, D. Suter, D.B. Zax, and A. Pines, "Spin-Echo Phenomena in Zero-Field NMR," LBL-24426.
20. S.-B. Liu, L.C. de Menorval, K. Takegoshi, R. Ryoo, M. Trecoske, and A. Pines, "Xenon-129 and Multiple-Quantum NMR Studies of Molecular Sorption in Na-Y Zeolite: The Effect of Thermal Treatment," submitted to J. Phys. Chem.; LBL-24425.
21. J.W. Chang, C. Connor, E.L. Hahn, H. Huber, and A. Pines, "Direct Detection of Aluminum-27 Resonance with a SQUID Spectrometer," J. Magn. Reson. (in press) ; LBL-26223.
22. N.Q. Fan, B. Heaney, J. Clarke, D. Newitt, L.L. Wald, E.L. Hahn, A. Bielecki, and A. Pines, "Nuclear Magnetic Resonance with DC Squid Preamplifiers," in *Proc. IEEE Conf. on Superconductivity* (in press); LBL-26610.
23. H. Cho, K.T. Mueller, A.J. Shaka, and A. Pines, "Frequency Selective NMR Pulse Sequences Generated by Iterative Schemes with Multiple Fixed Points," Mol. Phys. (in press); LBL-25943.
24. L.C. de Menorval, D. Raftery, S.-B. Liu, K. Takegoshi, R. Ryoo, and A. Pines, "Investigations of Adsorbed Organic Molecules in NaY Zeolite by Xenon-129 NMR," LBL-26371.
25. D.N. Shykind, G.C. Chingas, A. Pines, A.J. Shaka, "A Fast, Stable Quadrature Phase Generator for Multiple-Pulse NMR," Rev. Sci. Instrum. (in press); LBL-26372.
26. B.F. Chmelka, L.C. de Menorval, R. Csencsits, R. Ryoo, S.-B. Liu, C.J. Radke, E.E. Petersen, and A. Pines, "Calcination-Dependence of Platinum Cluster Formation in NaY Zeolite: A Xenon-129 NMR Study," in *Proc. European Conf. on Structure and Reactivity of Surfaces*, Trieste, Italy, Sept. 13–16, 1988 (in press); LBL-26609.
27. G.C. Chingas, K. Mueller, B.Q. Sun, T. Terao, and A. Pines, "Dynamic-Angle Spinning of Quadrupolar Nuclei," LBL-25683.
28. B.F. Chmelka, K.T. Mueller, A. Pines, Y. Wu, and J.W. Zwanziger, "Oxygen-17 NMR in Solids by Dynamic Angle Spinning (DAS) and Double Rotation (DOR)," Nature (in press); LBL-26607.
29. D. Shykind (Ph.D. Thesis), "Phase Shifting and Imaging in Solid State NMR," LBL-26608.

Invited Talks

30. A. Pines, "One and Two-Dimensional NQR Spectroscopy," Ninth International Symposium on Nuclear Quadrupole Resonance, Kanpur, India, Jan. 11–15, 1988.
31. A. Pines, "Multiple Quantum and Zero Field NMR," departmental seminar, Department of Physics, Indian Institute of Science, Bangalore, Jan. 14, 1988.
32. A. Pines, "Quantum Measurement and Topology," Raman Research Institute, Bangalore, India, Jan. 15, 1988.
33. A. Pines, "Frontiers in Chemistry" seminar series, Arizona State University, Tempe, Feb. 5, 1988.
34. A. Pines, "Multiple Quantum and Zero Field NMR," departmental physical chemistry seminar, University of Illinois, Urbana, Feb. 11, 1988.
35. A. Pines, "Some Magnetic Moments," departmental seminar, Temple University, Philadelphia, PA, Feb. 12, 1988.
36. A. Pines, "Counting Clusters by NMR," Physical Science Colloquium, IBM Almaden Research Center, San Jose, CA, Mar. 11, 1988.
37. A. Pines, "Phase in Quantum Measurement," chemical dynamics luncheon discussion, University of California at Berkeley, Apr. 6, 1988.
38. A. Pines, "Aharonov-Anandan Quantum Phase for the Brain Dead," SSC Seminar, LBL, Apr. 15, 1988.
39. A.J. Shaka, "Two-Dimensional NMR and Molecular Conformations in Liquid Crystals," 29th Experimental Nuclear Magnetic Resonance Spectroscopy Conference, Rochester, NY, Apr. 17–21, 1988.
40. A. Pines, "Bistable Maps," Chemical Dynamics Luncheon Discussion, University of California at Berkeley, Apr. 20, 1988.
41. A. Pines, "Quantum Phase in NMR and Optics," Bourke Lecture of the Royal Society, Department of Physics, University of Nottingham, England, Apr. 26, 1988.
42. A. Pines, "Some Magnetic Moments," Bourke Lecture of the Royal Society, Department of Chemistry, University of Nottingham, England, Apr. 27, 1988.
43. A. Pines, "More Magnetic Moments," Bourke Lecture of the Royal Society, University of Durham, England, Apr. 28, 1988.
44. A. Pines, "Berry's Phase in NMR and Optics," Bourke Lecture of the Royal Society, Cambridge University, England, May 4, 1988.
45. First Joint University of Manchester/Manchester Institute of Technology Colloquium, Chemistry

Department, University of Manchester, England, Apr. 29, 1988.

46. A. Pines, "Berry's Phase and Quantum Measurement," Chemistry Department, University of Bristol, England, May 3, 1988.
47. D. Suter, "Multiple-Quantum Transitions and Spin Clusters," GERM-X. RMN des phases adsorbees, Grenoble, May 5–6, 1988.
48. A. Pines, "Spin Precession and Phase in Optics and NMR," 9th European Experimental NMR Conference, Bad Aussee, Austria, May 16–20, 1988.
49. A. Pines, "Computers in Physical Chemistry," Symposium on How the Computer has Affected the Practice of Chemistry, 3rd North American Chemical Congress, Toronto, Ontario, June 5–11, 1988.
50. A. Pines, "Making NMR Count," Symposium on Coherence in Laser Spectroscopy, 3rd North American Chemical Congress, Toronto, Ontario, June 5–11, 1988.
51. A. Pines, "Multiple-Quantum Spectroscopy for Nationally Institutionalized Scientists," National Institutes of Health, Bethesda, MD, June 15, 1988.
52. A. Pines, "Magnetic Moments: Recent Developments in NMR," LBL Summer Lecture Series, July 13, 1988.
53. A. Pines, "New Angles in Sample Spinning," 30th Rocky Mountain Conference, Denver, CO, July 31–Aug. 5, 1988.
54. A. Pines, "New Advances in Instrumentation," XIIIth International Conference on Magnetic Resonance in Biological Systems, Madison, WI, Aug. 14–19, 1988.
55. A. Pines, "NMR Studies of Clusters in Solids," XXIVth Ampere Congress on Magnetic Resonance and Related Phenomena, Poznan, Poland, Aug. 29–Sept. 3, 1988.
56. G.C. Chingas, "Observation of Abundant Spins in the Solid-State (CRAMPS) with Applications," NATO Advanced Studies Institute Program, Maratea, Italy, Aug. 22–Sept. 2, 1988.
57. G.C. Chingas, "Zero Field NMR with Some Possible Applications," NATO Advanced Studies Program, Maratea, Italy, Aug. 22–Sept. 2, 1988.
58. A. Pines, "Quantum Measurement and Topology," Center for Pure and Applied Mathematics, University of California at Berkeley, Sept. 15, 1988.
59. A. Pines, "There's No Free Induction," Bay Area Nuclear Magnetic Resonance Group Meeting, Berkeley, CA, Sept. 28, 1988.
60. A. Pines, "1. Clustering in Solids; 2: Second Order Spinning," Eastern Analytical Symposium, Inc., Oct. 2–7, 1988.
61. A. Pines, "Berry's Phase and Quantum Measurement," Physics Department colloquium, University of Florida, Gainesville, Nov. 3, 1988.
62. A. Pines, "NMR with Lots of Photons," departmental seminar, Chemistry Department, University of Florida, Gainesville, Nov. 4, 1988.
63. A. Pines, "SQUID Detection of Magnetic Resonance," chemical dynamics luncheon discussion, University of California at Berkeley, Nov. 9, 1988.
64. K. Mueller, "NMR Research at Berkeley," Estonian Academy of Sciences, Institute of Chemical Physics and Biophysics, Tallinn, Estonia, USSR, Nov. 17, 1988.

Synthesis of Novel Solids*

Angelica M. Stacy, Investigator

INTRODUCTION

The general goal of this research is to synthesize advanced materials with novel properties. Current work is directed towards the synthesis and characterization of two classes of materials: high-temperature oxide superconductors and rare-earth transition-metal phosphides. In the area of high-temperature oxide superconductivity, research efforts are focused in three areas: (1) synthesis of superconductors using hydroxide fluxes, (2) investigations of partial substitution of ^{18}O in $YBa_2Cu_3O_7$, and (3) a search for new niobium oxide superconductors (supported through a contract with EPRI). Rare-earth compounds are being investigated because they exhibit cooperative phenomena, including valence fluctuations, heavy-fermion superconductivity, and unusual types of magnetic ordering. New classes of rare-earth transition-metal phosphides that exhibit cooperative phenomena (especially superconductivity) are sought. Several new compounds have been discovered, including $EuNi_5P_3$, which exhibits unusual steps in the magnetization-versus-field curves. Such synthetic studies will lead to numerous new classes of materials with novel magnetic and electronic properties.

1. Low-Temperature Synthesis of Superconducting $La_{2-x}M_xCuO_4$ (Publication 4)

W.K. Ham, G.F. Holland, and A.M. Stacy

The new superconductors generally have been prepared by reactions of intimate mixtures of the metal oxides, carbonates, oxalates, or nitrates at high temperatures (often up to 1100°C). Since this synthetic route often leads to impure, inhomogeneous products, there is a clear need to discover new synthetic routes. This group has isolated $La_{2-x}M_xCuO_4$ and $Ba_{1-x}K_xBiO_3$ from fused NaOH/KOH melts at temperatures as low as 300°C. The oxides are dissolved in wet, molten NaOH/KOH. Heating between 300°C and 450°C results in slow loss of water and precipitation of the product. The route is a single-step process that leads to high-T_c superconductors at temperatures much lower than those used in previous synthesis. Because the products are precipitated directly from solution, it is possible to control the stoichiometry precisely, and also the particle size. Single crystals can be grown, as well as thin films.

*This work was supported by the Director, Office of Energy Research, Office of Basic Energy Sciences, Materials Sciences Division, of the U.S. Department of Energy under Contract No. DE-AC03-76SF00098.

2. Partial Substitution of ^{18}O in $YBa_2Cu_3O_7$: Investigations of Inhomogeneities and Their Effect on T_c (Publication 10)

W.K. Ham, S.W. Keller, J.N. Michaels, A.M. Stacy, D. Krillov,† D.T. Hodul,† and R.H. Fleming‡

The possibility of site-selective substitution of ^{18}O into $YBa_2Cu_3O_7$ has been explored. Samples containing various quantities of ^{18}O were prepared by processing in $^{18}O_2$ at 950°C and 450°C. The samples were characterized by secondary-ion mass spectroscopy (SIMS), temperature-programmed desorption (TPD) and reduction (TPR), Raman spectroscopy, and magnetization measurements. Measurements of the shifts in the Raman active modes with ^{18}O substitution and of the ratios of ^{18}O to ^{16}O by TPD, TPR, and SIMS show that even for temperatures as low as 450°C and times as short as 2 hr, ^{18}O is not substituted exclusively into the chain site (O1) in $YBa_2Cu_3O_7$. This result indicates that other oxygen sites are involved in the mechanism for oxygen diffusion in $YBa_2Cu_3O_7$. In addition, there is no consistent variation in the shifts in T_c with the degree of substitution; therefore, the isotope effect for a sample with 100% ^{18}O substitution cannot be predicted by a linear extrapolation of data obtained for samples with partial ^{18}O substitution. The difficulties of measuring the true isotope shift have been explored.

†Permanent address: Varian Associates, Palo Alto, CA 94303.

‡Permanent address: Charles Evans and Associates, Redwood City, CA 94063.

3. Work in Progress

The synthesis of the superconducting oxides $Ba_{1-x}K_xBiO_3$ and $YBa_2Cu_3O_7$ using hydroxide melts is being explored. Large single crystals of $EuNi_5P_3$ are being synthesized for use in neutron-diffraction experiments; these experiments will help elucidate the complex magnetic structure.

1988 PUBLICATIONS AND REPORTS

Refereed Journals

1. G.F. Holland and A.M. Stacy, "Physical Properties of the Quaternary Oxide Superconductor $YBa_2Cu_3O_7$," Acc. Chem. Res. **21**, 8 (1988).
2. K.J. Leary, J.N. Michaels, and A.M. Stacy, "A Comparative Study of a Multisite Model and a Subsurface Diffusion Model for Temperature-Programmed Desorption," AIChE J. **34**, 263 (1988).
3. H.-C. zur Loye, A.M. Stacy, and R.H. Staley, "Effect of the Method of Preparation on the Interaction between Ni and TiO_2," Solid State Ionics **26**, 133 (1988).
4. W.K. Ham, G.F. Holland, and A.M. Stacy, "Low-Temperature Synthesis of Superconducting $La_{2-x}M_xCuO_4$: Direct Precipitation from NaOH/KOH Melts," J. Am. Chem. Soc. **110**, 5214 (1988).
5. K.J. Leary, J.N. Michaels, and A.M. Stacy, "Penetration of Hydrogen into Subsurface Sites of a Pd/SiO_2 Catalyst during Temperature-Programmed Desorption," Langmuir **4**, 1251 (1988).
6. H.-C. zur Loye and A.M. Stacy, "Changes in the Magnetic Properties of Ni/TiO_2 Composites with Reduction Temperature: Evidence for the Formation of Ni_yTiO_z," Langmuir **4**, 1261 (1988).

Other Publications

7. P.D. VerNooy, M.A. Dixon, and A.M. Stacy, "Copper Mixed-Valency in a New Aluminum-Barium-Copper Oxide," in *High-Temperature Superconductors*, MRS Symp. Proc. **99**, 651 (1988).
8. K. Khachaturyan, E.R. Weber, P. Tejedor, A.M. Stacy, and A.M. Portis, "Measurement of Microwave Frequency Magnetoresistance of High-T_c Superconducting Oxides," in *High Temperature Superconductors*, MRS Proc. **99**, 383 (1988).
9. M.A. Dixon, P.D. VerNooy, and A.M. Stacy, "Synthesis of a Low Temperature Form of Barium-Copper-Oxide From Barium Hydroxide Flux," MRS Symp. Proc. **EA14**, 69 (1988).
10. W.K. Ham, S.W. Keller, J.N. Michaels, A.M. Stacy, D. Krillov, D.T. Hodul, and R.H. Fleming, "Partial Substitution of ^{18}O in $YBa_2Cu_3O_7$: Investigations of Inhomogeneities and Their Effect on T_c," J. Mater. Res. (in press).

LBL Reports

11. H.W. Zandbergen, R. Gronsky, M.Y. Chu, L.C. DeJonghe, G.F. Holland, and A.M. Stacy, "The Structure and Properties of Twin Boundaries in Superconducting $YBa_2Cu_3O_7$," LBL-24139rev.

Invited Talks

12. A.M. Stacy, "Connections in Solid State Chemistry: from Superconductors to Chaos," IBM Almaden Research Center, San Jose, CA, Jan. 12, 1988; Harvard University, Cambridge, MA, Jan. 22, 1988; MIT, Cambridge, MA, Jan. 22, 1988; Department of Chemistry, University of California, Irvine, Feb. 23, 1988; Eastman Kodak, Rochester, NY, Mar. 31, 1988; Department of Chemistry, University of Rochester, Rochester, NY, Apr. 1, 1988; Union Carbide, Charleston, WV, June 14, 1988; W.R. Grace, Columbia, MD, June 15, 1988.
13. A.M. Stacy, "The Chemistry of the New High Temperature Superconductors," Lawrence Hall of Science, Berkeley, CA, Feb. 4, 1988; American Association for the Advancement of Science, Boston, MA, Feb. 11–15, 1988; Career Planning Day for high school students, Livermore, CA, Mar. 5, 1988; Gordon Conference on the Chemistry of Electronic Materials, Oxnard, CA, Mar. 7–11, 1988; Summer School on High Temperature Superconductivity, El Escorial, Spain, July 4–9, 1988; California Section, ACS, Berkeley, CA, Oct. 17, 1988.
14. A.M. Stacy, "Discovery and Physical Properties of Superconducting Compounds—Experiment and Theory," Phoebe Hearst Distinguished Lecture Series on Metals and Society, University of California at Berkeley, May 6, 1988.
15. A.M. Stacy, "The Use of Molten Hydroxides as Solvents for the Synthesis of New Copper Oxides," Department of Chemistry, University of California at Berkeley, May 6, 1988.
16. A.M. Stacy, "New Synthetic Routes to Quaternary Copper Oxides," Materials Research Society, Reno, NV, Apr. 5–9, 1988.
17. A.M. Stacy, "Solid State Chemistry of Mixed-Valent Copper Oxides," American Chemical Society, Toronto, Ontario, June 6–10, 1988.
18. A.M. Stacy, "Oxygen Isotope Effect in the New High Temperature Superconductors," Summer School on High Temperature Superconductivity, El Escorial, Spain, July 4–9, 1988.
19. A.M. Stacy, "Oxygen Diffusion in $YBa_2Cu_3O_{7-y}$ and Related Highly Oxidized Copper Oxides," Gordon Conference on Solid State Chemistry, Plymouth, NH, July 24–29, 1988.
20. A.M. Stacy, "High Temperature Superconductors: Grain Boundaries and Surface Chemistry," Gordon Conference on the Chemistry at Interfaces, Meriden, NH, July 24–29, 1988.
21. A.M. Stacy, "Synthesis of New Copper Oxides Using Molten Hydroxides as Solvents," Gordon Conference on Inorganic Chemistry, Wolfeboro, NH, July 30–Aug. 5, 1988.
22. A.M. Stacy, "Synthesis and Characterization of New Copper Oxides," American Chemical Society Meeting, Los Angeles, CA, Sept. 26, 1988.
23. A.M. Stacy, "New Synthetic Routes to High-T_c Superconductors and Related Materials," LBL, Aug. 17, 1988.

Chemical Sciences

FUNDAMENTAL INTERACTIONS

PHOTOCHEMICAL AND RADIATION SCIENCES

Photochemistry of Materials in the Stratosphere*

Harold S. Johnston, Investigator

INTRODUCTION

This research is concerned with global atmospheric photochemical modeling and with experimental gas-phase photochemistry. In collaboration with Lawrence Livermore National Laboratory (LLNL), theoretical studies are made of atmospheric transport, radiation balance, and photochemistry. One goal of the experimental work is to obtain optical and kinetic data in the laboratory that are needed by modelers of the atmosphere. Another goal is to measure the distribution of excess energy in the fragments produced after a molecule is broken apart by an energetic pulse of light. The experimental methods include laser flash photolysis, laser resonance absorption, resonance fluorescence, dispersed chemiluminescence from photolysis products, and infrared diode lasers. This research has applications to molecular dynamics, to problems of atmospheric ozone, and to problems of global change of trace gases in the atmosphere.

1. Nitrogen Oxides from High-Altitude Aircraft: An Update of Potential Effects on Ozone (Publication 5)

H.S. Johnston, D.C. Kinnison, and D.J. Wuebbles†

A sensitivity study was carried out using the LLNL one-dimensional (1D) and two-dimensional (2D) chemical-radiative-transport models of the global atmosphere to examine possible effects of future aircraft NO_x emissions on stratospheric ozone. A broad range in magnitude, altitude, and latitude of the assumed NO_x emissions was examined. Major findings of this initial study were: (1) Nitrogen oxides from the exhaust gases of stratospheric aircraft can reduce stratospheric ozone on a global basis. The degree of these calculated ozone reductions depends strongly on injection altitude and magnitude. (2) The altitude at which NO_x emissions cause the largest reduction in the ozone column is about 25 km, according to 1D model calculations. This altitude of maximum ozone sensitivity is weakly dependent on emission rate and Cl_y background mixing ratios. (3) For a given altitude and magnitude of NO_x emissions, the 2D model finds that the reduction of global ozone depends only weakly on latitude of the injections. For a given injection, the largest ozone-column reductions occur in the polar regions. (4) For very large Cl_y mixing ratios, NO_x emissions can increase the ozone column, partially counteracting the ozone reduction caused by Cl_x. This effect is found only in a highly Cl_x-perturbed stratosphere where ozone is already greatly depleted. (5) The effect of water vapor emission at a factor of 90 greater than the NO_x emissions has negligible effect on ozone, compared to the effects of the assumed NO_x emissions. (6) Calculated global reductions of ozone due to NO_x emissions are smaller in the 2D model than in the 1D model (see Figure 1-1).

*This work was supported by the Director, Office of Energy Research, Office of Basic Energy Sciences, Chemical Sciences Division, of the U.S. Department of Energy under Contract No. DE-AC03-76SF00098.

†Permanent address: Lawrence Livermore National Laboratory, Livermore, CA, 94550.

2. Use of Excess Carbon-14 Data to Test 2D Stratospheric Models (Publication 6)

H.S. Johnston

The excess carbon-14 data following the nuclear bomb tests of 1961–1962 have been organized in a form convenient to use for testing 2D models with respect to air transport in the middle to lower stratosphere. Detailed initial values for October 1963 are listed in tables, and extensive target values (observations made at specified altitudes) for the models to calculate are given at four latitudes, for each of four

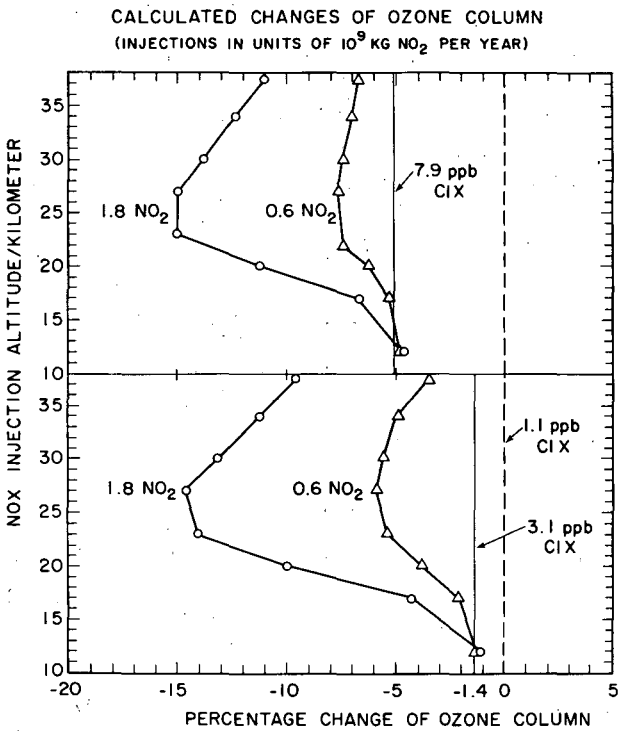

Figure 1-1. Calculated changes of the ozone vertical column for various conditions: NO_x injection quantities at 1.8×10^9 kg/yr (1971 SST standard value) and at 0.6×10^9 kg/yr (maximum anticipated engine modification, with same fleet size), injection altitude from 12 to 37.5 km, and with two stratospheric chlorine background values (3.1 ppb, the current value; 7.9 ppb, the anticipated maximum future value if current rate of chlorofluorocarbon manufacture is maintained for the indefinite future). Note the lesser ozone reduction due to aircraft at the higher chlorine background value. (XBL 894-1255)

seasons, and for 2.75 years. This method uses observed carbon-14 profiles as initial values, instead of a model for the rise of the bomb debris.

3. Collision-Free Fluorescence of Nitrogen Dioxide from the Photolysis of Nitryl Chloride and Nitrogen Pentoxide (Publication 3)

B.Y. Oh

Collision-free nitrogen dioxide fluorescence is induced by fast (15 nsec) excimer-laser photolysis of RNO_2 compounds at low pressure (5 mtorr). A large amount of such data was taken with variation of the photolyzed molecules and ultraviolet wavelength. The dispersed spectra give information about the internal energy distribution (first two moments) of the photolysis products, if one knows the fluorescence lifetime as a function of wavelength. A project is under way to measure the collision-free NO_2 fluorescence lifetimes, especially at wavelengths above 600 nm.

4. Work in Progress

The fluorescence spectrum of the nitrate free radical has been studied by a sensitive photon-counting method, and several previously unobserved features have been found. In collaboration with Professor William Lester, additional quantum mechanical calculations are under way in an effort to interpret these data and to determine the structure (D3h or C2v) of this free radical. A simple pulsed molecular-beam machine has been constructed and used for preliminary study of collision-free photolysis-induced fluorescence of nitrogen dioxide.

1988 PUBLICATIONS AND REPORTS

Refereed Journals

1. B. Kim, H.S. Johnston, D.A. Clabo, Jr., and H.F. Schaefer III, "The Vertical Electronic Spectrum of NO_3: $^2A_2'$, $^2E''$ ($^2A_2$, $^2B_1$) and $^2E'$ States," J. Chem. Phys. **88**, 3204 (1988); LBL-24204.
2. D. Kinnison, H. Johnston, and D. Wuebbles, "Ozone Calculations with Large Nitrous Oxide and Chlorine Changes," J. Geophys. Res. **93**, 14,165 (1988); LBL-24573.

LBL Reports

3. B.Y. Oh (Ph.D. Thesis), "Photodissociation of NO_2-X (X = ClO,NO_3,Cl) Molecules," LBL-26462.
4. D. Darwin, A.T. Young, H.S. Johnston, and C.B. Moore, "Rate Constants for $^3CH_2$ ($\tilde{X}$ $^3B_1$) Removal by O_2, NO, and C_2H_2 from Infrared Diode Laser Flash Kinetic Spectroscopy," accepted by J. Phys. Chem.; LBL-25112.
5. H. Johnston, D. Kinnison, and D. Wuebbles, "Nitrogen Oxides from High Altitude Aircraft: An Update of Potential Effects on Ozone," submitted to J. Geophys. Res.; LBL-26206.
6. H. Johnston, "Use of Excess Carbon-14 Data to Test Two-Dimensional Stratospheric Models," accepted by J. Geophys. Res.; LBL-25677.

CHEMICAL PHYSICS

Energy Transfer and Structural Studies of Molecules on Surfaces*

Charles B. Harris, Investigator

INTRODUCTION

The goal of this research is to study the mechanisms that are responsible for the transfer of energy from the excited states of molecules to metal surfaces and to develop new laser techniques for probing molecule-surface interactions. The research program is both theoretical and experimental in character, and it includes nonlinear optical, picosecond, and femtosecond laser techniques, in addition to a variety of standard surface-science tools for characterizing molecule-surface interactions. Recent work has centered on the development of picosecond infrared lasers; the elucidation of the mechanisms of surface-enhanced photochemistry, surface-enhanced photoelectron emission, and the breakdown of classical dielectric response theory for explaining energy transfer from molecules to noble metal surfaces; and the development of new techniques for studying the dynamics of electrons at interfaces on femtosecond time-scales. The results of this program have a direct bearing on high-speed technological devices and materials, and on other problems of general interest such as the dynamics of electrical transmission in conductors on ultrafast timescales and the optical properties of thin films.

*This work was supported by the Director, Office of Energy Research, Office of Basic Energy Sciences, Chemical Sciences Division, of the U.S. Department of Energy under Contract No. DE-AC03-76SF00098.

1. A New Method for Surface Structure Using a Combination of Second Harmonic Generation and Coverage-Dependence Fluorescence (Publication 4)

C.B. Harris and E. Peterson

A number of phenomena that occur at surfaces are sensitive to the geometry and orientation of adsorbate molecules. Two-dimensional energy transfer via dipole-dipole coupling, for example, varies both with intermolecular distance and with the relative orientation of the dipole moments. In addition, resonant second harmonic generation (SHG) is able to define the angle between the transition dipole of an absorption band and the surface normal, but not the position of the molecule about this surface normal. A combination of SHG and a simple dipole-dipole interaction model was developed as a new technique for determining adsorbate geometries on surfaces. General formulae for absorption-band shifts using the geometry constraints imposed by the SHG data were derived for a dimer constructed from two arbitrarily placed monomers on the surface. These formulae can be used to determine the orientation of the two monomers relative to each other. Finally, a simplified version of this formalism was used to interpret absorption band shifts for a system of rhodamine B adsorbed on quartz. A subclass of possible molecular geometries can be defined from the overlap of the distributions predicted by each method alone.

2. Picosecond Studies of the Electron-Hole Pair Dynamics in CdS_xSe_{1-x} Graded Semiconductors (Publication 5)†

C.B. Harris and J.K. Hane

Band-edge emission characteristics of CdS_xSe_{1-x} semiconductors provide a probe of electron-hole dynamics in a system with a graded composition region. Graded semiconductors are inhomogeneous samples in which the composition varies as a func-

tion of depth. A picosecond laser system was used to create a nonequilibrium distribution of electron-hole pairs in inhomogeneous samples. Using time-correlated single-photon counting, timeresolved fluorescence measurements were performed on materials with either decreasing or increasing S concentration over a 1–2 μm region from the surface. In both cases, the decay functions reflect a simple picture of carrier diffusion into deeper regions of the sample. However, other qualitative features suggest the influence of local effects associated with Se/S substitution. The dynamics of electron-hole pairs in this material may be quite different from an alloy semiconductor for which the virtual crystal approximation is valid. If the de Broglie wavelengths of the electrons and holes are short relative to the disorder, the unit cells in the disordered crystal cannot be represented by an average unit cell. In this case, the motion of carriers cannot be described in terms of an average band-gap gradient. The form of the decay function, when deconvoluted from the instrument response function, should reflect the dynamics of the relation process. The highly nonexponential data were fit by a Kohlrausch exponential, a functional form observed empirically for various relaxation processes occurring in disordered condensed phase. Further studies of this CdS_xSe_{1-x} system area in progress and present an opportunity to test various models of relaxation in localized systems.

†This program was sponsored by the Office of Naval Research using DOE equipment.

3. Fundamental Studies of Bond Breaking and Forming on Ultrafast Timescales (Publication 1)†

C.B. Harris, J.K. Brown, and D.E. Smith

A series of experiments has been completed that show that the traditional stochastic theories for chemical reaction dynamics in liquids are not valid without significant modification. Stochastic theories based on the Langevin or Fokker-Planck equations for describing physical phenomena break down when thermal fluctuations no longer look completely random. For many condensed-matter phenomena, this occurs on the picosecond or femtosecond timescale. For bond breaking and forming processes in liquids, this time corresponds to collision times. In addition, the first direct time-resolved measurement of predissociation and curve crossing in a solution-phase chemical reaction was made. Results show that predissociation may be much more rapid ($\leq$1 ps) than previously thought and that curve crossing in solution is extremely facile and not the rate-limiting step in recombination.

†This research was funded by the National Science Foundation using DOE equipment.

4. Studies of Chemical Reactivity in Condensed Phase (Publications 2 and 6)†

C.B. Harris, J.K. Brown, D.J. Russell, and D.E. Smith

The general question, "Are isolated binary collision theories valid for vibrational relaxation in liquids?" has been addressed. Several scaling theorems were developed that allow one to generically test the question of whether gas-phase theories for energy redistribution are valid at liquid-state densities. Simple isolated binary-collision models qualitatively reproduce molecular dynamics relaxation behavior, yet fail to scale properly with density. It is important to include effects of correlated and many-body collisions, especially correlated collisions that result from the amplitude of the vibrational motion perturbing the surrounding solvent molecules.

Using the experimental results discussed above and the results of large-scale molecular-dynamics simulations, a variety of theoretical approaches have been tested for bond formation and the resulting energy dissipation to the surroundings associated with the enthalpy of the bond. The utility of stochastic dynamics based on the generalized Langevin equations to quantitatively account for the observations has been examined. Several new approaches have been developed, including the application of spectral estimation techniques used for high-speed signal processing. In particular, the memory kernal use in stochastic dynamics (generalized Langevin equations) has been constructed from a class of techniques based on estimates of autoregressive and moving average (ARMA) parameters and applied to energy dissipation via vibrational relaxation in liquids on ultrafast timescales.

†This research was funded by the National Science Foundation using DOE equipment.

5. Work in Progress

The Dynamics of Electrons at Interfaces on Ultrafast Timescales

An extremely sensitive technique utilizing time-resolved angle-dependent multiphoton photoemission has been developed to study transient excitations of surface electrons on the femtosecond timescale. The technique yields the time-resolved energy and momentum distribution of electrons emitted from the surface and is applicable to a wide variety of problems. By using a high-repetition-rate (4 MHz) tunable fiber-compressed UV femtosecond laser, an "excite" pulse is used to cause transitions from the bulk states or from occupied surface states on metals to empty states above Fermi level but below the vacuum. The dynamics of electrons in these excited states can be followed by photoionizing electrons from these states with a visible "probe" pulse and measuring the electrons momentum by time of flight. On average, only one photoelectron is detected every 100 laser shots, so one eliminates all the incipient problems of space-charge broadening that can occur with other laser sources. Because of the high repetition rate, however, one can still detect 10^4 to 10^5 electrons per second. This provides unparalleled sensitivity yet retains the time resolution in the experiment, which is simply determined by the laser pulse width. Currently, 100–200 fs is available in our laboratory. Compensating for dispersion in a synchronously pumped dye laser, one can achieve 20–30 fs time resolution with no loss of sensitivity.

As an initial experiment, the dynamics of electrons on the image potential states on Ag(111) and Cu(100) have been investigated. The kinetic-energy distribution of photoelectrons ejected by the resonant absorption of two laser photons has been measured for Ag(111) after an initial pulse excites the short-lived image state from an occupied surface state below the Fermi energy, and a second delayed pulse photoemits the electron from the image potential state. The distribution of photoelectron kinetic energies reveals the binding energy of the image potential state. The dynamics to the N = 1 state of Ag(111) is currently pulse-width limited. Most recently, the effects of depositing controlled submonolayer coverages of xenon on silver have been initiated in order to determine whether the xenon interacts with electrons in image states as a polarizable dielectric continuum or whether isolated atom-electron interactions such as negative-ion formation predominate.

1988 PUBLICATIONS AND REPORTS

Refereed Journals

1. A.L. Harris, J.K. Brown, and C.B. Harris, "The Nature of Simple Photodissociation Reactions in Liquids on Ultrafast Time Scales," Ann. Rev. Phys. Chem. **39**, 341 (1988); LBL-24702.†
2. J.K. Brown, C.B. Harris, and J.C. Tully, "Studies of Chemical Reactivity in the Condensed Phase. IV. Density Dependent Molecular Dynamics Simulations of Vibrational Relaxation in Simple Liquids," J. Chem. Phys. **89**, 6687 (1988); LBL-25418.†

Other Publications

3. Y. Yajima, K. Yoshihara, C.B. Harris, and S. Shionoya, eds., "Ultrafast Phenomena VI, Springer Series Chemical Physics, Springer Verlag, Berlin, 1988.

LBL Reports

4. E.S. Peterson and C.B. Harris, "A New Technique for the Determination of Surface Adsorbate Geometries Utilizing Second Harmonic Generation and Absorption Band Shifts," submitted to J. Chem. Phys; LBL-26765.
5. J.K. Hane, M.G. Prisant, and C.B. Harris, "Time-Resolved Luminescence of Electron-Hole Pairs in CdS_xSe_{1-x} Graded Semiconductors," submitted to Appl. Phys. Lett.; LBL-26764.‡
6. J.K. Brown (Ph.D. Thesis), "Molecular Dynamics Simulations of Simple Liquid Phase Chemical Reactions," LBL-24353.‡

Invited Talks

7. C.B. Harris, "Do Gas Phase Binary Collision Theories Describe Reaction Dynamics in Condensed Phases?" Symposium on Molecular Dynamics and Spectroscopy, Northeast Regional Meeting, American Chemical Society, Rochester, NY, Nov. 9, 1987.
8. C.B. Harris, "Energy Transfer, and Photoemission at Metal and Semiconductor Interfaces," Third North American Chemical Congress Symposium on Photoprocesses at Surfaces, Toronto, Ontario, June 5–11, 1988.
9. C.B. Harris, "Fundamental Studies of Radicals in Liquids on the Femtosecond Timescale," Radical Ions Gordon Research Conference, Brewester Academy, Wolfeboro, NH, June 27–July 1, 1988.
10. C.B. Harris, "Energy Transfer at Metal and Semiconductor Interfaces," Adriatico Research Conference on "The Application of Lasers in Surface Science," Trieste, Italy, Aug. 23–26, 1988.
11. C.B. Harris, "Are Isolated Binary Collision Theories Valid for Vibrational Relaxation in Liquids," ACS Meeting on Dynamical Processes in Liquids, Los Angeles, CA, Sept. 25–30, 1988.

†Office of Naval Research Program using DOE equipment.

‡National Science Foundation Program using DOE equipment.

Selective Photochemistry*

C. Bradley Moore, Investigator

INTRODUCTION

The fundamental goals of this program are to understand the photophysics and photochemistry that occur following selective excitation of molecules and during the reactions of free radicals. Of particular interest are the chemical reactions of specifically excited states and the dynamics of energy transfer, both within a molecule and to surrounding molecules.

Molecules produced in bound excited singlet states may fragment following the conversion of electronic excitation energy into vibrational energy. Intersystem crossing to triplet states is often in competition with internal conversion to singlet states. In this work the dynamics of intersystem crossing and reaction of the triplet state are studied for both unimolecular and bimolecular systems.

For low levels of vibrational excitation in small molecules, individual quantum states may be excited, enabling the measurement of reaction and energy-transfer rate constants for each quantum state. For larger or more highly excited molecules, it is usually not possible to excite single eigenstates. Instead, a number of eigenstates are excited simultaneously, and a redistribution of the initial vibrational excitation occurs. This process, known as intramolecular vibrational-energy redistribution (IVR), is extremely rapid and severely limits the realization of truly mode-specific unimolecular reactions. Advances in mode-specific chemistry will come from a more complete understanding of the IVR process and the parameters that control its efficiency. By being able to predict the rates of IVR and the path of vibrational-energy flow through a molecule, experiments can be designed utilizing molecular systems that maximize the possibilities for mode-specific effects. Studies designed to elucidate the coupling mechanisms and dominant pathways for IVR are currently under way on a number of model systems.

The rates and mechanisms of free-radical reactions, such as are important in combustion, are often best studied by flash kinetic spectroscopy using lasers for thermal heating, for photolyzing, and for spectroscopic probing. Reactions can be studied as a function of individual quantum states. A fundamental understanding of the rate constants and product distributions for these reactions is sought to serve as a basis for modeling combustion processes.

*This work was supported by the Director, Office of Energy Research, Office of Basic Energy Sciences, Chemical Sciences Division, of the U.S. Department of Energy under Contract No. DE-AC03-76SF00098.

1. Rate Constants for $^3CH_2$ ($\tilde{X}^3B_1$) Removal by O_2, NO, and C_2H_2 from Infrared-Diode Laser Flash Kinetic Spectroscopy (Publication 5)

D.C. Darwin, A.T. Young, H.S. Johnston, and C.B. Moore

Removal rates of ground-state triplet methylene ($\tilde{X}^3B_1$, $^3CH_2$) due to the reaction with O_2, NO, and C_2H_2 have been measured using laser flash kinetic spectroscopy. Excimer-laser photolysis of ketene produced $^3CH_2$. The subsequent time behavior of the $^3CH_2$ transient was recorded by directly monitoring continuous-wave diode laser absorption due to $^3CH_2$. From analysis of $^3CH_2$ decay curves under pseudo-first-order conditions, the following rate constants were determined (293 ± 2 K):

$k_{O_2} = (3.24 \pm 0.26) \times 10^{-12}$ cm^3 molec^{-1} sec^{-1}

$k_{NO} = (2.91 \pm 0.24) \times 10^{-11}$ cm^3 molec^{-1} sec^{-1}

$k_{C_2H_2} < 1.4 \times 10^{-14}$ cm^3 molec^{-1} sec^{-1}.

Figure 1-1 shows the data set for NO. The results are in good agreement with recent, direct measurements made using flow-tube techniques, but are in poor agreement with earlier, indirect measurements. These results illustrate the importance of direct measurements of individual rate constants for input to models of complex phenomena such as combustion and atmospheric chemistry.

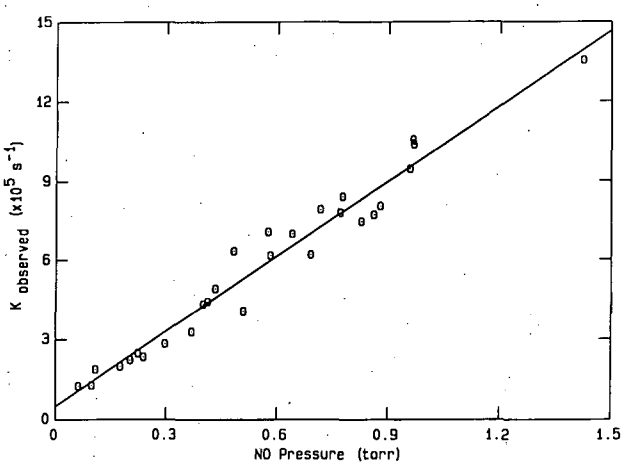

Figure 1-1. Measured rate vs NO pressure for reaction of $^3CH_2$. The rate constant is $(2.91 \pm 0.24) \times 10^{-11}$ cm^3 molec^{-1} sec^{-1} for the removal of $^3CH_2$ by NO. (XBL 894-1261)

2. Hydrogen-Atom Tunneling in the Thermal Tautomerism of Porphine Imbedded in a n-Hexane Matrix (Publication 4)

T.J. Butenhoff and C.B. Moore

Rate constants and the kinetic isotope effect for the tautomerization of porphine, Figure 2-1, imbedded in a n-hexane Shpol'skii matrix near 110 K have been measured using laser-induced fluorescence spectroscopy. A one-dimensional tunneling-model calculation has been used to compare the feasibility of the synchronous and asynchronous hydrogen-migration mechanisms. Only the asynchronous tunneling model is consistent with the rate constants and kinetic-isotope effects measured near 110 K and near room temperature. This work provides the reaction mechanism and potential-surface data needed for a study of mode selectivity in infrared photochemistry.

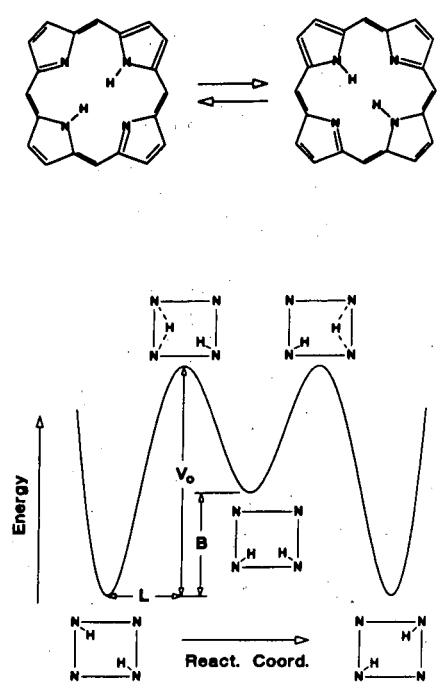

Figure 2-1. Tautomerism of free-base porphine (H_2P) (above) and a schematic diagram of the ground-state potential energy as a function of the reaction coordinate for the asynchronous migration in H_2P (below). The rate-constant data are fit well for L = 0.84 Å, $A_s = 1.0 \times 10^{14}\ sec^{-1}$, $V_0(H_2P) = 5450\ cm^{-1}$, $V_0(D_2P) = 5470\ cm^{-1}$, and $B = 1890\ cm^{-1}$. (XBL 894-1262)

3. The Small-Molecule Limit of Infrared Multiphoton Dissociation: Collisional Effects in D_2CO (Publication 1)

M.R. Berman† and C.B. Moore

In order to understand the mechanisms of infrared multiphoton excitation in the small-molecule limit, D_2CO was studied by monitoring infrared fluorescence from stretching modes of D_2CO following excitation in the bending modes. The dependence of the infrared multiphoton dissociation yield on laser wavelength, on laser power, and on reactant and foreign gas pressures was also studied. Severe bottlenecks to excitation through the first few steps are found. Vibration-to-vibration transfer of a bending quantum from one excited D_2CO molecule to another is a crucial step. Collision-induced changes of rotational quantum number must also play an important role.

†Present address: McDonnell Douglas Research Laboratories, P.O. Box 516, St. Louis, MO 63166.

4. Work in Progress

Energy transfer and chemical reaction rates are being studied for HCO and triplet CH_2 radicals. A diode laser infrared flash kinetic spectrometer has been constructed to extend this work beyond the 2–4 μm range available with our current difference-frequency spectrometer. Reaction rates of $^3CH_2$ with O_2 and NO have already been measured in collaboration with H.S. Johnston. Reaction rates for radical-radical reactions are being measured. Studies of reaction product distributions and formation kinetics are planned for the near future. Spectroscopy of radical-radical and radical-molecule reaction complexes is planned.

Unimolecular reaction dynamics are being studied by photofragment spectroscopy. A molecular-beam system has been constructed to use with the new VUV laser system developed together with Y.T. Lee and A.H. Kung. The fragmentation of ketene on its triplet potential energy surface will be studied by detection of CO using a tunable photolysis laser below the threshold for singlet fragmentation.

Infrared spectra of intermediates in organometallic photochemistry in gas and liquid phase are being studied jointly with R.G. Bergman. Emphasis is on CH activation chemistry. The work reported above has shifted to studies of CH activation systems studied in liquid Kr and Xe.

1988 PUBLICATIONS AND REPORTS

Refereed Journals

1. M.R. Berman and C.B. Moore, "The Small Molecule Limit of Infrared Multiphoton Dissociation: Collisional Effects in D_2CO," Laser Chem. **8**, 169 (1988); LBL-24761
2. C.B. Dane, D.R. Lander, R.F. Curl, F.K. Tittel, Y. Guo, M.I.F. Ochsner, and C.B. Moore, "Infrared Flash Kinetic Spectroscopy of HCO," J. Chem. Phys. **88**, 2121 (1988); LBL-24278.
3. E.P. Wasserman, R.G. Bergman, and C.B. Moore, "IR Flash Kinetic Spectroscopy of Transients Generated by Irradiation of $(\eta^5\text{-}C_5H_5)Co(CO)_2$ in the Gas Phase and in Solution," J. Am. Chem. Soc. **110**, 6076 (1988); LBL-24813.
4. T.J. Butenhoff and C.B. Moore, "Hydrogen Atom Tunneling in the Thermal Tautomerism of Porphine Imbedded in a n-Hexane Matrix" J. Am. Chem. Soc. **110**, 8336 (1988); LBL-26572.

LBL Reports

5. D.C. Darwin, A.T. Young, H.S. Johnston, and C.B. Moore, "Rate Constants for $^3CH_2$ ($\tilde{X}^3B_1$) Removal by O_2, NO, and C_2H_2 from Infrared Diode Laser Flash Kinetic Spectroscopy," J. Phys. Chem. Frederick Kaufman memorial issue (in press); LBL-25112.

Invited Talks

6. C.B. Moore, "Infrared Flash Kinetic Spectroscopy — Structure and Reactivity of Reaction Intermediates," Annual Review, Materials and Chemical Sciences Division, LBL, Feb. 11, 1988.
7. C.B. Moore, "State-Selected and State-Resolved Unimolecular Reaction Dynamics," USA-USSR Workshop on Lasers in Linear and Nonlinear Photochemistry, Mar. 1, 1988.
8. C.B. Moore, "State-to-State Studies of Unimolecular Reactions," Avco Everett Research Labs, Everett, MA, Mar. 15, 1988.
9. C.B. Moore, "Energy Flow in Unimolecular Reactions," Harvard University, Cambridge, MA, Mar. 16, 1988.
10. C.B. Moore, "Laser Studies of Unimolecular Reaction Dynamics," Society for Applied Spectroscopy, Northern California Section, Berkeley, CA, Mar. 24, 1988.
11. C.B. Moore, "State-to-State Dynamics of Unimolecular Reactions," Fudan University, Shanghai, People's Republic of China, Apr. 5, 1988.
12. C.B. Moore, "Energy Transfer in Unimolecular Reaction Dynamics," Institute for Chemical Physics, Academy of Sciences, Dalian, People's Republic of China, Apr. 7, 1988.
13. C.B. Moore, "Infrared Flash Kinetic Spectroscopy," Fudan University, Shanghai, People's Republic of China, Apr. 9, 1988.
14. C.B. Moore, "State-Resolved Dynamics of Unimolecular Reactions," University of Pennsylvania, Philadelphia, Apr. 28, 1988.
15. C.B. Moore, "Photochemical Reaction Dynamics," 1988 Combustion Research Contractors Meeting, Lake Geneva, WI, June 1–3, 1988.
16. T.J. Butenhoff, K.L. Carleton, I.-C. Chen, M.-C. Chuang, M.F. Foltz, W.H. Green, Jr., and C.B. Moore, "The Dynamics of Chemical Bond Breaking: State-Selected, State-Resolved, Photofragmentation of Ketene and Formaldehyde," Third Chemical Congress of North America, Toronto, Ontario, June 5–10, 1988.
17. W.C. Natzle, T.J. Butenhoff, H.-H. Limbach, R.S.H. Chuck, and C.B. Moore, "Vibrational Photochemistry in Condensed Phase," Third Chemical Congress of North America, Toronto, Ontario, June 5–10, 1988.
18. C.B. Moore, "Lasers in Chemistry," ICE Program in Chemical Instrumentation (Advanced Physical and Analytical Chemistry) for High School Teachers, Berkeley, CA, July 14, 1988.
19. C.B. Moore, "The Dynamics of Breaking Chemical Bonds," Department of Chemistry, University of California, Berkeley, Sept. 6, 1988.
20. C.B. Moore, "Dynamics of Chemical Bond Breaking," Department of Chemistry, University of Virginia, Charlottesville, VA, Oct. 26, 1988.
21. C.B. Moore, "IR Flash Kinetic Spectroscopy with the FEL," LBL/BNL Workshop on Scientific Opportunities of the Infrared Free Electron Laser, LBL, Nov. 1, 1988.
22. C.B. Moore, R.G. Bergman, I-C. Chen, D.C. Darwin, H.S. Johnston, E.P. Wasserman, and A.T. Young, "Infrared Flash Kinetic Spectroscopy of Free Radicals," Optical Society of American 1988 Annual Meeting Symposium on Laser Spectroscopy of Molecules, Santa Clara, CA, Nov. 3, 1988.
23. C.B. Moore, "Photofragmentation Dynamics," Workshop on Chemical Reaction Dynamics, LBL, Nov. 4, 1988.
24. C.B. Moore, "Dynamics of Bond Breaking at Threshold — a Test of Unimolecular Reaction Rate Theories," Physikalisch-Chemisches Institut, Heidelberg University, Heidelberg, Federal Republic of Germany, Dec. 14, 1988.
25. C.B. Moore, "The Dynamics of Chemical Bond Breaking," CNRS, Laboratoire de Photophysique Moléculaire, Université de Paris-Sud, Paris, France, Dec. 16, 1988.

Physical Chemistry with Emphasis on Thermodynamic Properties*

Kenneth S. Pitzer, Investigator

INTRODUCTION

The purpose of this program is the discovery and development of methods of calculation of thermodynamic and related properties of important chemical systems by the use of quantum and statistical mechanics together with experimental measurements for key systems. Current emphasis is on novel ionic systems and on properties close to the critical point. Systems comprising fused salts mixed in any proportion with water or other polar solvents are being studied experimentally and with theory. Current studies also include (1) dilute ionic solutions very close to the critical point of the solvent where anomalous properties are observed and (2) the representation of near-critical properties in an equation of state valid over the full range of temperature and density. Recent theoretical advances include treatments of the dielectric constant of H_2O, the thermodynamics of ionic solutions in H_2O above its critical temperature, and the critical properties of pure ionic fluids such as NaCl. Earlier advances yielded improved equations for electrolyte solutions. These various equations are now being applied to a wide variety of systems of industrial or geological interest, including geothermal brines. Other recent research involved the relativistic quantum chemistry of molecules containing very heavy atoms.

1. Near-Critical NaCl-H_2O: An Equation of State and Discussion of Anomalous Properties (Publications 5 and 7)

K.S. Pitzer and J.C. Tanger IV

The system NaCl-H_2O near the critical point of pure water shows not only the remarkable properties of any two-component system near the critical point of one component but also an anomalous curvature of the T-x and P-x projections of the critical line in the range below mole fraction 0.0005. An equation of state is presented that is based on the Haar-Gallagher-Kell equation for pure water with a few terms involving the mole fraction of NaCl together with the temperature and density. Parameters in this equation were selected that yield a good representation of the entire vapor-liquid coexistence surface[1,2] from 250 to 600°C and from the three-phase pressure to the critical pressure (or to the vapor pressure of pure water below its T_c) (see Figure 1-1). Derivatives of this equation yield densities, enthalpies, and heat capacities that are compared with experimental data. The values calculated for the apparent molar heat capacity at slightly supercritical pressure agree remarkably well with recent measurements[3] (see Figure 1-2). Also, the properties calculated for the vapor near the three-phase line are compared with those predicted by the successive hydration model previously developed for NaCl in steam in equilibrium with solid NaCl. Other related topics are discussed, including the anomalous features noted above.

1. K.S. Pitzer, J.L. Bischoff, and R.J. Rosenbauer, Chem. Phys. Lett. **134**, 60 (1987).

2. J.L. Bischoff, R.J. Rosenbauer, and K.S. Pitzer, Geochim. Cosmochim. Acta **50**, 1437 (1986).

3. D.E. White, R.H. Wood, and D.R. Biggerstaff, J. Chem. Thermo. **20**, 159 (1988).

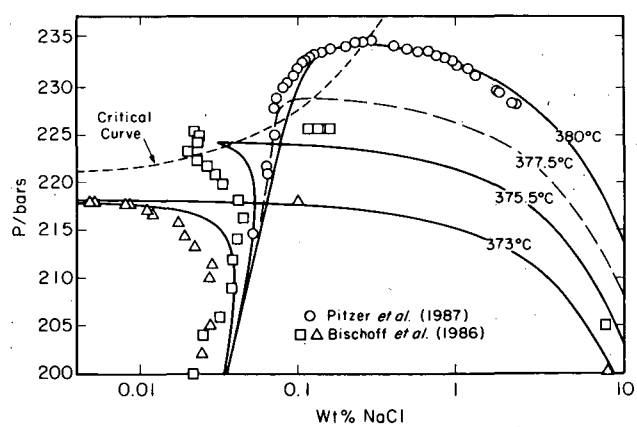

Figure 1-1. Vapor and liquid compositions along several near-critical isothermal coexistence curves. The curves are calculated, the points experimental.[1,2] (XBL 894-1256)

*This work was supported by the Director, Office of Energy Research, Office of Basic Energy Sciences, Chemical Sciences Division, of the U.S. Department of Energy under Contract No. DE-AC03-76SF00098.

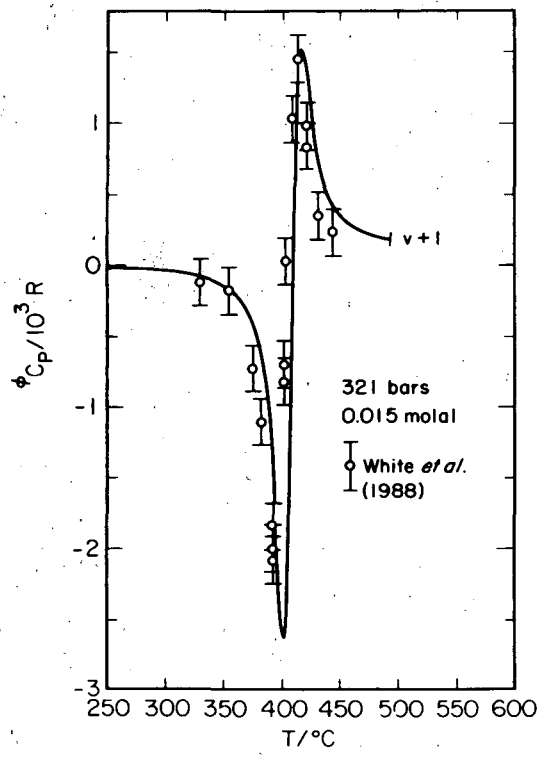

Figure 1-2. Apparent molar heat capacities for a 0.015 molal NaCl solution at 321 bars. The curve is calculated; the experimental[3] points show estimated uncertainties. (XBL 894-1257)

2. An Ionic System with Critical Point at 44°C (Publication 9)

R.R. Singh and K.S. Pitzer

The coexistence curves are known for only a very few ionic systems, but in each case they show an apparent critical exponent of 1/2 instead of the value near 1/3 shown by all nonionic systems. It is of great interest to determine whether this value of 1/2 for the critical exponent remains valid very close to the critical point or, possibly, shifts to a value near 1/3. In order to investigate this question, an ionic system was sought that had a critical point near room temperature where sensitive measurements and precise temperature control would be possible. Such a system has been discovered; it is composed of triethyl-n-hexylammonium triethyl-n-hexylboride in diphenyl ether and has a critical point at 316.7 K (43.6°C) with mole fraction 0.052 of salt. Its coexistence curve shows a critical exponent of 1/2 to within about 1° of the critical point; more sensitive measurements are now in progress. In the course of this investigation, the solubility of this liquid salt was measured for various solvents and an equation was developed that correlates these results with the two variables: (1) dielectric constant and (2) cohesive energy density (Hildebrand's solubility parameter).

3. Equation of State in the Acentric-Factor System (Publications 8 and 12)

D.R. Schreiber and K.S. Pitzer

The acentric factor theory for fluid properties was originally presented with tabulated functions for the compressibility factor and other properties because no convenient equation of state represented fluid behavior over a wide range of conditions to the required accuracy. Now much more complex equations are "convenient," and many equations have been developed that are completely defined when T_c, P_c, and ω are given. An equation is developed to best meet the following criteria: (1) accuracy of representation of measured properties over a wide range of conditions, (2) accurate agreement with the observed near-critical properties, (3) simplicity of form, and (4) computational convenience. The acentric-factor system is an approximation, and agreement to the best experimental accuracy is not expected. Comparisons with experiment are presented to indicate the precision that can be expected for various regions and for the critical isotherm[1] (see Figure 3-1). The equation is further tested by comparisons of calculated enthalpies. The behavior of the effective critical exponent β_e in the near-critical region is examined.

1. P.P. Dawson, I.H. Silberberg, and J.J. McKetta, J. Chem. Eng. Data **18**, 7 (1973).

4. Thermodynamics of Electrolyte Mixtures. Activity and Osmotic Coefficients Consistent with the Higher-Order Limiting Law for Symmetrical Mixing (Publication 2)

J-Z. Yang and K.S. Pitzer

The parameters for symmetrical mixing of ions of the same sign in the virial-coefficient (Pitzer) system are evaluated from literature data for 298.15 K in a manner consistent with the higher-order limiting law of Friedman.[1] Twenty-four systems involve cation mixing with a common anion, and fourteen involve anion mixing with a common cation. Heat

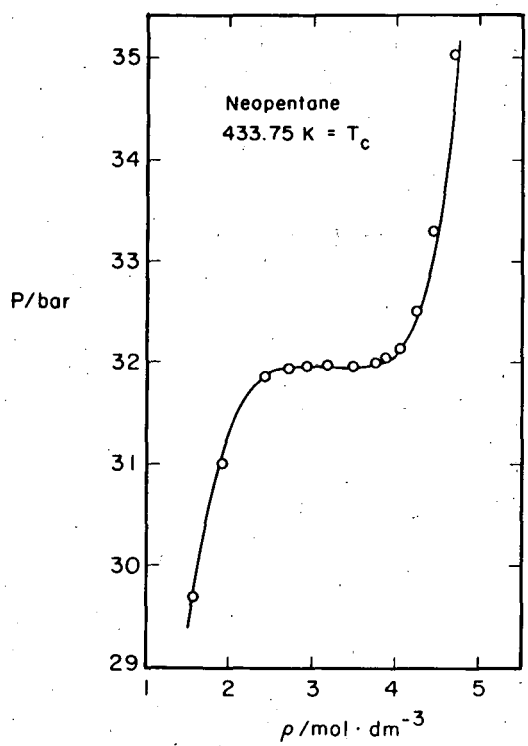

Figure 3-1. The critical isotherm for neopentane. The curve is calculated from the general equation in the acentric factor system; the points are experimental.[1] (XBL 894-1258)

of mixing data were similarly treated in a recent publication;[2] the results give the temperature coefficients of some of these same parameters. The combined results yield the mixing parameters as functions of temperature on a basis both self-consistent and in accord with the limiting law. The results also yield, for a few systems without a common ion, predicted values in good agreement with experimental data.

1. H. L. Friedman, *Ionic Solution Theory*, Interscience Pub., New York, 1962.

2. R.C. Phutela and K.S. Pitzer, J. Solution Chem. **15**, 649 (1986).

5. Work in Progress

The liquid-liquid coexistence curve for the newly discovered ionic system is being extended closer to the critical point at 43.6°C by refractive-index measurements at very precisely controlled temperatures. The study of differences between vapor-liquid and liquid-liquid coexistence curves (Publication 5) is being extended to the region very close to the critical point.

1988 PUBLICATIONS AND REPORTS

Refereed Journals

1. K.S. Pitzer and D.R. Schreiber, "Improving Equation-of-State Accuracy in the Critical Region: Equations for Carbon Dioxide and Neopentane as Examples," Fluid Phase Equilib. **41**, 1 (1988); LBL-24079.
2. J-Z. Yang and K.S. Pitzer, "Thermodynamics of Electrolyte Mixtures. Activity and Osmotic Coefficients Consistent with the Higher-Order Limiting Law for Symmetrical Mixing," J. Solution Chem. **17**, 909 (1988); LBL-25059.
3. R.T. Pabalan and K.S. Pitzer, "Apparent Molar Heat Capacity and Other Thermodynamic Properties of Aqueous KCl Solutions to High Temperatures and Pressures," J. Chem. Eng. Data **33**, 354 (1988); LBL-24085.†
4. R.T. Pabalan and K.S. Pitzer, "Heat Capacity and Other Thermodynamic Properties of Na_2SO_4(aq) in Hydrothermal Solutions and the Solubilities of Sodium Sulfate Minerals in the System Na-Cl-SO_4-OH-H_2O to 300°C," Geochim. et Cosmochim. Acta **52**, 2393 (1988); LBL-24706.†

LBL Reports

5. J.C. Tanger IV and K.S. Pitzer, "Thermodynamics of NaCl-H_2O: A New Equation of State for the Near-Critical Region and Comparisons with Other Equations for Adjoining Regions," accepted by Geochim. et Cosmochim. Acta; LBL-24814.
6. K.S. Pitzer, "Some Interesting Properties of Vapor-Liquid or Liquid-Liquid Coexistence Curves for Ionic and Nonionic Fluids," accepted by Thermochim. Acta; LBL-25058.
7. K.S. Pitzer and J.C. Tanger IV, "Near-Critical NaCl-H_2O: An Equation of State and Discussion of Anomalous Properties," accepted by Intl. J. Thermophys.; invited talk at 10th Symposium on Thermophysical Properties, Gaithersburg, MD, June 20–23, 1988; LBL-25330.
8. D.R. Schreiber and K.S. Pitzer, "Selected Equation of State in the Acentric Factor System," accepted by Intl. J. Thermophys.; presented at 10th Symposium on Thermophysical Properties, Gaithersburg, MD, June 20–23, 1988; LBL-25452.
9. R.R. Singh and K.S. Pitzer, "An Ionic System with Critical Point at 44°C," accepted by J. Am. Chem. Soc.; LBL-25646.
10. J-Z. Yang and K.S. Pitzer, "Thermodynamics of Aqueous Uranyl Sulfate to 559 K," accepted by J. Solution Chem.; LBL-25745.
11. K.S. Pitzer, "Fluids, Both Ionic and Nonionic, Over Wide Ranges of Temperature and Composition," Pure and Applied Chemistry (in press) (Rossini Lec-

ture at the 10th IUPAC Conference on Chemical Thermodynamics); LBL-25859.

12. D.R. Schreiber and K.S. Pitzer, "Equation of State in the Acentric Factor System," accepted by Fluid Phase Equilibria; LBL-25927.
13. J-Z. Yang and K.S. Pitzer, "The Application of the Ion-Interaction Model to Multicomponent 1-1 Type Electrolytes in Mixed Solvents," accepted by J. Solution Chem.; LBL-26023.
14. J.L. Bischoff and K.S. Pitzer, "Liquid-Vapor Relations for the System NaCl-H_2O: Summary of the P-T-x Surface from 300° to 500°C," accepted by Amer. J. Science; LBL-25108.†
15. J.C. Tanger IV and K.S. Pitzer, "Calculation of the Thermodynamic Properties of Aqueous Electrolytes to 1000°C and 5000 Bar from a Semicontinuum Model for Ion Hydration," submitted to J. Phys. Chem.; LBL-26261.†

Invited Talks

16. K.S. Pitzer and J.C. Tanger IV, "Near-Critical NaCl-H_2O: An Equation of State and Discussion of Anomalous Properties," 10th Symposium on Thermophysical Properties, Gaithersburg, MD, June 20–23, 1988.
17. K.S. Pitzer, "Fluids, Both Ionic and Nonionic, Over Wide Ranges of Temperature and Composition," the annual Rossini Lecture of the Commission on Thermodynamics of the International Union of Pure and Applied Chemistry, delivered at its Conference on Chemical Thermodynamics, Prague, Czechoslovakia, August 29, 1988.

†This work was supported by the Director, Office of Energy Research, Office of Basic Energy Sciences, Division of Engineering and Geosciences of the U.S. Department of Energy under Contract No. DE-AC03-76SF00098.

Molecular Interactions*

William A. Lester, Jr., Investigator

INTRODUCTION

This research program is directed at extending fundamental knowledge of atoms and molecules including their electronic structure, mutual interaction, collision dynamics, and interaction with radiation. The approach combines the use of *ab initio* methods—multiconfiguration Hartree-Fock (MCHF), configuration interaction (CI), and the recently developed quantum Monte Carlo (QMC)—to describe electronic structure, intermolecular interactions, and other properties, with various methods for characterizing inelastic and reactive collision processes, and photodissociation dynamics.

1. Damped-Core Quantum Monte Carlo: An Effective Treatment for Large-Z Systems (Publication 1)

B. L. Hammond, P.J. Reynolds, † and W.A. Lester, Jr.

In the past several years increasing attention has focused on quantum Monte Carlo (QMC) methods for obtaining atomic, molecular, and chemical properties, including electronic structure.[1-5] QMC is a method of solving the Schrödinger equation stochastically, and with suitable algorithms, exactly. Results obtained have been remarkably accurate and account explicitly for correlation effects. Recently, workers have begun to explore ways that treat only valence electrons[6-8] motivated by the steep dependence on nuclear charge Z of the computation time required to reduce statistical uncertainties to the level of chemical accuracy. This Z-dependence, estimated[7,9] at $Z^{6.5}$, arises partly from the increasingly large fraction of the energy associated with the core relative to the chemically active valence electrons. The core energy rises as Z^2, and, closely related, the time steps that may be taken in the simulations decrease as Z^2 due to the reduced phase space of the core electrons. This causes extremely poor sampling efficiency for the chemically important valence electrons, while leaving a large "background" energy and variance from the core. Increased sampling efficiency would greatly enhance the speed and broaden the applicability of QMC, a goal being actively pursued.[2,3,6-10] The advantage of treating valence electrons only, for example, using pseudopotentials, is that the overall $Z^{6.5}$ dependence weakens to $Z^{eff3.4}$, where Z^{eff} is a screened nuclear charge.[7]

In damped-core QMC we introduce a random-walk (QMC) method in which the core is treated separately from the valence space, although still by a Monte Carlo method, and valence energies are computed directly. Since most chemical properties derive from the behavior of the valence electrons, we make the approximation that the core may be adequately described by a trial wave function Ψ_{core}. We may, however, choose Ψ_{core} as accurately as desired, even including explicit interelectronic distance terms. Core electrons follow a random walk that distributes them with a probability $|\Psi_{core}|^2$ by a Metropolis algorithm.[11] The valence electrons are sampled using a separate trial function Ψ_{val}. They are, however, treated by a QMC method that "solves" the Schrödinger equation[12] and enables one to sample from the true wave function. From the valence walk, moving in the potential created by the core electrons, one obtains the valence energy to the system.

We calculate ionization potentials and electron affinities of C, Si, and Ge, and find excellent agreement with experiment. Effective speedup over standard QMC approaches is estimated to be as large as a factor of 5000.

*This work was supported by the Director, Office of Energy Research, Office of Basic Energy Sciences, Chemical Sciences Division, of the U.S. Department of Energy under Contract No. DE-AC03-76SF00098.

†Present address: Physics Division, Office of Naval Research, Arlington, VA 22217-5000.

1. D.M. Ceperley and B.J. Alder, Science **231**, 555 (1986).

2. R.N. Barnett, P.J. Reynolds, and W.A. Lester, Jr., J. Chem. Phys. **82**, 2700 (1985); R.N. Barnett, P.J. Reynolds, and W.A. Lester, Jr., J. Chem. Phys. **84**, 4992 (1986); P.J. Reynolds, R.N. Barnett, B.L. Hammond, and W.A. Lester, Jr., J. Stat. Phys. **43**, 1017 (1986).

3. F. Mentch and J.B. Anderson, J. Chem. Phys. **80**, 2675 (1984); D.R. Garmer and J.B. Anderson, J. Chem. Phys. **86**, 4025, 7237 (1987).

4. J.W. Moskowitz, K.E. Schmidt, M.A. Lee, and M.H. Kalos, J. Chem. Phys. **77**, 349 (1982); J.W. Moskowitz and K.E. Schmidt, J. Chem. Phys. **85**, 2868 (1986).

5. M. Caffarel and P. Claverie, J. Chem. Phys. **88**, 1088, 1100 (1988).

6. M.M. Hurley and P.A. Christiansen, J. Chem. Phys. **86**, 1069 (1987); P.A. Christiansen, J. Chem. Phys. **88**, 4867 (1988).

7. B.L. Hammond, P.J. Reynolds, and W.A. Lester, Jr., J. Chem. Phys. **87**, 1130 (1987).

8. T. Yoshida and K. Iguchi, J. Chem. Phys. **88**, 1032 (1988).

9. D.M. Ceperley, J. Stat. Phys. **43**, 815 (1986).

10. C.J. Umrigar, K.G. Wilson, and J.W. Wilkins, Phys. Rev. Lett. **60**, 1719 (1988).

11. N. Metropolis, A.W. Rosenbluth, M.N. Rosenbluth, A.H. Teller, and E. Teller, J. Chem. Phys. **21**, 1087 (1953).

12. See, e.g., P.J. Reynolds, D.M. Ceperley, B.J. Alder, and W.A. Lester, Jr., J. Chem. Phys. **77**, 5593 (1982), and references therein.

2. Monte Carlo Study of Electron Correlation Functions for Small Molecules (Publication 7)

Z. Sun,[†] P.J. Reynolds, [‡] R.K. Owen, and W.A. Lester, Jr.

A study is made of electron-electron correlation functions for use in trial wave functions for small molecules. New forms are proposed that have only a few variational parameters, and these parameters have physical meanings that are easily discerned. Total energies for H_2, LiH, and Li_2 computed using these correlation functions are presented, and comparison is made with previous forms, including the Jastrow-Pade form often used in Monte Carlo studies. We further treat the possibility that correlation depends not only on the separation of a pair of electrons but also on the location of the electron pair relative to the nuclei—indicative of a density-dependent or many-body correlation effect. Our results indicate that such a many-body correlation effect is weakly present.

[†]Permanent address: Institute of Mechanics, Chinese Academy of Sciences, Beijing, People's Republic of China.

[‡]Present address: Physics Division, Office of Naval Research, Arlington, VA 22217-5000.

3. Electronic Structure, Hyperfine Interactions, and Magnetic Properties for Iron Octahedral Sulfides (Publication 8)

M. Braga,[†] S.K. Lie,[‡] C.A. Taft,[§] and W.A. Lester, Jr.

Spin-polarized multiple-scattering calculations have been performed for FeS_6^{n-} (n = 8, 9, 10) clusters in order to study the electronic structure of the iron atom octahedrally coordinated to sulfur. The calculated total spin and charge densities together with the 3d and 4s atomic populations are used to interpret the Mössbauer hyperfine parameters. A detailed discussion of the hyperfine interaction and magnetic properties is given for the spinel greigite (Fe_3S_4). Possible existence of a Fe(IV) state in minerals containing only FeS is discussed, and it is concluded that it is highly unlikely.

[†]Permanent address: Departamento de Quimica Fundamental, Universidade Federal de Pernambuco, 50739 Recife, Pernambuco, Brazil.

[‡]Permanent address: Instituto de Fisica, Universidade Federal Fluminense, 24210 Niteroi, Rio de Janeiro, Brazil.

[§]Permanent address: Centro Brasileiro de Pesquisas Fisicas, Urca, 22290 Rio de Janeiro, Brazil.

4. Theoretical Study of the Interaction of Fe, Fe^+, and FeCO with Ar (Publication 2)

M. Braga,[†] A.L. Almeida,[‡] C.A. Taft,[‡] B.L. Hammond, and W. A. Lester, Jr.

Ab initio Hartree-Fock calculations were performed on $FeAr^+$ and $FeAr^+$ in order to determine the interaction of both neutral and singly ionized Fe atoms trapped in Ar, and on ArFeCO and FeCOAr in order to ascertain the effect of an Ar matrix on the FeCO molecule. Quadrupole splittings and isomer shifts are computed using *ab initio* orbital populations and charge densities scaled by a relativistic factor. Good agreement between calculated and experimental hyperfine parameters is found in each case. The interaction energy for Fe^+–Ar was computed using both *ab initio* Hartree-Fock and effective core potential (ECP) methods. Both approaches yield a minimum between Fe^+ and Ar at approximately 7.6 bohr.

[†]Permanent address: Departamento de Quimica Fundamental, Universidade Federal de Pernambuco, 50739 Recife, Pernambuco, Brazil.

[‡]Permanent address: Centro Brasileiro de Pesquisas Fisicas, Urca, 22290 Rio de Janeiro, Brazil.

1988 PUBLICATIONS AND REPORTS

Refereed Journals

1. B.L. Hammond, P.J. Reynolds, and W.A. Lester, Jr., "Damped-Core Quantum Monte Carlo: An Effective Treatment for Large-Z Systems," Phys. Rev. Lett. **61**, 2312 (1988); LBL-24680.
2. M. Braga, A.L. Almeida, C.A. Taft, B.L. Hammond, and W.A. Lester, Jr., "Theoretical Study of the Interaction of Fe, Fe^+, and FeCO with Ar," J. Chem. Phys. **89** 4867 (1988); LBL-25723.
3. C.A. Taft, J.C. Azevedo, J.G.R. Tostes, and W.A. Lester, Jr., "*Ab Initio* Studies of the Linear Complex

$HC_3N...HC_3N$," J. Mol. Struct. (Theochem) **168**, 169 (1988); LBL-25682.

4. M.N. Ramos, C.A. Taft, J.G.R. Tostes, and W.A. Lester, Jr., "An *ab initio* Spectroscopic Study of the HCN...HCN and HCN...HNC Linear Complexes," J. Mol. Struct. **175**, 303 (1988); LBL-25681.
5. P.R. Seidl, K.Z. Leal, J.G.R. Tostes, C.A. Taft, B.L. Hammond, and W.A. Lester, Jr., "An *ab initio* Investigation of the Effects of 2-Exo and Endo Substituents on Norbornane," Chem. Phys. Lett. **147**, 373 (1988); LBL-25246.
6. J.G.R. Tostes, C.A. Taft, M.N. Ramos, and W.A. Lester, Jr., "Role of Polarization Functions on the Bridge Hydrogen Atom in HCN...HCN," Int. J. Quantum Chem. **34**, 85 (1988); LBL-24683.

LBL Reports

7. Z. Sun, P.J. Reynolds, R.K. Owen, and W.A. Lester, Jr., "Monte Carlo Study of Electron Correlation Functions for Small Molecules," Theor. Chim. Acta (in press); LBL-24095.
8. M. Braga, S.K. Lie, C.A. Taft, and W.A. Lester, Jr., "Electronic Structure, Hyperfine Interactions and Magnetic Properties for Iron Octahedral Sulfides," Phys. Rev. B (in press); LBL-25939.

Invited Talks

9. P.R. Seidl, K.Z. Leal, J.W. de M.Carneiro, J.G.R. Tostes, C.A. Taft, B.L. Hammond, and W.A. Lester, Jr., "*Ab initio* Charge Distribution in Half-Cage Compounds," 3rd Chemical Congress of North America and 195th ACS National Meeting, Toronto, Ont., June 5–10, 1988; LBL-25474 abs.
10. W.A. Lester, Jr., "Quantum Monte Carlo for Molecules," Department of Condensed Matter and Statistical Physics, Brazilian Center of Physics Research, Rio de Janeiro, Brazil, Feb. 9, 1988.
11. W.A. Lester, Jr., "Diffusion Quantum Monte Carlo," Department of Fundamental Chemistry, Federal University of Pernambuco, Recife, Brazil, April 7, 1988.
12. W.A. Lester, Jr., "Computers in Chemistry: A Personal Perspective," Third Chemical Congress of North America, Toronto, Ont., June 5, 1988.
13. W.A. Lester, Jr., "Collisions and Electronic Structure of $H_2(B^1\Sigma_u^+)$," Satellite Meeting on Chemical Reaction Dynamics, Weizmann Institute, Rehovot, Israel, Aug. 28–31, 1988.
14. W.A. Lester, Jr., "Computational Sciences," White House Initiative on Historically Black Colleges and Universities Science and Technology Symposium, Washington, D.C., Sept. 25–27, 1988.

Spectroscopy and Structures of Reactive Intermediates*

Richard J. Saykally, Investigator

INTRODUCTION

The objective of this research is to develop new techniques for the detection of unstable forms of molecules, and to use these techniques to carry out detailed measurements of the structures, properties, and dynamics of these species with the goal of improving our large-scale understanding of chemical reactions and energy transfer, as applied to combustion systems.

Reactive forms of molecules, including neutral-free radicals and molecular ions, play extremely important roles as reaction intermediates in combustion processes, reactive plasmas, in the terrestrial atmosphere, and in interstellar space. The transient nature of these reactive species has made their detection and characterization a very difficult task, and comparatively few of these important reactive molecules have been studied in detail.

"van der Waals complexes"—molecules held together at low temperatures only by very weak dispersion or induction forces or by hydrogen bonds—constitute excellent prototypes of these same weak interactions that dominate the condensed phases. One of the chemical physicist's great dreams has been to bridge the gap from the gas phase, where detailed measurements of isolated species are possible, to the condensed phases, where this is clearly impossible, through the investigation of successively more complex van der Waals aggregates in the gas phase. This dream is still a long way from being realized, as these species, like the reaction intermediates, are extremely difficult to detect and characterize. Nevertheless, a new level of understanding of van der Waals forces is emerging from studies of the vibrational motions of the weak bonds.

The primary goal of this research, then, is to carry out detailed investigations of those reaction intermediates that are critical species in the combustion of important fuels. Exactly the same experimental and theoretical techniques employed to study reaction intermediates can be applied to van der Waals molecules; hence, studies of these two crucially important classes of molecules will be undertaken as well, with the long-range objective of correlating the measured properties of these species as a means of understanding condensed phases in more detail.

*This work was supported by the Director, Office of Energy Research, Office of Basic Energy Sciences, Chemical Sciences Division, of the U.S. Department of Energy under Contract No. DE-AC03-76SF00098.

1. Far-Infrared Laser Stark Spectroscopy of the Σ Bending Vibration of ArHCl (Publication 1)

R.L. Robinson,† Dz.-H. Gwo, and R.J. Saykally

A complete analysis of the far-infrared laser Stark/microwave double-resonance spectrum of the ℓ bending vibration of ArHCl is given. Hyperfine-resolved spectra of the R(0), R(1), R(2), and P(1) transitions were measured near 25 cm^{-1} for both chlorine isotopes. Accurate values for the band origins, rotational constants, dipole moments, and quadrupole hyperfine constants were obtained. Comparison with Hutson's close-coupling calculations provide very strong support for the existence of a secondary minimum in the intermolecular potential surface at the linear ArClH geometry.

†Present address: Joint Institute for Laboratory Astrophysics and Department of Chemistry, University of Colorado, Boulder, CO 80309.

2. Tunable Far-Infrared Laser Spectroscopy of van der Waals Bonds: Extended Measurements on the lowest Σ Bend of ArHCl (Publication 2)

K.L. Busarow, G.A. Blake,† K.B. Laughlin,‡ R.C. Cohen, Y.T. Lee, and R.J. Saykally

A tunable far-infrared laser system has been used to measure the vibration-rotation spectrum of the lowest Σ bending state of ArHCl near 24 cm^{-1} in a continuous-wave planar jet operating with a terminal jet temperature near 3 K. Over 60 transitions have been observed for both ^{35}Cl and ^{37}Cl isotopes with resolution of the quadrupole hyperfine structure. An improved set of molecular parameters was determined, including B, D, H, and eqQ for both upper and lower states. Very narrow linewidths (approximately 300 kHz) resulting in high resolution and sen-

sitivity make this technique a powerful new method for detailed investigation of intermolecular forces.

[†]Present address: Center for Cosmochemistry and Geochemistry, Division of Geology and Planetary Sciences, California Institute of Technology, Pasadena, CA 91125.

[‡]Present address: Department of Chemistry, Massachusetts Institute of Technology, Cambridge, MA 02139.

3. Tunable Far-Infrared Laser Spectroscopy of van der Waals Bonds: Vibration-Rotation-Tunneling Spectra of Ar-H_2O (Publication 3)

R.C. Cohen, K.L. Busarow, K.B. Laughlin,[†] G.A. Blake,[‡] M. Havenith,[§] Y.T. Lee, and R.J. Saykally

The first high-resolution spectra of a rare gas–H_2O cluster have been observed using a tunable far-infrared laser to probe the vibration-rotation-tunneling levels of Ar-H_2O formed in a continuous planar supersonic jet. The high sensitivity of this spectrometer facilitated extensive measurements of two perpendicular subbands, which are assigned to transitions from the ground state to the upper component of a hydrogen-exchange tunneling doublet (c-type) at 21 cm^{-1} and to $\nu_{b1} = 1^+$ (b-type) at 25 cm^{-1}, the lower tunneling component of a bending vibration that is perpendicular to the tunneling coordinate. The tunneling splitting is shown to be in the range 2.5–7 cm^{-1}, and the lower tunneling component of the excited bending vibration lies between 39 and 43 cm^{-1} above the ground state of the complex. The experimentally determined center-of-mass separation (R_{cm} = 3.7 Å) and harmonic stretching force constant (k_s = 0.0134 mdyn/Å) are compared to those of related first- and second-row hydrides. The large-amplitude motions occuring within this complex make it difficult to establish its structure.

[†]Present address: Department of Chemistry, Massachusetts Institute of Technology, Cambridge, MA 02139.

[‡]Present address: Center for Cosmochemistry and Geochemistry, Division of Geology and Planetary Sciences, California Institute of Technology, Pasadena, CA 91125.

[§]Present address: Institut für Angewandte Physik, Universität Bonn, Federal Republic of Germany.

4. Tunable Far-Infrared Laser Spectroscopy of Hydrogen Bonds: The $K_a = 0(u) \rightarrow 1$ (g) Rotation-Tunneling Spectrum of the HCl Dimer (Publication 4)

G.A. Blake,[†] R.C. Cohen, K.B. Laughlin,[‡] Y.T. Lee, and R.J. Saykally

The ground state $K_a = 0(u) \rightarrow 1(g)$ b-type subband of the rotation-tunneling spectrum of the symmetric $^{35}Cl-^{35}Cl$, $^{37}Cl-^{37}Cl$, and the mixed $^{35}Cl-^{37}Cl$ hydrogen chloride dimers have been recorded near 26.3 cm^{-1} with sub-Doppler resolution in a continuous two-dimensional supersonic jet with a tunable far-infrared laser spectrometer. Quadrupole hyperfine structure from the chlorine nuclei has been resolved. From the fitted rotational constants a $(H^{35}Cl)_2$ center-of-mass separation of 3.81 Å is derived for the $K_a = 1(g)$ levels, while the nuclear quadrupole coupling constants yield a vibrationally averaged angular structure for both tunneling states of approximately 20–25° for the hydrogen-bonded proton and at least 70–75° for the external proton. This nearly orthogonal structure agrees well with that predicted by *ab initio* theoretical calculations, but the observed splittings and intensity alterations of the lines indicate that the chlorine nuclei are made equivalent by a large-amplitude tunneling motion of the HCl monomers. A similar geared internal-rotation tunneling motion has been found for the HF dimers, but here the effect is much greater. The ground-state tunneling splittings are estimated to lie between 15–18 cm^{-1}, and the selection rules observed indicate that the *trans* tunneling path dominates the large-amplitude motion, as expected, provided the dimer remains planar. From the observed hyperfine constants, we judge the dimer and its associated tunneling motion to be planar to within 10°.

[†]Present address: Center for Cosmochemistry and Geochemistry, Division of Geology and Planetary Sciences, California Institute of Technology, Pasadena, CA 91125.

[‡]Present address: Department of Chemistry, Massachusetts Institute of Technology, Cambridge, MA 02139.

5. Work in Progress

We are now developing tunable far-infrared laser techniques for studying reactive molecules generated by excimer laser photolysis and van der Waals complexes. Ultimately these will possess extremely high sensitivity and resolution such that subtle effects on hydrogen tunnelling migration effects can be explored in fluxional radicals like vinylidene and vinyl radical.

1988 PUBLICATIONS AND REPORTS

Refereed Journals

1. R.L. Robinson, Dz.-H. Gwo, and R.J. Saykally, "Far Infrared Laser Stark Spectroscopy of the Σ Bending Vibration of ArHCl: Strong Evidence for a Double Minimum Potential Surface," Mol. Phys. **63**, 1021 (1988); LBL-24806.
2. K.L. Busarow, G.A. Blake, K.B. Laughlin, R.C. Cohen, Y.T. Lee, and R.J. Saykally, "Tunable Far Infrared Laser Spectroscopy of van der Waals Bonds: The Σ Bend of ArHCl," J. Chem. Phys. **89**, 1268 (1988); LBL-24859.
3. R. Cohen, K.L. Busarow, K.B. Laughlin, G.A. Blake, M. Havenith, Y.T. Lee, and R.J. Saykally, "Tunable Far Infrared Laser Spectroscopy of van der Waals Bonds: Vibration-Rotation-Tunnelling Spectra of Ar-H_2O," J. Chem. Phys. **89**, 4494 (1988); LBL-25399.
4. G. Blake, K.L. Busarow, R. Cohen, K. Laughlin, Y.T. Lee, and R.J. Saykally, "Tunable Far Infrared Laser Spectroscopy of van der Waals Bonds: Vibration-Rotation Tunneling Spectra of Ar-H_2O," J. Chem. Phys. **89**, 6577 (1988); LBL-25400.

LBL Reports

5. K.L. Busarow, R.C. Cohen, G.A. Blake, K.B. Laughlin, Y.T. Lee, and R.J. Saykally, "Measurement of the Perpendicular Rotation-Tunneling Spectrum of the Water Dimer by Tunable Far Infrared Laser Spectroscopy in a Planar Supersonic Jet," accepted by J. Chem. Phys.; LBL-26174.
6. R.J. Saykally, "Tunable Far-IR Laser Spectroscopy of van der Waals Bonds: A New Probe of Intermolecular Forces," accepted by Accts. Chem. Res.; LBL-26553.
7. Dz.-H. Gwo, M. Havenith, R. Cohen, K.L. Busarow, and R.J. Saykally, "Tunable Far-IR Laser Spectroscopy of van der Waals Bonds: The Intermolecular Stretching Vibration of Ar-NH_3," submitted to J. Chem. Phys.; LBL-26554.
8. M. Havenith, Dz.-H. Gwo, K.L. Busarow, R. Cohen, and R.J. Saykally, "Tunable Far-IR Laser Spectroscopy of van der Waals Bonds: The Intermolecular Stretching Vibration of Ammonia Dimer," submitted to J. Chem. Phys.; LBL-26555.

Theory of Atomic and Molecular Collision Processes*

William H. Miller, Investigator

INTRODUCTION

This research is primarily involved with the development and application of theoretical methods and models for describing atomic and molecular collision processes and chemical reaction dynamics. Specific topics of interest have included the theory of inelastic and reactive scattering, collision processes involving electronically excited atoms or molecules, collisional ionization phenomena, statistical theories of chemical reactions, scattering of atoms and molecules from surfaces, and the interactions of molecular systems with high-power laser radiation.

Most recently, research has focused on the development of theoretical methods for a first-principles treatment of dynamics in polyatomic molecular systems. The goal is to develop approaches that can utilize *ab initio* quantum chemical calculations of the potential energy surface (in the Born-Oppenheimer approximation) as direct input into the dynamical treatment, and thus, to as great an extent as possible, have a truly predictive theory.

The potential application of these methods is almost without limit. In this group hydrogen-atom transfer processes have been studied in a variety of systems. Other research groups have used these approaches to describe a variety of reactions that are relevant to the primary steps in combustion.

1. Monte Carlo Path Integration for the Real-Time Propagator (Publication 4)†

N. Makri and W.H. Miller

Monte Carlo methods are described for evaluating the Feynman path-integral representation of the (real-time) propagator (time-evolution operator), $\exp(-iHt/\hbar)$. The approach is based on the modified Filinov algorithm presented earlier by Makri and Miller.[1] Numerical calculations are presented for time evolution in a symmetric double-well potential, as well as in a Morse potential.

†Calculations were performed on the Berkeley Theoretical Chemistry computing facility, supported by the National Science Foundation Grant No. CHE84-16345.

1. N. Makri and W.H. Miller, Chem. Phys. Lett. **139**, 10 (1987).

2. Effect of Fluctuations in State-Specific Unimolecular Rate Constants on the Pressure Dependence of the Average Unimolecular Reaction Rate (Publication 6)†

W.H. Miller

The standard (i.e., Lindemann mechanism, strong-collision assumption, etc.) treatment of thermal unimolecular reactions expresses the effective, pressure-dependent unimolecular rate constant (usually called k_{uni}) in terms of the average unimolecular rate constant for a given total energy, k(E) (and, more rigorously, for a given total angular momentum). Several experimental and theoretical studies have shown, however, that unimolecular rate constants for individual quantum states (all of essentially the same total energy and angular momentum) can have significant variations about the average rate, i.e., a significant degree of state specificity. This paper examines the effect that these fluctuations have on the effective, pressure-dependent rate, k_{uni}. The general result is that fluctuations reduce the rate, most prominently at high pressures.

†Calculations were performed on the Berkeley Theoretical Chemistry computing facility, supported by the National Science Foundation Grant No. CHE84-16345.

3. A Diabatic Reaction-Path Hamiltonian (Publication 7)†

W.H. Miller, B.A. Ruf, and Y.-T. Chang

A reaction-path Hamiltonian is constructed that is based on a straight-line, least-motion path that interpolates linearly between equilibrium reactant and product geometries of the molecular system.

*This work was supported by the Director, Office of Energy Research, Office of Basic Energy Sciences, Chemical Sciences Division, of the U.S. Department of Energy under Contract No. DE-AC03-76SF00098.

Conservation of linear and angular momentum are correctly accounted for. The resulting Hamiltonian has a Cartesian-type kinetic energy, the coriolis coupling terms originally present in the kinetic energy having been transformed to potential energy coupling (hence the term "diabatic" reaction-path Hamiltonian). Curvature-coupling terms that appear in the original reaction-path Hamiltonian, which is based on the minimum-energy reaction path, are absent here because the present reaction path is straight. This new, diabatic reaction-path Hamiltonian should be especially useful for describing H-atom transfer reactions in polyatomic systems, a case for which the minimum-energy reaction path provides a poor description.

†Calculations were performed on the Berkeley Theoretical Chemistry computing facility, supported by the National Science Foundation Grant No. CHE84-16345.

4. Correct Short-Time Propagator for Feynman Path Integration by Power-Series Expansion in Δt (Publication 8)†

N. Makri and W.H. Miller

The most commonly used short-time propagator in a discretized Feynman path integral (and also several more sophisticated "improved" ones) is not correct through first order in the time increment Δt. The correct semiclassical result for the phase (i.e., the action) of the short-time propagator is developed in this paper as a power series in Δt, explicit expressions being given for the terms of order Δt^{-1}, Δt^{1}, and Δt^{3}. The proposed expression is also the correct quantum mechanical result through order Δt^{2}. Test applications to the standard harmonic oscillator and also to a double-well potential (typical for intramolecular H-atom transfer) show the first-order propagator (i.e., the correct result through order Δt) to be a significant improvement over previous ones; inclusion of the third-order term gives considerable additional improvement (i.e., faster convergence).

†Calculations were performed on the Berkeley Theoretical Chemistry computing facility, supported by the National Science Foundation Grant No. CHE84-16345.

5. Work in Progress

A new kind of semiclassical tunneling model is being developed for use in classical trajectory simulations of polyatomic dynamical processes. Although much is known about "rigorous" semiclassical approximations to quantum mechanics, the goal of the present work is a simple-to-use, necessarily approximate model that can be implemented within the framework of a standard trajectory simulation. Applications to multidimensional models of H-atom transfer reactions show that such models can be usefully accurate.

1988 PUBLICATIONS AND REPORTS

Refereed Journals

1. J.Z.H. Zhang, S.I. Chu, and W.H. Miller, "Quantum Scattering via the S-Matrix Version of the Kohn Variational Principle," J. Chem. Phys. **88**, 6233 (1988).
2. W.F. Polik, C.B. Moore, and W.H. Miller, "Quantum Interference Among Competing Unimolecular Decay Channels: Asymmetric D_2 Decay Profiles," J. Chem. Phys. **89**, 3584 (1988).
3. J.Z.H. Zhang and W.H. Miller, "Accurate 3-Dimensional Quantum Scattering Calculations for F + H_2 → HF + H," J. Chem. Phys. **88**, 4549 (1988).
4. N. Makri and W.H. Miller, "Monte Carlo Path Integration for the Real Time Propagator," J. Chem. Phys. **89**, 2170 (1988); LBL-25156.
5. J.Z.H. Zhang and W.H. Miller, "Comment on 'Quantum Scattering via the S-Matrix Version of the Kohn Variational Principle'," J. Chem. Phys. **89**, 4454 (1988).
6. W.H. Miller, "Effect of Fluctuations in State-Specific Unimolecular Rate Constants on the Pressure Dependence of the Average Unimolecular Reaction Rate," J. Phys. Chem. **92**, 4261 (1988); LBL-25280.
7. W.H. Miller, B.A. Ruf, and Y.T. Chang, "A Diabatic Reaction Path Hamiltonian," J. Chem. Phys. **89**, 6298 (1988); LBL-25669.
8. N. Makri and W.H. Miller, "Correct Short-Time Propagator for Feynman Path Integration by Power Series Expansion in Δt," Chem. Phys. Lett. **151**, 1 (1988); LBL-25670.
9. A.C. Peet and W.H. Miller, "A Pointwise Representation of the S-Matrix Kohn Variational Principle for Quantum Scattering," Chem. Phys. Lett. **149**, 257 (1988).
10. N. Makri and W.H. Miller, "Exponential Power Series Expansion for the Quantum Time Evolution Operator," J. Chem. Phys. **90**, 904 (1989); LBL-25701.

Other Publications

11. B.A. Ruf and W.H. Miller, "A New (Cartesian) Model for Reaction Dynamics in Polyatomic Systems, with Application to H-Atom Transfer in

Malonaldehyde," J. Chem. Soc., Faraday Trans. 2 **84**, 1523 (1988); LBL-24412.

12. W.H. Miller, "A New Variational Expression for the Scattering Matrix," Collect. Czech. Chem. Comm. **53**, 1873 (1988); LBL-24205.
13. W.H. Miller, "Recent Developments in Quantum Mechanical Reactive Scattering—the S-Matrix Version of the Kohn Variational

LBL Reports

14. W.H. Miller, "Theoretical Models for Reaction Dynamics in Polyatomic Molecular Systems," NATO Barcelona (1989); LBL-25671.
15. W.H. Miller, "Quantum Mechanics of Chemical Reactions: Recent Developments in Reactive Scattering and in Reaction Path Hamiltonians," Jerusalem ICQC; LBL-26377.

Photoelectron Spectroscopy*

David A. Shirley, Investigator

INTRODUCTION

This program addresses both experimental and theoretical aspects of electron spectroscopy for the investigation of electronic structure of matter in the gaseous and condensed phases. Research is conducted using both laboratory sources at LBL and synchrotron radiation in the 5–5000 eV energy range available at the Stanford Synchrotron Radiation Laboratory, where there is participation in developing the spectroscopy of this newly accessible range of the electromagnetic spectrum. Time-of-flight measurements with synchrotron radiation are used to measure angular distributions of photoelectrons and resonant photoemission phenomena in the gas phase. Ultrahigh-resolution photoelectron spectroscopy based on molecular beams is yielding new information about small molecules and about the transition from single metal atoms to behavior characteristic of a three-dimensional solid. Employing angle-resolved, variable-energy photoemission and electron-energy-loss spectroscopy, this program examines the electronic structure of solids. The program also studies the geometric and electronic structure of surface-adsorbate systems using photoelectron diffraction, angle-resolved photoemission extended fine structure (ARPEFS), and surface extended x-ray absorption fine structure (SEXAFS).

1. Observation of Correlation Effects in Zero Kinetic Energy Electron Spectra near the N1s and C1s Thresholds in N_2, CO, C_6H_6, and C_2H_4 (Publication 10)

L.J. Medhurst, T.A. Ferrett,† P.A. Heimann, D.W. Lindle,‡ S.H. Liu,§ and D.A. Shirley

Zero kinetic energy (ZKE) spectra of N_2, CO, C_2H_4, and C_6H_6 were taken across the N1s (N_2) and C1s ionization thresholds. Discrete resonances at subthreshold photon energies were observed and were found to become more intense as threshold is approached relative to the same peaks in absorption spectra. For N_2 the satellite/main-line branching ratios at threshold are 11(1)% for the 419.7(1) eV binding energy satellite, and 2.3(1.0)% for the 426.5(1) eV binding energy satellite. For CO, the branching ratio for the 304.6(1) eV binding energy satellite is 15(2)% at its threshold (see Figure 1-1). Branching ratios at threshold are also determined for the satellites of C_6H_6 and C_2H_4. Decay characteristics and assignments of the continuum features of C_6H_6 and C_2H_4 are also discussed.

*This work was supported by the Director, Office of Energy Research, Office of Basic Energy Sciences, Chemical Sciences Division, of the U.S. Department of Energy under Contract No. DE-AC03-76SF00098. It was performed at the Stanford Synchrotron Radiation Laboratory, which is supported by the Department of Energy's Office of Basic Energy Sciences.

†Present address: Department of Chemistry, Swarthmore College, Swarthmore, PA 19081.

‡Present address: National Bureau of Standards, Gaithersburg, MD 20899.

§Permanent address: Institute of Chemistry, Academia Sinica, People's Republic of China.

1. U. Gelius, J. Electron Spectros. Relat. Phenom. 5, 985 (1974).

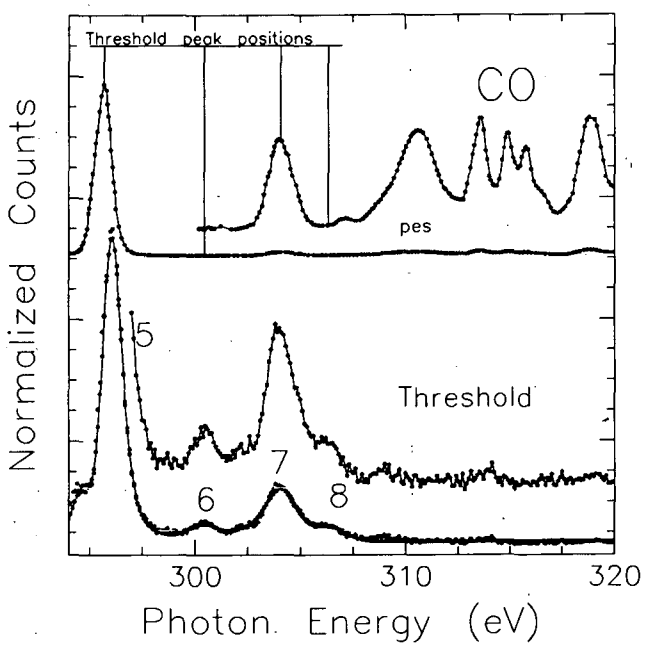

Figure 1-1. ZKE scan of CO above the C1s threshold. The solid line is a least-squares fit to the spectrum. Included for comparison is the potential-energy-surface spectrum of Gelius *et al.*[1] (XBL 885-1919)

2. Angle-Resolved Photoemission From the Ar 2p Subshell (Publication 7)

D.W. Lindle,[†] L.J. Medhurst, T.A. Ferrett,[‡] P.A. Heimann, M.N. Piancastelli,[§] S.H. Liu,[¶] D.A. Shirley, T.A. Carlson,[**] P.C. Deshmukh,[††] G. Nasreen,[‡‡] and S.T. Manson[‡‡]

The angular distribution for Ar 2p photoionization has been measured from just above threshold to 400 eV photon energy and calculated in the same energy range using the relativistic random-phase approximation (see Figure 2-1). The present experimental and theoretical results are in good agreement but disagree somewhat with earlier Hartree-Fock (HF) calculations. The HF values are found to be significantly higher in the near-threshold region. Possible reasons for this discrepancy are discussed with relevance to the general understanding of inner-shell photoionization phenomena.

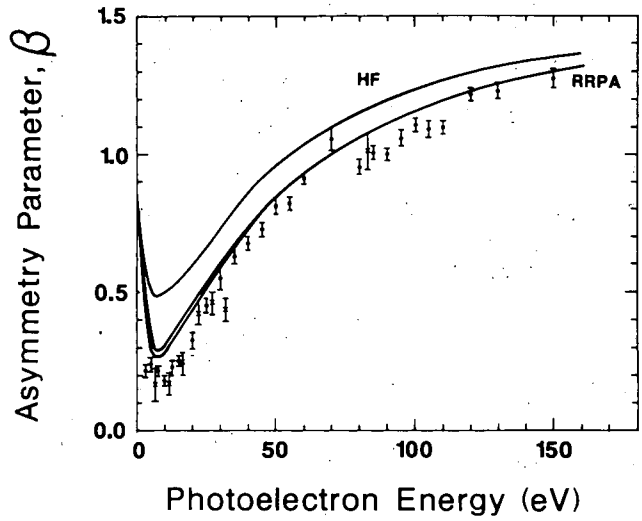

Figure 2-1. Angular-distribution asymmetry parameter for Ar 2p photoionization as a function of energy above the $2p_{3/2}$ ionization threshold at 248.4 eV. All of the β_{2_p} results are unresolved with respect to the 2p spin-orbit components. Experimental results are from the Berkeley group (solid circles) and the ORNL group (X). Theoretical curves represent the present relativistic random-phase approximation (RRPA) 5- and 14-channel calculations (upper and lower, respectively) and Hartree-Fock (HF) calculations from Ref. 1. (XBL 884-1087)

[†]Present address: National Bureau of Standards, Gaithersburg, MD 20899.

[‡]Present address: Department of Chemistry, Swarthmore College, Swarthmore, PA 19081.

[§]Permanent address: Department of Chemistry, Second University of Rome, 00100 Rome, Italy.

[¶]Permanent address: Institute of Chemistry, Academia Sinica, People's Republic of China.

[**]Permanent address: Chemistry Division, Oak Ridge National Laboratory, Oak Ridge, TN 37831-6201.

[††]Permanent address: Department of Physics, Indian Institute of Technology, Madras 600036, India.

[‡‡]Permanent address: Department of Physics and Astronomy, Georgia State University, Atlanta, GA 20202.

1. D.J. Kennedy and S.T. Manson, Phys. Rev. A **5**, 227 (1972).

3. Resonant Processes Above the Carbon 1s Ionization Threshold in Benzene and Ethylene (Publication 14)

M.N. Piancastelli,[†] T.A. Ferrett,[‡] D.W. Lindle,[§] L.J. Medhurst, P.A. Heimann, S.H. Liu,[¶] and D.A. Shirley

Resonant photoemission has been studied above the carbon 1s ionization thresholds in gas-phase benzene and ethylene. The experimental data for both molecules include relative partial cross-section and asymmetry-parameter measurements for the C1s main line and asymmetry-parameter measurements for one C1s shake-up satellite in each system (see Figure 3-1). Resonances above the C K-edge have been analyzed on the basis of their decay to either the C1s main-line or valence-hole states, and have

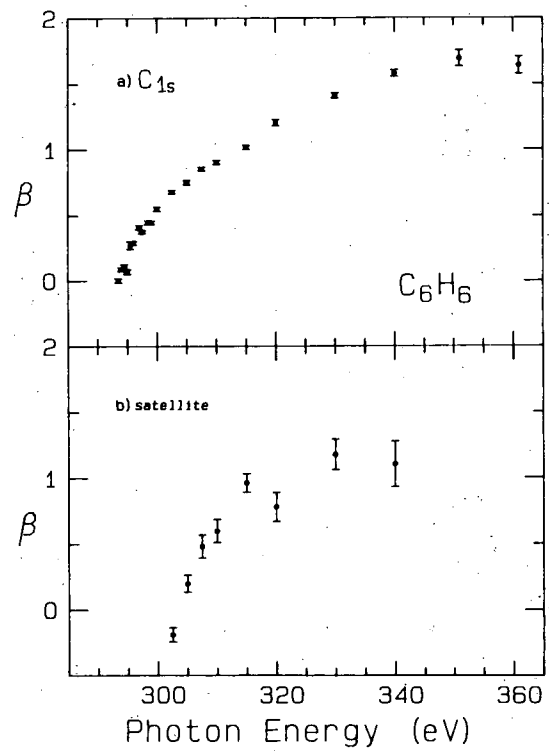

Figure 3-1. Angular-distribution parameter for the C1s main line and the 297-eV satellite in benzene. (XBL 885-1788)

been tentatively assigned as either shape resonances or doubly excited states according to their observed one-electron or many-electron decay, respectively. The importance of determining the resonant behavior of all available photoemission channels in the proximity of a resonance is thus illustrated.

[†]Permanent address: Department of Chemistry, Second University of Rome, 00100 Rome, Italy.

[‡]Present address: Department of Chemistry, Swarthmore College, Swarthmore, PA 19081.

[§]Present address: National Bureau of Standards, Gaithersburg, MD 20899.

[¶]Permanent address: Institute of Chemistry, Academia Sinica, People's Republic of China.

4. Adsorption and Surface Reactions of H_2S and SO_2 on Cu(100) Studied by Electron-Energy-Loss Spectroscopy (Publication 12)

K.T. Leung,[†] X.S. Zhang,[‡] and D.A. Shirley

The adsorption of H_2S and SO_2 on Cu(100) was investigated using electron-energy-loss spectroscopy as a function of coverage, temperature, and scattering angles. In particular, irreversible dissociation of H_2S and the formation of sulfhydryl (SH) species at low and intermediate coverage on Cu(100) were observed at low temperature. This was followed by molecular physisorption at higher coverage. In the case of SO_2 on Cu(100), decomposition of SO_2 and the formation of SO_3 surface species at room temperature were observed (see Figure 4-1). A surface reaction involving preadsorbed SO_2 on Cu(100) with H_2S is discussed.

[†]Present address: Department of Chemistry, University of Waterloo, Waterloo, Ontario N2L 3G1.

[‡]Permanent address: Department of Physics, Zhejiang University, Hangzhou, People's Republic of China.

5. Surface Bonding Geometry of (2×1)S/Ge(001) by Normal-Emission Angle-Resolved Photoemission Extended Fine Structure (Publication 9)

K.T. Leung,[†] L.J. Terminello,[‡] Z. Hussain,[§] X.S. Zhang,[¶] T. Hayashi,[**] and D.A. Shirley

The surface structure of (2×1)S/Ge(001) was determined using ARPEFS in the normal-emission

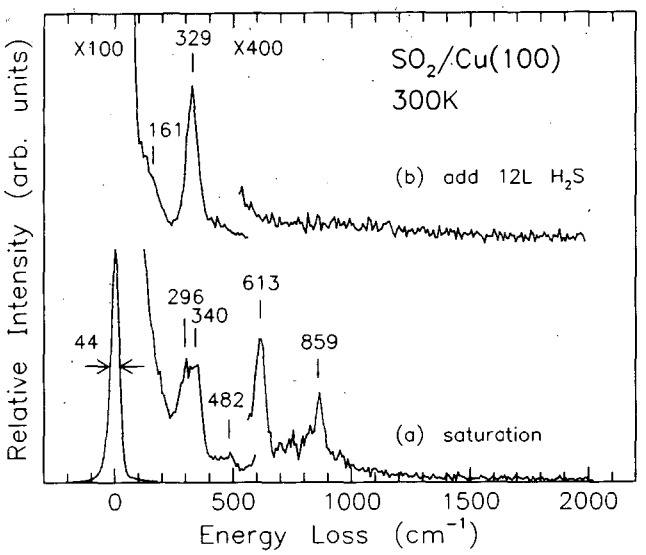

Figure 4-1. Electron-energy-loss spectra of a saturation coverage of SO_2 on Cu(100) at 300 K before (a) and after (b) exposing an additional 12 L of H_2S. (XBL 8811-3936)

direction. By comparing the experimental data with curved-wave, multiple-scattering calculations, quantitative information about the local-adsorption geometry was obtained. In particular, adsorption in a twofold bridge site, with a S-Ge bond length of 2.36 ± 0.05 Å, was found. The twofold S bridge appears most likely to occur between two partially intact symmetric Ge-Ge dimers, with the Ge dimer laterally displaced by 0.10 ± 0.05 Å from the bulk position. This result therefore provides evidence for S bonding to strong dangling bonds in the original dimers of the clean Ge(001) surface (see Figure 5-1). There is, however, no evidence of significant surface

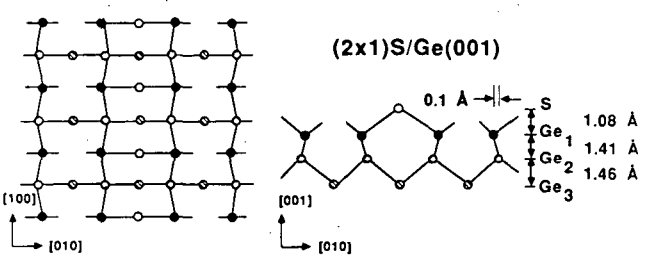

Figure 5-1. Surface bonding geometry of (2×1)S/Ge(001) determined by ARPEFS. Note that the result does not give information about the planarity of the Ge layers. Therefore only interlayer distances and the lateral displacement from the bulk position are indicated and are rounded off to the nearest 0.01 Å. (XBL 8812-4080)

contraction or expansion in the substrate layers, in contrast to the (2×2)S/Ge(111) case.

[†]Present address: Department of Chemistry, University of Waterloo, Waterloo, Ontario N2L 3G1.

[‡]Present address: IBM T.J. Watson Research Center, Yorktown Heights, NY 10598.

[§]Permanent address: Department of Physics, University of Petroleum and Minerals, Dhahran, Saudi Arabia.

[¶]Permanent address: Department of Physics, Zhejiang University, Hangzhou, People's Republic of China.

[**]Permanent address: Material Evaluation Section, NTT Electrical Communications Laboratories, Tokyo 180, Japan.

6. Surface Geometry of (1×1)PH_x/Ge(111) Determined with Angle-Resolved Photoemission Extended Fine Structure (Publication 13)

L.J. Terminello,[†] K.T. Leung,[‡] Z. Hussain,[§] T. Hayashi,[¶] X.S. Zhang,[**] and D.A. Shirley

ARPEFS obtained from the phosphorous 1s core level was studied to determine the chemisorption geometry of (1×1)PH_x/Ge(111), prepared by partial dissociation of PH_3 adsorbed on Ge(111). The most likely composition of the adsorbate dissociation product is PH_2. We determined that the phosphorous adsorbs 2.26 Å above a first-layer germanium atom, and preferentially tilts toward the second-layer germanium atom with a 0.63-Å lateral displacement from a true atop position. Other geometrical parameters determined from the multiple-scattering spherical-wave analysis (see Figure 6-1) of the ARPEFS include the first-to-second-layer germanium Ge(1)-Ge(2) spacing (0.68 Å) and the second-to-third-layer germanium Ge(2)-Ge(3) spacing (2.68 Å). This represents a 17% contraction for Ge(1)-Ge(2) and a 9% expansion for Ge(2)-Ge(3) (see Figure 6-2). The importance of adsorbate scattering and how it affects data interpretation is also discussed. Comparison of this chemisorption system with other systems is made.

[†]Present address: IBM T.J. Watson Research Center, Yorktown Heights, NY 10598.

[‡]Present address: Department of Chemistry, University of Waterloo, Waterloo, Ontario N2L 3G1.

[§]Permanent address: Department of Physics, University of Petroleum & Minerals, Dhahran, Saudi Arabia.

[¶]Permanent address: Material Evaluation Section, NTT Electrical Communications Laboratories, Tokyo 180, Japan.

[**]Permanent address: Department of Physics, Zhejiang University, Hangzhou, People's Republic of China.

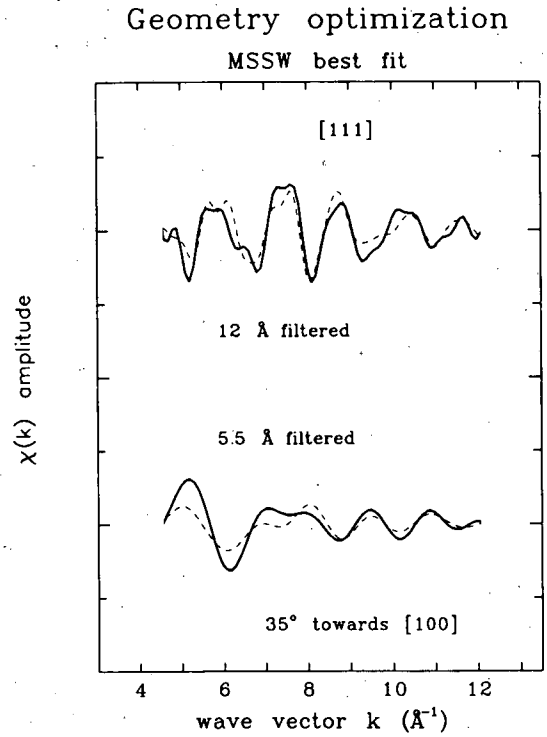

Figure 6-1. Fourier-filtered experimental data (solid lines) shown with the best-fit multiple-scattering spherical-wave calculation (dashed lines). (XBL 8812-4145)

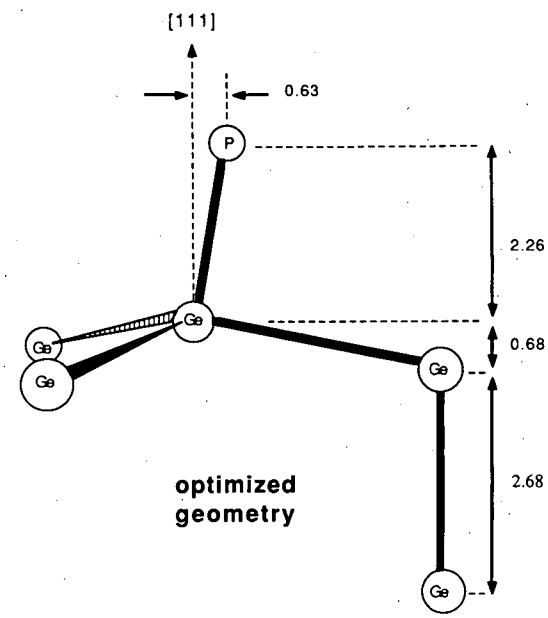

Figure 6-2. Local adsorption geometry, including the reconstructed Ge(111) surface and the tilted atop site (not drawn to scale). (XBL 8812-4146)

1988 PUBLICATIONS AND REPORTS

Refereed Journals

1. D.A. Shirley, U. Becker, P.A. Heimann, and B. Langer, "Near Threshold Behavior of Photoelectron Satellite Intensities," J. de Phys., Colloque C9, Supplement 12, 427 (1987); LBL-23989.
2. U. Becker, B. Langer, H.G. Kerkhoff, M. Kupsch, D. Szostak, R. Wehlitz, P.A. Heimann, S.H. Liu, D.W. Lindle, T.A. Ferrett, and D.A. Shirley, "Observation of Many New Argon Valence Satellites Near Threshold," Phys. Rev. Lett. **60**, 1490 (1988); LBL-22464.
3. D.W. Lindle, T.A. Ferrett, P.A. Heimann, and D.A. Shirley, "Photoemission from Xe in the Vicinity of the 4d Cooper Minimum," Phys. Rev. A **37**, 3808 (1988); LBL-22028.
4. L. Wang, J.E. Reutt, Y.T. Lee, and D.A. Shirley, "High Resolution UV Photoelectron Spectroscopy of CO_2^+, COS^+ and CS_2^+ Using Supersonic Molecular Beams," J. Electron Spectrosc. Rel. Phenom. **47**, 167 (1988); LBL-23936.
5. T.A. Ferrett, M.N. Piancastelli, D.W. Lindle, P.A. Heimann, and D.A. Shirley, "Si 2p and 2s Resonant Excitation and Photoionization in SiF_4," Phys. Rev. A **38**, 701 (1988); LBL-20742.
6. L.J. Terminello, X.S. Zhang, Z.Q. Huang, S. Kim, A.E. Schach von Wittenau, K.T. Leung, and D.A. Shirley, "c(2×2)S/Cr(001) Surface and Near-Surface Structure Determined using Angle-Resolved Photoemission Extended Fine Structure," Phys. Rev. B **38**, 3879 (1988); LBL-24247.
7. D.W. Lindle, L.J. Medhurst, T.A. Ferrett, P.A. Heimann, M.N. Piancastelli, S.H. Liu, D.A. Shirley, T.A. Carlson, P.C. Deshmukh, G. Nasreen, and S.T. Manson, "Angle-Resolved Photoemission from the Ar 2p Subshell," Phys. Rev. A **38**, 2371 (1988); LBL-24858.
8. T.A. Ferrett, D.W. Lindle, P.A. Heimann, M.N. Piancastelli, P.H. Kobrin, H.G. Kerkhoff, U. Becker, W.D. Brewer, and D.A. Shirley, "Shape-Resonant and Many-Electron Effects in the S 2p Photoionization of SF_6," J. Chem. Phys. **89**, 4726 (1988); LBL-18829.
9. K.T. Leung, L.J. Terminello, Z. Hussain, X.S. Zhang, T. Hayashi, and D.A. Shirley, "Surface Bonding Geometry of (2×1)S/Ge(001) by Normal Emission ARPEFS," Phys. Rev. B **38**, 8241 (1988); LBL-24616.
10. L.J. Medhurst, T.A. Ferrett, P.A. Heimann, D.W. Lindle, S.H. Liu, and D.A. Shirley, "Observation of Correlation Effects in Zero Kinetic Energy Electron Spectra Near the N1s and C1s Thresholds in N_2, CO, C_6H_6 and C_2H_4," J. Chem. Phys. **89**, 6096 (1988); LBL-25263.
11. X.S. Zhang, L.J. Terminello, S. Kim, Z.Q. Huang, A.E. Schach von Wittenau, and D.A. Shirley, "Chemisorption Structure of c(2×2)S/Fe(001) Determined by Angle-Resolved Photoemission Extended Fine Structure," J. Chem. Phys. **89**, 6538 (1988); LBL-24248.

LBL Reports

12. K.T. Leung, X.S. Zhang, and D.A. Shirley, "Adsorption and Surface Reactions of H_2S and SO_2 on Cu(100) Studied by Electron Energy Loss Spectroscopy," LBL-25552.
13. L.J. Terminello, K.T. Leung, Z. Hussain, T. Hayashi, X.S. Zhang, and D.A. Shirley, "Surface Geometry of (1×1) PH_x/Ge(111) Determined with Angle-Resolved Photoemission Extended Fine Structure," LBL-26151.
14. M.N. Piancastelli, T.A. Ferrett, D.W. Lindle, L.J. Medhurst, P.A. Heimann, S.H. Liu, and D.A. Shirley, "Resonant Processes Above the Carbon 1s Ionization Threshold in Benzene and Ethylene," LBL-22548.
15. L.J. Terminello (Ph.D. Thesis), "Surface Structures Determined Using Electron Diffraction," LBL-26300.

Invited Talks

16. D.A. Shirley, "Surface Structures Photoelectron Diffraction," Case Western Reserve University, Cleveland, OH, Dec. 1, 1988.
17. D.A. Shirley, "Selected Topics in High Energy Chemical Physics," Physics Colloquium, University of California, Santa Cruz, Nov. 3, 1988.

Crossed Molecular Beams*

Yuan T. Lee, Investigator

INTRODUCTION

The major thrust of this research project is to elucidate the details of the dynamics of simple elementary reactions that are theoretically important and to unravel the mechanism of complex chemical reactions or photochemical processes that play important roles in many macroscopic processes. Molecular beams of reactants are used to study individual reactive encounters between molecules or to monitor photodissociation events in a collision-free environment. Most of the information is derived from measurement of the product fragment energy and angular distributions. Recent activities are centered on the mechanisms of elementary chemical reactions involving oxygen atoms with unsaturated hydrocarbons, the dynamics of endothermic substitution reactions, the dependence of the chemical reactivity of electronically excited atoms on the alignment of excited orbitals, the primary photochemical processes of polyatomic molecules, intramolecular energy transfer of chemically activated and locally excited molecules, the energetics of free radicals that are important to combustion processes, the infrared-absorption spectra of carbonium ions and hydrated hydronium ions, and bond-selective photodissociation through electric excitation.

1. High-Resolution Photoionization Spectrum of Water Molecules in a Supersonic Beam (Publication 5)

R.H. Page, R.J. Larkin, Y.R. Shen, and Y.T. Lee

We have obtained high-resolution ($\sim$1.5 cm^{-1}) photoionization spectra of supersonically cooled (T_{rot} $\sim$50 K) H_2O and D_2O in the 1000–900 Å range. The light source, generated by frequency tripling in a pulsed free jet of gas, is described briefly. Spectra are rotationally resolved. Vibrationally excited autoionizing Rydberg series converging to the ground electronic state $[\tilde{X}; (1b_1)^{-1}]$ of the molecular ion are detected. This may well be the first example of a highly resolved Rydberg spectrum of a stable polyatomic molecule. From the convergence limit, the ionization potential H_2O is determined to be 101, 777 $\pm$ 7 cm^{-1}. Intensities of the Rydberg-state autoionization signals are smaller than predicted using known Franck-Condon factors, indicating that predissociation is a competitive decay channel. Rydberg-state lifetimes are $\sim$1 psec, deduced from homogeneous linewidths. Autoionizing features from Rydberg states associated with the ion's quasilinear $\tilde{A}$ $(3a_1)^{-1}$ state are observed with linewidths greater than 10 cm^{-1}, indicating that their lifetimes are less than $\sim$0.5 psec. Rotational assignments of some of the bands in this linear $\leftarrow$ bent transition show that the Rydberg- and ionic-state geometries are nearly identical. A consistent assignment of the controversial bending (v_2) quantum number and Rydberg-series quantum defect $\delta = -0.037$ have been provided.

2. Tunable Far-Infrared Laser Spectroscopy of van der Waals Bonds: Extended Measurements on the Lowest Σ Bend of ArHCl (Publication 9)

K.L. Busarow, G.A. Blake, K.B. Laughlin, R.C. Cohen, Y.T. Lee, and R.J. Saykally

A tunable far-infrared laser system has been used to measure the vibration-rotation spectrum of the lowest Σ bending state of ArHCl near 24 cm^{-1} in a continuous-wave planar jet operating with a terminal-jet temperature near 3 K. Over 60 transitions have been observed for both ^{35}Cl and ^{37}Cl isotopes with resolution of the quadrupole hyperfine structure. An improved set of molecular parameters was determined, including B, D, H, and eqQ for both upper and lower states. Very narrow linewidths (approximately 300 kHz) resulting in high resolution and sensitivity make this technique a powerful new method for the detailed investigation of intermolecular forces.

*This work was supported by the Director, Office of Energy Research, Office of Basic Energy Sciences, Chemical Sciences Division, of the U.S. Department of Energy under Contract No. DE-AC03-76SF00098.

3. Symmetric Stretch Excitation of CH_3 in the 193.3-nm Photolysis of CH_3I (Publication 11)

R.E. Continetti, B.A. Balko, and Y.T. Lee

New high-resolution photofragment translational-spectroscopy measurements on the 193.3-nm photolysis of CH_3I reveal up to four quanta of v_1 C-H symmetric stretch excitation in the C-I bond-fission channel. In addition, these experiments show for the first time that C-H bond fission occurs at wavelengths longer than 185 nm with a quantum yield of ~3%. The data yield upper bounds to the C-H bond-dissociation energy in CH_3I of 101 ± 1 kcal/mol and, for the C-I bond-dissociation energy, 55.0 ± 0.3 kcal/mol.

4. The Reactions of Ground- and Excited-State Sodium Atoms with Hydrogen Halide Molecules (Publication 12)

P.S. Weiss, J.M. Mestdagh, M.H. Covinsky, B.A. Balko, and Y.T. Lee

The reactions of ground- and excited-state Na atoms with hydrogen halide (HX) molecules have been studied using the crossed-molecular-beams method. With both increasing translational and increasing electronic energy, the reactive cross sections increase in the reactions of HCl and HBr. From product angular and velocity distributions, detailed center-of-mass information is derived. For the reactions of Na($3\,^2S_{1/2}$, $3\,^2P_{1/2}$, $4\,^2D_{5/2}$, $5\,^2S_{1/2}$) with HCl, the product NaCl is backscattered with respect to the incoming Na atom in the center-of-mass frame of reference. The reaction of each Na state studied with HCl is direct and proceeds via collinear and near-collinear Na-Cl-H approach geometries. For the Na($3\,^2P_{3/2}$) and Na($4\,^2D_{5/2}$) reactions with HCl, the predominant transition-state symmetry is $^2\Sigma$ in a collinear (C_{xv}) Na-Cl-H geometry. This is consistent with the reaction proceeding via electron transfer from the Na atom to the halide atom. Absolute reactive cross sections for each state of Na studied with HCl were determined by comparison with both small- and large-angle elastic scattering. We were unable to observe Na atoms with over 4 eV of electronic energy react with HF up to collision energies of 13 kcal/mol.

5. Tunable Far-Infrared Laser Spectroscopy of van der Waals Bonds: Vibration-Rotation-Tunneling Spectra of Ar-H_2O (Publication 13)

R.C. Cohen, K.L. Busarow, K.B. Laughlin, G.A. Blake, M. Havenith, Y.T. Lee, and R.J. Saykally

The first high-resolution spectra of a rare gas–H_2O cluster have been observed using a tunable far-infrared laser to probe the vibration-rotation-tunneling levels of Ar-H_2O formed in a continuous planar supersonic jet. The high sensitivity of this spectrometer facilitated extensive measurements of two perpendicular subbands assigned to transitions from the ground state to the upper component of a hydrogen-exchange tunneling doublet (c-type) at 21 cm^{-1}, and $\nu_{b1} = 1^+$ (b-type) at 25 cm^{-1}, the lower tunneling component of a bending vibration that is perpendicular to the tunneling coordinate. The tunneling splitting is shown to be in the range 2.5–7 cm^{-1}, and the lower tunneling component of the excited bending vibration lies between 39 and 43 cm^{-1} above the ground state of the complex. The experimentally determined center-of-mass separation ($R_{c.m.}$ = 3.75 Å) and harmonic-stretching force constant (k_s = 0.0134 mdyn/Å) are compared to those of related first- and second-row hydrides. The large-amplitude motions occurring within this complex make it difficult to establish its structure.

6. Dynamics of Endoergic Substitution Reactions: I. Br + Chlorinated Aromatic Compounds (Publication 14)

G.N. Robinson, R.E. Continetti, and Y.T. Lee

The endoergic substitution reactions Br + R-Cl → Cl + R-Br (R = o-, m-, and p-$CH_3C_6H_4$, C_6H_5, C_6F_5; $\Delta H^\circ \simeq 15$ kcal/mol) have been studied using the crossed-molecular-beams method in the collision energy (E_c) range 20–35 kcal/mol. The $CH_3C_6H_4Br$ and C_6F_5Br products were found to be mostly forward scattered with respect to the incident Br beam, indicating that the lifetimes of the Br-R-Cl collision complexes are short compared to their rotational periods. The product translational-energy distributions and excitation functions for these reactions are well reproduced by statistical calculations that

assume only a few vibrational modes in the collision complexes participate in intramolecular energy redistribution prior to Cl elimination. Ring substituents are found to affect both the extent of energy redistribution in the complexes and the probability of Br addition. For example, no substitution product was observed with m-$CH_3C_6H_4Cl$ or C_6H_5Cl. The relative magnitudes of the cross sections are explained in terms of possible features of the potential-energy surfaces along their reaction coordinates.

7. Dynamics of Endoergic Substitution Reactions. II: Br + $\{CH_2CCl_2\}$ → Cl + $\{CH_2CClBr\}$ (Publication 15)

G.N. Robinson, R.E. Continetti, and Y.T. Lee

We have extended the crossed-beams studies described in abstract 6 to the reactions of Br atoms with 1,1- and trans-dichloroethylene. The slopes of the product translational-energy distributions and excitation functions for both reactions support our previous conclusion that Cl elimination from Br-R-Cl collision complexes can compete with Br elimination only in the limit that few vibrational modes of the complex are active in energy redistribution. The substitution cross section for the Br + CH_2CCl_2 reaction is considerably lower than that for the Br + trans-CHClCHCl reaction in the collision-energy range 15–25 kcal/mol, suggesting that steric effects play a dominant role in determining the relative magnitudes of the cross sections.

8. Crossed-Molecular-Beam Studies of the Reactions of Methyl Radicals with Iodoalkanes (Publication 17)

G.N. Robinson, G.A. Nathanson, R.E. Continetti, and Y.T. Lee

The I-atom exchange reactions, $CH_3 RI \rightarrow CH_3I + R$ [R = CF_3, $(CH_3)_3C$], were investigated at a collision energy of ≈13 kcal/mol using the crossed-molecular-beams technique. The supersonic beam of methyl radicals was formed by pyrolyzing a mixture of ≈1% di-tert-butyl peroxide in helium in a quartz nozzle. A large fraction of the total energy available to the products from these reactions is channeled into relative translation [≈50% for R = $(CH_3)_3C$ and ≈70% for R = CF_3], suggesting that the dominant interaction among the products is repulsive. The CH_3I product from both reactions was observed to be entirely backward scattered with respect to the incident radical beam, indicating that a roughly collinear C-I-C transition-state geometry is favored. The present results are compared to those of earlier crossed-beam studies of the $CH_3 + IY \rightarrow CH_3I + Y$(Y = Cl, Br, I) reactions; the differences observed among these reactions are explained with reference to the CH_3I-Y and CH_3I-R interaction potentials.

9. Polarization Effects in Reactive Scattering of Na Atoms in the 4D Level (Publication 18)

P.S. Weiss, M.H. Covinsky, H. Schmidt, B.A. Balko, Y.T. Lee, and J.M. Mestdagh

Experiments performed using a crossed-beam apparatus have shown that the reactivity of Na(4D) with HCl and O_2 changes substantially as the 4d orbital alignment is varied. This change is different for the two reactions. The favorable alignment for the reaction with HCl has the d orbital aligned along the relative-velocity vector of the reactants. This result is consistent with a long-range electron transfer initiating the reaction and suggests that the Na-Cl axis dominates over the H-Cl axis in determining the favorable atomic orbital alignment. For the reaction with O_2, the NaO formation has a high translational-energy threshold, and the favored orbital alignment varies as a function of the NaO laboratory scattering angle. Very restricted conditions are found to be necessary for the reaction: near-collinear geometry and the d orbital perpendicular to the molecular axis.

10. Ultrahigh-Resolution (1 + 1) Photoionization Spectroscopy of KrI: Hyperfine Structures, Isotope Shifts, and Lifetimes for the n = 5,6,7 $4p^5ns$ Rydberg Levels (Publication 22)

T. Trickl, M.J.J. Vrakking, E. Cromwell, Y.T. Lee, and A.H. Kung

High-resolution measurements of the hyperfine structures and isotope shifts are reported for KrI n = 5,6,7 $4p^5ns$ Rydberg levels, obtained using a soft x-ray and extreme ultraviolet (XUV) laser with a bandwidth of 210 MHz in a resonant two-photon-ionization scheme. Use of known I_2 frequencies yields an improved absolute calibration of the Kr

energy levels by more than one order of magnitude. The nuclear-quadrupole hyperfine structure indicates that the $4p^5 6s$ and $4p^5 7s$ states are described by a pure jj-coupling scheme, whereas the $4p^5 5s$ states depart from a pure jj-coupling scheme by 0.37(6) %. The magnetic hyperfine structure shows that the $4p^5 ns$ states are mixed with $4p^5 n'd$ states. The isotope shifts can be described as pure mass effects within the precision of our experiment. For the $4p^5 6s$ and $4p^5 7s$ states, lifetimes were determined that differ markedly from theoretical literature values.

11. Ultranarrow-Bandwidth Vacuum Ultraviolet (VUV)-XUV Laser System (Publications 19 and 23)

E. Cromwell, T. Trickl, Y.T. Lee, and A.H. Kung

An ultrahigh-brightness laser system has been developed to study the spectroscopy and dynamics of molecules and clusters in the VUV-XUV spectral region. The laser utilizes pulse amplification of a single-mode ring dye laser, frequency doubling, and four-wave mixing in a pulsed jet. Pulse energies of >100 mJ in the visible and $>10^{11}$ photons/pulse in the VUV-XUV have been obtained. The bandwidth of the laser has been measured to be 91 MHz in the visible and 210 MHz in the XUV.

12. Dissociation of Cyclohexene and 1,4-cyclohexadiene in a Molecular Beam (Publication 24)

X. Zhao, R.E. Continetti, A. Yokoyama, E.J. Hintsa, and Y.T. Lee

Molecular-beam photofragmentation translational spectroscopy of cyclohexene and 1,4-cyclohexadiene was carried out using 193-nm and IR multiphoton excitation. At 193 nm, both the retro-Diels-Alder reaction of cyclohexene and H_2 elimination from both molecules were observed in the ground electronic state, indicating the occurrence of internal conversion of the electronically excited states. The retro-Diels-Alder reaction is shown to be concerted up to an internal energy higher than 148 kcal/mol. H-atom elimination was also observed for both molecules following 193-nm excitation. The H atom is eliminated from an excited state of cyclohexene and is assigned to be from a carbon next to the double bond with a corresponding C-H bond energy of 87 ± 3 kcal/mol. It is shown that the peak of the translational-energy distribution for concerted dissociation in the ground state is determined mainly by the dynamics of the potential-energy release along the reaction coordinate and is not sensitive to either the amount of internal energy or the form of excitation.

13. Work in Progress

Upon the completion of the investigation of the dynamics of $D + H_2 \rightarrow DH + H$ reaction, a series of substitution reactions of D atoms and unsaturated hydrocarbons will be carried out. Among the first reactions to be investigated are $D + C_2H_2 \rightarrow C_2HD + H$ and the possible ring-opening reaction of benzene induced by the addition of energetic D atoms. The reactions of electronically excited Ba atoms and transition-metal atoms with oxygen-containing molecules are also under preparation.

The production and dissociation of polyatomic radicals will be one of our major themes. Of particular interest is the $\cdot CH_2CH_2OH$ radical, which is the intermediate of $C_2H_4 + OH$ product reaction and can be produced from the photodissociation of $Br\cdot CH_2CH_2OH$ using 193-nm photons. Secondary dissociation of vibrationally excited $\cdot CH_2CH_2OH$ radicals will be investigated using molecular-beam photofragmentation translational spectroscopy. The other important area that will be intensely investigated is the systematic survey of the dynamics and mechanisms of primary dissociation processes of unsaturated hydrocarbons.

The solvation of NH_4^+ and H_3O^+ by NH_3 and H_2O will be investigated through the measurements of infrared absorption spectra. The investigation will cover the first and second solvation shells and will then move on to solvated metal ions such as $Na^+(H_2O)_n$.

1988 PUBLICATIONS AND REPORTS

Refereed Journals

1. R.H. Page, M.F. Vernon, Y.R. Shen, and Y.T. Lee, "Infrared Vibrational Predissociation Spectra of Large Water Clusters," Chem. Phys. Lett. **141**, 1 (1987); **144**, 104 (1988); LBL-24006.
2. G.N. Robinson, R.E. Continetti, and Y.T. Lee, "Dynamics of Endoergic Aromatic Substitution Reactions," Faraday Discuss. Chem. Soc. **84**, 25 (1987); LBL-23701.

3. J.M. Mestdagh, B.A. Balko, M.H. Covinsky, P.S. Weiss, M.F. Vernon, H. Schmidt, and Y.T. Lee, "Reactive Scattering of Electronically Excited Alkali Atoms with Molecules," Faraday Discuss. Chem. Soc. **84**, 145 (1987); LBL-23588.
4. M. Okumura, L.I. Yeh, and Y.T. Lee, "Infrared Spectroscopy of the Cluster Ions $H_3^+ \cdot (H_2)_n$," J. Chem. Phys. **88**, 79 (1988); LBL-23995.
5. R.H. Page, R.J. Larkin, Y.R. Shen, and Y.T. Lee, "High-Resolution Photoionization Spectrum of Water Molecules in a Supersonic Beam," J. Chem. Phys. **88**, 2249 (1988); LBL-24158.
6. R.H. Page, Y.R. Shen, and Y.T. Lee, "Local Modes of Benzene and Benzene Dimer; Studied by Infrared-Ultraviolet Double Resonance in a Supersonic Beam," J. Chem. Phys. **88**, 4621 (1988); LBL-24007.
7. R.H. Page, Y.R. Shen, and Y.T. Lee, "Infrared-Ultraviolet Double Resonance Studies of Benzene Molecules in a Supersonic Beam," J. Chem. Phys. **88**, 5362 (1988); LBL-23769.
8. J.R. Grover, Y. Wen, Y.T. Lee, and K. Shobatake, "Crossed-beam Reactive Scattering of $F_2 + C_6H_6$: Heat of Formation of Ipso-fluorocyclohexadienyl Radical," J. Chem. Phys. **89**, 938 (1988).
9. K.L. Busarow, G.A. Blake, K.B. Laughlin, R.C. Cohen, Y.T. Lee, and R.J. Saykally, "Tunable Far Infrared Laser Spectroscopy of Van der Waals Bonds: Extended Measurements on the Lowest Σ Bend of ArHCl," J. Chem. Phys. **89**, 1268 (1988); LBL-24859.
10. L. Wang, J.E. Reutt, Y.T. Lee, and D.A. Shirley, "High Resolution UV Photoelectron Spectroscopy of CO_2^+, COS^+, and CS_2^+ Using Supersonic Molecular Beams," J. Electron Spectrosc. **47**, 167 (1988); LBL-23936.
11. R.E. Continetti, B.A. Balko, and Y.T. Lee, "Symmetric Stretch Excitation of CH_3 in the 193.3 nm Photolysis of CH_3I," J. Chem. Phys. **89**, 3383 (1988); LBL-25355.
12. P.S. Weiss, J.M. Mestdagh, M.H. Covinsky, B.A. Balko, and Y.T. Lee, "The Reactions of Ground and Excited State Sodium Atoms with Hydrogen Halide Molecules," Chem. Phys. **126**, 93 (1988); LBL-25529.
13. R.C. Cohen, K.L. Busarow, K.B. Laughlin, G.A. Blake, M. Havenith, Y.T. Lee, and R.J. Saykally, "Tunable Far Infrared Laser Spectroscopy of van der Waals Bonds: Vibration-Rotation-Tunneling Spectra of Ar-H_2O," J. Chem. Phys. **89**, 4494 (1988); LBL-25399.
14. G.N. Robinson, R.E. Continetti, and Y.T. Lee, "Dynamics of Endoergic Substitution Reactions. I. Br + Chlorinated Aromatic Compounds," J. Chem. Phys. **89**, 6226 (1988); LBL-25530.
15. G.N. Robinson, R.E. Continetti, and Y.T. Lee, "Dynamics of Endoergic Substitution Reactions. II. $Br + (CH_2CCl_2) \rightarrow Cl + (CH_2CClBr)$," J. Chem. Phys. **89**, 6238 (1988); LBL-25531.
16. G. Blake, K.L. Busarow, R. Cohen, K. Laughlin, Y.T. Lee, and R.J. Saykally, "Tunable Far Infrared Laser Spectroscopy of van der Waals Bonds: Vibration-Rotation Tunneling Spectra of $(HCl)_2$," J. Chem. Phys. **89**, 6577 (1988); LBL-25400.
17. G.N. Robinson, G.M. Nathanson, R.E. Continetti, and Y.T. Lee, "Crossed Molecular Beam Studies of the Reactions of Methyl Radicals with Iodoalkanes," J. Chem. Phys. **89**, 6744 (1988); LBL-25553.
18. P.S. Weiss, M.H. Covinsky, H. Schmidt, B.A. Balko, Y.T. Lee, and J.M. Mestdagh, "Polarization Effects in Reactive Scattering of Na Atoms in the 4D Level," Zeitschrift für Physik D **10**, 227 (1988); LBL-25321.

Other Publications

19. E. Cromwell, A.H. Kung, T. Trickl, and Y.T. Lee, "XUV Source for Ultra-High Resolution Spectroscopy," SPIE O-E/LASE '88, Los Angles, CA, Jan. 10–17, 1988; LBL-24636.
20. L.I. Yeh, M. Okumura, J.D. Myers, and Y.T. Lee, "Vibrational Spectroscopy of Cluster Ions: Two Novel Methods," Workshop on Molecular and Cluster Beam Science, National Research Council, 57–66, 1988; LBL-23842.

LBL Reports

21. Y.T. Lee, "Reactive Scattering: Non-Optical Methods," in *Atomic and Molecular Beams Method*, G. Scoles and U. Buck, eds., Oxford University Press, 1988 (in press); LBL-20767.
22. T. Trickl, M.J.J. Vrakking, E. Cromwell, Y.T. Lee, and A.H. Kung, "Ultrahigh-Resolution (1 + 1) Photoionization Spectroscopy of KrI: Hyperfine Structures, Isotope Shifts and Lifetimes for the n = 5,6,7 $4p^5ns$ Rydberg States," submitted to Phys. Rev. A; LBL-25787.
23. E. Cromwell, T. Trickl, Y.T. Lee, and A.H. Kung, "Ultra-Narrow Bandwidth VUV-XUV Laser System," submitted to Rev. Sci. Instrum.; LBL-26041.
24. X. Zhao, R.E. Continetti, A. Yokoyama, E.J. Hintsa, and Y.T. Lee, "Dissociation of Cyclohexene and 1,4-Cyclohexadiene in a Molecular Beam," submitted to J. Chem. Phys.; LBL-26333.
25. G.N. Robinson (Ph.D. Thesis), "Crossed Molecular Beam Studies of Substitution and Exchange Reactions," LBL-24635.
26. L.I. Yeh (Ph.D. Thesis), "Infrared Spectroscopy of Weakly Bound Molecular Ions," LBL-26331.
27. X. Zhao (Ph.D. Thesis), "Photodissociation of Cyclic Compounds in a Molecular Beam," LBL-26332.

Invited Talks

28. Y.T. Lee, "Reaction of Electronically Excited Atoms," Memorial Symposium on the 100th Birthday of Otto Stern, University of Hamburg, Federal Republic of Germany, Feb. 4, 1988.

29. Y.T. Lee, "New Approach for IR Absorption Spectroscopy of Ionic Clusters," USA-USSR Linear and Non-Linear Laser Workshop, University of California, Santa Barbara, Mar. 3, 1988.
30. Y.T. Lee, "Elementary Chemical Reactions Involved in Combustion," University of Gothenburg, Sweden, Mar. 21, 1988.
31. Y.T. Lee, "Molecular Beam Studies of Chemical Reaction Dynamics," Department of Chemistry, University of Florida, Gainesville, Mar. 28, 1988.
32. Y.T. Lee, "Application of Molecular Beam and Laser Techniques in the Investigation of Spectroscopy and Photochemistry," Department of Chemistry, University of Florida, Gainesville, Mar. 30, 1988.
33. Y.T. Lee, "Crossed Molecular Beam Studies on Elementary Chemical Reactions," Mack Memorial Award Lecture, Department of Chemistry, Ohio State University, Columbus, Mar. 31, 1988.
34. Y.T. Lee, "Bond Selective Photodissociation Through Electronic Transitions," Department of Chemistry, Ohio State University, Columbus, Apr. 1, 1988.
35. Y.T. Lee, "Molecular Beam Studies on Atomic and Molecular Processes," Department of Physics, University of California, Berkeley, Apr. 13, 1988.
36. Y.T. Lee, "Molecular Beam Studies of Elementary Chemical Reactions," IBM Research Laboratory, San Jose, CA, Apr. 15, 1988.
37. Y.T. Lee, "Molecular Collisions and Dynamics of Elementary Chemical Reactions," Department of Chemistry, Nanjing University, People's Republic of China, May 16–20, 1988.
38. Y.T. Lee, "Endothermic Substitution Reactions of Aromatic Hydrocarbons," 2nd National Conference on Chemical Kinetics, Beijing, People's Republic of China, May 23, 1988.
39. Y.T. Lee, "Elementary Chemical Reactions Involved in Combustion Chemistry," DOE Combustion Contractor's Meeting, Lake Geneva, WI, June 3, 1988.
40. Y.T. Lee, "Molecular Beam Studies of Hot Atom Chemical Reactions," 3rd Chemical Congress of North America, Toronto, Ontario, June 7, 1988.
41. Y.T. Lee, "A New Approach for High Resolution Vibrational Spectroscopy on Solvated Ionic Species in the Gas Phase," 43rd Molecular Spectroscopy Symposium, Ohio State University, Columbus, June 15, 1988.
42. Y.T. Lee, "Chemistry in the Modern Society," University of Metropolitana, Caracas, Venezuela, June 27, 1988.
43. Y.T. Lee, "Application of Molecular Beam Techniques in the Investigation of Elementary Chemical Reactions," 1st Venezuela National Congress of Chemical Industry, Caracas, Venezuela, June 28, 1988.
44. Y.T. Lee, "Substitution Reactions of Br Atoms with o-, m-, and p-chlorotoluene," Institute of Atomic and Molecular Sciences, Taipei, Republic of China, July 8, 1988.
45. Y.T. Lee, "Recent Advances in Chemical Reaction Dynamics," Department of Chemistry, University of Hong Kong, July 11, 1988.
46. Y.T. Lee, "Infrared Absorption Spectroscopy of Hydrated Hydronium Ions," Department of Chemistry, University of Hong Kong, July 13, 1988.
47. Y.T. Lee, "Molecular Beam Chemistry," Naval Research Laboratory, Washington, DC, Aug. 5, 1988.
48. Y.T. Lee, "Unimolecular Decomposition of Benzene," Thermochemistry and Kinetics, Current Directions Symposium, University of Southern California, Los Angeles, Sept. 22, 1988.
49. Y.T. Lee, "Molecular Beam Chemical Kinetics," Department of Chemistry, Xiamen University, Xiamen, People's Republic of China, Oct. 12, 1988.
50. Y.T. Lee, "Investigation of Laser Induced Chemical Processes by the Molecular Beam Technique," Institute for the Structure of Matter, Chinese Academy of Sciences, Fuzou, People's Republic of China, Oct. 14, 1988.
51. Y.T. Lee, "Primary Photochemical Processes by Lasers and Molecular Beams," Department of Chemistry, University of Singapore, Oct. 21, 1988.
52. Y.T. Lee, "New Spectroscopy Method for the Investigation of Solvated Hydronium and Ammonium Ions," Chemistry Department, National University, Singapore, Oct. 21, 1988.
53. Y.T. Lee, "Molecular Collisions, Scientific Research, and Modern Society," Singapore, Oct. 22, 1988.
54. Y.T. Lee, "Molecular Beam Studies on Elementary Chemical Reactions," Haworth Lecture, Department of Chemistry, Brookhaven National Laboratory, Upton, NY, Nov. 15, 1988.
55. Y.T. Lee, "IR Absorption Spectroscopy of Solvated Hydronium Ions," Department of Chemistry, Brookhaven National Laboratory, Upton, NY, Nov. 17, 1988.
56. Y.T. Lee, "Molecular Beam Studies on Primary Photochemical Processes," Department of Physics, Kansas State University, Manhattan, Dec. 1, 1988.
57. Y.T. Lee, "Dynamics of Elementary Chemical Reactions," Cardwell Lecture, Department of Physics and Chemistry, Kansas State University, Manhattan, Dec. 1, 1988.
58. Y.T. Lee, "Molecular Collisions and Chemical Reactions," Ramon Areces Foundation, Madrid, Spain, Dec. 15, 1988.
59. Y.T. Lee, "Crossed Molecular Beams Studies on Elementary Chemical Reactions," University of Salamanca, Spain, Dec. 16, 1988.

ATOMIC PHYSICS

High-Energy Atomic Physics*

Harvey Gould, Investigator

INTRODUCTION

The goal of this program is to understand atomic collisions of relativistic ions and to test quantum electrodynamics (QED) in very high atomic-number atoms. These are new areas of research that involve physics that is not accessible at lower energies or with ions of lower atomic number. This research is conducted at the Lawrence Berkeley Laboratory's Bevalac, the world's only relativistic heavy-ion accelerator. Recent results include the first measurement of electron-impact ionization of highly ionized very heavy ions (U^{88+}, U^{89+}, U^{90+}, and U^{91+}). This measurement was done by channeling relativistic uranium ions through Si single crystals. These and earlier experiments in this program have led to an understanding of relativistic heavy-ion-atom collisions, which in most cases is now more complete than for nonrelativistic collisions. Present activities include a precision (0.1%) measurement of the Lamb shift in uranium. Future experiments will attempt to observe a new capture mechanism — electron capture from the production of electron-positron pairs by the motional Coulomb fields of relativistic nuclei passing within atomic distances of each other.

1. Electron-Impact Ionization of U^{88+} – U^{91+} (Publication 1)

N. Claytor,† B. Feinberg, H. Gould, C.E. Bemis, Jr., J. Gomez del Campo, C.A. Ludemann, and C.R. Vane.

We have made the first measurements of electron-impact ionization cross sections for very highly charged ions. We did this by channeling 407-MeV/nucleon U^{92+}, U^{91+}, U^{90+}, U^{89+}, and U^{88+}(bare uranium through berylliumlike uranium) along the <110> axis of 0.11-mm-thick and 0.37-mm-thick Si single crystals.

For channeled ions, we observe a large reduction in the probability for ionization and a reduction in the probability for electron capture. This is shown in Figure 1-1. We are able to determine the fraction of incident ions that channel and the density of electrons along the path of the ions that channel.

We use these determinations to interpret our ionization data to yield cross sections for electron-impact ionization. Electron-impact cross sections were done for hydrogenlike-berylliumlike uranium

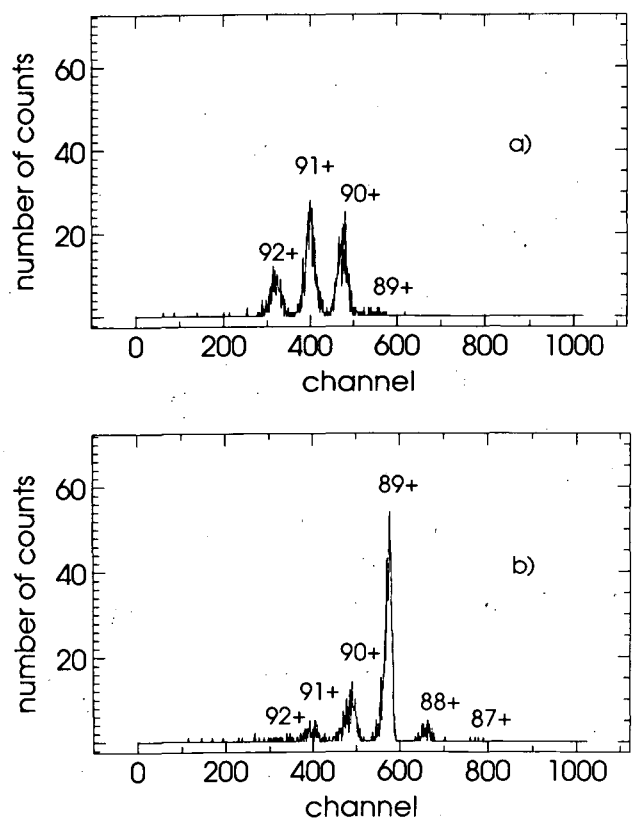

Figure 1-1. Observed charge-state distributions from 405-MeV/nucleon U^{89+} exiting the 0.37-mm-thick Si single crystal. In (a) the ions pass through a random direction of the crystal. In (b) the ions are aligned with the <110> axis of the crystal. Approximately 80% of the ions in (b) have channeled. (XBL 886-2102)

*This work was supported by the Director, Office of Energy Research, Office of Basic Energy Sciences, Chemical Sciences Division, of the U.S. Department of Energy under Contract No. DE-AC03-76SF00098.

by 220-keV electrons (the energy of the electrons seen in the rest frame of the 407-MeV/nucleon uranium). Our cross sections are 3.9, 11.0, 16.0, and 31.0 barns (+100%–50%), respectively, for ionizing 1s, $1s^2$, 2s, and $2s^2$ electrons. Our 1s and $1s^2$ results disagree with present theory. Our 2s and $2s^2$ results are not accurate enough to distinguish between theories.

[†]Present address: Department of Physics, University of Pennsylvania, Philadelphia, PA 19104.

2. Work in Progress

A measurement of the Lamb shift in lithiumlike uranium (U^{89+}) is in progress. The experiment uses a Doppler-tuned spectrometer (DTS) to measure the $2p_{1/2}$–$2s_{1/2}$ transition energy in lithiumlike uranium. The Lamb shift is about 75 eV out of a transition energy of about 280 eV.

A prototype DTS was successfully tested using boron ions at the SuperHILAC. (The n = 2 – n = 1 transition in hydrogenlike Boron is at 255 eV.) Six detectors for the Bevalac DTS were built and tested. The complete Doppler-tuned UV spectrometer, consisting of the six detectors, precision collimating slits, gas-absorber cells, target transporter, alignment apparatus, an electromagnet for suppressing scattered electrons, scintillators for charged-particle vetos (protons from nuclear disintegrations), beam-position detectors, etc., was assembled in a 6-foot-diameter vacuum chamber, tested, and installed in the B40 cave at the Bevalac. Two 10-inch-diameter diffusion pumps were placed on the chamber to maintain vacuum against the diffusion of gas through the 4-μm-thick detector windows. (Very thin windows are necessary to transmit the low-energy x rays.)

1988 PUBLICATIONS AND REPORTS

Refereed Journals

1. N. Claytor, B. Feinberg, H. Gould, C.E. Bemis, Jr., J. Gomez del Campo, C.A. Ludemann, and C.R. Vane, "Electron Impact Ionization of U^{88+}–U^{91+}," Phys. Rev. Lett. **61**, 2081 (1988); LBL-25534.

Other Publications

2. H. Gould, "Electron Impact Ionization of U^{91+}–U^{88+} Measured by Channeling," Spring Meeting, American Physical Society, Baltimore, MD, Apr. 18–21, 1988; Bull. Am. Phys. Soc. **33**, 1008 (1988); LBL-24668abs.
3. N. Claytor, "Channeling of Relativistic Uranium," 8th High Energy Heavy Ion Study, Lawrence Berkeley Laboratory, Berkeley, CA, Nov. 16–20, 1987; in *Proc. 8th High Energy Heavy Ion Study*, J.W. Harris and G.J. Wozniak, eds., 1988, p. 481; LBL-24580.

Invited Talks

4. H. Gould, "Measurement of the Lamb Shift in Heliumlike Uranium," Physics Department Colloquium, University of California, Davis, Feb. 9, 1988.

Atomic Physics*

Michael H. Prior, Investigator

INTRODUCTION

This program conducts experimental studies of atomic structure and collisional interactions in atomic systems or projectile-target combinations that have unique properties. At present, emphasis is on the study of highly charged ions, their energy-level structure, and their behavior in low-energy collisions with atomic targets. Among the broad range of possible research topics, those are selected that are best addressed by the unique facilities and expertise at LBL and that have impact as strong tests of atomic or collision theory. Often, topics studied have relevance to plasma diagnostics in tokamak devices, or to advanced laser technology. Collaborative efforts with investigators from outside LBL form a part of this program activity when they are consistent with research goals. Presently, efforts are under way that yield metastable energy-level structures of highly charged ions, reveal details of multiple electron-transfer processes, and reveal Auger electron and x-ray emission spectra from ion-atom collisions.

1. Double and Single Electron Capture in Slow Collisions of $Ar^{9,8+}$ Ions with He Atoms (Publication 7)

R. Hutton,[†] M.H. Prior, S. Chantrenne,[‡] M.H. Chen[‡] and D. Schneider[‡]

The process of double electron capture in a single collision between a slow, highly charged ion and an atomic target is the subject of a great deal of current interest, both theoretically and experimentally. This interest derives, in part, from the existence of competing processes, namely (i) sequential capture (during a single collision) of two electrons, one at each of two avoided crossings of the relevant molecular-orbital energy levels, and (ii) the process of correlated two-electron capture at a single avoided crossing. Much of the experimental data supporting the concept of correlated double capture have been obtained using He-like projectiles (e.g., O^{6+}). In contrast, this work reports experimental studies with F-like (9-electron) Ar^{9+} ions, which provide evidence of a double-capture process similar to those observed with He-like projectiles.

These experiments were performed using ion beams produced by the LBL electron cyclotron resonance (ECR) ion source and the associated atomic physics beamline facilities. A schematic diagram of the apparatus is shown in Figure 1-1. The method uses the technique of zero-degree (forward direction) electron spectroscopy, incorporating two electron spectrometers in tandem. The first, small, 45° analyzer serves primarily to direct forward-emitted electrons into the high-resolution hemispheric analyzer. The electrons come from the multiply excited projectile states formed by electron capture from He atoms in the gas cell. Pressure in the target cell was monitored by a capacitance manometer and regulated by an automatic leak valve; cell pressures ranged from 0.1 to 1.5 mTorr.

In this work we observed Auger lines using both Ar^{8+} and Ar^{9+} projectiles. Ar^{8+} is a Ne-like ion with a $2p^6\ {}^1S_0$ ground state, and neither single nor double electron capture has much probability, at these collison energies, of producing states with Auger decay channels. However, the Ne-like system has two long-lived metastable levels ($2p^5 3s$, $^3P_{0,2}$) 250 eV above the ground state; because of their long lifetimes, these states, made in the ion source, are present in the beam when it reaches the gas cell. Either one- or two-electron capture onto these metastable core levels can produce Auger-decay electrons. Figure 1-2a shows an Auger spectrum from Ar^{8+} + He collisions; all of the lines shown can be attributed to decay of core-excited Na-like (11-electron) levels formed by single electron capture onto the metastable Ar^{8+} beam component.

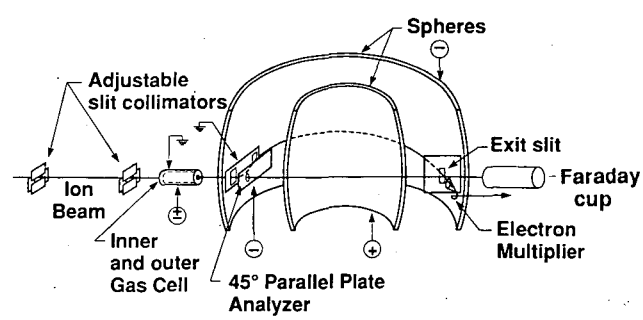

Figure 1-1. Experimental arrangement for zero-degree electron spectroscopy using a collimated beam from the LBL ECR ion source. The beam passes through the gas cell and 45° parallel-plate analyzer into the Faraday cup. Forward-emitted electrons are deflected by the 45° analyzer into the high-resolution hemispherical instrument. (XBL 891-140)

*This work was supported by the Director, Office of Energy Research, Office of Basic Energy Sciences, Chemical Sciences Division, of the U.S. Department of Energy under Contract No. DE-AC03-76SF00098.

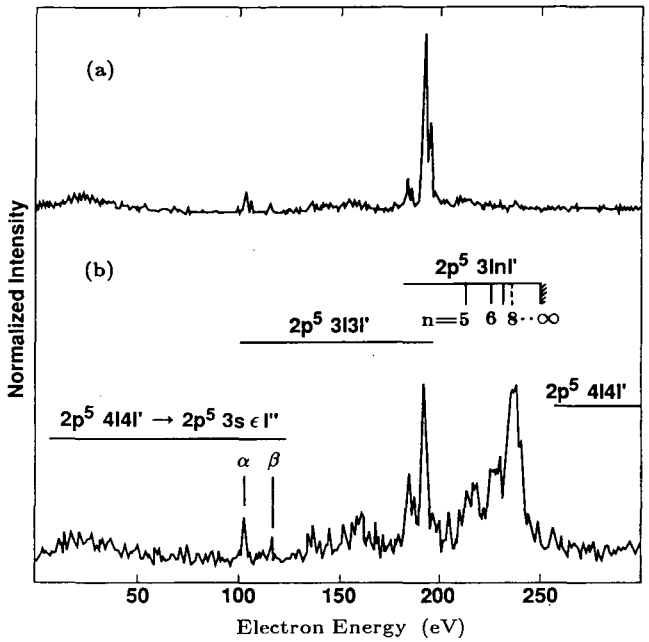

Figure 1-2. Auger electron spectra from (a) 80-keV Ar^{8+} and, (b) 90-keV Ar^{9+} collisions on a He gas target (pressure 0.4 mTorr). Electron energies are given in the projectile frame. The locations of lines (see text), which originate from several initial configurations, are indicated. In all cases the final state is $2p^6\epsilon l$ except for the lower-energy $2p^54l4l'$ group, where the final state is $2p^53s\epsilon l$. The lines labeled α and β are from $2p^53s^2\ ^2P_J$ and $2p^53s3p\ ^4D_J$ states. The latter contains the metastable $^4D_{7/2}$ component. (XBL 891-141B)

Ar^{9+} is F-like (9 electrons) with a $2p^5\ ^2P$ ground configuration; single electron capture will produce a Ne-like singly excited system and consequently no Auger electrons. Two-electron capture can produce Na-like core-excited states with configurations of the form $2p^5nln'l'\ ^2L$ and ^4L. Figure 1-2b shows a spectrum from Ar^{9+} + He collisions; one notes that the spectra in Figure 1-2 a and b are very similar up to energies near 200 eV. Careful pressure studies of the Ar^{9+} spectrum showed that essentially all the structure below 200 eV is produced by double collisions, the first of which populates the Ne-like metastable levels of Ar^{8+}, followed by a second, single-capture collision that populates the Na-like Auger state. However, above 200 eV the lines come from levels populated by true single-collision double-capture processes. We have identified the Na-like configurations responsible for the structure above 200 eV to be $2p^53lnl'$, with the n value showing the largest cross section around n = 8, although the distribution is very wide and appears to show population to states near the $2p^53s$ limit (250 eV). The production of such highly nonequivalent states in a single-collision double capture has been taken as evidence of the importance of dynamic correlation of the two active electrons in previous studies with He-like projectiles; this is the first study to show similar behavior in a multielectron projectile.

The Auger line labeled β in Figure 1-2 is of some special interest because it comes from the decay of the $2p^53s3d\ ^4D_J$ levels, one of which, J = 7/2, is metastable. This state is forbidden to decay by Coulomb autoionization or electric dipole (E1) photon emission, because it is essentially a pure state of total spin 3/2 (quartet). We established the metastability of a component of line β by biasing the He gas cell to −100 V, which shifts all prompt lines by 100 eV but leaves lines from metastable states that decay between the gas cell and the 45° analyzer unshifted. From such biased spectra we measured 114.10 ± 0.33 eV for the $^4D_{7/2}$ Auger line energy; the multiconfiguration Dirac-Fock (MCDF) calculations predict 114.09 eV. From high-resolution scans we also measured the prompt lines from the $2p^53s^2\ ^2P_{3/2}$ and $^2P_{1/2}$ states (these are blended within the line labeled α in Figure 1-2) to be 100.6 ± 0.33 eV and 102.8 ± 0.33 eV, in excellent agreement with the MCDF values of 100.58 and 102.78 eV. The metastable $^4D_{7/2}$ level, as demonstrated by our pressure studies, was populated by two collisions, and thus its observation in this work does not indicate spin reorientation in a single-collision double-capture event.

---

†Guest researcher, on leave from the University of Lund, Sweden.

‡Permanent address: Lawrence Livermore National Laboratory, Livermore, CA 94550.

2. Work in Progress

The study of Auger electron spectra from Na-like highly charged ions excited by double-electron-capture collisions is systematically being extended using F-like ion beams ranging from Si^{5+} to Cu^{20+}. This will yield an isoelectronic comparison of production and spectral features useful in understanding the role of dynamic correlation, possible spin reorientation in double-capture processes, and metastable level energies. This work is a collaboration with colleagues (D. Schneider *et al.*) from Lawrence Livermore National Laboratory.

To gain further insight into the "correlated" double-capture process, an experiment has been mounted to measure electron spectra in coincidence with the projectile final charge state, to determine the extent of capture into the "super" nonequivalent states consisting of one electron in a bound state of the projectile and one in the continuum moving with the projectile. Preliminary observations indicate that

nearly all the electrons captured to the continuum of the projectile (that is, unbound, but nearly at rest in the projectile frame) are associated with a projectile final charge state reduced by one unit. This is a collaborative effort with colleagues from Western Michigan University, University of Frankfurt, and Lawrence Livermore National Laboratory.

A detailed study of the scattering of Ne^{9+} (H-like) projectiles from Ne atoms, which identifies the final charge state of the target and projectile, is undergoing final analysis. This study shows details of the multielectron transfer process in slow (90 keV), highly charged ion-atom collisions, and reveals oscillatory structure in the scattering probability vs angle (or impact parameter) for certain final-charge-state combinations. This structure is due to interference effects in the probability for transfer of the projectile K-vacancy to the target during the collision. This work is a collaborative effort with colleagues (H. Schmidt-Boecking *et al.*) from the Institut für Kerphysik, University of Frankfurt.

1988 PUBLICATIONS AND REPORTS

Refereed Journals

1. H. Schmidt-Boecking, M.H. Prior, R. Doerner, H. Berg, J.O.K. Pedersen, C.L. Cocke, M. Stockli, and A.S. Schlachter, "Angular Dependence of Multiple Electron Capture in 90 keV Ne^{7+} – Ne Collisions," Phys. Rev. A **37**, 4640 (1988); LBL-24446.
2. H. Berg, R. Doerner, C. Kelbch, S. Kelbch, J. Ullrich, S. Hagmann, P. Richard, H. Schmidt-Boecking, A.S. Schlachter, M. Prior, H.J. Crawford, J.M. Engelage, I. Flores, D.H. Lloyd, J. Pedersen, and R.E. Olson, "Multuple Ionization of Rare Gases by High Energy Uranium Ions," J. Phys. B **21**, 3929 (1988).

Other Publications

3. M.H. Prior, "Collision and Spectroscopic Studies with Highly Charged Ions from the LBL ECR Ion Source," Bull. Am. Phys. Soc. **33**, 1713 (1988).
4. S.J. Chantrenne, D. Schneider, M.H. Prior, and R. Bruch, "Auger Electron Study of Slow Ion-Atom Collisions," Bull. Am. Phys. Soc. **33**, 1004 (1988).
5. H. Schmidt-Boecking, M.H. Prior, J.O.K. Pedersen, C.L. Cocke, R. Doerner, and H. Berg, "Quasi-Molecular X-ray Spectra from 117 keV Ne^{9+} + Ne Collisions," Bull. Am. Phys. Soc. **33**, 920 (1988).
6. M.H. Prior, H. Schmidt-Boeking, R. Doerner, H. Berg, J.O.K. Pedersen, C.L. Cocke, M. Stockli, and A.S. Schlachter, "Vielelektronentransfer in (90 keV - Ne^{7+} + Ne)-Stoessen," 9th Arbeitsbericht, Arbeitsgruppe "Energiereiche Atomare Stoesse," April 1988, p. 60, EAS-9, ISSN 0724-4975.

LBL Reports

7. R. Hutton, M.H. Prior, S. Chantrenne, M.H. Chen, and D. Schneider, "Double and Single Electron Capture in Slow Collisions of $Ar^{9,8+}$ Ions with He Atoms," Phys. Rev. A (in press); LBL-26581.

Invited Talks

8. M.H. Prior, "Research with Low Energy, Highly Charged Ions at the LBL ECR Ion Source," IXth Atomic Physics Program Workshop, Bethesda, MD, Aug. 31–Sept. 1, 1988.
9. M.H. Prior, "Collision and Spectroscopic Studies with Highly Charged Ions from the LBL ECR Ion Source," Physics Department Colloquium, University of Nevada, Reno, Dec. 2, 1988.

PROCESSES AND TECHNIQUES

CHEMICAL ENERGY

Formation of Oxyacids of Sulfur from SO_2*

Robert E. Connick, Investigator

INTRODUCTION

The stimulus for this research is the existence of acid rain. Coal-burning power plants produce sulfur dioxide, which is oxidized in air to form sulfuric acid, the principal component of acid rain. In most commercial flue-gas desulfurization processes, the sulfur dioxide is absorbed in an aqueous solution of low acidity, where it may be oxidized by O_2. Control of the rate of this latter reaction is of major importance to these processes. While recent research of this project has been concentrated on this reaction, investigation of the fundamental chemistry of species formed from sulfur dioxide and reactions of these species remains the primary goal. The oxidation-reduction chemistry of sulfur should be studied, particularly reactions between two oxidation states of the element, e.g., reactions involving HSO_3^-, H_2S, S_8, and the polythionates. A secondary and not closely related goal is to determine the factors controlling the rate of substitution reactions in the first coordination sphere of metal ions in solution. Computer modeling has been extended to three dimensions, and configurations of activated complexes have been determined. The usual concept of a transition state with reflection coefficient near unity is quite inadequate.

1. Work in Progress

Rate Law and Mechanism of the Oxidation of Bisulfite Ion by Oxygen.

Work continues on the mechanism of this important reaction. Monohydrogen peroxy monosulfate ion, HSO_5^-, appears to be an intermediate in the reaction. It has been found that HSO_5^- reacts with HSO_3^- to produce disulfate ion, $S_2O_7^{2-}$. Earlier work had shown that an intermediate with a lifetime of about one minute was formed in the HSO_3^- – O_2 reaction, and subsequently Chang, Littlejohn, and Hu[1] identified it as $S_2O_7^{2-}$. The HSO_5^- could be formed in a two-step chain:

$$SO_3 \cdot^- + O_2 \rightarrow SO_5 \cdot^-,$$

$$SO_5 \cdot^- + HSO_3^- \rightarrow HSO_5^- + SO_3 \cdot^-.$$

A puzzling inconsistency remains, however: Chang *et al.* find that all of the HSO_3^- goes through $S_2O_7^{2-}$, whereas our work consistently shows only half of it forming $S_2O_7^{2-}$ before forming sulfate ion. The likely existence of HSO_5^- as a short-lived intermediate raises the possibility that it is responsible for the apparent autocatalysis of the reaction by reacting with HSO_5^- to produce chain carriers.

Modeling of Displacement Reactions of Solvent in the First Coordination Sphere of Metal Ions.

In the computer simulation of the exchange of solvent from the first coordination sphere of a metal ion, release of a constrained solvent particle at different distances from the metal ion results in three types of activated complex. They can be crudely characterized by the geometry of the five remaining, closely coordinated particles as (1) tetragonal pyramid, (2) trigonal bipyramid, and (3) a nonsymmetric trigonal bipyramid in which the three common basal particles project at angles of 90°, 135°, and 135° relative to each other. All computations are for a radius ratio of metal to solvent that permits six particles to just contact the metal ion and each other. More extensive runs will be made to identify the dominant reaction path.

*This work was supported by the Director, Office of Energy Research, Office of Basic Energy Sciences, Chemical Sciences Division, of the U.S. Department of Energy under Contract No. DE-AC03-76SF00098.

1. S.G. Chang, D. Littlejohn, and K.Y. Hu, Science **237**, 756 (1987).

Potentially Catalytic and Conducting Polyorganometallics*

K. Peter C. Vollhardt, Investigator

INTRODUCTION

The task being carried out under this program is the design and execution of organic methodology aimed at allowing access to sequences of linked strong π-ligands to transition metals. The synthetic approaches are designed to be efficient, readily performed, and so adaptable as to allow control over the sequence of the attached metals. In this way, a number of novel transition-metal arrays have become available in which the metallic centers adopt "unnatural" linear and angular configurations. It is anticipated that these structures will give rise to hitherto unobserved reactivity and potential catalytic activity when exposed to small organic molecules. Moreover, such transition-metal chains provide ideal models for probing the elementary steps of multimetallic ligand and electron transfer. Continued progress is being made in the synthetic aspects of this project, resulting in novel systems in which several cyclopentadienyl units have been linked and complexed to transition metals. The first total syntheses of ter- and quatercyclopentadienyl tri- and tetrametals have been announced, including a trisheterometallic system containing the sequence molybdenum, rhenium, and tungsten. The discovery of exciting preliminary chemistry of these systems, including thermally and photochemically induced intramolecular ligand transfers, has justified the original premise of this research. Current efforts are focused on exploring the reactivity patterns of the structures under investigation and expanding the ligand chain.

*This work was supported by the Director, Office of Energy Research, Office of Basic Energy Sciences, Chemical Sciences Division, of the U.S. Department of Energy under Contract No. DE-AC03-76SF00098.

1. On the Way to Ligating Oligocyclopentadienyls: Synthesis and Preliminary Reactivity of the Two Isomeric Tercyclopentadienyls and their Transition-Metal Complexes (Publication 9)

D.A. Newman, K.P.C. Vollhardt, and R. Boese†

The first rational synthesis of trinuclear transition-metal complexes of the two isomeric tercyclopentadienyl ligands is described. The synthetic strategy, which is general, utilizes the alkylating ability of 3-chloro-2-cyclopentenone in the presence of cyclopentadienyl anions, including fulvalene dianion, to introduce a new masked cyclopentadienyl ligand. In this way, several trinuclear metal arrays with or without metal-metal bonds have been constructed attached to three linked cyclopentadienyl fragments and bearing additional ligands that may migrate along the trimetallic chain. The latter property seemingly depends on stereoelectronic factors. The intramolecular nature of such a transfer involving methyl has been established by a crossover experiment with specifically deuterium-labeled (tercyclopentadienyl)tritungsten(nonacarbonyl)methyl.

†Permanent address: Institute of Inorganic Chemistry, University–GH Essen, Federal Republic of Germany.

2. The Chemistry of (Fulvalene)-molybdenumruthenium(pentacarbonyl) (Publication 8)

M.A. Huffman and K.P.C. Vollhardt

Photolysis of $FvMoRu(CO)_5$ in the presence of alkynes leads to two types of molybdenum-bound alkyne complexes: $Fv(CO)_2RuMo(CO)(RC \equiv CR')$ ($R = R' = Ph$; $R = R' = 4\text{-}MeC_6H_4$; $R = Ph$; $R' = SiMe_3$) and $Fv(CO)_2RuMo(CO)_2$ ($RC \equiv CR'$) ($R = R' = Ph$; $R = Ph$; $R' = SiMe_3$). An x-ray crystallographic study of one of the tricarbonyl derivatives ($R = R' = Ph$) reveals the presence of a four-electron-donating alkyne ligand bound to Mo. Variable-temperature NMR studies indicate fluxionality via two processes, alkyne rotation ($\Delta H‡ = 10.1 \pm 1.1$ kcal mol^{-1}; $\Delta S‡ = -25 \pm 34$ eu) and side-to-side alkyne movement accompanied by terminal-to-bridging carbonyl exchange ($\Delta H‡ = 8.3 \pm 0.3$ kcal mol^{-1}; $\Delta S‡ = -24 \pm 1$ eu). Addition of O_2 to one of the tetracarbonyl analogs gives the

known oxo complex $Fv(CO)_2RuMo(O)$ (PhC ≡ CPh) and CO_2, and of S_8 the molybdenadithiolene $Fv(CO)_2MoRu(CO)$ [SC(Ph) = C(Ph)S]. Photosubstitution of the title complex by terminal alkynes provides side-bound, bridging vinylidenes $Fv(CO)_2MoRu(CO)[\mu = \eta^1{:}\eta^2\text{-}C = C(H)R]$ (R = Ph, R = $SiMe_3$), the first with this type of ligand bridging two different metals and the first containing ruthenium. For the phenylated example, the structure was confirmed by x-ray crystallography. Desilylation of the silylated compound with $Bu_4N^+F^-$ results in the parent vinylidene complex. Spin-saturation transfer NMR spectroscopy shows the latter to be fluxional in a process that exchanges the vinylidene hydrogens, presumably via rotation ($\Delta H‡$ = 14.8 ± 0.8 kcal mol^{-1}; $\Delta S‡$ = − 15.3 ± 2.4 eu). Desilylation of $Fv(CO)_2RuMo(CO)$ (PhC ≡ $CSiMe_3$) furnishes an intermediate that contains a four-electron-donating, Mo-bound phenylethyne that isomerizes to its vinylidene form as above, an unprecedented transformation. Under 80 psi, CO adds reversibly to this isomer, yielding $Fv(CO)_2MoRu(CO)_2[\mu\text{-}\eta^1\text{-}C{=}C(H)Ph]$, characterized by x-ray crystallography. The phenylated two-carbon fragment is semibridging, a type of structure not previously reported. In contrast, PMe_3 produces a zwitterionic bridging alkenyl complex $Fv(CO)_2MoRu(CO)[\mu\text{-}\eta^1{:}\eta^2\text{-}C(PMe_3){=}C(H)Ph]$ that rearranges thermally to the vinylidene analog $Fv(CO)_2MoRu(CO)(PMe_3)[\mu\text{-}\eta^1\text{-}C{=}C(H)Ph]$. Protonation of the original tetracarbonyl relative with HBF_4 leads to a cationic, bridging alkenyl system $\{Fv(CO)_2RuMo(CO)_2[\mu\text{-}\eta^1{:}\eta^2\text{-}C(H){=}C(H)Ph]^+\}[BF_4^-]$. These reactions are completely distinct from those of the analogous dimolybdenum and diruthenium metallomers, providing considerable encouragement for a continuation of the search for active catalysts among such structures.

3. Models for Organometallic Polymers: Zigzag Chains of $Mo_2(O_2CCH_3)_4$ Units Linked by Dimethylphosphinoethane (dmpe) and Tetramethylethylenediamine (tmeda) Ligands (Publication 12) TEXT

M.C. Kerby,† B.W. Eichhorn,‡ A.J.A. Creighton,‡ and K.P.C. Vollhardt

Attempted oligomerization of dinuclear metal complexes is frequently hampered by the alternative formation of clusters. This work describes a potential solution to this problem by the utilization of bidentate ligands. Thus, infinite zigzag chains with repeating $Mo_2(O_2CCH_3)_4$ units are recovered from neat solutions containing dmpe and tmeda. X-ray studies of the light yellow dmpe polymer, $1/\infty[Mo_2(O_2CCH_3)_4(dmpe)_2]$, and its light yellow tmeda analog, $1/\infty[Mo_2(O_2CCH_3)_4(tmeda)_2]$, shown in Figures 3-1 and 3-2, reveal nearly isomorphic structures. The former belongs to the space group P1 (−135°C), with a = 8.473 (2) Å, b = 9.562 (3) Å, c = 7.654 (3) Å, α = 110.59 (2)°, β = 100.06 (2)°, γ = 69.26 (2)°, Z = 1, V = 541.9 (3) $Å^3$, R = 0.058, and R_w = 0.058. The latter belongs to the space group P1 (20°C), with a = 8.388 (1) Å, b = 8.445 (2) Å, c = 8.840 (2) Å, α = 105.95 (2)°, β = 115.62 (1)°, γ = 91.63 (2)°, Z = 1, V = 535.1 (2) $Å^3$, R = 0.025, and R_w = 0.033. The dmpe and tmeda links are coordinated axially through weak Mo-L bonds to a relatively unperturbed Mo_2^{4+} core. A solid-state Raman spectrum of the tmeda analog demonstrates a small

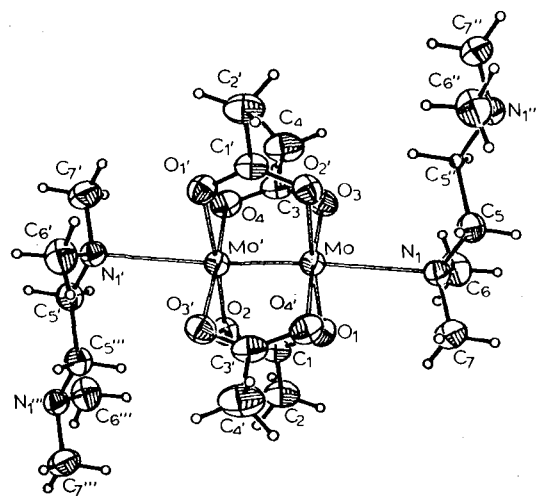

Figure 3-1. Chem-X representation of $[Mo_2(O_2CCH_3)_4(tmeda)_2]$, the repeating unit in a polymer. (XBL 894-1263)

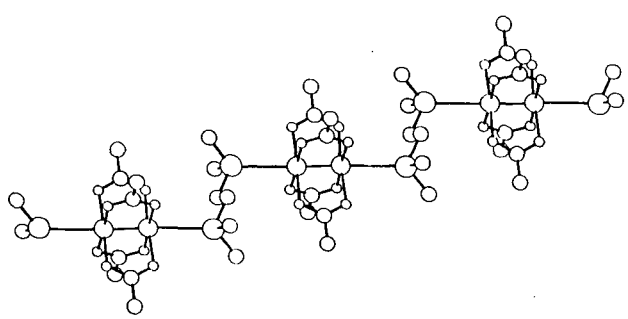

Figure 3-2. The corresponding polymer containing the repeating unit shown in Figure 3-1. (XBL 894-1264)

decrease in the Mo-Mo stretching frequency ($\nu_{Mo\text{-}Mo}$ = 391 cm^{-1}) compared to Mo_2 $(O_2CCH_3)_4$ ($\nu_{Mo\text{-}Mo}$ = 405 cm^{-1}).

---

†M.C. Kerby received an Exxon postdoctoral fellowship.

‡Permanent address: Exxon Research and Engineering Co., Corporate Research Science Laboratories, Annandale, NJ 08801.

1988 PUBLICATIONS AND REPORTS

Refereed Journals

1. K.P.C. Vollhardt and E.C. Walborsky, "Intramolecular Carbyne-carbyne Coupling on Exposure of $[\mu 3\text{-}\eta^1\text{-}CR^1]$ $CpCo]_3$ Clusters to Sulphur and Selenium: A Novel Synthesis of 1-Cobalta-2,5-Diheterocyclopent-3-enes," Polyhedron **7**, 1023 (1988); LBL-26645.
2. M.S. El-Shall and K.P.C. Vollhardt, "Molecular Structure and Electronic Properties of Hexaethynylbenzene," J. Mol. Struct. (Theochem) **183**, 175 (1989); LBL-26647.
3. D. Bläser, R. Boese, W.A. Brett, P. Rademacher, H. Schwager, A. Stanger, and K.P.C. Vollhardt, "Structure, Deformation Electron Densities, Photoelectron Spectra, and Reactivity of 3,4-Dihydro-1H-cyclobuta[a]cyclopropa[d]benzene," Angew. Chem. **101**, 209 (1989); Angew. Chem., Int. Ed. Engl. **28**, 186 (1989); LBL-26643.
4. A. Stanger and K.P.C. Vollhardt, "The Origin of the Symmetrical Structure of Benzene. Is the σ or the π Frame Responsible? An Ab-initio Study of the Effect of HCC Bond Angle Distortion," J. Org. Chem. **53**, 4889 (1988); LBL-26648.

Other Publications

5. K.P.C. Vollhardt, *Organic Chemistry*, W.H. Freeman and Co., New York, 1987.
6. K.P.C. Vollhardt, *Organische Chemie*, Verlag Chemie GmbH, Weinheim, 1988.

LBL Reports

7. K.P.C. Vollhardt, "Metallacyclopentadiene and Metallacyclopentene Complexes by Cyclodimerization of Alkynes with Alkynes or Alkenes," in *Inorganic Reactions and Methods*, J.J. Zuckerman and A.P. Hagen, eds., VCH Publishers, Weinheim (in press); LBL-26642.
8. M.A. Huffman (Ph.D. Thesis), "Reactions of (Fulvalene)molybdenumruthenium(pentacarbonyl) with Alkynes," LBL 26649.
9. D. A. Newman, K.P.C. Vollhardt, and R. Boese, "On the Way to Ligating Oligocyclopentadienyls: Synthesis and Preliminary Reactivity of the Two Isomeric Tercyclopentadienyls and Their Transition Metal Complexes," LBL-26646.
10. J.A. King, Jr., and K.P.C. Vollhardt, "The Thermal and Photochemical Degenerate 'Walk' of (η^5-Cyclopentadienyl)cobalt Along η^4-Bound 1,3,5-Hexatriene," J. Organomet. Chem. (in press); LBL-26644.
11. B.W. Eichhorn, M.C. Kerby, R.C. Haushalter, and K.P.C. Vollhardt, "Activated Mo-Mo Quadruple Bonds. Synthesis, Structure, and Properties of the Solvent Separated Ion Pair $[Mo_2(O_2CCH_3)_2(en)_4]$ $[(O_2CCH_3)_2] \cdot en$," LBL-26774.
12. M.C. Kerby, B.W. Eichhorn, A.J.A. Creighton, and K.P.C. Vollhardt, "Models for Organometallic Polymers. Zigzag Chains of $Mo_2(O_2CCH_3)_4$ Units Linked by Dmpe and Tmeda Ligands," LBL-26775.

Invited Talks

13. K.P.C. Vollhardt, "Oligocyclopentadienylmetals: Remarkable Organometallic Materials," University of California at Davis, May 17, 1988; Exxon Research and Engineering Co., Annandale, NJ, July 18, 1988; University of Cologne, Federal Republic of Germany, Dec. 12, 1988; Free University of Berlin, Federal Republic of Germany, Dec. 16, 1988.
14. K.P.C. Vollhardt, "Transition-metal Mediated Total Synthesis of Natural and Unnatural Products," Eastman Kodak Co., Rochester, NY, May 6, 1988; Shell Sittingbourne Research Centre, Kent, England, Sept. 12, 1988; Bayer AG Pflanzenschutzzentrum, Monheim, Federal Republic of Germany, Sept. 16, 1988; Technical University of Berlin, Federal Republic of Germany, Dec. 9, 1988; Schering AG, Berlin, Federal Republic of Germany, Dec. 13, 1988.

High-Energy Oxidizers and Delocalized-Electron Solids*

Neil Bartlett, Investigator

INTRODUCTION

The main aim of this program is the synthesis and characterization of new materials that may have value in electrochemical applications or in the efficient conversion of light to electrical energy. The synthetic work tests models and theories that correlate physical properties (such as electrical conductivity) with chemical composition and structure. Major aims in the synthetic strategies are (1) to tailor make the band gap in semiconductor materials and (2) to achieve high carrier concentration and mobility in the conductive materials. The present emphasis is on two-dimensional networks, such as those related to graphite. Electron oxidation of such materials (with accompanying intercalation to form salts) generates durable and conductive materials (some conducting better than aluminum). The layered materials can often be oxidized (and intercalated) electrochemically in reversible processes, and some may find use in high-energy electrodes. Physical and chemical studies are being applied to such materials to determine the structure and bonding changes that accompany oxidation and reduction. Salts that are either proton conductors or fluoride-ion conductors, and that are resistant to oxidation but are not metallic, are being sought as solid electrolytes for use with the metallic layer-material salts.

1. The Preparation of Planar-Sheet Graphite Fluorides C_xF with $X < 2$ (Publication 5)

R. Hagiwara, M. Lerner, and N. Bartlett

The chemical fluorination of second- and third-stage graphite fluoroarsenate salts with elemental fluorine in liquid anhydrous hydrogen fluoride (AHF) at ambient temperatures produces a mixture of first-stage hexafluoroarsenate, C_yAsF_6, and planar-sheet graphite fluoride, C_xF, with x as small as 1.3. X-ray powder diffraction data indicate hexagonal symmetry for $C_{1.3}F$, with an a_o parameter only slightly greater than that of pristine graphite. This fluoride has proved to be remarkably inert to oxidation and survives the oxidative attack by perchloric acid at 150°C, which destroys the C_yAsF_6. The black, insulating $C_{1.3}F$ has a density of 2.6 g /cm^3 (by flotation), which is in satisfactory agreement with that of 2.7 g/cm^3 calculated for the composition $C_{1.3}F$, using the cell parameters given in Table 1-1. The hexagonal cell a_o parameter is slightly greater than that of pristine graphite and in harmony with the earlier results[1] for sp^2 carbon fluorides with x values in the range 2 to 6. The cell parameters, and the diffraction patterns from which they derive, show no relationship to those of the puckered-sheet (sp^3 carbon) carbon fluorides $(C_2F)_n$ and $(CF)_n$, as may be seen from the data included in Table 1-1. The IR spectra of $C_{1.3}F$ exhibit the most intense ν (C-F) absorption at $\sim$1125 cm^{-1} and C_2F at[1] $\sim$1100 cm^{-1}, whereas ν (C-F) for puckered-sheet $(C_2F)_n$ or $(CF)_n$ is at[2] $\sim$1220 cm^{-1}. The C_{1s} electron spectroscopy for chemical analysis (ESCA) spectra of $C_{1.3}F$ show two peaks, that at 284.7 eV being graphite-like and that at 287.7 eV being attributable to sp^2 carbon with an F ligand attached. In the puckered-sheet fluoride $(C_2F)_n$, the binding energy[2] for carbon without F is 288.5 eV, and that with F attached is 290.4 eV. The F_{1s} ESCA of $C_{1.3}F$ exhibits a binding energy of 686.6 eV, similar to that previously noted for sp^2-type $C_{2.5}F$ and much lower than

Table 1-1
Lattice parameters (Å) for graphitic fluorides (sp^2 carbon), puckered-sheet carbon fluorides (sp^3 carbon), and graphite.

Graphite fluoride	Interlayer spacing(lc)(Å)[a]	a_o (Å)[a]
Planar-sheet graphite fluoride[b]		
$C_{1.3}F$	6.4	2.478
C_2F	5.9	2.472
C_3F	5.9	2.459
C_4F	5.5	2.459
C_6F	4.7	2.458
Puckered-sheet carbon fluoride[b]		
$(CF)_n$	6.0	2.53–2.57
$(C_2F)_n$	8.1	2.51
Graphite	3.34	2.461

a. σ for c_o = 0.05 Å; σ for a_o = 0.055 Å.

b. Planar-sheet graphite fluorides, C_xF ($x \geq 2$) were prepared by fluorination of original sp^1 graphite in AHF.

*This work was supported by the Director, Office of Energy Research, Office of Basic Energy Sciences, Chemical Sciences Division, of the U.S. Department of Energy under Contract No. DE-AC03-76SF00098.

that observed[2] for puckered-sheet $(C_2F)_n$ or $(CF)_n$, where the binding energy is ~689.3 eV.

For a composition $C_{1\text{-}3}F$, most F atoms must be placed in *meta* disposition to others on the same side of the C_6 rings of the carbon atom network. This places most F atoms only 2.48 Å (the unit-cell a_o value) from each of two F-atom neighbors. The F-ligand array on each side of a carbon sheet must be close packed. There is no space for significant nestling of the adjacent F-ligand layers of adjacent sheets. The large interlayer spacing of 6.4 Å implies a large van der Waals gap between the two F-ligand layers.

Galvanostatic discharge of a Li/1M $LiClO_4$–propylene carbonate/$C_{1\text{-}3}F$ cell (see Figure 1-1) at 100 $\mu A/cm^2$ shows a longer plateau at ~3 V than a comparable C_2F cell at the same current density.[3]

1. T. Mallouk and N. Bartlett, J. Chem. Soc., Chem. Commun., 103 (1983).
2. Y. Kita, N. Watanabe, and Y. Fujii, J. Am. Chem. Soc. **101**, 3832 (1979).
3. R. Hagiwara, M. Lerner, N. Bartlett, and T. Nakajima, *J. Electrochem. Soc.* **135**, 2393 (1988).

2. A Lithium/C_2F Primary Battery (Publication 1)

R. Hagiwara, M. Lerner, N. Bartlett, and T. Nakajima

The true graphitic fluoride (sp^2 carbon) C_2F, lithium metal, and a 1M $LiClO_4$–propylene carbonate solution as electrolyte constitute a primary battery, with discharge curves shown in Figure 1-1.

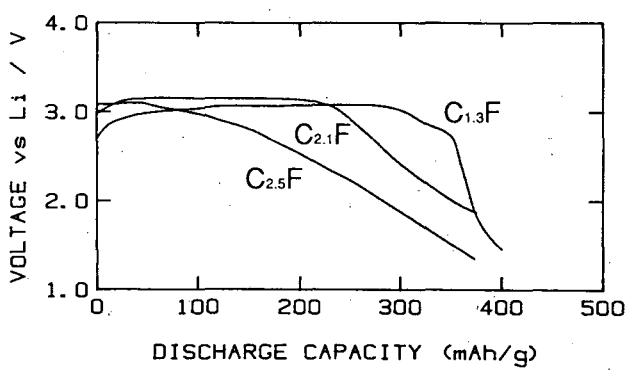

Figure 1-1. Galvanostatic discharge (100 $\mu A/cm^2$) curves of lithium-C_xF battery. (Electrolyte: 1M $LiClO_4$ in propylene carbonate. (XBL 894-1338)

An open-circuit voltage (OCV) of 3.5 to 3.6 V was observed (Li reference) at a discharge depth of 100 to 200 $mAhg^{-1}$. A much faster polarization decay was observed than for the puckered-sheet (sp^3 carbon) carbon fluorides $(CF)_n$ and $(C_2F)_n$. A flat discharge potential of greater than 3 V was observed at a current density of 100 μAcm^{-2}. The discharge capacity above 1 V for 100 μAcm^{-2} current density was approximately 70% of the theoretical capacity of ~600 $mAhg^{-1}$.

3. A General Method for the Synthesis of Polymeric Binary Fluorides Exemplified by AgF_3, NiF_4, RuF_4, and OsF_4 (Publication 4)

B. Zemva,† K. Lutar,† A. Jesih,† W.J. Casteel, Jr., and N. Bartlett

Fluoride-ion capture from their anion relatives in anhydrous hydrogen fluoride solution by strong fluoride-ion acceptors such as AsF_5 has provided a general approach to the synthesis of polymeric binary fluorides that is particularly advantageous in the synthesis of the highest-oxidation-state transition-metal polymeric fluorides.

The highest attainable oxidation state of an element is usually obtained in anionic species. This is commonly so for fluorides; yet, although salts of anions such as NiF_6^{2-} and AgF_4^- have been known for ~40 years, neither NiF_4 nor AgF_3 has been established, although a structurally undefined AgF_3 was described recently by Bougon and his coworker.[1] Each of these fluorides has been obtained by this new approach:

$$< -60°C$$

$$NiF_6^{2-} + 2AsF_5 \rightarrow 2AsF_6^- + NiF_4 \downarrow ;$$

$$\sim 20°C$$

$$AgF_4^- + AsF_5 \rightarrow AsF_6^- + AgF_3 \downarrow .$$

The brown solid NiF_4 loses elemental fluorine above −60°C and has not yet been structurally characterized. AgF_3 precipitated at or below room temperature is a bright red solid that slowly (>> 24 hr at 20°C) transforms to a dark brown solid of different structure. The freshly precipitated material is isos-

tructural[2] with AuF_3, but the hexagonal unit cell [a_o = 5.088(10) Å, c_o = 15.43(3) Å, V = 346 Å^3, Z = 6, with extinctions conforming with space group P6, 22-D_6^2 or its enantiomer] is 27 Å^3 smaller than that of its gold relative. This smallness of AgF_3 relative to AuF_3 is probably associated with a contraction of ~4.5 Å^3 of the d_z^2 valence electron pair of the AgIII relative to that of the Au(III). This contraction is in harmony with the resistance of AgIII to further oxidation, whereas AuF_3 and AuF_4 are readily oxidized to AuF_5 and AuF_6, respectively.

Each of RuF_4 and OsF_4 is readily obtained from its respective K_2MF_6 salt (where M is Ru, Pd, Ir, or Pt)[3] dissolved in AHF and then treated with AsF_5. OsF_4 is isostructural with RhF_4 and is orthorhombic, with a_o = 9.85(3) Å, b_o = 9.28(3) Å, c_o = 5.69(2) Å, V = 520 Å^3, and Z = 8; the observed extinctions conform to the space group F dd2, which is the one adopted by the tetrafluorides. The RuF_4 x-ray powder pattern is not complex but has not yet been indexed. The structure of RuF_4 is evidently not identical to that of OsF_4, but it could be closely related.

---

†Collaborators working at The Institute Jozef Stefan, Ljubljana, Yugoslavia.

1. R. Bougon and M. Lauce, Comptes Rendues Sceances Acad. Sci. Ser. 2, **297**, 117 (1963).

2. F.W.B. Einstein, P.R. Rao, J. Trotter, and N. Bartlett, J. Chem. Soc. (A) 478 (1967).

3. P. R. Rao, A. Tressaud, and N. Bartlett, J. Inorg. Nucl. Chem., Supplement, 23 (1958); A.F. Wright B.E.F. Fender, N. Bartlett, and K. Leary, Inorg. Chem. **17**, 748 (1978).

4. Work in Progress

Examination of the C_xN products of the chlorination of C_5H_5N at temperatures above 700°C shows that the composition close to the reaction threshold is close to C_5N but that at higher temperatures $(CN)_2$ loss gives sharply lower nitrogen content. There is the possibility that the N atoms of C_5N are not coplanar with the carbon-atom network (which appears to be graphite-like). Electron-energy-loss spectroscopy and the determination of the electronic properties of the C_xN and other B/C and B/C/N graphites are also in hand. To further our understanding of the bonding principles that determine structural type, the synthesis and structural characterization of other unknown binary fluorides is continuing.

1988 PUBLICATIONS AND REPORTS

Refereed Journals

1. R. Hagiwara, M. Lerner, N. Bartlett, and T. Nakajima, "A Lithium/C_2F Primary Battery," J. Electrochem. Soc. **135**, 2393 (1988); LBL-24847.

Other Publications

2. N. Bartlett, "Helium Can Form Stable Bonds," Nature **331**, 487 (1988).

LBL Reports

3. K. Lutar, A. Jesih, I. Leban, B. Zemva, and N. Bartlett, "The Crystal Structures of $XeF_5^+MF_4^-$ (M = Ag and Au) and their Relevance to the Basicity and Oxidizability of MF_4^-," LBL-25395.
4. B. Zemva, K. Lutar, A. Jesih, W. J. Casteel, Jr., and N. Bartlett, "A General Method for the Synthesis of Polymeric Binary Fluorides Exemplified by AgF_3, NiF_4, RuF_4, and OsF_4," LBL-25805.
5. R. Hagiwara, M. Lerner, and N. Bartlett, "The Preparation of Planar-Sheet Graphite Fluorides C_xF with $x < 2$," LBL-25774.
6. M. Lerner and N. Bartlett, "Electrochemical Oxidation of Graphite in an Anhydrous Hydrogen Fluoride/Alkali Fluorometallate Salt Electrolyte," LBL-26527.
7. N. Bartlett, "Valency in the Periodic Table—Concerning the Limits of Oxidation of the Elements," LBL-26528.
8. M. Lerner (Ph.D. Thesis), "Preparation and Characterization of Graphite Fluorometallate Salts and Graphite Fluorides by Chemical and Electrochemical Methods," LBL-25860.
9. S.G. Mayorga (Ph.D. Thesis), "Preparation and Characterization of Novel Boron Nitride Intercalation Compounds and Silver (111) Fluoro-Complexes," LBL-26132.

Invited Talks

10. N. Bartlett, "Metallic and Semiconductive Graphite-Related Materials," 3rd Gordon Conference on Chemistry of Electronic Materials, Ventura, CA, Mar. 7–11, 1988.
11. N. Bartlett, "Novel Metals, Semiconductors and Insulators in New Families of Materials Related to Graphite," J. Clarence Karcher Lecture, Department of Chemistry, The University of Oklahoma, Norman, Mar. 24, 1988.
12. N. Bartlett, "Valency in the Periodic Table—Concerning the Limits of Oxidation of the Elements," The Robert E. Welch Foundation, Houston, TX, Nov. 2, 1988.

Transition Metal–Catalyzed Conversion of CO, NO, H_2, and Organic Molecules to Fuels and Petrochemicals*

Robert G. Bergman, Investigator

INTRODUCTION

The goal of this program is the development of new chemical reactions in which transition metals interact with organic materials, and the understanding of how these reactions work. A recent discovery on this project was the finding that certain hydridoiridium and -rhodium complexes undergo oxidative addition into the carbon-hydrogen bonds of completely saturated hydrocarbons (M + R-H → R-M-H). This finding was the first example of this long-sought "alkane C-H activation" reaction; research is now being directed at examining the scope, selectivity, and mechanism of the process, and in developing ways to convert the activated metal complex R-M-H into functionalized organic molecules. During the current year, progress was made on the functionalization problem by uncovering a modified iridium system that effects dehydrogenation of the activated alkane. In a second study, activation of the very strong vinyl C-H bond in ethylene was investigated; evidence for the intervention of a transient intermediate other than the iridium-ethylene π-complex was obtained. Further progress was made toward understanding the thermodynamic driving force of the C-H oxidative addition process, and a flash kinetics spectrometer was constructed that is capable of infrared detection of transient organometallic species (similar to those involved in C-H activation) and measurement of the rates of their rapid reactions.

*This work was supported by the Director, Office of Energy Research, Office of Basic Energy Sciences, Chemical Sciences Division, of the U.S. Department of Energy under Contract No. DE-AC03-76SF00098.

1. Synthesis of an (η^3-Allyl)(Hydrido)Iridium Complex and its Reactions with Arenes and Alkanes. Sequential Intermolecular C-H Oxidative Addition and Hydride-to-Alkene Migratory Insertion Reactions (Publication 1)

W.D. McGhee and R.G. Bergman

The iridium allyl hydride complex (η^5-C_5Me_5)(η^3-C_3H_5)(H)Ir (**1** in Figure 1-1) has been prepared from $[(\eta^5\text{-}C_5Me_5)IrCl_2]_2$, and its reaction with arenes and alkanes has been investigated. The hydride reacts with C-H bonds in benzene and cyclopropane in the presence of phosphines L, leading to the phenyl and cyclopropyl complexes (η^5-C_5Me_5)(L)Ir(*n*-propyl)(R). Irradiation of **1** in the presence of PMe_3 takes a different course, giving the previously uncharacterized (η^5-C_5Me_5)Ir(PMe_3)$_2$. Thermal reaction of **1** in alkane solvents such as *n*-butane and *i*-butane, which are capable of β-elimination, leads to products formed by replacement of the allyl group in **1** by a substituted allyl ligand generated by overall dehydrogenation of the alkane. Thermolysis of **1** in the presence of arenes such as *n*-propylbenzene and cumene leads to more complicated products resulting from intermolecular C-H activation followed by cyclometallation and/or dimerization. Mechanistic studies, including kinetics, isotope tracer experiments, and intra- vs intermolecular isotope-effect determinations, suggest the mechanism outlined in Figure 1-1 is responsible for the alkane dehydrogenation reactions induced by hydride **1**. The coordinatively unsaturated species (η^5-C_5Me_5)(η^2-propene)Ir (complex **A** in Figure 1-1) plays a critical role in this mechanism; significant differences exist between the behavior of this intermediate and that of the closely related phosphine-substituted complex (η^5-C_5Me_5)(PMe_3)Ir studied earlier.

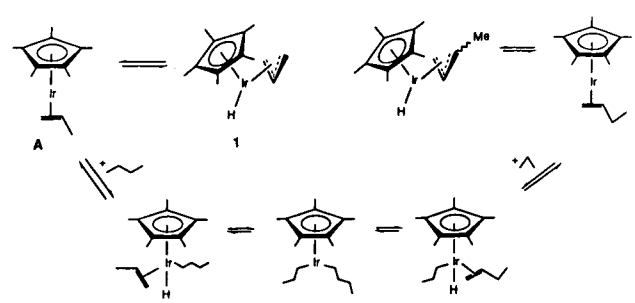

Figure 1-1. Proposed mechanism for the dehydrogenation of *n*-butane induced by (η^5-C_5Me_5)(η^3-C_3H_5)(H)Ir (**1**). (XBL 893-1197)

2. C-H Insertion and π-Complex Formation Reactions of $(\eta^5\text{-}C_5Me_5)(PMe_3)Ir$ with Ethylene: An Intra- and Intermolecular Isotope-Effect Study (Publication 2)

P.O. Stoutland and R.G. Bergman

Thermolysis of $(\eta^5\text{-}Me_5C_5)(PMe_3)Ir(C_6H_{11})(H)$ at 130–160°C in cyclohexane in the presence of ethylene results in formation of $(\eta^5\text{-}Me_5C_5)(PMe_3)Ir(HC{=}CH_2)(H)$ (**1**) and $(\eta^5\text{-}Me_5C_5)(PMe_3)Ir(H_2C{=}CH_2)$ (**2**) in a ratio of 2:1. The x-ray structure of complex **1** has been determined (see Figure 2-1); this is the first simple transition-metal vinyl hydride that has been fully characterized in this way. The π-complex **2** is completely stable to the reaction conditions, and thermolysis of **1** in cyclohexane or benzene above 180°C results in quantitative conversion to **2**. Therefore, the π-complex cannot be an intermediate in the C-H oxidative addition reaction leading to **1**. To determine the mechanism of the vinyl C-H insertion, thermolysis of $(\eta^5\text{-}Me_5C_5)(PMe_3)Ir(C_6H_{11})(H)$ in the presence of several deuterated ethylenes was carried out. The reaction with ethylene-d_2 results in insertion into both the C-H and the C-D bonds and allows determination of an intramolecular isotope effect: $k_H/k_D = 1.18 \pm 0.03$. Competition experiments involving ethylene and ethylene-d_4 allow determination of an intermolecular isotope effect for insertion into a C-H(D) bond: $k_H/k_D = 1.49 \pm 0.08$. The intermolecular isotope effect for formation of **2** was found to be 0.82 ± 0.05. The different intra- and intermolecular isotope effects for C-H insertion require an intermediate (other than the π-complex **2**) on the reaction pathway leading to **1**. A complex having an ethylene C-H bond coordinated to iridium is suggested as the structure of this intermediate.

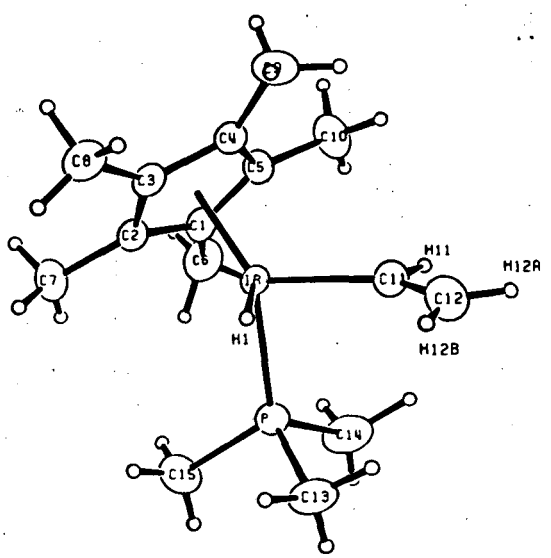

Figure 2-1. Molecular geometry of $(\eta^5\text{-}Me_5C_5)(PMe_3)Ir(HC{=}CH_2)(H)$ (**1**), as determined by x-ray diffraction. The thermal ellipsoids are scaled to represent the 50% probability surface. Hydrogen atoms are shown as small spheres for clarity. (XBL 893-1198)

3. Infrared Flash Kinetic Spectroscopy of Transients Generated by Irradiation of $(\eta^5\text{-}C_5H_5)Co(CO)_2$ in the Gas Phase and in Solution (Publication 3)

P. Wasserman, R.G. Bergman, and C.B. Moore

The photoinduced ligand substitution chemistry of $(\eta^5\text{-}C_5H_5)Co(CO)_2$ in the gas and solution phases has been studied by using laser flash kinetic spectroscopy with fast infrared detection. The data are consistent with primary loss of one CO to form an unsaturated species that is trapped rapidly by solvent to give a reactive solvate complex; Figure 3-1 illustrates transient spectra that demonstrate the formation of this complex in cyclohexane. In the absence of other ligands, the solvate reacts with starting dicarbonyl, leading to $Cp_2Co_2(CO)_3$. Dative ligands L [e.g., C_2H_4 in the gas phase or $P(n\text{-}C_4H_9)_3$ in cyclohexane solution] react rapidly with the solvate, leading to adducts of general formula CpCo(CO)(L). The rates of these bimolecular addition reactions have been

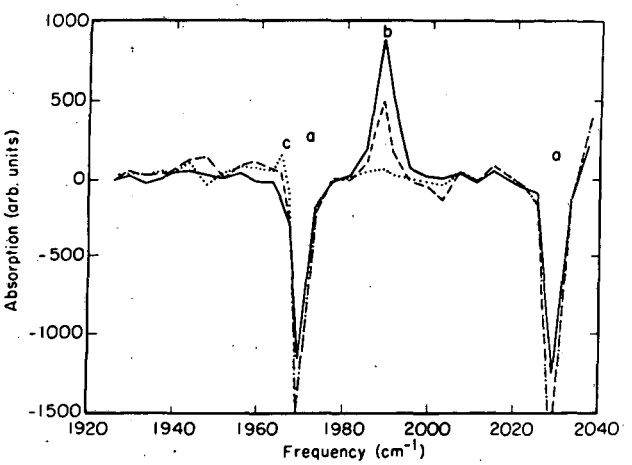

Figure 3-1. Transient spectra obtained 0.25 (solid line), 0.75 (dashed line), and 1.5 μs (dotted line) after the 308-nm photolysis of a 2.9×10^{-4} M solution of $CpCo(CO)_2$ in cyclohexane. a: $CpCo(CO)_2$; b: the solvate CpCo(cyclohexane); c: $Cp_2Co_2(CO)_3$. (XBL 893-1199)

measured for several ligands. In general, the unsaturated intermediate reacts with the ligands at rates close to those of diffusion in both media, which indicates that the open site of the coordination sphere may be only weakly solvated in alkane solutions. Solvation complexes of this intermediate with benzene and tetrahydrofuran in cyclohexane solution were produced; these solvates are far less reactive than the cyclohexane solvate. The benzene solvate appears to react with the ligand through both direct and indirect pathways. The rate constants for these reactions have been determined.

4. The Thermodynamic Driving Force for C-H Activation at Iridium (Publication 4)

P.O. Stoutland, R.G. Bergman, S.P. Nolan,† and C. Hoff†

This paper discusses the relationship between the intermolecular oxidative addition reaction of carbon-hydrogen bonds in organic molecules to transition-metal centers, and the dissociation energies of the C-H, M-H, and M-R bonds that undergo changes during this process. Earlier studies of transition-metal M-H and M-R bond energies are reviewed, followed by a summary of relative and absolute bond energies measured more recently for the C-H inserting (η^5-C_5Me_5)(PMe_3)Ir system. Table 4-1 lists a number of these recently measured metal-X bond energies. The M-H and M-R energies are unsually large in this system compared with most others that are presently known; important exceptions are those in the thorium series, where intermolecular C-H activation is also observed. The (η^5-C_5Me_5)(PMe_3)Ir(X)(Y) bond-energy values are utilized in discussing the propensity of iridium for intermolecular C-H insertion, and in predicting thermochemistries for its R-H insertion and M(H)(R) reductive elimination reactions. Finally, the physical basis for the strong metal-carbon and -hydrogen bonds in the iridium system is discussed.

Table 4-1
Ir-C bond-dissociation enthalpies for (η^5-Me_5C_5)(PMe_3)Ir(H)(X).

X	D_{Ir-X}(kcal/mol)
$CH_2C(CH_3)_3$	48
CH_6H_{11}	52
C_5H_9	52
CH_3	56
$CH_2CH(CH_3)CH(CH_3)_2$	56
C_5H_{11}	58
$CH=CH_2$	71
C_6H_5	82
H	74
Cl	90
Br	76
I	64

†Permanent address: Department of Chemistry, University of Miami, Coral Gables, FL 33124.

5. Work in Progress

Nearly all the metal complexes that so far have been found to undergo efficient oxidative addition to carbon-hydrogen bonds have a cyclopentadienyl (Cp)-type ligand attached to the metal. In current work, efforts are under way aimed at developing non-Cp-containing C-H activation systems, so that the role played by this ligand in the oxidative addition process can be better understood. In a second line of investigation, utilizing the knowledge gained in studying C-H activation systems involving complexes with one metal center, projects are under way aimed at developing two-center (dinuclear) complexes that will activate C-H bonds. In such systems, the second metal center will be employed to introduce functionalizing reagents and to help rationally modify the reactivity and selectivity of the activation process.

1988 PUBLICATIONS AND REPORTS

Refereed Journals

1. W.D. McGhee and R.G. Bergman, "Synthesis of an (η^3-Allyl)(Hydrido)Iridium Complex and Its Reaction with Arenes and Alkanes. Sequential Intermolecular C-H Oxidative Addition and Hydride-to-Alkene Migratory Insertion Reactions," J. Am. Chem. Soc. **110**, 4246 (1988); LBL-24231.
2. P.O. Stoutland and R.G. Bergman, "C-H Insertion and π-Complex Formation of (η^5-C_5Me_5)(PMe_3)Ir with Ethylene: An Intra- and Intermolecular Isotope Effect Study," J. Am. Chem. Soc. **110**, 5732 (1988); LBL-24358.
3. E.P. Wasserman, R.G. Bergman, and C.B. Moore, "IR Flash Kinetic Spectroscopy of Transients Generated by Irradiation of $CpCo(CO)_2$ in the Gas Phase and in Solution," J. Am. Chem. Soc. **110**, 6076 (1988); LBL-25460.

4. P.O. Stoutland, R.G. Bergman, S.P. Nolan, and C.D. Hoff, "The Thermodynamic Driving Force for C-H Activation at Iridium," Polyhedron **7**, 1429 (1988); LBL-24357.
5. W.D. McGhee, F.J. Hollander, and R.G. Bergman, "C-H Oxidative Addition and Reductive Elimination Reactions in a Dinuclear Iridium Complex," J. Am. Chem. Soc. **110**, 8428 (1988); LBL-25459.

LBL Reports

6. J.F. Hartwig, R.A. Andersen, and R.G. Bergman, "Synthesis of a Highly Reactive (Benzyne)Ruthenium Complex: C-C, C-H, N-H, and O-H Activation Reactions," submitted to J. Am. Chem. Soc.; LBL-26480.

Invited Talks

7. R.G. Bergman, "Synthesis and Reactivity of Metal Oxo and Alkoxide Complexes," H. King Lecturer, Department of Chemistry, Kansas State University, Manhattan, Jan. 28, 1988.
8. R.G. Bergman, "Formation and Cleavage of Carbon-Carbon and Carbon-Hydrogen Bonds at Transition Metal Centers," "Models for Metal-Mediated Oxidation Reactions: The Chemistry of Complexes with Metal-Oxygen Bonds," and "Organotransition Metal Enolates," Nieuwland Lectures, Department of Chemistry, University of Notre Dame, South Bend, IN, Mar. 21–25, 1988.
9. R.G. Bergman, "Insertion of Metals into the C-H Bonds of Organic Compounds," and "Synthesis and Reactions of Complexes with Metal-Oxygen and Metal-Nitrogen Bonds," Department of Chemistry, Florida State University, Tallahassee, Mar. 31, 1988.
10. R.G. Bergman, "Transformations of Organic Compounds Mediated by Transition Metal Complexes," "Studies of the Mechanism of Metal Alkoxide Insertion Reactions," and "The Role of Sigma Complexes in C-H Activation Reactions," Glenn Brown Visiting Scholar, Department of Chemistry, Case-Western Reserve University, Cleveland, OH, Apr. 27–29, 1988.
11. R.G. Bergman, "Application of Thermochemical Kinetics to Problems in Organic and Organometallic Reaction Mechanisms," Symposium on Thermochemistry and Kinetics: Current Directions, organized in honor of Prof. Sidney W. Benson, University of Southern California, Los Angeles, Sept. 22–23, 1988.
12. R.G. Bergman, "Transformations of Organic Compounds Mediated by Transition Metal Complexes," Clarence Karcher Lecturer, Department of Chemistry, University of Oklahoma, Norman, Oct. 27, 1988.
13. R.G. Bergman, "Reactions of Metal Oxo and Alkoxide Complexes with Organic Compounds," Syntex Distinguished Lecturer, Department of Chemistry, University of Colorado, Boulder, Jan. 25, 1988; Department of Chemistry, Texas A & M University, College Station, Apr. 21, 1988; Pettit Memorial Lecture, Department of Chemistry, University of Texas, Austin, Apr. 22, 1988; Symposium on the Chemistry of Transition Metal Alkoxides and Related Oxo Compounds, American Chemical Society Meeting, Los Angeles, Sept. 25–30, 1988; Department of Chemistry, University of California, Santa Cruz, Nov. 7, 1988; Department of Chemistry, Stanford University, Stanford, CA, Nov. 16, 1988.
14. R.G. Bergman, "Activation of Carbon-Hydrogen Bonds in Alkanes Using Organotransition Metal Complexes," Department of Chemistry, Harvey Mudd College, Pomona, CA, Nov. 8, 1988.
15. R.G. Bergman, "Activation of Carbon-Hydrogen Bonds Using Soluble Transition Metal Complexes," Department of Chemistry, Swarthmore College, Swarthmore, PA, Dec. 5, 1988.
16. R.G. Bergman, "The Use of Organotransition Metal Complexes in the Formation and Cleavage of Bonds to Carbon, Nitrogen and Oxygen," Department of Chemistry, Syracuse University, Syracuse, NY, Dec. 6, 1988; Department of Chemistry, State University of New York at Stony Brook, Dec. 8, 1988.

HEAVY-ELEMENT CHEMISTRY

Actinide Chemistry*

Norman M. Edelstein, Richard A. Andersen, Kenneth N. Raymond, Andrew Streitwieser, Jr., and Alan Zalkin, Investigators

INTRODUCTION

The purpose of this project is to study actinide materials in order to provide the basic knowledge necessary for their safe and economic utilization in present and future technology. The program includes the preparation of new gaseous, liquid, and solid phases and studies of their physical and chemical properties. Techniques for characterization include x-ray diffraction, optical and vibrational spectroscopy, magnetic resonance, and magnetic susceptibility. Equilibrium and kinetic data for complex formation are measured. From these complementary studies, new insights into the structural and chemical principles of actinide compounds are obtained with which to design new synthetic schemes to produce new materials.

A major aspect of the program is the design and synthesis of sequestering agents for actinide ions. These compounds are intended for use in the treatment of actinide poisoning and for possible application in the treatment of spent reactor fuels. Preparative, structural, and physical studies of new types of organoactinide, related organolanthanide, and new actinide inorganic complexes are continuing. Studies on optical spectra of free ions and actinide ions in crystals are being pursued in order to understand their electronic structure.

ACTINIDE-SPECIFIC SEQUESTERING AGENTS

The primary goal of this work is to develop and characterize chelating agents that specifically and effectively sequester actinide ions. Such chelating agents are intended to provide treatment for actinide contamination in humans and in systems related to the nuclear fuel cycle. Techniques such as x-ray crystallography, electrochemistry, potentiometry, and ultraviolet-visible spectrophotometry are used to examine the coordination properties of the actinide complexes. Biological studies are also performed in collaboration with Dr. P.W. Durbin of the Biology and Medicine Division at LBL to assess the effectiveness of the chelating agents to remove actinides *in vivo*.

1. Kinetically Inert Lanthanide Amine Complexes (Publications 1 and 3)

P.H. Smith,† Z.E. Reyes,‡ C.W. Lee,§ and K.N. Raymond

Chelating agents to complex actinide(IV) ions have been developed using a biomimetic approach founded on the ligand structures of naturally occurring iron(III) sequestering agents called siderophores. The present study emphasizes the encapsulation aspects of such metal-ion binding. A series of macrocyclic lanthanide amine complexes has been prepared by the addition of bis(dimethylamino)methane to one equivalent of lanthanide ion and two equivalents of triaminotriethylamine in acetonitrile. These compounds have been structurally characterized, and the electrochemical potential of a ytterbium complex in acetonitrile suggests a large stabilization of the +3 state.

A normal-pulse polarogram observed with 2mM Yb^{3+}(L) [L = 1,9-bis(2-aminoethyl)-1,4,6,9,12,14-hexaazacyclohexadecane] in acetonitrile solution (0.3M sodium triflate) using a dropping electrode (DME) as the working electrode is illustrated in Figure 1-1. The log plot shown in the inset is linear with a slope of 60 mV, indicating that the electrode reaction is a Nernstian one-electron process. The half-wave potential is −1.44 V vs SCE. This measured reduction potential is directly related to the stabilities, K_{III} and K_{II}, of the Yb(III) and Yb(II) with the macrocyclic ligand by the relationship

$$E_c^o - E_s^o = 0.059 \log (K_{II}/K_{III}) \quad ,$$

*This work was supported by the Director, Office of Energy Research, Office of Basic Energy Sciences, Chemical Sciences Division, of the U.S. Department of Energy under Contract No. DE-AC03-76SF00098.

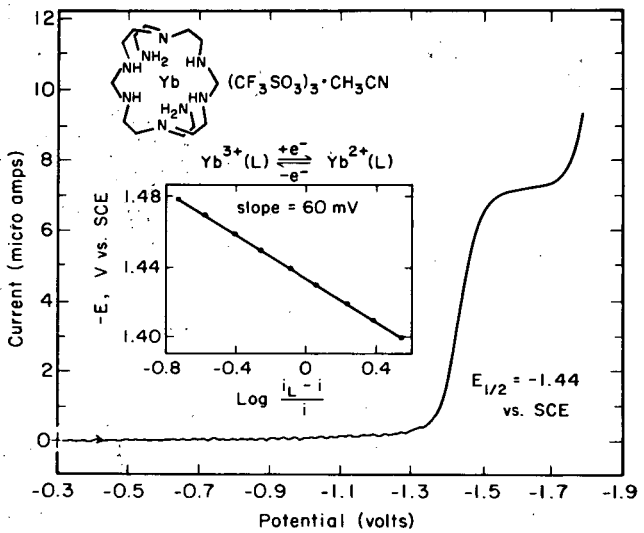

Figure 1-1. Normal-pulse polarogram of $Yb^{3+}(L)$ in 0.3M sodium triflate acetonitrile solution. Negative potentials (V vs SCE) are plotted to the right, and reduction currents are plotted upward. The inset shows a plot of E vs log $(i_L - i/i)$ for the normal-pulse polarogram. (XBL 866-2155)

where E_c^o and E_s^o are the standard reduction potentials of the Yb(III,II) redox couple with and without being encapsulated by the ligand in acetonitrile. Since the standard reduction potentials can be approximately identified with half-wave potentials, using the half-wave potentials of -0.6 V vs SCE for the Yb(III,II) couple in the absence of coordinating ligands in acetonitrile, K_{III}/K_{II} is calculated to be 10^{14}. A part of the explanation for the observed remarkably larger stabilities for Yb(III) vs Yb(II) amine macrocycle may be found in the significantly smaller size of the Yb(III) ionic radius compared to Yb(II),[1] yielding a better fit within the ligand cavity. The 3+ ion is also a stronger acid than the 2+ ion. The advantages associated with the smaller size of the central metal ion in forming a stable conformation of these macrocycles have been demonstrated by the single-crystal x-ray structural studies of the La(III) and Yb(III) complexes for this macrocyclic ligand.[2] Another important factor may originate from the low solvation energy in acetonitrile, suggesting that there is not a considerably greater desolvation energy for encryptation of the Yb(III) ion in acetonitrile.

[†]Present address: Los Alamos National Laboratory, Los Alamos, NM 87545.

[‡]Present address: Departmento de Quimica, Colegio Universitario de Humacao, Humacao, Puerto Rico 00661.

[§]Present address: Department of Chemistry, Korea University, 208, Seochang, Jochiwon, Choong-nam 339-800, Korea.

1. R.D. Shannon, Acta Crystallogr. **A32**, 751 (1976).

2. P.H. Smith and K.N. Raymond, Inorg. Chem. **24**, 3469 (1985).

2. Complexation of Lanthanide(III) Ions by Catechol and Similar Ligands (Publication 2)

D.H. Zhu,[†] M.J. Kappel,[‡] and K.N. Raymond

The solution complexation chemistry of Eu(III) and Lu(III) with catechol and several monocatecholates (e.g., tiron, DMBS) were investigated using potentiometric and spectrophotometric methods. These two trivalent lanthanides form complexes of the same composition, with those of Lu(III) more stable. Complexes of Eu(III) with catechol of 1:1, 1:2, and 1:3 are formed at pH 8.0, 10.0, and 12.0, respectively, as shown by the continuous variation plot in Figure 2-1. The overall formation constant, log β, of trivalent lanthanides with tetracatechol is $\sim$20. This value is to be compared with a log $\beta \geqslant 50$ for lanthanide(IV) and actinide(IV) with tetracatechol. The latter value demonstrates that very stable actinide(IV) tetracatecholate complexes are formed, thereby making catechol a potential chelating agent for actinide(IV) *in vivo*.

[†]Present address: Institute of Atomic Energy, Academic Sinica, Beijing, People's Republic of China.

[‡]Present address: Rohm and Haas, Spring House, PA 19477.

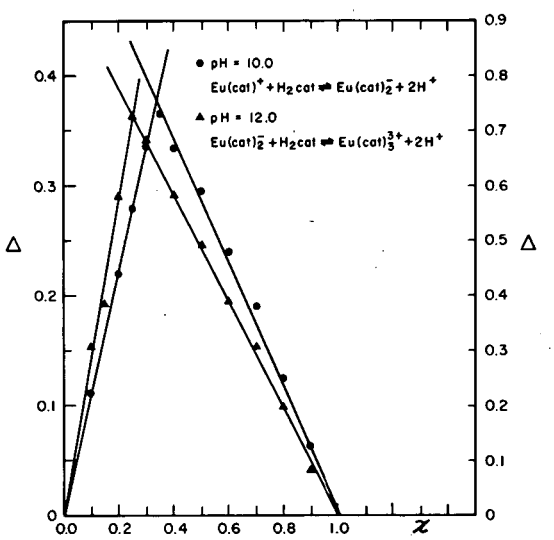

Figure 2-1. Continuous various plot of the optical-density difference vs mole fraction of Eu(III) at $[Eu^{3+}] + [cat] = 1.6 \times 10^{-4}$M, pH 10 and pH 12. (XBL 838-11177)

SYNTHETIC AND STRUCTURAL STUDIES OF ACTINIDES AND OTHER COMPOUNDS

3. $[Li(Me_2NCH_2CH_2NMe_2)_2]$-$[Li_2(Me_2NCH_2CH_2NMe_2)_2$ (μ-η^5, η^5-MeC_5H_4)]-$[(\eta^5$-$MeC_5H_4)_6U_2(\mu$-Me)$]_2$: A Compound with Symmetrically Bridging MeC_5H_4 and Me Groups (Publication 22)

S.D. Stults, R.A. Andersen, and A. Zalkin

Reaction of eqimolar amounts of MeLi and $(MeC_5H_4)_3U$(thf) in $Me_2NCH_2CH_2NMe_2$ and diethyl ether gives red crystals of $[Li(Me_2NCH_2CH_2NMe_2)_2]$-$[Li_2(Me_2NCH_2CH_2NMe_2)_2(\mu$-$\eta^5$,$\eta^5$-$MeC_5H_4)][(\eta^5$-$MeC_5H_4)_6U_2(\mu$-Me)$]_2$ in 19% yield. Single-crystal x-ray crystallography; monoclinic, $C_{2/c}$, a = 18.093(4) Å, b = 21.706(6) Å, c = 27.233(6) Å, b = 97.53(3)°, Z = 4, R = 0.053 [2165 data, $F^2 > 3\sigma(F^2)$], shows that the compound is composed of two cationic fragments, $[Li(Me_2NCH_2CH_2NMe_2)_2]$ and $[Li_2(Me_2NCH_2CH_2NMe_2)_2(\mu$-$\eta^5$,$\eta^5$-$MeC_5H_4)]$ (see Figure 3-1), the latter of which contains two Li(tmed) units on opposite sides of the planar MeC_5H_4 ring, i.e., an inverted sandwich structure. The bonding in this inverted sandwich fragment may be viewed in the following way. Each lithium atom in the LiN_2^+ fragment can use one s-orbital and two p-orbitals for four electrons in bonding to the tmed ligand. The empty sp^2-hybridized orbital of σ-symmetry on each LiN_2^+ fragment can interact with the filled σ-symmetry orbital on the MeC_5H_4-anion, forming bonding, antibonding, and nonbonding combinations. The two electrons are located in the bonding molecular orbital; this description is the familiar one given for three-center–two-electron bonding. The filled, π-symmetry orbitals on the MeC_5H_4- fragment can act as π-donors toward the empty, unhybridized, orthogonal p-orbitals on each $Li(tmed)^+$ fragment, accounting for the perpendicular orientation of the two $Li(tmed)^+$ fragments. On the other hand, the perpendicular orientation minimizes the repulsion between the Me_2N groups across the MeC_5H_4 ring, and steric rather than electronic factors may be responsible for the observed geometry. The anion portion contains a symmetrically bridging methyl group sandwiched between two $(MeC_5H_4)_3U$ units so that the methyl group has $D_{3h}-$ symmetry (see Figure 3-2). It is difficult to describe the bonding in the anion, since the idealized C_{3v} symmetry $(MeC_5H_4)_3U$ fragment has many orbitals (s, p, d, f) of σ-symmetry, though the following description appears to be reasonable. The D_{3h}- symmetry methyl anion is formed from one s-orbital and two p-orbitals, giving a sp^2-hybridized set that contains six electrons for the C-H bonds and an unhybridized p-orbital with its two electrons that can be used in bonding with the σ-orbitals on the Lewis acid $(MeC_5H_4)_3U$.

4. The Structures of Bis[bis(trimethylsilyl)-cyclopentadienyl](chloro)uranium(III)-[bis(t-butylisocyanide)] and Bis[bis(trimethylsilyl)cyclopentadienyl]-(chloro)uranium(III) [bis(t-butylcyanide)] (Publication 42)

S.M. Beshouri and A. Zalkin

In an attempt to explore the lability of the uranium(III) chloro-bridged dimer $(Cp_2''UCl)_2$, [Cp'' = $C_5H_3(SiMe_3)_2$], toward Lewis bases, reactions were undertaken using *tert*-butylcyanide $[NC-C(CH_3)_3]$ and *tert*-butylisocyanide [CN-

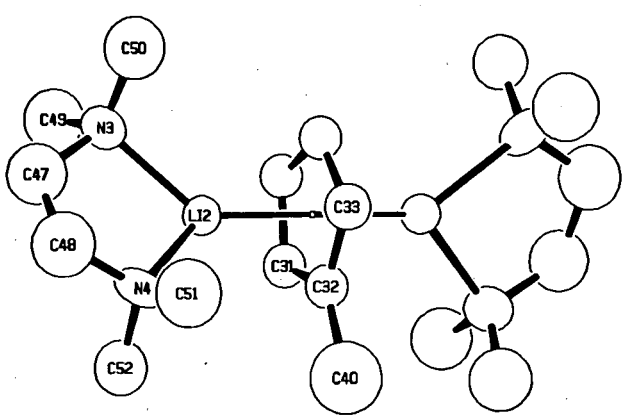

Figure 3-1. ORTEP drawing of $[Li_2(Me_2NCH_2CH_2NMe_2)_2(\mu$-$\eta^5$,$\eta^5$-$MeC_5H_4)]$ fragment. (XBL 891-307)

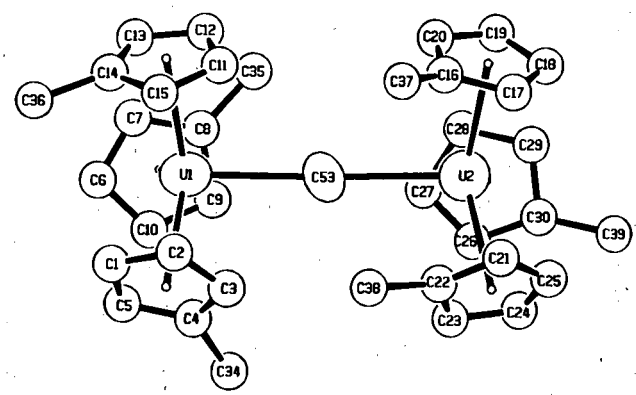

Figure 3-2. ORTEP drawing of $[(\eta^5$-$MeC_5H_4)_6U_2(\mu$-Me)] fragment. (XBL 891-306)

$C(CH_3)_3$]. The reaction of $\langle Cp_2''UCl\rangle_2$ with these ligands (L) is facile, forming five coordinate uranium(III) complexes of the general formula $Cp_2''UCl{\cdot}2L$. Both complexes were prepared via the same synthetic procedure. $\langle Cp_2''UCl\rangle_2$ was dissolved in diethyl ether under an N_2 atmosphere. CN-CMe_3 or NC-CMe_3 was added and the color of the solution immediately darkened. The residue was extracted with hexane, filtered, and cooled to −20°C. Dark crystals were isolated after several days and sealed inside thin-walled quartz capillaries under an inert and dry atmosphere of argon. The crystals, $[(Me_3Si)_2C_5H_3]_2ClU{\cdot}CNCMe_3$ (I) and $[(Me_3Si)_2C_5H_3]_2ClU{\cdot}NCCMe_3$ (II), are monoclinic, $P2_1/n$, with (I) a = 22.211(3) Å, b = 11.484(2) Å, c = 18.026(3) Å, and β = 110.43(2)°; (II) a = 22.206(4) Å, b = 11.457(2) Å, c = 18.030(3) Å, and β = 110.46(2)°. For Z = 4, the calculated densities are 1.324 and 1.327 g/cm^3, respectively. The structures were refined by full-matrix least-squares to R factors of R = 0.030 for 3271 data [$F^2 > 3\sigma(F^2)$] and 0.033 for 3090 data [$F^2 > 3\sigma(F^2)$] for (I) and (II), respectively. The molecule adopts a five-coordinate, distorted trigonal bipyramidal structure, where the donor L ligands occupy the axial sites. The uranium(III) atom is in a plane with chlorine and the centroids of two cyclopentadienyl rings; the two coordinating groups (t-butylcyanide in I, Figure 4-1, or t-butylisocyanide in II, Figure 4-2) lie above and below this plane. Some interatomic distances (in Å) are: ⟨U-Cp⟩: (I) 2.51, (II) 2.53; ⟨U-C(Cp)⟩: (I) 2.79(2), (II) 2.80(2); U-Cl: (I) 2.694(3), (II) 2.698(3); ⟨U-C(isocyanide)⟩: 2.66(1); ⟨U-N(cyanide)⟩: 2.62(1).

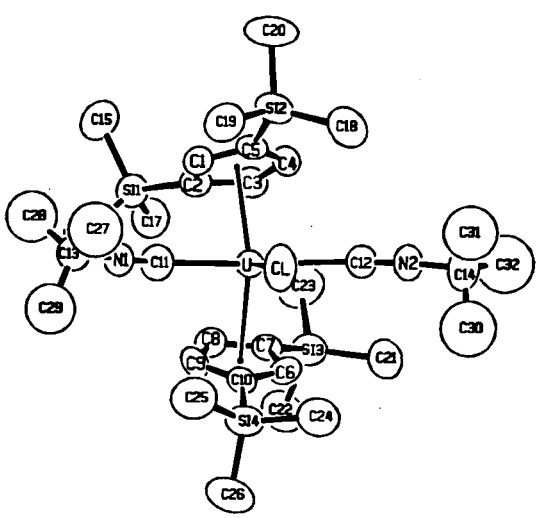

Figure 4-1. ORTEP drawing of (I) $[(Me_3Si)_2C_5H_3]_2ClU{\cdot}CNCMe_3$ showing atomic numbering; 50% probability ellipsoids. (XBL 891-65)

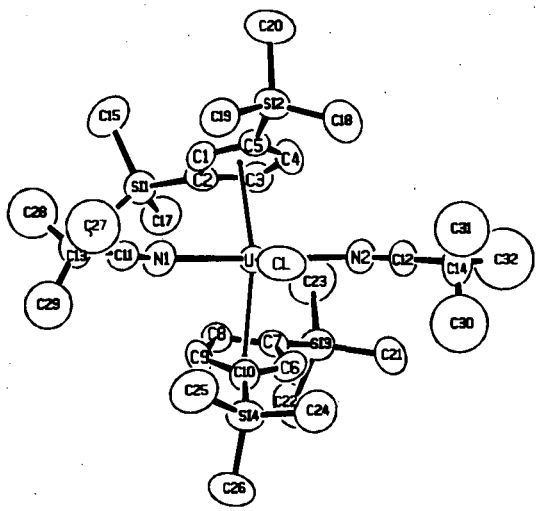

Figure 4-2. ORTEP drawing of (II) $[(Me_3Si)_2C_5H_3]_2ClU{\cdot}NCCMe_3$ showing atomic numbering; 50% probability ellipsoids. (XBL 891-66)

5. Tris(methylcyclopentadienyl)uranium(III)-ammonia (Publication 43)

R.K. Rosen and A. Zalkin

The crystal structure of $(MeC_5H_4)_3U{\cdot}NH_3$ was determined in order to examine the role of steric effects on the U-L bond length in a series of $(MeC_5H_4)_3U{\cdot}L$ compounds, where L = ammonia, 4-dimethylaminopyridine, and quinuclidine. The compound was prepared by the addition of an ammonia-saturated toluene solution to a solution of $(MeC_5H_4)_3U{\cdot}OC_4H_8$, and the red-brown needles were crystallized from ether at −20°. The crystals are monoclinic, Im, with cell dimensions a = 12.129(3) Å, b = 24.197(5) Å, c = 8.725(3) Å, and β = 92.85°. For Z = 6 the calculated density is 1.92 g/cm^3. The structure was refined to an R factor of 0.037 [4247 data, $F^2 > 3\sigma(F^2)$]. There are two independent molecules in the unit cell. In the first molecule (see Figure 5-1), the atoms are all in general positions; the second molecule is astride the mirror plane and is shown in Figure 5-2. Although the orientation of components of the two molecules is different, the bond distances and angles are comparable within the estimated statistics, and chemically the two are identical. The uranium atom is bonded to three cyclopentadienyl rings and to an ammonia molecule, with ⟨U-C⟩, ⟨U-ring⟩, and ⟨U-N⟩ distances of 2.81(5), 2.55(3), and 2.61(3) Å, respectively.

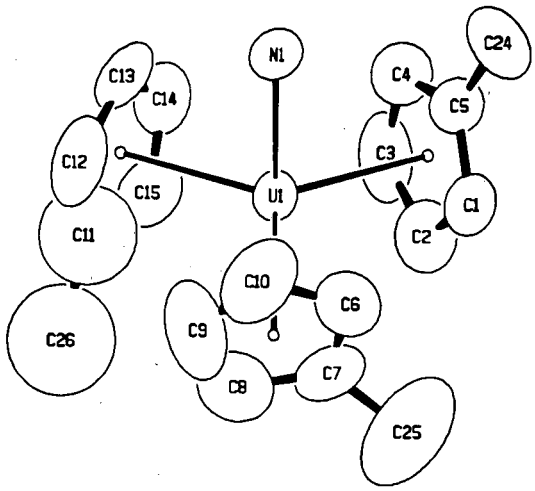

Figure 5-1. ORTEP drawing of the $(MeC_5H_4)_3U{\cdot}NH_3$ molecule in the general position; thermal ellipsoids at 50% probability level. (XBL 891-67)

6. Tris[bis(trimethylsilyl)amido](trimethylsilylimido)uranium(V) (Publication 14)

A. Zalkin, J.G. Brennan, and R.A. Andersen

$\{[(CH_3)_3Si]_2N\}_3{=}UNSi(CH_3)_3$ was prepared during a systematic synthetic and comparative x-ray crystallographic study of monomeric pentavalent uranium compounds. The crystals are rhombohedral, R3c, with a = 12.495(4) Å and α = 89.83(3)° at 23°C; for Z = 2 the calculated density is 1.373 g/cm^3. The structure was refined to an R factor of 0.027 for 1194 data with $F^2 > 3\sigma F^2$. The uranium(V) atom is on a threefold axis at the center of a tetrahedron of nitrogen atoms (see Figure 6-1). Distances are: U=N, 1.910(16) Å; U-N 2.295(10) Å; ⟨Si-N⟩, 1.728 ± 0.027 Å; ⟨Si-C⟩, 1.91 ± 0.04 Å.

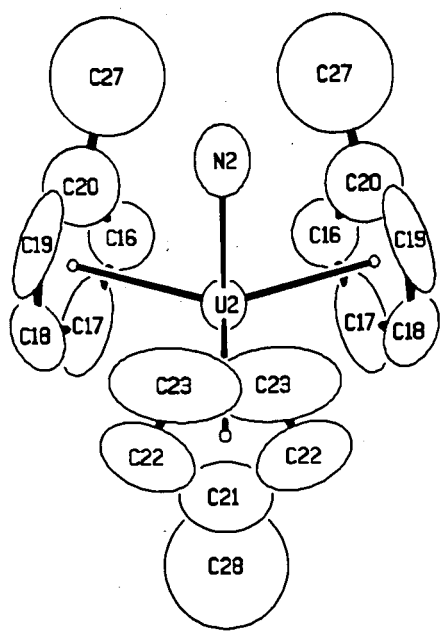

Figure 5-2. ORTEP drawing of the $(MeC_5H_4)_3U{\cdot}NH_3$ molecule on the mirror plane; thermal ellipsoids at 50% probability level. (XBL 891-68)

7. Di-μ-oxo-bis{bis[bis(trimethylsilyl)cyclopentadienyl]uranium(IV)} (Publication 15)

A. Zalkin and S.M. Beshouri

$(\{[(CH_3)_3Si]_2C_5H_3\}_2UO)_2$ was generated as a side product of the reaction of bis(trimethylsilyl)cyclopentadienyl uranium(III) complexes with unsaturated molecules, and it is believed to be formed as a result of oxygen contamination. The crystals are monoclinic, $P2_1/n$, with a = 15.648(3) Å, b = 15.951(3) Å, c = 12.195(3) Å, and β = 99.99(2)° at 23°C; for Z = 2 the calculated density is 1.49 g/cm^3. The structure was refined by full-matrix least squares to an R factor of 0.036 for 2997 data $[F^2 > 2\sigma(F^2)]$. The dimeric complex, in which two $(Me_3Si)_2C_4H_3U$ moeities are bridge bonded by two oxygen atoms, lies on a center of symmetry (see Figure 7-1). Distances are: U-O, 2.096(6), 2.129(6) Å; ⟨U-C⟩, 2.77(3) Å; ⟨U-Cp⟩, 2.497(4) Å.

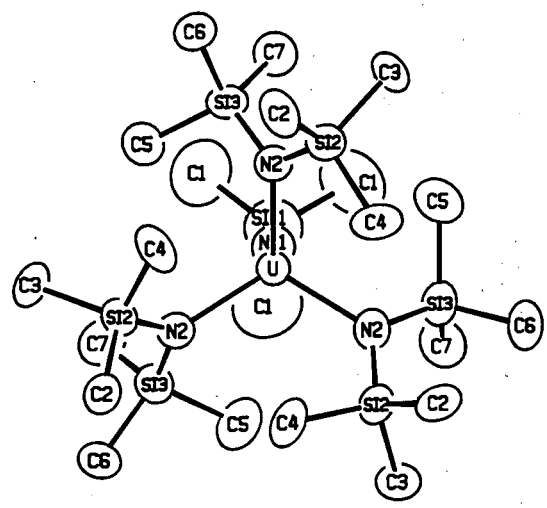

Figure 6-1. ORTEP drawing of the $(MeC_5H_4)_3U(NC_6H_5)$ molecule looking down and slightly off the threefold axis. (XBL 891-57)

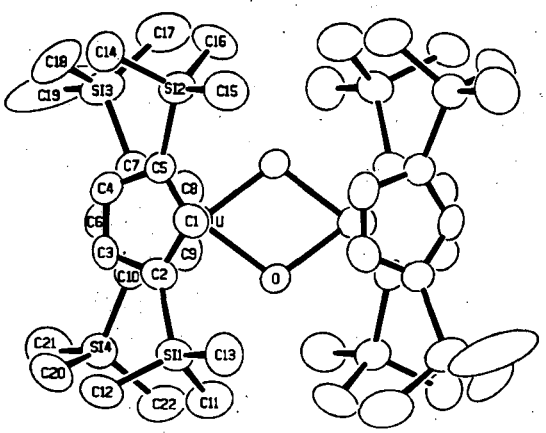

Figure 7-1. ORTEP drawing of $(\{[(CH_3)_3Si]_2C_5H_3\}_2UO)_2$ with thermal ellipsoids at 50% probability level. (XBL 891-59)

8. Bis[bis(t-butyl)cyclopentadienyl]uranium Chloride (Publication 17)

A. Zalkin, A.L. Stuart, and R.A. Andersen

$\{[(Me_3C)_2C_5H_3]_2UCl\}_2$ was prepared as part of a systematic synthetic and x-ray crystallographic study aimed at elucidating the solid-state stereochemistry and geometrical alterations in trivalent uranium metallocenes as a function of coordination environment. The crystals are orthorhombic, Pccn, with a = 13.040(3) Å, b = 17.086(3) Å, and c = 24.587(3) Å at 23°C; for Z = 4 the calculated density is 1.523 g/cm^3. The structure was refined by full-matrix least squares to an R factor of 0.027 for 1293 data with $F^2 > 2\sigma(F^2)$. Two $[(Me_3C)_2C_5H_3]UCl$ groups form a double chlorine-bridged dimer (see Figure 8-1) in which the uranium atom is bonded to two cyclopentadienyl rings and to two chlorine atoms with U-Cp and U-Cl distances of 2.516 and 2.856(4) Å, respectively.

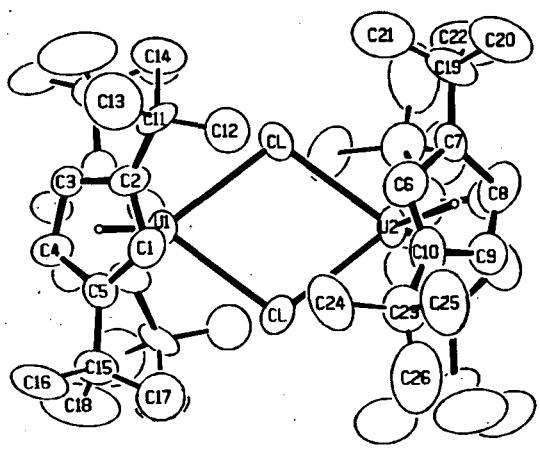

Figure 8-1. ORTEP drawing of $\{[(Me_3C)_2C_5H_3]_2UCl\}_2$ with thermal ellipsoids at 50% probability level. (XBL 891-60)

9. Bis[bis(trimethylsilyl)cyclopentadienyl]-chloro)uranium(III) bis(2,6-dimethylphenylisocyanide) (Publication 39)

A. Zalkin and S.M. Beshouri

$[(Me_3Si)_2C_5H_3]_2ClU{\cdot}2(CNC_6H_3Me_2)$ was prepared by reaction of one equivalent of $[\langle C_5H_3(SiMe_3)_2\rangle_2UCl]_2$ with four equivalents of $CN(Me_2C_6H_3)$ in diethyl ether solution. The product was dissolved in hexane solution, and dark crystals were isolated after cooling at −20°C. The crystals are monoclinic, $P2_1/n$, with a = 16.000(4) Å, b = 22.806(4) Å, c = 13.093(3) Å, and β = 92.85(2)° at 23°C. For Z = 4 the calculated density is 1.33 g/cm^3. The structure was refined by full-matrix least squares to an R factor of 0.031 for 4116 $[F^2 > 2\sigma(F^2)]$ of 8437 total unique data. The uranium atom is five coordinate, with the following distances: U-Cl, 2.6865(20) Å; U-Cp, 2.505, 2.508 Å; U-C(isocyanide), 2.654(9), 2.681(9) Å; and ⟨U-C(cyclopentadiene)⟩, 2.781(11) Å (see Figure 9-1).

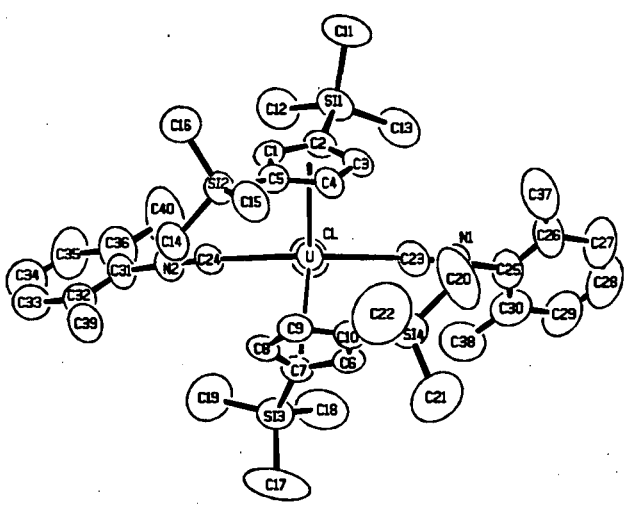

Figure 9-1. ORTEP drawing of $[(Me_3Si)_2C_5H_3]_2ClU{\cdot}2(CNC_6H_3Me_2)$ with thermal ellipsoids at 50% probability level. (XBL 891-62)

10. Bis[bis(trimethylsilyl)cyclopentadienyl]-(bromo)uranium(III)bis (t-butylisocyanide) (Publication 40)

S.M. Beshouri and A. Zalkin

$[(Me_3Si)_2C_5H_3]_2UBr{\cdot}2[CNCMe_3]_2$ was prepared by reaction of one equivalent of $[\langle C_5H_3(SiMe_3)_2\rangle_2UBr_2]$ with four equivalents of $CN(CMe_3)$ in diethyl ether solution; the product was dissolved in hexane, and dark crystals were isolated after cooling to −20°C. The crystals are monoclinic, $P2_1/n$, with a = 11.765(3) Å, b = 12.135(2) Å, c = 30.125(5) Å, β = 92.29(2)°, and V = 4297.5; for Z = 4 the calculated density is 1.396 g/cm^3. The crystal structure was determined using monochromated MoKα x rays. The structure was refined by full-matrix least squares to an R factor of 0.033 using 4281 $[F^2 > 2\sigma(F^2)]$ of 7592 total unique data. The uranium atom is five coordinate, with the following distances: U-Br, 2.8761(10) Å; U-Cp, 2.514, 2.520 Å; U-C(isocyanide), 2.662(8), 2.697(7) Å; and ⟨U-C(cyclopentadiene)⟩, 2.791(18) Å (see Figure 10-1).

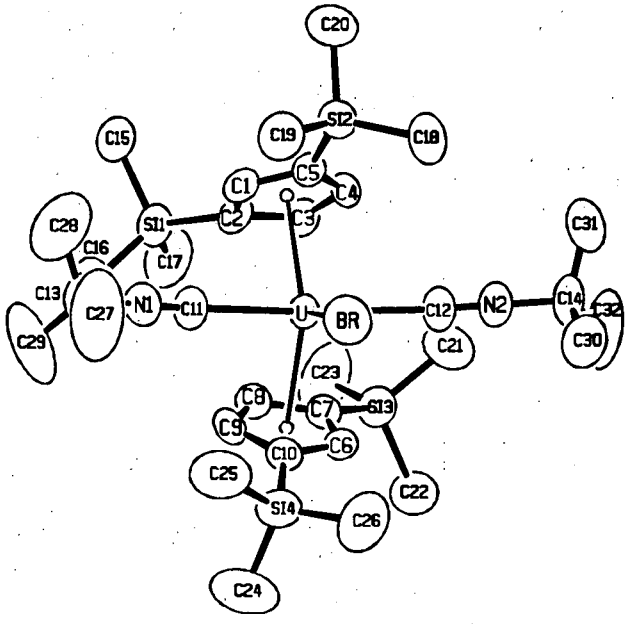

Figure 10-1. ORTEP drawing of $[(Me_3Si)_2C_5H_3]_2UBr{\cdot}2[CNCMe_3]_2$ showing atomic numbering; 50% probability ellipsoids. (XBL 891-63)

11. Bis[bis(trimethylsilyl)cyclopentadienyl]-(chloro)uranium(III)bis-(trimethylsilylcyanide) (Publication 41)

A. Zalkin and S.M. Beshouri

$[(Me^3Si)_2C_5H_3]_2UCl{\cdot}2[NCSiMe_3]_2$ was prepared by reaction of one equivalent of $[\langle C_5H_3(SiMe_3)_2\rangle_2UCl]_2$ with four equivalents of $NCSiMe_3$ in diethyl ether solution. The product was dissolved in hexane, and dark green crystals were isolated after cooling at −20°C. The crystals are monoclinic, $P2_1/n$, with a = 11.602(2) Å, b = 36.947(5) Å, c = 10.999(2) Å, and β = 99.31(2)°. For Z = 4, the calculated density is 1.272 g/cm^3. The structure was refined to an R factor of 0.041 for 4138 $[F_2 > 2\sigma(F_2)]$ of 6929 total unique data. The uranium atom is five coordinate, with the following distances: U-Cl, 2.698(3) Å; U-Cp, 2.510, 2.520 Å; U-N(cyanide), 2.592(11), 2.619(10) Å; and ⟨U-C(cyclopentadiene)⟩, 2.789(22) Å (see Figure 11-1).

12. Structure of Rubidium Uranyl(VI) Trinitrate (Publication 38)

A. Zalkin, L.K. Templeton, and D.H. Templeton

Crystals of $RbUO_2(NO_3)_3$ were prepared for study of x-ray dichroism with synchrotron radiation,

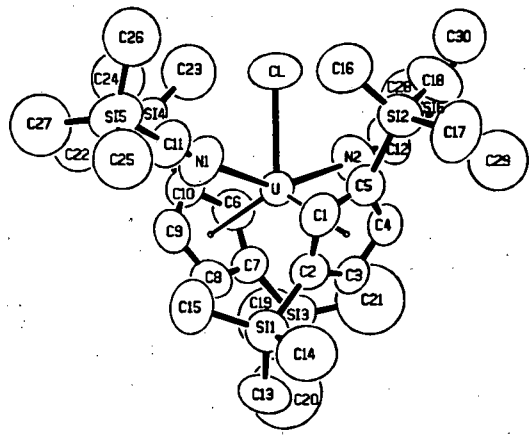

Figure 11-1. ORTEP drawing of $[(Me_3Si)_2C_5H_3]_2UCl{\cdot}2[NCSiMe_3]_2$ showing atomic numbering; 50% probability ellipsoids. (XBL 891-64)

and the structure was redetermined to check the symmetry and molecular orientation, to obtain the anisotropic thermal parameters, and as part of an investigation of uranium-oxygen bond distances. The crystals are hexagonal, R3c, with dimensions a = 9.384(4) Å and c = 18.899(6) Å. For Z = 6 the x-ray density is 3.743(4) g/cm^3. Least-squares refinement of the structure resulted in an R factor of 0.014 for 261 independent reflections with $I > 2\sigma(I)$. The uranyl ion is coordinated in bidentate fashion by three nitrate ions in its equatorial plane (see Figure 12-1). Bond lengths are U-O = 1.746(4) Å (uranyl), 2.474(3) Å (nitrate); N-O = 1.205(6) Å (terminal), 1.268(4) Å (bridge). The anomalous scattering term f' for U measured at 0.71 Å is −10.7(2).

13. Bis[bis(pentamethylcyclopentadienyl)-ytterbium(III)]ditelluride (Publication 13)

A. Zalkin and D.J. Berg

The complex was isolated from the reaction of $Yb[C_5(CH_3)_5]_2{\cdot}O(C_2H_5)_2$ with a large excess of tellurium powder in hexane after stirring for two days at room temperature. Crystals of $[(Me_5C_5)_2Yb]_2Te_2$ are monoclinic, $P2_1/n$, with a = 15.517(3) Å, b = 10.611(2) Å, c = 13.166(3) Å, and β = 114.34(2)°; for Z = 2 the calculated density is 1.92 g/cm^3. The structure was refined to an R factor of 0.036 for 3330 $[F_2 > 2\sigma(F_2)]$ of 4560 total unique data. The Te_2^{-2} ion is on a center of symmetry and lies perpendicular to and in between the two Yb atoms (see Figure 13-1). Each Yb atom is bonded approximately tetrahedrally to two cyclopentadienyl rings centers and the Te_2^{-2} ion. Distances are: ⟨Yb-C⟩, 2.626(17) Å; ⟨Yb-Cp(centroid)⟩, 2.332(18) Å; and Te-Te, 2.7686(11) Å.

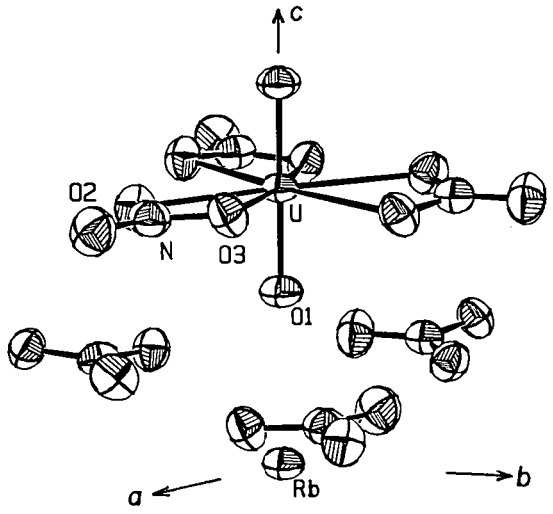

Figure 12-1. ORTEP view of the rubidium uranyl(VI) trinitrate structure with 50% probability thermal ellipsoids. Labels identify atoms in the asymteric unit. (XBL 891-69)

14. $(Me_5C_5)_2Yb(\mu\text{-}H_3B)(PMe_3)$: A Complex with a Near-Linear BH_3 Bridging Group (Publication 21)

C.J. Burns and R.A. Andersen

Addition of $(Me_5C_5)_2Yb$ to H_3BPMe_3 gives the 1:1 coordination compound, $(Me_5C_5)_2Yb(\mu\text{-}H_3B)(PMe_3)$, with BH_3 bridging the Yb and P centers so that $(Me_5C_5)_2Yb$ is a Lewis acid and the borane portion of H_3BPMe_3 is the Lewis base; the crystal structure is shown in Figure 14-1. The small perturbations upon coordination and the similarity between $(Me_5C_5)_2Yb(\mu\text{-}Me)BeC_5Me_5$, in which the hydrogen atoms on the bridging methyl group were located and refined, and $(Me_5C_5)_2Yb(\mu\text{-}H_3B)PMe_3$ strongly suggest that the CH_3- and BH_3 portions are bonded to $(Me_5C_5)_2Yb$ in a similar fashion, i.e., by way of Yb···H-B and Yb···B interactions. The BH_3 portion in the 1:1 coordination compound may be viewed in much the same way as the bridging BH_4- group (BH_3L is isolobal with BH_4- and CH_4) in metal tetrahydroborate complexes is viewed.

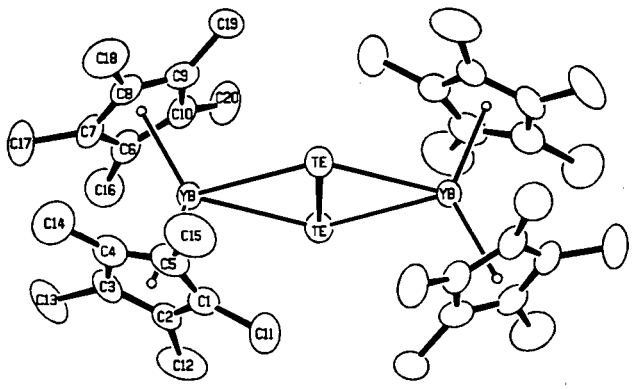

Figure 13-1. ORTEP drawing of the $Yb[C_5(CH_3)_5]_2{\cdot}O(C_2H_5)_2$ molecule; 50% probability ellipsoids. (XBL 891-58)

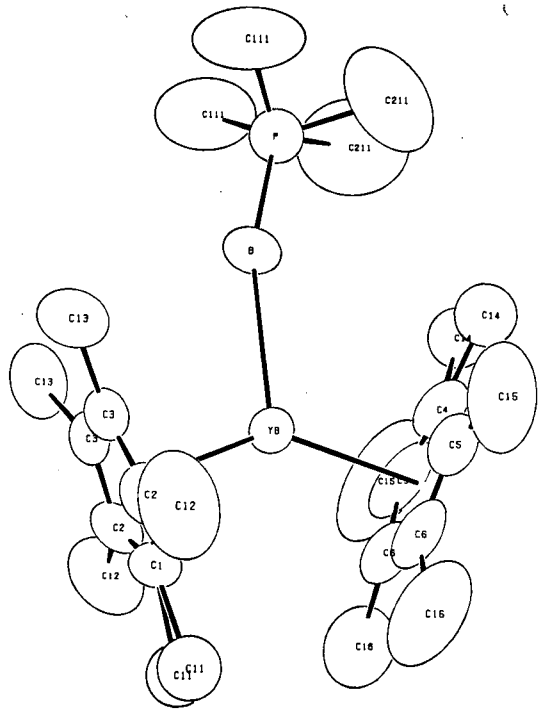

Figure 14-1. ORTEP diagram of $(Me_5C_5)_2Yb(\mu\text{-}BH_3)(PMe_3)$. (XBL 891-305)

15. Reaction of $(Me_5C_5)_2Yb$ with Fluorocarbons: Formation of $(Me_5C_5)_4Yb_2(\mu\text{-}F)$ by Intermolecular C-F Activation (Publication 20)

C.J. Burns and R.A. Andersen

Addition of C_6F_6 and other fluoroaromatics and fluoroolefins, though not C_2F_6 or 1,1,1-CF_3CH_3, to $(Me_5C_5)_2Yb$ gives the mixed-valence complex $(Me_5C_5)_4Yb_2(\mu\text{-}F)$ with a linear, asymmetric Yb(II)-F-Yb(III) bond, the structure of which is shown in Figure 15-1. The unusual intermolecular reaction of fluorocarbons with $(Me_5C_5)_2Yb$ is complex. In a qualitative sense, the C-F activation does not depend only upon the averaged C-F bond dissociation energy, since C_6F_6 (D = 154 kcal/mol) is activated whereas C_2F_6 (D = 127 kcal/mol) is not. The functional group and solvent dependence suggest that a polarizable functional group on the fluorocarbon and a vacant coordination site on the metal is necessary for efficient activation, forming perhaps a weak complex similar to the isolated molecule, $(Me_5C_5)_2Yb(\eta^2\text{-}MeC{\equiv}CMe)$. In addition, the electron affinity of the fluorocarbon and the strength of the metal-to-fluorine bond are important.

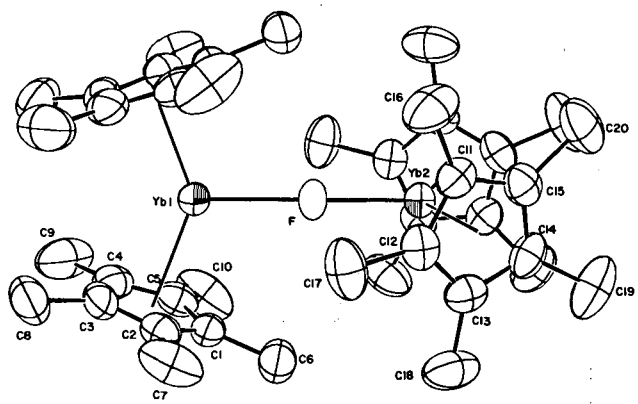

Figure 15-1. ORTEP diagram of $(Me_5C_5)_4Yb_2(\mu\text{-}F)$. The averaged Yb(1)-C distance is 2.69(2) Å, and the averaged Yb(2)-C distance is 2.58(2) Å, the Yb(1) ring-centroid distance is 2.41 Å, the Yb(2) ring-centroid distance is 2.29 Å, the ring centroid-Yb(1)-ring centroid angle is 140°, and the ring centroid-Yb(2)-ring centroid angle is 139°. (XBL 868-2899)

16. Electron-Transfer Chemistry of $(Me_5C_5)_2Yb$: Cleavage of Diorganoperoxide and Related Chalcogenides to give $(Me_5C_5)_2Yb(ER)(L)$ Where E is O, S, Se, or Te and L is a Lewis Base; Crystal Structure of $(Me_5C_5)_2Yb(TePh)(NH_3)$ (Publication 8)

D.J. Berg, R.A. Andersen, and A. Zalkin

The divalent metallocenes of ytterbium, $(Me_5C_5)_2Yb(OEt_2)$ or $(Me_5C_5)_2Yb(NH_3)_2$, react with molecules of the type REER to give the trivalent ytterbium complexes $(Me_5C_5)_2Yb(ER)(L)$, where L is OEt_2 or NH_3; E is S, Se, or Te; and R is a phenyl or substituted phenyl group. The ammonia complexes are easier to characterize than the diethyl ether complexes, since the latter complexes lose ether in the solid state and give unsatisfactory microanalytical data whereas the ammonia complexes give satisfactory elemental analyses. In addition, the line width of the Me_5C_5 protons in the ^1H NMR spectra of the diethyl ether complexes is ~500 Hz whereas the line width at half height is ~50 Hz for the ammonia complexes, consistent with the notion that the barrier to chemical exchange is higher for the ammonia complexes. The peroxides, ROOR, where R is Me_3C or Me_3Si, give the alkoxides $(Me_5C_5)_2Yb(OR)(NH_3)$, and $Et_2NC(S)SS(S)CNEt_2$ gives the known $(Me_5C_5)_2Yb(S_2CNEt_2)$. In contrast, dialkyldithiophosphinates give $(Me_5C_5)_2Yb(S_2PR_2)$ and R_2PPR_2, where R is Me or Et. The synthetic routes developed in this work are the best methods currently available for synthesis of these trivalent

species. The crystal structure of $(Me_5C_5)_2Yb(TePh)(NH_3)$ has been done. The crystals are orthorhombic, $P2_12_12_1$, with a = 11.823(3) Å, b = 25.917(6) Å, c = 8.539(2) Å, and V = 2616.5 Å. For Z = 4, the calculated density is 1.69 g/cm^3. The structure was refined by full-matrix least squares to a conventional R factor of 0.046 [4991 data, $F^2 > \sigma(F^2)$]. The Yb-Te distance is 3.039(1) Å, and the Yb-Te-C(Ph) angle is 113.0(3)°. An ORTEP drawing of $(Me_5C_5)_2Yb(TePh)(NH_3)$ is shown in Figure 16-1.

17. Electron Exchange Between Potassium Bis(t-butyl[8]annulene)ytterbate(II) and Potassium Bis(t-butyl[8]annulene)ytterbate(III) (Publication 26)

D.C. Eisenberg, S.A. Kinsley, and A. Streitwieser, Jr.

Exchange on the ^1H NMR time scale has been observed between potassium bis([8]annulene)ytterbate(II) and potassium bis([8]annulene)ytterbate(III). The absence of exchange between potassium bis([8]annulene)calcate(II) and potassium bis([8]annulene)ytterbate(III) demonstrates that the measured exchange is electron exchange rather than ligand exchange. Rates of exchange have been determined between the corresponding t-butyl derivatives, potassium bis(*t*-butyl[8]annulene)ytterbate(II) and potassium bis(*t*-butyl[8]annulene)ytterbate(III), by NMR line-broadening techniques; typical second-order rate constants are $5 \times 10^7\ M^{-1}\ sec^{-1}$ at 19.3°C in tetrahydrofuran (THF), and $1 \times 107\ M^{-1}\ sec^{-1}$ in THF containing diglyme. The enthalpy of activation is about 7 Kcal mol^{-1}, and the entropy of activation is close to zero. From these activation parameters and the effect of the more strongly solvating diglyme, a mechanism is proposed that involves change in coordination of solvating diglyme, as summarized in Figure 17-1.

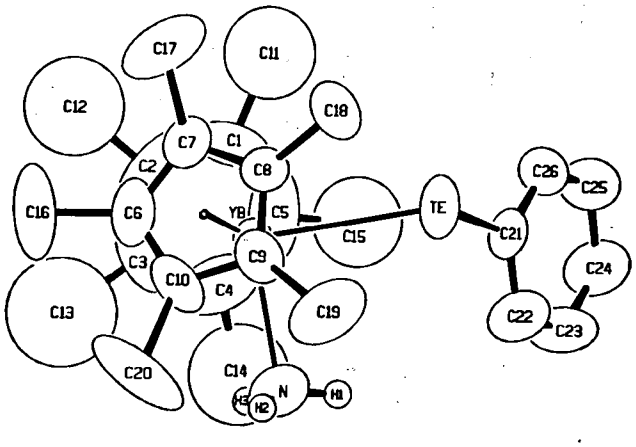

Figure 16-1. ORTEP drawing of $(Me_5C_5)_2Yb(TePh)(NH_3)$. All atoms are shown as 50% probability surfaces except those of the hydrogen atoms, which are arbitrary. The carbon atoms C1-C5 and C11-C15 are refined isotropically. (XBL 891-304)

18. 1,5-Disubstituted Cyclooctatetraenes (Publication 27)

M.H. Lyttle, A. Streitwieser, and M.J. Miller

Bulky groups in cyclooctatetraene rings have been shown earlier to confer marked air stability to uranocene derivatives. New and improved routes have been developed for the preparation of 1,5-di-t-butylcyclooctatetraene, 1B, and 1,5-diphenylcyclooctatetraene, 1P. These compounds were prepared from 1,5-cyclooctadiene in ten steps and in 11% and 1% overall yield, respectively. An alternative route gave the diphenyl compound in 10% overall yield in eight steps, but this route was

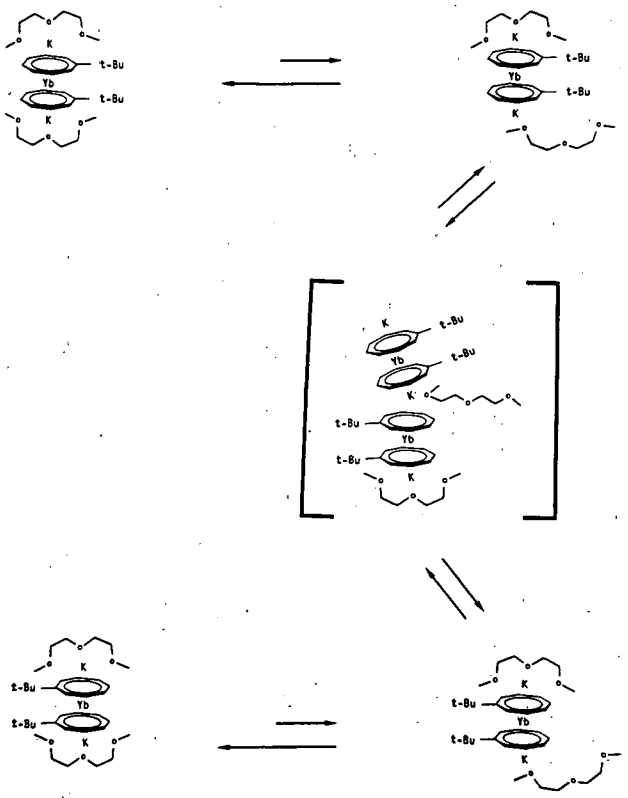

Figure 17-1. Proposed mechanism for electron transfer between [8]annulene derivatives of Yb(II) and Yb(III). (XBL 891-358)

not effective for the t-butyl derivative. Both pathways share a common, appropriately substituted intermediate, 5-phenyl-9-oxabicyclo[3.3.1.]nonan-1-o1, and 5-*t*-butyl-9-oxabicyclo[3.3.1.]nonan-1-o1. The syntheses are shown schematically in Figure 18-1. 1,1′,5,5′-tetra-*t*-butyluranocene prepared from 1B was stable to water and substantially insensitive to air.

PHYSICAL AND SPECTROSCOPIC PROPERTIES

19. Analysis of the $5f^1 \rightarrow 6d^1$ Transitions in PaX_6^{2-} (X = Cl, Br) and $Pa^{4+}/ThBr_4$ (Publication 10)

N. Edelstein, J.C. Krupa,[†] R.C. Naik,[†,‡] K. Rajnak,[§] B. Whittaker,[‖] and D. Brown[‖]

The $5f^1$ configuration is an attractive system to study because of the simplicity of its electronic spectrum. In addition, for Pa^{4+} in compounds, absorption bands due to the interconfigurational $5f^1 \rightarrow 6d^1$ occur in the visible region. Thus one has the almost unique opportunity to study the $6d^1$ configuration in a solid compound.

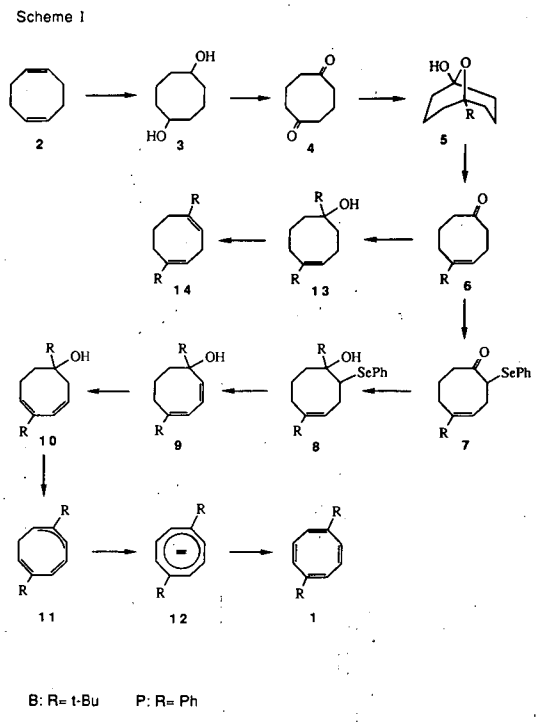

Figure 18-1. Outline of synthetic routes to 1,5-di-t-butyl- and 1,5-diphenylcyclooctatetraenes. (XBL 891-359)

The optical spectra of $Pa^{4+}/ThBr_4$ and M_2PaX_6 (M = Cs, X = Cl; M = NEt_4, X = Cl, Br) in the visible and ultraviolet ranges have been obtained and are analyzed in terms of a Hamiltonian including the crystal-field and spin-orbit interactions for the 6d configuration. A lower limit of $\sim 13800\ cm^{-1}$ is obtained for the total crystal-field splitting of PaX_6^{2-}. Spin-orbit coupling constants of $\zeta_{6d} = 2050\ cm^{-1}$ (PaX_6^{2-}) and $\zeta_{6d} = 1570\ cm^{-1}$ ($Pa^{4+}/ThBr_4$) are obtained. Figure 19-1 shows the energy-level diagram of the $5f^1$ and $6d^1$ configurations of $Pa^{4+}/ThBr_4$ and assignments of the observed fluorescent transitions. The crystal-field analyses of the $6d^1$ configuration have shown that both the crystal-field and spin-orbit coupling parameters are much smaller than might have been expected by extrapolation of the data available for the $5d^1$ systems, Ce^{3+} and $TaCl_6^{2-}$.

[†]Present address: Université de Paris-Sud, Paris, France.

[‡]Permanent address: Spectroscopy Division, Bhabha Atomic Research Center, Trombay, Bombay-400085, India.

[§]Permanent address: Kalamazoo College, Kalamazoo, MI.

[‖]Permanent address: AERE Harwell, Oxfordshire, England.

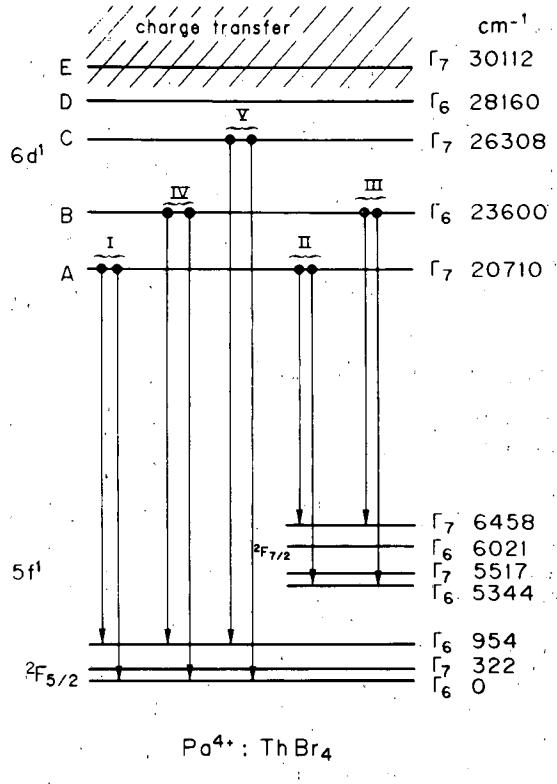

Figure 19-1. Energy levels of the $5f^1$ and $6d^1$ configurations of $Pa^{4+}/ThBr_4$ and assignments of fluorescent transitions. (XBL 883-851)

20. Optical Study and Analysis of Pu^{4+} in Single Crystals of $ZrSiO_4$ (Publication 30)

I.S. Poirot,[†] W.K. Kot, N.M. Edelstein, M.M. Abraham,[‡] C.B. Finch,[‡] and L.A. Boatner[§]

Optical spectroscopic investigations of the narrow absorption and fluorescence spectra of trivalent lanthanide and actinide ions doped in single crystals of various hosts have been studied for over 30 years. The parametric theory used to interpret these spectra has been quite successful for these ionic systems. The same theory applied to the tetravalent actinide ion U^{4+}, however, results in fits to the experimental spectra that are much worse than those found for the trivalent lanthanide or trivalent actinide ions. At the beginning of the actinide series, the 5f orbitals have their maximum spatial extension, which results in maximum covalent bonding between the metal ion and the ligands. In addition, the excited $5f^{n-1}6d^1$ configuration is close in energy relative to the $5f^n$ ground configuration, and for tetravalent ions, the crystal field due to the ligands is generally much larger than that found for trivalent ions. As the atomic number Z increases, the 5f orbitals contract and the excited $5f^{n-1}6d^1$ configuration is raised in energy relative to the ground configuration. Although the exact reasons for the relatively poor results found for the U^{4+} ion have not been established, the electronic properties of the heavier Z tetravalent actinides should be more ionic or lanthanide-like. Thus one would expect the conventional parametric theory, which works so well for the trivalent ions, to be more successful when applied to the heavier Z actinides.

Optical data have been reported and analyzed previously for the actinide ions U^{4+} and Np^{4+} diluted in $ZrSiO_4$. In this paper, the electronic structure of tetravalent plutonium incorporated as a dilute impurity in single crystals of the tetragonal host $ZrSiO_4$ has been studied using polarized optical spectroscopy. Fifty-three crystal-field levels were assigned and used to obtain a fit to a parametric Hamiltonian to within an rms deviation of 33 cm^{-1}. The resulting crystal-field parameters were similar to those obtained for the U^{4+}:$ZrSiO_4$ and Np^{4+}:$ZrSiO_4$ systems. The parametric fit improved with increasing atomic number from U^{4+} to Pu^{4+}, suggesting that the tetravalent actinides are indeed more "lanthanide-like" as the atomic number increases.

[†]Permanent address: Organization for Economic Cooperation and Development, Nuclear Energy Agency, 91191 Gif-Sur-Yvette Cedex, France.

[‡]Permanent address: Solid State Division, Oak Ridge National Laboratory, Oak Ridge, TN 37831.

21. Revisions and Additions to the Energy Levels of Neutral Cerium, ^{244}CmI (Publication 12)

J. Blaise,[†] E.F. Worden,[‡] and J.G. Conway

New spectroscopic data obtained using isotopically different samples have led to revisions and additions to the energy levels of neutral curium, ^{244}Cm I. There are now 491 odd and 432 even energy levels with J-values. Almost all the levels have isotope shifts, and many have g-values and configuration designations. Ten odd configurations and nine (one tentative) even configurations have been identified. Figure 21-1 shows the range of $^{246-244}$Cm isotope shifts observed for a number of configurations.

[†]Permanent address: Laboratoire Aimé Cotton, Centre National de la Recherche Scientifique, 91405 Orsay, France.

[‡]Permanent address: Lawrence Livermore National Laboratory, Livermore, CA 94550.

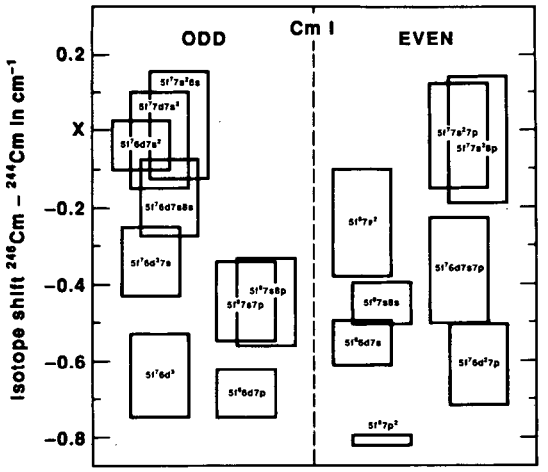

Figure 21-1. Range of observed isotope shifts for 17 electronic configurations of Cm I. The value of X is about 0.85 cm^{-1}. (XBL 891-357)

22. On the Stability and Bonding in Bis(η-arene)lanthanide Complexes (Publication 37)

D.M. Anderson,[†] F.G.N. Cloke,[†] P.A. Cox,[‡] N. Edelstein, J.C. Green,[‡] T. Pang,[†] A.A. Sameh,[†] and G. Shalimoff

Cocondensation of atoms of the lanthanide elements with 1,3,5-tri-t-butylbenzene gives the thermally stable bis(η-arene)lanthanide(0) sandwich compounds for the lanthanides Nd, Tb, Dy, Ho, Er, and Lu, thermally unstable complexes for La, Pr, and Sm, and unisolable materials for Ce, Eu, Tm, and Yb.

In considering the bonding in these compounds, $[Y(\eta\text{-}^tBu_3C_6H_3)_2]$ is taken to be the prototype molecule. In an 18-electron bis(η-arene) transition-metal sandwich complex, the highest occupied molecular orbitals (HOMOs) are the largely metal-based a_{1g} and e_{2g} orbitals. The e_{2g} electrons are more stable and more delocalized onto the arene rings than the a_{1g} electrons, and therefore the 15-electron yttrium complex is expected to have a $^3E_{2g}$ configuration. This ground state (^2E) is in accordance with the electron-spin resonance (ESR) observations and the effective magnetic moment of 1.74 B.M. Application of the same bonding model to the lanthanide complexes leads to the notion that three electrons are required to contribute to the e_{2g} orbitals in order to form a stable complex.

By analogy with the yttrium compound, it is reasonable to propose that, to a first approximation, a $4f^nd^1s^2$ (n = 0–14) configuration is required in either the ground or an easily accessible excited state of the lanthanide atom in order to form a stable bis-arene lanthanide compound. The magnetic properties of the complexes provide a testing ground for this model of their electronic structure. However, it is not easy to predict what coupling scheme should apply in such unusual compounds. The initial assumption is that the orbital angular momentum of the three e_2 electrons is quenched. Three limiting cases for interaction between the three e_2 electrons and the f electrons can be found. Table 22-1 gives the calculated and experimental values for the compounds. Cases 2 and 3 provide the same calculated values of the magnetic moments.

Examination of Table 22-1 shows that most of the experimental magnetic moments tend to lie between the two values predicted by Cases 2 and 3 and Case 1. In general, the success of these rather naive models in explaining the magnetic properties of these unusual compounds, plus the systematics of the promotion energies to the $4f^nd^1s^2$ configuration, support the proposed bonding scheme whereby three of the valence electrons of the lanthanide are involved in bonding to the arene rings and the rest remain in the f shell.

[†]Permanent address: School of Chemistry and Molecular Sciences, University of Sussex, Brighton BN1 9QJ, U.K.

[‡]Permanent address: Inorganic Chemistry Laboratory, South Parks Road, Oxford OX1J3QR, U.K.

Table 22-1
Predicted and experimental magnetic moments.

		μ(B.M.)				
Metal	Atomic Config.	Atom	Ln^{3+}	Case 1	Cases 2 & 3	Expt.
Y	d^1s^2		0	1.73	1.73	1.74
Nd	f^4s^2	2.68	3.62	4.01	2.68	1.57[a]
Gd	$f^7d^1s^2$	6.51	7.94	8.12	8.94	8.75
Tb	f^9s^2	10.64	9.7	9.87	10.74	10.69
Dy	$f^{10}s^2$	10.61	10.64	10.79	11.67	11.20
Ho	$f^{11}s^2$	9.58	10.61	10.75	11.63	10.10
Er	$f^{12}s^2$	7.56	9.58	9.74	10.61	11.00[b]
Lu	$f^{14}d^1s^2$		0	1.73	1.73	1.69

a. The value given is that at <20 K. At temperatures >200 K a value of 5.3 is found for μ.
b. The value given is that at <125 K. At temperatures >200 K a value of 9.7 is found for μ.

23. Anomalously Small 4f-5d Oscillator Strengths and 4f-4f Electronic Raman Scattering Cross Sections for Ce^{3+} in Crystals of $LuPO_4$ (Publication 33)

G.M. Williams, N. Edelstein, L.A. Boatner,[†] and M.M. Abraham[‡]

The oscillator strengths for the $4f^1 \rightarrow 5d^1$ transitions of Ce^{3+} in $LuPO_4$ were measured from absorption spectra and compared to calculated values. The energy-level diagram for Ce^{3+} ($4f^1$ and $5d^1$ configurations) is shown in Figure 23-1. The measured oscillator strengths were found to be between 2.5 to 20 times smaller than the corresponding theoretical values. In addition, absolute cross sections for electronic Raman scattering between the levels of the $4f^1$ configuration of Ce^{3+} in $LuPO_4$ were measured and found to be significantly smaller than those expected from theory. When the calculated values of the absolute cross sections were weighted empirically by the measured $4f^1 \rightarrow 5d^1$ oscillator strengths, good agreement was obtained between the experimental and calculated values, as shown in Table 23-1. Both of these discrepancies may be explained by a reduction in the radial integral, $\langle 4f|r|5d\rangle$, for Ce^{3+} in the solid state. Absorption data obtained from the literature for the $4f^1 \rightarrow 5d^1$ transitions of Ce^{3+} in a number of host crystals were used to establish an inverse correlation between the magnitude of the cerium ion-ligand distance and the reduction in the $\langle 4f|r|5d\rangle$ integral.

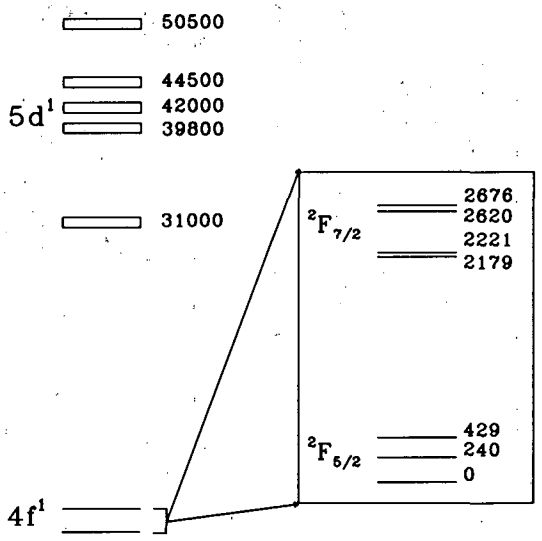

Figure 23-1. Schematic representation of the energy level structure of Ce^{3+} in a crystal of $LuPO_4$. All numbers are in cm^{-1}. (XBL 892-432)

[†]Permanent address: Solid State Division, Oak Ridge National Laboratory, Oak Ridge, TN 37831.

Table 23-1
Observed and calculated electronic Raman differential scattering cross sections for Ce^{3+} in $LuPO_4$. The values shown in the last column were obtained by empirically weighting the $\langle 4f|r|rd\rangle$ matrix element by the measured values of the $4f^1 \rightarrow 5d^1$ oscillator strengths.

	$\frac{d\sigma}{d\Omega} \times 10^{30}$, cm^2/steradian		
Transition Δ cm^{-1}	Observed	Calculated 5d wavefunctions	Calculated weighted 5d wavefunctions
240	0.3	31	2.8
429	7.4	74	7.8
2,179	3.25	20	2.9
2,221	1.9	5.3	1.9
2,620	1.35	6.7	1.9
2,676	0.55	3.5	0.5

24. Intensities of Electronic Raman Scattering Between Crystal-Field Levels of Ce^{3+} in $LuPO_4$: Nonresonant and Near Resonant Excitation (Publication 34)

G.M. Williams, P.C. Becker,† J.G. Conway, N. Edelstein, L.A. Boatner,‡ and M.M. Abraham‡

The relative intensities of the electronic Raman scattering between individual crystal-field states of the $4f^1$ configuration of Ce^{3+} in $LuPO_4$ are compared to those calculated using the standard second-order theory and also by explicitly evaluating the sum over the virtual intermediate states using the crystal-field wavefunctions for the $5d^1$ configuration. The results (Figure 24-1) show that the explicit calculation predicts the observed relative intensities much more accurately than the standard theory. In addition, a change in the incident laser energy from the argon ion green line (514.5 nm, 19429.7 cm^{-1}) to that of the frequency-tripled output of a Nd^{3+}:YAG (355 nm, 28191.5 cm^{-1}) results in enhancements of the electronic Raman scattering intensities by factors on the order of 100 (see Figure 24-2). These enhancements are accurately predicted by the explicit calculation.

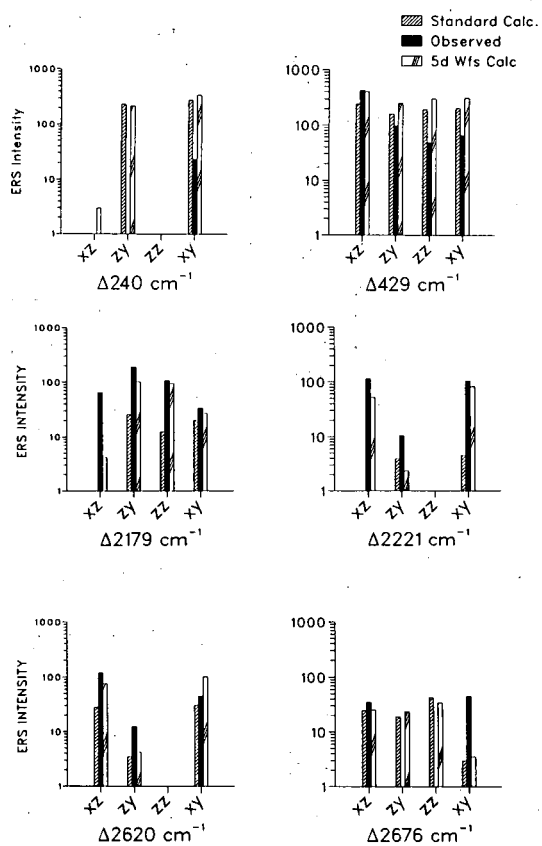

Figure 24-1. Observed electronic Raman scattering intensities for the nominally $Ce_{0.20}Lu_{0.80}PO_4$ crystal and the intensities calculated using either the standard second-order theory or by explicit evaluation of the sum over the 5d intermediate states. (XBL 892-434)

†Present address: AT&T Bell Laboratories, Murray Hill, NJ 07974.

‡Permanent address: Solid State Division, Oak Ridge National Laboratory, Oak Ridge, TN 37831.

25. The Electronic Structure of Organometallic Complexes of the f Elements—XXIII. Interpretation of the Magnetochemical and Optical Data of a Tetrahydrofuran Adduct Derived from Tris(η ^{5}cyclopentadienyl)-ytterbium(III) (Publication 29)

H.-D. Amberger,† H. Schultze,† H. Reddmann,† G.V. Shalimoff, and N.M. Edelstein

Numerous optical and magnetic studies have been performed for adducts of $Cp_3Yb{\cdot}L(Cp = \eta^5\text{-}C_5H_5)$, where L is a Lewis base. In contrast to $Cp_3Ln{\cdot}L$ (Ln = Ce−Er) compounds of the lighter lanthanides, optical spectra of $Cp_3Yb{\cdot}L$ compounds exhibit vibronic transitions with intensities comparable to the purely electronic transitions. Recently

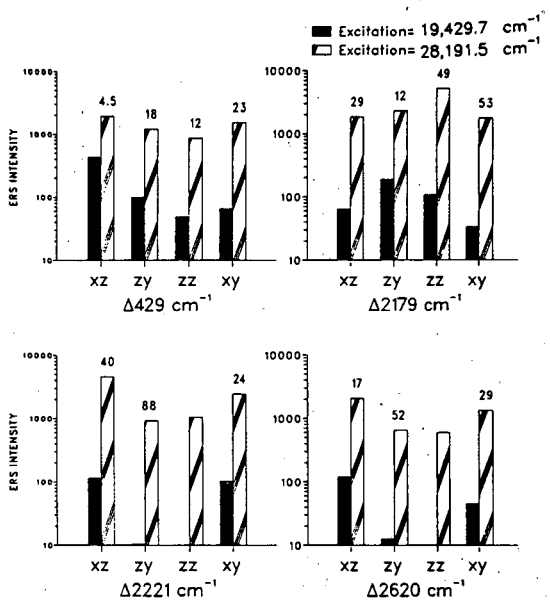

Figure 24-2. Intensities of electronic Raman scattering for the nominally $Ce_{0.20}Lu_{0.80}PO_4$ crystal excited with an argon-ion laser 514.5-nm line and the frequency-tripled output of a Nd^{3+}:YAG laser (355-nm). The numbers above the bars indicate the resonance-enhancement ratios. (XBL 892-433)

Amberger and Schultze[1] have assigned the vibronic sidebands of the hypersensitive $^4I_{9/2} \rightarrow {}^4G_{5/2}$ transition of $Cp_3Nd{\cdot}THF$ and its perdeuterated analog. They assumed comparable vibrational frequencies should be found for $Cp_3Yb{\cdot}THF$ and $(Cp\text{-}d_5)_3Yb{\cdot}THF\text{-}d_8$ and on this basis assigned the vibronic and purely electronic transitions for these molecules.

The magnetic susceptibilities of $Cp_3Yb{\cdot}L$ (L = THF, γ picoline) in the temperature range 5–300 K and the electron paramagnetic resonance spectra of these two compounds at low temperature have been measured. In this paper the assignments of Amberger and Schultze derived from the optical spectrum of $Cp_3YB{\cdot}THF$ and the new magnetic data have been used to derive preliminary values of the spin-orbit coupling constant and the crystal-field parameters for $Cp_3Yb{\cdot}L$ compounds. Given the limited data available, satisfactory fits have been obtained.

---

†Permanent address: Institüt für Anorganische und Angewandte Chemie der Universität Hamburg, D-2000 Hamburg 13, Federal Republic of Germany.

1. H.-D. Amberger and H. Schultze, Spectrochem. Acta **43A**, 1301 (1987).

1988 PUBLICATIONS AND REPORTS

Refereed Journals

1. P.H. Smith, Z.E. Reyes, C.-W. Lee, and K.N. Raymond, "Characterization of a Series of Lanthanide Amine Cage Complexes," Inorg. Chem. **27**, 4154 (1988); LBL-24530.
2. D.H. Zhu, M.J. Kappel, and K.N. Raymond, "Coordination Chemistry of Lanthanide Catecholates," Inorg. Chim. Acta **147**, 115 (1988); LBL-24690.
3. K.N. Raymond and P.H. Smith, "Biomimetic Ligands: Metal Ion Specificity and Encapsulation," Pure Appl. Chem. **8**, 1141 (1988); LBL-24810.
4. D.L. White, P.W. Durbin, N. Jeung, and K.N. Raymond, "Specific Sequestering Agents for the Actinides. 16. Synthesis and Initial Biological Testing of Polydentate Oxohydroxypyridine-carboxylate Ligands," J. Medicinal Chem. **31**, 11 (1988); LBL-21714.
5. J.L. Stewart and R.A. Andersen, "Preparation and Crystal Structure of Addition Compound $MeLi{\cdot}U[OCH(CMe_3)_2]_4$, a Compound with a Uranium to Carbon Sigma Bond," J. Chem. Soc. Chem. Comm. 1846 (1987); LBL-23513.
6. J.G. Brennan, R.A. Andersen, and A. Zalkin, "Crystal Structures of $(MeC_5H_4)_4U_2(\mu\text{-}NR)_2$. Unsymmetrical Bridging, R=Ph, and Symmetrical Bridging, R=$SiMe_3$, Organoimide Ligands in Organoactinide Compounds," J. Am. Chem. Soc. **110**, 4554 (1988); LBL-24055.
7. J.G. Brennan, S.D. Stults, R.A. Andersen, and A. Zalkin, "Crystal Structures of $(MeC_5H_4)_3M(L)$ Where M is Uranium or Cerium and L is Quinuclidine or $P(OCH_2)_3CEt$; Evidence for Uranium to Phosphorus π-Backbonding," Organometallics **7**, 1329 (1988); LBL-22025.
8. D.J. Berg, R.A. Andersen, and A. Zalkin, "Electron Transfer Chemistry of $(Me_5C_5)_2Yb$: Cleavage of Diorganoperoxide and Related Chalcogenides to Give $(Me_5C_5)_2Yb(ER)(L)$, Where E is O, S, Se, or Te and L is a Lewis Base; Crystal Structure of $(Me_5C_5)_2Yb(TePh)(NH_3)$," Organometallics **7**, 1858 (1988); LBL-24673.
9. I. Poirot, W. Kot. G. Shalimoff, N. Edelstein, M.M. Abraham, C.B. Finch, and L.A. Boatner, "Optical and EPR Investigations of $Np4^+$ in Single Crystals of $ZrSiO_4$," Phys. Rev. B **37**, 3255 (1988); LBL-23518.
10. N. Edelstein, J.C. Krupa, R.C. Naik, K. Rajnak, B. Whittaker, and D. Brown, "Analysis of the $5f^1 \rightarrow 6d^1$ Transitions in PaX_6^{2-} (X = Cl, Br) and $Pa^{4+}/ThBr_4$," Inorg. Chem. **27**, 3186 (1988); LBL-24551.
11. P.A. Tanner and N.M. Edelstein, "Infrared Luminescence Spectrum and Crystal-Field Analysis of Neodymium-Doped Yttrium Vanadate," Chem. Phys. Lett. **152**, 140 (1988); LBL-26027.
12. J. Blaise, E.F. Worden, and J.G. Conway, "Revisions and Additions to the Energy Levels of Neutral Curium, ^{244}Cm I," J. Opt. Soc. Am. B **5**, 2093 (1988); LBL-25462.
13. A. Zalkin and D.J. Berg, "Bis[bis(pentamethylcyclopentadienyl)ytterbium(III)] Ditelluride," Acta Crystallogr. C **44**, 1488 (1988); LBL-24977.
14. A. Zalkin, J.G. Brennan, and R.A. Andersen, "Tris[bis(trimethylsilyl)amido](trimethylsilylimido)-uranium(V)," Acta Crystallogr. C **44**, 1553 (1988); LBL-24904.
15. A. Zalkin and S.M. Beshouri, "Di-m-oxo-bis{bis[bis(trimethylsilyl)cyclopentadienyl]uranium-(IV)}," Acta Crystallogr. C **44**, 1826 (1988); LBL-24978.
16. A. Zalkin, J.G. Brennan, and R.A. Andersen, "Tris(trimethylsilylcyclopentadienyl)uranium(III)," Acta Crystallogr. C **44**, 2104 (1988); LBL-21180.
17. A. Zalkin, A.L. Stuart, and R.A. Andersen, "Bis[bis(tert-butyl)cyclopentadienyl]uranium chloride," Acta Crystallogr. C **44**, 2106 (1988); LBL-25152.

LBL Reports

18. P.W. Durbin, D.L. White, N. Jeung, F.L. Weitl, L.C. Uhlir, E.S. Jones, F.W. Bruenger, and K.N. Raymond, "Specific Sequestering Agents for the Actinides. 18. In Vivo Chelation of $^{238}Pu(IV)$ by 3,4,3-LICAM(C): Effects of Ligand Methylation and pH," Health Phys. J. (in press); LBL-23564.

19. P.W. Durbin, N. Jeung, S.J. Rodgers, P.N. Turowski, F.L. Weitl, D.L. White, and K.N. Raymond, "Removal of ^{238}Plutonium(IV) from Mice by Poly-Catecholate, -Hydroxamate or -Hydroxypyridininonate Ligands," Rad. Prot. and Dosimetry (in press); LBL-25626.
20. C.J. Burns and R.A. Andersen, "Reaction of $(Me_5C_5)_2Yb$ with Fluorocarbons: Formation of $(Me_5C_5)_4Yb_2(\mu\text{-}F)$ by Intermolecular C-F Activation," LBL-26006.
21. C.J. Burns and R.A. Andersen, "$(Me_5C_5)_2Yb(\mu\text{-}H_3B)(PMe_3)$: A Complex with a Near-Linear BH_3 Bridging Group," LBL-26032.
22. S.D. Stults, R.A. Andersen, and A. Zalkin, "$[Li(Me_2NCH_2CH_2NMe_2)_2][Li_2(Me_2NCH_2CH_2NMe_2]_2(\mu\text{-}\eta^5,\eta^5\text{-}MeC_5H_4)][(\eta^5\text{-}MeC_5H_4)_6U_2(\mu\text{-}Me)]_2$: A Compound with Symmetrically Bridging MeC_5H_4 and Me Groups," LBL-26155.
23. J.L. Stewart (Ph.D. Thesis), "Tris[bis(trimethylsilyl)amido]Uranium: Compounds with Tri-, Tetra-, and Penta-valent Uranium," LBL-25240.
24. S.D. Stults (Ph.D. Thesis), "Tris(cyclopentadienyl)-Cerium and Uranium: Relative Basicity, Structure, and Reactions," LBL-26124.
25. M.D. Fabiano (M.S. Thesis), "Basicity of Coordinated Ligands in Trivalent Uranium and Cerium Metallocene Complexes," LBL-26010.
26. D.C. Eisenberg, S.A. Kinsley, and A. Streitwieser, Jr., "Electron Exchange Between Dipotassium Bis([8]annulene)ytterbate(II) and Potassium Bis([8]annulene)ytterbate(III)," submitted to J. Am. Chem. Soc.; LBL-25585.
27. M.H. Lyttle, A. Streitwieser, Jr., and M.J. Miller, "1,5-Disubstituted Cyclooctatetraenes," submitted to J. Org. Chem.; LBL-26326.
28. D.C. Eisenberg (Ph.D. Thesis), "Electron Transfer in Bis([8]annulene)f-Element Systems," LBL-25834.
29. H.-D. Amberger, H. Schultze, H. Reddmann, G.V. Shalimoff, and N.M. Edelstein, "The Electronic Structure of Organometallic Complexes of the f Elements—XXIII. Interpretation of the Magnetochemical and Optical Data of a Tetrahydrofuran Adduct Derived from Tris(η^5-cyclopentadienyl)-ytterbium(III)," J. Less-Common Metals (in press); LBL-25354.
30. I.S. Poirot, W.K. Kot, N.M. Edelstein, M.M. Abraham, C.B. Finch, and L.A. Boatner, "Optical Study and Analysis of Pu^{4+} in Single Crystals of $ZrSiO_4$," submitted to Phys. Rev. B; LBL-25729.
31. X. Shangda, G.M. Williams, and N.M. Edelstein, "Contributions of the Energy Level Structure of the $4f^15d^1$ Intermediate Configuration to the Electronic Raman Scattering Intensities of $TmPO_4$," submitted to Phys. Rev. B; LBL-26122.
32. G.M. Williams (Ph.D. Thesis), "Resonance Electronic Raman Scattering in Rare-Earth Crystals," LBL-26344.
33. G.M. Williams, N.M. Edelstein, L.A. Boatner, and M.M. Abraham, "Anomalously Small 4f–5d Oscillator Strengths and 4f–4f Electronic Raman Scattering Cross Sections for Ce^{3+} in Crystals of $LuPO_4$," LBL-26348.
34. G.M. Williams, P.C. Becker, J.G. Conway, N.M. Edelstein, L.A. Boatner, and M.M. Abraham, "Intensities of Electronic Raman Scattering Between Crystal-Field Levels of Ce^{3+} in $LuPO_4$: Non-Resonant and Near Resonant Excitation," LBL-26350.
35. G.M. Williams, P.C. Becker, N.M. Edelstein, L.A. Boatner, and M.M. Abraham, "Excitation Profiles of Resonance Electronic Raman Scattering from Er^{3+} in Crystals of $ErPO_4$," LBL-26351.
36. W. Kot, G. Shalimoff, N.M. Edelstein, M.M. Abraham, L.A. Boatner, and C.B. Finch, "Electron Paramagnetic Resonance Study and the Zero-Field Splitting of Cm^{3+} in Single Crystals of $LuPO_4$," LBL-26347abs.
37. D.M. Anderson, F.G.N. Cloke, P.A. Cox, N. Edelstein, J.C. Green, T. Pang, A.A. Sameh, and G. Shalimoff, "On the Stability and Bonding in Bis(η-arene)lanthanide Complexes," submitted to J. Chem. Soc., Chem. Commun.; LBL-26402.
38. A. Zalkin, L.K. Templeton, and D.H. Templeton, "Structure of Rubidium Uranyl(VI) Trinitrate," Acta Crystallogr. (in press); LBL-25869.
39. A. Zalkin and S.M. Beshouri, "Bis[bis(trimethylsilyl)-cyclopentadienyl](chloro)uranium(III)bis(2,6-dimethylphenylisocyanide)," submitted to Acta Crystallogr.; LBL-26150.
40. S.M. Beshouri and A. Zalkin, "Bis[bis(trimethylsilyl)-cyclopentadienyl](bromo)uranium(III)bis(t-butylisocyanide)," submitted to Acta Crystallogr.; LBL-26175.
41. A. Zalkin and S.M. Beshouri, "Bis[bis(trimethylsilyl)-cyclopentadienyl](chloro)uranium(III)bis(trimethylsilylcyanide)," submitted to Acta Crystallogr.; LBL-26238.
42. S.M. Beshouri and A. Zalkin, "Structure of Bis[bis-(trimethylsilyl)cyclopentadienyl](chloro)uranium(III)-[bis(t-butylisocyanide)] and Bis[bis(trimethylsilyl)cyclopentadienyl](chloro)uranium(III)bis(t-butylcyanide)," submitted to Acta Crystallogr.; LBL-26270.
43. R.K. Rosen and A. Zalkin, "Tris(methylcyclopentadienyl)uranium(III)ammonia," submitted to Acta Crystallogr.; LBL-26273.

Invited Talks

44. K.N. Raymond, "Template Synthesis of Ligands for Highly Charged Metal Cations," Joint Japan-U.S. Seminar, Miami, FL, Nov. 27, 1987.
45. K.N. Raymond, "Specific Sequestering Agents for Iron and the Actinides," Department of Chemistry, University of Colorado, Boulder, Feb. 29, 1988.
46. K.N. Raymond, "Specific Sequestering Agents for Lanthanides and Actinides," Los Alamos National Laboratory, Los Alamos, NM, Feb. 25, 1988.
47. K.N. Raymond, "Biomimetic High Oxidation State Metal Ion Sequestering Agents," Florida Conference

on Chemistry in Biotechnology, Palm Coast, FL, Apr. 26–29, 1988.

48. K.N. Raymond, "Metal Ions in Bondage—From Nature to the Unnatural," DuPont Distinguished Lecturer, Indiana University, Bloomington, Nov. 2, 1988.
49. K.N. Raymond, "Sequestration of the Lanthanide and Actinide Elements," Fisher Lecturer, Vanderbilt University, Nashville, TN, Nov. 3, 1988.
50. K.N. Raymond, "Specific Sequestering Agents for Higher Oxidation State Metal Cations—Molecular Bondage," University of California, Los Angeles, Dec. 1, 1988.
51. R.A. Andersen, "Bridging Alkyls in f-Transition Metal Chemistry," Chemistry Department, Massachusetts Institute of Technology, Cambridge, MA, Nov. 10, 1988.
52. R.A. Andersen, "Bridging Alkyls in f-Transition Metal Chemistry," Chemistry Department, Harvard University, Cambridge, MA, Nov. 11, 1988.
53. N. Edelstein, "Electronic Raman Scattering in Lanthanide Crystals with Resonant and Nonresonant Excitation," NATO Advanced Research Workshop on Selective Excitation and Activation of Lanthanide Levels in Molecules, Institut d'Etudes Scientifiques de Cargese, Corsica, June 28, 1988.
54. N. Edelstein, "Optical and Magnetic Properties of Actinide and Lanthanide Compounds," Departement de Physico-Chimie, Division d'Etudes de Separation Isotopique et de Chimie Physique, Centre d'Etudes Nucleaires de Saclay, France, July 4, 1988.
55. A. Streitwieser, "f-Element Chemistry of Cyclooctatetraene," Department of Chemistry, University of California, Berkeley, Apr. 8, 1988.
56. A. Streitwieser, "Uranocene and Related Chemistry," DOE Savannah River Laboratory, Aiken, SC, Apr. 21, 1988.
57. D.H. Templeton, "f-Prime and f-Double Prime," NSF-CNRS Seminar on Anomalous X-Ray Scattering, Bendor, France, June 16, 1988.
58. D.H. Templeton, "Scattering of Polarized X Rays," University of Lausanne, Switzerland, June 20, 1988.
59. D.H. Templeton, "Origin of X-Ray Dispersion," Annual Meeting, American Crystallographic Association, Philadelphia, PA, June 26, 1988.
60. D.H. Templeton, "The Chemistry of X-Ray Dispersion," Gilbert Newton Lewis Memorial Lecture, University of California, Berkeley, Oct. 20, 1988.
61. D.H. Templeton, "Anomalous Scattering of Polarized X Rays," Fall Meeting, Materials Research Society, Boston, MA, Nov. 30, 1988.

CHEMICAL ENGINEERING SCIENCES

High-Pressure Phase Equilibria in Hydrocarbon-Water (Brine) Systems*

John M. Prausnitz, Investigator

INTRODUCTION

Phase equilibria are required for design of efficient large-scale separation processes (e.g., distillation and extraction) in the chemical and related industries. In this context, "efficient" refers to optimum use of raw materials and to conservation of energy.

Since the variety of technologically important fluid mixtures is extremely large, it is not possible to obtain all desired equilibria from experiment. Therefore, the objective of this research is the development of molecular thermodynamics for interpretation and correlation of limited, selected phase-equilibrium data toward reliable prediction of phase equilibria for computer-aided engineering design. The correlations are expressed through semitheoretical physicochemical models. In this research, particular attention is given to those systems that are of primary interest in energy-related industries, especially those concerned with fossil fuels, aqueous mixtures containing electrolytes, fossil-fuel/water mixtures, agricultural products, and mixtures encountered in biotechnology.

Development of molecular thermodynamics calls for a combination of theoretical computations and experimental work. Further, it demands simultaneous awareness first, of progress in molecular science and second, of realistic requirements for engineering design.

*This work was supported by the Director, Office of Energy Research, Office of Basic Energy Sciences, Chemical Sciences Division, of the U.S. Department of Energy under Contract No. DE-AC03-76SF00098.

1. Correlation of Liquid Heat Capacities for Fossil Fuels Using Characterization Data (Publication 1)

P.A. Rodgers, A. L. Creagh, and J.M. Prausnitz

Heat capacities for liquid fossil-fuel fractions are correlated as a function of characterization data. The correlation uses molecular weight from freezing-point-depression or gel-permeation-chromatography measurements, molar hydrogen-to-carbon ratio from elemental analysis, hydrogen distribution from proton nuclear-magnetic-resonance data, and, if available, number of methyl, hydroxyl, primary amine, and secondary amine groups per molecule from infrared spectroscopy. The correlation is established for temperatures below 500 K using characterization data for 118 pure hydrocarbons; the average deviation from experiment is 2.3%. When the correlation is used to predict the heat capacities of nine petroleum fractions, the average deviation is 2.6%. Average deviations for 14 coal-derived liquids are about 6.6%, but for those liquids containing more than about 3 wt% oxygen, the average deviation is somewhat lower. For high-oxygen-containing fractions, the correlation presented here is significantly better than that of Mraw *et al.*[1]

1. S.G. Mraw, J.L. Heidman, S.-C. Hwang, and C. Tsoupoulos, Ind. Eng. Chem. Proc. Des. Dev. **23**, 577 (1984).

2. A Correlation for Thermodynamic Properties of Heavy Fossil-Fuel Fractions (Publication 8)

B.J. Schwarz and J.M. Prausnitz

A correlation is developed for calculation of thermodynamic properties of heavy fossil fuels, based on a recent version of the perturbed-hard-chain equation of state. Since the correlation does not require experimental vapor pressures or densities as input data, it is useful for heavy fossil fuels where vapor pressures and densities are difficult or impossible to

measure. For fossil-fuel fractions, equation-of-state parameters are found from approximate molecular-structure (characterization) data coupled with a calibration based on pure-component (model compound) data. Interaction parameters are given for mixtures of fossil fuels with methane, ethane, carbon dioxide, hydrogen, and hydrogen sulfide. While the correlation presented here is useful for calculating vapor-liquid equilibria, it is not intended for conventional fossil fuels, where other correlations are satisfactory. Instead, it is intended for heavy fossil fuels where conventional correlations are often not reliable and where the usual input data are often unavailable.

3. Molecular Thermodynamics of Partially Ordered Fluids: Microemulsions (Publication 4)

Y. Hu and J.M. Prausnitz

Mixtures of water, oil, and surfactant often form microemulsions where tiny drops of oil (or water) are dispersed in a matrix of water (or oil). A microemulsion is a partially ordered fluid in which the surfactant molecules exist in an oriented layer at the boundary between the continuous phase and the discontinuous phase. This work proposes a molecular thermodynamic model that is useful for calculating a variety of phase diagrams observed in microemulsion-forming systems.

The model is based on a revised form of Widom's abstract representation of a microemulsion: that representation provides a procedure for calculating essential contributions to the configurational entropy. In Widom's representation, all molecules are difunctional dumbbells such that all the hydrophilic ends are situated together in some lattice sites and all the lipophilic ends are situated together in other sites. A form of Guggenheim's quasichemical theory is used to evaluate the combinatorial contributions that correspond to Widom's picture. Chemical association of surfactant molecules and physical interactions are also taken into account. Minimization of the Gibbs energy yields a distribution function for representing micelle sizes.

Calculated ternary phase diagrams are in good agreement with experimental results. Different types of diagrams can be obtained upon changing physically significant model parameters. A study of how these parameters affect phase behavior provides insight on microemulsion stability.

4. Computational Aspects of a Noncubic Equation of State for Phase Equilibrium Calculations. Effect of Density-Dependent Mixing Rules (Publication 7)

R.J. Topliss, D. Dimitrelis, and J.M. Prausnitz

An efficient procedure is presented for solving a noncubic equation of state for density. In phase-equilibrium calculations, the costly computing step is not the density calculation but the calculation of the equation-of-state constants for the mixture. Illustrative calculations are given for high-pressure phase equilibria for hydrogen/ethane and methane/water. These calculations show the superiority of noncubic equations with density-dependent mixing rules.

5. High-Temperature Mutual Solubilities for Some Binary and Ternary Aqueous Mixtures Containing Aromatic and Chlorinated Hydrocarbons (Publication 9)

H.H. Hooper, S.M. Michel, and J.M. Prausnitz

Mutual solubilities at the three-phase equilibrium pressure have been measured for binary mixtures of water with 1,2-dichloroethane and chlorobenzene in the temperature range 75–200°C. Liquid-liquid equilibria were measured for ternary aqueous mixtures containing toluene and phenol at 150 and 200°C and for ternary aqueous mixtures containing thiophene and pyridine at 100 and 150°C. Results are given for equilibrium compositions of both liquid phases and for three-phase equilibrium pressures.

6. Extraction of Fatty-Acid Methyl Esters with Supercritical Carbon Dioxide (Publication 10)

A.H. Wu, A. Stammer, and J.M. Prausnitz

A flow apparatus was constructed to measure vapor-phase compositions of systems containing fatty-acid methyl esters as solute and supercritical carbon dioxide as solvent at 65 to 200 bar. The equilibrium cell consists of a packed bed of liquid (or solid) solute coated on an inert solid support that is commonly used in gas-chromatographic columns.

Experimental measurements were obtained for five binary systems containing methyl myristate, methyl stearate, methyl oleate, methyl linoleate, or methyl laurate. Each system was measured at 40°C and 60°C and at pressure below the critical point of the mixture. In addition. a ternary system containing carbon dioxide, methyl oleate, and methyl linoleate was measured at 40°C and 107 bar.

The measured solubility data were correlated using an equation of state that has a perturbation term of the van der Waals form and a reference system proposed by Boublik and Mansoori. A quadratic mixing rule with one binary parameter is suitable for these mixtures.

7. Correlation of Liquid-Liquid Equilibria for Some Water–Organic Liquid Systems in the Region 20–250°C (Publication 11)

H.H. Hooper, S. Michel, and J.M. Prausnitz

A group-contribution model of the UNIFAC type is used to correlate liquid-liquid equilibria for water–organic liquid systems over a wide temperature range. Good agreement with experiment is obtained using temperature-dependent water-organic interaction parameters. This correlation may be useful for engineering design for processing of fossil fuels.

8. Explicit Approximations to the Mean Spherical Approximation (MSA) for Electrolyte Systems with Unequal Ion Sizes (Publication 17)

A.H. Harvey, T.W. Copeman, and J.M. Prausnitz

A systematic investigation is presented for explicit approximations to the MSA for ionic systems with ions of different size. Solution of the exact MSA for this case requires an implicit solution for the screening parameter; that implicit feature makes it particularly undesirable for use in iterative equation-of-state calculations. This work first compares with the exact MSA solution, an approximation based on a linear mixing rule for a single effective ion size, and second, a low-ion-density approximation due to Copeman and Stein. These comparisons are for the electrostatic contributions to the Helmholtz energy, the pressure, and the chemical potentials because these quantities are of primary interest in phase-equilibrium calculations using an equation of state. Over a wide range of reduced temperatures, reduced densities, and ion-diameter ratios, the simple linear rule produces good results. However, for diameter ratios differing greatly from unity, better results are obtained at low ion densities from the method of Copeman and Stein. Comparison with published Monte Carlo data suggests that, when the MSA is used for the primitive model applied to aqueous electrolyte solutions, little error is introduced by the use of these approximations.

9. Thermodynamics of Liquid-Liquid Equilibria including the Critical Region (Publication 13)

J.J. de Pablo and J.M. Prausnitz

To obtain good representation in the liquid-liquid critical region, a semitheoretical correction is added to a conventional expression (e.g., van Laar or NRTL) for the excess Gibbs energy of a binary or ternary system along the coexistence curve. This correction is an exponential function of a suitable distance from the critical point; it is significant in the critical region but not elsewhere. In the correction function. the preexponential factor is determined from stability considerations. In the exponential argument, two parameters are determined from theoretical power laws. While the coordinates of the critical point must be known (or estimated), no phase-equilibrium data in the critical region are required to determine parameters. The correction presented here provides an excellent approximation for phase equilibria along the coexistence curve close to and remote from critical conditions. Further, the correction facilitates simultaneous representation of isothermal vapor-liquid and liquid-liquid equilibria, including the liquid-liquid critical region.

10. Molecular Thermodynamics of Aqueous Two-Phase Systems for Bioseparations (Publication 14)

R.S. King, H.W. Blanch, and J.M. Prausnitz

Aqueous polymer-polymer two-phase systems provide a powerful method for separating biomolecules by extraction. When a complex mixture of biomolecules (e.g., a fermentation broth or a solution of lysed cells) is added to such a system,

biomolecules partition uniquely between the two phases achieving separation.

A thermodynamic framework is presented for optimizing extraction performance in biological separations. First, a molecular-thermodynamic model, based on the osmotic virial equation, is proposed to describe phase equilibria for dilute aqueous mixtures containing polymers and protein. Second, experimental phase-equilibrium data (protein partition coefficients) are reported for a number of model proteins, including albumin, lysozyme, and α chymotrypsin. To interpret and correlate the experimental data, low-angle laser-light scattering (LALLS) measurements were made to determine osmotic second virial coefficients for aqueous mixtures containing polymers, proteins, salts (KCl, KH_2PO_4, and K_2SO_4 at concentrations of 50 and 100 mM), and several combinations of polymer-polymer and polymer-protein pairs. Combined with electrochemical measurements (differences in potential between the two phases and protein net charge), these data provide parameters for the model to calculate the desired phase equilibria. A comparison of calculated and experimental results indicates that the virial-equation model provides good prediction of binodals and a reliable basis for estimating infinite-dilution protein partition coefficients for biotechnical process design.

11. Work in Progress

Efforts are directed at experimental and molecular-thermodynamic studies of: (a) high-pressure vapor-liquid equilibria in multicomponent aqueous systems containing salts and common gases; (b) liquid-liquid equilibria for aqueous systems containing organic fluids; (c) high-pressure liquid-liquid equilibria in aqueous systems containing polymers, salts, and carbon dioxide; (d) solubilities and micellization of agricultural products in compressed carbon dioxide; (e) phase equilibria in aqueous mixtures containing water-soluble polymers, salts, and biomolecules; (f) enzyme-catalyzed transesterification in compressed carbon dioxide; (g) phase equilibria in the critical region of binary and ternary mixtures; and (h) phase equilibria for aqueous systems containing gels and organic solutes.

1988 PUBLICATIONS AND REPORTS

Refereed Journals

1. P.A. Rodgers, A.L. Creagh, and J.M. Prausnitz, "Correlation of Liquid Heat Capacities for Fossil Fuels Using Characterization Data," Fuel **67**, 134 (1988); LBL-22201.
2. T.W. Randolph, D.S. Clark, H.W. Blanch, and J.M. Prausnitz, "Enzymatic Oxidation of Cholesterol Aggregates in Supercritical Carbon Dioxide," Science **239**, 387 (1988).
3. B.J. Schwarz and J.M. Prausnitz, "Correlation for Thermodynamic Properties of Heavy Fossil-Fuel Fractions," Ind. Eng. Chem. Res. **27**, 882 (1988); LBL-23918.
4. Y. Hu and J.M. Prausnitz, "Molecular Thermodynamics of Partially-Ordered Fluids, Microemulsions," AIChE J. **34**, 814 (1988); LBL-24266.
5. T.W. Randolph, D.S. Clark, H.W. Blanch, and J.M. Prausnitz, "Cholesterol Aggregation and Interaction with Cholesterol Oxidase in Supercritical Carbon Dioxide," Proc. Natl. Acad. Sci. **85**, 2979 (1988).
6. E.G. de Azevedo and J.M. Prausnitz, "Effects of Molecular Size and Shape on Thermodynamic Properties of Fluid Mixtures," Fluid Phase Equilib. **41**, 109 (1988).
7. R.J. Topliss, D. Dimitrelis, and J.M. Prausnitz, "Computational Aspects of a Non-Cubic Equation of State for Phase-Equilibrium Calculations. Effect of Density-Dependent Mixing Rules," Comput. Chem. Eng. **12**, 483 (1988); LBL-22470.
8. T.W. Randolph, H.W. Blanch, and J.M. Prausnitz, "Enzyme-Catalyzed Oxidation of Cholesterol in Supercritical Carbon Dioxide," AIChE J. **34**, 1354 (1988).
9. H.H. Hooper, S. Michel, and J.M. Prausnitz, "High-Temperature Mutual Solubilities for Some Binary and Ternary Aqueous Mixtures Containing Aromatic and Chlorinated Hydrocarbons," J. Chem. Eng. Data **33**, 502 (1988); LBL-24818.
10. A. Wu, A. Stammer, and J.M. Prausnitz, "Extraction of Fatty-Acid Methyl Esters with Supercritical Carbon Dioxide," Int. Symp. on Supercritical Fluids (*Societe Francaise de Chimie*), Nice, p. 107 (1988); LBL-24201.
11. H.H. Hooper, S. Michel, and J.M. Prausnitz, "Correlation of Liquid Liquid Equilibria for Some Water-Organic Liquid Systems in the Region 20–250°C," Ind. Eng. Chem. Res. **27**, 2182 (1988); LBL-24968.

12. A.H. Harvey, T.W. Copeman, and J.M. Prausnitz, "Explicit Approximations to the Mean Spherical Approximation for Electrolyte Systems with Unequal Ion Sizes," J. Phys. Chem. **92**, 6432 (1988); LBL-24876.
13. J.J. de Pablo and J.M. Prausnitz, "Thermodynamics of Liquid-Liquid Equilibria Including the Critical Region," AIChE J. **34**, 1595 (1988); LBL-24207.
14. R.S. King, H.W. Blanch, and J.M. Prausnitz, "Molecular Thermodynamics of Aqueous Two-Phase Systems for Bioseparations," AIChE J. **34**, 1585 (1988).

Other Publications

15. J. M. Prausnitz, "Molecular Thermodynamics of Fluid Mixtures," in *Essays in Physical Chemistry* (A Source book for Physical Chemistry Teachers), W.T. Lippincott, Ed., American Chemical Society, 1988.

LBL Reports

16. D. Dimitrelis and J.M. Prausnitz, "Solubilities of N-Octadecane, Phenanthrene, and N-Octadecane/phenanthrene Mixtures in Supercritical Propane at 390 and 420 K and Pressures to 60 bar," submitted to J. Chem. Eng. Data; LBL-25528.
17. A. Wu and J.M. Prausnitz, "Fractionation of a Polydisperse Polymer Using an Anti-Solvent: Application of Continuous Thermodynamics," submitted to J. Appl. Polymer Sci.; LBL-25575.
18. J.J. de Pablo and J.M. Prausnitz, "Liquid-Liquid Equilibria Including the Critical Region. Transformation to Non-Classical Coordinates," submitted to J. Phys. Chem.; LBL-25709.
19 A.H. Harvey and J.M. Prausnitz, "The Nonadditive Hard-Sphere Mixture as a Reference System in Equation-of-State Calculations," submitted to Fluid Phase Equilib.; LBL-25823.
20 A.H. Harvey and J.M. Prausnitz, "Thermodynamics of High-Pressure Aqueous Systems Containing Gases and Salts," accepted by AIChE J.; LBL-26001.
21. G.A. Krei, A.H. Harvey, and J.M. Prausnitz, "Molecular Thermodynamics of Aqueous Solutions Containing Volatile Weak Electrolytes," submitted to Chem. Eng. Commun.; LBL-26002.
22. G.F. Chou, R.F. Forbert, and J.M. Prausnitz, "High-Pressure Vapor-Liquid Equilibria for CO_2/n-Decane, CO_2/Tetralin, CO_2/n-Decane/Tetralin at 71.1 and 104.4°," submitted to J. Chem. Eng. Data; LBL-26039.
23. G.F. Chou and J.M. Prausnitz, "A Phenomenological Correction to an Equation of State for the Critical Region," submitted to AIChE J.; LBL-26040.
24. G.F. Chou and J.M. Prausnitz, "Condensation Behavior of Natural Gas Mixtures in the Retrograde Region," LBL-26048.

Invited Talks

25. J.M. Prausnitz, "Molecular Thermodynamics for Chemical Process Design," Chemical Engineering Department, University of California at Los Angeles, Feb. 1988; Chemical Engineering Department, Clarkson University, Potsdam, NY, Apr. 1988; Chemical Engineering Department, University of Arizona, Tucson, Nov. 1988.
26. J.M. Prausnitz, "Molecular Thermodynamics for Biotechnology," German Society of Chemical Engineering, Berlin, Federal Republic of Germany, June 1988.
27. J.M. Prausnitz, "Chemical Engineering Thermodynamics: Past, Present and Future," 100th Birthday Convocation, Chemical Engineering Department, MIT, Cambridge, MA, Oct. 1988.
28. M. Prange (speaker) and J.M. Prausnitz, "Thermodynamics of Hydrophilic Gels," Chemical Engineering Department, University of Minnesota, Minneapolis, Mar. 1988.
29. G.F. Chou (speaker) and J.M. Prausnitz, "A Phenomenological Correction to an Equation-of-State for the Critical Region," AIChE Meeting, New Orleans, LA, Feb. 1988.
30. H.H. Hooper (speaker), S. Michel, and J.M. Prausnitz, "High-Temperature Mutual Solubilities of Hydrocarbons and Water," 3rd International Symposium on Solubility Phenomena, Guildford, England, Aug. 1988.
31. A. Stammer (speaker), A. Wu, and J.M. Prausnitz, "Extraction of Fatty Acid Methyl Esters with Supercritical Carbon Dioxide," International Symposium on Supercritical Fluids, Nice, France, Oct. 1988.
32. A.H. Harvey (speaker) and J.M. Prausnitz, "The Nonadditive Hard Sphere Mixture as a Reference System for Equation-of-State Calculations," National Bureau of Standards, Gaithersburg, MD, Sept. 1988.
33. A.H. Harvey (speaker) and J.M. Prausnitz, "Equation of State for Fluids Containing Electrolytes," AIChE Meeting, Washington, DC, Nov. 1988.
34. J.J. de Pablo (speaker) and J.M. Prausnitz, "Thermodynamics of Liquid-Liquid Equilibria Including the Critical Region," Exxon Research & Engineering, Annandale, NJ, Dec. 1988.

Fossil Energy

Studies of Materials Erosion in Coal Conversion and Utilization Systems*

Alan V. Levy, Investigator

INTRODUCTION

The erosion and erosion-corrosion studies have been primarily directed toward the problem of metal wastage of heat transfer tubes in fluidized bed combustors (FBCs), of both bubbling and circulating types. Cooperation with major U.S. boiler manufacturers has presented the opportunity to use bed material erodents from a number of operating FBCs that have a range of chemical and physical characteristics to determine how their variations relate to metal wastage in both laboratory and in-service exposures. The operation of laboratory erosion-corrosion test equipment to simulate the conditions in FBCs necessitated the determination of how test variables such as particle size and solids loading affected material wastage at lower particle velocities and temperatures than had been used in previous work. Based upon observations of how scales form on steels being eroded-corroded, low Cr content steel alloys were formulated with somewhat higher than normal silicon contents that demonstrated marked reductions in metal wastage. Ongoing and future research will continue in the direction of understanding how and why real materials behave as they do in simulated and real FBC environments. Increased cooperative efforts with industry are planned.

1. Behavior of Tubing Steels in FBC In-Service Testing (Publication 14)

G.Q. Geng

The metal wastage rates and mechanisms of superheater tubes in the convection pass region of commercial circulating fluidized bed combustors (CFBCs) were determined by the analysis of 2 1/4Cr-1Mo steel tubes from a CFBC secondary superheater and 1018 steel tubes from a cooler location in the primary superheater of the same CFBC. The tubes had been in service for a 4000 hour period.

It was determined that the basic metal wastage mechanism was the formation of an outer scale layer of mixed bed material and iron oxide that was eroded away in a brittle manner by the cracking and chipping of a segmented scale. The in-service behavior correlated well with laboratory tests of the same alloys at similar exposure conditions. The laboratory metal wastage rate was 1.58 μm/hr, while the in-service rate was 1.17 μm/hr. Beneath the outer scale was generally an iron oxide scale with little or no bed material in it. The composition and structure of the outer scale layer directly related to the metal wastage rate in both laboratory and in-service exposures. The means by which metal loss occurred is thought to be cation diffusion of iron atoms outward and anion diffusion of oxygen inward to form more oxide and mixed bed material–oxide scale to replace that which had been eroded from the surface.

In order to determine the relative metal wastage behavior of four candidate FBC heat exchanger tubing alloys with increasing chromium for the primary and secondary superheaters of the convection pass of a circulating fluidized bed combustor, flat specimens 2 in. long $\times$ 0.14 in. thick were tack welded directly onto the tops ($\alpha = 90°$) and sides ($\alpha = 30°$) of superheater tube shields in an operating CFBC. One group of 20 specimens was exposed for 950 hours and another for 1885 hours. After exposure the metal wastage was measured and microscopic observations of the specimens' surfaces and cross sections were made. It was found that the metal wastage decreased with increasing chromium content of the alloys no matter which location the specimens occupied in the convection pass region, how long they were exposed, or how high the exposure temperature was. The performance characteristics of the tubing steels tested were affected by factors that included their location, temperature, duration of exposure, and the characteristics of the FBC particles.

2. The Erosion-Corrosion of Modified Chromium Steels (Publication 5)

B.Q. Wang

Low alloy steels containing 2–9% chromium and other alloying elements with either regular silicon or additional silicon content were tested at the velocities and temperatures that can occur in AFBCs, i.e., low velocity (10 m/s and 20 m/s) and low elevated

*This work was supported by the U.S. Department of Energy under DOE/FEAA 15 10 10 0, Advanced Research and Technical Development, Fossil Energy Materials Program, Work Breakdown Structure Element LBL-3, and under Contract No. DE-AC03-76SF00098.

temperatures (450°C, 650°C) using CFBC bed material as the erodent. It was determined that the particular characteristics of the scale that formed on each of the alloys affected the metal wastage that occurred. The low chromium content (2–3%) steels that contained additional silicon (1.4–1.5 wt%) had markedly lower metal loss than regular silicon content steels with the same or even higher chromium content.

At the lower temperature and particle velocity, a thicker mixed bed material–iron oxide protective scale layer formed on the surface of the additional silicon steel compared to the normal silicon steel than at the higher particle temperature and velocity. It also had more bed material in it. This layer helped to protect the surface of the metal and to reduce the metal wastage.

Metallographic analysis of tested specimens showed that the metal wastage caused by erosion-corrosion of the normal silicon content steels occurred by higher loss rate spalling of the weaker scale during the test. The additional silicon content steels with the same chromium content failed by lower loss rate cracking and chipping of a stronger mixed bed material–iron oxide scale. This behavior pattern was also observed earlier on similar low chromium steels with and without additional silicon at higher test temperatures and velocities. The occurrence of the same metal wastage mechanisms at the milder test conditions that are representative of FBC environments is very promising.

3. Work in Progress

Erosivity of Particles in FBCs (G.Q. Geng)

An investigation was carried out to determine what kinds of metal loss rates and mechanisms occurred when the various types of particles in AFBCs were used as erodents in a laboratory blast nozzle type tester. Sixteen different particles were obtained from 10 different combustors; they included bed material, sand, limestone, and precipitator ash. Tests were carried out at conditions that nearly simulated those in AFBCs. It was determined that several characteristics of the particles contributed to the metal wastage that occurred. Among them were composition, shape, size, and strength. The erosion of mixed bed material–iron oxide scales that formed on the target metal surfaces was the primary mechanism of metal wastage.

The more hard/strong particles that were present in a bed material, primarily SiO_2, the greater was the amount of metal wastage that occurred. The more angular the SiO_2 in the bed material was, the more erosive was the bed material. The greater the amount of limestone in the charge and the larger the resultant CaO content of the bed material, the lower was the bed material's erosivity. When the CaO content of the bed material was low and the SiO_2 particles were angular, a thin, intermittent scale was produced that permitted the base metal to directly participate in the metal wastage process, generally resulting in a higher metal loss rate.

When bed materials are relatively high in CaO compared to SiO_2 metals, they cause relatively thick, brittle, segmented mixed bed material–iron oxide or straight bed material layers to form on the metal surface. This provides a level of protection that results in lower metal wastage rates with maximum metal loss occurring at an impact angle of $\alpha = 90°$. It was determined that there was a threshold ratio of sand to limestone, under which the protective, calcium rich layer formed and above which it was eroded off the surface relatively rapidly. The threshold ratio was affected by the erosion-corrosion test conditions, i.e., temperature, particle velocity, and impact angle.

The Effect of Particle Size and Feed Rate on Erosion (M. Liebhard)

The effects of several particle variables on the erosivity of gas-solid particle streams were determined. They included shape, mass, size, impact velocity, and feed rate. Tests were carried out at room temperature on 1018 steel using spherical shape glass beads and angular shape SiC, neither of which shattered upon impact. The range of the test variables, particularly the particle velocities, used in the investigation were considerably different from those reported in the literature. It was determined that there was a major difference in the erosivity of the spherical and angular shaped particles as a function of particle size. Spherical particles had increased erosivity with particle size to a peak, and then erosivity decreased at still larger particle sizes. Angular particles' erosivity increased with particle size to a level that became more or less constant with size at lower velocities, but increased continuously at higher velocities. Low solids loading caused more mass loss than higher solids loadings for both spherical and angular particles if the feed rate difference was large. The shape of particles was a major factor in determining their erosivity, angular particles generally being an order of magnitude more erosive than spherical particles.

1988 PUBLICATIONS AND REPORTS

Refereed Journals

1. A.V. Levy, "The Erosion of Structural Alloys, Cermets, and In-Situ Oxide Scales on Steels," Wear **127**, 31 (1988).
2. A.V. Levy, Z.R. Shui, and B.Q. Wang, "Erosion of Solid Solution Strengthened Alloys," Wear **127**, 193 (1988).
3. A.V. Levy, "The Erosion-Corrosion Behavior of Protective Coatings," Surf. Coatings Technol. **36**, 387 (1988).

Other Publications

4. A.V. Levy, Z.R. Shui, and B.Q. Wang, "The Erosivity of 600 μm Diameter AFBC Bed Material," NACE Corrosion 88, St. Louis, MO, Mar. 1988, Paper No. 145.
5. A.V. Levy and B.Q. Wang, "The Effect of Test Conditions on the Erosion-Corrosion of Alternate Low Alloy Steel Tubing Alloys," NACE Corrosion 88, St. Louis, MO, Mar. 1988, Paper No. 147.

Invited Talks

6. A.V. Levy, "The Mechanism of Erosion of Ductile Metals," People's Republic of China, Sept. 1988.
7. A.V. Levy, "The Effects of Thermal and Mechanical Hardening Treatments on Erosion Behavior of Alloys," People's Republic of China, Sept. 1988.
8. A.V. Levy, "Erosion of Brittle Materials," People's Republic of China, Sept. 1988.
9. A.V. Levy, "Erosion-Corrosion of Steels," People's Republic of China, Sept. 1988.
10. A.V. Levy, "Fluidized Bed Combustion (FBC) In-Service Erosion-Corrosion of Steels," People's Republic of China, Sept. 1988.
11. A.V. Levy, "Erodent Particles Effects on Erosion-Corrosion of Steels," People's Republic of China, Sept. 1988.
12. A.V. Levy, "Slurry Erosion," People's Republic of China, Sept. 1988.
13. B.Q. Wang, "Studies of Materials Erosion in Coal Conversion and Utilization Systems," DOE-ORNL Fossil Energy Materials Conference, Oak Ridge, TN, Aug. 1988.
14. A.V. Levy, "Erosion-Corrosion of Steels in Circulating Fluidized Bed Combustors," Babcock and Wilcox Co., Barberton, OH, June 1988.

Energy Storage Systems

ELECTROCHEMICAL ENERGY STORAGE

Lutgard C. DeJonghe, James W. Evans, Rolf H. Muller, John Newman, Philip N. Ross, Jr., and Charles W. Tobias, Investigators

Surface Morphology of Metals in Electrodeposition*

Charles W. Tobias, Investigator

INTRODUCTION

The objective of this project is to gain understanding of the partial processes and their interactions involved in the deposition and dissolution of metals by electrolysis. Of particular interest is the influence of hydrodynamic flow on electrocrystallization, and the distribution of charge-transfer rates on advancing and receding metal profiles, as determined by the electric and concentration fields in the solution, and by the kinetics of the charge-transfer reaction. Control of the morphology of metallic deposits has been traditionally effected by addition agents that interfere with the crystallization process. In energy-storage applications, however, other means may have to be employed for the control of morphology.

- Rotating-disk, rotating-cylinder, or planar electrodes in channel-type electrolyzers are used for the preparation of metal deposits on substrates with precisely defined surface topography. The genesis of surface textures is studied, using *in situ* motion-picture microphotography, videorecording, and *post mortem* examination by electron microscopy.
- Developing surface contours are simulated by solving the Laplace equation, using either the finite-difference, finite-element, or boundary-element method. The effects of transport of metal ions and additives by convective diffusion are concurrently evaluated.

*This work was supported by the Assistant Secretary of Conservation and Renewable Energy, Office of Energy Storage and Distribution, Energy Storage Division, of the U.S. Department of Energy under Contract No. DE-AC03-76SF00098.

1. Application of Video Microscopy to *in situ* Studies of Electrodeposition (Publication 4)

L. McVay, R.H. Muller, and C.W. Tobias

The development of the morphology of growing electrodeposits has not, until recently, received sufficient emphasis in electrochemical research. Part of the difficulty lies in the relative slowness of deposition processes, which often require many hours even for the formation of relatively thin layers. Observation of the deposition process *in situ*, through microscopes, over extended periods of time would place a very heavy burden on the researcher. Video recording offers a great advantage over time-lapse photography, in that the quality of images can be immediately evaluated and suitable adjustments made, as opposed to waiting for developed motion picture film after the experiment is completed.

The traveling videomicroscope built in our laboratories has several unique features that make it possible for us to study microscopic processes *in situ* in flow cells (see Figure 1-1). Three-dimensional

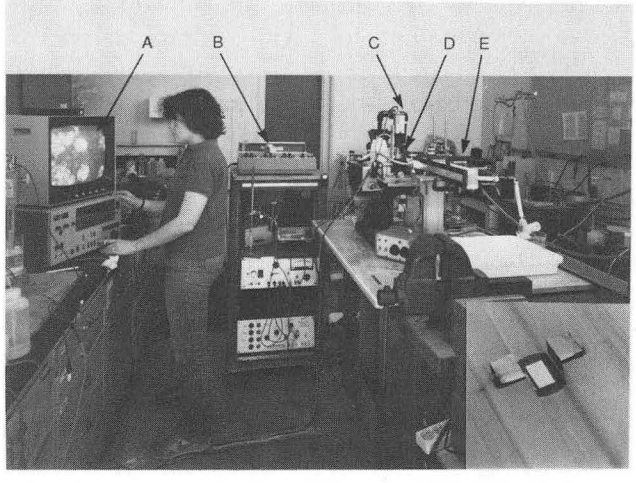

Figure 1-1. Video microscope for studies of electrodeposition in a flow cell. A: video screen showing image of developing deposit (the width of the image on the screen corresponds to 0.8 mm of the electrode surface); B: electrical instrumentation; C: video camera and microscope; D: fiber-optic illumination; E: flow channel for deposition of zinc from acid chloride solution. Inset shows electrode arrangement in the channel; placement of anodes in the side walls allows illumination and optical observation of the cathode surface. (XBB 891-535)

movement permits easy observation of any portion of the electrode surface. The traveling stage, capable of oscillatory movement, allows the simultaneous observation of extended electrode areas. This stage is very helpful in studying flow-related phenomena, as one can examine both upstream and downstream effects of perturbations in the boundary layer that are caused by protrusions in the deposit. A maximum traveling distance of more than 2 cm is possible. A dual eyepiece enables the experimenter to observe the experiment in progress, or to record still photos, without destroying the video camera's alignment. Adequate light for good-quality micrographs is provided by fiber-optic illumination.

In situ observations at high magnifications are desirable in morphological studies, yet difficulties arise because of the small working distances required by most large-magnification objective lenses. In our system, we use retrofocusing lenses in applications requiring the objective lens to be kept away from the specimen. These retrofocusing lenses have working distances up to 10 times that of a normal objective lens; thus they can be placed outside the electrochemical cell. Since the clearance between the objective lens and the specimen plane is substantially wider, thicker-gapped electrochemical cells can be employed, thereby eliminating the experimental difficulties involved in using small-gapped cells. The gap in the current cell is 3 mm; when coupled with a 2-mm optical glass window, the 50×, 5.6-mm working distance lens can be used.

The videomicroscope system is able to record the progress of deposition at magnifications up to 375×, corresponding to a video image of approximately 300 × 200 μm. A maximum magnification of 600× can be attained with a more intense light source. Using the 50×, N.A. = 0.6 long-focusing objective lens, the diffraction-limited resolution is 0.5 μm, although the actual resolution is somewhat less because a nonstandard cover-glass thickness is used. In spite of this image degradation, the video quality is still good, and videomicroscopy is a valuable resource in exploring macroscopic deposition phenomena.

2. Work in Progress

The initiation and growth mechanism of mossy zinc deposits is being investigated in a channel-type flow cell. *In situ* videomicroscopic observations, scanning electron microscopy, and transmission electron microscopy have shown that moss is generally initiated only after a substantial thickness of compact zinc is deposited, and that it usually forms around a protruding nodule. Distinctly crystalline mossy deposits are obtained in both unsaturated or saturated, flowing alkaline zincate electrolytes. Hydrodynamic models are being evaluated to account for the instability phenomena responsible for the initiation of moss. (Jointly directed with R.H. Muller)

Over considerable ranges of current densities, zinc deposited from flowing acid electrolytes forms regular striated patterns. Micropatterned electrodes with precisely defined roughness geometry have been prepared in the Berkeley microfabrication facility. These electrodes are being used as substrates in the study of the emergence and development of macroscopic morphological patterns in zinc deposits. Profiles are being evaluated using Fourier analysis; autocorrelation distances are determined to extract the characteristic frequency of striae as a function of the nature of substrate, current density, and charge passed. (Jointly directed with R.H. Muller)

Copper deposition from acid electrolyte onto a rotating-disk electrode, in the presence of thiourea, is the vehicle for the study of the role of transport of inhibitors in leveling or brightening. The flux of the inhibitor is set by the rotational rate while the flux of the cupric ions is defined by the current density. Leveling is obtained at high metal/inhibitor flux ratio, while in the reverse case the surface actually becomes rougher. The dependence of overpotential of copper deposition on this ratio allows quantitative explanation of this anomaly. The model developed earlier in this laboratory concerning the role of microscopic flows in the development of surface contour is being adapted to take into account the changing contour during electrodeposition.

Engineering Analysis of Electrolytic Gas Evolution

Charles W. Tobias, Investigator

INTRODUCTION

Electrolytic gas evolution is among the most common reaction types in electrolysis and in advanced rechargeable batteries. Modern applications in energy storage and transmission (e.g., hydrogen) require much higher energy efficiency and lower capital cost than achieved in gas-generating processes in the past. This project is directed toward the quantitative description of partial processes and their interactions involved in the nucleation, coalescence, and detachment of gas bubbles. Of special interest are the effects of moving individual bubbles and of gas-electrolyte emulsions on ohmic cell resistance and on mass transport of charged and uncharged species to and from electrode surfaces. A thorough understanding of the physical processes involved in the liberation and movement of gases at electrodes and in the electrolyte should lead to improved energy efficiency and lower capital costs in process and device technology.

1. Microscopic Resolution of Mass-Transfer Enhancement at Vertical Gas-Evolving Electrodes (Publication 3)

G.M. Whitney and C.W. Tobias

Mass-transfer enhancement by a stream of bubbles rising near a mass-transfer surface is resolved spatially and temporally, using a micromosaic electrode. The center of this electrode is sectioned into 100-μm square, coplanar elements set in a 10 by 10 array, with 2 to 5 μm gaps between segments. The electrode simulates a continuous surface but is composed of electrically isolated elements. The array is surrounded by a larger 5 by 5 mm electrode that ensures that the concentration and electric fields are linear at the segmented area.

The effect of hydrogen bubbles rising past the electrode is detected by measuring limiting currents of the reduction of ferric to ferrous sulfate at individual segments of the mosaic electrode. Bubbles are generated either in the plane of the electrode, immediately below the mosaic square (see Figure 1-1), or at the tip of a platinum wire facing the electrode at precisely known distances.

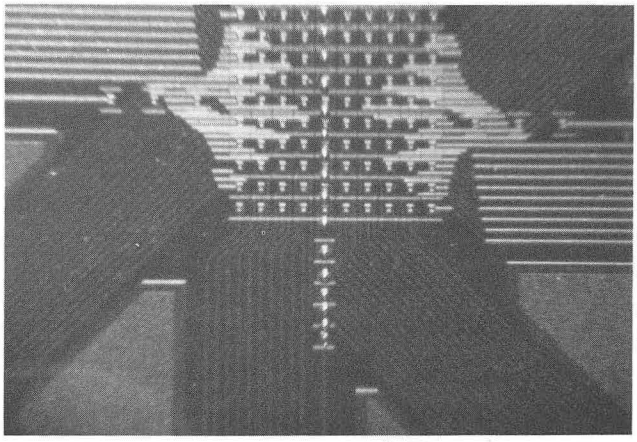

Figure 1-1. Stream of 60-μm-diameter bubbles rising parallel to vertical micromosaic electrode. Bubbles originate at a site 500 μm below the array of monitoring electrodes, at a rate of 8.5 μA. (XBC 853-2187)

The mass-transfer enhancement by bubble streams rising within the boundary layer is analyzed in terms of a modified surface-renewal theory. The enhancement, localized to a renewal path of approximately 5 bubble diameters wide, is fluctuating and intense. Mass transfer resulting from bubble streams rising outside the boundary layer receives a steady, laminar enhancement (see Figure 1-2). This case is analyzed in terms of a steadily rising column of bubbles and entrained fluid. It is concluded that the

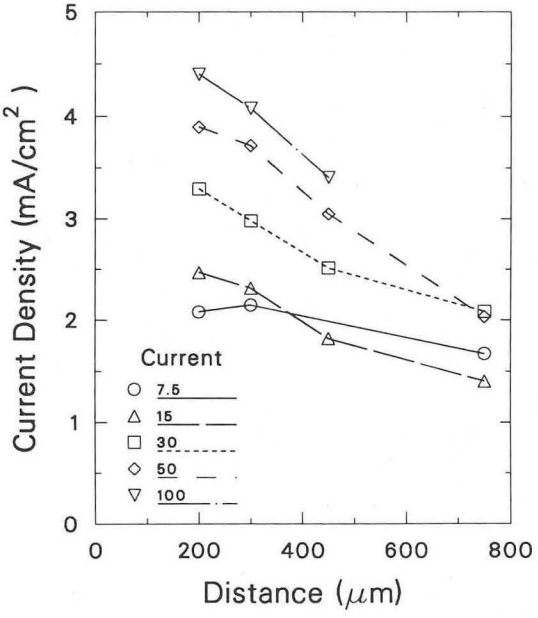

Figure 1-2. Average mass-transfer enhancement to segmented portion of the micromosaic electrode, as a function of the distance L of the bubble stream rising parallel to it, showing dependence on current used for bubble generation. (XBL 876-2605)

mass transfer due to bubble streams within the boundary layer is aided predominantly by the motion of individual bubbles that disturb the boundary layer, while enhancement caused by bubbles rising outside the boundary layer is the result of an increased velocity gradient at the mass-transfer surface.

1988 PUBLICATIONS AND REPORTS

Refereed Journals

1. G.M. Whitney and C.W. Tobias, "Mass Transfer Effects of Bubble Streams Rising Near Vertical Electrodes," AIChE J. **34**, 1981 (1988); LBL-24618.

LBL Reports

2. J.O. Dukovic and C.W. Tobias, "Simulation of Leveling in Electrodeposition," accepted by J. Electrochem. Soc.; LBL-26435.
3. G.M. Whitney, "Microscopic Resolution of Mass Transport Enhancement at Vertical Gas-Evolving Electrodes," Second International Symposium on Electrolytic Bubbles, May 31–June 1, 1988, Imperial College, London, UK; LBL-24618.
4. L. McVay, R.H. Muller, and C.W. Tobias, "Application of Video Microscopy to *in situ* Studies of Electrodeposition," LBL-26426.

Invited Talks

5. C.W. Tobias, "In Pursuit of Electrolytic Gas Evolution" and "Electrodeposition of Metals: An Old Art and a New Science," University of Trondheim, Norway, May 9–10, 1988.
6. C.W. Tobias, "Galvanizing, An Old Art or a New Science," Hungarian Chemical Society, Budapest, Hungary, May 23, 1988.
7. C.W. Tobias, "Novel Trends in Chemical Engineering Education in the USA," Technical University of Budapest, Hungary, May 25, 1988; Institute of Chemical Engineering, Veszprem, Hungary, May 20, 1988.
8. C.W. Tobias, "Technical Electrochemistry; The Engineering Side of Electrochemical Science," Hungarian National Academy of Science, Budapest, Hungary, May 26, 1988.

Surface Layers on Battery Materials*

Rolf H. Muller, Investigator

INTRODUCTION

The structure and composition of surface layers for rechargeable galvanic cells are determined in order to identify film-formation mechanisms and to find means to control film properties that result in high power density, cycle life, and energy efficiency. Anodic oxide formation and cathodic metal deposition of interest for battery applications in aqueous media are presently investigated.

Experimental measurements are centered on *in situ* optical techniques: elastic light scattering and Raman spectroscopy have recently been added to spectroscopic ellipsometry and video microscopy for the determination of structure and composition of surface layers, as has scanning tunneling microscopy. Electrochemical and *ex situ* techniques of surface analysis continue to be used. Experimental results are employed in theoretical models for the quantitative description of the formation of surface layers.

Studies on the effect of adsorbed materials on the electrocrystallition of metals and the exploration of new means to accelerate electrochemical mass transfer for high-rate metal deposition are reported under "Electrochemical Phase Boundaries."

1. *In situ* Laser Raman Spectroscopy of Copper Anodization in Alkaline Media (Publication 3)

S.T. Mayer and R.H. Muller

Anodic surface films formed on copper in 1M KOH were studied, using new Raman spectroscopy equipment. During a potential sweep, Cu_2O (633 cm^{-1}) was observed to form at the potentials of the first current peak (−350 mV vs Hg/HgO). Figure 1-1 shows the appearance of the oxide peak at 633 cm^{-1} at a potential of −350 mV. Near the second current peak (0 mV), $Cu(OH)_2$ (488 cm^{-1}) was observed to form, although CuO is thermodynamically more stable than the hydroxide. Figure 1-1 shows that the Cu_2O peak disappears only gradually as $Cu(OH)_2$ is formed. Near the anodic potential of oxygen evolution (650 mV), a broad Raman band around 550 cm^{-1} has been observed (Figure 1-2) and is proposed to result from the presence of a trivalent copper surface species. The mechanism of reduction of the different oxide species to copper metal is complex and is affected by illumination.

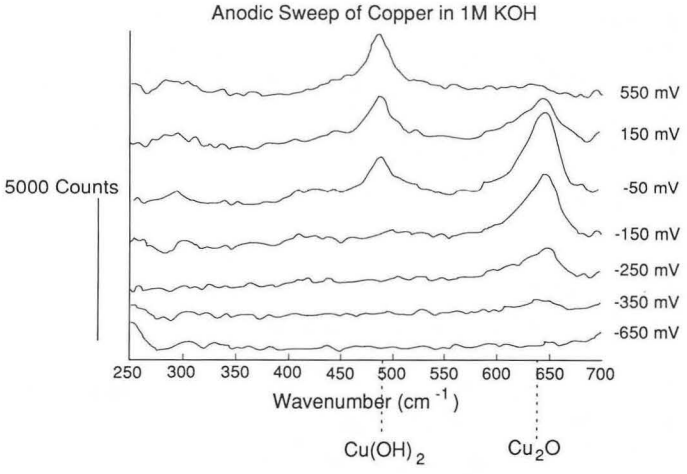

Figure 1-1. Raman spectra of a Cu electrode in 1M KOH during anodic potential sweep (1 mV/sec). Onset of Cu_2O (633 cm^{-1}) and $Cu(OH)_2$ (488 cm^{-1}) formation. Potentials vs Hg/HgO, collection time 100 sec per spectrum, successive spectra offset. (XBL 891-346)

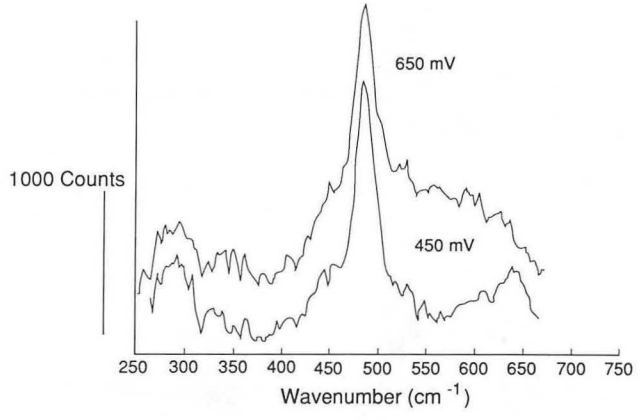

Figure 1-2. Raman spectra of a Cu electrode in 1M KOH during anodic potential sweep (1 mV/sec) near oxygen evolution. Appearance of broad peak (550 cm^{-1}) at 650 mV indicative of trivalent copper species. (XBL 891-347)

*This work was supported by the Assistant Secretary of Conservation and Renewable Energy, Office of Energy Storage and Distribution, Energy Storage Division, of the U.S. Department of Energy under Contract No. DE-AC03-76SF00098.

2. *In Situ* Scanning Tunneling Microscopy of Pb Multilayer Deposits on Ag (Publication 4)

S.T. Mayer, R.H. Muller, and P.N. Ross

The multilayer electrodeposition of Pb on evaporated polycrystalline Ag was studied using new *in situ* scanning tunneling microscopy (STM) equipment. At the onset of bulk deposition, a large number of small (50–100 Å) growth centers are seen to form at the rougher portions of the substrate (see Figure 2-1 A). The growth of these centers results in a reduction of the short-range roughness (Figure 2-1 B), and a longer-range (500 Å) waviness of the surface develops (Figure 2-1 C). Another roughening cycle is initiated by renewed nucleation (Figure 2-1 D). Amplitude density and autocorrelation functions of surface profiles have been used for the quantitative analyses of STM images. Such functions are shown in Figure 2-2 for the substrate and the four surfaces of Figure 2-1. The successive changes in the width of the distributions illustrate the repeated roughening and smoothing cycles ascribed to nucleation and growth in recessed regions of the surface.

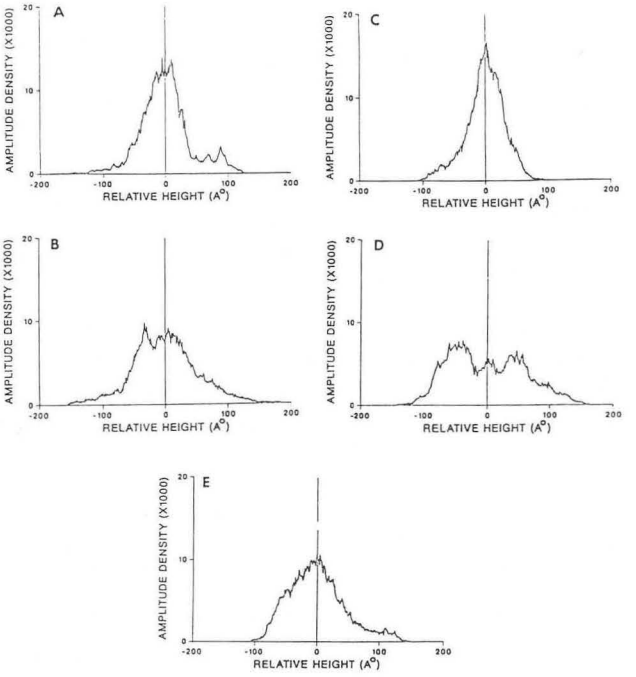

Figure 2-2. Amplitude density function of STM surface profiles during deposition of Pb on Ag at −650 mV vs Ag/AgCl. (A) substrate, (B) to (E) as in (A) to (D) of Figure 2-1. (XBL 891-76)

3. Structural Changes of Oxide Films during Anodization of p-Doped Silicon in Aqueous Ammonium Fluoride (Publication 5)

R.W. Crocker and R.H. Muller

The growth of anodic oxide layers on silicon in 0.1M NH_4F, pH 3.5, was measured by spectroscopic ellipsometry during the application of potential steps. The film grows to a steady-state thickness that increases with increasing potential, as shown in Figure 3-1 for a series of potential steps of approximately 5 min duration, separated by open-circuit periods of approximately 10 min. Surprisingly, the film does not dissolve at open circuit. Current oscillations observed above 3.0 V are therefore not caused by dissolution-limited film growth, and other models are being investigated to explain this phenomenon.

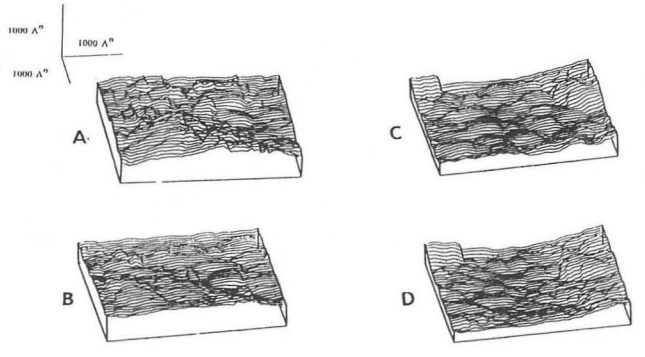

Figure 2-1. *In situ* STM line plot of the electrodeposition of Pb on Ag (evaporated on glass) from 5mM PbAc, 1M NaAc; 650 mV vs Ag/AgCl: (A) 100 sec, (B) 300 sec, (C) 1000 sec, (D) 1200 sec. (XBL 891-75)

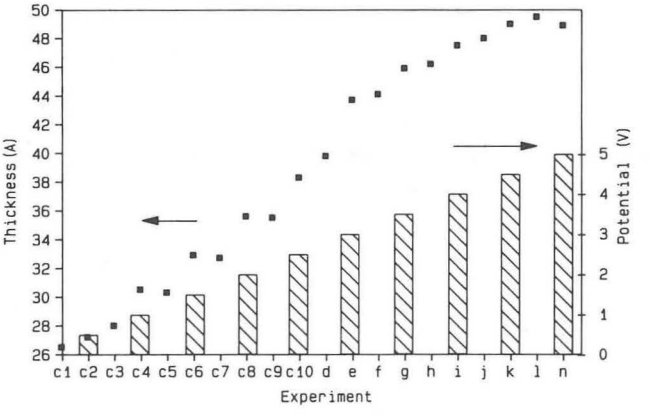

Figure 3-1. Growth of anodic oxide on silicon in acidic ammonium fluoride solution. Steady-state oxide thickness during application of repeated 5-min potential steps and during open circuit between steps. (XBL 889-3204A)

4. Work in Progress

An instrument for the *in situ* measurement of elastically scattered light from electrode surfaces has been built. Information on surface roughness is derived from the measurements. The scattered light is collected over an angle of 5° to 85° from the incident direction in 1° increments with fiber optic probes. Light-scattering measurements during the anodic oxidation of Cu showed a very small (200 Å) surface roughness, which slowly increased during growth of the Cu_2O layer, consistent with the formation of a compact film derived from ellipsometer measurements. During the formation of $Cu(OH)_2$ at greater anodic potentials, roughness is found to increase further, in agreement with the formation of hydroxide needles observed by SEM.

The early oxidation and reduction of a Cu(111) surface in KOH has been determined by spectroscopic ellipsometry to involve a compact cuprous oxide layer. The thickness of this layer is, however, only half of that expected on the basis of a charge analysis, indicating a loss due to a soluble material.

Light-scattering measurements and scanning tunneling microscopy have confirmed earlier conclusions from ellipsometer observations on the redistribution of silver oxide during the early stages of anodic film formation. A high number of small nuclei is transformed to a lesser number of large crystals during this redistribution by the action of a dissolved silver species.

The anodic oxidation of nickel, which proceeds by a solid-state diffusion mechanism, has been observed by spectroscopic ellipsometry and a prototype ellipsometer microprobe. Measurements during the conversion of $Ni(OH)_2$ to NiOOH could not be interpreted by optical models based on a uniform change of valence throughout the film. Optical changes also depend on charge and discharge rates. Domains of differing composition and thickness with transverse dimensions on a 50-μm scale have been identified in a 100-Å film.

The enhancement of mass transfer by microscopic surface irregularities in a flow field has been investigated by use of electrodes with artificial hillocks and ridges of 5 and 10 μm height, respectively, in a flow field. These protrusions mimic the effects of metal growth centers on an electrode. The morphology at zinc deposits from acidic zinc chloride solutions has been found to strongly depend on the initial surface topography (directed jointly with C.W. Tobias).

The formation of mossy, nonadherent zinc deposits from flowing alkaline electrolytes has been found to set in after a compact layer of substantial thickness (100 μm) has been formed. The abrupt change in the character of the deposit is not explained by present theories. It is initiated at protrusions in the compact layer but does not depend on the complexation of the zinc ion (directed jointly with C.W. Tobias).

1988 PUBLICATIONS AND REPORTS

Refereed Journals

1. S.T. Mayer and R.H. Muller, "Nucleation of Silver (I) Oxide Investigated by Spectroscopic Ellipsometry," J. Electrochem. Soc. **135**, 2133 (1988); LBL-23844rev.
2. H-C. Tsai, D.M. Bogy, M.K. Kundmann, D.K. Veirs, M.R. Hilton, and S.T. Mayer, "Structure and Properties of Sputtered Carbon Overcoats on Rigid Magnetic Media Disks," J. Vac. Sci. Technol. **A6**, 2307 (1988).

LBL Reports

3. S.T. Mayer and R.H. Muller, "In situ Laser Raman Spectroscopy of Copper Anodization in Alkaline Media," LBL-26453.
4. S.T. Mayer, R.H. Muller, and P.N. Ross, "In situ Scanning Tunneling Microscopy of Pb Multilayer Electrodeposits on Ag," LBL-26454.
5. R.W. Crocker and R.H. Muller, "Structural Changes of Oxide Films During Anodization of P-Doped Silicon in Aqueous Ammonium Fluoride," LBL-26064.

Electrode Kinetics and Electrocatalysis*

Philip N. Ross, Investigator

INTRODUCTION

Carbon blacks are important materials used in a variety of battery systems, and each system often makes use of a specific property of the carbon, e.g., conductivity, corrosion resistance, capacitance, catalytic activity, etc. In spite of their importance and wide use, the relation of their chemical properties to precursor and treatment history is not well understood, and considerable advancement in technologies using carbon materials appears possible. In the case of air electrodes in metal-air batteries, the carbon is used as a support for the active catalyst, i.e., to achieve and maintain high dispersion, and as a current collector, since the active catalyst may not have high bulk conductivity and may be relatively expensive and/or heavy. Thus, the unique properties of carbon of interest in this application are conductivity, surface area, and corrosion resistance. It is known that dramatic changes in structure and chemical properties occur when carbon blacks are heat-treated in an inert atmosphere at temperatures varying from 1000 to 3000°C. Heat-treatment conditions can be combined with selection of the carbon precursor to tailor the properties of the carbon black to suit the application. The particular technical challenge in air electrodes is to develop a carbon with sufficient corrosion resistance, conductivity, and surface area to meet the lifetime and performance requirements for electric-vehicle applications.

1. The Corrosion of Carbon Black Anodes in Alkaline Electrolyte: IV. Current Efficiencies for Oxygen Evolution from Metal Oxide–Impregnated Graphitized Furnace Blacks (Publication 5)

N. Staud,† H. Sokol, and P.N. Ross

A quantitative method for determining the number of oxygenated carbon atoms in a carbon black sample was developed and applied to the study of oxygen chemisorption on graphitized furnace blacks. It was found that chemisorption of oxygen atoms produced in a low-pressure microwave discharge of argon/oxygen results in the formation of an oxygen complex on every carbon atom exposed on the edge-plane surface of these carbons. These combined procedures were then used to titrate the surfaces of a variety of graphitized furnace blacks for the number of edge atoms. The corrosion rate of these carbons was found to be directly proportional to the number of sites titrated by oxygen-atom chemisorption, i.e., the number of edge atoms. The number of edge atoms exposed on the surface of graphitized furnace blacks depends on the microstructure of the precursor carbon black and the conditions of graphitization. Catalyzation of these graphitized carbons by NiO has little or no effect on their corrosion rate, which results in current efficiencies for oxygen evolution greater than 98%. The absence of an effect of NiO on the corrosion rate is attributed to the specificity of the corrosion reaction to edge-plane sites and an apparent necessity for contact between NiO particles and edge-plane carbon atoms for catalyzation of the corrosion reaction by NiO. NiO particles sitting on basal planes, which comprise at least 90% of the surface area in these carbons, catalyze only the oxygen-evolution reaction.

*This work was supported by the Assistant Secretary of Conservation and Renewable Energy, Office of Energy Storage and Distribution, Energy Storage Division, of the U.S. Department of Energy under Contract No. DE-AC03-76SF00098.

†Present address: IBM Magnetic Recording Institute, Almaden Research Center, San Jose, CA 95120-6099.

2. Work in Progress

A new study was initiated last year on modified platinum electrocatalysts for the direct oxidation of methanol in acid electrolyte. This study uses modern surface analytical methods [(e.g., low-energy electron diffraction (LEED), Auger electron spectroscopy (AES), x-ray photoelectron spectroscopy (XPS), ion scattering spectroscopy (ISS)] coupled with electrochemical methods to determine the dependence of catalytic activity on the composition and structure of modified platinum surfaces.

The best known catalysts for the direct oxidation of methanol are platinum surfaces modified by underpotential deposition (UPD) of certain adatoms, most especially tin. However, virtually all experiments with UPD catalysts were done using the potentiodynamic method, and attempts to translate the enhancement of UPD adatoms to practical electrodes operated at steady state have met with considerable difficulty. The stability of the adatom structure under steady-state conditions is questionable. We have addressed this question initially by prepar-

ing a Pt-Sn surface having Sn atoms in known atomic positions, e.g., using Pt-Sn alloy surfaces prepared by UHV methods. In the bulk-alloy structure, Sn is substituted for Pt at the corners of the unit cell. In vacuum, the surfaces of the alloy would ideally have Sn substituted in an ordered manner for Pt atoms in the surface. It is postulated that the intermetallic bonding in these substitutional positions will stabilize the Sn atoms in these positions in the surface, and that they will remain in these positions by equilibrium with stannous ions in solution.

The early results with a Pt_3Sn (100) surface have been very encouraging. LEED and AES analysis indicated that the surface has the composition and structure expected for the bulk truncation at the (100) plane, with the 50% Sn atoms substituting for every other Pt atom in the surface. The voltammetry in dilute HF, even without Sn ions in solution, indicated a reversible redox state at 0.4 V vs reversible hydrogen electrode, which is stable with time, and does not result in Sn dissolution, as confirmed by AES analysis of the emersed electrode. However, slightly more anodic potential initiates Sn dissolution from the surface concurrent with another reversible redox process, possibly involving the soluble Sn ion. It is believed that the redox state at 0.4 V is unique to the alloy surface and cannot be produced by underpotential deposition from solution. It is possible that the state can be produced on a pure Pt surface by electrodeposition of bulk Sn, then anodically stripping the bulk Sn leaving the surface alloy. This latter mechanism is still under study. It is postulated that the redox state at 0.4 V is water dissociation at the Sn atom sites to form OH, which may then react with methanol fragments (either CO or COH) adsorbed at neighboring Pt sites to form the final product CO_2. On the Sn-free surface, i.e., the pure Pt surface, there is no mechanism for removal of the methanol at 0.4 V, since OH does not form on the pure Pt surface at this potential. At more anodic potential, the Sn surface atoms are oxidized to $Sn(II)_{ads}$, with some fraction of these adsorbed ions being dissolved to form Sn(IV) in solution (probably complexed as SnF_6^{2-}). Thus, there are three redox processes on the alloy surface:

$$Sn(O) + H_2O \rightarrow Sn{-}OH + H^+ + e^-,$$

$$E_o = 0.4 \text{ V},$$

$$Sn{-}OH + H_2O \rightarrow Sn(OH)_2 + H^+ + e^-,$$

$$0.4 < E < 0.7 \text{ V},$$

$$Sn(OH)_2 + 2\,H^+ \rightarrow Sn(IV) + 2\,H_2O + 2\,e^-,$$

$$E < 0.7 \text{ V}.$$

The first and last reactions are reversible, but the middle reaction is very irreversible (does not occur cathodically), leading to an irreversible loss of Sn from the alloy surface if the potential is scanned too anodic. However, the preliminary data for methanol electro-oxidation indicate that the reaction is catalyzed by the higher (more anodic) redox states of Sn, and does not involve the unique alloy redox state at $E < 0.4$ V.

1988 PUBLICATIONS AND REPORTS

Refereed Journals

1. F.T. Wagner and P.N. Ross, "Long-Range Structural Effects in the Anomalous Voltammetry on Ultra-High Vacuum Prepared Pt(111)," J. Electroanal. Chem. **250**, 301 (1988); LBL-22488.
2. P.N. Ross and M. Sattler, "The Corrosion of Carbon Black Anodes in Alkaline Electrolyte: III. The Effect of Graphitization on the Corrosion Resistance of Furnace Blacks," J. Electrochem. Soc. **135**, 1464 (1988); LBL-22725rev.

Other Publications

3. P.N. Ross, "Long-Range Structural Effects in Anomalous Voltammetry of Pt(111)," ACS Symp. Ser. 378, The American Chemical Society, Washington, DC, 1988, Chapter 3; LBL-25050.

LBL Reports

4. P.N. Ross, "Zinc-Air Battery Design Concept for the DOE-EHP IDSEP Van," LBL-24639.
5. N. Staud, H. Sokol, and P.N. Ross, "The Corrosion of Carbon Black Anodes in Alkaline Electrolyte: IV. Current Efficiencies for Oxygen Evolution from Metal Oxide Impregnated Graphitized Furnace Blacks," J. Electrochem. Soc. (in press); LBL-26927.

Electrical and Electrochemical Behavior of Particulate Electrodes*

James W. Evans, Investigator

INTRODUCTION

This work is concerned with the use of particulate electrodes (especially zinc) in the storage of electrical energy. One of the major difficulties encountered in the use of monolithic (e.g., slablike) zinc electrodes in batteries is the change in the morphology of the electrode as the battery is cycled. For example, there is a tendency for zinc to form nodular or dendritic growths; this growth can have an impact on battery performance by forming shorts or penetrating cell diaphragms. These problems might be overcome by use of a particulate electrode where the zinc is present either as particles or as a thick coating on a particle substrate; the morphology and mechanical integrity of the particle is then of less concern.

Possible particulate electrodes are slurry electrodes (where the particles move into and out of the cell suspended in the electrolyte), fluidized-bed electrodes, moving-bed electrodes, and fixed-bed electrodes. Fluidized-bed electrodes have been extensively investigated at LBL and are suitable for charging of the particles (electrodeposition of zinc). However, they appear to be unsuitable for particle discharge (electrodissolution of zinc), and attention has shifted to a different kind of electrode. Laboratory studies with this new cell indicate a performance comparable with that of another zinc-air cell successfully developed at LBL .[1]

*This work was supported by the Assistant Secretary of Conservation and Renewable Energy, Office of Energy Storage and Distribution, Energy Storage Division, of the U.S. Department of Energy under Contract No. DE-AC03-76SF00098.

1. P.N. Ross, Jr., "Feasibility Study of a New Zinc-Air Battery Concept Using Flowing Alkaline Electrolyte," LBL-21437.

1. Fluid Flow and Mass Transport in Small Cavities (Publication 1)

J.W. Evans

Mass transport within small cavities is of technological interest in many practical activities, including battery development. Previous investigators[1] have carried out computations of the effect of fluid flow on this mass transport. Unfortunately, the generality of their results was hidden by their definition of Reynolds and Peclet numbers in terms of a velocity that is inaccessible experimentally, and obtained by calculation only with difficulty. By adopting definitions in terms of a different velocity in the present study, it became possible to recast the results in a way that is more readily used by both theoreticians and experimentalists.

1. J. Alkire, D.B. Reiser, and R.L. Sani, J. Electrochem. Soc. **131**, 2795 (1984).

2. Work in Progress

The novel zinc-air cell, which has shown good discharge performance in laboratory studies, is undergoing further development.

1988 PUBLICATIONS AND REPORTS

Refereed Journals

1. J.W. Evans, "Effect of Fluid Flow on Mass Transport within Small Cavities — A Reinterpretation of the Results of Alkire and Coworkers," J. Electrochem. Soc. **135**, 1999 (1988); LBL-24500.

Invited Talks

2. J.W. Evans, "Electrochemical Reactor Design," keynote address, 7th Australian Electrochemical Conference, Sydney, Australia, Feb. 1988.

Electrochemical Properties of Solid Electrolytes*

Lutgard C. De Jonghe, Investigator

INTRODUCTION

The goals of this research program include the definition of key factors governing the high- and intermediate-temperature performance and reliability of sodium β''-alumina electrolytes, the investigation of intermediate- and ambient-temperature alkali metal/organosulfur batteries, and fundamental electrochemical studies of the properties of organosulfur redox couples. Probably the best known and most extensively researched solid electrolyte is sodium β''-alumina; the chemical, electrochemical, and mechanical properties of this ceramic have been evaluated, both *ex situ* and *in situ*, as the separator in sodium/sulfur cells. In fact, the sodium/β''-alumina/sulfur battery, which operates at 350°C, has already achieved high energy and power density, long cycle life, and high reliability. Still, the impressive performance of these cells is offset somewhat by the technical difficulties of operating batteries at high temperatures. Accordingly, there has been a considerable amount of research effort invested in the pursuit of solid electrolyte cells operating at reduced temperatures, notably the Zebra cell and the sodium/organosulfur battery. However, in order to lower the operating temperature of solid electrolyte cells without prohibitive losses in power density, the electrical properties of the electrolyte must be suited to the temperature range chosen. Until very recently, the targeted temperature range for β''-alumina electrolyte has been 300 to 350°C, and the commercial ceramic has been engineered accordingly. It is well known that at low temperatures (ambient to 200°C), the grain-boundary resistivity of β''-alumina contributes significantly to the total resistivity of the ceramic. For high-temperature applications, the large activation energy for grain-boundary conductivity minimizes its contribution, and consequently the ceramic is optimized for mechanical strength by producing fine-grained electrolytes. However, fine-grained structures are not entirely suitable for lower-temperature applications, where the constraints for mechanical durability are not as stringent, but the requirements for conductivity are of primary importance. The grain-boundary contribution to electrolyte resistance can be controlled in two obvious ways: (1) reducing the number of grain boundaries through appropriate sintering schedules; (2) reducing the grain-boundary resistivity and/or activation energy through the addition of grain-boundary active dopants. The success of intermediate-temperature batteries based on β''-alumina electrolytes is fortunately not entirely limited by improvements in the electrolyte conductivity. Advanced cells operating in the temperature range of 100 to 200°C have two important advantages that will effect the attainable power densities with these cells. First, the above temperature range permits the use of polymeric seals such as elastomers and/or epoxies. This not only reduces the cell complexity but reduces cell weight, thereby increasing the specific power (power/weight) of the battery. Second, the diminished stresses on the solid electrolyte using these types of seals, as opposed to the rigid glass seals necessary for high-temperature operation, allow the use of electrolyte of smaller wall thickness, which lowers the total resistance of the cell and also increases its power and power density. Also, the use of polymeric seals in these types of batteries encourages the design of prismatic cells (a design that was abandoned for Na/S cells), which should bring the energy and power density to levels acceptable for commercial application.

*This work was supported by the Assistant Secretary of Conservation and Renewable Energy, Office of Energy Storage and Distribution, Energy Storage Division, of the U.S. Department of Energy under Contract No. DE-AC03-76SF00098.

1. Chemical Stability of Sodium Beta''-Alumina Electrolyte in Sulfur/Sodium Polysulfide Melts (Publication 1)

M. Liu and L.C. De Jonghe

Degradation of the electrolyte separator in the Na/β''-alumina/Na_2S_x battery is one of the major limitations determining cell reliability and useful life. There has been considerable effort in establishing the mechanism of degradation of the electrolyte in contact with the negative molten sodium electrode.[1] In 1981 De Jonghe *et al.* reported evidence of degradation of β''-alumina electrolyte in contact with sodium polysulfide melts,[2] but little was known as to the nature of the electrolyte/polysulfide melt interface and the ensuing corrosion reactions. In the present investigation, β''-alumina samples were exposed to polysulfide melts of varying composition (from Na_2S_2 to Na_2S_5 to pure sulfur) with and without impurity contamination for a period of 5 to 10 weeks, and the resulting corroded electrolytes were

examined by Auger electron spectroscopy and electron microscopy techniques. The impurities introduced to the melts included water, moist air, oxygen, Na/S battery case material, and carbon felt. Examination of the deteriorated electrolytes led to the conclusion that β''-alumina ceramics were indeed chemically attacked by Na_2S_x melts and pure sulfur at high temperatures (see Figure 1-1). The likely thermodynamic reactions for corrosion of these electrolytes were written for each set of conditions encountered in the tests. The thermodynamically stable corrosion products are Na_2SO_4, $NaAl(SO_4)_2$, $Al_2(SO_4)_3$, $NaHSO_4$, Na_2CO_3, and NaOH. Most of these compounds have high melting points and were found deposited on the electrolyte surface. The degree of corrosion of the electrolytes was found to increase with content of sulfur in the melt in going from Na_2S_x to pure sulfur. Furthermore, all of the corrosion reactions were greatly accelerated by the presence of impurities such as water, oxygen, and transition metals contained in cell casement alloys.

1. L.C. De Jonghe, L. Feldman, and A. Buechele, Solid State Ionics **5**, 267 (1981).

2. L.C. De Jonghe, L. Feldman, and A. Buechele, J. Mater. Sci. **16**, 780 (1981).

2. Sodium/Beta″-Alumina/Organosulfur Batteries Operating at Intermediate Temperatures (Publication 5)

S.J. Visco and L.C. De Jonghe

Sodium-beta″-alumina solid electrolyte is particularly well suited to intermediate-temperature applications, due to both its high ionic conductivity and low activation energy for conduction. The current

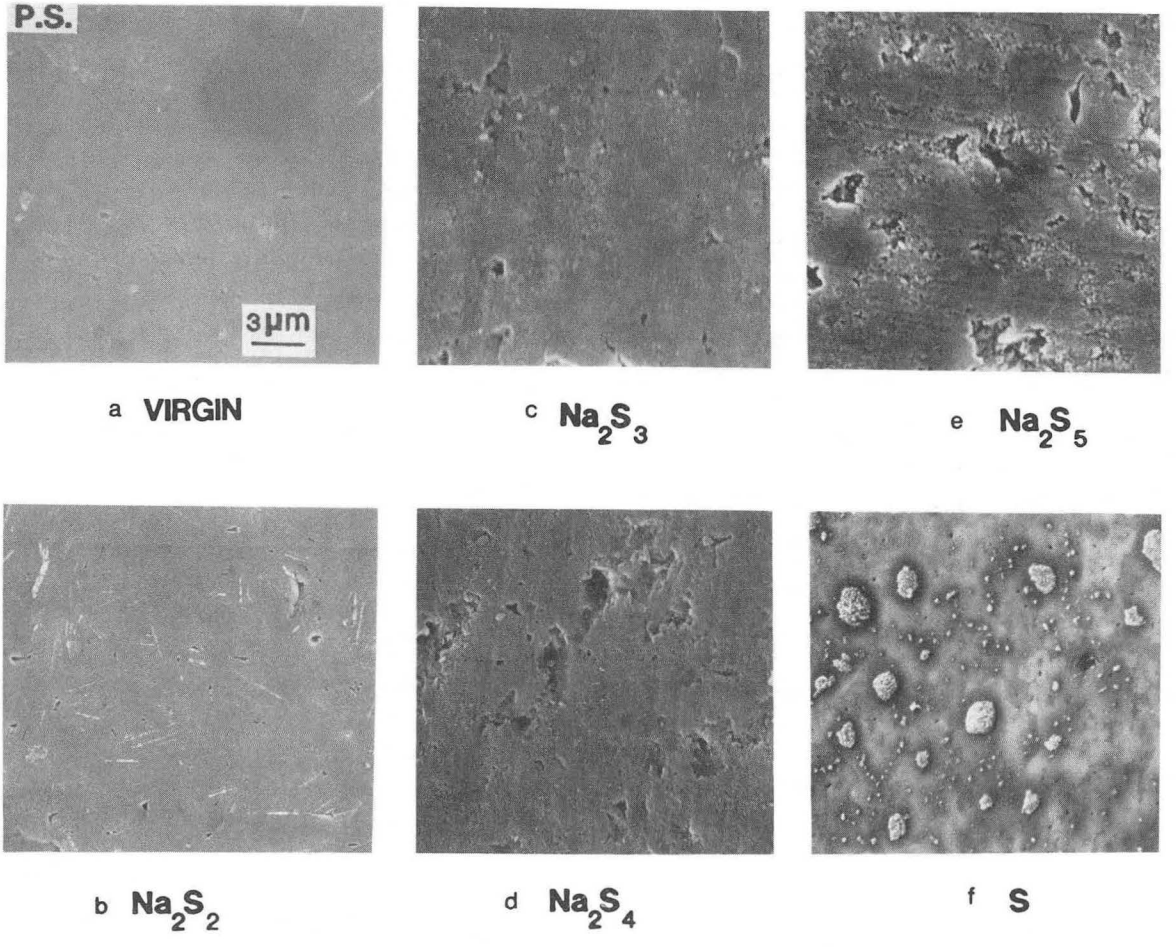

Figure 1-1. Scanning electron micrographs of the polished surface of the electrolyte before and after five weeks of immersion in sodium polysulfide melts with different compositions. (a) As-polished before immersion; (b) immersed in Na_2S_2 (350°C); (c) immersed in Na_2S_3 (400°C); (d) immersed in Na_2S_4 (400°C); (e) immersed in Na_2S_5 (400°C); (f) immersed in pure sulfur (350°C). (XBB 864-2699)

study highlights Na/β''/organosulfur cells operating in the temperature range of 100 to 130°C. The organosulfur electrodes are based on the reversible redox dimerization of thio anions to disulfides, $RSSR + 2\,e^- = 2\,RS^-$, where R is an organic moiety. The general cell reaction for a sodium-based cell using these positive electrodes is $2\,Na + RSSR = 2\,NaRS$. All the disulfide electrodes tested to date have been liquid at the cell operating temperature, but only a few of the thiolate salts have been molten at these temperatures. Consequently, the sodium thiolate salts must either be soluble in the parent disulfide up to a saturation limit,[1] or an appropriate solvent must be included in the positive electrode to facilitate complete discharge of the cell. The current study highlights Na/RSSR cells having ethereal or hydroxy-based organosulfur electrodes. Sodium/β''/hydroxyethyl disulfide cells were discharged at high rates at 120°C without the aid of solvents or other additives. However, the hydroxyethyl disulfide electrode was irreversibly polymerized by nucleophilic attack of the thio anion on the hydroxy end group and consequently did not accept full recharge. Ethoxyethyl disulfide (EEDS), $C_2H_5OCH_2CH_2SSCH_2CH_2OC_2H_5$, electrodes were also tested in Na/RSSR cells operating in the temperature range of 105 to 145°C. The pure EEDS electrodes were thermally and chemically stable but did require the addition of high-dielectric-constant/low-viscosity solvents such as dimethyl sulfoxide (DMSO) to dissolve the $NaSCH_2CH_2OC_2H_5$ salts generated on cell discharge. These cells could be cycled at reasonably high rates, but there was evidence of electrolysis and/or chemical reaction with the DMSO solvent. The dilution of DMSO with dimethyl sulfone (DMSF) served to increase the stability of the positive electrode; as the composition of the solvent in the positive electrode approached pure sulfone, the pressure rise seen with DMSO diminished to negligible levels. Although the EEDS/DMSF electrodes exhibited enhanced stability, the current denities for the Na/RSSR cells using these electrodes were lower than for the EEDS/DMSO electrodes. Consequently, studies are under way to increase EEDS electrode performance by using mixed sulfone solvent systems and/or other suitable mixed solvents.

1. M. Liu, S.J. Visco, and L.C. De Jonghe, submitted to J. Electrochem. Soc.

3. Electrochemical Investigations of Organodisulfide/Thiolate Redox Couples (Publication 4)

M. Liu, S.J. Visco, and L.C. De Jonghe

The redox behavior, kinetic reversibility, chemical reversibility and stability, and specific adsorption or chemisorption at various electrode interfaces was investigated for a homologous group of organosulfur compounds, including tetraethyl thiuram disulfide (TETD), tetramethyl thiuram disulfide (TMTD), phenyl disulfide (PDS), and fluorophenyl disulfide (FPDS), dissolved in appropriate nonaqueous solvents. Although a few cursory electrochemical experiments had been reported for thio/disulfide redox couples in nonaqueous solvents, neither the overall redox reaction nor the detailed redox mechanism for this couple had been established prior to this study. Results from chronoamperometry and/or chronocoulometry studies were combined with data obtained from rotating-disk-electrode studies to establish the number of electrons transferred in the overall redox reaction as well as the diffusion coefficients of the various electroactive materials. These parameters as derived from the experimental data are shown in Table 3-1. The culmination of the data indicated that the overall, stoichiometric reaction of these redox couples is

$$RSSR + 2\,e^- = 2\,RS^- \quad ,$$

where R represents an organic moiety. The double-pulse chronocoulometric response of all disulfides studied exhibited close adherence to the theoretical

Table 3-1
Number of electrons transferred in the electrode reaction and diffusion coefficients of RSSR species at 293 K.

	RDE + chronocoul.		RDE + chronoamp.	
Organodisulfide	n	$D \times 10^6$ (cm^2/sec)	n	$D \times 10^6$ (cm^2/sec)
TMTD	2.05	3.51	2.03	3.57
TETD	1.98	2.62	2.00	2.57
PDS	2.02	2.96	1.98	3.04
FPDS	2.10	3.29	2.10	3.32

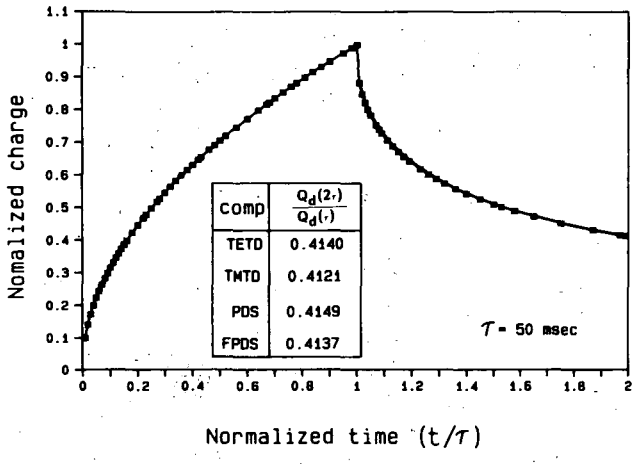

Figure 3-1. Normalized chronocoulometric response, $Q_d(t)/Q_d(\tau)$, for a group of organodisulfides in DMSO containing 0.1M tetraethylammonium perchlorate. Surface area of the microplatinum working electrode was 4×10^{-3} cm^2. The working electrode potential (vs Ag/AgCl) was stepped from a rest potential (−0.25 V) to the diffusion-limited cathodic potential (−2.1 V), then to the active anodic potential (+0.4 V), and finally back to the rest potential. The duration of these potential steps was 50 msec. (XBL 887-2484)

ratio for the total charge at t = 2τ to the charge at 1τ (τ = 50 msec), $Q_d(2\tau)/Q_d(\tau)$ = 0.414, as shown in Figure 3-1, which is a necessary condition for complete chemical reversibility. The organosulfur redox couples studied were chemically reversible, yet kinetically hindered, particularly at ambient temperatures. The microscopic reversibility of the RSSR/RS$^-$ couple ensures the validity of constructing secondary energy-storage systems based on these materials. The slow electrode kinetics observed for the couples studied, however, implies that the use of suitable electrocatalysts may improve the performance of organosulfur-based positive electrodes. This electrocatalytic effect was in fact later observed.[1] The negligible adsorption of these materials at platinum electrodes, in addition, implies that the electrode kinetics can be formulated by simple electrodic equations without consideration of surface coverage.

1. M. Liu, S.J. Visco, and L.C. De Jonghe, "Electrochemical Properties of Disulfide/Thiolate Redox Couples," accepted by J. Electrochem. Soc.; LBL-25638.

4. Work in Progress

Electrical and mechanical properties of sodium beta″-alumina electrolytes are being studied as a function of ceramic-processing conditions and dopant levels in order to optimize the polycrystalline Na^+ conductors for use at intermediate temperatures (100 to 250°C). Optimized electrolytes are targeted for a variety of intermediate-temperature cells, including the Na/β″/RSSR batteries, which operate in the range of 100 to 150°C.

1988 PUBLICATIONS AND REPORTS

Refereed Journals

1. M. Liu and L.C. De Jonghe, "Chemical Stability of Sodium Beta″-Alumina in Sulfur/Sodium Polysulfide Melts," J. Electrochem. Soc. **135**, 741 (1988); LBL-21712.
2. S.J. Visco and L.C. De Jonghe, "Ionic Conductivity of Organosulfur Melts for Advanced Storage Electrodes," J. Electrochem. Soc. **135**, 2905 (1988); LBL-24464.

Other Publications

3. S.J. Visco and L.C. De Jonghe, "Effect of R groups on Na/RSSR Battery Characteristics," in *174th Meeting Electrochem. Soc.*, Chicago, IL, Oct. 9–14, 1988, Ext. Abs. No. 76; LBL-25518.
4. M. Liu, S.J. Visco, and L.C. De Jonghe, "Electrochemical Investigations of Organodisulfide/Thiolate Redox Couples," in *174th Meeting Electrochem. Soc.*, Chicago, IL, Oct. 9–14, 1988, Ext. Abs. No. 75; LBL-25539.

LBL Reports

5. S.J. Visco and L.C. De Jonghe, "Sodium/Beta″-Alumina/Organosulfur Batteries Operating at Intermediate Temperatures," Mat. Res. Soc. Symp., Fall Meeting, 1988 (in press); LBL-26061.
6. M. Liu, S.J. Visco, and L.C. De Jonghe, "Electrochemical Properties of Disulfide/Thiolate Redox Couples," accepted by J. Electrochem. Soc.; LBL-25638.

Analysis and Simulation of Electrochemical Systems*

John Newman, Investigator

INTRODUCTION

This program involves fundamental investigations of the transport and interfacial phenomena important in electrochemical systems. Results of this work are used to analyze experimental data, to identify important system parameters, and to aid in the design and scale-up of electrochemical systems. Specific projects include the analysis of transient and steady-state transport processes in solid polymer electrolytes, mathematical modeling of the Li-Al/FeS, the Li-Al/FeS_2, and the Na/$FeCl_2$ batteries, theoretical investigations of inductance effects in high-power batteries, an investigation of the ac impedance behavior of porous electrodes, and the rigorous interpretation of cyclic voltammetry and ac impedance experiments.

1. Current Distribution near an Electrode Edge as a Primary Distribution is Approached (Publication 10)

A.C. West and J. Newman

When ohmic resistances dominate over electrode kinetic resistances, the distribution of current density on an electrode can be highly nonuniform. In the limit of zero kinetic resistance (i.e., a primary current distribution), the current density at the edge of an electrode will be infinite if the interior angle of intersection between the electrode and insulator is obtuse. In practical cases, nonzero kinetic resistances exist, and the current density remains finite.

Previous results demonstrate that, when the ohmic resistance is large compared to the kinetic resistance, the current distribution can be described by the primary distribution everywhere except the edge region. The purpose of this paper is to describe the deviations from the primary distribution and to show explicitly the manner in which the current density at the edge of the electrode approaches extreme values as the ohmic resistance becomes large.

The analysis is valid for any angle of intersection and can be applied in the edge region (for a large ohmic resistance) regardless of the geometric details of the rest of the electrochemical cell. Results are given for linear and Tafel kinetics.

2. Modeling and Optimization of Li-Alloy/Metal-Sulfide Molten-Salt Batteries (Publication 7)

A.A. Mason

An optimization of Li-Al/FeS_x molten-salt batteries is presented. The computer model uses input data from experimental test cells and is valid for prismatic cell geometries. Emphasis is placed on the negative-to-positive capacity ratio and the number of electrodes per cell. The Li-Al/FeS, Li-Al/FeS_2 (two-plateau operation), and Li-Al/FeS_2 (upper-plateau operation) battery systems are compared. While the specific energies are similar for all three systems, the specific power near the end of discharge is highest for the upper-plateau FeS_2 system.

A similar model for a multielectrode Li-Al/FeS_2 cylindrical cell (upper-plateau operation) is also presented. The effects of the positive-current collector radius, the cell height, and the number of positive electrodes on the specific energy and specific power are examined. Sufficient experimental data are not present for this geometry, so detailed conclusions are difficult to draw.

3. Determination of the Diffusion Coefficient from Impedance Data in the Low-Frequency Range (Publication 1)

B. Tribollet, W.H. Smyrl, and J. Newman

A new method is given for determining the diffusion coefficient or the Schmidt number of an electroactive species. The variation of the real part, relative to the imaginary part, of the electrochemical impedance, or of the electrohydrodynamic (EHD) impedance, at a rotating disk yields the diffusion coefficient without any assumption about the kinetics or any specific values for the electrode area or the solution concentration. This method may be used for all ordinary Schmidt number values (greater than 100).

*This work was supported by the Assistant Secretary of Conservation and Renewable Energy, Office of Energy Storage and Distribution, Energy Storage Division, of the U.S. Department of Energy under Contract No. DE-AC03-76SF00098.

4. Transference Number Calculations for Sodium Polysulfides (Publication 2)

T. Risch and J. Newman

Transference numbers for sodium cations and sulfur anions in sodium polysulfide melts are calculated from previously determined experimental data. Concentrated electrolyte theory, assuming a binary electrolyte consisting of sodium anions and sulfide cations in a neutral sulfur solvent, is used to relate the transference numbers to fundamental solution transport properties. Slopes of open-circuit potential measurements vs melt composition on sodium-sulfur cells with and without transference are used to determine the sulfur anion and sodium cation transference numbers. The transference number of sodium cations is calculated from previous experimental data for two temperatures, 573 and 633 K, and range from 0.88 to 0.93 for sodium sulfide mole fractions between 0.20 and 0.34. These values for transference numbers presented here are more accurate than previous interpretations of these data where unity sodium cation transference numbers were assumed. The results of this work are shown to be important in the design of sodium-sulfur cells.

5. The Effect of Schmidt Number on the Faradaic Impedance (Publication 6)

A.K. Hauser and J. Newman

Frequency-response analysis results calculated by a Stefan-Maxwell impedance model are presented for a copper rotating disk in chloride solutions. The algorithm accounts for multicomponent diffusion, migration, and homogeneous and heterogeneous reactions, as well as a finite Schmidt number and interfacial velocity. The validity of the model was checked by comparing its results with analytic solutions valid in the limit of dilute solutions, excess supporting electrolyte, and infinite Schmidt number. Good agreement was obtained. Results for copper dissolution are plotted in various forms, enabling easier interpretation of the system. The effect of the Schmidt number on the faradaic impedance has been examined, and an alternative way of plotting the dimensionless convective-diffusion impedance is proposed to reduce the Schmidt number dependence of the frequency response nearly to one curve by stretching the abscissa using $(\omega/\Omega)Sc^{1/3}$.

6. Work in Progress

A model that will permit the quantitative interpretation of experimental observations of solid polymer electrolytes is being developed. More specifically, the model will help in determining fundamental transport properties from transient and steady-state experiments. The effects of membrane water content and temperature on these properties will be elucidated.

A mathematical model of the $Na/FeCl_2$ battery has been developed. The model predicts the cell voltage as a function of the state of discharge and has been useful in showing porosity and volume fraction profiles and how they can affect cycle life. Mass-transfer limitations are being incorporated into the model and should permit greater agreement with experiments.

A model that uses Duhamel's theorem to simulate cyclic-voltammetry experiments at stationary and rotating-disk electrodes is being improved. The model can account for mass-transfer effects, faradaic reactions, and adsorption phenomena, which will permit the quantitative interpretation of data. In particular, it is being used to study linear sweep voltammograms of the reduction of nitrate in acidic, nickel solutions.

Inductance effects found in high-power batteries are being investigated. Results from simplified and highly idealized systems have provided insight into how a realistic model should be developed. Emphasis is placed on identifying the proper scale-up parameters and the optimum configuration for a high-power battery.

A mathematical model of the electrode/electrolyte interface is being developed to calculate the frequency response of a rotating disk. The algorithm accounts for the effect of surface coverage owing to specific adsorption and charge-transfer reactions. Double-layer theory is used to calculate the potentials at the interfacial planes and the surface excesses of all the electroactive species present in the solution. This model of the interface will be coupled with a previously developed macroscopic model accounting for convection, migration, and multicomponent diffusion in concentrated solutions, in addition to homogeneous and heterogeneous reactions.

Ring-disk electrodes are being used to investigate porous ferrous sulfate films that form during the dissolution of iron in sulfuric acid solutions. Specifically, the reaction kinetics of film dissolution and precipitation and estimates of the film thickness are being investigated.

A theoretical investigation of the growth and dissolution of salt films is under way. These films are important in a wide variety of battery systems, and it is felt that an understanding of these films is necessary to develop more quantitatively correct models. Emphasis is placed on how different growth mechanisms can influence overall battery behavior.

Laplace's equation arises in the description of many systems. Its solution is often expensive and difficult to obtain accurately. Tools are being developed that will facilitate its numerical solution. In particular, boundary-integral techniques for axisymmetric and two-dimensional geometries are being developed. Additionally, a singular-perturbation analysis, valid for fast kinetics, has been performed and will be used as a tool for verifying the accuracy of other numerical procedures.

Additional work includes an experimental and theoretical impedance study of redox reactions in porous flow-through electrodes and studies of corrosion processes, with an emphasis on developing criteria for adequate corrosion protection.

1988 PUBLICATIONS AND REPORTS

Refereed Journals

1. B. Tribollet, W.H. Smyrl, and J. Newman, "Determination of the Diffusion Coefficient from Impedance Data in the Low Frequency Range," J. Electrochem. Soc. **135**, 134 (1988).
2. T. Risch and J. Newman, "Transference Number Calculations for Sodium Polysulfides," J. Electrochem. Soc. **135**, 1715 (1988); LBL-24721.
3. D. Bernardi, E.M. Pawlikowski, and J. Newman, "Mathematical Modeling of LiAl/LiCl,KCl/FeS Cells," J. Electrochem. Soc. **135**, 2922 (1988); LBL-22265.

LBL Reports

4. A.K. Hauser and J. Newman, "Effects of Finite Rates of a Homogeneous Reaction on the Dissolution of Copper in Chloride Solutions," submitted to J. Electrochem. Soc.; LBL-25584.
5. A.K. Hauser and J. Newman, "Potential and Concentration Variations of a Reacting, Supporting Electrolyte," submitted to J. Electrochem. Soc.; LBL-25608.
6. A.K. Hauser and J. Newman, "The Effect of Schmidt Number on Faradaic Impedance," submitted to J. Electrochem. Soc.; LBL-25721.
7. A.A. Mason (M.S. Thesis), Modeling and Optimization of Li-Alloy/Metal-Sulfide Molten Salt Batteries, LBL-26159.
8. A.K. Hauser and J. Newman, "Singular Perturbation Analysis of the Faradaic Impedance of Copper Dissolution Accounting for the Effects of Finite Rates of a Homogeneous Reaction," submitted to J. Electrochem. Soc.; LBL-25706.
9. A.K. Hauser and J. Newman, "Data Reduction and Analysis of the Dissolution of Copper in Chloride Solutions," LBL-26066.
10. A.C. West and J. Newman, "Current Distribution near an Electrode Edge as a Primary Distribution is Approached," submitted to J. Electrochem. Soc.; LBL-26153.

Invited Talks

11. J. Newman, "Transport Theory for Electrolytes," Fuel Cell Workshop, U.S. Department of Energy, Morgantown, WV, Apr. 5, 1988.
12. A.K. Hauser and J. Newman, "Electrolytic Mass Transfer to a Rotating Disk in Dilute Solutions: Concentration Variations of the Reacting, Excessive Supporting Electrolyte," Atlanta meeting, The Electrochemical Society, Atlanta, GA, May 16, 1988.
13. A.K. Hauser and J. Newman, "A Macroscopic Impedance Model for a Rotating Disk Electrode: Analysis of the Dissolution of Copper in Chloride Solutions," Chicago meeting, The Electrochemical Society, Chicago, IL, Oct. 10, 1988.
14. A.C. West and J. Newman, "Effects of Nonuniform Current Distributions on the Interpretation of Kinetic Data," Chicago meeting, The Electrochemical Society, Chicago, IL, Oct. 12, 1988.

Health and Environmental Sciences

Semiconductor Materials and Devices*

Eugene E. Haller, Investigator

INTRODUCTION

The recently achieved ultrahigh purity and crystalline perfection of large germanium single crystals and, to a lesser degree, silicon and gallium arsenide single crystals have led to the discovery of a large number of novel impurity and defect complexes that exhibit energy levels in the band gap of these semiconductors. Understanding the composition and electronic structure of these novel acceptors and donors through the use of sensitive far-infrared spectroscopy techniques and radioactive tracer schemes represents one component of this research effort.

Two factors have helped in identifying the structure and composition of these novel shallow acceptors and donors: (1) unusual electronic ground-state structures with reduced symmetry, and (2) correlation with the materials involved in the crystal growth and purification, such as the crucible material (typically synthetic silica or graphite) and the ambient (typically H_2, N_2, or vacuum). One of the major findings is that atomic hydrogen plays an important role in the formation and composition of many of the new impurity complexes. Hydrogen is found to passivate donors and acceptors in Ge, Si, and GaAs. In Ge hydrogen also forms electrically active centers present at rather low concentrations ($\leq 10^{11}cm^{-3}$). The information gained through this research is of immediate use to LBL's semiconductor radiation-detector program, which originated this research.

The use of ultrapure crystals as starting material for specially doped crystals is studied in connection with the development of sensitive far-infrared photoconductors for low-photon-flux applications in outer space and neutron-transmutation-doped germanium for bolometer applications. The high ratio of intentional-dopant concentrations and residual-impurity concentrations has led to photoconductors with very high responsivity working at or close to the photon noise limits.

The close coupling between crystal synthesis and analysis has enabled us to effectively study and use these extremely pure and structurally perfect materials.

1. Study of the Fundamental Linewidths of 1S → nP Donor Transitions in Ultrapure Germanium (Publication 7)†

H. Navarro,‡ E.E. Haller, and F. Keilmann§

The fundamental linewidths of dipole transitions of donor-bound electrons in ultrapure germanium were investigated. The experiments were performed on the stress-insensitive D(H,O) donor complex, which is present in concentrations of 10^{11} cm^{-3}. Various transitions (n = 2, 3, 4, 5, and 6) were tuned with a variable magnetic field to the frequencies of several far-infrared laser lines, and the photothermal response was recorded (see Figure 1-1). The transitions 1S → 2P_ and 1S → 3P_ lead to Lorentzian lines with a full width at half maximum (FWHM) of 8.2 ± 0.4 μeV. Higher excited states produce lines

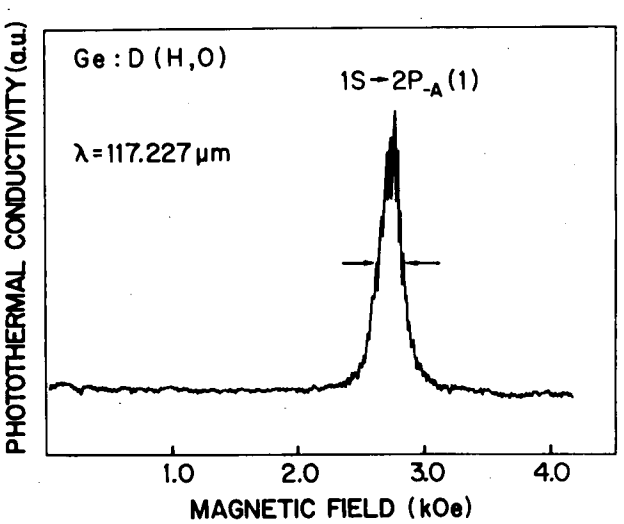

Figure 1-1. Photothermal-conductivity signal generated by a laser of indicated wavelength against the sweeping magnetic field. The arrows indicate where the linewidth was measured. The Lorentzian character of the line shows clearly. (XBL 892-541)

*This work was supported by the Director, Office of Energy Research, Office of Health and Environmental Research, U.S. Department of Energy under Contract No. DE-AC03-76SF00098, and in part by NASA Contract No. W-14,606 under Interagency Agreement with the Department of Energy.

with a FWHM of around 6.4 μeV, the narrowest lines for electronic transition ever recorded. The experiments show that the observed linewidths do not depend on the sample temperature below 9 K, the applied electric field below 1.4 eV cm^{-1}, or band-edge light. The last process creates free electrons and holes, which in turn are captured by ionized donors and acceptors. Stark broadening by random Coulomb fields from ionized impurities is thereby greatly reduced. The experimentally determined linewidths are dominated by the excited-state lifetime that results from the electron-acoustic-phonon interaction. This interaction couples the bound excited states to all the other nearby states. The excited-state lifetimes derived from the linewidths are in agreement with the values predicted by the theory of Barrie and Nishikawa.[1]

†Parts of the experiments for this work were performed at the Max-Planck-Institute for Solid State Research, Heisenbergstr. 1, D-7000 Stuttgart, Federal Republic of Germany.

‡Permanent address: Departamento de Fisica, ICUAP, Universidad Autonoma de Puebla, Apartado J-48, Pueblo, Pue. 72570, Mexico.

§Permanent address: Max-Planck-Institute for Solid State Research, D-7000 Stuttgart 80, Federal Republic of Germany.

1. R. Barrie and K. Nishikawa, Can. J. Phys. **41**, 1823 (1963); K. Nishikawa and R. Barrie, Can. J. Phys. **41**, 1135 (1963).

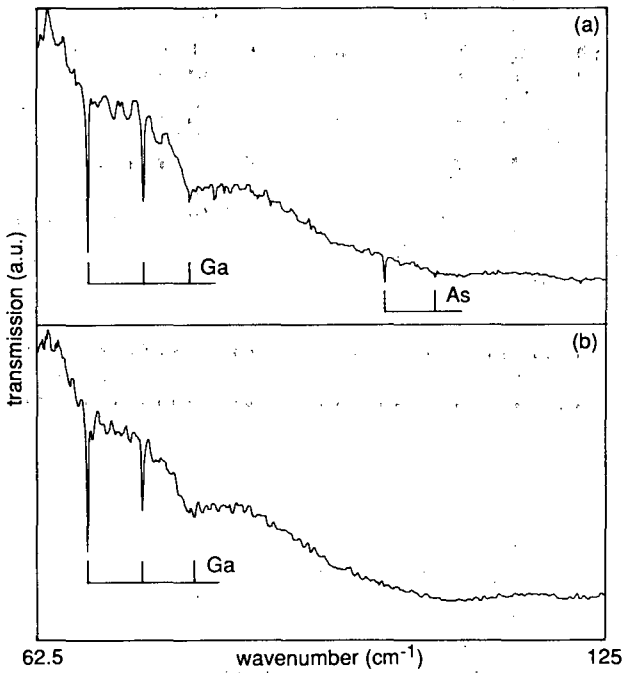

Figure 2-1. Absorption spectra of a NTD Ge sample: (a) annealed at 500°C for 1 hr; (b) unannealed. The lines of the shallow acceptor Ga are visible in both spectra and are unaffected by radiation damage. In contrast, the shallow As donors form deep-level complexes with point defects. Annealing is required to activate the As donors. (XBL 882-406)

2. Infrared Absorption Study of Neutron-Transmutation-Doped Germanium (Publication 9)

I.S. Park† and E.E. Haller

Using high-resolution far-infrared Fourier-transform absorption spectroscopy and Hall-effect measurements, we have studied the evolution of the shallow acceptor and donor impurity levels in germanium during and after the neutron-transmutation-doping process. Our results show unambiguously that the gallium acceptor-level concentration equals the concentration of transmutated Ge atoms during the entire doping process, indicating that neither recoil during transmutation nor gallium-defect complex formation play significant roles (see Figure 2-1). The arsenic donor levels appear at full concentration only after annealing for 1 hr at 450°C. We show that this is due to donor-radiation-defect complex formation. Again recoil does not play a significant role (see Figure 2-2).

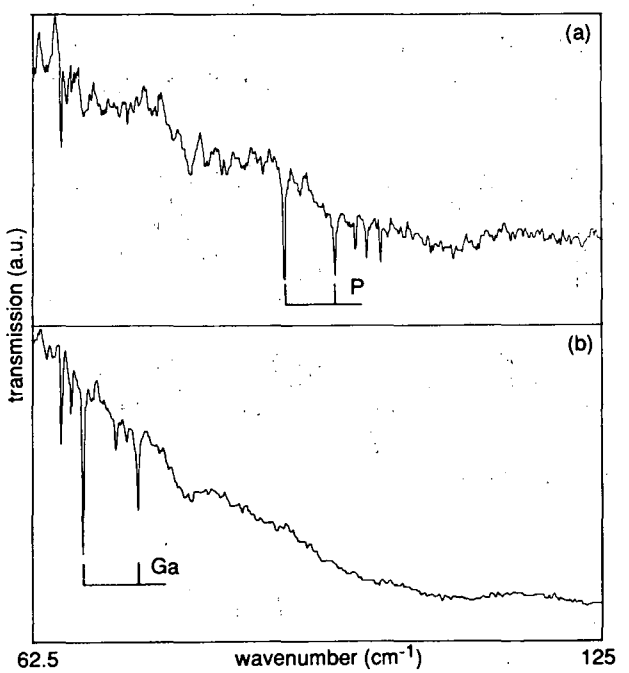

Figure 2-2. Absorption spectra of a phosphorus-doped Ge sample ($N_p = 6 \times 10^{13}$ cm^{-3}). (a) Spectrum of the sample before NTD: the lines of the shallow donor P are visible; (b) spectrum after NTD and without annealing: the NTD-produced Ga acceptor lines are visible, while both the P and As donor lines are absent. This shows that donors interact with mobile radiation damage centers, forming deep-level centers. (XBL 882-407)

†Present address: GoldStar Cable Co., Ltd., 555 Hogye-Dong, Anyang-Shi, Kyungki-Do, 430-080, Republic of Korea.

1988 PUBLICATIONS AND REPORTS

Refereed Journals

1. H. Navarro, J. Griffin, E.E. Haller, and R.E. McMurray, Jr., "Experimental Study of Three Ground-State Components of the Hydrogen-Oxygen Donor in Germanium," Solid State Commun. **64**, 1297 (1987).
2. J.Q. Wang, P.L. Richards, J.W. Beeman, and E.E. Haller, "A Stressed Photoconductive Detector for Far-Infrared Space Applications," Appl. Opt. **26**, 4767 (1987); LBL-23222.
3. H. Navarro, J. Griffin, and E.E. Haller, "The Zeeman Spectra of Phosphorus and the D(H,O) Donor Complex in Ultra-Pure Germanium," J. Phys. C: Solid State Phys. **21**, 1511 (1988).
4. N. Wang, B. Sadoulet, T. Shutt, J. Beeman, E.E. Haller, A. Lange, I. Park, R. Ross, C. Stanton, and H. Steiner, "Search for a 20 mK Temperature Sensor," IEEE Trans. Nucl. Sci. **NS-35**, No. 1, 55 (1988); LBL-24301.
5. D. Labrie, I.J. Booth, M.L.W. Thewalt, and E.E. Haller, "Piezospectroscopy of the Ground and Excited States of Zinc Double Acceptors in Germanium," Phys. Rev. B **38**, 5504 (1988).
6. E.E. Haller, "Far Infrared Fourier Transform Spectroscopy of Semiconductors," in *Proc. 6th FTS Conference,* Mikrochimica Acta (Wien) **III**, 241 (1988); LBL-23244.
7. H. Navarro, E.E. Haller, and F. Keilmann, "Study of the Fundamental Linewidths of 1S → n P Donor Transitions in Ultra-Pure Germanium," Phys. Rev. B **37**, 10822 (1988).
8. I.S. Park, E.E. Haller, E.N. Grossman, and D.M. Watson, "Germanium: Gallium Photoconductors for Far-Infrared Heterodyne Detection," Appl. Opt. **27**, 4143 (1988); LBL-24901.
9. I.S. Park and E.E. Haller, "Infrared Absorption Study of Neutron-Transmutation-Doped Germanium," J. Appl. Phys. **64**, 6775 (1988); LBL-24902.
10. D.D. Nolte and E.E. Haller, "Thermal Emission of Holes from Defects in Uniaxially Stressed p-type Silicon," Phys. Rev. B **38**, 9857 (1988); LBL-25315.
11. N.M. Haegel, J.W. Beeman, P.N. Luke, and E.E. Haller, "Transient Photoconductivity in Ge:Be Due to Be^+ Center Formation," Phys. Rev. B **39**, 3677 (1989).

Other Publications

12. M. Helm, K. Unterrainer, E. Gornik, and E.E. Haller, "New Results on Stimulated Emission from p-Germanium in Crossed Fields," in *Proc. Fifth Intl. Conf. on Hot Carriers in Semiconductors,* Boston, MA, July 20–24, 1987.
13. C. Rossington and E.E. Haller, "Germanium Blocked Impurity Band Infrared Detectors," in *Proc. CIRP4, Fourth Intl. Conf. On Infrared Physics,* Zurich, Switzerland, Aug. 22–26, 1988.
14. T. Yamamoto, H. Sukede, S. Komiyama, T. Kurosawa, and E.E. Haller, "Evidence for Bunching of Streaming Carriers in Momentum Space," in *Proc. ICPS 19,* Warsaw, Poland, Aug. 15–19, 1988, W. Zawadski and J.M. Langer, eds., DHM, Ltd., Warsaw, Poland.
15. B.L. Gel'mont, V.G. Golubev, V.I. Ivanov-Omskii, G.I. Kropotov, and E.E. Haller, "Magnetospectroscopic Studies of the D(H,O) Complex in Germanium," in *Proc. ICPS 19,* Warsaw, Poland, Aug. 15–19, 1988, W. Zawadski and J.M. Langer, eds., DHM, Ltd., Warsaw, Poland.
16. T. Theiler, F. Keilmann, and E.E. Haller, "Nonlinear Effects in Impurity Pumping and in Impurity Ionization," in *Proc. 3rd Intl. Conf. on Shallow Impurities in Semiconductors,* Linkoping, Aug. 10–12, 1988, B. Monemar, Ed., The Institute of Physics Conf. Ser., Vol. 95, London, England.

LBL Reports

17. D.D. Nolte, E.E. Haller, L.M. Falicov, and P. Omling, "The Effect of Uniaxial Stress on Iron-Boron and Iron-Aluminum Defects in Silicon," LBL-22110.
18. E.E Haller, "Hydrogen-Related Effects in Crystalline Semiconductors," in *Proc. 3rd Intl. Conf. on Shallow Impurities in Semiconductors,* Linkoping, Aug. 10–12, 1988, B. Monemar, Ed., The Institute of Physics Conf. Ser., Vol. 95, London, England; LBL-25708.
19. T.W. Kenny, P.L. Richards, I.S. Park, E.E. Haller, and J. Beeman, "Bias-Induced Nonlinearities in Neutron-Transmutation-Doped Germanium at ^4He Temperatures," submitted to Phys. Rev. B; LBL-25633.

Invited Talks

20. E.E. Haller, "GaAs Crystal Growth and Characterization," AT&T Engineering Center, Princeton, NJ, May 10, 1988.
21. E.E. Haller, "GaAs Research at the Center for Advanced Materials," Bel COR, Redbank, NJ, May 11, 1988.
22. E.E. Haller, "Hydrogen Related Complexes in Ge," Shanghai Institute for Technical Physics, Shanghai, People's Republic of China, May 29, 1988; Institute for Semiconductors, Beijing, People's Republic of China, June 6, 1988.
23. E.E. Haller, "IR-Photoconductive Detectors," Toshiba Corp., Japan, June 22, 1988.
24. E.E. Haller, "Far IR Semiconductor Photoconductors and Bolometers," Hamamatsu Photonics, Japan, June 23, 1988.
25. E.E. Haller, "GaAs Research at CAM," Lawrence Livermore National Laboratory, Livermore, CA, June 30, 1988.

26. E.E. Haller, "Hydrogen Related Effects in Semiconductors," Max-Planck-Institute for Solid State Research, Stuttgart, Federal Republic of Germany, Aug. 8, 1988.
27. E.E. Haller, "Hydrogen-Related Effects in Crystalline Semiconductors," 3rd International Conference on Shallow Impurities in Semiconductors, Linkoping, Sweden, Aug. 10–12, 1988.
28. E.E. Haller, "Hydrogen in Semiconductors," Physics Department Seminar, University of California at Berkeley, Oct. 26, 1988; Department of Materials Science and Mineral Engineering, University of California at Berkeley, Oct. 27, 1988; Department of Materials Science and Engineering, University of California at Los Angeles, Nov. 11, 1988.

Exploratory Research and Development Funds

Raman Studies of Surface Processes*

Gerd M. Rosenblatt, Investigator

INTRODUCTION

This project is designed to utilize and develop new instrumentation for the study of surfaces using unenhanced surface Raman spectroscopy (SRS). The project's goals are to use SRS to study surface composition; to provide new information concerning rotational and vibrational energy levels, dynamics, and reactivity of molecules adsorbed on a variety of surfaces; to study fundamental processes under ultrahigh-vacuum (UHV) conditions; and to extend the technique to a range of chemically important pressures, temperatures, and interfaces. An apparatus has been constructed that uses an imaging photomultiplier tube (PMT) to obtain Raman spectra that have unprecedented sensitivity and that yield a one-dimensional Raman image of sample composition along a few millimeters of an illuminating, focused laser beam. A unique capability to obtain spatially resolved compositional profiles and maps of a material's surface using the one-dimensional Raman images is under development. The Raman system is coupled to an UHV chamber that enables Raman spectra to be obtained from solid samples and films at temperatures between 15 K and 900 K. The UHV chamber has low-energy electron-diffraction (LEED) and Auger surface-analysis capabilities. This project provides a dramatic new analytical capability that compliments and contributes to other LBL surface and materials science projects.

1. Unenhanced Surface Raman Spectroscopy of Nitrogen Physisorbed on Ag(111) (Publications 4 and 7)

D.K. Veirs, V.K.F. Chia, and G.M. Rosenblatt

The Raman spectrum of N_2 physisorbed on Ag(111) at 15 K has been obtained at low nitrogen exposures (4L) with low laser intensities (see Figure 1-1). The Raman intensity is unenhanced and is linear with nitrogen exposure between 1 and 353 L and with laser power from 100 to 1000 mW

*This work was supported by the Director's Exploratory Research and Development Funds of the Lawrence Berkeley Laboratory under Contract No. DE-AC03-76SF00098.

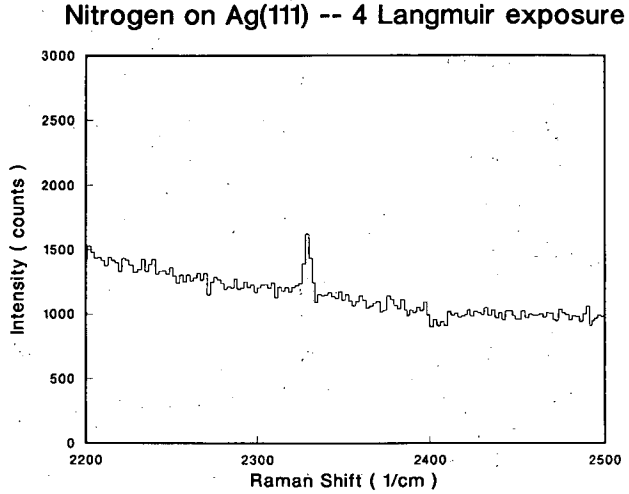

Figure 1-1. Unenhanced surface Raman spectrum of the Q-branch of physisorbed N_2 on a clean, smooth Ag(111) surface at 15 K is observed at low exposures and low laser intensities. Exposure was 4L, laser power was 100 mW, and integration time was 450 sec. (XBL 887-2513)

(see Figure 1-2). The observed intensity of 7.6 counts sec^{-1} W^{-1} L^{-1} is in good agreement with an intensity calculated using the gas-phase Raman cross section. The observed line positions of multilayer physisorbed nitrogen are consistent with Raman spectra in the literature for the α-phase of bulk solid nitrogen. Background scattering associated with carbon contamination (see Figure 1-3), and with silver

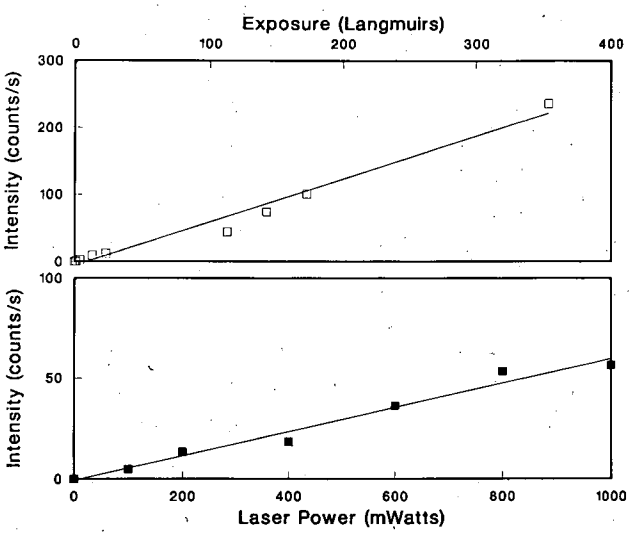

Figure 1-2. The integrated intensity of the vibrational Raman peak of nitrogen varies linearly with both exposure and laser power. In the top graph the exposure is varied while the laser power is kept constant at 75 mW; in the bottom graph Raman spectra are obtained as the laser power is increased after a 100-L exposure. In both cases the Ag(111) surface was at 15 K. (XBL 883-857)

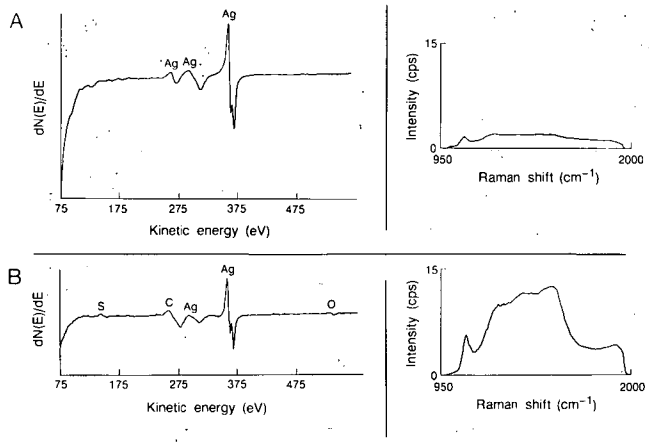

Figure 1-3. Small amounts of carbon on a smooth silver surface are accompanied by a large, broad Raman signal between 1000 and 1600 cm^{-1} and a significant increase in the background signal. In (A) no carbon is observed in the Auger spectrum, although it is weakly observed in the Raman signal. In (B) the Auger spectrum shows the presence of a small amount of carbon with trace amounts of sulfur and oxygen; however, the Raman signal is dominated by a large carbon signal and a dramatically increased background. (XBL 886-8046A)

islands produced during surface cleaning by alternative ion bombardment and annealing, affects the minimum detectable level of physisorbed species on silver. On a smooth, clean silver surface with a minimum of background scattering, a detection limit of less than 0.1 monolayer is calculated.

2. Ultrahigh-Vacuum Apparatus for Surface Spectroscopy and Characterization at Cryogenic Temperatures (Publications 2 and 8)

V.K.F. Chia, D.K. Veirs, and G.M. Rosenblatt

An ultrahigh-vacuum apparatus has been designed and constructed that enables the study of molecular adsorbates on well-defined single crystals at controlled temperatures from 15 to 900 K. Sample and sample-holder cooling curves from room temperature to below 15 K are shown in Figure 2-1. Sample cooling is achieved with a closed-cycle helium refrigerator coupled to the sample holder via a flexible copper cable. This configuration maintains a 3-K temperature differential from the 11-K cryocold head to the sample and damps vibrations from the cyrocold head. The cyrogenic sample manipulator allows X,Y,Z translations, tilt, and rotation of an arm holding the sample about the vertical central axis of the vacuum chamber. The sample, displaced from the central axis, may also be rotated about its vertical axis. A detailed drawing of the sample-

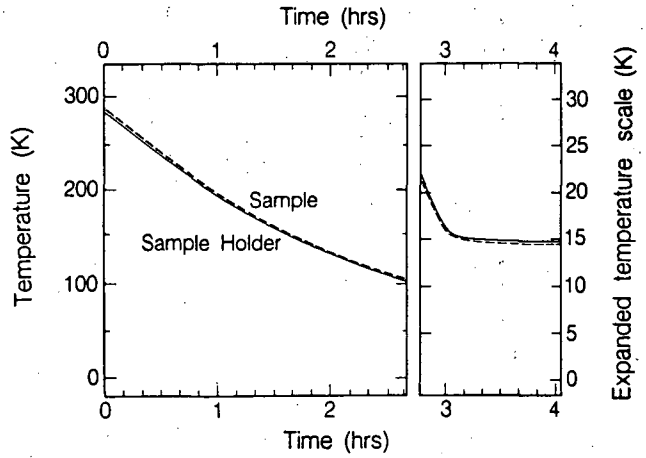

Figure 2-1. Temperature of the sample and sample holder versus time, starting when the closed-cycle helium refrigerator is started. The lowest final temperature achieved is 13.4 K in three hours. (XBL 894-1295)

mounting arrangement is shown in Figure 2-2. Rotation of the sample about a working circle radius of 12.7 cm allows the sample to be accessed for surface cleaning, characterization, and study by instrumentation whose physical size does not allow access by sample rotation about the chamber central axis

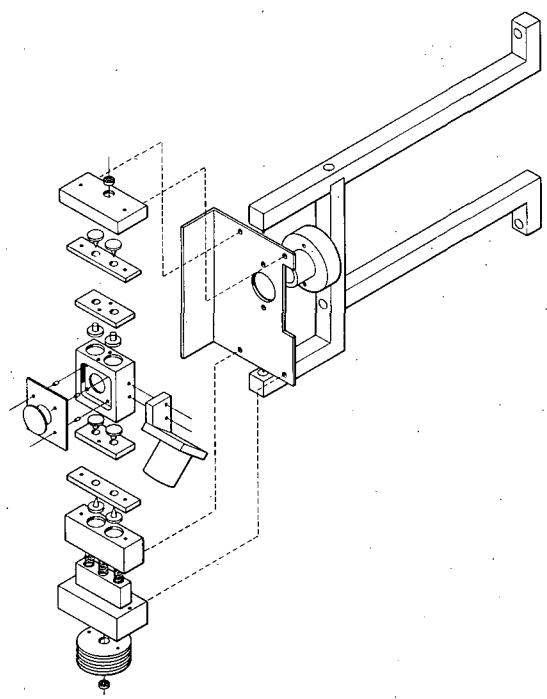

Figure 2-2. Exploded view of the manipulator arm, sample holder, and sample-holder mount used to obtain sample temperatures down to 15 K in an UHV system with surface Raman spectroscopy, LEED, and Auger spectroscopy capabilities. The sample holder and sample-holder mount rotate by 90° on the bearings seen at the top and bottom of the left-hand side of the drawing. (XBL 879-3901B)

alone. In our application, unenhanced SRS, LEED, and Auger spectroscopy are carried out while maintaining a controlled sample temperature. Laser entry ports at two incident angles permit the study of substrates with differing optical properties.

3. Spatially Resolved Raman Spectroscopy in the Study of Transformed Zones in PSZ (Publications 3, 5, 6, and 9)†

D.K. Veirs, G.M. Rosenblatt, R.O. Ritchie, and R.H., Dauskardt

Raman vibrational spectroscopy provides an effective phase-characterization technique in materials systems containing particle dispersions of the three polymorphs of ZrO_2; the tetragonal and monoclinic phases each have a unique Raman spectrum (see Figure 3-1). We have investigated the utilization of LBL's novel, spatially resolved Raman spectroscopy system in the study of transformed zones surrounding cracks in partially stabilized MgO-ZrO_2 (PSZ). The experimental arrangement makes use of an imaging (2D) photomultiplier tube to produce a one-dimensional Raman profile of phase compositions along a slit-like laser beam without translation of either the sample or laser beam and without scanning the spectrometer. The estimated spatial resolution is equivalent to the detector resolution of 28 μm and is not measurably reduced by secondary scattering events in the PSZ. Phase-characterization studies of the size, frontal morphology, and extent of transformation of transformation zones surrounding cracks produced under monotonic and cyclic loading conditions have been carried out. Particularly large zones were observed in peak-toughened PSZ material, extending 1300 μm ahead of the crack tip with widths of up to 3000 μm (see Figure 3-2). Good agreement was found with transformed-zone areas determined using optical interference microscopy.

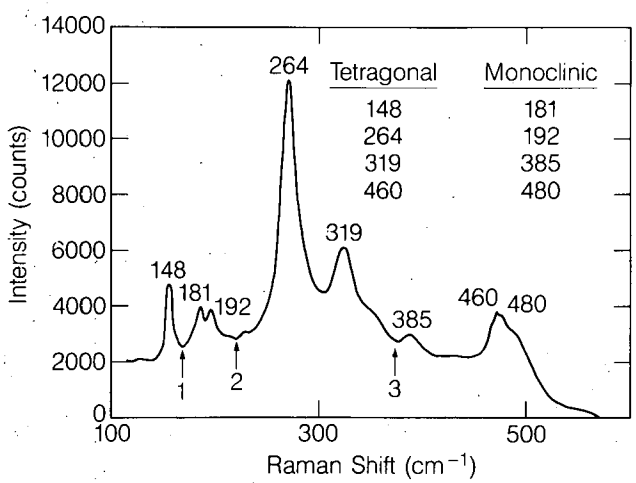

Figure 3-1. Characteristic Raman spectrum of MgO-PSZ ceramic containing monoclinic and tetragonal precipitates. The integrated intensity of the 181 and 192 cm^{-1} peaks are used to estimate the relative fraction of the monoclinic phase when compared to the integrated intensity of the 264 cm^{-1} tetragonal peak. (XBL 883-6010)

†Research in collaboration with R.O. Ritchie and R.H. Dauskardt was also supported by the Director, Office of Energy Research, Office of Basic Energy Sciences, Materials Sciences Division, of the U.S. Department of Energy under Contract No. DE-AC03-76SF00098.

4. Work in Progress

Interactions between physisorbed molecules and metal surfaces are being examined using Raman spectroscopy of N_2 and H_2 physisorbed on clean, well-characterized single-crystal silver. Preliminary investigations indicate that N_2 forms an ordered structure on Ag much like the low-temperature α-phase of solid N_2. Further studies are under way to determine the low-coverage limit of unenhanced SRS and to extend the measurements to chemisorbed systems.

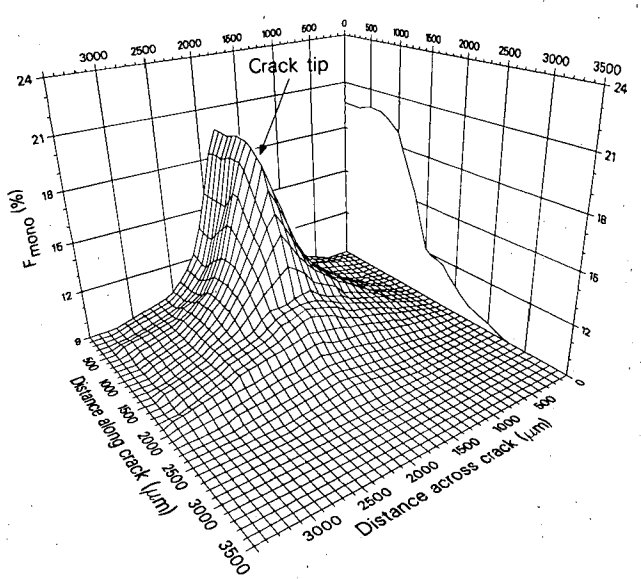

Figure 3-2. Two-dimensional Raman map of the fraction of monoclinic phase across the face of a partially stabilized zirconia sample in which a crack has been grown, showing the phase-transformation zone associated with the crack. Using this map, the extent of transformation within the zone, the width of the zone, and the shape of the zone ahead of the crack tip can be determined. (XBL 882-388)

Other collaborative projects that are being actively pursued include: (1) Raman studies of hard carbon films, "diamond-like" films, and individual carbon fibers; and (2) using spatially resolved Raman to ascertain the extent of the phase-transformation zone in partially stabilized zirconia induced by crack propagation under various cyclic and monotonic loads, and dynamic *in situ* studies of changes in the phase-transformation zone accompanying cyclic loading of the crack.

1988 PUBLICATIONS AND REPORTS

Refereed Journals

1. H.-c. Tsai, D.B. Bogy, M.K. Kundmann, D.K. Veirs, M.R. Hilton, and S.T. Mayer, "Structure and Properties of Sputtered Carbon Overcoats on Rigid Magnetic Media Disks," J. Vac. Sci. Technol. A **6**, 2307 (1988); LBL-22762.

Other Publications

2. D.K. Veirs, G.M. Rosenblatt, R.H. Dauskardt, and R.O. Ritchie, "Two-Dimensional Spatially Resolved Raman Spectroscopy of Solid Materials," in *Microbeam Analysis—1988*, D.E. Newbury, Ed., San Francisco Press, San Francisco, 1988, p. 179; LBL-24971.
3. D.K. Veirs, V.K.F. Chia, and G.M. Rosenblatt, "Unenhanced Surface Raman Spectroscopy of Adsorbed Films," in *Proc. Eleventh Int. Conf. on Raman Spectroscopy*, R.J.H. Clark and D.A. Long, eds., John Wiley and Sons, New York, 1988, p. 243; LBL-24566.
4. D.K. Veirs and G.M. Rosenblatt, "Spatially Resolved Raman Spectroscopy Using a Two-Dimensional Detector," in *Proc. Eleventh Int. Conf. on Raman Spectroscopy*, R.J.H. Clark and D.A. Long, eds., John Wiley and Sons, New York, 1988, p. 961; LBL-24565.
5. D.K. Veirs, R.O. Ritchie, and R.H. Dauskardt, "Application of Spatially Resolved Raman Spectroscopy in the Study of Transformed Zones in PSZ," Bull. Am. Phys. Soc. **3**, 697 (1988); LBL-24565abs.

LBL Reports

6. V.K.F. Chia, D.K. Veirs, and G.M. Rosenblatt, "Cryogenic Sample Manipulator for Multipurpose Sample Analysis," J. Vac. Sci. Technol. A. (in press); LBL-24865.
7. D.K. Veirs, V.K.F. Chia, and G.M. Rosenblatt, "Unenhanced Surface Raman Spectroscopy of Nitrogen Physisorbed on Ag(111)," submitted to Langmuir; LBL-24566abs.
8. V.K.F. Chia, D.K. Veirs, and G.M. Rosenblatt, "Ultrahigh Vacuum Apparatus for Surface Spectroscopy and Characterization at Cryogenic Temperatures," submitted to Rev. Sci. Instrum.; LBL-24567.
9. R.H. Dauskardt, R.O. Ritchie, and D.K. Veirs, "Spatially-Resolved Raman Spectroscopy in the Study of Transformed Zones in PSZ," J. Am. Ceram. Soc. (in press); LBL-25251.

Invited Talks

10. G.M. Rosenblatt and D.K.Veirs, "Raman Spectroscopy of Surfaces, Interfaces, and Films," Chemical Biodynamics Chemistry Seminar, University of California at Berkeley, Feb. 1988.
11. D.K. Veirs, R.O. Ritchie, and R.H. Dauskardt, "Application of Spatially Resolved Raman Spectroscopy in the Study of Transformed Zones in PSZ," 1988 March Meeting, American Physical Society, New Orleans, LA, Mar. 1988.
12. D.K.Veirs, V.F.K. Chia, and G.M. Rosenblatt, "Raman Spectroscopy of Surfaces, Interfaces, and Films," Surface Chemistry Seminar, University of California at Berkeley, Apr. 1988.
13. D.K. Veirs and G.M. Rosenblatt, "Unenhanced Surface Raman Spectroscopy of Adsorbed Films," 62nd Colloid and Surface Science Symposium, American Chemical Society, Pennsylvania State University, State College, PA, June 1988.
14. M.R. Khan, N. Heilman, S. Smith, M. Smallen, G.F. Hughes, D.K. Veirs, B. Marchon, M. Salmeron, D.F. Ogletree, and W. Siekhaus, "Carbon Overcoat and the Process Dependence on its Microstructure and Wear Characteristics," 4th Joint MMM-Intermag Conference, Vancouver, BC, July 12–15, 1988.
15. G.M. Rosenblatt and D.K. Veirs, "Spatially Resolved, High Sensitivity Raman Spectroscopy of High Temperature Materials," High Temperature Chemistry Gordon Conference, Plymouth, NH, July 1988.
16. D.K. Veirs, G.M. Rosenblatt, R.H. Dauskardt, and R.O. Ritchie, "Two-Dimensional Spatially Resolved Raman Spectroscopy of Solid Materials," Annual Meeting, Microbeam Analysis Society, Milwaukee, WI, Aug. 1988.
17. D.K.Veirs, V.F.K. Chia, and G.M. Rosenblatt, "Unenhanced Surface Raman Spectroscopy of Nitrogen Physisorbed on Ag(111)," Vibrational Spectroscopy Gordon Conference, Wolfeboro, NH, Aug. 1988.
18. D.K. Veirs and G.M. Rosenblatt, "Spatially Resolved Raman Spectroscopy Using a Two-Dimensional Detector," International Conference on Raman Spectroscopy, London, England, Sept. 1988.
19. D.K. Veirs, V.K.F. Chia, and G.M. Rosenblatt, "Unenhanced Surface Raman Spectroscopy of Adsorbed Films," International Conference on Raman Spectroscopy, London, England, Sept. 1988.

20. D.K. Veirs and G.M. Rosenblatt, "Recent Developments in Compositional Mapping Using Raman Spectroscopy," ACS Pacific Conference, San Francisco, Oct. 1988.

21. G.M. Rosenblatt and D.K. Veirs, "Recent Developments in Raman Spectroscopy of High Temperature Materials," 25th Bay Area Conference on High Temperature Science and Technology, LBL, Nov. 9, 1988.

Novel Properties of Matter at Megabars of Pressure*

Marvin L. Cohen, Raymond Jeanloz, and Peter Y. Yu, Investigators

INTRODUCTION

The purpose of this research project is to investigate the properties of matter at megabars of pressure both experimentally and theoretically. The objective is to combine the expertise of experimentalists and theorists in the area of high-pressure technology, materials characterization techniques, inorganic synthesis, and theoretical computation of properties of matter to synthesize and investigate new materials with unusual properties or with potential applications to energy technology. Examples of these new materials are ultrahard solids with strength comparable to or exceeding that of diamond, and solids with unusual electrical, superconducting, optical, and magnetic properties.

What distinguishes this project from other high-pressure projects is the close interaction between the theoretical group of Marvin Cohen and the two experimental groups under Raymond Jeanloz and Peter Yu. The theoretical group uses the *ab initio* pseudopotential method to calculate the ground-state properties of solids as a function of volume. These properties include the total energy of the solid, the bulk modulus of the different phases, the transition pressure and volume from one phase to another, the electronic and vibrational spectra of the high-pressure phases, electron-phonon interaction, and superconducting transition temperatures. The theoretical predictions are tested by experiments performed by the Yu and Jeanloz groups. These two investigators have broad experience in materials science and with a wide range of high-pressure techniques, such as high-temperature synthesis of inorganic materials, x-ray crystallography, Raman and emission spectroscopies, Fourier-transform infrared spectroscopy, and low-temperature electrical-transport measurements.

*This work was supported by the Director's Exploratory Research and Development Funds of Lawrence Berkeley Laboratory under Contract No. DE-AC03-76SF00098.

1. Properties of Cubic BN Under High Pressure and Temperature (Publication 2)

E. Knittle, R.M. Wentzcovitch, R. Jeanloz, and M.L. Cohen

In spite of the fact that cubic BN has many properties that make it attractive in the manufacture of machine tools and other industrial applications, there has been no determination of its equation of state and other basic properties. Cohen and Jeanloz have performed the first complete theoretical and experimental study of the static compression of cubic BN and show that the experimental results are in excellent agreement with theoretical results based on a first-principles (LCAO) pseudopotential approach. Similar studies on compounds of B, C, and N under high pressure have also been carried out. These compounds have been synthesized inside diamond anvil cells under high-pressure and high-temperature conditions. After synthesis the compression of the samples is measured *in situ* inside the cell. Samples containing different ratios of C and BN have been studied, and these results are being analyzed.

2. Nonlinear Pressure Dependence of T_c in Single-Crystal Superconducting BiCaSrCuO (Publication 3)

H.F. Goldstein, L.C. Bourne, P.Y. Yu, and A. Zettl

In a previous work,[1] the pressure dependence of T_c in ceramic LaSrCuO superconductors was found to be highly nonlinear. The polycrystalline nature of these materials made it difficult to interpret the nonlinear pressure dependence. It has now been shown that, even in single-crystal BiCaSrCuO compounds, a similar nonlinear dependence exists and, furthermore, the pressure dependence is reproducible on increasing and decreasing pressure cycles. None of the existing theories on superconductivity can explain this nonlinear pressure dependence satisfactorily.

1. D. Erskine, E. Hess, P.Y. Yu, and A.M. Stacy, J. Mat. Res. 2, 783 (1987).

3. Work in Progress

The temperature and pressure dependence of electrical resistance in high-quality single crystals of Cu_2O have been studied under pressures exceeding 0.5 Mbar. The resistance of Cu_2O dropped by several orders of magnitude around 100 kbar. The temperature dependence of the resistance suggested that Cu_2O had transformed into a semimetallic state. Above 300 kbar the temperature dependence suggested a metallic state that is not superconducting at temperatures down to 4.2 K. Single crystals of CuO have been grown at Berkeley and obtained from France. These single crystals have been characterized by polarized Raman scattering for the first time, and their electrical resistance has been studied as a function of temperature and pressure. The activated resistance characteristic of a semiconductor has been observed up to pressures as high as 700 kbar. However, the activation energy of the resistivity decreased monotonically with pressure. Extrapolating from these results, CuO is expected to become metallic above 1 Mbar.

Some other projects that should yield interesting results include novel properties of semiconductor superlattices under pressure, the study of laser-induced melting and synthesis under high pressure, and studies of dynamics of glasses under high pressure.

1988 PUBLICATIONS AND REPORTS

Refereed Journals

1. D. Erskine, P.Y. Yu, and S.C. Freilich, "High Pressure Visible Spectroscopy of Polyimide Film," J. Polymer Sci. C **26**, 465 (1988); LBL-24553.

Other Publications

2. E. Knittle, R.M. Wentzcovitch, R. Jeanloz, and M.L. Cohen, "Experimental and Theoretical Equation of State of Cubic BN," Nature (in press).

LBL Reports

3. H.F. Goldstein, L.C. Bourne, P.Y. Yu, and A. Zettl, "Pressure Dependence of Superconductivity in Single-Crystal $Bi_2Sr_2CaCu_2O_8$," LBL-25595.
4. S.B. Zhang, D. Erskine, M.L. Cohen, and P.Y. Yu, "Metallic Properties of Orthorhombic High Pressure Phase of GaAs: Theory and Experiment," LBL-26543.

Invited Talks

5. P.Y. Yu, "Superconductivity and Other Studies of Electrical Properties under High Pressure," Gordon Research Conference on Research at High Pressures, Meriden, NH, June 27–July 1, 1988.

Novel Materials from Nanocrystalline Aggregates*

U. Dahmen and K.H. Westmacott, Investigators

INTRODUCTION

Materials with extremely small grain size, in the range from a few Angstroms to a few hundred Angstroms, are termed nanocrystals or nanocomposites. By virtue of their very high grain-boundary area, such materials show unusual properties such as greatly enhanced diffusivity, low sintering temperatures, limited grain growth, and shifts in magnetic properties.

Nanocomposites with a narrow range of size distributions and with varying degrees of texture are of particular interest because of their potential for controllable packing density and anistropy. Ceramic materials of this nature can be produced by thermal-decomposition reactions. The resulting porous microstructure may be considered a composite of small oriented crystallites (nanocrystals) and pores.

The highest degree of texture is obtained by ionized-cluster beam deposition of metals on a single-crystal substrate, a technique that allows formation of thin films with unique continuous bicrystal structure.

The purpose of this program is to explore new materials synthesized from ultrafine grains (nanocrystals) or clusters, to study the potential for producing novel microstructures with unique properties, and to conduct a detailed microstructural investigation to understand effects of processing variables.

1. The Use of Heteroepitaxy in the Fabrication of Bicrystals for the Study of Grain-Boundary Structure (Publication 1)

U. Dahmen and K.H. Westmacott

Experiments on grain-boundary structure can be grouped into two categories—those that provide limited structural information on a large number of boundaries and those that give detailed structural information on a limited sampling of boundaries.

The first category is typified by the elegant rotating-sphere-on-plate experiments pioneered by Gleiter and coworkers.[1] In this technique single-crystal spheres are placed in a random array on a single-crystal plate and annealed to promote their relaxation into low-energy orientations. The resulting orientation distribution is recorded in an x-ray pole figure, and, assuming all boundary planes are parallel to the plate surface, statistically significant data on misorientation and type of boundary (twist/tilt, symmetrical/asymmetrical) can be obtained rapidly. However, this macroscopic method does not give any direct information on the grain-boundary structure.

This report describes a new method for producing specimens that are particularly suitable for high-resolution observations of grain-boundary structures. Unlike the bicrystals produced by conventional methods, the specimens contain boundaries that display a continuous variation in boundary orientation. The technique simply relies on heteroepitaxy as a means of controlling the misorientation between grains during thin-film growth. For example, if the substrate surface has fourfold rotational symmetry and epitaxial overgrowth occurs in an orientation with twofold rotational symmetry, then two orientation variants are equally probable. As illustrated schematically in Figure 1-1 and in a high-resolution micrograph in Figure 1-2, the two variants are at

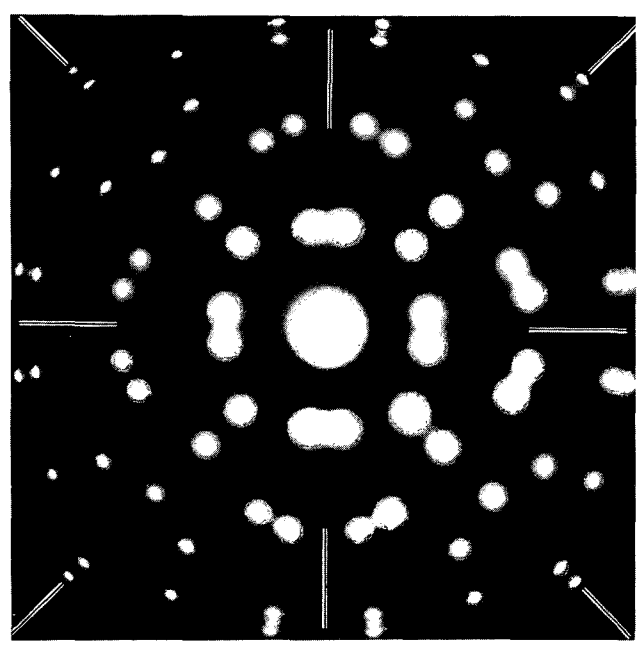

Figure 1-1. Selected-area diffraction pattern of the two orientation variants resulting from the deposition of a film with twofold rotational symmetry on a substrate with fourfold rotational symmetry. (XBB 889-8861)

*This work was supported by the Director's Exploratory Research and Development Funds of Lawrence Berkeley Laboratory under Contract No. DE-AC03-76SF00098.

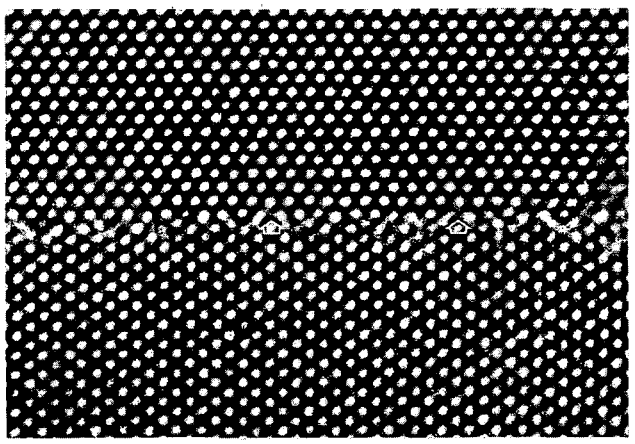

Figure 1-2. High-resolution micrograph of 90° <110> asymmetrical tilt boundary in thin-film aluminum bicrystal with boundary plane parallel to electron beam. Recorded by C.J.D. Hetherington at 800 kV on LBL's Atomic Resolution Microscope. (XBB 880-10319)

right angles due to the 90° rotation symmetry of the substrate. A systematic investigation of thin-film bicrystal structures grown by heteroepitaxy is in progress.

1. H. Gleiter and P. Marquart, Z. Metall. **75**, 263 (1984).

2. TEM Characterization of Nanocrystals Produced by Decomposition Reactions (Publication 6)

U. Dahmen and K.H. Westmacott

Nanocrystalline particles and structures are by definition ideal subjects for study by transmission electron microscopy. By the combined use of high-resolution, high-voltage *in situ* and microanalytical electron microscopy, direct information on crystalline structures and morphologies and their orientation relationships and interactions can be obtained. In the present work, metal oxide nanocrystals are produced by thermal decomposition of Mg and Al hydroxide crystals or powders. Decomposition is observed during either *in situ* heating or electron irradiation. High-resolution studies show that the resulting structures consist of fine dispersions of nanocrystallites slightly misoriented with respect to each other. Since the decomposition produces large areas of clean internal surface, consolidation of these materials should in principle yield high-purity, high-density oxides. To explore the potential for such processing, the effects of variables such as the initial form, source, and purity of the hydroxides on the final microstructure is being studied. Preliminary results comparing the microstructures derived from single crystals and powders produced by commercial and spark erosion methods were obtained.

1988 PUBLICATIONS AND REPORTS

Refereed Journals

1. U. Dahmen and K.H. Westmacott, "The Use of Heteroepitaxy in the Fabrication of Bicrystals for the Study of Grain Boundary Structure," Scripta Metall. **22**, 1673 (1988); LBL-25750.
2. M.G. Kim, U. Dahmen, and A.W. Searcy, "Shape and Size of Crystalline MgO Particles Formed by the Decomposition of $Mg(OH)_2$," J. Am. Ceram. Soc. **71**, C-373 (1988); LBL-22159.
3. U. Dahmen and K.H. Westmacott, "High Resolution Imaging of Near-Σ17 Tilt Boundaries in Aluminum," EMSSA Proc. **18**, 147 (1988); LBL-25879abs.

Other Publications

4. M.G. Kim, U. Dahmen, and A. W. Searcy, "Origin of Cracking Phenomena Observed in Decomposition Reactions," in *Ceramic Microstructures '86, Role of Interfaces*, J. Pask and A.G. Evans, eds, p. 145; LBL-22160.

LBL Reports

5. U. Dahmen and K.H. Westmacott, "A Small Angle Electron Diffraction Technique for Nanophase Analysis," LBL-24956.
6. U. Dahmen and K.H. Westmacott, "TEM Characterization of Nanocrystals Produced by Decomposition Reactions," LBL-24077abs.

Invited Talks

7. U. Dahmen and K.H. Westmacott, "TEM Characterization of Nanocrystals Produced by Decomposition Reactions," Micrometallurgy 1988, Lake Tahoe, CA, Mar. 10–11, 1988.
8. U. Dahmen and K.H. Westmacott, "High Resolution Imaging of Near-Σ17 Tilt Boundaries in Aluminum," EMSSA Meeting, Durban, South Africa, Dec. 6–8, 1988.

Work for Others

UNITED STATES OFFICE OF NAVAL RESEARCH

Normal and Superconducting Properties of New High-T_c Materials*

Vladimir Z. Kresin, Investigator

INTRODUCTION

This research is carried out in two directions: (1) analysis of normal and superconducting properties of new materials (proximity effect, normal parameters, etc.), (2) and origin of high superconducting transition temperature (T_c).

1. Origin of High T_c (Publications 1, 5, and 7)

V.Z. Kresin and H. Morawitz

The observed high superconducting transition temperatures are caused, in our view, by the coexistence of strong electron-phonon coupling and the plasmon mechanism. A generalized Eliashberg equation describing the effects of phonons and plasmons on the pairing is presented. Our approach is based on the method of thermodynamic Green's functions. The structure of the plasmon and phonon bands in conducting, highly anisotropic layered materials is studied.

2. Proximity Effect (Publication 3)

V.Z. Kresin

A proximity system containing a high-T_c superconductor cam be used to strengthen the field effect. The use of the proximity contact S_h-Nb in the Josephson junction S_h-Nb-InAs-Nb-S_h (where S_h is a high-T_c film) is promising from the point of view of making a three-terminal device. The proximity effect can also be used to increase the values of the parameters of a conventional superconductor, such as T_c, critical field, and critical current.

3. Major Parameters of the High-T_c Oxides (Publications 2 and 8)

V.Z. Kresin, G. Deutscher, and S.A. Wolf

A general fundamental feature of the high-T_c oxides is a very small value of the Fermi energy. We point out that this leads to peculiar thermodynamic and transport properties in the normal and superconductive states, which in fact require unconventional analysis. We show that the electronic heat capacity can be separated at high temperature, and it can be used to determine the electron-phonon coupling constant. The unusual temperature dependences of the kinetic coefficients can also be explained.

4. Search for Nonphonon Mechanisms of Superconductivity (Publication 4)

K.E. Kihlstrom, P.D. Hovda, V.Z. Kresin, and S.A. Wolf

We present the results of a quantitative test to separate phonon from nonphonon contributions to the superconductivity in A-15 (Nb_3Ge). This test is based on analysis of heat capacity, tunneling $a^2F(\omega)$ data, and neutron-scattering data. We obtained evidence for a substantial contribution of a nonphonon mechanism to the superconducting state in Nb_3Ge. In contrast, our results suggest the superconducting state in Pb and V_3Si is due to phonons.

*This work was supported by the U.S. Office of Naval Research under Contract No. N00014-86-F0015 through an agreement with the U.S. Department of Energy under Contract No. DE-AC03-76SF00098.

5. Fluctuations and High-T_c Superconductivity (Publication 6)

R.S. Thompson and V.Z. Kresin

The leading correction due to thermodynamic fluctuations to the dependence of the heat capacity on temperature and applied magnetic field is calculated for anisotropic high-T_c superconductors. Experimental data are discussed.

1988 PUBLICATIONS AND REPORTS

Refereed Journals

1. V.Z. Kresin and H. Morawitz, "Layer Plasmons and High T_c Superconductivity," Phys. Rev. B **37**, 7854 (1988); LBL-25640.
2. V.Z. Kresin and S.A. Wolf, "Effect of the Structure of the Fermi Surface on the Normal and Superconducting Parameters of the High T_c Oxide Superconductors," J. Superconductivity **1**, 143 (1988); LBL-25208.
3. V.Z. Kresin, "Proximity Effect and High T_c Superconductivity," Cryogenics **28**, 409 (1988); LBL-26793.
4. K.E. Kihlstrom, P.D. Hovda, V.Z. Kresin, and S.A. Wolf, "Evidence of Nonphononic Superconductivity in Nb_3Ge," Phys. Rev. B **38**, 4588 (1988); LBL-25481.
5. V.Z. Kresin and H. Morawitz, "Plasmons and Phonon in Anisotropic Systems and Their Effect on High T_c Superconductivity," J. Superconductivity **1**, 89 (1988); LBL-25209.
6. R.S. Thompson and V. Z. Kresin, "Fluctuation Pairing and Heat Capacity of High T_c Superconductors," Mod. Phys. Lett. B **2**, 1159 (1988); LBL-25480.
7. V.Z. Kresin and H. Morawitz, "Plasmon and Phonon Mechanisms of Superconductivity in the Layered High T_c Copper Oxides," Physica C **153**, 1327 (1988); LBL-25641.
8. V.Z. Kresin, G. Deutscher, and S.A. Wolf, "Small Value of the Fermi Energy and the Unusual Normal and Superconducting Properties of High T_c Oxides," J. Superconductivity **1**, 327 (1988); LBL-25642.

Other Publications

9. V.Z. Kresin, G. Deutscher, and S.A. Wolf, "Exotic Normal and Superconducting Properties of High T_c Oxides," in *First Latin-American Conference on High T_c*, R. Nicolsky, R. Barrio, O. de Lima, and R. Escudero, eds., World, 1988, p. 159; LBL-25483.
10. V.Z. Kresin and H. Morawitz, "Phonon-Plasmon Mechanism of High T_c," in *First Latin-American Conference on High T_c*, R. Nicolsky, R. Barrio, O. de Lima, and R. Escudero, eds., World, 1988, p. 166; LBL-25482.

Invited Talks

11. V.Z. Kresin, "High T_c and Superconducting Films," Gordon Conference on High T_c, Santa Barbara, CA, Jan. 1988.
12. V.Z. Kresin, "Proximity Effect and High T_c," Conference on Applications of Superconductivity, Los Angeles, CA, Feb. 1988.
13. V.Z. Kresin, "High T_c Superconductivity," University of North Carolina, Charlotte, Apr. 1988.
14. V.Z. Kresin, "Plasmons in Layered Crystals," University of Maryland, College Park, Apr. 1988.
15. V.Z. Kresin, "Normal and Superconducting Properties of the High T_c Oxides," Latin-American Conference on High Temperature Superconductivity, Rio de Janeiro, Brazil, May 1988.
16. V.Z. Kresin, "Origin of High T_c," Conference on Mechanisms of High T_c, Gaithersburg, MD, Oct. 1988.
17. V.Z. Kresin, "High T_c Films and Proximity Effect," International Conference on High T_c Films, Colorado Springs, CO, Nov. 1988.
18. V.Z. Kresin, "Properties of High T_c Materials," Naval Research Laboratory, Washington, D.C., Nov. 1988.
19. V.Z. Kresin, "Mechanisms of High T_c" Argonne National Laboratory, Argonne, IL, Nov. 1988.

UNITED STATES DEPARTMENT OF TRANSPORTATION

Materials for Enhanced Heavy Fuel Capability Marine Diesels*

Alan V. Levy, Investigator

1. Work in Progress

The application of thin, 0.1 mm thick partially stabilized Y_2O_3 and $CeO\text{-}ZrO_2$ plasma sprayed ceramic coatings on the piston domes and exhaust manifolds of several test diesel engines has been completed. The engines propel large, off-the-road ore hauling trucks at an open pit copper mine. The modified engines will be installed in the trucks for an approximately two year test period, at the end of which the ceramic coated parts will be destructively analyzed.

1988 PUBLICATIONS AND REPORTS

Other Publications

1. A.V. Levy and S. MacAdam, "Durability of Ceramic Coatings in 14,000 Hours Service in a Marine Diesel Engine," ASME Energy Technology Conference, New Orleans, LA, Jan. 1988, Paper No. 88-ICE-19.
2. A.V. Levy, "The Performance of Ceramic Coatings on Diesel Engine Combustion Zone Components," in *Proc. ASM National Thermal Spray Conf.*, Cincinnati, OH, Oct. 1988 (in press).

Invited Talks

3. A.V. Levy, "Use of Thin Ceramic Coatings on Diesel Engine Combustion Zone Components," Utah Copper Mine, Port Hardy, B.C., Dec. 1988.

*This work was supported by the U.S. Department of Transportation, Maritime Administration, P.O. No. 400-49002, through an agreement with the U.S. Department of Energy under Contract No. DE-AC03-76SF00098.

ELECTRIC POWER RESEARCH INSTITUTE

A Cold Model Study of Wear on Fluidized Bed Combustor Tubes*

Alan V. Levy, Investigator

INTRODUCTION

Energy production from the fluidized bed combustion of coal has many advantages over conventional coal burning methods. A large reduction in emission of the pollutants NO_x and SO_x, as well as a high combustion efficiency and wider fuel tolerance, make fluidized bed combustion an attractive technology. A significant problem encountered in the burning of coal by this process has been the material wastage of heat exchanger tubes and other components immersed in the fluidized bed. A major probable contribution to heat exchanger tube wastage in bubbling fluidized beds is mechanical in nature. It arises from the impact of aggregates of defluidized particles thrown against tube undersides during either the passage of rising bubbles, or the collapse of "teardrop" like voids that form periodically under the tubes. In an effort to investigate this process, isolated from other erosive or corrosive effects, a novel wear testing rig has been designed and built. This device simulates the particle aggregate impact environment by the fast movement of a specimen rod vertically within a minimally fluidized bed.

*This work was supported by Electric Power Research Institute through Agreement No. RP8000-6.

1. Work in Progress

Operational Characteristics of Test Device (S. MacAdam)

Tests conducted during a cold model study indicate that the device reproduces most aspects of the tube wastage in bubbling beds. Wear rates and distributions for a wide variety of metallic and plastic materials were very similar to those found in other cold wear studies that utilized conventional fluidized beds.

The mechanism of material removal was found to be one of a combination of micromachining and plowing due to the dragging of partially constrained particles across the tube surface. Wear resistance was found to increase linearly with the hardness of pure annealed metals, but was not affected by hardness induced through heat treatment.

The type of particle used as the bed material had a major effect on wear behavior. The degree of particle rounding and the nature of the particle debris governed wear. Olivine particles became very round and produced much submicron dust that remained in the bed. This dust deposited on the tube surface and prevented any significant wear. Silicon carbide particles also became round but primarily produced debris larger than 1 μm, which did not form any protective layer on the tube surface. Quartz remained relatively sharp throughout testing and resulted in the greatest wear, even though a partially protective submicron particle layer did form.

A new testing rig of basically the same design has been constructed that will operate at the elevated temperatures characteristic of in-bed tubes in fluidized bed combustors. The combined effects of wear and corrosion in this environment will be studied over the next two years to develop a fundamental understanding of the system and to suggest means of reducing tube material wastage.

Appendices

APPENDIX A

DIVISION PERSONNEL*

1988 Scientific Staff

Investigators	Postdoctoral and Other Scientists	Graduate Students		Participating Guests
Neil Bartlett	R. Hagiwara	W. Casteel	B. Shen	
Robert Bergman		K. Bharucha M. Burn J. Duncan T. Foo D. Glueck J. Hartwig	M. Hostetler D. Klein R. Michaelman R. Simpson P. Walsh E. Wasserman	
Leo Brewer		B. Ebbinghaus K. Krushwitz	S. Leonard	
John Clarke		A. Cleland N. Fan M. Heaney	A. Miklich J. Schmidt	R. Dalven
Marvin Cohen		S. Zhang		A. Garcia
Eugene Commins		K. Abdullah		
Robert Connick	R. Adamic			
Didier de Fontaine		A. Berera	P. Huang	M. Kraitchman S. Menon M. Wiedenmeier
Lutgard De Jonghe	S. Visco		M. Liu	
Norman Edelstein Richard Andersen Kenneth Raymond Andrew Streitwieser, Jr. David Templeton Allan Zalkin	D. Ball S. Beshouri J. Bucher G. Shalimoff	T. Boussie T. Franczyk W. Kot W. Lukens P. Matsunaga D. Piehler	R. Rosen M. Smith L. Uhlir M. Weydert Q. Yu	C. Jenson J. Karpishin S. Konetschny-Rapp B. Lulay M. Neu S. Schmitt L. Templeton T. Westmoreland D. White
James Evans	O. Rego-Monteiro	L. Feng B. Li	G. Savaskan S. Shieh	
Leo Falicov	C. Chen	D. Chrzan	J. Freericks	
Andreas Glaeser	A. Tomsia	J. Roedel	M. Shalz	
Harvey Gould	C. Carlberg J. Schweppe	V. Kostroun		

*Does not include Division personnel affiliated only with CAM.

Investigators	Postdoctoral and Other Scientists	Graduate Students		Participating Guests
Ronald Gronsky	A. Meike N. Merk M. Sluiter J. Ulan	K. Atwal M. Fendorf	K. Fortunati M. Tidjani	C. Burmester F. Dupont C. Willis L. Yamamoto
Eugene Haller*				
Charles Harris		R. Jordan	E. Peterson	J. Brown E. Haas R. Hoff M. Lee W. Merry M. Paige D. Pennington D. Russell K. Schultz B. Schwartz D. Smith
Carson Jeffries		Y. Kim	Q. Lam	
Harold Johnston		J. Burley P. Hunter C. Miller	K. Patten W. Sisk	
Yuan Lee	D. Anex M. Cote	J. Allman B. Balko P. Chu R. Continetti M. Covinsky E. Cromwell H. Davis	J. Meyers T. Miau J. Price A. Schmoltner A. Suits M. Vrakking	M. Crofton D. Liu P. Weber
William Lester, Jr.	V. Kresin	R. Barnett	R. Owen	J. Andrews B. Hammond S. Huang P. Pernot M. Soto Z. Sun C. Tsai
Alan Levy	S. MacAdam			G. Gangqiang Y. Liu B. Wang
Steven Louie		J. Zhu		
William Miller		Y. Chang L. Gaucher T. Gray	A. Makri B. Ruf P. Teal	S. Auerbach A. Peet W. Yang J. Zhang
C. Bradley Moore	J. Harrison	T. Butenhoff Y. Choi	D. Darwin S. Kim	R. Alverez A. Kung
Rolf Muller	D. Schwartz	M. Armstrong R. Crocker	S. Mayer	L. Kim
John Newman		V. Battaglia T. Fuller A. Grabowski C. Haili	A. Hauser P. Shain A. West	
Donald Olander	J. Abrefah A. Motta	Y. Kim M. Moalem	K. Park L. Wang	M. Ballooch H. Harrell
Norman Phillips		S. Kim B. Woodfield	Y. Wu	A. Amato R. Caspary R. Fisher

*Also affiliated with the Engineering Division

Investigators	Postdoctoral and Other Scientists	Graduate Students		Participating Guests
Alexander Pines	G. Chingas P. Grandinetti Z. Peng J. Zwanziger	B. Black D. Caplan J. Chang C. Connor T. Jarvie R. Jelinek H. Long	K. Mueller J. Pearson M. Raferty M. Rosen S. Rucker J. Sachleben B. Sun	B. Chmelka C. Schmidt Y. Wu
Kenneth Pitzer	R. Singh			J. Hovey
John Prausnitz		E. Anderson J. De Pablo	H. Hooper	
Michael Prior				R. Dorner R. Herrman R. Hutton
Paul Richards		G. Bernstein M. Fischer C. Mears	D. Miller R. Phelps	P. Timbie
Gerd Rosenblatt	J. Ager K. Viers			J. Roe
Philip Ross	A. Haner			L. Johnson
Richard Saykally		K. Busarow R. Cohen	D. Gwo D. Steyert	
Alan Searcy	P. Hou D. Meschi	J. Bierach J. Bullard	R. Cinque D. Fenwick	
Y. Ron Shen		W. Chen R. Chin M. Feller A. Karn	T. Moses C. Mullin X. Zhu	M. Haner D. Pauschinger
David Shirley	P. Heimann M. Siggel	Z. Huang E. Hudson L. Medhurst B. Niu A. Schach von Wittenau	T. Shulman R. Vanzee L. Wang L. Wang J. Zhang	Z. Li J. Liesgang
Angelica Stacy		J. Badding M. Geselbracht W. Ham R. Hoskins	S. Keller S. Stoll P. Vernooy	R. Bornick V. Carlson G. Holland
Gareth Thomas		M. Chandramouli K. Lin	L. Tang	D. Callahan M. Cinibulk T. Epicier J. Kim C. Koehler C. Koestler K. Liu
Charles Tobias		D. Gibbons S. Hessami K. Jordan	L. McVay D. Sutija	R. Anderson
K. Peter Vollhardt		A. Kahn R. Myrabo	M. West	
Kenneth Westmacott	U. Dahmen C. Hetherington R. Kilaas K. Krishnan M. O'Keefe			
Peter Yu		D. Kim		P. Seguy

Support Staff*

Division Administrative Staff

M. Alper — Associate Division Director
Division Administrators: L. Maio, M. Montgomery

Administration

L. English
J. Leonard
T. Lynem
R. Rodriguez

Personnel/Financial

C. Coolahan
L. Dunnivant
C. Gerardi
M. Graham
S. Nasman
S. Waters

Purchasing

S. Stewart
P. Conant

Technical Editor

R. Albert

Travel

S. Quarello

Administrative/Secretarial Staff

T. Allyn
R. Arcol
M. Atkinson
C. Bauer
C. Becker
H. Benson
M. Bishop
G. Brazil
D. Carmichael
T. Crawford
J. Denney
E. Edelson
S. Ewing
N. Facher
S. Gangwer
C. Gliebe
L. Gloria
R. Jones
B. Kuchinsky
M. Momii
M. Moore
B. Moriguchi
V. Narasimhan
M. Noyd
G. Osterloh
M. Ragsdale
P. Ray
R. Rodriguez
B. Salisbury
V. Savitt
P. Southard
K. Steele
A. Weightman
A. Wingfield
K. Wong
S. Yamagishi
B. Zambrano
J. Zissler

Technical Staff

Technical Coordinator: J. Holthuis

D. Ackland
H. Ackler
D. Ah Tye
H. Brendel
R. Cardenas
N. Claytor
D. Colomb
K. Desai
C. Echer
R. Ellis
C. Flor
C. Gleeson
A. Gronsky
J. Holthuis
J. Jacobsen
D. Jurica
E. Mah
J. Miles
E. Nelson
M. Ng
D. Owen
T. Prussin
P. Ruegg
L. Rumaner
J. Severns
W. Smith
H. Sokol
B. Sun
L. Sun
G. Tabler
J. Turner
J. Wu

*Support staff affiliated only with CAM not included.

APPENDIX B

DIVISION COMMITTEES

DIVISIONAL COUNCIL

A. Bell
L. De Jonghe
H. Johnston
W. Lester (Alternate)
S. Louie
K. Raymond
R. Ritchie
P. Ross
A. Searcy (Alternate)
G. Thomas
K. Westmacott

DIVISIONAL RESEARCH STAFF COMMITTEE

R. Bergman
N. Edelstein
L. Falicov
R. Muller*
R. Ritchie
K. Westmacott

ELECTRON MICROSCOPE USERS COMMITTEE

R. Gronsky
P. Ross*
K. Westmacott

EQUIPMENT REVIEW COMMITTEE

J. Clarke
H. Johnston
R. Muller*
R. Ritchie
P. Yu

TECHNICAL STAFF AND SHARED FACILITIES COMMITTEE

M. Alper
L. De Jonghe*
R. Gronsky
J. Holthuis
L. Maio
J. Morris
M. Prior
P. Ross*
G. Somorjai
G. Thomas

*Chairman

ADMINISTRATIVE STAFF COMMITTEE

M. Alper
L. Maio*
M. Montgomery
C. Peterson
A. Searcy

MCSD SAFETY COORDINATOR

D. Meschi
R. Ellis (Alternate)

SAFETY AND LABORATORY STANDARDS COMMITTEE

Buildings 62, 66, and 72

H. Brendel
D. Colomb
R. Ellis (Alternate)
L. English
J. Haley
J. Holthuis
L. Johnson
D. Jurica
E. (Fong) Mah
D. Meschi*
B. Muhammad
R. Muller
E. Nelson
E. Perez
C. Peterson
P. Ruegg
M. Salmeron
J. Severns
G. Shalimoff
S. Stewart
D. Tribula
M. Van Hove
D. Zeglinski

Building 70A

E. Bourret-Courchesne
G. Shalimoff*
R. Van Zee

Buildings 62 and 66 Building Manager:
D. Meschi/R. Ellis
(Alternate: C. Peterson)

Building 72 Building Manager:
K. Westmacott
(Alternate: E. Nelson)

APPENDIX C

LIST OF DIVISIONAL SEMINARS

Chemical Dynamics Seminars

Date	Speaker and Affiliation	Seminar Title
2-24-88	Y. Haas, Department of Chemistry, Hebrew University of Jersualem, Israel	Photodynamics of Molecules Excited to the $n\pi^*$ State
2-29-88	K. Eisenthal, Department of Chemistry, Columbia University, New York	Laser Studies of Liquid Surfaces
3-7-88	C. Nikitin, Insitute of Chemical Physics, Moscow, USSR	Modeling of Nonadabatic Effects In Rotational Structure of NH_3 Overtone Bands
3-10-88	D. McKean, Department of Chemistry, University of Aberdeen, Scotland	Expermental and *Ab Initio* Studies of CH and SiH Bonds
3-18-88	A. DePristo, Department of Chemistry, Iowa State University, Ames	Reactions of H_2 on Ni Surfaces and Clusters
4-1-88	D. Thompson, Department of Chemistry, Oklahoma State University, Stillwater	Intramolecular Vibrational Energy Redistribution and Mode Specificity in Unimolecular Reactions
4-7-88	J. Fenn, Department of Chemical Engineering, Yale University, New Haven, CT	Electrospray Mass Analysis of Large Molecules
4-8-88	D.G. Fleming, Department of Chemistry, University of British Columbia, Vancouver	Muonium Reactivity in Gases: Isotope Effects and Quantum Tunneling in Thermal Abstraction and Addition Reactions
4-13-88	R. Pitzer, Department of Chemistry, Ohio State University, Columbus	Electronic Structure and Spectra of Uranocene
5-13-88	C. Sorensen, Department of Chemistry, Kansas State University, Manhattan	Aggregation Kinetics in Colloids and Aerosols
7-21-88	H. Pickett, Jet Propulsion Laboratory, Pasadena, CA	A Far-IR Limb Observing Spectrometer for the Stratosphere: Studies of the Ozone Hole
7-22-88	B. Friedrich, Department of Chemistry, Harvard University, Cambridge, MA	Collision Dynamics and the Change of Electronic State
7-26-88	C. Zhang, Dalian Institute of Chemical Physics, Chinese Academy of Sciences, Dalian, PRC	ODR-MPI E-E Energy Transfer in Diatomics with Rotational Resolution
8-22-88	F. Temps, Max-Planck Institut für Strömungsforschung, Göttingen, FRG	The Reactions of Methylene Radicals in the Gas Phase
9-22-88	J. Hutson, Department of Chemistry, University of Durham, England	Intermolecular Potentials from the Spectroscopy of van der Waals Dimers and Trimers

Date	Speaker and Affiliation	Seminar Title
9-29-88	R.G. Littlejohn, Department of Physics, University of California at Berkeley	Periodic Orbits in Chaotic Spectra
9-30-88	K. Lehmann, Department of Chemistry, Princeton University, Princeton, NJ	Spectroscopy and Intramolecular Dynamics of Ammonia
10-5-88	M. Quack, Laboratorium für Physikalische Chemie der ETH, Zürich, Switzerland	Intramolecular Dynamics and Statistical Mechanics from High Resolution Spectroscopy and *Ab Initio* Theory
10-14-88	A.D.J. Haymet, Department of Chemistry, University of California at Berkeley	Water and Aqueous Solutions
11-8-88	J. Driessen, Eindhoven University of Technology, Eindhoven, The Netherlands	Polarization Effects in Collisions Involving Excited Rare Gas Atoms
11-18-88	C.A. Taft, Centro Brasileiro de Pesquisas Fisicas, Rio de Janeiro, Brazil	Electronic Structure, Hyperfine Interactions, and Magnetic Properties of Transition Metal and Rare Earth Complexes
11-22-88	D. Herschbach, Department of Chemistry, Harvard University, Cambridge, MA	Bent Atoms (a Tribute to Otto Stern)
12-2-88	S. Mukamel, Department of Chemistry, University of Rochester, Rochester, NY	A Unified Description of Electron Transfer and Molecular Nonlinear Optical Lineshapes
12-8-88	H. Petek, Institute for Molecular Science, Okazaki, Japan	Isomerization Dynamics of Stilbene in Rare Gas Clusters

Electron Microscopy Seminars

4-4-88	M. Ignat, CNRS, France	*In situ* Studies of Deformation and Fracture of Composites
4-13-88	M.C. Pienkowski, University of Oxford, England	HREM of Mixed UO_2 Oxides ... Evidence for Ordering?
4-18-88	K. Ishizuka, Kyoto University, Japan	3-D Effect of Dynamical Electron Diffraction
4-25-88	M. Mills, Sandia National Laboratories, Livermore, CA	A Study of Dislocation Cores Using HREM
6-10-88	H. Zandbergen, Gorlaeus Laboratories, The Netherlands	Electron Microscopy of Tl and Bi High T_c Superconductor Compounds
6-15-88	J. Lepinoux, CNRS, Poitiers, France	Simulation of the Dynamic Organization of Dislocation Structures
8-16-87	S. Iijima, NEC Corporation, Japan	Natural Superstructure in MOCVD-Grown GaInP
9-12-88	R.G. Faulkner, Leicestershire, UK	Grain Boundary Segregation and its Relation to Embrittlement in Steels
10-7-88	D. Lestrat, École des Mines des Paris, France	Performance and Structure of New PM Nickel Base Superalloys for Turbine Discs
12-5-88	P. Veyssiere, CNRS-ONERA, Chatillon, France	Dislocation Properties in Ordered Intermetallic Alloys: a Weak-Beam Study

Other Seminars Hosted

Date	Speaker and Affiliation	Seminar Title
2-88	G.Z. Yin, Intel Corp., San Jose, CA	Orthogonal Design Optimization
6-23-88	A.L. Johnson, National Bureau of Standards, Gaithersburg, MD	Surface Structure Investigated by ESDIAD: Electron Stimulated Desorption, Ion Angular Distributions
7-13-88	J. Peterson, University of Tennessee and Oak Ridge National Laboratory	Bulk Phase Chemical Studies on the Edge of Matter: The Transcurium Elements
8-2-88	J. Liesegang, Department of Physics and Research Centre for Electron Spectroscopy, La Trobe University, Melbourne, Australia	Ion Interference Studies (XPS) on the Surface of the Fluoride Ion Selective Membrane LaF_3
8-24-88	C.F. Geraldes, Department of Chemistry, University of Coimbra, Portugal	Lanthanide Macrocyclic Chelates as NMR Shift Probes and MRI Contrast Agents: Some Selected Applications
8-30-88	C-H. Wong, Texas A & M University	Enzymes in Organic Synthesis
9-5-88	G. Kaindl, Institut für Atom und Festkörperphysik, Fachbereich Physik, Freie Universität, Berlin	Photoemission Studies of Schottky-Barrier Formation in Metal/Semiconductor Interfaces
9-6-88	D.E. Koshland, Jr., University of California at Berkeley	Propagation of Conformational Changes in Membrane Proteins
9-6-88	C.H. Heathcock, University of California at Berkeley	Daphniphyllum Alkaloids: Biomimetic Synthesis or Chemomimetic Synthesis?
9-20-88	S.F. Pedersen, University of California at Berkeley	Practical Applications of Low-Valent Early Transmission Metal Halides in Organic Synthesis
9-21-88	G. Cloke, School of Chemistry and Molecular Sciences, University of Sussex, Brighton, England	Organo f-Element Compounds in High and Low Oxidation States
9-22-88	H-J. Knölker, Institut für Organische Chemie der Universität Hannover, FRG	Novel Approaches to Imidazoles, Spiroquinolines, and Carbazoles: First Total Synthesis of Carbazomycine A
9-27-88	W. Pfleiderer, University of Konstanz, Switzerland	The Oligoribonucleotide Problem
9-28-88	H.-D. Amberger, Institute for Inorganic Chemistry, University of Hamburg, FRG	Interpretation of the Magnetochemical, Magnetooptical, and Optical Properties of Adducts Derived from the Tris(cyclopentadienyl)-Lanthanides on the Basis of Crystal-Field Theory
10-4-88	E. Nakamura, Tokyo Institute of Technology	New Aspects of Reactivities and Selectivities in Organocopper Chemistry
10-13-88	S. Danishefsky, Yale University	The Enediyne and Glycoside Problem
10-18-88	J.L. Sessler, University of Texas at Austin	Quinone Substituted Porphyrin Dimers: New Photosynthetic Model Systems
10-19-88	S.V. Ley, Imperial College, London	New Methods for Natural Product Synthesis
10-25-88	J.A. Marshall, University of South Carolina	Synthesis of Cembranolide Natural Products

Date	Speaker and Affiliation	Seminar Title
11-1-88	R.L. Funk, Pennsylvania State University	On the Way to Periplanone A...
11-8-88	J.D. Winkler, University of Chicago	Synthesis of Natural and Unnatural Products
11-15-88	G.W. Gokel, University of Miami	New Chemistry of Lariat Ethers
11-22-88	D.E. Cane, Brown University	Cell Free Studies of the Biosynthesis of Isoprenoids
11-29-88	K. Biemann, Massachusetts Institute of Technology	Recent Developments and Applications of Tandem Mass Spectrometry
12-5-88	W. Wurth, IBM Almaden Research Center, San Jose, CA	$X\alpha$ Calculations of Molecular Photoabsorption Spectra
12-6-88	M. Kuehne, University of Vermont	New Syntheses of Indole and Indoline Alkaloids
12-15-88	E. Paparazzo, Istituto di Teoria e Struttura Elettronica, CNR, Rome, Italy	Oxides at Surfaces and Interfaces
12-16-88	B. Olsson, The Royal Institute of Technology, Stockholm, Sweden	Recent Results in Molecular Dynamics using the HFD Method

APPENDIX D

INDEX OF INVESTIGATORS*

*Boldface numbers indicate investigators' main programs.

LAWRENCE BERKELEY LABORATORY
TECHNICAL INFORMATION DEPARTMENT
1 CYCLOTRON ROAD
BERKELEY, CALIFORNIA 94720